ICP Mass Spectrometry Handbook

Edited by

Simon M. Nelms

Blackwell Publishing

CRC Press

Inductively Coupled Plasma Mass Spectrometry Handbook

Inductively Coupled Plasma Mass Spectrometry Handbook Edited by Simon M. Nelms
 ISBN: 978-1-405-10916-1

Inductively Coupled Plasma Mass Spectrometry Handbook

Edited by

Dr Simon M. Nelms
Thermo Electron,
Ion Path, Road Three,
Winsford, Cheshire, CW7 3BX

Blackwell
Publishing

CRC Press

Editorial offices:
Blackwell Publishing Ltd, 9600 Garsington Road, Oxford OX4 2DQ, UK
Tel: +44 (0)1865 776868
Blackwell Publishing Asia Pty Ltd,
550 Swanston Street, Carlton, Victoria 3053, Australia
Tel: +61 (0)3 8359 1011

ISBN10: 1-4051-0916-5
ISBN-13: 978-1-4051-0916-5

Published in the USA and Canada (only) by
CRC Press LLC, 2000 Corporate Blvd., N.W., Boca Raton, FL 33431, USA
Orders from the USA and Canada (only) to
CRC Press LLC

USA and Canada only:
ISBN10: 0-8493-2381-9

First published 2005

Library of Congress Cataloging-in-Publication Data:
A catalog record for this title is available from the Library of Congress

British Library Cataloguing-in-Publication Data:
A catalogue record for this title is available from the British Library

Set in 9.5/12pt Times and Optima
by Techbooks, India
Printed and bound in India
by Gopsons Paper Ltd, Noida

The publisher's policy is to use permanent paper from mills that operate a sustainable forestry policy, and which has been manufactured from pulp processed using acid-free and elementary chlorine-free practices. Furthermore, the publisher ensures that the text paper and cover board used have met acceptable environmental accreditation standards.

For further information on Blackwell Publishing, visit our web site: www.blackwellpublishing.com

To all the many authors of this book, for their hard work and dedication in preparing the manuscripts and to my wife, Liz, whose encouragement and support throughout the production of this text proved so valuable to me.

Contents

Foreword

Inductively coupled plasma – mass spectrometry (ICP-MS) had a humble beginning in the mid-1970s. Loops of twisted wire were important structural components, at least in the instrument built in Ames, and a barricade of human bodies between the ICP and the recording electronics was found to be an effective way to shield RF noise. For humanitarian reasons, the latter method was used only when necessary to produce data to show at a conference, usually the day before departure! The thrill of generating such last-minute results remains in ICP-MS research to this day.

From these dubious origins, ICP-MS has become a highly developed analytical technique for elemental and isotopic analysis. Over 4000 such instruments have been produced, and they are widely used in many important scientific applications. For example, the laptop computer used to write this Foreword would not have anything like its present performance without ICP-MS to determine trace metal impurities in the purity of the reagents and chips used. The success of ICP-MS in this application also illustrates the value of plain old good luck in science. Four elements for which performance is improved greatly by use of the cool ICP are Na, K, Ca and Fe. By great good fortune, these just happen to be key impurity elements in semiconductor production!

It is this widespread application base, the enabling of new types of multielement measurements at concentration levels previously inaccessible, that represents the scientific value of ICP-MS. Indeed, the detection limits are now restricted more by the cleanliness of the blank than by the sensitivity of the ICP-MS instrument, at least for most samples and elements.

ICP-MS has improved substantially since the earlier Handbook by Jarvis, Gray and Houk, published in 1991; the use of low-flow nebulizers, magnetic sectors and collision cells was just beginning back then. Some instruments now fit onto a benchtop; most have something like the Nike Swoosh emblazoned somewhere on the cover. Decorations aside, the present book provides detailed descriptions of current instrumentation and capabilities, analytical considerations like interferences, and key applications of ICP-MS. The information herein is very valuable to scientists using ICP-MS, as well as those seeking further improvements in performance. The method is not quite plug-and-play, and background knowledge of the instrumentation, its strengths and limitations is important in the production of valid results. This book fills that need, and I congratulate the editor and the authors for this very valuable contribution.

R. S. Houk
Professor of Chemistry
Ames Laboratory U. S. Department of Energy
Iowa State University
Ames, Iowa 50011 USA

Preface

Inductively coupled plasma mass spectrometry (ICP-MS) is arguably the most versatile trace elemental analysis technique available today. Depending on the individual instrument configuration, sample types ranging from sea waters and rock digests to ultra-pure semiconductor grade chemicals can be routinely analysed, for almost all the elements in the Periodic Table, from low pg/mL (in most cases) to high μg/mL concentration levels. It is this versatility that has led to the rapid acceptance and subsequent growth of the technique. Since the launch of the first commercial quadrupole ICP-MS instruments in 1983, the technology has evolved from large, floor-standing, manually operated systems, with limited functionality and relatively poor detection limit capabilities, to compact, sensitive and highly automated routine analytical instruments. From the outset, it was observed that although ICP-MS spectra were much less complex than ICP optical emission spectra, interferences were nonetheless present and as ICP-MS has grown, considerable attention has been focused on achieving wholly interference-free analysis. The first step towards achieving this objective was the development of high resolution ICP-MS in the late 1980s, whereby analytes could be resolved from interferences using a magnetic field, by virtue of the mass differences between analyte/interference pairs. This technology, although effective in resolving a wide range of polyatomic interferences, lacks the power to resolve isobaric interferences (i.e. overlap between isotopes of the same nominal mass, such as ^{87}Rb and ^{87}Sr). More recently, the advent of collision/reaction cell technology has revolutionised quadrupole ICP-MS. Born out of existing technology for triple quadrupole organic mass spectrometers, collision/reaction cells have taken interference reduction a dramatic step forward. Through collision and reaction with appropriate gases in a cell preceding the analyser quadrupole, interferences such as $^{40}Ar_2^+$ can be almost completely eliminated whilst leaving analyte ions (^{80}Se in this case) relatively unaffected. As with high resolution ICP-MS, collision/reaction cells cannot provide a complete solution to isobaric interference, although through the use of carefully selected reaction conditions, some isobaric interferences can be shifted to higher masses as molecular species (for example separating Rb and Sr using CH_3F as the reaction gas to selectively form SrF). Collision/reaction cell technology makes up a large part of current research into ICP-MS and this is reflected in the substantial section devoted to the subject in this book.

The aim of truly interference-free analysis may ultimately be realised by the future development of Fourier transform ion cyclotron resonance (FT-ICR) ICP-MS. This technique, although in its infancy (and currently prohibitively expensive), has demonstrated a resolution capability of 88000 and is theoretically capable of resolution in excess of 1×10^6, rendering it the only currently available technique that has the potential to directly resolve isobaric interferences. The principles and applications of this exciting technology are discussed in the second chapter of this book.

Extensive advances and improvements have been made in the area of sample introduction for ICP-MS and this subject forms a large part of this text. The currently available liquid and solid sampling systems, from nebulisers and spray chambers to electrothermal vaporisation and laser ablation, are described and discussed in detail herein.

In addition to the advances in ICP-MS instrument and sample introduction accessories design that have occurred, applications of the technique, particularly in the field of speciation analysis, have also evolved considerably during this time. Speciation analysis (the science of measuring elemental species) has grown significantly in importance and application in recent years, as a result of the realisation that the bioavailability and corresponding nutritional or toxic properties of an element depend on the chemical form in which it is present. In practice, species separation is performed using chromatographic techniques such as CE, HPLC or GC, prior to on-line detection using a variety of detectors. The popularity of ICP-MS as a detector for speciation studies at the trace levels encountered in real-world samples can be attributed to the relative ease with which it can be coupled to chromatography equipment and its ability to handle low concentration, transient signals. The present state-of-the-art and future potential of speciation analysis with ICP-MS detection is described in Chapter 7 of this book.

This book aims to provide a background to this exciting technology, with chapters devoted to plasma generation, ion sampling and focusing, mass analysis, ion detection and sample introduction. Calibration and quantitative analysis methodologies are also reviewed together with substantial discussion on quality assurance and result validation. Finally, this book also aims to update the reader with recent developments in the main application areas.

Contributors List

Andrew Fisher	School of Earth, Ocean and Environmental Sciences, Plymouth University, Drake Circus, Plymouth, Devon, PL4 8AA, United Kingdom
Alison Holliday	LCABIE CNRS UMR 5034, Helioparc, 2, Avenue du President Angot, 64053 Pau, Cedex 9, France
Bill Spence	Thermo Electron, Ion Path, Road Three, Winsford, Cheshire, CW7 3BX, United Kingdom
Carla Vogt	Institute of Inorganic Chemistry, Department of Analytical Chemistry, University of Hannover, Callinstrasse 9, D-30167 Hannover, Germany
Christopher Latkoczy	Gloriasteig 5, 8044 Zurich, Switzerland
Diethard K. Bohme	Department of Chemistry, York University, 4700 Keele Street, Toronto, Ontario, M3J 1P3, Canada
David Wray	Earth and Environmental Sciences Department, University of Greenwich at Medway, Pembroke, Central Avenue, Chatham Maritime, Kent, ME4 4AW, United Kingdom
Dick Stresau	ETP Electron Multipliers, 31 Hope Street, P.O. Box 143, Ermington, 2115 New South Wales, Australia
Dmitry R. Bandura	MDS Sciex, 71 Four Valley Drive, Concord, Ontario, L4K 4V8, Canada
Eva Krupp	LCABIE CNRS UMR 5034, Helioparc, 2, Avenue du President Angot, 64053 Pau, Cedex 9, France
Frank Vanhaecke	Laboratory of Analytical Chemistry, Gent University, Proeftuinstraat 86, B-9000 Gent, Belgium
Fabienne Saby	LCABIE CNRS UMR 5034, Helioparc, 2, Avenue du President Angot, 64053 Pau, Cedex 9, France

Geoff M. Nowell	Department of Earth Sciences, University of Durham, Science Laboratories, Durham, DH1 3LE, United Kingdom
Gregory C. Eiden	Analytical Chemistry Group, Pacific Northwest National Laboratory, Mail Stop P7-07, Richland, WA 99352, USA
Gunda Köllensperger	Institute of Chemistry, University of Agricultural Sciences (BOKU), Muthgasse 18, A-1190 Vienna, Austria
Gregory K. Koyanagi	Department of Chemistry, York University, 4700 Keele Street, Toronto, Ontario, M3J 1P3, Canada
Heidi Goenaga-Infante	Laboratory of the Government Chemist (LGC), Specialised Techniques, Queens Road, Teddington, Middlesex, TW11 0LY, United Kingdom
José L. Todoli	Department of Analytical Chemistry, University of Alicante, P.O. Box 99, 03080 Alicante, Spain
Jackie Morton	Biological Monitoring, Health and Safety Laboratory, Harpur Hill, Buxton, SK17 9JN, United Kingdom
Jean-Marie Collard	Analytical Technologies Division, Solvay Research and Technology, 310 Rue de Ransbeek, B-1120 Brussels, Belgium
Jochen Vogl	Bundesanstalt für Materialforschung und –prüfung, Leiter AG Isotopenanalytik, Unter den Eichen 87, 12205 Berlin, Germany
Jonathan H. Batey	Thermo Electron, Ion Path, Road Three, Winsford, Cheshire, CW7 3BX, United Kingdom
Kevin Hunter	ETP Electron Multipliers, 31 Hope Street, P.O. Box 143, Ermington, 2115 New South Wales, Australia
Matthew S. A. Horstwood	NERC Isotope Geoscience Laboratory, British Geological Survey, Kingsley Dunham Centre, Keyworth, Nottingham, NG12 5GG, United Kingdom
Mariella Moldován	LCABIE CNRS UMR 5034, Helioparc, 2, Avenue du President Angot, 64053 Pau, Cedex 9, France
Martin Liezers	Thermo Electron, Ion Path, Road Three, Winsford, Cheshire, CW7 3BX, United Kingdom
Olivier F. X. Donard	LCABIE CNRS UMR 5034, Helioparc, 2, Avenue du President Angot, 64053 Pau, Cedex 9, France

Rosa Rodríguez Martín-Doimeadios	LCABIE CNRS UMR 5034, Helioparc, 2, Avenue du President Angot, 64053 Pau, Cedex 9, France
Scott D. Tanner	MDS Sciex, 71 Four Valley Drive, Concord, Ontario, L4K 4V8, Canada
Steve J. Hill	School of Earth, Ocean and Environmental Sciences, Plymouth University, Drake Circus, Plymouth, Devon, PL4 8AA, United Kingdom
Simon M. Nelms	Thermo Electron, Ion Path, Road Three, Winsford, Cheshire, CW7 3BX, United Kingdom
Stephan Hann	Institute of Chemistry, University of Agricultural Sciences (BOKU), Muthgasse 18, A-1190 Vienna, Austria
Thomas Prohaska	Institute of Chemistry, University of Agricultural Sciences (BOKU), Muthgasse 18, A-1190 Vienna, Austria
Vladimir I. Baranov	MDS Sciex, 71 Four Valley Drive, Concord, Ontario, L4K 4V8, Canada
Yoko Kishi	IAS Incorporated, 4-39-5-916 Fujimidai, Kunitachi-shi, Tokyo, 186-0003, Japan
Yuichi Takaku	Department of Radioecology, Institute for Environmental Sciences, 1-7 Ienomae Obuchi, Rokkasho-mura, Kamikata-gun, Aomori 039-3212, Japan
Zoë A. Quinn	MDS Sciex, 71 Four Valley Drive, Concord, Ontario, L4K 4V8, Canada

Chapter 1
Plasma Generation, Ion Sampling and Focusing

Steve J Hill, Andy Fisher and Martin Liezers

1.1 PLASMA GENERATION

Steve J Hill and Andy Fisher

The inductively coupled plasma (ICP) is the most widely used ionisation source for inorganic mass spectrometry. When argon gas passes through a quartz torch placed in an induction coil (also called the load coil) to which a radio frequency (RF) power between 750 and 1700 W is applied, an alternating current oscillates within the field. The frequency of oscillation is governed by the type of RF generator used, but most commercial instruments use a frequency of either 27.1 MHz or 40.6 MHz. These oscillations set up electrical and magnetic fields at the top of the torch. If a spark is then applied to the argon gas via a Tesla coil, electrons are stripped from some of the argon atoms. These electrons then become trapped in the magnetic field and are accelerated in closed circular paths. This process is known as inductive coupling and hence the plasma so formed is referred to as an inductively coupled plasma (ICP). As these rapidly moving electrons collide with neutral argon atoms, further electrons are stripped from the atoms and hence a chain reaction is established. It is also this collision process that generates the high temperature of the plasma. The annular plasma fireball that is formed therefore consists of neutral argon atoms, positively charged argon ions and electrons. The plasma will exist for as long as radio frequency power is supplied to the induction coil. The function of the plasma in analytical instruments is to transform the sample, usually a liquid, into ions. The plasma is at a temperature between 6000 and 10 000 K, depending on the region in the plasma, and therefore, the sample aerosol is readily desolvated, vaporised, atomised and then at least partially ionised. The extent of the ionisation, which is primarily a function of the first ionisation potential of the element relative to that of argon (15.76 eV), influences a number of factors including sensitivity and susceptibility to certain sample matrix effects. In argon plasmas, under hot plasma conditions, most of the elements in the periodic table produce predominantly singly charged ions at yields ranging from 5% to 100%. Some elements, such as Ce and Ba, have second ionisation potentials low enough to yield significant quantities of doubly charged ions. Fortunately, for the large majority of applications, interference from doubly charged ions is not a major problem but this source of interference does need to be considered for unusual applications such as measuring Na in novel Ti based semiconductor materials (interference from $^{46}Ti^{2+}$ on monoisotopic ^{23}Na). The ICP and its role as an ion source has been extensively described in the literature and will not be discussed further here. For more detailed information, the interested reader is directed to the reference texts of Hill et al.[1] and Janis et al.[2]

Inductively Coupled Plasma Mass Spectrometry Handbook Edited by Simon M. Nelms
 ISBN: 978-1-405-10916-1

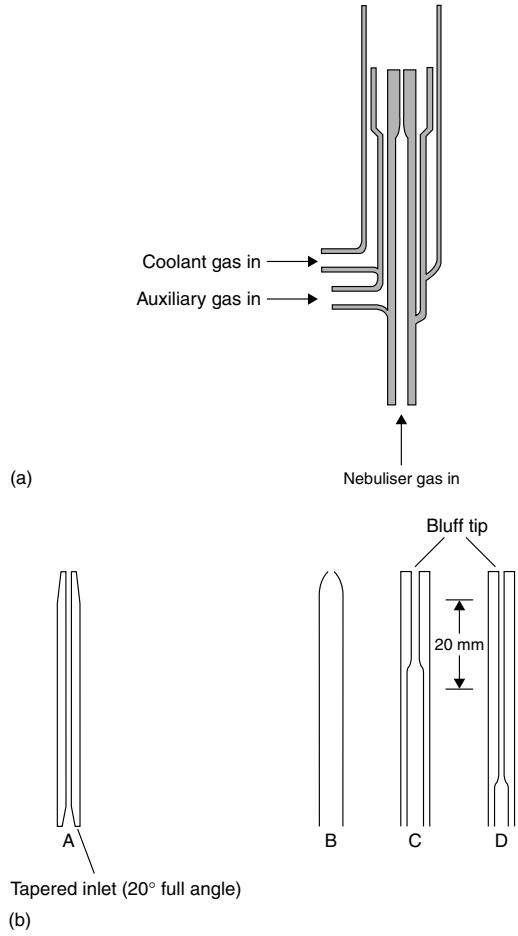

Figure 1.1 A schematic diagram of a typical torch (a) and different designs of injectors (b). Injectors C and D are more prone to blocking than injector A because of the sharp reduction in bore.

1.1.1 Torches

The vast majority of torches used today are of the basic Fassel style, as shown schematically in Figure 1.1. These torches consist of three concentric tubes through which the argon flows. The outermost of the flows contains the plasma or coolant gas typically operated at a flow rate of 11–15 L of argon min^{-1}. It is this gas flow that constitutes the plasma. The gas is introduced tangentially into the torch to push the plasma away from the sides of the quartz torch, and hence preventing it from melting. The tangential flow also gives rise to the characteristic tear-drop shape of the plasma. The middle of the three tubes carries the intermediate or auxiliary flow, typically operated at a flow rate of 0.5–1.5 L of argon min^{-1}. The main function of this gas flow is to push the plasma away from the innermost tube (the injector tube) to again prevent it from melting. The injector tube carries the gas flow from the nebuliser which is therefore often called the nebuliser gas flow. The flow rate will depend on the type of nebuliser used, but for a standard

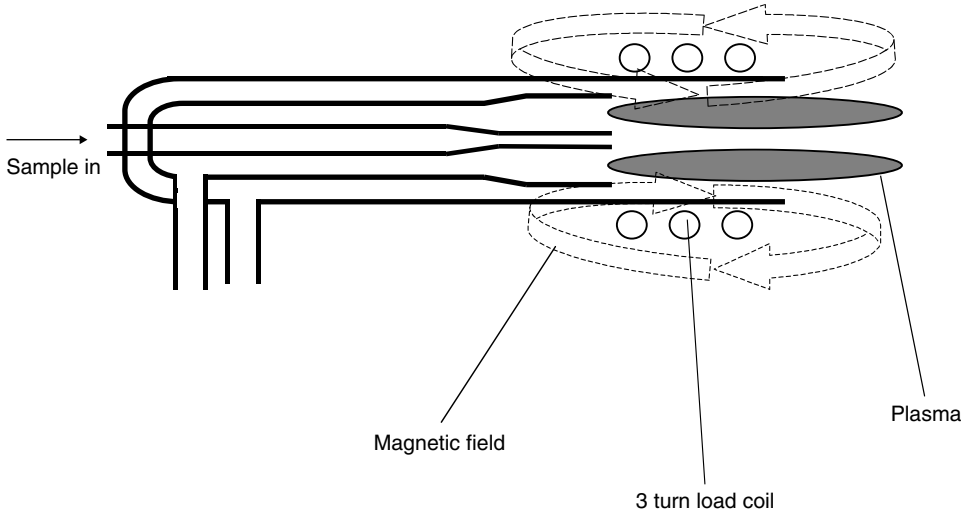

Figure 1.2 A schematic diagram of a plasma.

nebuliser/spray chamber assembly, 0.5–1.5 L min^{-1} is common. The nebuliser gas flow impacts on the centre of the annular fireball and, assuming the flow rate is sufficient, a hole will be punched through the centre of the plasma (the torus), forming a channel (the annulus). It is through this channel that the sample passes. A schematic diagram of a plasma is shown in Figure 1.2.

The standard Fassel-style torch is 18 mm in diameter and the injector has a typical bore of 1.5 mm. There are torches that have smaller dimensions, lower gas flow rates and operate at a reduced power.[3] It has been demonstrated that the figures of merit for these torches, in terms of limit of detection and precision, are only marginally inferior to those from the standard-size torch, but they are also less tolerant of samples with a high content of dissolved solids. For such samples, the injector becomes blocked relatively easily and will become unusable after only a few samples. Conversely, the low-flow torch is more capable of sustaining a plasma when organic solvents are introduced.

Many torches currently in use are partially demountable. Here, the injector may be removed and replaced with another of a different bore, a different configuration or machined from a different material. The injector used will depend on the type of sample to be analysed. For samples such as blood, even a ten-fold dilution leaves a substantial content of solid material, and this will eventually block a standard 1.5 mm bore injector. It is therefore useful to be able to replace this standard injector with one of larger bore, i.e. 2 mm or perhaps even 2.5 mm. Wide-bore injectors are less likely to become blocked and, if blockage does occur, it will occur more slowly, enabling a larger number of samples to be analysed prior to cleaning. The drawbacks with larger bore injectors are that they 'punch' through the plasma less readily, so require operation with higher nebuliser gas flows, and generally yield lower sensitivity than narrower injectors as the aerosol transmitted to the plasma is less dense. This property has the benefit, however, of producing reduced matrix effects, such as ionisation suppression, in the plasma as less dense aerosols are more efficiently processed in the plasma.

Torch injectors also come in a number of different configurations, some of which are shown in Figure 1.1. Injectors that have a step reduction in the bore are more likely to block than those that

have a more gradual decrease. This is because samples with high solid content tend to condense on the angular step reduction. As discussed previously, the main torch body is manufactured from quartz. Some injectors are however made from other materials, such as alumina, platinum, sapphire or ceramic. Such injectors are more resilient to corrosive samples, e.g. those containing hydrofluoric acid, and in the case of platinum and sapphire can be manufactured in a highly pure form for ultra-trace analysis applications.

A number of torches are available for use with more specialised techniques. In torch vaporisation (ITV) and direct sample insertion (DSI) are techniques whereby a sample is injected onto a probe or cup, made from graphite or a refractory metal, and this is inserted directly up the injector of a modified torch. Both of these approaches are capable of introducing very small volumes of liquid sample and very small masses of solid materials into the plasma. These techniques are more commonly used with radial ICP-AES instrumentation, but they may find application with ICP-MS.[4,5] A schematic diagram of such a torch is shown in Figure 1.3. The main modification is a widening of the injector bore to accommodate the probe. Low-pressure torches for use with ICP-MS have also been described. In one particular application[6] the torch was used to sustain a helium-based ICP that could be used as a detector for gas chromatography. In this study, organotin compounds were detected at low levels and then, by using a lower power, fragmentation patterns of the compounds could also be identified. Thus the plasma could be used as both a hard ionisation source, i.e. where the compounds are completely destroyed to provide the elemental composition, and as a much gentler ionisation source to characterise the analyte in much the same way as a traditional GC-MS instrument.

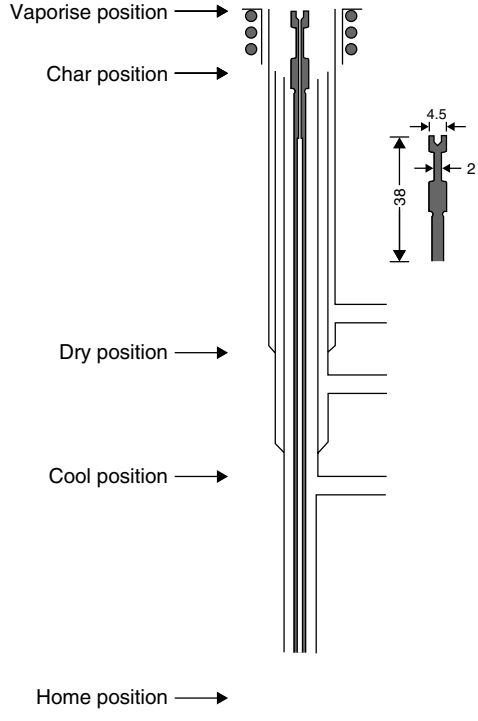

Figure 1.3 Schematic diagram of a modified torch used for DSI.

1.1.2 Mixed gas plasmas

Although the vast majority of plasmas are formed entirely of argon, the introduction of alternative gases can have very beneficial effects. The Fassel-style torch is not very tolerant of alternative gases that, even at relatively low concentrations, can extinguish the plasma. The ease with which they are extinguished will depend on the quality of the instruments' RF tuning network. The introduction of gas incrementally often avoids problems. Some instruments have an alternative gas input together with a separate mass flow controller to enable accurate and reproducible alternate gas introduction. Alternatively, a gas blender may be used.

Nitrogen has been used in ICP-MS to decrease interference effects. The nitrogen can be introduced either into the coolant gas flow[7] or into the nebuliser gas flow[8] to overcome assorted interferences including that of $^{40}Ar^{35}Cl^+$ on $^{75}As^+$, and oxide based interferences. If it is introduced to the coolant gas flow, a larger volume (5–10% v/v) is required to have an effect; i.e. it is less efficient than when it is introduced via the nebuliser flow. Introduction via the nebuliser flow, at levels of 4.5% v/v, has been shown to be sufficient to overcome the interference effects from 1% chloride. The mechanism by which the interference is removed is uncertain, but inspection of the mass spectrum gives some indication of what is happening. A decrease in signal at *m/z* 75 corresponding to $^{40}Ar^{35}Cl^+$ (and at *m/z* 77 attributable to $^{40}Ar^{37}Cl^+$) is accompanied by a concomitant increase in signal at both *m/z* 49 and 51 ($^{35}Cl^{14}N^+$ and $^{37}Cl^{14}N^+$, respectively). It would therefore appear that a favourably competitive reaction occurs, with the nitrogen reacting with the chloride preferentially when compared with the argon. Introduction of nitrogen has a substantial effect on the physical and electrical properties of the plasma. If introduced to the nebuliser gas flow, the width of the annulus increases significantly. In addition, the presence of nitrogen in the nebuliser gas flow leads to a decrease in the electron temperature by 3000–5000 K together with a smaller, but still significant, decrease in the gas kinetic temperature. Hence, although the presence of nitrogen in the nebuliser gas can significantly decrease the interference effects, there can also be an unfortunate decrease in sensitivity.[9] This, however, is insufficient to affect the analysis of most samples. Other workers have introduced nitrogen into the coolant gas, reporting only a marginal signal depression, and for some elements, sensitivity was actually reported to be improved slightly.[10] A plasma comprising mainly nitrogen (plus a small amount of argon in the coolant) has been described by Uchida and Ito.[11] It was found that such a plasma decreased the interference effects caused by argon species, thereby facilitating the determination of arsenic and selenium, but increased nitrogen-based interferences. In addition, analytes with a first ionisation potential of <6.5 eV showed increased sensitivity, whereas those with first ionisation potential >6.5 eV had decreased sensitivity.

Oxygen is a commonly introduced gas in ICP-MS analyses where the sample contains organic solvents. The presence of organic solvents, with their increased vapour pressure and decreased surface tension, often causes problems in plasma spectrometry because of the increased transport efficiency to the plasma. Numerous methods have been used to decrease the solvent loading, e.g. desolvation devices, but the presence of any solvent will make the plasma less energetic. An additional problem is that thermal decomposition of the organic solvent will result in carbon deposition. This may then clog the sampler cone and coat the ion lens system, causing excessive signal drift. The presence of oxygen transforms the thermal decomposition process to give oxidative combustion. The carbon deposits are therefore removed as carbon dioxide. The amount of oxygen to be added will depend on the concentration of organic solvent being introduced. Particular problems occur when gradient chromatography is being used, where the organic

solvent composition may change drastically over a period of 10–15 min. If an excess of oxygen is introduced, oxidative attack on the sampler cone may occur. Under extreme conditions this may mean that a new sampler cone could be rendered useless in only a few minutes. Some sampler cones are either made from platinum or have a platinum insert and these tend to be more resilient to oxidative attack than standard nickel or copper cones.

Hydrogen has been less frequently introduced into plasmas. Hydrogen has a very high thermal conductivity and therefore if it is introduced to the nebuliser gas flow, thermal energy is more readily transferred from the toroidal region to the annular region of the plasma. This means that the plasma becomes more energetic and the rotational temperature increases. This can be particularly useful when analytes that form refractory oxides are to be analysed, as these may be dissociated more efficiently in the more energetic plasma. The analysis of slurries of refractory samples, e.g. ceramic, firebrick, etc., has been shown to benefit from the introduction of hydrogen.[12] Although this study was performed on an ICP-emission instrument, the basic principles still hold true for ICP-MS. Polyatomic ion interferences during ICP-MS analyses have also been reported to be diminished when hydrogen is added to the nebuliser gas flow.[13] In this study, it was reported that the MO^+ polyatomic interferences were decreased by a factor of 10 when compared with an all-argon plasma. However, other potentially interfering molecular ions e.g. $ArCl^+$, ArO^+ and ClO^+ were not found to be alleviated. Additional drawbacks associated with the use of hydrogen in ICP-MS analyses include the degradation of signal-to-noise and signal-to-background ratios and the suppression of the response of heavier analytes compared with lighter ones.

The noble gases (helium, neon and xenon) have occasionally been used either as an additional gas added to argon plasmas, or as the sole plasma gas. These gases tend to be much more expensive than argon and so are not in common usage, although they do offer some advantages. Many of the interferences observed in an argon ICP originate from a combination of some of the constituents of the sample with the argon used to form the plasma e.g. ArO^+ on Fe determinations, $ArCl^+$ on As and Se, Ar_2^+ on Se, $ArNa^+$ on Cu, etc. If the plasma is formed from a gas other than argon, such interferences do not arise. Helium is the most frequently used of the noble gases.[14] In addition to having fewer interferences, it also has other benefits, for example its higher ionisation potential (24.59 eV compared with 15.76 eV for argon). This means that for analytes that are hard to ionise in all-argon plasmas (e.g. the halogens, phosphorus, sulfur, etc), ionisation in helium plasmas becomes more efficient and hence improved sensitivity is obtained. It should be noted, however, that commercial instrumentation tends to be optimised for the use of argon and therefore substantial modification may be required to the RF generator/matching network to enable a stable plasma to be formed using helium. The first report of the use of a helium plasma as an ion source for mass spectrometry was by Montaser and co-workers.[15] A recent publication by Iacone and co-workers reported the use of an all-helium plasma operated at a power of 500–1000 W and using less than 10 L min^{-1} helium.[16] Using high-speed video images, the authors demonstrated that the helium discharge rotated with a frequency of 80–250 Hz depending on the forward power. Detection limits at the part per trillion level were reported. It should be noted that for some helium-based plasmas, the normal three-turn copper induction coil is insufficient to sustain a stable plasma. Iacone *et al*. have also described the generation of a free-running helium plasma that required a 14.5-turn coil.[17] This paper describes the modifications required to convert a commercial free running generator into one capable of supporting a helium plasma. As discussed previously, work on low-pressure plasmas often utilise helium as the plasma gas. In one example, Rosenkranz *et al*.[18] used a pure helium plasma to obtain atomic mass spectra (when a power of 9–12 W was used) and molecular spectra (when 5 W power was used). The use of further gases (methane, isobutane and ammonia) to aid ionisation was also investigated.

In a rare application of the other noble gases, a neon plasma has been used in conjunction with laser ablation (LA)-ICP-MS analysis of solid mineral reference materials.[19] The authors reported that, in general, the neon plasma yielded lower sensitivity than an argon plasma, but that it successfully alleviated many interference problems. These included those arising from $^{63}Cu^{40}Ar^+$ and $^{65}Cu^{40}Ar^+$ on the determinations of $^{103}Rh^+$ and $^{105}Pd^+$ respectively during the analysis of copper sulfide and from $^{58}Ni^{40}Ar^+$ and $^{60}Ni^{40}Ar^+$on the determination of $^{98}Ru^+$and $^{100}Ru^+$ respectively during the analysis of nickel sulfide. The authors also reported that very different plasma operating parameters were required when compared with an argon plasma, with the nebuliser gas flow being the most significantly different. Houk and co-workers have succeeded in reducing polyatomic ion interferences by introducing small amounts of xenon to the nebuliser gas flow of plasmas.[20] The introduction of as little as 10–37 ml min^{-1} to the nebuliser flow was found to reduce the interferences arising from N_2^+, HN_2^+, ClO^+, ArN^+ and ArO^+, thereby facilitating the determination of analytes such as Si, K, V, Cr and Fe. The same group has also explored some of the more mechanistic aspects of xenon addition, and reported that 1.5% v/v xenon in the nebuliser flow enhanced the ionisation of iron. To explain this, they proposed a charge transfer mechanism between Xe^+ and neutral Fe atoms.[21]

Hydrocarbon gases have been used to overcome polyatomic interferences in ICP-MS determinations. Methane has been used by several workers, with varying degrees of success. One of the more successful applications was published by Hill *et al.*[22], who successfully overcame ArCl-based polyatomic interferences by introducing 1% v/v methane into the nebuliser gas flow. The addition of methane does, however, complicate the mass spectrum and may clog the sampler cone orifice with carbon. Thus care must be taken to ensure that one problem is not solved at the expense of causing another. Ethene at a concentration of 0.5% v/v in the nebuliser gas has also been used successfully to overcome numerous polyatomic interferences[23] including a number of chloride- and oxide-based interferences. Although more successful at interference removal than methane, the use of ethene does have disadvantages, for example the need to constantly aspirate water through the nebuliser to prevent carbon deposition on the sampler cone.

Finally, a number of more esoteric applications of mixed gas plasmas have been reported. Halogenated gases have been used to increase the volatility of very refractory analytes for sample introduction techniques such as electrothermal vaporisation, DSI or ITV. One example is the introduction of sulfur hexafluoride to aid the volatilisation of analytes that form refractory carbides with the graphite cup DSI device.[4] An air plasma has also been described by Uchida and Ito.[24] Although the nebuliser and coolant gas flows consisted entirely of air, argon at a flow rate of 1.5 L min^{-1} was necessary in the auxiliary flow to sustain a stable plasma. In general, the air ICP was reported to share some of the same advantages and disadvantages as nitrogen-based plasmas.

For additional information regarding the various gases that have been used and the range of applications to which this approach has been applied, the interested reader is directed to reviews elsewhere.[25–28]

1.1.3 Alternative plasmas

The argon ICP is by far the most common type of plasma to be coupled with mass spectrometric detection. As discussed above, alternative gas and mixed gas plasmas have been used, but several other types of plasma have also been employed; one such plasma is the microwave-induced plasma (MIP). The MIP usually utilises helium and is therefore very highly ionising. It suffers far fewer interference problems than argon-based plasmas, although traditionally it has had the reputation of not being a very robust plasma, i.e. it is easily extinguished by the

ingress of any solvent. The majority of applications therefore couple gas chromatography with the MIP detector[29], but even so, in many cases there is a need to vent the solvent away to prevent plasma extinction. In recent years this problem has been largely overcome, with the advent of high-power MIPs that can tolerate aspiration of aqueous samples. In one application[30], a high powered MIP (1.3 kW) was sustained with nitrogen, indicating that it is not only helium that may be used. It should be noted however that this particular application used an ultrasonic nebuliser and these are usually associated with a desolvation device. The use of MIP-MS, especially when helium is used as the support gas, enables the determination of extremely difficult to ionise analytes. Coupled with a GC, MIP-MS has been used to determine pesticides in both qualitative and quantitative analyses.[31]

Glow discharge has also been used as an ionisation source for mass spectrometric detection. Glow discharge is especially good at sputtering the surface from solid samples and therefore has found use for the analysis of difficult-to-dissolve samples and for depth profiling studies. Recently the development and evaluation of a glow discharge, MIP tandem source for time-of-flight mass spectrometry has been reported.[32]

References

1. Hill, S. J. (1999) *Inductively Coupled Plasma Spectometry and its applications*, Sheffield Academic Press, Sheffield, UK.
2. Jarvis, K. E., Gray, A. L., and Houk, R. S. (1992) *Handbook of Inductively Coupled Plasma Mass Spectrometry*, Blackie and Son Ltd., Glasgow, UK.
3. Evans, E. H. and Ebdon, L. (1991) Comparison of normal and low-flow torches for inductively coupled plasma mass-spectrometry using optimized operating-conditions. *J. Anal. At. Spectrom.*, **6**, 421.
4. Karanassios, V. and Wood, T. J. (1999) Development and characterization of an automated direct sample insertion inductively coupled plasma atomic emission spectrometry system. *Appl. Spectrosc.*, **53**, 197.
5. Karanassios, V., Drouin, P., and Reynolds, G. G. (1995) Electrically heated wire-loop, in-torch vaporization (ITV) sample introduction system for ICP-AES with photomultiplier tube detection and ICP-MS. *Spectrochim. Acta*, **50B**, 415.
6. O'Connor, G., Ebdon, L., Evans, E. H., Ding, H., Olson, L. K., and Caruso, J. A. (1996) Feasibility study of low pressure inductively coupled plasma mass spectrometry for qualitative and quantitative speciation. *J. Anal. At. Spectrom.*, **11**, 1151.
7. Lam, J. W. and McLaren, J. W. (1990) Use of aerosol processing and nitrogen–argon plasmas for reduction of oxide interference in inductively coupled plasma mass-spectrometry. *J. Anal. At. Spectrom.*, **5**, 419.
8. Hill, S. J., Ford, M. J., and Ebdon, L. (1992) Simplex optimization of nitrogen argon plasmas in inductively coupled plasma mass-spectrometry for the removal of chloride-based interferences. *J. Anal. At. Spectrom.*, **7**, 719.
9. Sesi, N. N., MacKenzie, A., Shanks, K. E., Yang, P. Y., and Hieftje, G. M. (1994) Fundamental-studies of mixed-gas inductively-coupled plasmas. *Spectrochim. Acta*, **49B**, 1259.
10. Xiao, G. and Beauchemin, D. (1994) Reduction of matrix effects and mass discrimination in inductively-coupled plasma-mass spectrometry with optimized argon-nitrogen plasmas. *J. Anal. At. Spectrom.*, **9**, 509.
11. Uchida, H. and Ito, T. (1995) Inductively-coupled nitrogen plasma-mass spectrometry assisted by adding argon to the outer gas. *J. Anal. At. Spectrom.*, **10**, 843.

12. Ebdon, L. and Goodall, P. (1992) Slurry atomization using hydrogen-modified inductively coupled plasmas. *J. Anal. At. Spectrom.*, **7**, 1111.
13. Ebdon, L., Ford, M. J., Goodall, P., and Hill, S. J. (1993) Hydrogen addition to the nebulizer gas for the removal of polyatomic ion interferences in inductively-coupled plasma-mass spectrometry. *Microchem. J.*, **48**, 246.
14. Nam, S.-H., Zhang, H., Cai, M. X., Lim, J.-S., and Montaser, A. (1996) Status report on helium inductively coupled plasma mass spectrometry. *Fresenius' J. Anal. Chem.*, **355**, 510.
15. Montaser, A., Chan, S. K., and Koppenaal, D. W. (1987) Inductively coupled helium plasma as an ion-source for mass-spectrometry. *Anal. Chem.*, **59**, 1240.
16. Iacone, L. A., Minnich, M. G., Masamba, W. R. L., Nam, S.-H, Montaser, A., and Michel, R. G. (1999) High-speed video images of helium inductively coupled plasmas for mass spectrometry. *Spectrochim. Acta*, **54B**, 1919.
17. Iacone, L. A., Masamba, W. R. L., Nam, S.-H., Minnich, M. G., Okino, A., and Montaser, A. (2000) Formation and fundamental characteristics of novel free-running helium inductively coupled plasmas. *J. Anal. At. Spectrom*., **15**, 491.
18. Rosenkranz, B., O'Connor, G., and Evans, E. H. (1999) Low pressure inductively coupled plasma ion source for atomic and molecular mass spectrometry: investigation of alternative reagent gases for organomercury speciation in tissue and sediment. *J. Anal. At. Spectrom*., **15**, 7.
19. Petibon, C. M., Longerich, H. P., Horn, I., and Tubrett, M. N. (2002) Neon inductively coupled plasma for laser ablation-inductively coupled plasma-mass spectrometry. *Appl. Spectrosc.*, **56**, 7.
20. Smith, F. G., Wiederin, D. R., and Houk, R. S. (1991) Argon xenon plasma for alleviating polyatomic ion interferences in inductively coupled plasma mass-spectrometry. *Anal. Chem.*, **63**, 1458.
21. Bricker, T. M., Smith, F. G., and Houk, R. S. (1995) Charge transfer reactions between xenon ions and iron atoms in an argon–xenon inductively coupled plasma. *Spectrochim. Acta*, **50B**, 1325.
22. Hill, S. J., Ford, M. J., and Ebdon, L. (1992) Investigations into the application of methane addition to the nebulizer gas in inductively coupled plasma mass-spectrometry for the removal of polyatomic interferences. *J. Anal. At. Spectrom*., **7**, 1152.
23. Ebdon, L., Ford, M. J., Hutton, R. C., and Hill, S. J. (1994) Evaluation of ethene addition to the nebulizer gas in inductively-coupled plasma-mass spectrometry for the removal of matrix-gas-derived, solvent-gas-derived, and support-gas-derived polyatomic ion interferences. *Appl. Spectrosc.*, **48**, 507.
24. Uchida, H. and Ito, T. (1997) Evaluation of an inductively coupled air–argon plasma as an ion source for mass spectrometry. *J. Anal. At. Spectrom.*, **12**, 913.
25. Sheppard, B. S. and Caruso, J. (1994) Plasma-mass spectrometry—consider the source invited lecture. *J. Anal. At. Spectrom*., **9**, 145.
26. Durrant, S. F. (1993) Alternatives to all-argon plasmas in inductively-coupled plasma-mass spectrometry (ICP-MS)—an overview. *Fresenius' J. Anal. Chem.*, **347**, 389.
27. Montaser, A. and van Hoven, R. L. (1987) Mixed-gas, molecular-gas, and helium inductively coupled plasmas for analytical atomic spectrometry—a critical-review. *Crit. Rev. Anal. Chem.*, **18**, 45.
28. Hill, S. J., Fisher, A., O'Connor, G., and Evans, E. H. (1999) Alternative plasmas and sample introduction systems. In: *Inductively Coupled Plasma Spectrometry and its Applications* (ed. S. J. Hill), Sheffield Academic Press, Sheffield, UK.
29. O'Connor, G., Rowland, S. J., and Evans, E. H. (2002) Evaluation of gas chromatography coupled with low pressure plasma source mass spectrometry for the screening of volatile organic compounds in food. *J. Sep. Sci.*, **25**, 839.
30. Chatterjee, A., Shibata, Y., Yoshinaga, J., and Morita, M. (2000) Determination of arsenic compounds by high-performance liquid chromatography-ultrasonic nebulizer-high power

nitrogen-microwave-induced plasma mass spectrometry: An accepted coupling. *Anal. Chem.*, **72**, 4402.
31. Zapata, A. M., Bock, C. L., and Robbat, A. (1999) Performance evaluation of a gas chromatograph coupled to a capillary microwave-induced plasma mass spectrometer. *J. Anal. At. Spectrom.*, **14**, 1187.
32. Su, Y. X., Duan, Y. X., and Jin, Z. (2000) Development and evaluation of a glow discharge microwave-induced-plasma tandem source for time-of-flight mass spectrometry. *Anal. Chem.*, **72**, 5600.

1.2 SAMPLING INTERFACE DESIGN AND FUNCTION

Martin Liezers

If the response versus mass of a typical modern ICP-MS is considered under normal operating conditions, then for most if not all commercial instruments (quadrupole, time of flight and magnetic sector), sensitivity increases with mass. Therefore, for example, 1 ng/mL of ^{238}U is found to yield a larger signal than 1 ng/mL of ^{7}Li. However, when one considers this in terms of the actual number of atoms in the solution, then in the case of the 1 ng/mL of Li and U example, there are 238/7 times more ^{7}Li atoms in that solution than there are ^{238}U atoms, since 7 g of ^{7}Li contains the same number of atoms as 238 g of ^{238}U. If ionisation of these elements in the ICP is presumed to approach ~100% and ICP-MS sensitivity was relatively constant across the mass range, then the expected response should decrease with increasing mass. As noted above, in reality the opposite behaviour is usually observed in ICP-MS, so where are all the low-mass ions lost?

The answer is largely due to collisional scattering and space charge effects that occur within the plasma sampling interface and the following ion optics. Even after some 25 years of development it is still comparatively rare to achieve detection efficiencies where having one million atoms of a particular element in 1 mL of solution translates to a single detected count for that element. While this may be of little importance for routine ICP-MS analysis, since most low mass elements are naturally more abundant and their detection limits are rarely challenged, this simple exercise illustrates that there remain enormous research possibilities to locate and count the other 999 999 potential ions in the 1 mL of solution that are not detected, even on a good day.

The role of the sampling interface is to extract analyte ions from the ICP, as efficiently as possible and present them to the mass spectrometer side of the instrument where mass analysis takes place. Fundamentally this involves transporting the analyte ions from the high temperature (~7500 K), atmospheric pressure (~1000 mbar) environment of the ICP into the spectrometer operating at room temperature (~300 K) and reduced pressures (10^{-5}–10^{-9} mbar) under which conditions mass analysis and detection of selected analyte ions actually take place. An enormous pressure change is required (reduction by a factor of 10^{8}–10^{12}) and most of this has to be accomplished over a very short distance (<10 cm) using relatively small vacuum pumps, if the whole instrument is to be kept compact. Operating pressures and cone shapes within the sampling interface strongly influence analyte sensitivity, mass response, matrix tolerance and levels of molecular interference. The problem facing early ICP-MS development was how to design this interface to transfer ions from the atmospheric pressure ICP into a moderate vacuum system where mass selection and detection could be made.

The quadrupole mass filter is probably the most robust type of mass analyser, being capable of operating at relatively high pressures, approaching 10^{-4} mbar. So it was unsurprising that all early interface development focused on using quadrupole mass filters, rather than magnetic

mass analysers that require substantially lower operating pressures (10^{-8} mbar or lower). The earliest work focussed on using a dc capillary arc argon plasma as the ion source.[1–5] In later work the argon dc arc was replaced by the ICP[6,7] and MIP[8] as the ion source. Initial approaches to sampling atmospheric pressure plasmas were made using a single metal cone with tiny tip apertures in the range 0.05–0.1 mm to maintain safe operating pressures in the quadrupole whilst allowing relatively small vacuum pumps to be used. Ions from injected analytes could be detected in reasonable numbers, with both elemental and isotopic analyses possible, but some analytical problems remained. It was recognised that when the plasma contacted the metal cone surface, a cool boundary layer formed through which the plasma-generated ions only migrate reluctantly and quite often end up in a modified form such as molecular ions (oxides, etc.). In addition such tiny apertures were very prone to sample clogging, hindering practical sample analysis. To puncture this cooled boundary layer and sample the ions directly from the plasma, larger sampling apertures >0.5 mm were required. If a single sampling aperture of these dimensions was employed, then huge vacuum pumps were required to maintain an adequate operating pressure for the quadrupole mass analyser and detector. Fortunately, a simple solution[8] was discovered in earlier work on the physics of molecular beam formation.[9–11] A second cone with a moderately sized aperture (>0.5 mm) was inserted behind the first and the intervening space between the two cones pumped to an intermediate pressure (~4–5 mbar). This allowed the front sampling cone to run with an enlarged aperture (~0.5–1 mm) without creating pressure problems in the quadrupole mass analyser or detector, while the vacuum pumps required remained small and therefore relatively inexpensive. Experiments have been performed using three aperture interfaces;[12,13] however, despite some promising results this design has not yet been widely adopted in modern commercial ICP-MS instruments. Most commercial designs have continued to favour the original two-cone approach to step down the pressure from the ICP to the mass spectrometer.

Additional discussions on the physics of the plasma sampling interface can be found in the literature.[14–18] This continues to be a dynamic research field and considerable advances remain to be made given the high loss of analyte ions between the ICP source and the mass spectrometer.

All modern ICP-MS instruments (magnetic sector, time of flight and quadrupole) employ a broadly similar sampling interface in which there are a number of common components. The basic layout is shown in Figure 1.4. It has become a standard feature of ICP-MS that the ICP is always mounted horizontally, although there are no special physical reasons why alternative orientations could not be adopted as effectively. The ICP flame is centred on an aperture, typically ~1 mm in diameter formed at the tip of a metal cone, usually manufactured from nickel, although platinum, copper and aluminium have characteristics that can be advantageous in certain applications. The important physical properties of the cone material are: its melting point, thermal conductivity, resistance to thermal shock and chemical resistance (principally to oxidation and to a lesser extent acid attack). The front cone is normally referred to as the sample cone. In order to prevent the sample cone melting in the ICP, it is mounted on a water cooled plate. A vacuum seal is achieved between the cone and mounting plate using either a graphite gasket or Viton O-ring. The sample cone is held in place either by a screw fitting or in some instruments simply by a combination of friction between the O-ring and the recess in which the cone is located and the suction effect of the interface vacuum. Providing a mechanism for easily removing and replacing the sample cone is essential since (a) the cone aperture slowly erodes in the plasma (leading to the periodical requirement to replace it) and (b) during high matrix content sample analyses (e.g. sea water) the cone orifice may gradually block as a result of sample matrix condensation and must be cleaned before further use. Behind the sample cone is the expansion chamber that is pumped by a single- or double-stage rotary pump with a pumping capacity

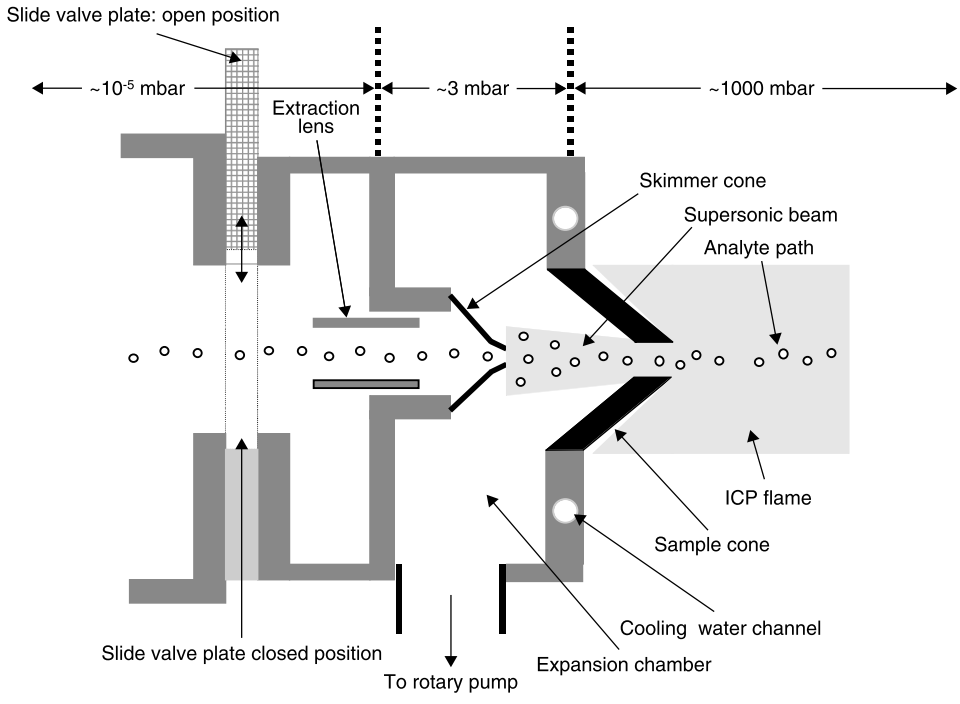

Figure 1.4 A cross section through a typical ICP-MS ion sampling interface region.

normally in the range of 18–30 m^3/h, producing an operating pressure in the range 2–5 mbar. As a result of the reduced pressure region behind the sample cone, a significant portion of the plasma is drawn through the sample cone aperture into the expansion chamber. The argon ICP is considered to be a weakly ionised plasma (~0.1%), with the bulk of the argon gas drawn through the sampler orifice un-ionised. The cloud of gas atoms, molecules, ions and electrons entering the expansion chamber quickly increases in speed and expands outwards under the influence of the reduced pressure in this region, resulting in the formation of a free jet. The flow speed of the expanding gas exceeds the local speed of sound, resulting in supersonic expansion. The rapid increase in gas velocity requires energy, which is acquired by converting the thermal energy of the gas into kinetic energy, resulting in a reduction of the gas kinetic temperature to 100–200 K from a source temperature of 5000–7500 K,[14] over a very short distance (<1 cm). The gas at this point is not in thermal equilibrium as the electron temperature remains close to the source temperature, but the drop in density occurs so rapidly (<5 μs) that ion–electron recombination is prevented. Effectively the plasma composition is frozen as it was at the instant of sampling. This process, often called adiabatic expansion, is fundamental to ICP-MS analysis as it allows practically useful measurements of elemental ions to be made. The supersonic jet formed is bounded radially by a 'barrel shockwave' and axially by a Mach disc that are generated where the rapidly expanding plasma gas meets the more slowly moving background gas in the chamber as illustrated in Figure 1.5.

This region of free expansion is called the zone of silence. Spaced behind the sample cone is a second cone with a smaller orifice in its tip (0.4–0.7 mm), called the skimmer cone. For the skimmer cone to sample the expanding plasma gas effectively, the orifice must be situated

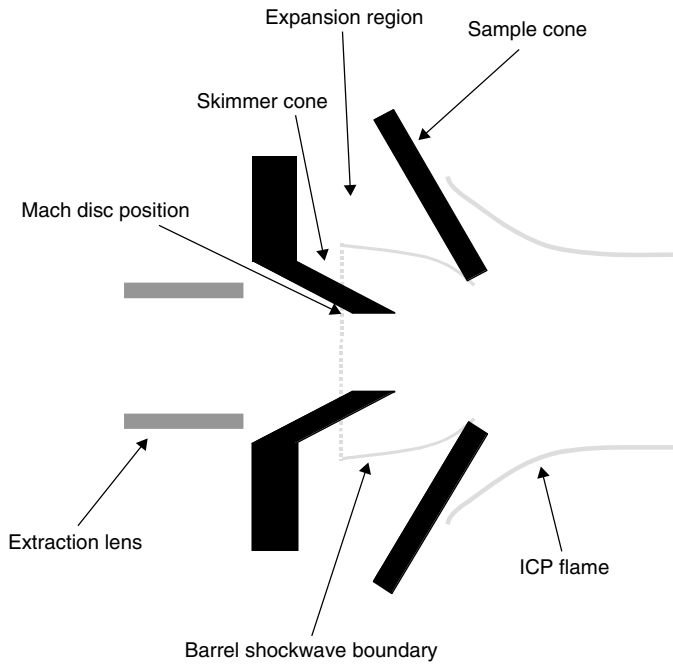

Figure 1.5 A stylised cross section through the expansion region illustrating the location of the barrel shockwave and the Mach disc.

within the zone of silence, ahead of the Mach disc. The position of the Mach disc (X_M) is given by the equation:[19]

$$X_M = 0.67 D_0 (p_s / p_e)^{1/2}$$

where D_0 is the sampling orifice diameter and p_s and p_b are the source and expansion chamber pressures, respectively. Under typical operating conditions X_M is $\sim$1 cm, so to ensure the skimmer is sampling well within the zone of silence, its tip is placed $<$1 cm from the rear of the sample cone orifice. Most evidence to date suggests that the ion and electron populations from the ICP in the supersonic gas flow between the sample and skimmer cones remain balanced. No charge separation appears to take place in this region.

Skimming the gas outside the zone of silence produces very low sensitivity. The profile of the skimmer cone tip is sharper than that of the sample cone, because the presence of the skimmer tip in the zone of silence disturbs the gas expansion and in order to maintain optimum ion sampling, this disturbance should be minimised.[18] The shape of the skimmer and the condition of the skimmer tip both have a profound effect on instrument transmission, mass response, molecular backgrounds, matrix effects and even the subsequent geometry of the ion optics.

Skimmer cones can be manufactured from the same range of materials as the sample cone. While the skimmer aperture does not normally erode in the reduced pressure environment of the expansion chamber, they can accumulate a build-up of solid material resulting from the condensation of high boiling point compounds from the injected sample. If the level of total dissolved solids in the solutions analysed is high ($>$0.2% (m/v)) then clogging of the skimmer cone aperture may occur. If this happens, then cleaning of the skimmer cone is required. Carefully controlling the skimmer tip temperature through the appropriate selection of materials

with the desired thermal characteristics minimises or in some cases virtually eliminates orifice clogging from high matrix samples. As noted earlier, the condition of the skimmer cone tip profoundly affects ICP-MS sensitivity. A sharp clean edge around the orifice generally gives good performance. In contrast, a blurred or distorted orifice edge may disturb the supersonic gas flow through the skimmer and poor sensitivity is usually the result. The wall thickness in the skimmer tip is much lower than that of the sample cone, and consequently the skimmer is much more sensitive to rough handling or poor cleaning practices than the sample cone. Consequently, removal and cleaning probably account for most skimmer failures rather than any gradual plasma erosion of the skimmer aperture.

The optimum expansion chamber pressure depends on the sample–skimmer cone apertures and spacing. In older model ICP-MS instruments it may be possible to adjust the sample–skimmer cone distance using spacing rings, but on most, if not all modern instruments, the spacing is fixed. Changing the sample–skimmer spacing in this way, whilst ensuring that the skimmer tip remains within the zone of silence, affects the instrument mass response. Replacing the argon ICP with a helium plasma creates pressure problems in a conventional ICP-MS instrument since helium is a more difficult gas to pump. These problems are largely cured by raising the expansion pumping capacity from about 25 m^3/h to ~100 m^3/h. Operating the argon ICP under these conditions produces an expansion pressure in the range 1–2 mbar. The lowered pressure has been found to improve the instrument sensitivity for elements heavier than argon.[20–22] Sensitivity for elements lighter than argon was reduced. This seems to be in conflict with earlier experiments on improved interface pumping where no gains in sensitivity were reported.[14] The degree of sensitivity enhancement is markedly sensitive to skimmer geometry, especially rear cone angle, when operating at these reduced expansion chamber pressures. On operating the ICP under reduced power settings such as in 'cool plasma' mode, the lower plasma gas temperature causes a corresponding increase in expansion chamber pressure. Under these special conditions greatly improved sensitivity is obtained by lowering the expansion chamber pressure, even for elements much lighter than argon. This behaviour results from the reduced ion current flowing through the interface under these conditions, causing a corresponding reduction in the 'space charge' losses of low-mass ions, as discussed later in this chapter.

Skimmer geometry affects certain molecular backgrounds, such as ArO^+ at mass 56, which interferes with the principle isotope of iron.[23] Skimmers with wide rear angles that yield high sensitivity also often yield high molecular backgrounds at some masses. Reducing the rear angle of the skimmer reduces sensitivity, but even without 'conditioning' the cones it is usually possible to obtain a significant reduction in the background equivalent concentration (BEC) of these interferences, resulting in improved detection limits. The reduction in these interferences may result from collisional dissociation of the molecular ions in the narrow channel at the rear of the skimmer, promoted as a result of local pressure increases in this constricted region. It is presently unclear as to exactly why 'conditioning' the skimmer by aspirating a solution containing for example, ~500 mg/L of sodium for a short period (e.g. 15–20 min) also suppresses the relative levels of these molecular ions to even lower levels. It is possible that the cone surface, when unconditioned (i.e. clean), plays a role in the formation of some molecular ions. In addition, conditioning the cones in this way also leads to considerable reductions in the background signals of cone-derived ions, such as Ni. It is therefore worth noting that sometimes used cones can yield superior detection limits for some elements than an equivalent brand new set.

In magnetic sector ICP-MS instruments, irrespective of whether the instruments have high resolution, multi-collection or a combination of both capabilities, the overall process performed by the plasma sampling interface remains essentially the same as for a quadrupole ICP-MS

instrument. Their sensitivity can also be boosted further by lowering the expansion chamber pressure. The only difference is that for a magnetic sector instrument to deliver the highest sensitivity, analyte ions must be moving at a significantly higher speed than in a quadrupole-based system. This is achieved by accelerating the positive ions through the application of a large negative voltage (typically 5–8 kV) after the ions have been sampled. Two designs have been developed to accomplish this ion acceleration. In the first approach, the expansion chamber and interface rotary pump are electrically isolated from the rest of the vacuum system and held at the accelerating potential, while the rest of the vacuum system is held at ground.[24] In the second method, the expansion chamber and pump are held at ground potential, while the rest of the mass spectrometer is held at the accelerating potential.[25] In both approaches, some part of the vacuum chamber and pumps have to be floated to a potentially hazardous voltage. This kind of approach has been attempted in quadrupole ICP-MS where improved sensitivity and reduced matrix effects were claimed, but has not found widespread use. In quadrupole instruments it is necessary to decelerate the ions before they enter the mass analyser or poor resolution and severe peak tailing result.[26]

1.3 ION EXTRACTION AND FOCUSING

Martin Liezers

1.3.1 Ion extraction

When the ICP is switched off, the expansion chamber returns to atmospheric pressure, while high vacuum ($\sim 10^{-7}$–10^{-8} mbar) is generally maintained for most of the ion optics, quadrupole and detector. These two regions of the instrument are isolated by a 'gate' or 'slide' valve (shown in Figure 1.4), which only opens when the ICP is operational and the expansion chamber is pumped out to the required operating pressure. Failure of the ICP during operation normally triggers the slide valve to close immediately to prevent excessive pressure causing damage to the detector or quadrupole in the high vacuum region of the mass spectrometer. It has been demonstrated that it is possible to operate an ICP-MS without a slide valve and to pump the whole vacuum system from atmospheric pressure to a workable vacuum ($\sim 10^{-5}$ mbar) in a period of less than 10 min.[27] However, this has implications for quadrupole and detector operation, so these had to be specifically designed to perform reliably at the higher operating pressure.

When the ICP-MS is operating with the slide valve open, the region behind the skimmer (often referred to as the 'intermediate' chamber) is pumped by a high vacuum pump, which in modern instruments is almost invariably a turbomolecular pump with a pumping speed typically in the range 200–500 L/s. Under these conditions the small skimmer cone orifice acts as a differential pumping aperture and the pressure measured off-axis, downstream of the skimmer typically lies in the range of 10^{-5} mbar. However, if the pressure is measured on-axis close (<6 cm) to the skimmer then pressures in the range 0.01–0.001 mbar may be recorded, because a definite gas beam develops behind the skimmer cone.

It has been suggested from Langmuir probe,[15] fluorescence[28] and pressure[29] measurements that the gas beam downstream of the skimmer cone does not attain the qualities of a true molecular beam for a typical plasma sampling interface. A disturbance or shockwave caused by the presence of the skimmer tip or even formed inside the skimmer tip may be responsible for disturbing molecular beam formation. The intensity and dimensions of the gas beam formed

downstream of the skimmer depend on a number of factors. These include sample–skimmer spacing, skimmer orifice size, skimmer shape and expansion/intermediate chamber pressures. Reducing the pressure in one or both of these chambers raises the on-axis intensity of the gas beam and shrinks the radial beam profile.[18,30] In effect, harder pumping can raise on-axis pressure by more intense focusing of the largely neutral dominated gas beam formed behind the skimmer. This phenomenon has not been heavily investigated, but given the relatively short mean free path (0.1–1 mm) of ions actually inside and immediately downstream of the skimmer there is a possibility that some undesirable interactions might still be taking place within the bulk un-ionised gas. Blocking the direct path of the neutral gas beam early into the following ion optics may be analytically advantageous, although this is often already performed to suppress background and is discussed in the following section on ion optics.

As all ions tend to assume the velocity of the bulk argon gas as they travel through the interface, downstream of the skimmer cone (if no electrostatic fields are applied) the ion kinetic energies exhibit a mass dependence given by the expression $0.5mv^2$ where m = ion mass and v = ion velocity (of the order of ~2500 m/s). This translates to a Li to U ion energy spread of typically 0.5–10 eV. In reality the ion kinetic energy may be raised by an additional amount caused by the plasma potential[31] generated at the ICP–sample cone contact, although instrument designs have evolved to minimise this effect, which is crucial for achieving good cool plasma operation.

Actual charge separation is believed to start taking place just behind the skimmer cone orifice, even in the absence of any applied external electric field,[17,30] although there have been suggestions that it may take place even earlier than the plasma sampling interface (i.e. within the plasma).[32–34] In the skimmer region, differences between ion and electron mobilities caused by the pressure drop, relative size difference and high electron temperature create a net negative charge diffusion radially towards the inner walls of the skimmer cone. This leaves a net positive charge on-axis in the bulk neutral gas flow. Applying an electric field in this region magnifies the charge separation process, thereby creating a high concentration of positive charge in a relatively small volume. As a consequence the positive ions in the gas beam begin to repel each other. In effect the ion beam becomes increasingly self-defocusing when it is collimated into a small volume as the positive ion current rises. This phenomenon, often referred to as the space-charge effect is believed to be responsible for matrix suppression effects and poor low-mass transmission, as well as limiting the ultimate achievable sensitivity. It also strongly influences the operation of the following ion optics. Electrically selecting the positive ions from the gas beam, which contains positive ions, negative ions, electrons and uncharged species (atoms and molecules), is usually called ‘extraction’. The extraction process is generally performed by a circular metal tube placed near the rear of the skimmer cone. Conceptually it is easier to imagine a negative voltage being applied to the metal tube (which is electrically insulated from the main vacuum chamber) to accelerate positive ions from the gas beam into the following ion optics, whilst repelling electrons, in essence creating a beam of positively charged ions. However, some instruments actually utilise a small positive voltage for this purpose and achieve the same effect, even ramping the extraction voltage with mass to reduce the effects of the mass-dependent ion kinetic energy generated by the plasma sampling interface.

Positive ions are favoured for ICP-MS since most elements in the Periodic Table form positive ions more efficiently than negative ions in the ICP. These survive long enough in the mass spectrometer to allow mass selection and detection. Nonetheless, a small amount of work has been undertaken running ICP-MS in negative ion mode.[35] This offers improved detection for the most electronegative elements, such as the halogens, that prefer to exist as negative ions, but

the high electron-generated instrument background and limited element range have restricted the practical use of this approach. Consequently, all current commercially available ICP-MS instruments have been designed to analyse only positive ions.

The magnitude of the extraction voltage depends on several factors such as the operating conditions of the plasma, expansion chamber pressure, ion current, skimmer cone shape and acceptance angle of the following ion optics. Depending on the ICP-MS instrument and the operational conditions, the extraction voltage can range from typically +10 to −1000 V. High (very negative) extraction voltages often produce the highest sensitivity for high-mass elements, but may also give higher backgrounds (molecular, instrumental and elemental), especially at low masses (<80 amu). Lower extraction voltages often favour low-mass element sensitivity. For routine work where very high sensitivity is not required, the background equivalent concentration (BEC) on some masses, especially those elements that possess a low ionisation potential, can be improved by operating with a low extraction voltage. A more open (wider angle) rear skimmer cone surface allows better electric field penetration from the extraction lens. While this often results in the highest sensitivity, the extraction lens optimises at a more negative voltage because a larger positive ion current is extracted with a greater potential for space-charge beam defocusing. Skimmer cones with a narrow rear angle produce a less divergent ion beam, either as a result of the mechanical constraint or poor extraction field penetration producing a lower positive ion current (and hence reduced space charge effects). As a result the extraction voltage optimises at a less negative voltage. Operating under 'cool plasma' conditions where the level of ionisation and the number of ions in the central channel of the ICP are dramatically reduced drops the optimum extraction voltage to very low values. Such behaviour results from a large reduction in the degree of space-charge repulsion. Under such conditions the positive ion current is reduced dramatically as plasma conditions are optimised to eliminate Ar^+ from the central channel of the ICP. In normal ICP operation, the Ar^+ ion carries a significant portion of the total positive charge in the ion beam.

Space-charge and to a lesser extent other collisional effects contribute to poor low-mass response, because low-mass ions possess lower ion kinetic energies than high-mass ions. As a result low-mass ions may be more readily ejected to the fringes of the beam or even lost all together, compared to high-mass ions. If the ion kinetic energies for both low- and high-mass ions were identical then both would be equally affected by space-charge effects. Practically, this behaviour fits the observed mass response, where highest sensitivity is usually observed for heavier ions in most if not all ICP-MS instruments.

As yet there appears to be no single satisfactory solution to the problems caused by space charge in ICP-MS, although a number of solutions have been proposed. Accelerating the positive ions should reduce space-charge effects, so it might be supposed that magnetic sector instruments, with their high ion acceleration voltage, would exhibit fewer apparent effects from this problem. However, evidence to date suggests that the effects are still present, irrespective of the ion acceleration method adopted.[36–40] An alternative interface design has been proposed that adds another differential pumping stage between the expansion and intermediate chambers together with sampling the directed gas flow from the skimmer cone through an offset flattened aperture plate.[12,13] This, it was claimed, reduces the mass-dependent kinetic energy spread. Good results were reported, but there appears to be no commercial adoption of this approach at present. A novel approach to reducing space-charge effects was made by attempting to neutralise the positive charge imbalance behind the skimmer by flooding the region with electrons from a hot filament. The results reported an overall improvement in sensitivity across the mass range, especially for the lower masses and reduced matrix effects.[41,42]

The effect of pressure on instrument sensitivity in the intermediate region of the vacuum system appears to be slight, at least for quadrupole ICP-MS, once the pumping rate exceeds about 250 L/s. A larger turbomolecular pump in this second stage can yield increased sensitivity across the mass range if the pumping rate is not restricted by the port size on the vacuum chamber. However, the cost of larger turbomolecular pumps increases quite steeply with pumping speed. The commercial movement towards compact–low-cost ICP-MS instruments has restricted further development in this direction, although this remains another area where transmission efficiency could potentially be improved across the mass range, beyond what is currently available.

1.3.2 Ion focusing

Many designs now exist for ion focusing optics specifically tailored for ICP-MS applications. The purpose of the ion optics is to guide analyte ions to the quadrupole where mass analysis takes place. It should be recognised that the ion optics act as an ion energy filter and as such have to be compatible with the range of ion kinetic energies emerging from the plasma sampling interface. If this condition is not met poor transmission will result.

Even matrix tolerance (in particular matrix induced signal suppression) is affected by the ion optics, since ion trajectories are not just dependent on ion kinetic energy. In practice space-charge effects tend to dominate ion trajectories in most situations. The principal factors influencing ICP-MS ion optics design have until quite recently been simplicity, sensitivity and background. Following work initially by Douglas[43] and Houk[44] using a triple quadrupole and later by Koppenaal[45,46] using the ion trap, it was realised after a slow start that the role of the ion optics could be widened to include selectively suppressing interferences. This was most readily performed using the rf driven quadrupole, hexapole or octopole (multipoles) as gas pressurised 'collision' or 'reaction' cells. Even operating unpressurised, rf-only multipoles efficiently transmit ions, and so can be treated like any other element in the ion optics. For this reason, they are sometimes referred to as ion guides. As this area of ICP-MS research has developed rapidly in the last decade, readers are referred to Part 2.4 of Chapter 2 and Chapter 8 of this book and the detailed review by Tanner *et al.*[47] that give a thorough description of the physics and applications of these devices, especially their role in removing interferences.

Modelling ICP-MS ion optics has been and continues to be a challenge.[48] A number of commercial software programs have been developed for other ion/electron optics applications. These predict the probable ion trajectories through a given design under a nominal set of conditions and have been widely used as a starting point in ICP-MS ion optics design. None incorporate all the physical effects encountered in ICP-MS. The complexity and cost of these programs often go hand in hand. One of the least expensive and probably mostly widely used programs, called SIMION, was originally written by Don McGilvery in support of his doctoral dissertation.[49] This particular modelling program has been refined since its inception in the mid-1970s and undergone a series of revisions and improvements. Currently it is offered as the commercial product SIMION 7.0.[50] Other packages include MUNRO[51] and CPO.[52] The latter, though much more expensive, offers much higher resolution than SIMION and allows improved handling of space charge. These software packages allow designers to test out the probability of a possible design functioning reasonably well. If the effects of space charge or other physical effects from the ICP sampling interface cannot be incorporated without resorting to actual practical tests, the predicted results can only be used as a guide to possible performance. The more expensive

software modelling programs, despite allowing incorporation of space-charge effects to some degree, still suffer from other deficiencies and do not provide a total design solution.

Most of the ion optic components in an ICP-MS are situated in the intermediate region between the expansion and analyser chambers. One of the ion lens elements often serves as a differential pumping aperture, with the operating pressure in the intermediate chamber running at $\sim 10^{-5}$ mbar, and the pressure in the analyser chamber that houses the quadrupole and detector running at 10^{-7}–10^{-6} mbar. Pressurised multipole cells used to selectively suppress interferences usually operate in the intermediate chamber. The gas used to pressurise these devices depends on the target interference(s) but can include hydrogen, helium, oxygen, methane or ammonia. Operating cell pressures typically lie in the range 0.01–0.001 mbar. In magnetic sector instruments it is not unusual to find four stages of differential pumping from the expansion chamber to the detector. The operating pressure in the mass filter sections of magnetic sector ICP-MS instruments has to be substantially lower than for quadrupoles (10^{-8}–10^{-9} mbar), otherwise serious peak tailing occurs as a result of positive ion – residual gas atom collisions. This phenomenon is less significant for quadrupole instruments, where a low operating pressure, although necessary to allow ion transmission (10^{-4}–10^{-5} mbar suffices for this purpose), is also required to prevent internal high voltage flash-over in either the quadrupole (when operating at high mass i.e. high applied voltage) or the electron multiplier, when operated in pulse counting mode. Figure 1.6 shows the overall layout of the three differential pumping stages in a typical modern quadrupole ICP-MS.

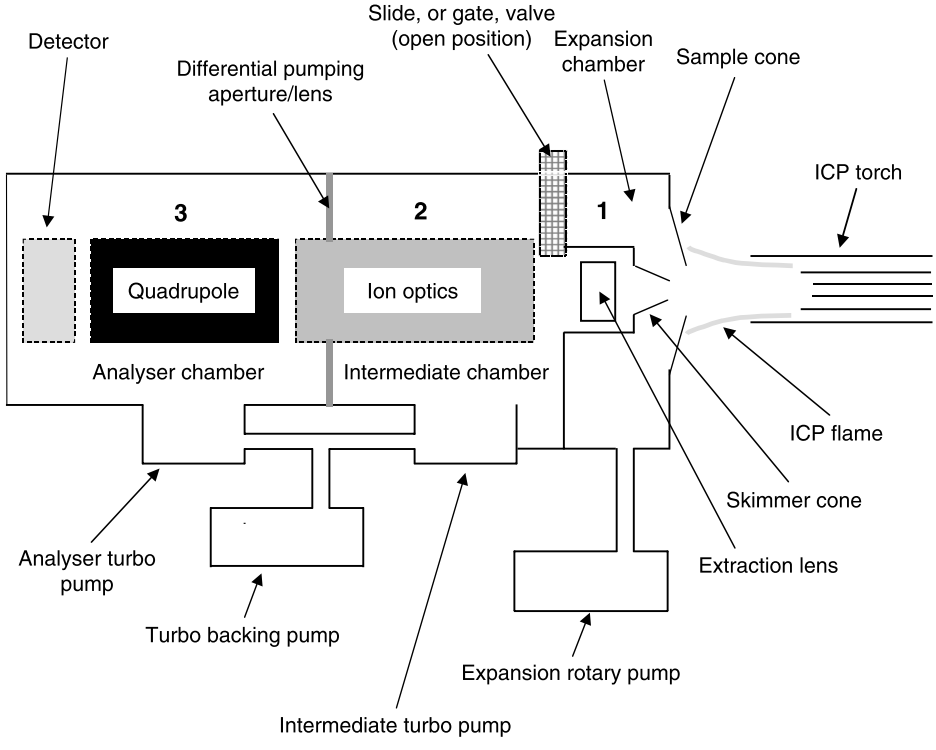

Figure 1.6 A cross section through a typical quadrupole ICP-MS showing the three stages of differential pumping.

Light can be focused or defocused using an appropriately shaped optical lens. In much the same manner, the trajectory of ions can be altered by an electric field. Such a field is readily created by applying a potential difference between a suitably shaped electrically conducting surface and ground, in effect forming an electrostatic lens. One beauty of an electrostatic lens over an optical lens is that by simply changing the magnitude or polarity of the voltage applied to the electrostatic lens it becomes possible to change the ion trajectory or in effect the degree of focusing or de-focusing. To perform the same change optically would require physically changing the position shape or the refractive index gradient of the optical lens, an operation that would normally require actual physical intervention.

If ions of different masses have the same kinetic energy, they should all follow the same trajectory in a constant electrostatic field. This would greatly simplify ion optics design. Unfortunately, in normal ICP-MS ion optics operation, ions of different masses possess a spread of kinetic energies and are present in sufficiently large numbers to create their own space-charge field, which continuously tries to defocus the formed beam.

Ion lenses generally take the form of metal discs with a central hole, tubes or plates. As the ion beam effectively starts as a point source from the back of the skimmer cone, the ion beam shape is effectively circular, so most ion lenses are cylindrically symmetrical in quadrupole-based instruments. The exception only appears where the ion beam is deflected off-axis for reasons related to background reduction (discussed later in this section). In magnetic sector ICP-MS instruments, the ion beam shape is deliberately modified from circular to rectangular by compressing the ion beam on one axis. This change is made so that the ions can be focused through slits, which effectively mirror the same role in an optical system, where slit width controls wavelength resolution. On a magnetic sector instrument, slit width controls mass resolution. All ion lenses must be electrically isolated from one another to operate correctly. Depending on their location within the instrument, those closer to the plasma sampling interface may require periodic cleaning to maintain optimum instrument performance, especially when samples with high total dissolved solids ($>0.1\%$ m/v) are run on a routine basis. Contamination of the ion optics results in the development of a non- or poorly conducting surface coating. Often virtually invisible, the coating can allow positive ions to collect on the surface of the ion optics in sufficient numbers to affect the trajectory of incoming ions in an unpredictable manner, resulting in signal drift and low transmission. As a result ion optical components (especially after they have been cleaned) should only be handled with gloves.

The fundamental role of the ion optics is to transport the positive ions left after charge separation behind the skimmer to the quadrupole where they are separated according to their mass-to-charge ratio before being counted by the detector. This role on its own would be simplified if the detector (usually an electron multiplier) could be left on the same central axis as the ICP ion source. However, it was noticed very early on in ICP-MS development that such an arrangement produces a very high background count rate from a pulse counting electron multiplier, even when the quadrupole is set to transmit a mass that is free of isotope or interference signals (e.g. mass 220.5). This high background is speculated to be caused by photons (and possibly high-energy ions or metastable species as well) striking the detector and triggering electron pulses, although its exact origin remains a subject open to debate. Early in the development of ICP-MS, reduction of this background was achieved by inserting a disc-shaped obstruction either within the ion optics or between the rear of the skimmer cone and the extraction lens to block the line-of-sight path between the electron multiplier detector and the ICP. This obstruction in the ion optics of the early instruments was often referred to as a ‘photon’ or ‘shadow’ stop and usually comprised a metal disc held at ground potential, located on the central axis and held by two or three supporting legs. This approach never really eliminated the background completely, but reduced

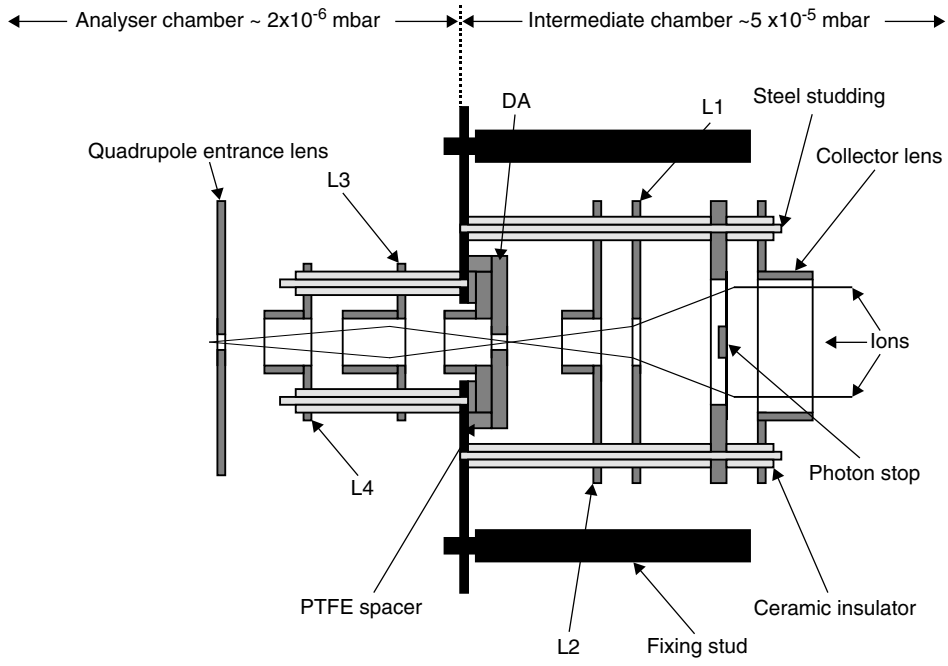

Figure 1.7 A cross section through the VG PlasmaQuad 2 quadrupole ICP-MS ion optics illustrating the path normally followed by ions traversing the stack. Background 5–50 cps.

it to a level of 5–50 cps),[53] where for all but the most demanding applications (e.g. ultra-trace analysis) background was not normally considered a problem. Figure 1.7 shows a cross section through an early VG PlasmaQuad 2 ion lens stack illustrating the position of the photon stop and the typical trajectory of an ion traversing the stack. While some ions do hit the photon-stop and are lost, space-charge defocusing may actually aid transmission in the early stages since a broad diffuse ion beam ensures more ions pass around the stop.

The ion flight path through a magnetic sector ICP-MS instrument to the detector is curved and it was noticed early on in the development of the first high resolution instruments that the off-peak backgrounds could be <0.1 cps.[24] This was most useful since when operating under high resolution conditions analyte transmission could fall dramatically, so in order to maintain good analyte detection limits, low background became essential. The search for high transmission and low background (<2 cps) in quadrupole instruments did not really make much progress until the ion optics design was changed to deliberately deflect the ions off the same axis as the apertures in the sampling interface and the ICP[54,55] before passing them into matching offset quadrupole and detector. Under these conditions the offset can be <1 cm. However designs have been developed that deflect ion trajectories by 90° to achieve a similar effect.[56,57] Figure 1.8 illustrates a cross section view through the Thermo Elemental PQ Excell ion optics, which incorporated a hexapole ion guide, and the typical ion path through the optics. Ions entering are focused through apertures into an enclosed rf-only hexapole. This may be pressurised if desired to selectively remove interferences when operating as a collision cell, although it functions efficiently unpressurised, transporting ions on-axis as a narrow beam. After passing through a differential pumping aperture, the fast moving ions are deflected off-axis in the vertical plane by about 5 mm into the aperture of a matched offset quadrupole mass analyser.

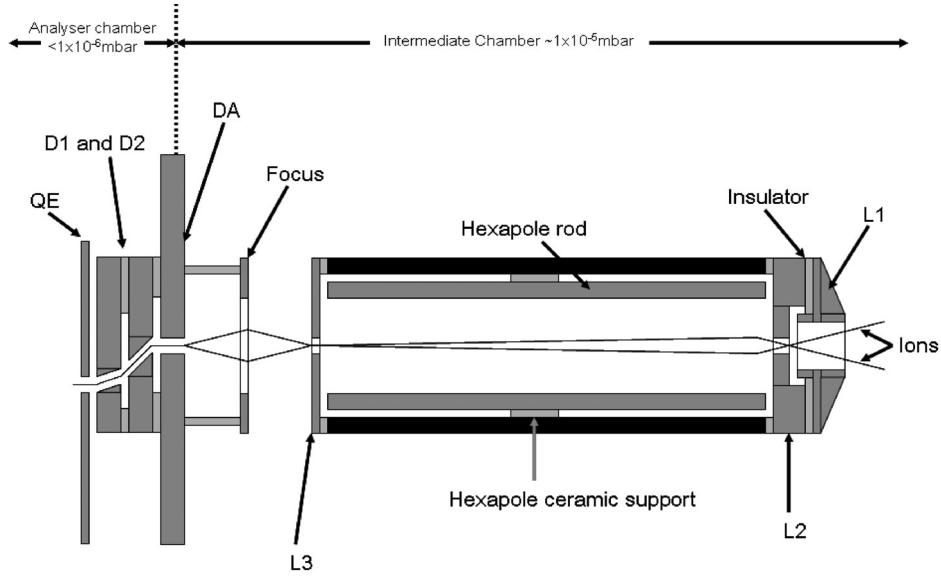

Figure 1.8 A cross section through the Thermo Elemental PQ Excell quadrupole ICP-MS ion optics, illustrating the path normally taken by ions traversing the stack. Background 0.1–0.5 cps.

Adopting an ion-deflection approach has allowed quadrupole ICP-MS instruments to maintain or increase transmission over the earlier photon-stop ion optics, as well as reduce the instrument background to <1 cps. In exceptional instances, <0.1 cps background has been achieved, whilst simultaneously maintaining a transmission of $>1 \times 10^9$ cps/ppm over the bulk of the mass range.[30,58] Developments in ion optics design have clearly reduced off-peak backgrounds to very low levels, but it is interesting that this has been achieved without a clear understanding of exactly what the causes of the background are. Advances in the future are more likely to arise from efforts to reduce 'on peak' elemental backgrounds (i.e. contamination) that arise from internal sources between the interface cones and the mass analyser than in chasing further reductions of off-peak backgrounds.

ICP-MS was slow to adopt multipole ion optics, despite their routine use in organic mass spectrometry for some considerable time. Commercial ICP-MS models have to date employed the quadrupole[59,60] and higher order multipoles such as the hexapole[61] and octopole[62] as gas pressurised collision cells/unpressurised ion guides. A photograph of an exposed hexapole assembly is shown in Figure 1.9. The unit comprises six highly polished rods with a circular profile, held parallel in an accurately machined ceramic former, effectively forming a tube.

In practice, separate flat apertured plates are normally fitted to the entrance and exit of the multipole to ensure ions enter and exit along the main central axis. These apertures also control gas escape from the multipole cell when it is pressurised. In operation, alternate rods are electrically connected with an rf voltage of opposing polarity applied to adjacent rods, forcing ions that enter the multipole towards the field-free region of the device along the central axis. A small dc bias is also normally superimposed to either speed ions up or slow them down. Optimum mass transmission depends on the applied rf voltage, which is normally ramped with mass. For rf frequencies >500 kHz, there is little effect on mass transmission except at very low mass, so the applied rf frequency normally remains fixed. The principle difference between hexapoles and

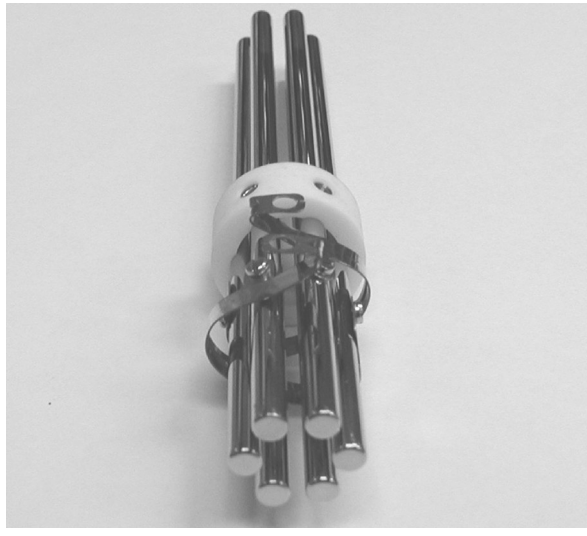

Figure 1.9 A basic hexapole assembly.

octopoles is that the central field-free region increases with higher order multipoles, effectively allowing ions to be confined and transmitted over a wider mass range. When operated as a pressurised collision cell this may be a mixed blessing, since, while some interferences can be virtually eliminated and analyte transmission maintained, new interference ions can be created. Transmission of these ions can be suppressed because of their different kinetic energy, but they are not rejected in these devices by selective mass transmission (see Chapter 8). The advantage of the quadrupole in this application is that the range of mass transmission can be selectively tuned to reject the precursor ions of cell formed interferences before these interferences have the opportunity to form. The down side of this approach is that analyte transmission drops as mass selectivity is raised. One other benefit of operating multipoles in pressurised mode is that they can deliver higher sensitivity as a result of the process of collisional focusing. In effect, collisions between the ions and the cell gas reduce the ion kinetic energy which ensures that the ions are forced more readily by the applied rf field to the central axis of the multipole. Narrowing the ion kinetic energy not only improves transmission through the subsequent ion optics, but has also been employed to improve mass resolution.

Manual optimisation of the ion lens voltages was standard in early ICP-MS instruments and some degree of skill was required to achieve good sensitivity and stability. This made rapid switching to different analytical conditions to obtain the best possible performance for the widest range of elements almost impossible. The use of 'auto-tune' algorithms in modern ICP-MS instruments has now become fairly routine. The optimisation routines incorporate adjustments in not only the ICP operating parameters, but also those of the ion optics. These routines can optimise a variety of performance parameters including sensitivity, stability and oxide/doubly charged ion levels. Their use has reduced the skill level required to operate an ICP-MS to a degree. However, these are by no means infallible programs and do not overcome problems created by poor practices elsewhere such as failing to perform routine instrument maintenance on the interface cones or ion optics. Good settings can be stored on the instrument computer and subsequently applied automatically for different analytical conditions required for analysis. Changing the operating conditions of the ICP-MS (e.g. switching to collision cell mode) to obtain

optimum analysis for the widest possible range of elements usually requires some changes to be made to the operating voltages applied to the ion optics. The changes may be required because of shifts in the ion kinetic energies, changes in the level of the ion current (which in turn affects space-charge defocusing), interface pressure changes or gas flow rates in collision/reaction cells. All can be accomplished quite readily without any operator intervention once 'good' settings have been established. Despite this progress, no one has yet manufactured an ICP-MS that can be treated completely like a 'black box' where, at least from the user's point of view, no tuning is required irrespective of the analysis performed.

References

1. Gray, A. L. (1975) *Analyst*, **100**, 289.
2. Gray, A. L. (1975) *Anal. Chem.*, **47**, 600.
3. Gray, A. L. (1976) *Dynamic Mass Spectrometry* (eds D. Price and J. F. J. Todd), Heyden & Son Ltd., London, Vol. 4, Chapter 10, p. 153.
4. Gray, A. L. (1976) *Proc. Anal. Div. Chem. Soc.*, **13**, 284.
5. Gray, A. L. (1978) *Dynamic Mass Spectrometry* (eds D. Price and J. F. J. Todd), Heyden & Son Ltd., London, Vol. 5, Chapter 8, p. 106.
6. Houk, R. S., Fassel, V. A., and Svec, H. J. (1981) *Dynamic Mass Spectrometry* (eds D. Price and J. F. J. Todd), Heyden & Son Ltd., London, Vol. 6, Chapter 19, p. 234.
7. Gray, A. L. (1981) *Dynamic Mass Spectrometry* (eds D. Price and J. F. J. Todd), Heyden & Son Ltd., London, Vol. 6, Chapter 20, p. 252.
8. Douglas, D. J. and French, J. B. (1981) *Anal. Chem*., **53**, 37.
9. Campargue, R. (1964) *Rev. Sci. Instrum*., **35**, 111.
10. Campargue, R. (1969) *Entropie*, **30**, 15.
11. Campargue, R. (1970) *J. Chem. Phys*., **52**, 1795.
12. Tanner, S. D., Cousins, L. M., and Douglas, D. J. (1994) *Appl. Spectrosc*., **48**(11), 1367.
13. Tanner, S. D., Douglas, D. J., and French, J. B. (1994) *Appl. Spectrosc*., **48**(11), 1373.
14. Douglas, D. J. and French, J. B. (1988) *J. Anal. At. Spectrosc*., **3**, 743.
15. Niu, H. and Houk, R. S. (1994) *Spectrochimica Acta* B, **49**, 1283.
16. Niu, H. and Houk, R. S. (1996) *Spectrochim. Acta* B, **51**, 779.
17. Douglas, D. J. and Tanner, S. D. (1998) *Inductively Coupled Plasma Mass Spectrometry* (ed. A. Montaser), Wiley-VCH, Inc., New York, Chapter 8, p. 615.
18. Olney, T. N., Chen, W., and Douglas, D. J. (1999) *J. Anal. At. Spectroc*., **14**, 9.
19. Ashkenas, H. and Sherman, F. S. (1966) Rarefied gas dynamics, In: *4th Symposium IV* (ed. J. H. De Leeuw), Academic Press, New York, Vol. 2.
20. Liezers, M., Tye, C. T., Mennie, D., and Koller, D. (1995) *Standard Technical Publication 1291*, American Society for Testing and Materials, West Conshohocken, PA, USA, p. 61.
21. Gunther, D., Longerich, H. P., and Jackson, S. E. (1995) *Can. J. Appl. Spectrosc*., **40**(4), 111.
22. Chiappini, R., Taillade, J. M., and Brebion, S. (1996) *J. Anal. At. Spectrosc*., **11**, 497.
23. Jarvis, K. E., Mason, P., Platzner, T., and Williams, J. G. (1998) *J. Anal. At. Spectrosc*., **13**, 689.
24. Bradshaw, N., Hall, E. F., and Sanderson, N. E. (1989) *J. Anal. At. Spectrosc*., **4**, 801.
25. Giessmann, U. and Greb, U. (1994) *Fresenius' J. Anal. Chem.*, **350**, 186.
26. Turner, P. J. (1991) Paper presented at *39th ASMS Conference of Mass Spectrometry and Related Topics*, Nashville, TN, 19–24 May.
27. Hitchen, P., Hutton, R., and Tye, C. T. (1992) *J. Autom. Chem*., **14**(1), 17.
28. Duersch, B. S., Chen, Y., Ciocan, A., and Farnsworth, P. B. (1998) *Specrochim.* Acta B, **53**, 569.

29. Douglas, D. J. (1995) Paper presented at the *Annual FACSS Meeting*, Cinncinati, OH, Paper 216, October.
30. Liezers, M. and Batey, J. (1998) Paper presented at the *25th Annual FACSS Meeting*, Austin, TX, Paper 613, October.
31. Turner, I. A. and Montaser, A. (1998) *Inductively Coupled Plasma Mass Spectrometry* (ed. A. Montaser), Wiley-VCH, Inc., New York, Chapter 4, p. 294.
32. Chambers, D. M., Poehlman, J., Yang, P., and Hieftje, G. M. (1991) *Spectrochim. Acta* B, **46**, 741.
33. Chambers, D. M. and Hieftje, G. M. (1991) *Spectrochim. Acta* B, **46**, 761.
34. Chambers, D. M., Ross, B. S., and Hieftje, G. M. (1991) *Spectrochim. Acta* B, **46**, 785.
35. Chtaib, M. and Schmit, J. P. (1988) *J. Anal. At. Spectrosc.*, **3**, 315.
36. Moens, L., Vanhaecke, F., Riondato, J., and Dams, R. (1995) *J. Anal. At. Spectrosc*., **10**, 569.
37. Vanhaecke, F., Riondato, J., Moens, L., and Dams, R. (1996) *Fresenius' J. Anal. Chem*., **355**, 397.
38. Rodushkin, I., Ruth, T., and Klockare, D. (1998) *J. Anal. At. Spectrosc*., **13**, 159.
39. Nonose, N. and Kubota, M. (2001) *J. Anal. At. Spectrosc*., **16**, 551.
40. Nonose, N. and Kubota, M. (2001) *J. Anal. At. Spectrosc*., **16**, 560.
41. Praphairaksit, N. and Houk, R. S. (2000) *Anal. Chem*., **72**, 2351.
42. Praphairaksit, N. and Houk, R. S. (2000) *Anal. Chem*., **72**, 2356.
43. Douglas, D. J. (1989) *Can. J. Spectrosc*., **34**, 38.
44. Rowan, T. J. and Houk, R. S. (1989) *Appl. Spectrosc*., **43**, 976.
45. Barinaga, C. J. and Koppenaal, D. W. (1994) *Rapid Commun. Mass Spectrosc*., **8**, 71.
46. Koppenaal, D. W., Barinaga, C. J., and Smith, M. R. (1994) *J. Anal. At. Spectrosc*., **9**, 1053.
47. Tanner, S. D., Baranov, V. I., and Bandura, D. R. (2002) *Spectrochim. Acta* **57B**, 1361.
48. Tanner, S. D. (1997) *Plasma Source Mass Spectrometry Developments and Applications* (eds G. Holland and S. D. Tanner), Special Publication 202, Royal Society of Chemistry, Cambridge, UK, p. 13.
49. McGilvery, D. C. (1997) Ph.D. Dissertation, Latrobe University, Bundoora, Victoria, Australia.
50. SIMION Version 7.0, Ion Source Software, P.O. Box 2726, Idaho Falls, ID 83403, USA. (www.sisweb.com/simion.htm)
51. MUNRO (http://www.mebs.co.uk)
52. CPO (http://www.electrouoptics.com)
53. Montaser, A., Mclean, J. A., Liu, H., and Mermet, J. M. (1998) *Inductively Coupled Plasma Mass Spectrometry* (ed. A. Montaser), Wiley-VCH, Inc., New York, Chapter 1, p. 1.
54. Jarvis, K. E., Gray, A. L., and Houk, R. S. (1992) *Handbook of Inductively Coupled Plasma Mass Spectrometry*, Blackie & Son Ltd., Glasgow, UK, p. 34.
55. Hu, K., Clemons, P. S., and Houk, R. S. (1993) *J. Mass Spectrosc*., **4**, 16.
56. Model SPQ 9000 Seiko Instruments Inc. Oyama Plant, 36-1, Takenoshita, Oyama-cho, Sunto-gun, Shizuoka 410-13 Japan.
57. Elliott, S., Knowles M., and Kolinitchenko, I. (2004) *Spectroscopy* **19**(1), 30.
58. Liezers, M., Farmer, O. T., Koppenaal, III, D. W., and Grate, J. W. (1999) Paper presented at the *26th Annual FACSS Meeting*, Vancouver, Canada, Paper 340, October.
59. Baranov, V. I. and Tanner, S. D. (1999) *J. Anal. At. Spectrosc*., **14**, 1133.
60. Tanner, S. D. and Baranov, V. I. (1999) *J. Am. Soc. Mass Spectrosc*. **10**, 1083.
61. Turner, P., Merren, R., Speakman, J., and Haines, C. (1997) *Plasma Source Mass Spectrometry Developments and Applications* (eds G. Holland and S. D. Tanner), Special Publication 202, Royal Society of Chemistry, Cambridge, UK, p. 28.
62. Leonhard, P., Pepelinik, R., Prange, A., Yamada, N., and Yamada, T. (2002) *J. Anal. At. Spectrosc*., **17**, 189.

Chapter 2
Mass Spectrometers

Jonathan H Batey, Thomas Prohaska, MSA Horstwood, GM Nowell, Heidi Goenaga-Infante and Gregory C Eiden

2.1 QUADRUPOLE MASS SPECTROMETERS

Jonathan H Batey

2.1.1 Introduction

The origins of mass spectrometry can be traced back to instruments that were designed and built during the second decade of the 20th century.[1] They shared the characteristic that mass separation was achieved by passing ions through a steady (that is, time-invariant) magnetic field. Of course, the magnetic field might be varied in order to scan through a mass spectrum, but the rate of change of the field was very slow compared to the transit time of the ions. The same principle is still used today. These instruments are classified as 'static' mass spectrometers.

An alternative approach is to use time-varying electric fields to separate the masses. The quadrupole mass filter (QMF) is probably the most familiar example; the ion trap and the time-of-flight mass spectrometer are also widely used and the application of these devices for ICP-MS is described later in this chapter. In all these instruments, electric fields are varied at a rate that is rapid compared with the transit time of the ions. They are known as 'dynamic' mass spectrometers.

2.1.1.1 Electrostatic fields

An electrostatic field **E** and its associated potential Φ are linked by the equation

$$\mathbf{E} = -\nabla\Phi = \mathbf{x}\frac{\partial}{\partial x}(\Phi) + \mathbf{y}\frac{\partial}{\partial y}(\Phi) + \mathbf{z}\frac{\partial}{\partial z}(\Phi) \tag{2.1.1}$$

where **x**, **y** and **z** are unit vectors directed along the Cartesian axes. Note that bold type is used to indicate vectors in this discussion.

An ion that carries an electric charge e (in coulombs) and which is subjected to the field **E** experiences a force **F,** where

$$\mathbf{F} = -e \cdot \mathbf{E} \tag{2.1.2}$$

From Newton's second law of motion, the corresponding acceleration is

$$\frac{\mathrm{d}^2}{\mathrm{d}t^2}(\mathbf{U}) = \mathbf{F}/m = -e \cdot \mathbf{E}/m \tag{2.1.3}$$

where **U** is the position vector of the ion, and m is its mass.

Inductively Coupled Plasma Mass Spectrometry Handbook Edited by Simon M. Nelms
 ISBN: 978-1-405-10916-1

Note that the force **F** and the resulting acceleration are both in the same direction as the electric field **E**. Therefore, if the ion starts at rest, it will move initially in the direction of the local electrostatic field. However, if the field is non-uniform (for example because of potentials applied to electrostatic lenses), once the ion is moving its velocity will not usually point in the same direction as the local field. The situation is somewhat analogous to the motion of a golf ball as it passes across a region of hills and valleys on a crazy golf course.

We usually think of an ion as having originated at a particular potential, measured relative to ground. This potential is known as the ion energy. In the case of ICP-MS, this corresponds to the plasma potential, and is typically a few volts. If the ion comes under the influence of an electrostatic field it will speed up or slow down, depending on whether the local potential is positive or negative with respect to ground. If it enters a region that is bounded by grounded surfaces (for example, a vacuum chamber), then energy conservation dictates that it will accelerate until its kinetic energy is equivalent to its original potential energy. That is,

$$e \cdot E_{\mathrm{I}} = \frac{1}{2} \cdot m \cdot |\mathbf{v}|^2$$

where **v** is the ion velocity and E_{I} is the ion energy (in electron volts (ev)).

Clearly, we have

$$E_{\mathrm{I}} = \frac{m \cdot |\mathbf{v}|^2}{2 \cdot e} \tag{2.1.4}$$

Note that it is the magnitude of the ion's velocity that appears in equation (2.1.4). The ion energy is independent of the direction in which the ion is travelling.

2.1.1.2 The quadrupole field

There are many descriptions in the literature of the theoretical basis of the QMF. Dawson[2] gives a wide-ranging treatment. Steel and Henchman[3] present a more recent and less detailed description.

Figure 2.1 is a schematic of a QMF, showing the electrodes and some equipotentials (voltage contours) in a plane perpendicular to the ion optical axis (the z axis).

For simplicity, we ignore the effect of fringing fields, so these equipotentials are constant along the whole length of the device. In Figure 2.1 a potential of +10 V is applied to the two electrodes (X_1, X_2) that are disposed in the horizontal direction, and −10 V is applied to the other two electrodes (Y_1, Y_2). The total potential difference between the two sets of rods, conventionally given the symbol Φ_0, is in this case 20 V.

In an idealised QMF the potential Φ is given by

$$\Phi(x, y, z) = \Phi_0 \cdot \frac{(x^2 - y^2)}{2{r_0}^2} \tag{2.1.5}$$

where r_0 is the inscribed radius of the cylinder enclosed by the quadrupole rods. The x coordinate is aligned horizontally and the y coordinate is aligned vertically as shown in Figure 2.1. The origin is at the centre of the entrance plane (where the 0 V contours intersect). The potential is independent of z, so there is no field component along the z axis.

The contours are analogous to those seen on a relief map, but here they indicate electrical potential rather than height. They are to be envisaged as extending along the length of the QMF.

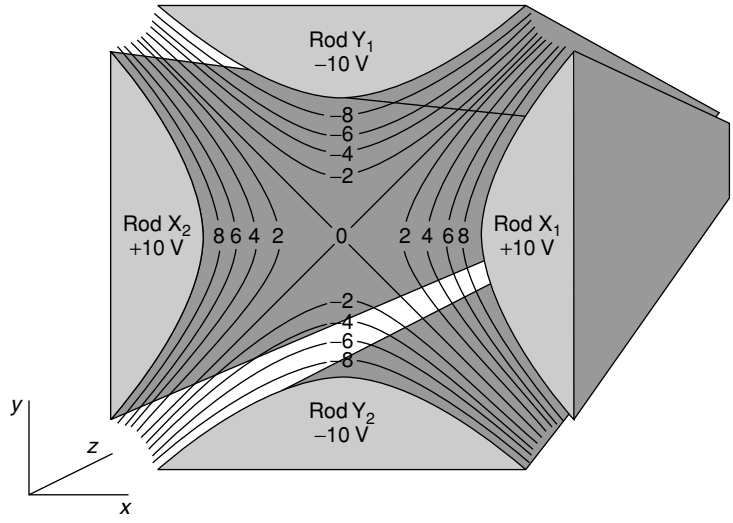

Figure 2.1 Schematic of a QMF. A potential of +10 V is applied to the electrode rods X_1 and X_2, while a potential of −10 V is applied to Y_1 and Y_2. Equipotentials (voltage contours) are drawn at intervals of 2 V

There is symmetry about the *XZ* and the *YZ* planes. The potential increases as we move away from the origin along the *X* axis whereas it decreases as we move away from the origin along the *Y* axis. The action of an electric field on an ion can be visualised by considering how an object would slide or roll down a saddle-shaped surface. Indeed, during the 1930s, electron optical designs were optimised by observing the trajectories of small ball bearings rolling on a stretched rubber sheet.

The required potential distribution can be generated by using electrodes whose cross section is hyperbolic, but cylindrical electrodes are found to generate a potential distribution that is close enough to hyperbolic for most purposes. Since they are much easier to manufacture and align to the necessary precision, cylinders are usually preferred in practice.

The components of the electric field along the axes are

$$E_x = \frac{\partial}{\partial x}(\Phi) = -x \cdot \Phi_0/({r_0}^2) \tag{2.1.6}$$

$$E_y = \frac{\partial}{\partial y}(\Phi) = y \cdot \Phi_0/({r_0}^2) \tag{2.1.7}$$

$$E_z = \frac{\partial}{\partial z}(\Phi) = 0 \tag{2.1.8}$$

The component E_x is independent of the y coordinate and vice versa. This can be seen in Figure 2.2(a) in which the electric field vector is plotted for points on a Cartesian grid.

Another view of the vector field is presented in Figure 2.2(b), in which the points are on a polar grid. Note that the magnitude of the electric field is constant at a given radius from the origin. There is no field along the z axis.

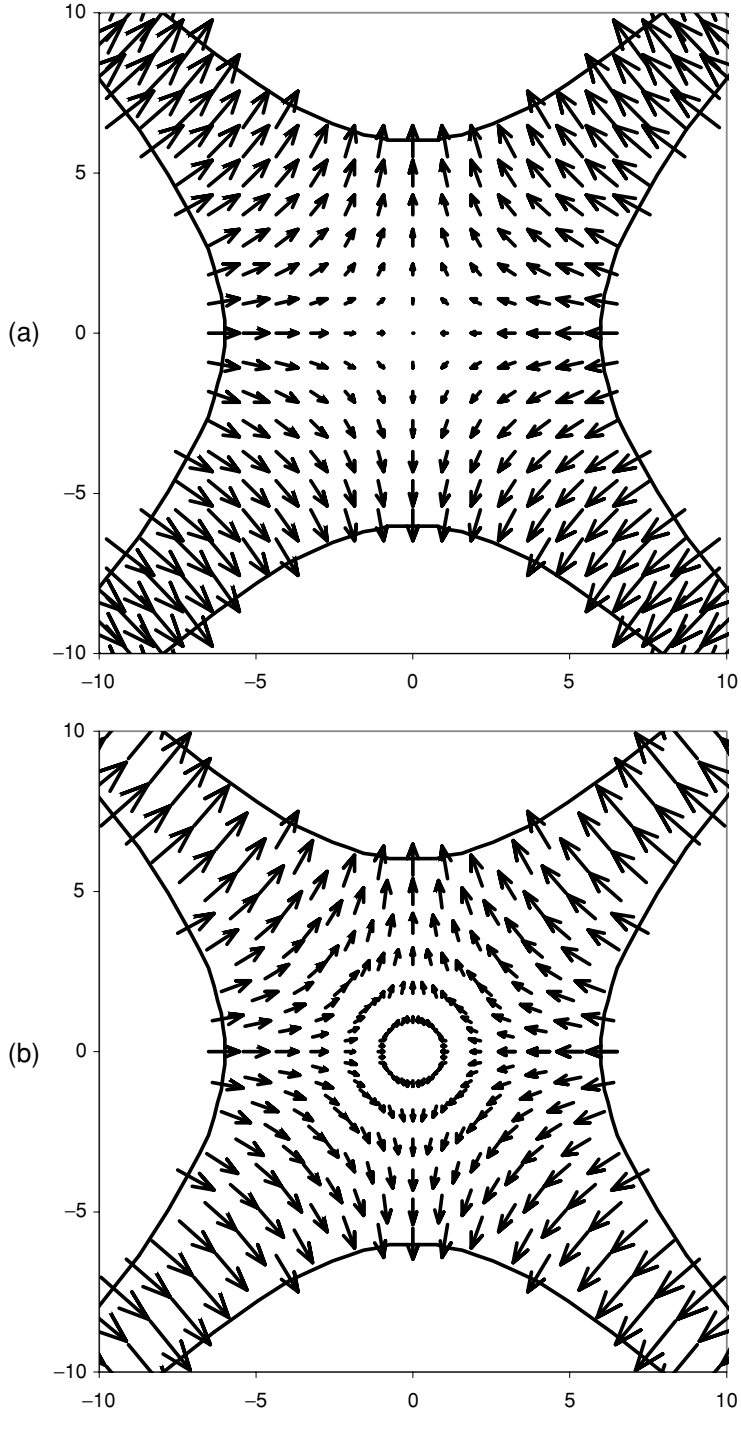

Figure 2.2 (a) Electric field vector, Cartesian grid and (b) electric field vector, polar grid

2.1.1.3 Ion motion

The quadrupole structure can be used as a static device (that is, one in which Φ_0 is constant) for steering and shaping an ion beam, with no mass selection. However, for a mass filter, the potential Φ_0 consists of a constant and an alternating component. Specifically,

$$\Phi_0 = U - V\cos(2\pi f(\mathrm{t} - \mathrm{t}_0)) \tag{2.1.9}$$

where U is the constant ('DC') potential;
V is the alternating ('RF') potential;
f is the frequency of the RF supply;
t is the time;
t_0 is the initial phase of the RF component.

The equations of motion are then

$$\frac{\mathrm{d}^2U_x}{\mathrm{d}t^2} = -E_x \cdot (e/m) = -(e/(m{r_0}^2)) \cdot (U - V\cos(2\pi f(t - t_0))) \cdot U_x \tag{2.1.10}$$

$$\frac{\mathrm{d}^2U_y}{\mathrm{d}t^2} = -Ey \cdot (e/m) = (e/(m{r_0}^2)) \cdot (U - V\cos(2\pi f(t - t_0))) \cdot U_y \tag{2.1.11}$$

$$\frac{\mathrm{d}^2U_z}{\mathrm{d}t^2} = 0 \tag{2.1.12}$$

where U_x, U_y and U_z are the coordinates of the ion.

Note that the x and y components of the ion motion are governed by the same differential equation; only the algebraic sign changes, because of the inherent symmetry of the applied field.

In a perfect QMF there is no acceleration along the z axis, so the ion is transmitted with a constant axial velocity. This velocity is determined essentially by the difference between the ion's energy (that is, the kinetic energy that it would have were it to enter a grounded environment) and the (constant) potential along the axis of the QMF. In equation (2.1.9) the axial potential is zero, but often a constant unipolar potential is superimposed. This is known as the 'pole bias' or sometimes the 'field axis' potential. It causes the ions to speed up or slow down within the QMF, so that they can be transmitted with optimal axial velocity.

Note that although an ion may speed up or slow down as it passes through intermediate lenses before it reaches the QMF, such lenses do not themselves influence the axial velocity within the QMF. In practice, fringing fields always exist near the entrance and exit of the QMF. These give rise to non-zero field components in the z direction, and will therefore alter the axial velocity. The influence of these fields extends into the mass filter to a distance of about $3r_0$ from the entrance and exit. For simplicity this influence is largely ignored in this treatment, which applies specifically to ion motion in a perfect quadrupole field (but see Section 2.1.1.9).

By substituting

$$a_x = 4eU/\left(mw^2{\mathrm{r}_0}^2\right) \qquad q_x = 2eV/\left(mw^2{r_0}^2\right)$$
$$a_y = -a_x \qquad q_y = -q_x$$

where $w = 2\pi f$

and introducing the dimensionless parameter $\xi = \pi ft$ as the independent variable, equations (2.1.10) and (2.1.11) become

$$\frac{d^2U_x}{d\xi^2} + (a_x - 2q_x \cos(2(x - x_0)))\,U_x = 0 \tag{2.1.13}$$

$$\frac{d^2U_y}{d\xi^2} + (a_y - 2q_y \cos(2(x - x_0)))\,U_y = 0 \tag{2.1.14}$$

which are both of the form

$$\frac{d^2u}{d\xi^2} + (a_u - 2q_u \cos(2(x - x_0)))\,u = 0 \tag{2.1.15}$$

where u represents either x or y.

2.1.1.4 Stability diagram

Equation (2.1.15) is the Mathieu equation. It is named after Emile Mathieu (1835–1890), who used it to study the vibrations of elliptical membranes.[4] It can be solved by numerical integration[5] or analytically[6] and its general behaviour is well known.[7] The solutions are generally divergent, but stable solutions are obtained when a_u and q_u lie within the bounded region of Figure 2.3.

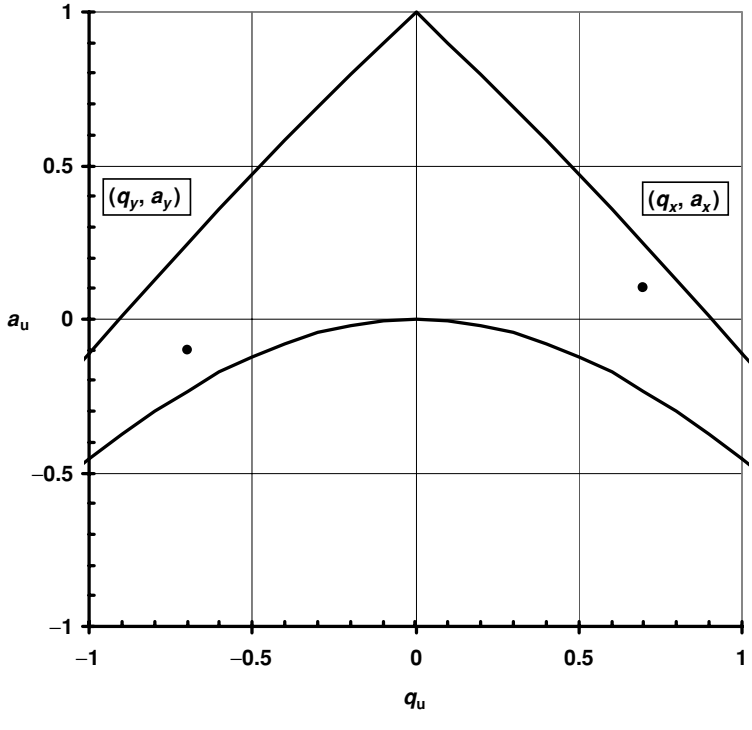

Figure 2.3 Mathieu stability diagram. The ion motion is stable if both operating points lie within the bounded region. The plotted points are for ($q_x = 0.7$, $a_x = 0.1$) and ($q_y = -0.7$, $a_y = -0.1$)

Although not shown in Figure 2.3, other regions of stability exist. These regions have been employed[8] to demonstrate improved mass resolution in ICP-MS, but at the expense of considerably reduced sensitivity. They have also been used for specialised residual gas analysis.[9]

If either U_x or U_y is an unstable solution of (2.1.15), then the ion motion is divergent in the corresponding direction, so one would expect the ion not to be transmitted by the mass filter. Conversely, if both U_x and U_y are stable solutions of (2.1.15), then we would expect the ion to be transmitted. U_x is characterised by the point (a_x, q_x) in the first quadrant of Figure 2.3, while U_y is characterised by (a_y, q_y) in the third quadrant. Because (a_y, q_y) can be obtained from (a_x, q_x) by rotating 180° about the origin, it is convenient to combine the operating point for the x and y motion into one diagram as shown in Figure 2.4.

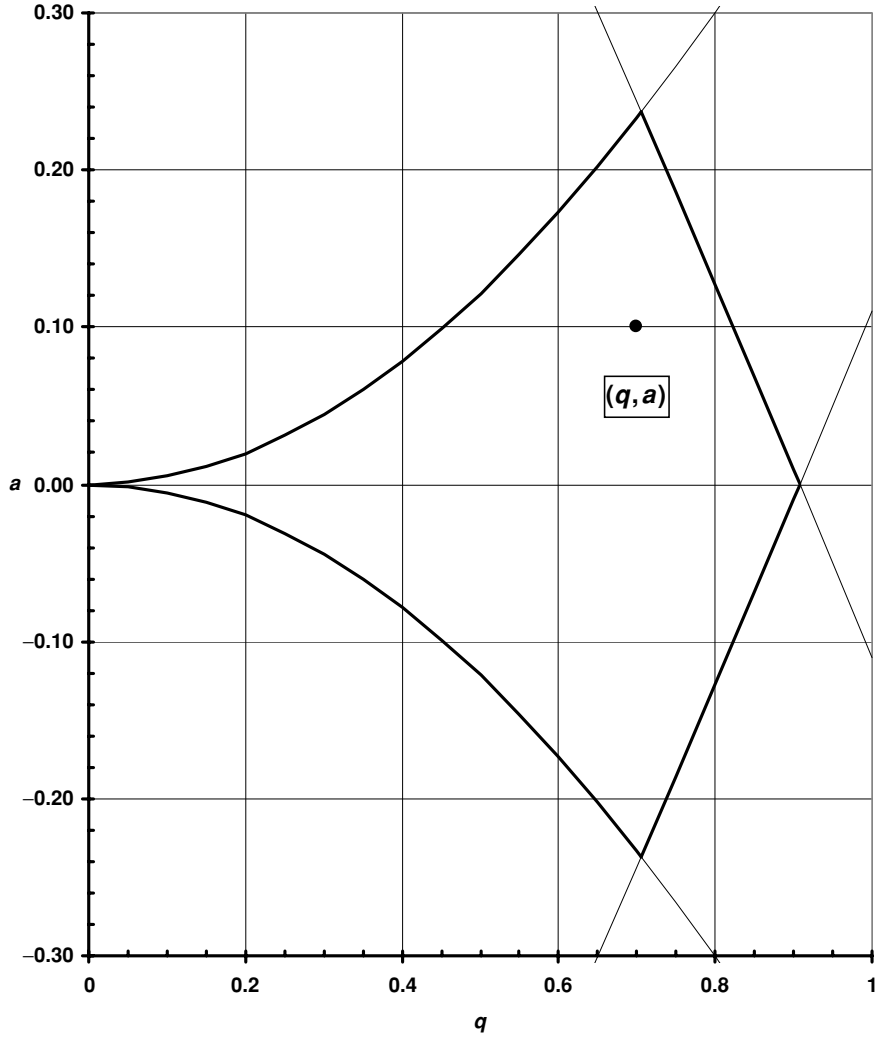

Figure 2.4 Mass filter stability diagram. The ion motion is stable if the operating point lies within the kite-shaped region. The operating point ($q = 0.7$, $a = 0.1$) is indicated

The ion motion is stable only if the operating point lies within the kite-shaped region, which is known as the 'stability region'. Because the stability region is symmetrical about the horizontal axis, the lower portion ($a < 0$) of the plot is usually omitted. As will be seen in the following section, it is necessary to include this portion to account fully for the observed behaviour of the QMF at low mass.

2.1.1.5 Scan lines

The significance of the stability region becomes clearer when it is plotted in terms of V and U for a particular case, as shown in Figure 2.5.

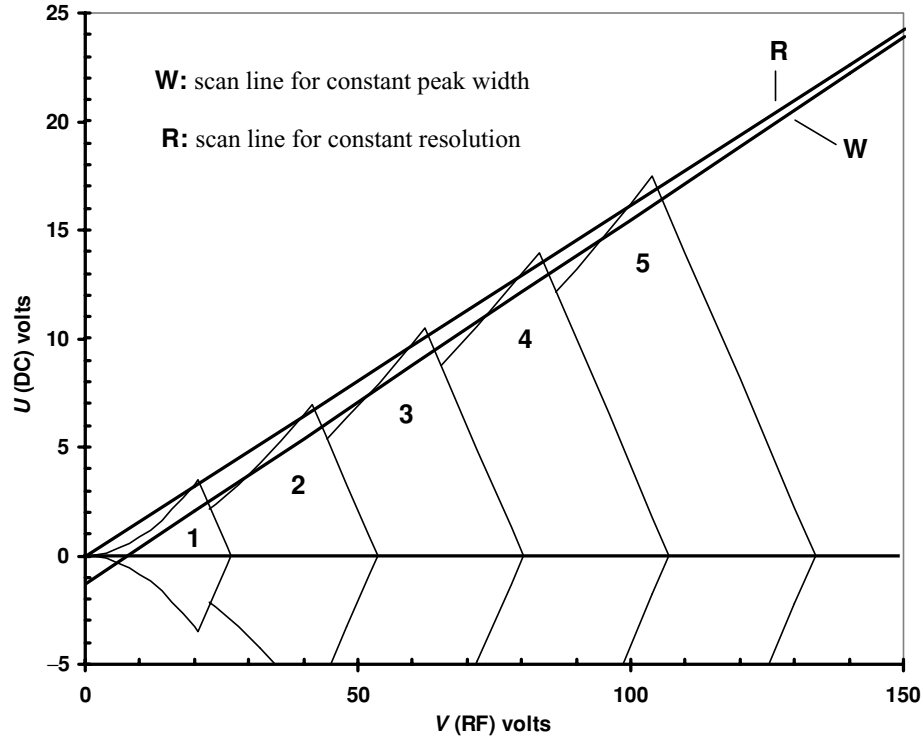

Figure 2.5 Stability plots for low masses

This shows data for $r_0 = 6$ mm and $f = 2 \times 10^6$ Hz; these values are typical for a quadrupole ICP-MS. Stability regions are shown for several ions of low mass. Ions of a particular mass are stable if V and U lie within the appropriate kite-shaped region. For example, ions of mass 1 amu are stable if V and U lie within the region labelled **1.**

Now suppose that we scan V from 0 to 150 V, whilst keeping U constant at 0 V. While U is between 0 V and 26.7 V, all of masses 1–5 are stable, and are therefore transmitted. Above 26.7 V, mass 1 is unstable and is not transmitted. For V greater than 133.8 V, none of the masses 1–5 are stable. For illustrative purposes, suppose now that we are able to inject equal numbers of ions per second of masses 1–5 into the mass filter. We expect to see a mass spectrum of the

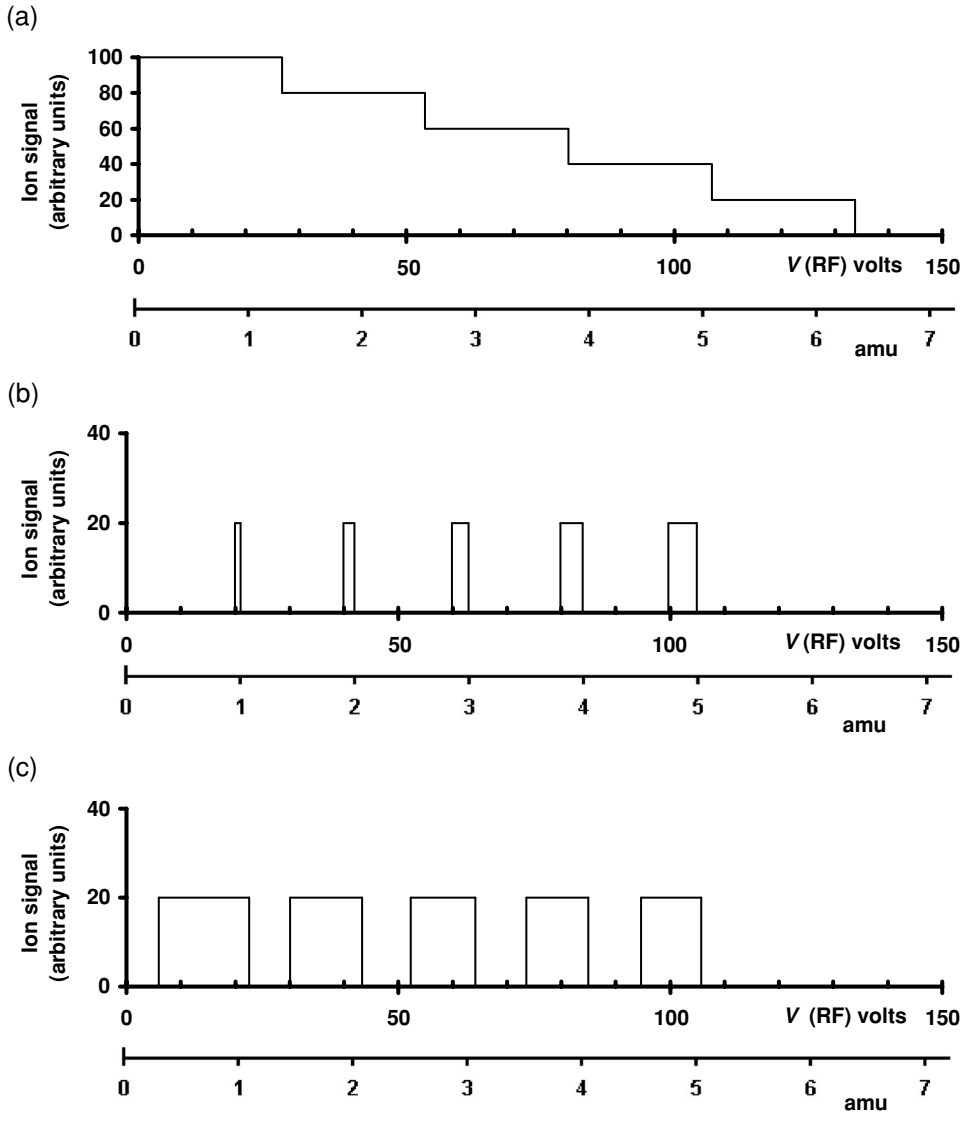

Figure 2.6 Conceptual mass spectra. (a) Scan line along V axis (RF only), (b) scan line **R** (constant resolution) and (c) scan line **W** (constant peak width)

general form shown in Figure 2.6(a). This is an idealised version of what is generally known as a 'total ion' or 'RF-only' spectrum. It is characterised by a large signal at low mass, and successive rapid reductions in signal as the scan renders successive masses unstable.

If we make U vary in direct proportion to V, that is as

$$U = k \cdot V \tag{2.1.16}$$

we have a scan line such as **R** in Figure 2.5, where k is a constant, corresponding to the slope of line R. This generates a very different spectrum, as shown in Figure 2.6(b). As **R** passes

through each stability region, the corresponding ion is transmitted. The stability regions scale linearly with mass, so the range of V for which each ion is transmitted is itself proportional to mass, and the peak width is also proportional to mass. This corresponds to constant resolving power, which is the operational mode for magnetic sector instruments. It is customary however to use a different technique for quadrupoles, where, usually, a constant offset is applied to the scan line. The result is a scan line such as **W**, for which

$$U = k_0 \cdot V - c \tag{2.1.17}$$

The slope k_0 is the same as the slope of the scan line that aligns with the tips of the stability regions and c is a constant offset, often known as the 'delta-m' offset. For all but the lowest masses, the boundaries of the relevant portion of the stability region are essentially linear. Consequently the range of V for which each ion is transmitted is constant, and so the peak width is also constant. This is seen in Figure 2.6(c). The peak width increases slightly for low-mass ions. This is because the low-mass edge of the stability region is slightly curved. The effect on peak width is particularly noticeable for the peak at 1 amu. Indeed, in Figure 2.5, we see that U has become negative before **W** has intersected the low-mass boundary of the stability region. Had we plotted only the positive values of U in Figure 2.5, it would not be clear where to locate the low-mass edge of the peak. Operating the QMF in this way actually corresponds to varying the resolving power across the mass range. However, this mode of operation is often somewhat confusingly referred to as operating with 'unit mass resolution'.

2.1.1.6 Ion trajectories

The trajectory of an ion in the mass filter can be obtained by numerical integration of equations (2.1.10)–(2.1.12). Typical trajectories are shown in Figure 2.7, for an ion of mass 5 amu with the quadrupole drive (V, U) set to three positions along the scan line **W** of Figure 2.8, which is an enlargement of the tip of the stability region for mass 5 in Figure 2.5.

Operating point	V(RF)	U(DC)
L	93.0	14.3
M	100.2	15.5
H	107.0	16.6

The operating point **M** corresponds to the nominal centre of the peak; it is at the midpoint of the portion of the scan line that is bounded by the stability region. The ion trajectories in both the X and Y directions are stable, so the ion is transmitted. At point **L**, the operating point is outside the stability region. The Y trajectory is unstable, so the ion is rejected from the filter. Conversely, at point **H**, the X trajectory is unstable. This illustrates the underlying concept of the mass filter i.e. that the ion is transmitted only when the operating point lies within the stability region, and that ions are rendered progressively more unstable as the operating point is taken further from the centre of the peak. Ions that follow unstable trajectories through the QMF eventually strike the quadrupole rods, where they are neutralised and, in principle, remain until the rods are cleaned.

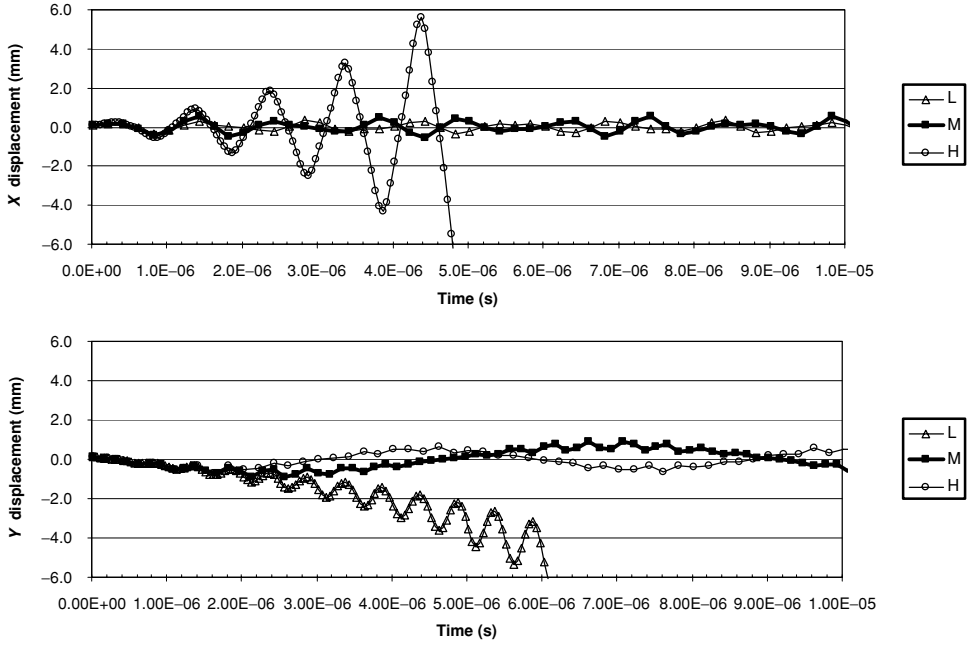

Figure 2.7 Ion trajectories

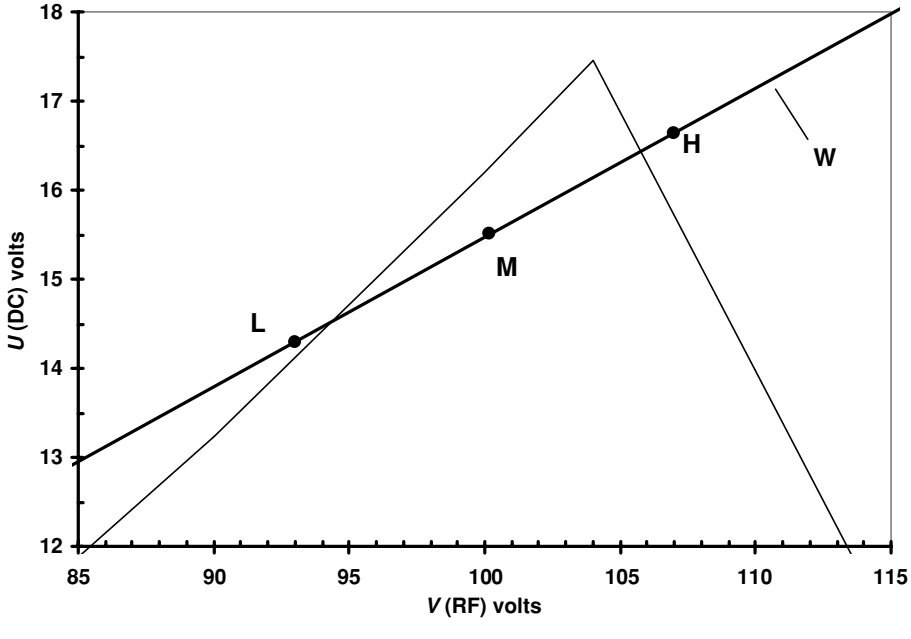

Figure 2.8 Stability plot for mass 5. The operating points **L**, **M** and **H** are the same as for the trajectory plots in Figure 2.7. They all lie on the scan line **W**

One can also visualise the operation of the QMF as the result of combining a 'low-pass' mass filtering action in the *y* direction with a 'high-pass' mass filtering action in the *x* direction. Of course, it is not possible to physically separate the two actions. Each is a fundamental consequence of the quadrupole field.

Note that Figure 2.7 shows the ion trajectory plotted as a function of time. Whether an ion that follows a divergent trajectory is actually rejected from the mass filter depends on how long the ion takes to traverse the length of the filter. If the filter is short, or if the ion energy is high or the ion is injected close to the axis of the quadrupole field, the ion may be transmitted, even though the trajectory is unstable mathematically. This causes peak tailing, which is discussed in more detail below.

2.1.1.7 Mass peaks

Of course, Figure 2.7 shows the trajectories for only one particular set of entry conditions. The ion trajectory is actually very dependent on these conditions, and also on the relative phase of the RF drive (t_0 in equations (2.1.10) and (2.1.11)). By varying the conditions systematically, one can determine the fate of a large number of ions, and thus generate a simulated mass spectrum.

Examples of simulated spectra are shown in Figure 2.9, in which the peak shapes have been calculated using a program similar to that described by Gibson and Taylor.[5] The following parameters were used:

Field radius (r_0)	6 mm	Radio frequency	2 MHz
Field length	200 mm	Input radius	1 mm
Exit radius	6 mm	Ion energy	5 eV
Beam divergence	5°	Ion masses	1, 2, 3, 4 and 5 amu

The simulated peaks are consistent with the conceptual spectra of Figure 2.6, but the peak shapes are more realistic. In general the tops of the peaks are rounded and the leading edge of the peaks are noticeably tailed. More recent work seeks to model the geometry of the quadrupole more realistically, taking account of field imperfections such as those introduced by the use of cylindrical electrodes.[10]

Of course, it would be near impossible to generate a 'real' mass spectrum to correspond with those in Figure 2.9, because the ion distribution is quite artificial. Figure 2.10 shows a mass spectrum of indium from a modern commercial ICP-MS.[11] The sample was 100 ppb of indium in 2% nitric acid. The main peaks, at 112.9 amu and 114.9 amu, are from the isotopes ^{113}In and ^{115}In. Also plotted is the simulated peak for ions of mass 114.9 amu. It is clear that the model accounts for the basic features of the observed mass spectrum.

In addition to the expected peaks from indium, there are also small peaks at neighbouring masses. These are due to trace levels of tin in the sample.

2.1.1.8 Peak tailing

An ICP-MS is required to operate over a wide range of analyte concentrations. The range of signals displayed in Figure 2.10 covers more than six orders of magnitude. There is a characteristic

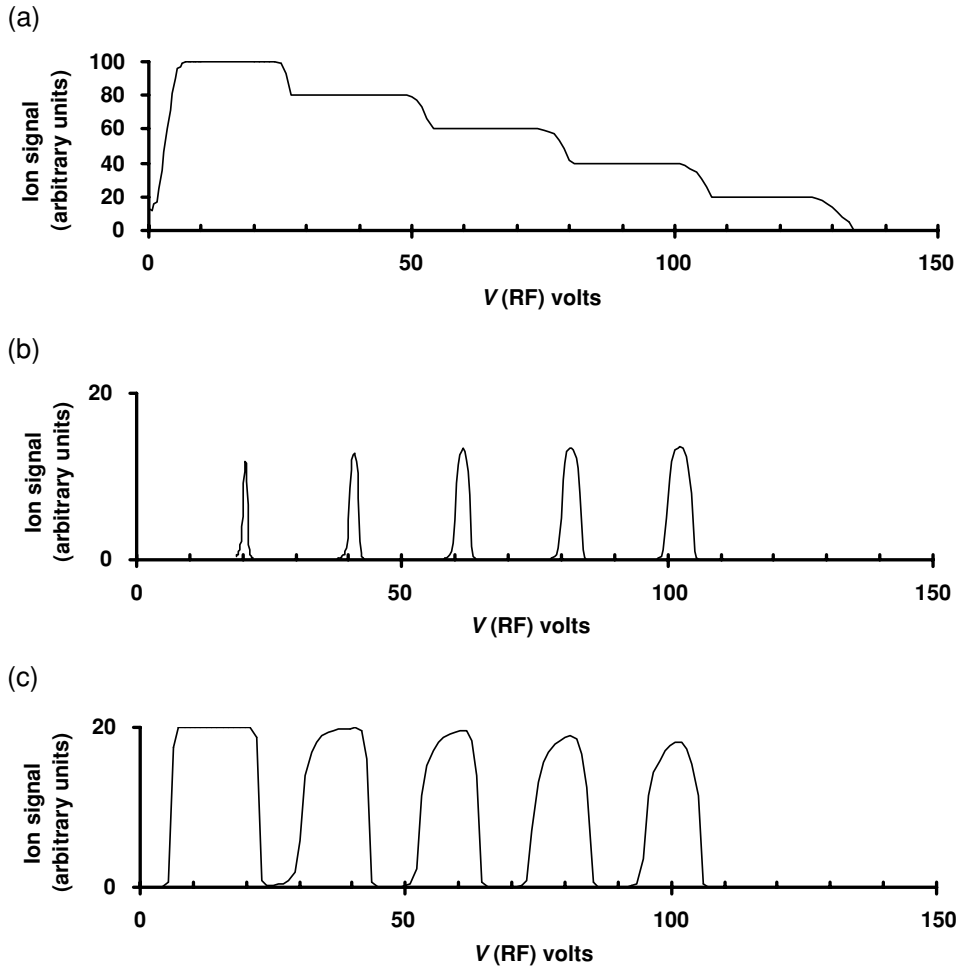

Figure 2.9 Simulated mass spectra. (a) Scan line along the *V* axis (RF-only spectrum), (b) Scan line **R** (constant resolution) and (c) Scan line **W** (constant peak width)

'tail' on the low-mass side of the peak. In Figure 2.10 this is most evident for the ^{115}In peak. As already mentioned, the tailing is caused by the failure of the mass filter to reject completely all the ions that follow divergent trajectories. The ions must remain under the influence of the quadrupole field for many cycles of the radio-frequency drive for peak tailing to be minimised. Qualitatively therefore, minimal peak tailing calls for a long mass filter, driven at a high radio frequency, and for the ions to traverse the filter as slowly as possible. Practical and economic considerations limit how far these parameters can be taken, but quadrupole rods of length 150–250 mm combined with a drive radio frequency of 2–3 MHz are usually employed for quadrupole ICP-MS instruments, in which ions from the plasma may be expected to have energies in the range 2–10 eV and an energy spread of 2–5 eV.

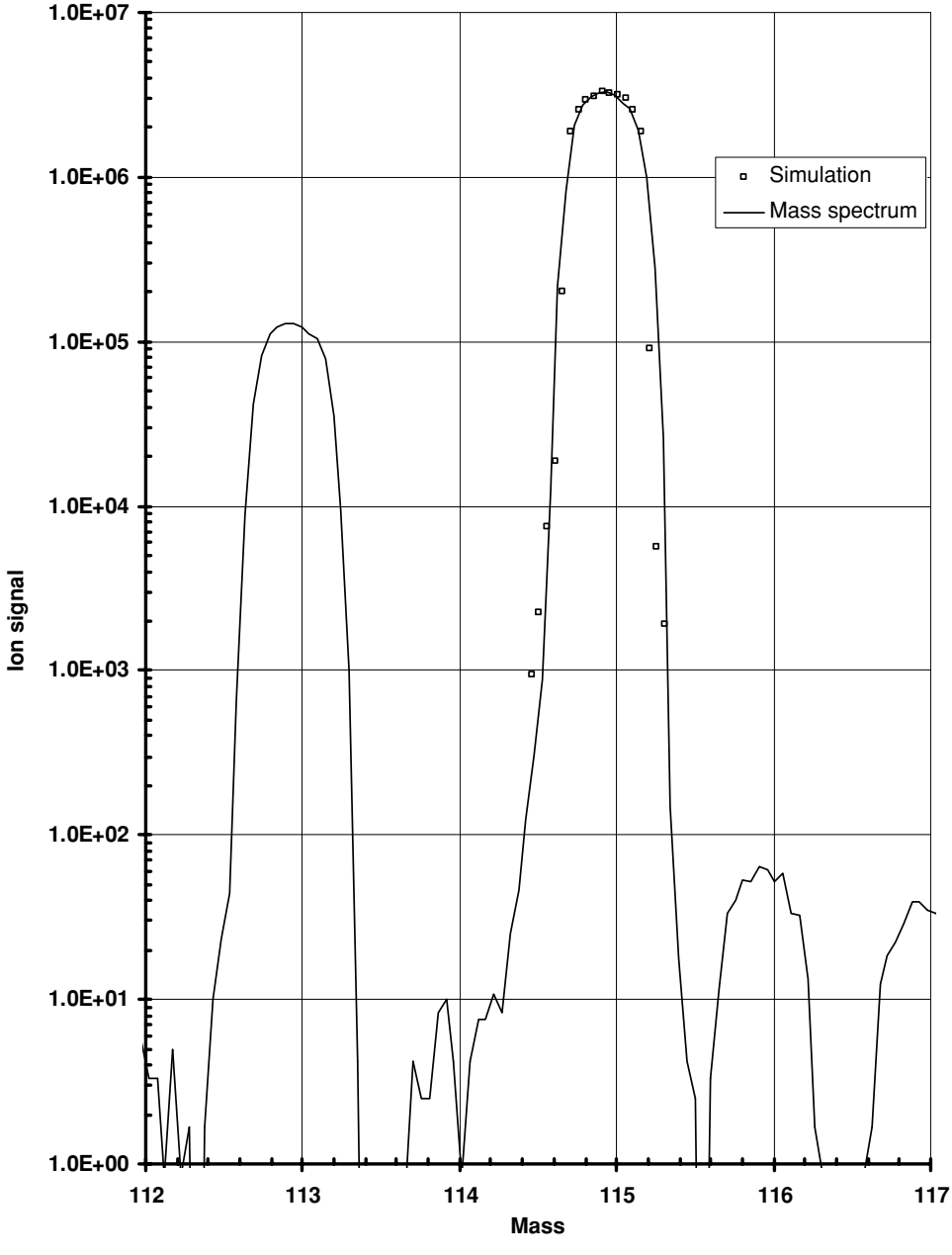

Figure 2.10 Spectrum from a commercially available quadrupole ICP-MS

Peak tailing is usually expressed as 'abundance sensitivity', which is defined[12] by IUPAC as 'the ratio of the maximum ion current recorded at a mass m to the ion current arising from the same species recorded at an adjacent mass ($m \pm 1$)'.

The abundance sensitivity of a quadrupole instrument can be 10^6 or better. This performance is not influenced strongly by the operating vacuum pressure; typically around 10^{-4} Pa (10^{-6} mbar) is quite adequate. This contrasts with magnetic sector instruments, in which ultra-high vacuum conditions are needed to minimise beam scattering when good abundance sensitivity is required.

2.1.1.9 Ion entry and exit

Ions are lost in the region of the mass filter near the entrance, and to a lesser extent in the region near the exit. In these 'fringing field' regions, the ion motion is destabilised because the local electric field is different from the value in the main part of the filter. For ion entry it is usual to minimise these losses by controlling carefully the ion entry conditions. This is often achieved using a short 'RF-only' pre-filter, driven from the same RF supply as the main quadrupole, but with no DC component. An alternative approach is to use an entrance lens, driven with a voltage that scans proportionately to the RF amplitude.

In practice, the conditions for ions leaving the mass filter are less critical. Often, field penetration from the high voltage applied to an electron multiplier detector helps to sweep ions efficiently out of the filter.

References

1. Grayson, M. A. (ed.). (2002) *Measuring mass: from positive rays to proteins.* Chemical Heritage Press, Philadelphia.
2. Dawson, P. H. (ed.) (1976) *Quadrupole Mass Spectrometry and its Applications*, Elsevier, Amsterdam.
3. Steel, C. and Henchman, M. (1998) Understanding the quadrupole mass filter through computer simulation. *J. Chem. Ed.*, **75**, 1049–54.
4. Mathieu, É. (1868) Mémoire sur le mouvement vibratoire d'une membrane de forme elliptique. *J. Math. Pure Appl.* **13**, 137–203.
5. Gibson, J. R., Taylor, S., and Leck, J. H. (2000) Detailed simulation of mass spectra for quadrupole mass spectrometer systems. *J. Vac. Sci. Technol.* **A18**(1), 237–43.
6. Baranov, V. (2003) Analytical approach for description of ion motion in quadrupole mass spectrometer. *J. Am. Soc. Mass Spectrom.*, **14**, 818–24.
7. McLachlan, N. W. (1947) *Theory and Application of Mathieu Functions*, Oxford University Press, Oxford.
8. Du, Z., Douglas, D. J., and Konenkov, N. (1999) Elemental analysis with quadrupole mass filters operated in higher stability regions. *J. Anal. At. Spectrom.*, **14**, 1111–9.
9. Hiroki, S., Abe, T., and Murakami, Y. (1992) Separation of helium and deuterium peaks with a quadrupole mass spectrometer by using the second stability zone in the Mathieu diagram. *Rev. Sci. Instrum.*, **63**(8), 3874–6.
10. Gibson, J. R. and Taylor, S. (2003) Asymmetrical features of mass spectral peaks produced by quadrupole mass filters. *Rapid Commun. Mass Spectrom.*, **17**, 1051–5.
11. Thermo Electron Corporation X Series ICP-MS.
12. IUPAC Compendium of Chemical Technology 1997.

2.2 MAGNETIC SECTOR FIELD INSTRUMENTS

2.2.1 SINGLE COLLECTOR INSTRUMENTS

Thomas Prohaska

Magnetic sector field ICP-MS instruments use a magnetic field to separate ions of a given mass/charge ratio. The first instrument of this type was introduced to the market in 1989.[1,2] Sector field analysers had been used for many years in molecular spectrometry for the identification and structural analysis of complex organic compounds. They had, however, the attribute of being very complex and thus expensive. The acceptance of the first instruments remained restricted to applications in which high mass resolution was an absolute prerequisite, although limitations from interferences became more and more troublesome with the ever increasing demand for analytical tasks in many biological, medical, geological and environmental applications.[3] At present, the availability of double-focusing ICP-MS instruments has not only facilitated improved accuracy ICP-MS based qualitative and quantitative investigations but also triggered new applications. Elimination of several spectral interferences, improved detection limits and better precision of isotope ratio measurements are important achievements in this respect.

Figure 2.11 shows as an example the schematic setup of a commercially available single-collector device.[4] The figures of merit and advantages/disadvantages are highlighted in Table 2.1.

2.2.1.1 Operation principle (mass separation)

The magnetic sector analyser consists of a curved flight tube, which is located between the poles of either a permanent magnet or, in practice, an electromagnet with variable field strength. The ions which are generated in the ICP, are accelerated up to 10 keV after passing the interface region (sampler and skimmer cone) by a high extraction potential. The high voltage is supplied to the interface (with the analyser at ground potential) or the interface is kept at ground and the analyser floated at high voltage. From the user safety point of view, the advantage of the second setup is that the sample introduction system is fully accessible whilst the high voltage is on. In addition, with this configuration a reduction of the capacitive coupling of the RF plasma to the interface can be observed. High vacuum is kept at 10^{-8} mbar by a differential pumping system (vane-type rotary pump and turbo molecular pumps). This vacuum is considerably lower than in quadrupole ICP-MS but is absolutely necessary to be this low for an adequate reduction of ion scattering with respect to the longer flight path of the ions.

After acceleration, positively charged ions from the plasma (now with uniform kinetic energy) are focused through a sequence of ion lenses before travelling through a narrow slit of adjustable width (the source slit). After passing through the source slit, the ions are injected perpendicular to the magnetic field and traverse the field in different circular trajectories according to their mass/charge ratio. A second slit (the collector slit) positioned at the exit of the magnet at the focus point results in the selection of a specific mass. Decreasing source and/or collector slit widths can be used to increase the mass resolution if the energy distribution is uniform (see later for a detailed description).

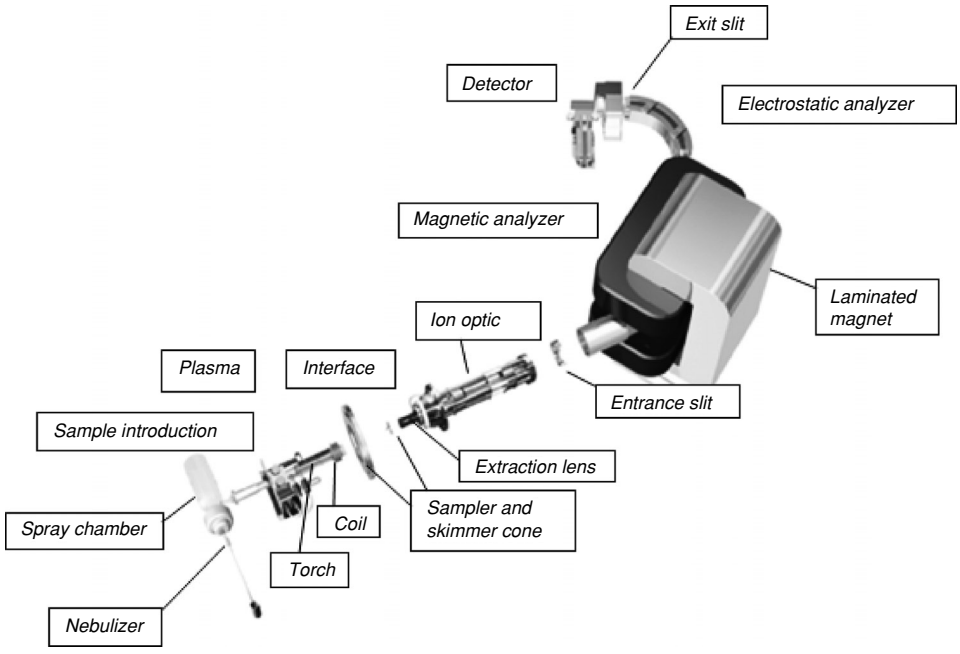

Figure 2.11 Schematic setup of a magnetic sector field ICP-MS (in this example of the Element 2). The system is a single-collector double-focusing magnetic sector field device with reversed Nier-Johnson geometry. The system consists of (i) sample introduction system (nebulizer+spray chamber or other coupled devices) (ii) plasma source (torch+load coil forming an inductively coupled Ar ion plasma), (iii) ion optics (including acceleration lens, different focusing lenses and the entrance slit), (iv) magnet (magnetic analyser for separating ions with respect to their m/z ratio), (v) ESA (electrostatic field for energy focusing) and the detector (secondary electron multiplier or Faraday cups (in case of multi-collector devices))

The equations of the separation process of charged particles in a magnetic field are given in Table 2.2.[5] The kinetic energy of an ion of mass m and charge z is given by equation (2.2.1.1). The path in the sector described by the ions of a given mass and charge is determined by a balance between the magnetic force F_m (equation (2.2.1.2)) and the centripetal force F_c (equation (2.2.1.3)). The combination of the two equations leads to an expression for the velocity of the ion (equation (2.2.1.4)). Substitution of equation (2.2.1.4) into equation (2.2.1.1) leads to an expression for m/z (equation (2.2.1.5)). This equation shows that the path that a particular ion takes through the magnet depends on the applied field strength and the acceleration voltage. Thus by adjusting the field strength, different masses are focused in turn on to the collector slit and then on to the detector. These equations assume that all ions entering the magnet have uniform kinetic energy. However, this assumption is only approximately true, because ions possess a statistical distribution of kinetic energy upon generation in the plasma and subsequent acceleration into the ion optics. This kinetic energy distribution arises from the Boltzmann distribution of energies and from electrostatic field inhomogeneities within the interface and ion optics. The effect of this spread in ion energies is a corresponding spread in the ion beam exiting the magnet, which results in a limitation of the maximum resolution achievable with magnetic sector instruments.

Table 2.1 Selected figures of merit of a magnetic sector field ICP-MS (single-collector instrument)

Sensitivity (single collector)	$>1 \times 10^6$ cps for 1 ng/g ^{115}In (Element2)
Instrumental detection limit (single collector)	<1 fg/g for noninterfered isotopes
Dark noise (single collector)	<0.2 cps
Linear dynamic range (single collector with SEV detector)	$> 10^9$
Isotope ratio precision:	
• Single-collector devices	>0.02% RSD
• (Multi-collector devices)	>0.002% RSD
Mass resolution	Up to 12 000 in commercial instruments (43 000 with experimental devices)
Advantages	• High mass resolution (up to 12 000) • High sensitivity • Low noise • Good isotope ratio precision • Flat-top peaks (trapezoidal shape) • High linear dynamic range over nine orders of magnitude
Disadvantages	• High cost • Duty cycles limited by hysteresis of magnetic field • Loss of sensitivity at higher mass resolution • Loss of trapezoid peak shape at high mass resolution • No solution for interferences with mass resolutions of more than 12 000

Table 2.2 Basic equations for the mass/charge separation of ions within a magnetic field

Equation	Description	Equation	Variables
2.2.1.1	Kinetic energy of an ion	$KE = zeV = \frac{1}{2}mv^2$	V: acceleration voltage v: velocity of the ion after acceleration e: elementary charge z: charge of the ion m: mass of the ion B: magnetic field strength r: radius of the magnetic field
2.2.1.2	Magnetic force	$F_m = Bze$	
2.2.1.3	Centripetal force	$F_c = \frac{mv^2}{r}$	
2.2.1.4	Velocity of an ion in a magnetic field	$v = \frac{Bzer}{m}$	
2.2.1.5	m/z with respect to the field strength	$\frac{m}{z} = \frac{B^2 r^2 e}{2V}$	

2.2.1.2 Double-focusing spectrometers

The mean energy of ions generated in an ICP source is of the order of 10–20 eV, with an ion kinetic energy distribution between 5 and 10 eV. It has been found that the ion energy can be reduced to around 5 eV by capacitive decoupling (CD) of the plasma from the load coil (although, at least for quadrupole instruments, the ion energy spread remains substantially the same). Capacitive decoupling can be accomplished by inserting a metal (usually Pt or Ag) shield between the load coil and the torch. This approach, referred to as operating with a screened or shielded torch, is also applied in quadrupole ICP-MS. The major advantages of this approach are improved sensitivity and the suppression of secondary discharge effects. Moreover, with a screen in place, the system can be operated under 'cool' (low power) plasma conditions to provide improved data for easily ionized elements, such as Li and Na, and relatively easily ionised elements that suffer from Ar-based interferences at high plasma power, such as Ca and Fe.[6]

The term 'double-focusing' is applied to mass spectrometers in which the directional and energy aberrations of a population of ions are simultaneously minimized, thereby improving the resolution capabilities of the instrument. Double focusing is achieved by the use of the combination of an energy-focusing electrostatic field (electrostatic analyser (ESA)), located either prior to or after the magnetic field, and the magnet (Figure 2.12).

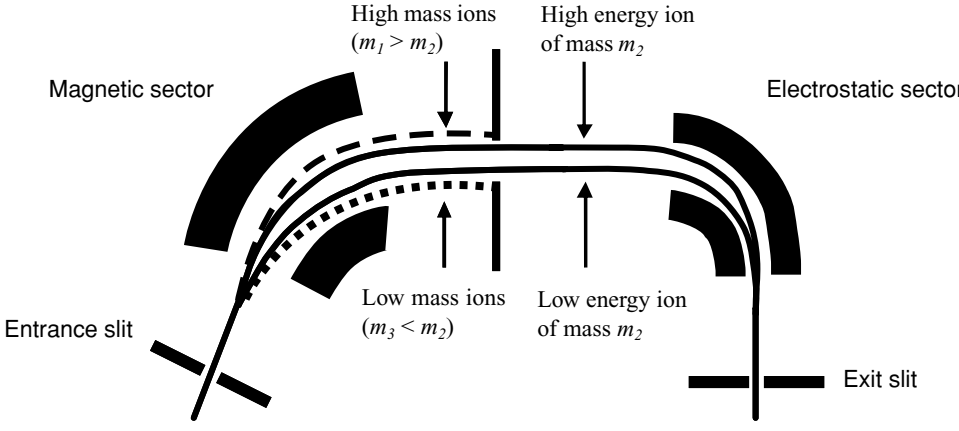

Figure 2.12 Operation principle of a double-focusing mass spectrometer

The electrostatic analyser field is used to compensate for the energy dispersion of the ions so that only mass dispersion is left. The electrostatic analyser consists of two curved parallel plates to which a DC voltage is applied. Traditionally, the electrostatic analyser is placed before the magnetic sector field. Instruments in which a 90° electrostatic analyser is combined with a 60° magnetic sector are known as Nier–Johnson geometry devices and this geometry is used in multi-collector instruments. The so-called reverse geometry places the electrostatic analyser behind the magnetic sector. This setup shows advantages since only the ions of the selected mass are subjected to subsequent energy focusing after mass separation. This configuration improves abundance sensitivity and reduces noise[14] and is applied in single-collector magnetic sector field ICP-MS instruments such as the Element2 (Thermo Electron Corp., Bremen, Germany).

Moreover, the bent geometry keeps the noise level low (since no photons pass directly to the detector) and allows high transmission.[7]

The Isoprobe MC-ICP-MS[8] (GV instruments, Wythenshawe, UK), a multi-collector device, is equipped with a pressurized hexapole collision cell to reduce the energy spread of the incoming ion before it enters the magnetic sector. Since it is a prerequisite that all ions must be accelerated by the same potential, all ions exit the hexapole at < 1 V potential and are then accelerated. The optional wide aperture retarding potential (WARP) filter is applied to enhance abundance sensitivity in this device. The WARP filter was originally developed for thermal ionization mass spectrometers in an attempt to improve the abundance sensitivity by two orders of magnitude. The principle of the WARP filter is that it excludes those ions that are not at the full accelerating potential. Any ions that have collided with residual gas molecules in the analyser are not transmitted by the WARP filter.

2.2.1.3 High resolution magnetic sector devices

Spectroscopic and non-spectroscopic interferences have been considered to be a severe impediment since the first days of the ICP-MS technique, limiting the maximum achievable analytical figures of merit. Several strategies have been applied to overcome the problem of spectral interferences (Table 2.3). Operating a mass spectrometer at higher mass resolution is one of the most straightforward ways to address this problem. High mass resolution allows separation of the peak of the isotope of interest and the interfering species. Although mass spectrometers of different

Table 2.3 Strategies to cope with spectral interferences in ICP-MS

Strategy	Difficulty
Theoretical approaches	
Mathematical corrections (via isotopic abundance or ion formation, which involve instrumental performance)	• Measurement of more isotopes • Uncertainty attached to isotopic abundance • Mass bias has to be considered
Maximum entropy calculations	• Problematic if interfering ion has higher signal intensity than the isotope of interest • Complex mathematical approach
Matrix matched calibration or standard addition	• Predictions are not always provable • Complicated to mix the adequate matrix
Sample/standard comparison	• More sample is required to produce standard addition standards • One standard has to be prepared for each sample • Time and material consuming • Interfering matrix elements have to be mixed together • Formation probability of polyatomic ion can only be estimated and is not always reproducible

Table 2.3 Strategies to cope with spectral interferences in ICP-MS *(Continued)*

Strategy	Difficulty
Instrumental approaches	
Nebulizer with cryogenic desolvation	• Only reduction of solvent induced interferences • Not 100% reduction of interferences • Not reproducible with significantly changing matrix
Nebulizer with membrane desolvation (tubular microporous Teflon membranes; polyimide fibers; Nafion tubes)	• Only for selected elements (mainly solvent-induced interferences or interfering elements that can be transferred to the gaseous phase (e.g. HCl, which is formed in acidified Cl containing matrices) • Not reproducible • Clogging of membranes causes instable desolvation
Matrix separation of interfering species: Offline/online chromatographic systems	• Time consuming • Sometimes a new separation method has to be developed first • Expensive tools • Possible source of additional contamination;
Cold (cool) plasma conditions: reduction of Ar-based interferences from the plasma; reduction of interferences formed by secondary discharge (shielded torch, balanced torch, reversed torch, screened torch)	• Increase of MeO^+ interferences by direct ionisation of neutral oxides • Not possible for all elements (decreased energy) • Matrix-depending effects
Mixed gases/alternative plasma sources (alternative gases; mixed plasma gases: competitive formation of polyatomic species; reduction of ionization temperatures by N_2; reduction by Xe due to lower ionization and excitation energy; addition of hydrocarbons; alternative plasma sources (MIP, N2-MIP))	• Reduces only Ar-based interferences; new interferences may occur • More expensive • Adaptation of system necessary • Methodologically challenging approach
Collision/reaction cell technologies	
High mass resolution	• Not reproducible for significantly different matrices • Instrumentally more expensive • loss of sensitivity

types can be operated applying high mass resolution (Table 2.4), until now only ICP-MS instruments based on double-focusing sector field mass spectrometers using a slit system to provide high mass resolution have become commercially available. Commercial instruments show maximum mass resolutions of generally about 10 000, although mass resolution up to 43 000 has been reported for a magnetic sector field ICP-MS.[9] The significant reduction in cost in recent years has led to a significant increase in the number of instruments used compared to quadrupole ICP-MS. The result is that now almost 20% of ICP-MS instruments worldwide are magnetic

Table 2.4 High mass resolution devices

ICP-MS device	Mass resolution
Quadrupole ICP-MS operated in higher regions of stability	Second region: $m/dm = 5000$ (reference 10) Third region of stability: $m/dm = 4000$ (reference 10)
Tandem quadrupole mass separators	Up to 20 000 for multiple pass quadrupoles (reference 11)
Time-of-flight instruments	Up to 2200 (FWHM) (reference 12)
Ion trap analyser	200–2000 (FWHM) (reference 13)
Ion cyclotron resonance FT analyser	200 000–200 000 000 (FWHM) (reference 13)
Double focusing magnetic sector field instruments	<12 000 (reference 9) (Up to 43 000 in special devices (reference 8))

sector field devices. Currently, the Element 2 (Thermo Electron Corp., Bremen, Germany) is the most prevalent commercially available high resolution single-collector sector field mass spectrometer. Recently, even multi-collector instruments (Neptune, Thermo Electron Corp., Bremen, Germany; NU-Plasma, NU Instruments, Wrexham, UK; Isoprobe, GV Instruments, Wythenshawe, UK) have been developed to allow operation using higher mass resolution. Multi-collector instruments will be described in more detail later in this chapter.

2.2.1.4 Spectral (or spectroscopic) interferences

Spectroscopic interferences can be sub-divided into isobaric atomic ions, multiply charged ions, polyatomic ions or intense adjacent signals, which overlap with the analytical signal of the isotope of interest.[14] Therefore, the accuracy and precision of the determination may considerably deteriorate.

Atomic (isobaric) interferences are caused by overlapping isotopes of different elements with the same nominal mass. For natural elements they can be found from mass 36 to mass 204 and for non-natural isotopes in the mass range above m/z 230, derived from nuclear processes. These interferences are easily predictable and alternative isotopes that show no isobaric interference are available in most cases (with the exception of In, which is interfered by ^{113}Cd and ^{115}Sn). Mathematical correction via the known isotopic abundances of the interfering element can be applied in cases where the preferred isotope is interfered by isobaric overlaps. The mass difference for isotopes of the same nominal mass is in general very small, so the required mass resolution for atomic interferences is very high (in the range of $10^4 - 6 \times 10^7$ (for Os/Re at mass 187)). This level of resolution cannot be accomplished by magnetic sector field instruments (of practical dimensions and geometries), so alternative instrumentation is required (see later in this chapter).

Multiply charged ions are found at fractions of their nominal mass, such that the observed mass = the nominal mass/N, where N is the charge on the ion (for example $^{88}Sr^{2+}$ on $^{44}Ca^{+}$). These ions have a smaller formation probability, because the second and higher ionisation potentials are larger than the first and are not generally a significant problem unless the source of

the multiply charged ion is a relatively easily ionized matrix element of very high concentration (e.g. the $^{135}Ba^{3+}$ interference on $^{45}Sc^{+}$, reference 15). Multiply charged ions are mainly found in the low mass range and require in general mass resolutions between 2000 and 10 000, easily within the reach of magnetic sector ICP-MS instruments.

Molecular or polyatomic ion interferences are formed by the matrix elements, the atoms of the solvent and/or the atoms of the plasma gas. The latter two sources contribute a significant amount since the high number of atoms present increases the quantity of interference generated, even for interferences of low formation probability. The mass difference to the elemental isotope of interest is usually relatively large for polyatomic species and separating them from the analyte of interest typically requires resolutions of about 2000–5000 for most of the polyatomic interferences in the medium mass range (up to mass 70). Resolutions of about 10 000 and more are required in the higher mass range and significantly higher mass resolution is necessary for special interferences (e.g. $m/\Delta m > 10^6$ for the Ar–Ti^{+} interference on ^{86}Kr). Formation of polyatomic species is believed to result from processes including condensation reactions in the expansion region, collisional reactions in the boundary layer around the outside of the sampler cone and survival of the species through the plasma (e.g. refractory metal oxide ions).[3] The formation of polyatomic ions is difficult to predict and depends on the matrix composition and concentration, as well as on nebulization and plasma conditions, resulting in significantly increased uncertainty on the measured analytical signal.

In the case of very high signal intensities, the adjacent lower abundant peak can be significantly interfered by the tailing of the major signal (e.g. measurement of ^{206}Pb in a ^{205}Tl matrix or tailing of ^{232}Th into the lower abundant Th isotopes). As discussed in Part 1 of this chapter (quadrupole ICP-MS), the parameter that quantifies the ability of a mass spectrometer to measure low signals at adjacent masses to very high signals is called abundance sensitivity. Since this parameter is defined by the ratio of the larger signal at mass M to the smaller signals at masses $M \pm 1$, application of high mass resolution can offer some apparent improvement in abundance sensitivity in cases where increasing the resolution has a larger relative effect on reducing the contribution of the peak tail to an adjacent mass than it does on signal reduction of the more intense peak.

2.2.1.5 Resolution of mass spectrometers

The capability of a mass spectrometer to differentiate between masses is usually stated in terms of its mass resolution, R, which is defined as

$$R = \frac{m}{\Delta m} \tag{2.2.1.6}$$

where Δm is the mass difference between two adjacent peaks that are just resolved and m is the nominal mass of the first peak. Two peaks are considered to be separated if the height of the valley between them is no more than some percentage of their height. The definition of Δm is different for different types of mass analysers. The 10% valley definition is commonly used for magnetic sector mass analysers. According to this definition, resolution is measured for two neighboring peaks of equal intensity using the point between the peaks (i.e. in the 'valley') where the signal intensity is 10% of the peak height. Since the intensities of neighboring peaks are rarely identical, however, an alternative definition is much more useful. In this definition Δm

is derived from the peak width at the points in the profile that correspond to 5% of the height. This approach leads in general to the same value for R as is obtained with the 10% definition mentioned before when the analyte and interferent peaks are of equal height. These definitions are shown in Figure 2.13(a). Quadrupole mass spectrometers are usually characterized using the full-width–at-half-maximum (FWHM) definition (Figure 2.13(b)). Hence, it has to be taken into account that the numerical resolution values based on the FWHM definition are about twice as high as with the 10% valley definition.

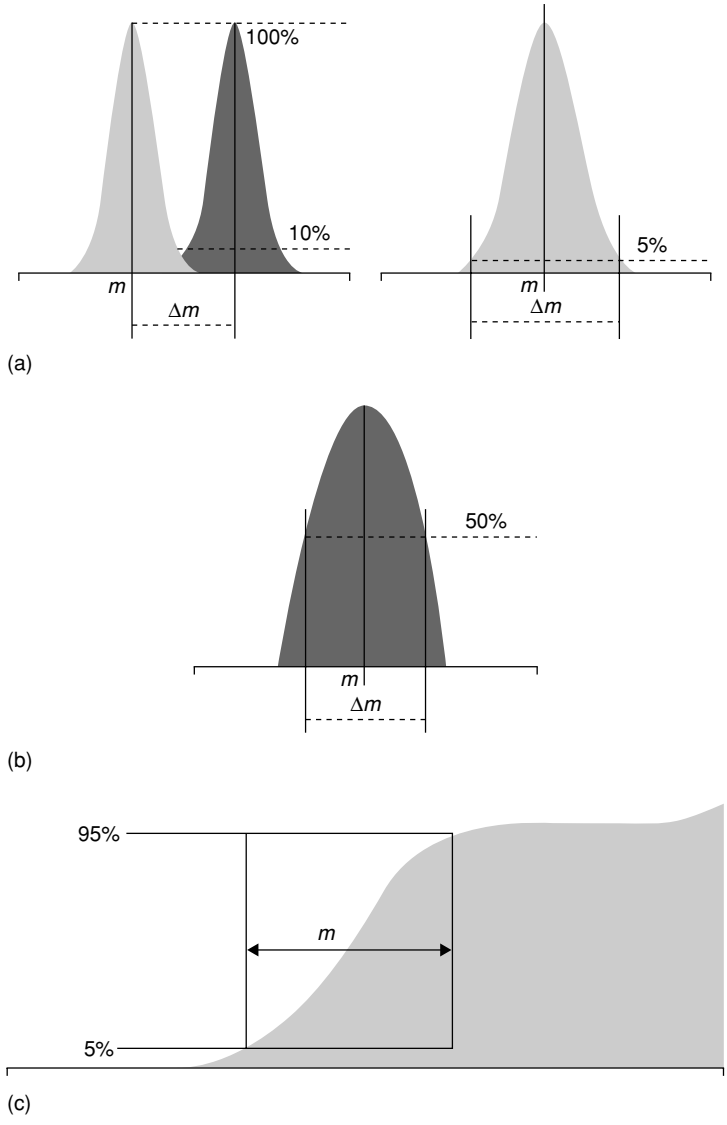

Figure 2.13 Definition of mass resolutions: (a) 5 and 10% valley definition, (b) full width at half maximum and (c) mass resolution for 'pseudo' high mass resolution

With respect to the pseudo-high mass resolution currently utilized in most MC-ICP-MS systems, the mass resolution $m/\Delta m$ is set such that Δm is defined as the difference between the masses where the analyte intensity amounts to 95% and 5% of the maximum signal intensity (Figure 2.13(c)). This approach, which does not fully resolve interferences, is taken to maintain high precision isotope ratio measurement by ensuring that adequate interference separation is achieved whilst retaining flat-top peak profiles. For the currently available routine MC-ICP-MS systems, if the resolution is set to achieve complete interference separation, the peaks lose their flat-top profiles as the magnets and flight tubes on these instruments are not physically large enough to allow higher resolution, flat-top peaks to be generated at the exit of the magnet (see later in this section).

2.2.1.6 Accomplishment of high mass resolution in double-focusing magnetic sector field instruments

Magnetic sector instruments are ion optical systems, which define the trajectory of ions from the entrance into the system to the exit. Mass resolution is accomplished by means of two mechanical slits, which are changed simultaneously. One slit is located between the acceleration lenses and the mass analyser (source, or entrance slit) and the other between the mass analyser and the detector (collector or exit slit) of the ion optical system. Because of the mechanical definition of the ion-beam-using slits, the peak shapes produced by magnetic sector instruments are ideally triangular or flat-topped (Figure 2.14(a)) compared to the rounded peaks of quadrupole based instruments. The advantage of flat-topped peaks is that the measured ion beam intensity is constant over a small mass range, so small errors in the mass calibration are not problematic and more importantly, improved isotope ratio precision can be achieved compared to quadrupole instruments.

The combination of entrance and exit slits defines the resolution of the system. In the case of the Element ICP-MS, both slit units can be set in parallel to three different slit widths, corresponding to three different nominal resolution values: low ($m/\Delta m = 300$), medium ($m/\Delta m = 4000$) and high resolution ($m/\Delta m = 10\,000$). The slit units are pneumatically operated. Resolution switching can be performed in less than 2 and is therefore ideally suited for multi-element analysis using all three resolutions.

Increases in mass resolution are not only accompanied by a loss in ion transmission efficiency and hence signal intensity (Figure 2.15), but also by a change in peak shape from flat topped to triangular (Figure 2.14(b)).[16] Moreover, the extremely narrow peaks at high mass resolution require an absolutely stable mass calibration (especially for isotope ratio applications).

Since polyatomic interferences are mainly located on the higher mass side of the peak of interest, 'pseudo' high resolution mode can be applied in MC-ICP-MS.[17] Thereby, the source slit is changed whereas the collector slit is not adjusted. In this way, the flat section of the spectral peak is maximized and finally there is no need to place a slit in front of every single collector of the MC device when measuring the analyte signal on one side (Figure 2.14(c)).

2.2.1.7 Accomplishing mass scans in single-collector instruments

Whereas multi-collector devices are operated at a constant magnetic field and collect the isotopes of interest simultaneously in different detectors, single-collector instruments have to scan over

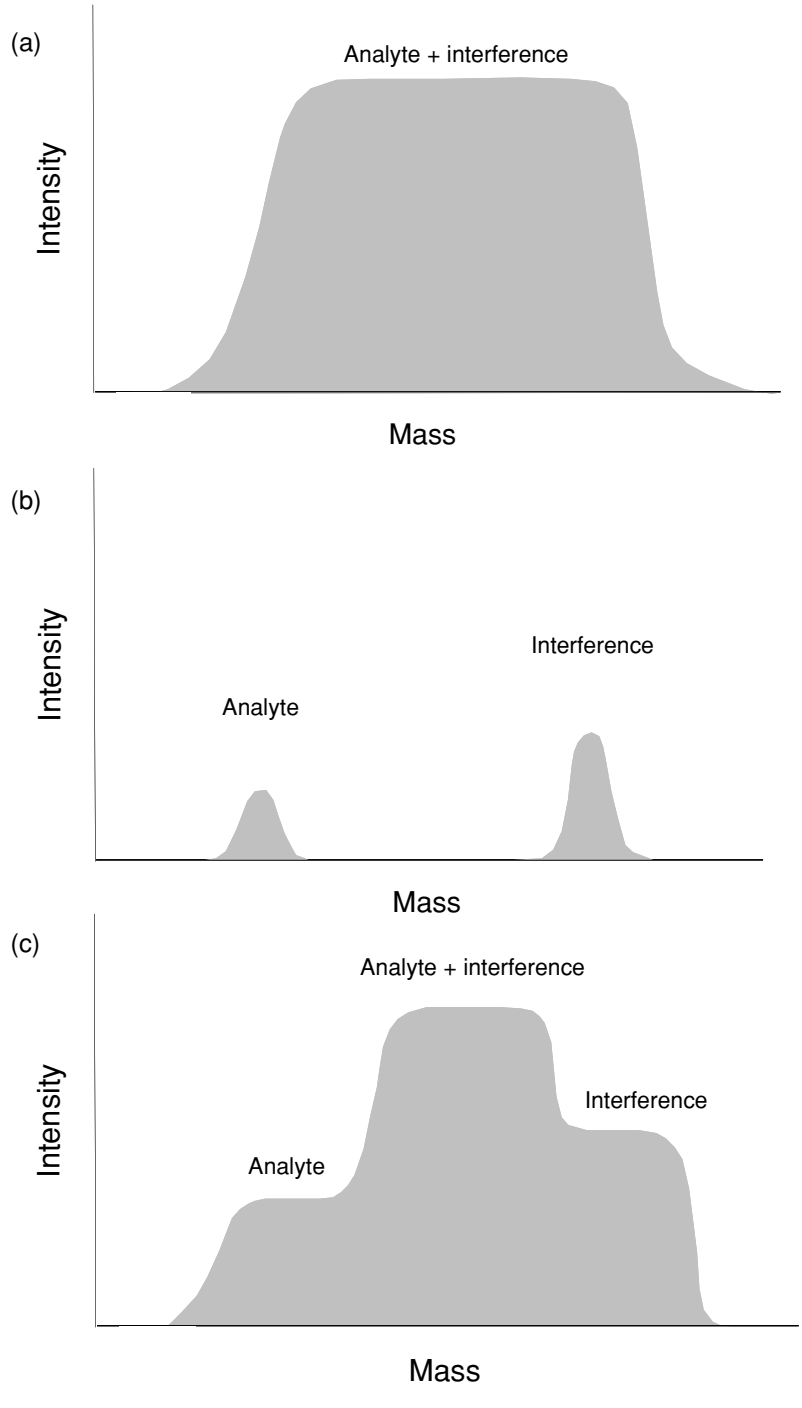

Figure 2.14 Peak in a mass spectrum (intensity vs mass) of a sector field ICP-MS at (a) low mass resolution, (b) high mass resolution and (c) 'pseudo' high mass resolution

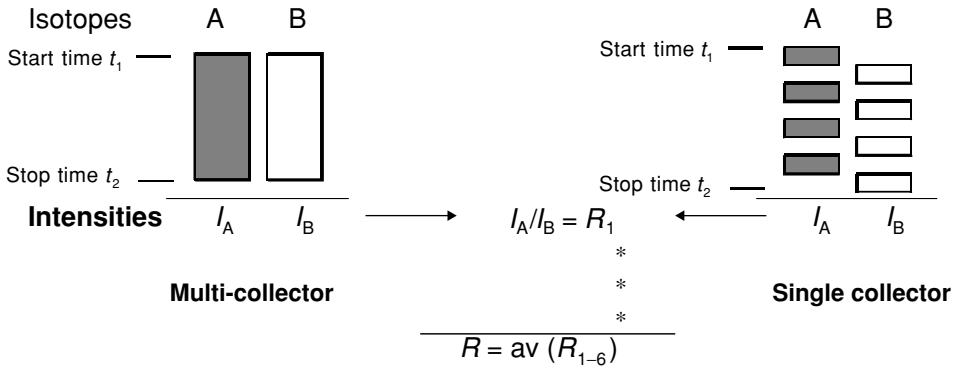

Figure 2.15 Operation principle for isotope ratios of single- and multi-collector devices. The signals of the isotopes are measured over a period of time resulting in signal intensities I. This signal intensities lead to ratio R_1. This procedure is repeated several times resulting in a number (six in this example) of ratios. These are averaged and their RSD gives the so-called internal precision. In the case of the single-collector devices, the isotopes cannot be measured simultaneously and are therefore analyzed in a fast hopping between the isotopes over a period of time. This is the so-called quasi-simultaneous measurement

the mass range to detect all masses of interest sequentially. The mass scans can be performed in different scan modes: by scanning the magnet (magnetic scan) or by scanning the acceleration (i.e. extraction) voltage (electric scan).

Magnetic scan: the accelerating voltage and the ESA voltage are kept constant, while the magnetic field is scanned from the value of the start mass to the value of the end mass. This mode is used for scanning large, continuous mass ranges. Its drawback is that, for repeated scanning, a settling time must be allowed to take into account the time needed by the magnet to recover from the hysteresis of each cycle.

Electric scan: the start mass is set magnetically, at full accelerating voltage. The scan from this start mass is performed electrically by reducing the accelerating voltage (and the coupled ESA voltage) at a constant magnetic field strength. The electric scan can cover a mass range extending from −5% to +30% above this magnet mass in the case of the Element2. The main characteristic of the electric scan is that since the magnetic field is not changed there is no need to incorporate a magnet settling time, so faster scanning across the selected mass range can be achieved than is possible with the magnet. In general, a combination of both scan modes is applied for multi-element analysis to cover a wider mass range. Therefore, the instrumental setup allows analyzing the whole mass range within one run. Due to fast switching times between the resolutions, the whole mass range can be analyzed in different mass resolutions for interfered (and non-interfered) isotopes within subsequent runs in one sample within a short time.[18]

Isotope ratio measurements using single-collector devices are performed using the electric scan in order to ensure a fast switch between the isotopes of interest, referred to as a 'quasi-simultaneous' measurement.[16] The operation principle of isotope ratio measurements by single-collector instruments compared to multi-collector instruments is schematized in Figure 2.15. Within this operation principle, the magnetic field is held at a constant value and the isotopes of interest are measured within a small mass window by electric scans.[19] Therefore, no settling time is necessary and both isotopes can be measured within milliseconds of each other over a selected period of time (in general about 2 min in total, to achieve acceptable counting statistics). Hence,

signal fluctuations arising from sample nebulization, ion formation processes in the plasma and general plasma flicker noise can be minimized. Isotope ratio precisions down to 0.05% have been reported for single-collector ICP-MS systems[19] and for 'large ratios' (i.e. ratios > 1:10) single-collector results are reported to be close to multi-collector data[10]. Finally, it is important to take into account that additional mass discrimination effects can be observed by changing the acceleration voltage, compared to switching the magnet between isotopes with the acceleration voltage fixed.[10] Mass discrimination effects are discussed in detail later in this Chapter and in Chapter 4.

References

1. Bradshaw, N., Hall, E. F. H., and Sanderson, N. E. (1989) Inductively coupled plasma as an ion source for high resolution mass spectrometry. *J. Anal. At. Spectrom.*, **4**, 801–3.
2. Morita, M., Ito, H., Uehiro, T., and Otsuka, K. (1989) Attempting to locate at present. *Anal. Sci.*, **5**, 609–10.
3. Evans, E. H. and Giglio, J. J. (1993) Interferences in inductively coupled plasma mass spectrometry. *J. Anal. At. Spectrom.*, **8**, 1–18.
4. http://www.finnigan.de
5. Turner, P. J., Mills, D. J., Schröder, E., Lapitajs, G., Jung, G., Iacone, L., Haydar, G., and Montaser, A. (1998) Instrumentation for low and high-resolution ICP-MS. In: *Inductively Coupled Plasma Mass Spectrometry* (ed. A. Montaser), Wiley-VCH, New York, pp. 422–94.
6. Appelblad, P. K., Rodushkin, I., and Baxter, D. C. (2000) The use of PT guard electrode in inductively coupled plasma sector field mass spectrometry: advantages and limitations. *J. Anal. At. Spectrom.*, **15**(4), 359–64.
7. Feldmann, I., Tittes, W., Jakubowski, N., and Stuewer, D. (1994) Performance characteristics of inductively coupled plasma mass spectrometry with high mass resolution. *J. Anal. At. Spectrom.*, **9**, 1007–14.
8. http://www.gvinstruments.co.uk/isoprobe1.htm
9. Morita, M., Ito, H., Linscheid, M., and Otsuka, K. (1994) Resolution of inter-element spectral overlaps by high resolution inductively coupled plasma mass spectrometry. *Anal. Chem.*, **66**, 1588–90.
10. Quétel, C. R., Prohaska, T., Hamester, M., Kerl, W., and Taylor, P. D. P. (2000) Examination of the performance exhibited by a single collector ICP-MS instrument for uranium isotope abundance ratio measurements over almost three orders of magnitude and down to pg/g concentration levels. *J. Anal. At. Spectrom.*, **15**, 353–8.
    Ying, J. F. and Douglas, D. J. (1996) High resolution inductively coupled plasma mass spectra with a quadrupole mass filter. *Rapid Commum Mass Spectrom.*, **10**, 649–52.
11. Amad, M. H. and Houk, R. S. H. (2000) Mass resolution of 11 000 to 22 000 with a multiple pass quadrupole mass analyzer. *J. Am. Soc. Mass Spectrom.*, **11**(5), 407.
12. Sturgeon, R. E., Lam, J. W. H., and Saint, A. (2000) Analytical characteristics of a commercial orthogonal acceleration time of flight mass spectrometer. *J. Anal. At. Spectrom.*, **15**, 607–16.
13. Duckworth, D. C. and Barshick, C. M. (1998) Ion traps: what do they hold for elemental mass analysis? *Anal. Chem.*, **1**, 709A–717A.
14. Moens, L. and Jakubowski, N. (1998) Double-focusing mass spectrometers in ICPMS. *Anal. Chem. News Features*, **70**(7), 251A–256A
15. Prohaska, T., Hann, S., Latkoczy, C., and Stingeder, G. (1999) Determination of rare earth elements U and Th in environmental samples by inductively coupled plasma double focusing sectorfield mass spectrometry. *J. Anal. At. Spectrom.*, **14**, 1–8.

16. Vanhaecke, F., Moens, L., and Dams, R. (1998) The accurate determination of copper in two groundwater candidate reference materials by means of high resolution inductively coupled plasma mass spectrometry using isotope dilution for calibration. *J. Anal. At. Spectrom.*, **13**, 1189–92.
17. Weyer, S. and Schwieters, J. (2003) High precision Fe isotope ratio measurements with high mass resolution MC-ICP-MS. *Int. J. Mass Spectrom.*, **226**, 355–68.
18. Latkoczy, C., Prohaska, T., Stingeder, G., and Wenzel, W. W. (2000) Simultaneous multi-element analysis of trace elements in soil samples by means of high resolution inductively coupled plasma sector field mass spectrometry. *Fresenius' J. Anal. Chem.*, **368**, 256–62.
19. Vanhaecke, F., Taylor, P., and Moens, L. (1998) Use of ICP-MS for isotope ratio measurements. In: *Inductively Coupled Plasma Spectrometry and its Applications* (ed. S. J. Hill), Sheffield Academic Press, Sheffield.

2.2.2 MULTI-COLLECTOR DEVICES

MSA Horstwood and GM Nowell

2.2.2.1 Principles of MC-ICP-MS design

For ultimate measurement precision in isotope-ratio ICP-MS, a multiple collector (MC) array is required to negate the various sources of noise inherent to a plasma ion source.[1] Multi-collector arrays have long been used in thermal ionisation mass spectrometry (TIMS) showing the level of precision that can be achieved (<5 ppm – parts per million of average value, $2\sigma_m$ – standard error of the mean; <20 ppm, 2σ – standard deviation of the population). Thermal ionisation produces ions with a very narrow spread of energies (~1 eV), at which level ion optic chromatic aberrations are insignificant. However, an ICP source produces ions with a significantly larger energy spread (20–30 eV) and chromatic aberrations become important. Currently, there are two solutions to this problem in commercially available mass spectrometers. One option is to use a multipole cell (e.g. a hexapole) containing an atmosphere of additional 'collision' gas (usually Ar, He or H) to reduce the energy spread of the ions before they enter the ion optics of the mass analyser. Collisions between the analyte ions and the 'collision' gas reduce the energy spread of the ion beam to <1 eV, a process known as 'thermalising', without compromising transmission.[2] For both a TIMS source and an ICP source with a thermalised beam, only single-focusing ion optics are required using a magnetic sector to correct for angular aberration of the beam.

For an ICP source without a thermalised beam however, double-focusing ion optics are required to correct for both chromatic and angular aberrations of the beam. This is accomplished by combining an electrostatic analyser (ESA) with a magnetic sector. The ESA focuses ions of differing energy along the focal plane as described earlier in this chapter (Part 2.2.1). This energy dispersion is exactly compensated by the energy dispersion of the magnet, so that ions of equal mass/charge, irrespective of their ion energy, end up at exactly the same point in the focal plane of the mass spectrometer.

In contrast to the reverse geometry commonly used for high-resolution single-collector (SC) sector field ICP-MS instruments, double-focusing MC-ICP-MS devices have the ESA *before* the magnetic sector, in the forward Nier–Johnson geometry. This is essential for MC instruments,

to allow a large mass range to be transmitted to the focal plane of the mass analyser without impediment by the entrance slit of the ESA. In SC-ICP-MS, only a very small mass range of about 1–2% mass dispersion is required, allowing the ESA to be placed after the magnetic sector in a reverse geometry and conveying the advantage of decreased ion scattering and improved abundance sensitivity and backgrounds compared to a MC instrument. Abundance sensitivity can, however, be improved in MC instruments by use of a second energy filter behind the main collector array (for example the WARP filter described in Part 2.2.1), allowing accurate measurement of large isotope ratios (>100).

Compared to TIMS, MC-ICP-MS has the potential to produce data of equal quality for a greater range of elements (including those with first ionisation potentials > 7 eV) as a result of the high ionisation temperature of its source (approximately 10 000 K vs approximately 2000 K for TIMS). Walder and Freedman[3] were the first to describe the use of such an instrument and MC-ICP-MS has since established itself as a valuable addition to TIMS and ICP-quadrupole(Q)-MS techniques.

2.2.2.2 Instrumentation and hardware

The primary purpose for employing MC-ICP-MS is to obtain high-precision isotope ratio measurements with uncertainty of the order of 10–100 ppm (2σ), depending on the isotope system of interest. To achieve this precision a relatively low mass resolution ($m/\Delta m = 400$–500) is usually used to maximise sensitivity and to ensure a flat-topped peak profile, in conjunction with a highly linear analogue detector such as a Faraday detector. These graphite-based collectors generally operate over a current range of 10^{-15} A (approximately 6.24×10^3 cps) to 10^{-10} A (approximately 6.24×10^8 cps), or up to 5×10^{-10} A (approximately 3.12×10^9 cps) in some designs of the Faraday, using a 10^{11} Ω resistor. Operating with higher signal intensities (i.e. increased sample concentrations or instrument sensitivity) reduces the effect on accuracy of smaller isobaric interferences and improves precision and reproducibility. At its lower count range (10 kcps) the Faraday easily overlaps with the ion-counting detectors (0–2 Mcps). MC-ICP-MS instruments have the capacity for one or more ion counters to be included in the detector array either in addition to or in substitution for some of the Faradays. At least one of the ion counters is usually on the axial channel and exposed through vertical or lateral movement of the Faraday or through deflection of the beam between or around collectors. Some MC-ICP-MS systems use a Daly-photomultiplier rather than electron-multiplier system for ion counting. The Daly system has more stable long-term gain characteristics compared to electron-multiplier systems. It consists of an aluminium-covered cathode 'Daly knob' held at approximately -20 kV, which emits a number of electrons for each ion impact. These electrons are repelled by the knob and impact a scintillator window where they are converted to photons that are received by a vacuum-housed photomultiplier tube, generating an electron shower and amplifying it in the same way as a conventional electron multiplier.[4] A retarding potential (e.g. WARP® or an RPQ®) or an electrostatic filter situated behind the main Faraday array improves the abundance sensitivity from 2–5 ppm to $<$50–500 ppb (manufacturers' specifications). Coupled with quiet electronics allowing dark noise of <0.1 cps, the Daly ion-counting system is capable of accurately measuring ion beams down to 1 cps.

Relatively new developments in MC technology include the 'virtual' amplifier® and zoom optics. Instead of each Faraday cup having a dedicated amplifier, the virtual or rotating amplifier

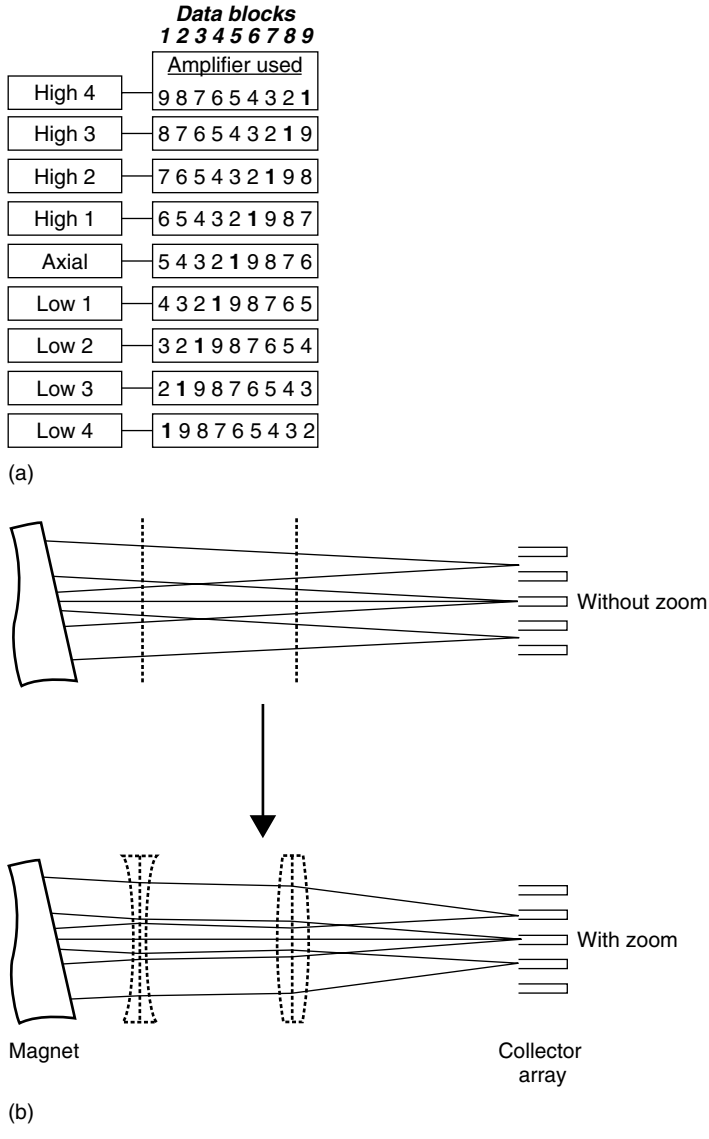

Figure 2.16 (a) The virtual amplifier® concept—each collector response is cycled through each of nine amplifiers over the course of a nine-block analysis to eliminate differential amplifier gains. (b) Zoom optic (diagram reproduced by permission from Nu Instruments, Wrexham, UK)

system® passes the current from each Faraday sequentially through each amplifier (see Figure 2.16(a)). This eliminates any variation in amplifier response, usually corrected for before analysis by measuring a constant current applied to each amplifier. Rotation of amplifiers can only be performed between data blocks with the number of blocks dictated by the number of collectors in use. Differences in Faraday efficiencies (generally <100 ppm relative deviation from the

reference (usually axial) collector) are not corrected by this system. Variable dispersion zoom optics can be used instead of or in addition to a moveable multi-collector array. Changing the voltage applied across this ion lens changes the dispersion of the beam, allowing any isotope system to be aligned in a fixed multi-collector array and/or perfect cup alignment to be maintained (Figure 2.16(b)) during multi-dynamic acquisition protocols (see below) using fixed or moveable collector arrays. In conjunction with a fixed multi-collector array, variable dispersion zoom optics render collector motor drives unnecessary, reducing the number of entry flanges in the collector block and thereby helping improve the vacuum properties and abundance sensitivity of the instrument. Compared to moveable collector arrays, rapid changeover between isotope systems is also possible with the zoom optics approach simply by changing the voltage applied to the 'zoom', although a full peak-jumping routine using this facility is yet to be adopted.

2.2.2.3 Data acquisition principles

Use of a multi-collector array allows the simultaneous measurement of multiple ion beams, thereby compensating for any fluctuation in beam intensity. This is an important consideration for ICP-MS systems, where signal intensity fluctuation or 'plasma flicker' is unavoidable. This 'static' mode of acquisition, where the mass analyser remains centred on a specific mass, produces high precision data but with the accuracy limited by slight differences in the individual response characteristics of each Faraday collector and its associated amplifier. Use of a 'dynamic' or 'peak-jumping' multi-collector acquisition protocol can improve precision and accuracy over the more conventional 'static' protocol, by adjusting the mass analyser between sequences to cycle the measurement of individual isotopes through a series of different collectors. A mathematical algorithm is used to cross-correlate the response of different Faraday-amplifier pairs for the same ion beam,[5] eliminating collector biases and improving accuracy. Dynamic routines require increased beam stability, time and therefore quantity of sample and consequently static or multi-static protocols (in which each cup is used only once in a series of static sequences) are more routinely used in MC-ICP-MS.

Before an analysis can be made, appropriate corrections for baseline and background signal must be performed. Baselines are most commonly measured $\pm$ 0.5 amu either side of the mass analysed in a given collector. This measurement represents the 'zero' level relative to which the ion beam intensity is measured. Peak tailing due to poor abundance sensitivity, and/or non-flat baselines resulting from small interferences, scattered ions or high electronic noise, can result in non-representative baseline measurements, which can lead to inaccurate data.[6] Characterisation of the baseline during set-up of a new analytical protocol or when analysing high matrix samples is important in determining the most appropriate mass at which to measure the baseline.

Having correctly measured the baseline, inaccurate data can still result from cross-contamination between samples and/or standards. This can be a problem even after extensive washout between samples and often increases over the course of an analytical session as the sample introduction system and cones become increasingly contaminated. This cross-contamination can, however, be corrected by measuring the residual signal on each peak once the background has stabilised. These on-peak zero (OPZ) signals can then be subtracted from the appropriate peaks. Using an OPZ baseline correction method usually requires manual analysis of the samples. An alternative to this that enables automation is to derive a washout protocol, which successfully washes out the previous sample to a pre-determined level considered negligible

for the subsequent analysis. The difference in isotopic composition between analyte and potential contaminant is an important consideration in determining the level of washout required, with contaminants of more disparate compositions having a more significant effect. Both OPZs and washout protocols assume a constant level of background signal without random fluctuations ('spiking') of the background during analysis of the sample. However, this is difficult to ensure.

2.2.2.4 Correcting for mass bias

The accurate measurement of elemental or isotopic compositions is compromised on all ICP-MS instruments by the phenomenon known as mass bias. A more complete description of the fundamentals of mass bias, its causes and correction algorithms is detailed in Albarède *et al.*[7] and Chapter 3, but some aspects are described here to aid understanding of the methods of mass bias correction in MC-ICP-MS.

Mass bias or mass discrimination results from ions of different mass having different kinetic energies, and charge repulsion between these ions in the region behind the skimmer cone of the mass spectrometer.[8] These 'space-charge' effects concentrate the heavier isotope in the axial region of the ion beam and therefore bias the isotopic ratio in its favour. The degree of mass bias is instrument dependent but is primarily determined by the absolute mass of the isotope of interest, its ion kinetic energy and the density of ions and degree of repulsion (space-charge effects) in the critical zone. Since isotopic mass and to a lesser extent kinetic energy are constant during analysis, the difference in mass bias observed between analyses is largely determined by space-charge effects. Therefore additional matrix components can severely affect the mass bias of one analysis compared to another, requiring careful monitoring and correction to avoid systematic variations of the sample relative to the standard run at the time. Mass bias is also very sensitive to matrix and analyte concentration in 'cold plasma' applications where the analyte ions represent a much greater proportion of the dominant ion species compared to normal 'hot plasma' applications where Ar^+ ions are by far the dominant ion species.

The mass–bias relationship between isotopes is usually described using an exponential function but power and linear laws are also sometimes appropriate, particularly for the light masses of Li and B (see Chapter 3). Ingle *et al.*[9] recently illustrated how the mass bias function is a direct measure of the instrument response function, which logically has to be smooth with change in mass. An exponential function calculated using the absolute masses of interest was shown to give the best fit of the more common correction expressions but when significant matrices were involved a polynomial expression modelling the response curve, determined using a multi-element solution, produced the best correction of all.

The ability to accurately correct for mass bias in MC-ICP-MS is critical to achieving high-accuracy isotope ratio analyses. The ideal way of doing this is to use a stable isotope pair internal to the element system of interest. This internal normalisation approach is applicable for multi-isotope systems where one or more isotopes are partly radiogenic in origin (e.g. $^{176}Lu \rightarrow^{\beta} {}^{176}Hf$) (i.e. not of fixed abundance in nature, so potentially different between samples), while at least one isotope pair is fixed in nature (e.g. $^{179}Hf/^{177}Hf$). Correcting for mass bias experienced by all the isotopes using the two stable isotopes, knowing they have an invariant composition in nature, allows resolution of the radiogenic/stable ratio. For non-radiogenic or 'stable' isotope systems (e.g. Zn, Cd, Sn) where the process of fractionation is mass dependent and affects all the

isotopes, internal normalisation is not appropriate. MC-ICP-MS investigation of stable isotope systems, or indeed radiogenic systems that do not contain two stable isotopes with which to monitor the mass bias (e.g. Pb), requires a different approach. Two options are available, namely standard-sample bracketing and spiking with an adjacent mass element (AME).

Standard-sample bracketing consists of measuring samples of interest between appropriate certified isotopic standards, and applying a correction to the samples according to the ratio measurements of these standards. Accurate and precise analysis relies on a stable instrument and complete matching between sample and standard matrices to avoid any variations of mass bias or introduced interferences (see later). This external normalisation approach is also more time consuming due to the increased number of standards analysed.

Alternatively, in a variation of internal normalisation, the analyte element can be spiked with an element of adjacent mass that does not interfere isobarically with the analyte, and the isotopes of both elements measured. The ability to simultaneously monitor and correct more than one element system is unique to MC-ICP-MS and is the main advantage of the technique over TIMS or SC-SF-ICP-MS. The classic example demonstrating the capability of using an AME for mass bias correction of another is the Tl–Pb system.[10] Thallium has two isotopes, ^{205}Tl and ^{203}Tl, which overlap the mass range of Pb without isobaric or atomic interference. The ^{205}Tl/^{203}Tl ratio (2.3871) (reference 11) can be used to calculate the degree of mass bias across the 208–204 mass range. Whether Tl is an *exact* proxy for Pb has been the subject of much debate[12,13] but will be taken as such in this work since it represents the most accurate inter-element proxy so far discovered in MC-ICP-MS. This approach does not, however, work for all AMEs. For example, in the first instance ^{109}Ag/^{107}Ag would appear an appropriate proxy for Cd with isotopes of 106–116. However, Ag behaves quite differently to Cd in the plasma and cannot be used to monitor mass bias as an appropriate proxy for Cd (see Figure 2.17).[14]

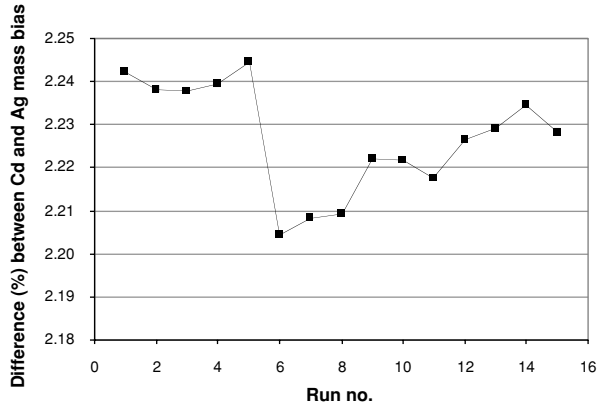

Figure 2.17 Absolute and temporal variation between Cd and Ag mass bias

2.2.2.5 Instrument-related and other primary corrections

The analysis of U isotopes by MC-ICP-MS highlights a number of instrument-related corrections, which must be performed to achieve accurate and precise data. Mass bias, ion counter gain and

linearity, hydride formation, abundance sensitivity, spike and procedural blank corrections must all be applied to data collected over one or more sequences using a combination of Faraday and ion-counting detectors. A typical multi-static acquisition protocol for the analysis of a sample of uranium is shown below, where the prefixes L and H refer to Faraday detectors located on the low- and high-mass sides, respectively, of the axial collector.

L4	L3	L2	L1	Axial (ion counter)	H1	H2	H3	H4
–	–	^{233}U	^{235}U	^{236}U	^{238}U	–	–	–
–	–	–	–	^{233}U	–	–	^{238}U	–
–	–	–	^{234}U	^{235}U	–	^{238}U	–	–
–	–	–	^{233}U	^{234}U	–	–	–	–

Currently a topical area of research, the determination of depleted or indeed enriched uranium in human urine and environmental samples, is providing a significant challenge. Firstly, complete chemical separation from all other constituents of the urine is essential if depleted-U (DU) signatures of ~1% (^{238}U/^{235}U ~140) are to be distinguished from natural U (^{238}U/^{235}U = 137.88). With no stable isotope pair within the U system or a suitable AME, a standard-sample bracketing protocol is usually employed to correct for mass bias. Human urine generally contains very low concentrations of U (generally 1–5 ng/L), so an isotope dilution strategy is required, together with ion-counting detection (ideally a Daly photomultiplier or discrete dynode secondary electron multiplier) and a multi-static (rather than multi-dynamic) peak-jumping routine, for precise measurement of the total U concentration and the minor isotopes of ^{234}U, ^{235}U and even ^{236}U. In this example ^{233}U is used as the spike for isotope dilution and aids in the correction for the 'Daly gain' (efficiency of the Daly ion counter relative to the Faraday – usually around 85%). An internal gain correction is preferable to an external calibration using a set of analysed standard solutions, as the gain can change with time and the error on the gain at the time of the sample analysis is significantly less than the uncertainty on the standards. Some ion counters also have non-linear responses at low count rates and this must also be monitored and corrected by measuring a well-characterised U standard run at different concentrations down to count rates typical of the samples being analysed. Count rates for the minor isotopes can range from many thousands (for ^{235}U) to zero counts per second (cps) for ^{236}U, a non-natural isotope produced by neutron capture on ^{235}U in the nuclear fuel cycle. At such low count rates, abundance sensitivity and hydride corrections are significant, usually 0.5–1 ppm and 1–2 ppm respectively of the adjacent peak. These corrections are essential to enable the confident determination of ^{236}U at <10 cps. The proportion of UH^+ interference can be measured using a standard solution and applied as a correction to ^{236}U (from $^{235}U^1H^+$) and even ^{234}U should the ^{233}U peak (and hence $^{233}U^1H^+$) be sufficiently high (this will not normally be the case if ^{233}U is being used for the ion counter gain correction). Abundance sensitivity can also be corrected by measuring signal intensities at 0.25 amu intervals between ^{236}U and ^{238}U, and deriving a correction curve. After all analytical corrections have been made, corrections for spike and total procedural blank must be made, accompanied by full error propagation for the entire set of corrections.

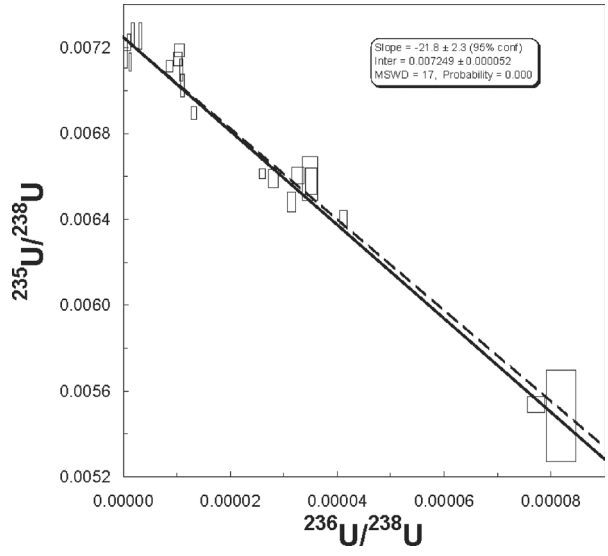

Figure 2.18 Correlation of $^{236}U/^{238}U$ versus $^{235}U/^{238}U$ ratios illustrating the ability to accurately measure very low concentrations of ^{236}U using a mixed Faraday-ion counter acquisition protocol. All errors 2σ (note that all sources of $2^{36}U/^{238}U$ uncertainty have yet to be identified); dashed line represents mixing line between known end-member compositions

The robustness of the resulting data set can be determined through correlation of $^{235}U/^{238}U$ versus $^{236}U/^{238}U$ as shown in Figure 2.18. This correlation is expected if the samples contain ^{236}U-bearing DU and as such gives confidence to the measurements.

2.2.2.6 Interfering element corrections

One of the major difficulties in making high-precision measurements involves accurate correction for spectral and isobaric interferences. In MC-ICP-MS, making interfering element corrections (IECs) for these interferences is not completely straightforward and introduces an additional component of error that must be propagated into the final uncertainty. In the Hf isotope system ^{176}Lu and ^{176}Yb isobarically interfere with ^{176}Hf and this provides a good example of the mechanism of IECs.

Simultaneous acquisition of all relevant Yb, Lu and Hf isotopes is possible in MC-ICP-MS using a static acquisition protocol similar to the one shown below.

L4	L3	L2	L1	Axial	H1	H2	H3	H4
^{172}Yb	^{173}Yb	^{175}Lu	^{176}Hf–Lu–Yb	^{177}Hf	^{178}Hf	^{179}Hf	^{180}Hf	–

Hf isotope ratios can be corrected for instrumental mass bias using the measured $^{179}Hf/^{177}Hf$ assuming an invariant ratio of 0.7325.[15] Invariant ratios of $^{176}Lu/^{175}Lu$ (0.026 59) (reference 11)

and $^{176}Yb/^{173}Yb$ (0.791 07) (reference 11) can be used to determine the degree of isobaric interference on ^{176}Hf by measuring the intensity of the non-interfering ^{175}Lu and $^{172\text{ or }173}Yb$ isotopes during analysis and subtracting the appropriate intensity of interference from the 176 peak. Firstly, however, the invariant Lu and Yb ratios must be inversely corrected for mass bias to reflect the fractionated nature of the lighter isotope relative to the 176 interfering on ^{176}Hf during the measurement. In practice, the Hf mass bias value is used for this since Hf, Lu and Yb all appear to behave similarly in the plasma and as such Hf is a reasonable proxy for the mass bias characteristics of Lu and Yb at the level of correction normally applied (note that Yb mass bias can be determined internally using $^{172}Yb/^{173}Yb$ but Yb intensities are usually too low to determine an accurate correction). For more accurate correction of ^{176}Yb on ^{176}Hf, Nowell and Parrish[16] calibrated a series of Yb-doped Hf standards to derive a reliable invariant $^{176}Yb/^{173}Yb$ ratio, allowing correction of Yb/Hf ratios up to ~0.3. This relationship is instrument specific but once determined it remains constant with time. Re-determination of the $^{176}Lu/^{175}Lu$ ratio is not required as the ^{176}Lu correction on ^{176}Hf is so small that any inaccuracy in the ratio has little effect on the final corrected $^{176}Hf/^{177}Hf$ ratio.

Other spectral interferences include argide complexes (XAr), oxides (XO), hydrides (XH), doubly charged species (X^{2+}, interfering at half the isotopic mass of X) and complex polyatomic molecules such as the nitric acid complex $^{1}H_2{}^{14}N^{16}O_3$ on ^{64}Zn.[17] A number of methods have been used to resolve, remove and correct for these interferences including high-resolution techniques (as detailed in Part 2.2.1), cool plasma and use of collision and reaction cells (Chapter 6).

2.2.2.7 Interferences, matrix effects and inter-element fractionation in isotope ratio measurement

Problems of correcting for mass bias and interferences are generally exacerbated when a sample with significant matrix is introduced to the plasma. Early misconceptions surrounding high-precision isotope ratio determination using MC-ICP-MS assumed that the high temperature and ionisation efficiency of the plasma source would allow samples to be analysed directly, avoiding laborious chemical purification of the sample. With MC-ICP-MS now a decade old, the opposite has been demonstrated – for ultimate precision isotope ratio data from MC-ICP-MS, samples require as much chemical processing and separation as is required for TIMS analyses. Anomalous matrix effects, differential oxide formation and polyatomic interferences, which may occur at levels insignificant for quadrupole ICP-MS elemental analysis, are very significant to MC-ICP-MS where ppm levels of precision and accuracy are usually required.

Introduction of a significant amount of matrix changes the space-charge relationship behind the skimmer cone[18] and the degree of mass bias. If a sample-standard bracketing protocol is adopted, small amounts of matrix present in the sample may change the mass bias relative to that determined from the standard. This may be small but can result in significant inaccuracy at the level of 10–100 ppm. Hence, efficient chemical separation procedures are essential for high-precision isotope ratio determination to ensure that chemically pure standards and samples run equivalently. Using an internal isotope pair for mass bias correction (e.g. $^{179}Hf/^{177}Hf$), small

shifts in mass bias between samples and standards can be corrected. The change in plasma (and indeed cone) conditions resulting from additional matrix also affects the level and stability of inter-element fractionation. As a result, great care must be taken when attempting simultaneous acquisition of isotope and parent/daughter ratios by non-isotope dilution methodologies (see, for example, Nowell and Parrish[16]), where significant (1–3%) shifts in the inter-element ratio can occur using an external calibration of the Lu–Hf ratio.

Increasingly, inter-element isotopic analyses (e.g. $^{206}Pb/^{238}U$, $^{176}Lu/^{177}Hf$, $^{87}Rb/^{86}Sr$,) are being conducted. Understanding, quantifying and correcting for the effect of fractionation on inter-element isotope ratio measurement and any necessary interference corrections is therefore critical if high-precision measurements are to be achieved. Accurate determination of inter-element isotope ratios can be affected by differential oxide formation. For example, U, Th and Pb oxidise differentially in the plasma, therefore biasing Th/U, Pb/U and Pb/Th inter-element isotope ratios important for geochronology. Mechanisms for minimising oxide formation include reducing the injector gas flow rate, desolvation of the sample aerosol and introducing a small amount of an additional gas (e.g. N_2 or He) to the plasma.[19] Such measures can reduce oxide formation to negligible levels (UO^+/U^+ = approximately 30 ppm and ThO^+/Th^+ = approximately 450 ppm (Horstwood, unpublished data)).

Polyatomic spectral interferences also present a significant problem. Complex molecules can form unexpected spectral interferences on analytes of interest. As an example, Figure 2.19(a) displays a mass scan across the 204–208 mass range whilst analysing a desolvated sample of dental enamel in a HNO_3–H_3PO_4 matrix after extensive chemical pre-treatment and ion-exchange chromatography. A polyatomic molecule with a mass of approximately 204.85 constitutes a significant interference on the ^{205}Tl peak that is used for correction of mass bias. A mass resolution of around 1500 ($=m/\Delta m$ (205/0.15)) would resolve this polyatomic interference and enable determination of its exact mass and possible composition, allowing methods for its minimisation or elimination to be developed. Using normal, low-resolution (400–500) MC-ICP-MS, problems of peak overlap can sometimes still be solved as illustrated in Figure 2.19(b). Here, the overlap is less severe and although not completely resolved, part of the true flat-top peak of the analyte can still be distinguished from that of the interferent or the combination of the two, and analysis conducted at this mass.

The complexity of some of these problems of interference, matrix and inter-element fractionation is exemplified by the analysis of Sr isotopes in both solution mode and laser ablation (LA-) MC-ICP-MS. Sr isotope studies have been traditionally carried out using TIMS although MC-ICP-MS can also be used but requires correction (or monitoring) for mass bias, interfering elements, doubly charged ions, argides and dimers, and unidentified interferences. Primarily, isobaric interferences from Rb and Kr (present in trace quantities within the Ar plasma gas) must be corrected but this is not wholly straightforward.

A single static acquisition is usually employed, similar to the set-up shown below.

^{89}Y is monitored as it can be aspirated during laser ablation applications where a small bleed is useful for tuning and centring purposes.

L4	L3	L2	L1	Axial	H1	H2	H3	H4
^{82}Kr	^{83}Kr	^{84}Sr-Kr	^{85}Rb	^{86}Sr-Kr	^{87}Sr-Rb	^{88}Sr	(^{89}Y)	–

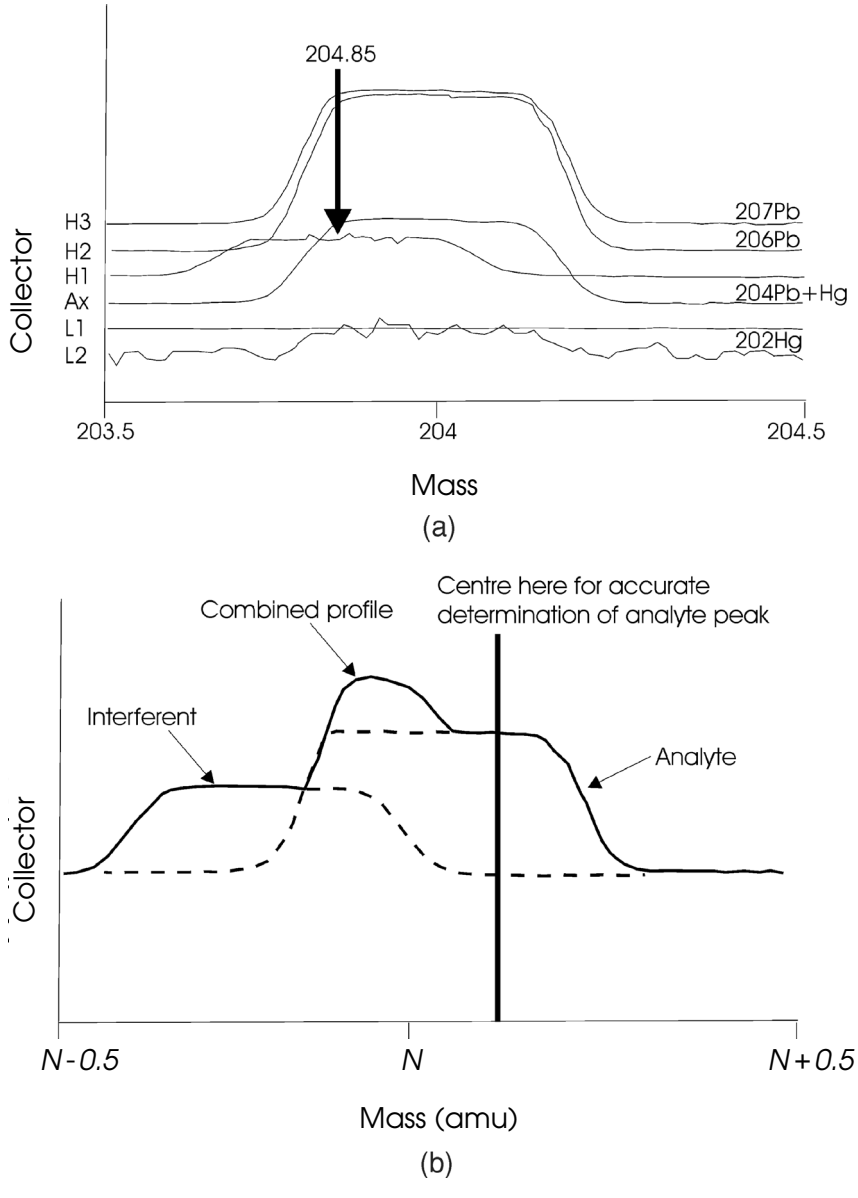

Figure 2.19 (a) Mass scan demonstrating polyatomic interference at mass 204.85. (b) Resolution of overlapping analyte and interferent peaks at $m/\Delta m = 400$

Correcting for Kr interference on Sr is made difficult due to an interferent variously apparent on ^{82}Kr and/or ^{83}Kr. This causes the ^{82}Kr/^{83}Kr ratio to deviate from its invariant value of around unity to values of 2–4. Reducing the sampling depth of the plasma and/or introducing N_2 serves to reduce this ratio but it is also possible to achieve a ^{82}Kr/^{83}Kr ratio of $\ll$1 (Horstwood, unpublished data), suggesting that an Ar_2H_2 interference on ^{82}Kr is not the only problem. Nowell *et al.*[20] describe a two-step iterative protocol for correcting ^{86}Kr on ^{86}Sr using either the ^{82}Kr or ^{83}Kr ion beam (whichever is the smaller and presumably lesser interfered signal). Initially, the non-corrected measured ^{86}Sr/^{88}Sr ratio, (assuming a true ^{86}Sr/^{88}Sr of 0.1194) is used to inversely mass bias correct the true ^{86}Kr/^{83}Kr or ^{86}Kr/^{82}Kr ratio before applying a ^{86}Kr correction on the ^{86}Sr. This yields a first-pass 'corrected measured' ^{86}Sr/^{88}Sr ratio, which is used again to inversely mass bias correct the true Kr ratios prior to performing a second, slightly more accurate correction of ^{86}Kr on ^{86}Sr. This gives a more accurate determination of the true ^{86}Sr/^{88}Sr mass bias. This final mass bias value is then used to correct for ^{87}Rb interference on ^{87}Sr, again after inverse mass bias correction of the true ^{87}Rb/^{85}Rb ratio (0.3857),[11] and also for the final (normal) mass bias correction of the ^{87}Sr/^{86}Sr ratio. In this way, the problem of accurately determining mass bias when one of the isotope pairs has an interference is satisfactorily corrected, resulting in highly precise and reproducible data.[20] In practice, Rb correction can only be performed on Rb/Sr ratios $<$0.2 before the correction begins to break down, largely because of error amplification resulting from the number of interference corrections and their inter-element nature.[21]

More problems become apparent during laser ablation. Waight *et al.*[22] detailed some of the problems including doubly charged REEs interfering on and off peak across the Kr–Sr mass range, and inaccurate ^{87}Sr/^{86}Sr and ^{84}Sr/^{86}Sr ratios (by 1.8–5.3% for the ^{84}Sr/^{86}Sr) during ablation of carbonates, silicates and phosphates. Similar data are presented here. Figure 2.20 shows ID-TIMS and LA-MC-ICP-MS results from analysis of a phosphate material. Previous data show solution-mode MC-ICP-MS and ID-TIMS to give results identical within uncertainty (0.709 67 $\pm$ 0.04% 2σ). For LA, however, a ^{87}Sr/^{86}Sr ratio of 0.7106 $\pm$ 0.06% (2σ) was obtained, representing a shift of 0.13%, clearly outside the uncertainty reported for the solution results. Data for other phosphate samples (not shown) demonstrate even larger shifts ($>$0.3%). Causes of these shifts are as yet largely unclear but are likely to be interferences from $ArCa^+$ and Ca dimers, which potentially contribute isobars at each mass in the Sr mass range (see Table 2.5). Polyatomic molecules such as ^{40}Ca–^{31}P–$^{16}O^+$ have also been implicated. A mass resolution of 16 500 is required to resolve, for example, $^{44}Ca_2^+$ from ^{88}Sr,

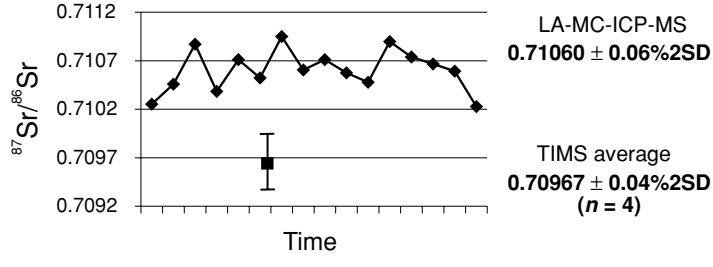

Figure 2.20 Comparison of ID-TIMS and LA-MC-ICP-MS ^{87}Sr/^{86}Sr ratios of a phosphate material. An interference consistently elevates the LA data

Table 2.5 Summary of potential interferences in the Kr–Sr mass range during analysis of carbonates and phosphates

Mass	Dimers	Hydrides	REE and polyatomics
82 (Kr)	$^{40-42}Ca_2$, $^{40(38)}Ar$–$^{42(44)}Ca$	$^{40}Ar_2{}^1H_2$, $^{40}Ca_2{}^1H_2$, $^{40}Ar^{40}Ca^1H_2$	$^{164}Er^{2+}$, $^{148}Sm/Nd^{16}O^{2+}$ $^{40}Ar^{16}O^{12}C^{14}N$, $^{40}Ca^{16}O^{12}C^{14}N$
83 (Kr)	$^{40-43}Ca_2$, ^{40}Ar–^{43}Ca	$^{40-42}Ca_2{}^1H$, $^{40(38)}Ar$–$^{42(44)}Ca^1H$, $^{40}Ar^{40}Ca^1H_3$	$^{166}Er^{2+}$, $^{150}Sm/Nd^{16}O^{2+}$, ^{36}Ar–^{31}P–^{16}O, $^{40}Ca^1H^{16}O^{12}C^{14}N$, $^{31}P^{14}N_2^{12}C_2$, $^{40}Ar^{12}C^{31}P$
84 (Kr and Sr)	$^{40-44,42}Ca_2$, ^{40}Ar–^{44}Ca	$^{40-42}Ca_2{}^1H_2$, ^{40}Ar–$^{42}Ca^1H_2$	$^{168}Er^{2+}$, $^{168}Yb^{2+}$, $^{152}Sm/Gd^{16}O^{2+}$, $^{136}Ce^{16}O_2{}^{2+}$, $^{40}Ca^1H^{12}C^{31}P$, $^{40}Ar^{16}O^{14}N_2$
85 (Rb)	$^{42-43}Ca_2$	$^{40(42)-44(42)}Ca_2{}^1H$, ^{40}Ar–$^{44}Ca^1H$	$^{170}Er^{2+}$, $^{170}Yb^{2+}$, $^{154}Sm/Gd^{16}O^{2+}$, $^{138}Ce/La^{16}O_2{}^{2+}$, $^{40}Ar^{14}N^{31}P$, $^{12}C^{14}N_3{}^{31}P$
86 (Kr and Sr)	$^{42(43)-44(43)}Ca_2$	$^{42-43}Ca_2{}^1H$ $^{40-44,42}Ca_2{}^1H_2$, ^{40}Ar–$^{44}Ca^1H_2$	$^{172}Yb^{2+}$, $^{156}Gd^{16}O^{2+}$, $^{140}Ce^{16}O_2{}^{2+}$, $^{40}Ar^1H^{14}N^{31}P$, $^{40}Ar^{16}O_2{}^{14}N$, $^{12}C_2{}^{31}P_2$
87 (Rb and Sr)	$^{43-44}Ca_2$	$^{42(43)-44(43)}Ca_2{}^1H$ $^{42-43}Ca_2{}^1H_2$	$^{174}Yb^{2+}$ $^{158}Gd^{16}O^{2+}$, $^{142}Ce/Nd^{16}O_2{}^{2+}$, $^{40}Ca/Ar^{31}P^{16}O$, $^{40}Ca/Ar^1H^{16}O_2{}^{14}N$, $^{40}Ca/Ar^1H_2{}^{14}N^{31}P$
88 (Sr)	$^{44}Ca_2$, $^{40-48}Ca_2$, ^{40}Ar–^{48}Ca	$^{43-44}Ca_2{}^1H$ $^{42(43)-44(43)}Ca_2{}^1H_2$	$^{176}Yb/Lu^{2+}$, $^{160}Gd/Dy^{16}O^{2+}$, $^{144}Sm/Nd^{16}O_2{}^{2+}$, $^{40}Ca/Ar^1H^{31}P^{16}O$, $^{12}C^{14}N^{31}P_2$

but due to the reduction in sensitivity and loss of the flat-top peak profile at these resolutions high-precision analyses cannot be achieved. Conditions allowing correction, minimisation or elimination of some of these interferences must therefore be found (at least for some materials) if high-quality LA-MC-ICP-MS analyses are to be performed. Clearly then, high-precision, and more importantly accurate, analysis of Sr isotope ratios by MC-ICP-MS is not straightforward.

2.2.2.8 Summary of Applications

MC-ICP-MS has revolutionised the scope and application of high-precision isotope analysis, through the ability to analyse much of the periodic table. From its birth through geological and

Table 2.6 Applications of MC-ICP-MS

Applications	Solution	Laser ablation
Environmental	Hg, Pb, Zn, Cu, Cd, Fe, U, Pu, Sr, Ca, Se, Cr	Pb, Sr
Biological, medical and forensic	Sr, Fe, U, Pb, Sb, Pt	Pb, Sr
Geology and geochronology	Pb, Fe, Hf, Sr, Re–Os, U–Th, Rb, Nd, Nb–Zr, Zr–Hf, Lu–Hf, Mo, In, Sn, Hg, Ra–Th–U, Dy, Th, Li, Sm–Nd, Ni	Pb, Fe, Hf, Sr, Re–Os, U–Pb, U–Th, Zr, Os, Lu–Hf
Science-based archaeology	Sn, Pb, Cu, Os, Zn	Pb, Sr, Cu, Os
Cosmogenesis and meteoritics	Zr, W, Ag, Tl, Ge, Sm–Nd, Lu–Hf, Ti, Ru, Pd–Ag, Fe, Mg, Cr, Al, Ni, Re, Os	Mg, Zr, W
Oceanography and climate	Si, Tl, Li, Mg, B, U–Th–Ra, Hf	

nuclear applications, environmental, archaeological, biological, medical and forensic scientists are now recognising what isotope ratio analysis can offer. Without the advent of MC-ICP-MS this would have been almost impossible or at least severely limited.

The range of applications now possible by MC-ICP-MS is almost unlimited and discussion of all of them is clearly well beyond the scope of this chapter. Table 2.6 summarises the use of MC-ICP-MS isotope ratio analysis in terms of both discipline and element. Research into fractionation mechanisms of non-traditional isotope systems will continue to increase the range of elements useful for isotope research and the diversity of applications, keeping MC-ICP-MS at the forefront of isotope research for many years to come.

References

1. Gray, A. L., Williams, J. G., Ince, A. T., and Liezers, M. (1994) Noise sources in inductively coupled plasma mass spectrometry: an investigation of their importance to the precision of isotope ratio measurements. *J. Anal. At. Spectrom.*, **9**, 1179–81.
2. Turner, P. J., Mills, D. J., Schröder, E., Lapitajs, G., Jung, G., Iacone, L. A., Haydar, D. A., and Montaser, A. (1998) Instrumentation for low- and high-resolution ICPMS. In: *Inductively Coupled Plasma Mass Spectrometry* (ed. A. Montaser), Wiley-VCH, New York, pp. 421–501.
3. Walder, A. J. and Freedman, P. A. (1992) Isotopic ratio measurement using a double focussing magnetic sector mass analyser with an inductively coupled plasma as an ion source. *J. Anal. At. Spectrom.*, **7**, 571–5.
4. Gill, R. (ed.) (1997) *Modern Analytical Geochemistry*, Longman, Singapore.
5. Thirlwall, M. F. (1991) Long-term reproducibility of multicollector Sr and Nd isotope ratio analysis. *Chem. Geol.* (Isot. Geosci. Sect.), **94**, 85–104.
6. Thirlwall, M. (2001) Inappropriate tail corrections can cause large inaccuracy in isotope ratio determination by MC-ICP-MS. *J. Anal. At. Spectrom.*, **16**, 1121–5.

7. Albarède, F., Telouk, P., Blichert-Toft, J., Boyet, M., Agranier, A. and Nelson, B. (2004) Precise and accurate isotopic measurements using multiple-collector ICPMS. *Geochimica et Cosmochimica Acta*, **68**(12), 2725–44.
8. Turner, P. J., Mills, D. J., Schröder, E., Lapitajs, G., Jung, G., Iacone, L. A., Haydar, D. A., and Montaser, A. (1998) Instrumentation for low- and high-resolution ICPMS. In: *Inductively Coupled Plasma Mass Spectrometry* (ed. A. Montaser), Wiley-VCH, New York, pp. 421–501.
9. Ingle, C. P., Sharp, B. L., Horstwood, M. S. A., Parrish R. R., and Lewis, D. J. (2003) Instrument response functions, mass bias and matrix effects in isotope ratio measurements and semi-quantitative analysis by single and multi-collector ICP-MS. *J. Anal. At. Spectrom.*, **18**, 219–29.
10. Longerich, H. P., Fryer, B. J., and Strong, D. F. (1987) Determination of lead isotope ratios by inductively coupled plasma-mass spectrometry (ICP-MS). *Spectrochim. Acta*, **42B**, 39–48.
11. Rosman, K. J. R. and Taylor, P. D. P. (1999) Isotopic compositions of the elements 1997. *J. Anal. At. Spectrom.*, **14**, 5N–24N.
12. White, W. M., Albarède, F. and Télouk, P. (2000) High-precision analysis of Pb isotope ratios by multi-collector ICP-MS. *Chem. Geol.*, **167**, 257–70.
13. Thirlwall, M. F. (2002) Multicollector ICP-MS analysis of Pb isotopes using a ^{207}Pb–^{204}Pb double spike demonstrate up to 400 ppm/amu systematic errors in Tl-normalisation. *Chem. Geol.*, **184**, 255–79.
14. Mason, T. F. D. (2003) High precision transition metal isotope analysis by plasma source mass spectrometry and implications for low-temperature geochemistry. Ph. D. Thesis, Imperial College, London.
15. Patchett, P. J. and Tatsumoto, M. (1980) A routine high-precision method for Lu–Hf isotope geochemistry and chronology. *Contrib. Mineral. Petrol.*, **75**, 263–7.
16. Nowell, G. and Parrish, R. R. (2001) Simultaneous acquisition of isotope compositions and parent/daughter ratios by non-isotope dilution solution-mode plasma ionisation multi-collector mass spectrometry (PIMMS). *Plasma Source Mass Spectrometry: The New Millennium* (eds G. Holland and S. D. Tanner), Royal Society of Chemistry, Cambridge pp. 298–310.
17. Mason, T. F. D., Weiss, D. J., Horstwood, M., Parrish, R. R., Russell, S. S., Mullane, E., and Coles B. J. (2004) High-precision Cu and Zn isotope analysis using MC-ICP-MS, Part 1: Spectral interferences and their correction. *J. Anal. At. Spectrom.*, **19**, 209–17.
18. Douglas, D. J. and Tanner, S. D. (1998) Fundamental considerations in ICPMS. In: *Inductively Coupled Plasma Mass Spectrometry* (ed. A. Montaser), Wiley-VCH, New York pp. 615–79.
19. Horlick, G. and Montaser, A. (1998) Analytical characteristics of ICPMS. In: *Inductively Coupled Plasma Mass Spectrometry* (ed. A. Montaser), Wiley-VCH, New York pp. 503–88.
20. Nowell, G. M., Pearson, D. G., Ottley, C. J., Schwieters, J., and Dowall, D., (2003) Long-term performance characteristics of a plasma ionisation multi-collector mass spectrometer (PIMMS): the ThermoFinnigan Neptune. In: *Plasma Source Mass Spectrometry* (eds G. Holland and S. D. Tanner), Royal Society of Chemistry Cambridge.
21. Davidson, J. D., Tepley, F., Palacz, Z. and Meffan-Main, S. (2001) Magma recharge, contamination and residence times revealed by in-situ laser ablation isotopic analysis of feldspar in volcanic rocks. *Ear. Planet. Sci. Lett.*, **184**, 427–42.
22. Waight, T., Baker, J. and Peate, D. (2002) Sr isotope ratio measurements by double-focusing MC-ICPMS: techniques, observations and pitfalls. *Int. J. Mass Spectrom.*, **221**, 229–44.

2.3 ICP-TIME-OF-FLIGHT MASS SPECTROMETRY

Heidi Goenaga-Infante

2.3.1 Introduction

The potential of the most commonly used mass spectrometers (quadrupoles and magnetic sector-field single collectors) for elemental analysis has been discussed in detail in Parts 2.1 and 2.2.1 of this chapter. However, some intrinsic limitations still remain with these sequentially scanned systems, particularly when transient or time-dependent signals (such as those produced by laser ablation (LA), electrothermal vaporisation (ETV), flow injection (FI) and chromatography) are used to analyse a large number of isotopes. These scan-based systems can measure only a single m/z at a unit of time. Hence, truly simultaneous determination of multiple isotopes, particularly when fast transient signals are analysed, is not possible without the introduction of 'spectral skew'.[1]

The limitation of measuring only a single isotopic peak at a time also constrains the precision that can be realised in the measurement of isotope ratios. Changes in nebulisation efficiency, variations in the plasma (plasma flicker) and the sampling of inhomogeneous plasma zones are all considered sources of instability in ICP-MS. Precision can best be improved using a ratioing method such as internal standardisation. Isotope dilution is also a method that can give more reliable and potentially very accurate determinations. Unfortunately, the signal fluctuations are often rapid enough that ratioing-based compensation is effective only if the target isotopes or elements are measured within microseconds of each other, otherwise the signal instability becomes additive. With quadrupole ICP-MS, the dwell time per isotope can be minimised in order to achieve high speed but even then, only a limited number of isotopes can be measured before this speed enhancement becomes ineffective in improving isotope ratio precision. The problem is even more difficult in sector-field instruments, as they often cannot be scanned as rapidly as quadrupoles.

Much effort has been made in order to overcome the problems of spectral skew, using modified instruments based on sequential scanning mass analysers, to determine more than one isotope simultaneously. An example is the twin-quadrupole instrument described by Allen *et al*.[2–4] Multi-collector ICP-MS based on double focusing magnetic sector mass analysers with multiple Faraday cup collectors (or electron multipliers) can determine several isotopes simultaneously and avoids the disadvantages of scanned systems for the analysis of transient signals[5–7] (see also Part 2.2.2 of this chapter). Furthermore, multi-collector magnetic sector field ICP-MS instruments are, up until now, the equipment in plasma source mass spectrometry with which the best precision (in the range of 0.02–0.005% RSD) can be achieved. This performance is comparable with that of isotope ratio measurements by thermal ionisation (an extremely stable ion source) mass spectrometry.[8] However, these multi-detector systems are typically limited to monitoring less than 10 isotopes per analysis.[9] Detector-array systems based upon Mattauch–Herzog sector-field instrument geometry have been used to simultaneously collect large mass spectral sections or even a complete elemental mass spectrum,[10] but to date the application of these systems to elemental analysis is limited by the performance of the currently available detector technology.

The coupling of trapping mass analysers, such as the quadrupole ion trap (IT) and the Fourier transform ion cyclotron resonance (FT-ICR) (see Part 2.4 of this chapter), offers simultaneous multi-elemental measurements, thus eliminating spectral skew and the trade-off between sensitivity, precision and mass coverage. However, using IT, individual m/z values are measured sequentially, resulting in a loss of sampling speed and duty cycle. Additionally, limited ion capacity (10^4–10^6) of IT limits its dynamic range.[11] Although the high resolution capability of FT-ICR-MS for elimination of most isobaric, as well as polyatomic, interferences that occur in ICP-MS also makes this type of mass analyser particularly attractive,[12] its routine application has to date been limited by cost, ultra-high vacuum requirements, restricted ion-storage capability and lengthy measurement time.

Time-of-flight mass spectrometers for ICP-MS offer the potential for truly simultaneous multi-isotopic detection, at lower cost and greater speed than the alternatives currently available. This part of the book aims to describe the operation of ICP-time-of-flight mass spectrometry (ICP-TOF-MS) and to discuss the most relevant applications of this instrumentation.

2.3.2 Principles of ICP-TOF-MS

Contrary to scanning mass spectrometers, in ICP-TOF-MS the ions are detected according to their m/z ratio by means of their flight times.[13] After being sampled from the plasma, all the ions are accelerated to the same kinetic energy of approximately 1 keV, resulting in ions of a specific m/z ratio having a well-defined flight time to the detector, determined by the following equation:

$$E_{\text{kin}} = \frac{1}{2}\, mv^2 = zqU \quad \Leftrightarrow \quad \frac{m}{z} = 2\, qU \left(\frac{t}{L}\right)^2 \tag{2.3.1}$$

where E_{kin} is the kinetic energy of the ion, m is the ion mass, v is its velocity, z is its charge, q is the electronic charge (i.e. 1.6×10^{-19} C), U is the electrostatic potential and L is the length of the electrostatic field-free drift region through which the ion travels to the detector.

As a consequence of this acceleration process, the ions acquire different m/z-dependent velocities (with lighter ions achieving higher velocities than heavier ions) within the field-free drift region (referred to as the flight tube), resulting in different flight times. Measurements of the intensity and flight times of ions arriving at the detector produce a mass spectrum directly.

2.3.3 Attractive features of TOF-MS for ICP-MS

TOF-MS is an inherently simple type of mass spectrometer with high transmission efficiency. With TOF-MS, all ions are extracted simultaneously for mass analysis, resulting in complete absence of the above-mentioned spectral skew. This simultaneous multi-element ion extraction also results in the achievement of RSDs below 0.05% for isotope ratio measurements of a number of elements in the bulk mode of operation (continuous measurement).[14,15] The precision of isotope ratio measurements using TOF-MS is therefore dictated mainly by fundamental noise effects rather than by the time-dependent signal fluctuations encountered with scanning mass spectrometers, as shown by Myers, Mahoney, Vanhaecke, Ray, Sturgeon and their co-workers.[14,16,17] Other important advantages of ICP-TOF-MS are the high data acquisition rate

achievable over the whole mass spectrum (ICP-TOF-MS systems can produce a complete atomic mass spectrum in less than 50 μs, thus generating more than 20 000 complete mass spectra per second) and the quasi-simultaneous nature of spectral generation. Because of the high spectral generation rate (considered as the main advantage of ICP-TOF-MS) and quasi-simultaneous detection capabilities, complete elemental coverage in micro-volumes and for rapid transient signals is possible. In other words, multi-elemental quasi-simultaneous transient signal analysis can be performed without sacrificing precision or detection limits, regardless of the number of isotopes monitored or the duration of the transient signal. Another consequence of the high data acquisition rate of ICP-TOF-MS is the 8- to 10-fold improvement in sample throughput compared with that of quadrupole ICP-MS, thus minimising the problem of interface cone orifice clogging caused by the introduction of high total dissolved solid samples (e.g. some environmental and biological materials) over extended periods of time into the ICP, and significantly reducing the cost of the analysis. Whereas analysis time using quadrupole ICP-MS is directly proportional to the number of isotopes multiplied by the integration time, with ICP-TOF-MS it is determined only by the integration time and the number of replicates selected and is independent of the number of isotopes being measured.[18] This results in considerable time-saving.

2.3.4 TOF-MS geometries for ICP-MS

In ICP-TOF-MS instrumentation, the time-of-flight mass spectrometer can be placed either orthogonal or axial to the plasma. The common and contrasting design concepts, operating principles and experimental performance of both orthogonal acceleration and axial time-of-flight ICP MS instruments have been examined and contrasted in detail by Hieftje[19] and co-workers and reviewed by Guilhaus.[20]

Hieftje and co-workers pioneered the use of both the orthogonal and axial TOF-MS geometries for ICP-MS,[21,22] resulting in the development of commercially available instruments by GBC Scientific Instruments (Melbourne, Victoria, Australia) (orthogonal geometry) and LECO Instruments (St Joseph, MI, USA) (axial geometry).

ICP-TOF-MS with orthogonal acceleration (oa) was first introduced in 1993. A simple schematic diagram of this system is depicted in Figure 2.21.

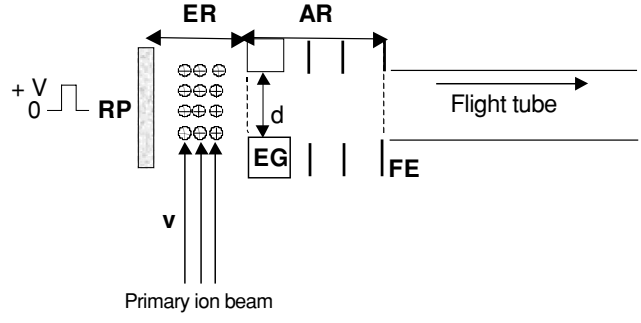

Figure 2.21 Schematic diagram of the orthogonal acceleration ICP-TOF-MS system. RP, repeller plate; ER, extraction region; AR, acceleration region; EG, extraction grid; d, extraction region width; v, beam velocity; FE, flight tube entrance grid (size relations not correct)

Briefly, in this system, the primary ion beam enters the extraction region between the repeller plate and the extraction grid. The ions within this region are accelerated into the flight tube (positioned at a 90° angle to the original axis of ion propagation) when the repeller is pulsed to a positive voltage. With this approach, the velocity of the primary ion beam in the orthogonal direction is much smaller than the final velocity of the accelerated ions. This is favourable to the duty cycle obtainable with this geometry since the primary ion beam slowly refills the extraction region while the ion packet extracted in the previous cycle is being analysed. However, the perpendicular velocity component of the ions affects their trajectory in the flight tube. The isokinetic ion beam extracted from the ICP source results in a mass-dependent energy perpendicular to the flight tube axis, leading to beam broadening.[19] First attempts to correct for this mass-dependent ion trajectory, by means of steering plates positioned within the flight tube, have led to reduced beam divergence but also to some loss in mass resolving power.[23] A 'spontaneous drift' design, which allows the ions to follow their original mass-dependent path, was first introduced by Guilhaus and co-workers[20] and subsequently modified by Bandura *et al*.[24] and Davis *et al*.[25] to eliminate the deleterious effects of the steering plates. The modified 'spontaneous drift' strategy[24,25] greatly minimises the above-mentioned mass-dependent ion trajectory problem when oa-TOF-MS systems are coupled with isokinetic sources due to the selective sampling of an energy range from an extracted ion packet of large size.[19] Axial ICP-TOF-MS was developed to address several of the limitations of oa-TOF-MS. Since the introduction of the axial Renaissance ICP-TOF-MS system by LECO in 1998, most of the applications of ICP-TOF-MS to elemental analysis have employed axial acceleration TOF-MS.[20]

A schematic overview of the LECO Renaissance axial acceleration ICP-TOF-MS design is given in Figure 2.22.

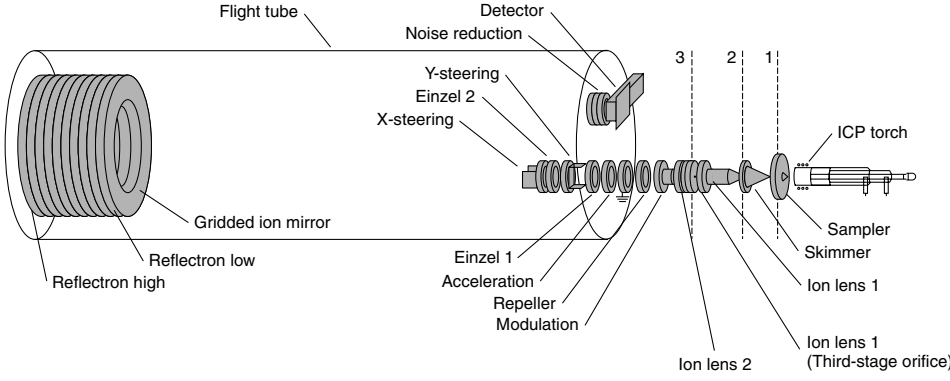

Figure 2.22 Schematic diagram of the LECO Renaissance axial ICP-TOF-MS system

Here, the ion segment is extracted in the same direction as the motion of the plasma ion beam, avoiding the mass bias problems inherent to the orthogonal geometry. Focusing of the ion beam, extraction of the ion packets and detection using axial ICP-TOF-MS instrumentation are achieved as follows.[18]

The ion flow through the ICP-TOF-MS is controlled using ion optics. Ions, electrons and neutral gas are all transported through the consecutive orifices in the instrument to the mass spectrometer; however, in common with all ICP-MS instruments, the flow of positive ions can be optimised and controlled with the ion lenses. The sampler and skimmer orifices are maintained

at ground potential. Ions are extracted from the skimmed beam with an ion lens and then focused through the third-stage orifice, which is kept at the same potential as the ion lens. The first lens in the third stage transmits the ions into the modulation region of the TOF-MS. The ICP is a continuous ion source, but TOF-MS requires time limited segments of ions in order to operate correctly. The term modulation refers to the process of creating a pulsed ion beam from a continuous one. The modulation optic is a cylinder, which selects a 1.5 cm long ion packet from the continuous stream emanating from the ICP for acceleration into the drift region of the mass spectrometer. A negative voltage applied to the modulation optic transmits ions to the acceleration region of the TOF-MS. When enough ions have been sampled, the modulation optic is switched to a positive potential. This prevents more ions from entering the drift region.

The ions selected by the modulation optic enter the region in front of the repeller electrode. This electrode is pulsed to a positive voltage and remains at this voltage for 1 μs, which sends all the positive ions into the dc acceleration region of the TOF-MS. Here the ions are brought to their final kinetic energy. Once the flight tube is clear of all accelerated ions, the rejection fields are dropped and the acceleration region is allowed to refill with ions from the plasma. Then the entire process is repeated, at a spectral generation frequency of 20 kHz. With current technology, the instrument data acquisition electronics are typically constrained to a maximum sampling rate of 78 Hz (12.75 ms integration time), so collecting every signal spectrum at this high spectral generation rate is not practical. Therefore each point of the signals provided (every 12.75 ms) from the data acquisition system corresponds to 256 integrated mass spectra. The integration time is controlled by the instruments' software and can be set to higher values than 12.75 ms if a particular application does not require such fast data reporting.

The ions enter the flight tube after acceleration and pass through focusing and steering optics to increase the ion transmission through the time-of-flight mass analyser. Due to the fact that ions of all masses present in the flight tube reach the detector, matrix ions or ions generated by the plasma gas have to be removed in order to prevent them from entering the flight path and subsequently overloading the detector. These ions are selectively deflected using the so-called transverse rejection ion pulse (TRIP) by applying sideways high-voltage pulses to the X-steering plate with the pulse timing and voltage being controlled by the instruments' software. The narrowest setting of a deflection window (0.03 μs) affects approximately 5 amu, but for lower m/z values ($\leq$ 40 amu) it can diminish to 1–3 amu.[18] Efforts to minimise the region (in the flight tube axis) in which ions experience the applied deflection pulse (proportional to the deflection window) by using alternative systems such as comb deflectors may result in a deterioration of the deflection efficiency in comparison with the traditional parallel-plate system.[26]

Efficient deflection of ^{40}Ar (one of the major background peaks under normal plasma conditions) requires the use of deflection windows with widths of about 0.1 μs or larger, so difficulties in the sensitive measurement of ^{39}K after deflection of ^{40}Ar are usually encountered. However, the use of cool plasma conditions (see Chapter 1) leads to considerable reduction of Ar-related ions, making it possible to measure ^{39}K using ICP-TOF-MS.[18]

The ions are detected by means of a discrete dynode multiplier (ETP Model AF831H, Ermington, NSW, Australia). It is located above the ion-optics, opposite the ion mirror. In front of the detector, three grids are placed in order to reduce the background originating from low-energy ions, by inhibiting them from striking the detector surface. The detector converts ions exiting the flight tube into electrons with gains of up to 10^7. The signals are recorded simultaneously in two different detection modes, the ion counting (digital) mode, which is used for the most sensitive work near the detection limit and the analog mode, which is used to extend the dynamic

range (up to 10^6–10^7) at high signal levels, since the signal from the ion counting mode is not linear at concentrations above 10 ng/mL for the most sensitive isotopes.[18] Losses of linearity at high ion count rates affect the accuracy of isotope ratio measurements, and require application of dead time correction of the signal intensities. This was illustrated in a study by Carrión *et al.*,[27] in which the ion counting data obtained using axial ICP-TOF-MS for transient isotope ratio measurements of Pb and Rb at absolute concentrations $\geq$ 1.5 ng had to be dead-time corrected.[27] However, the detection of high intensity signals (such as those produced by ultrasonic nebulisation (USN)[18,27] and flow injection pre-concentration[28] systems) using the analog mode has been shown to produce the best quality isotope ratio data using ICP-TOF-MS. No dead time correction is necessary using the analog mode and the contribution from fundamental noise is smaller at higher concentrations (i.e. high signal intensities).

2.3.5 Comparing the performance of ICP-TOF-MS systems

For both TOF-MS geometries, at the opposite end of the vacuum chamber, the ions arrive at an ion mirror, the so-called reflectron, which is composed of a series of charged flat rings. Two electrodes define two fields that reflect ions back down the flight tube to the detector surface. The first field is characterised by an electrode called 'reflectron low' and the second field is a linear potential drop between 'reflectron low' and 'reflectron high'. The ions that fly into the reflectron slow down under the influence of the successive fields and are then turned and accelerated back out of the mirror under the influence of the same fields. The ion mirror has the following beneficial effects. First of all the flight path length of the ions is doubled. This permits the construction of smaller vacuum chambers, which allows the use of smaller and less expensive turbomolecular pumps reducing the cost of the instrument. Another advantage is that photons and neutral species are not reflected to the detector where they would otherwise increase the background noise. As a result, the orthogonal acceleration system demonstrates very low detector background with less than one count per second per m/z for most non-interfered elements.[17] For the axial acceleration system, the contribution of photons and neutrals to the background level can be anticipated to be more significant, since the source, interface and ion optics are situated in-line with the flight tube. Indeed, instruments with axial acceleration are found to exhibit slightly higher background (1–10 cps per m/z) in comparison with oa-ICP-TOF-MS instruments.[18] This leads to the achievement of slightly better detection limits using the orthogonal TOF-MS since the sensitivities shown by both systems are comparable (in the range of 500–10 000 cps per μg/L depending on the ion mass).[19]

Finally, the ions are refocused by the reflectron as illustrated in Figure 2.23.

If two ions of the same m/z ratio travel with slightly different velocities, then the faster one will penetrate the ion mirror layers more deeply than the slower one, therefore taking longer to be turned around by the reflectron, allowing the slower ion to catch up. The effect is that both ions arrive at the same time at the detector, despite their slightly different initial velocities, thus reducing the signal peak width and improving the mass resolution.

In the ICP-TOF-MS system, the resolving power depends on the initial velocity spread and spatial distribution of the ion packet along the flight tube axis. For the orthogonal geometry, the resolving power is relatively insensitive to the distribution of ion velocities in the primary ion beam since ion packets are extracted along an axis in which their velocity distribution is low. Conversely, in the axial geometry, the large velocity spread of the ions in the primary ion beam

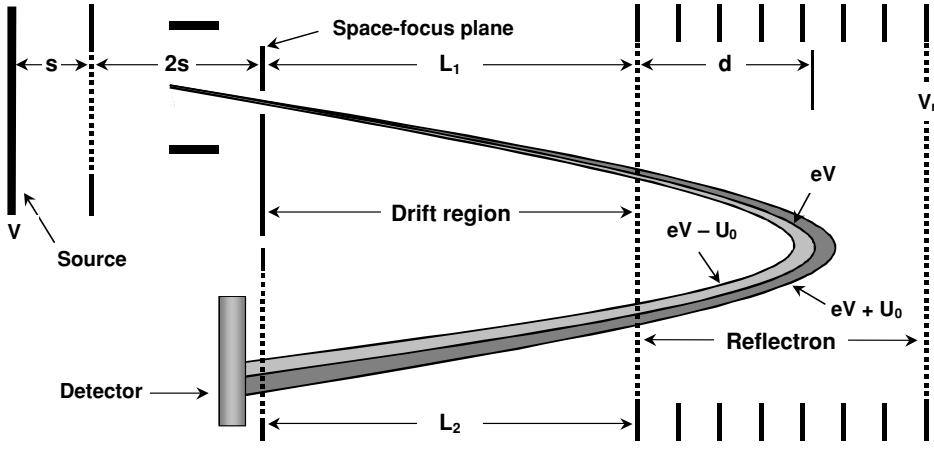

Figure 2.23 Principle of energy focusing in ICP-TOF-MS (size relations not correct)

is oriented in the direction of the flight tube. Thus, it can contribute directly to a spread in the observed flight times of a particular m/z, compromising resolving power. Additionally, to limit the initial spatial distribution of ions in the direction of the flight tube, whereas the oa-ICP-TOF-MS can make use of ion-optics to achieve this without compromising the duty cycle, the on-axis geometry requires improved space focusing if a large extraction region is completely filled with ions to obtain the greatest possible duty cycle. As a result, although a two-stage acceleration technique and a reflectron are implemented to improve the resolving power of the on-axis ICP-TOF-MS, this system specifies lower resolving powers (full width at half maximum, FWHM) (from 410 for ^{7}Li to 1140 for ^{209}Bi) than the oa-ICP-TOF-MS (500 for ^{6}Li and 2200 for ^{238}U).[17]

The precision of isotope ratio measurements achieved with both commercial instruments has been found to be similar and dependent on the integration time and, of course, on analyte concentration. As discussed above, analog mode is recommended for the highest possible precision on isotope ratios. Instrumental mass bias for the two commercial systems decreases with increasing m/z and is found to be similar in magnitude to that reported for quadrupole- and magnetic-sector-based instruments.[19]

2.3.6 Challenges of TOF for ICP-MS

Despite the figures of merit of TOF for elemental analysis by ICP-MS, there are still a number of significant challenges.[11,20] The fact that the transmission and detection efficiencies of the current systems are not as high as would be desired and that the duty cycle (percentage of ions utilised) is only about 6–10% at present leads to the achievement of poorer detection limits than those obtained by the scanning counterparts (quadrupole and magnetic sector instruments). The sensitivity of ICP-TOF-MS instruments is as much as an order of magnitude poorer than comparable quadrupole systems, and the detection limits correspondingly worse by a similar margin.[11] Since the RSD of a ratio measurement is partly governed by the magnitude of the signal, the poorer sensitivity of ICP-TOF-MS systems has also led to deterioration of isotope ratio measurement

precision, especially for fast transient ratio measurements of a few isotopes (less than 7), in comparison with that of the analogous quadrupole ICP-MS. For all these reasons, efforts are currently being made for improving the duty cycle and transmission efficiency of ICP-TOF-MS instruments.[11] The elimination of the heavy-mass bias still present in both instruments[17,18] also remains a challenge.

A significant difference in ion abundance of neighboring masses ($\geq 10^6$) within a single mass spectrum may lead to detector saturation. In such a case, the quasi-simultaneous nature of spectral generation of ICP-TOF-MS instruments demands an extension of their dynamic range. Currently, this problem can be minimised by limiting the intensity of the major peak (e.g. by m/z deflection, detuning the ion optics and reducing the detector gain). However, this does not occur without affecting the intensity of any other m/z within the mass spectrum.

Finally, although the TRIP pulse approach can reject ions in a small mass window (1–5 amu, depending on the mass range to which it is applied, as discussed earlier) currently there exists no effective means of deflecting a single m/z by ICP-TOF-MS while leaving other m/z unaffected. Future instrument designs would benefit from the ability to reduce the ion rejection window to values of ≤ 1 amu.

2.3.7 Applications of ICP-TOF-MS

Results on the evaluation of the analytical and isotope ratio performance of ICP-TOF-MS measurements in steady-state signals[14–23,17] were discussed earlier in this chapter. However, the major application field of ICP-TOF-MS involves the multi-element and multi-isotope analysis of rapid transient signals such as those commonly encountered in flow injection, [27,28,29–35] electrothermal vaporisation,[36] laser ablation,[37–40] capillary electrophoresis, (CE)[41] and chromatography.[1,42–55] From the number of references related to the coupling of ICP-TOF-MS with a separation system, TOF-MS seems to be an attractive alternative to scanning-based systems for hyphenated speciation analysis. Leach *et al.*[56] have recently reviewed the different hyphenated speciation systems that employ ICP-TOF-MS.

2.3.7.1 Hyphenated ICP-TOF-MS flow injection analysis

The capabilities of ICP-TOF-MS as a detector for simultaneous determination of a large number of isotopes in a transient flow injection peak have recently been reviewed by Adams and co-workers.[35] Flow injection as a means of sample introduction for ICP-MS offers a number of advantages,[35] namely, the ability to use small volume samples, the reduction of sample loading (particularly useful for measurement of samples containing high levels of dissolved solids) in the plasma and the facility for achieving high sample throughput (see Chapter 5 for further information about FI techniques for ICP-MS). FI methodologies are particularly advantageous for elemental analysis by ICP-TOF-MS when separation and pre-concentration methods and more efficient sample introduction devices (e.g. hydride generation (HG) and USN) are involved. The use of these devices leads to increased sensitivity, provides the selectivity required for multi-elemental analysis of complex matrices and eliminates the deleterious effects of organic solvents, often employed for analyte elution in FI applications, in the plasma i.e. increased carbon-based

interferences, higher reflected plasma power and the need to add oxygen to combust the carbon (to CO_2) before it blocks the interface cones.

Centineo *et al*.[33] developed a method based on the use of FI-HG-ICP-TOF-MS for the quasi-simultaneous determination of seven elements forming hydrides (As, Bi, Ge, Hg, Sb, Se and Sn). Analytical figures of merit such as detection limits in the low pg/mL region, linearity over more than five orders of magnitude and repeatability of 2–5% RSD allowed application of this strategy for highly accurate analysis of urine samples.

Benkhedda *et al*.[31] demonstrated the unique performance of ICP-TOF-MS for the simultaneous multi-element detection of 22 isotopes of rare earth elements (REEs) in a FI peak of about 5 s width (at 50% height) without the introduction of any spectral skew. Figure 2.24 represents the profiles obtained by USN-ICP-TOF-MS for three replicates of 250 μL injections of a 0.1 mg/L multi-elemental standard of REE's after FI on-line pre-concentration in a fkr (KR) pre-coated with the chelating reagent 1-phenyl-3-methyl-4-benzoyl-pyrazol-5-one (PMBP).

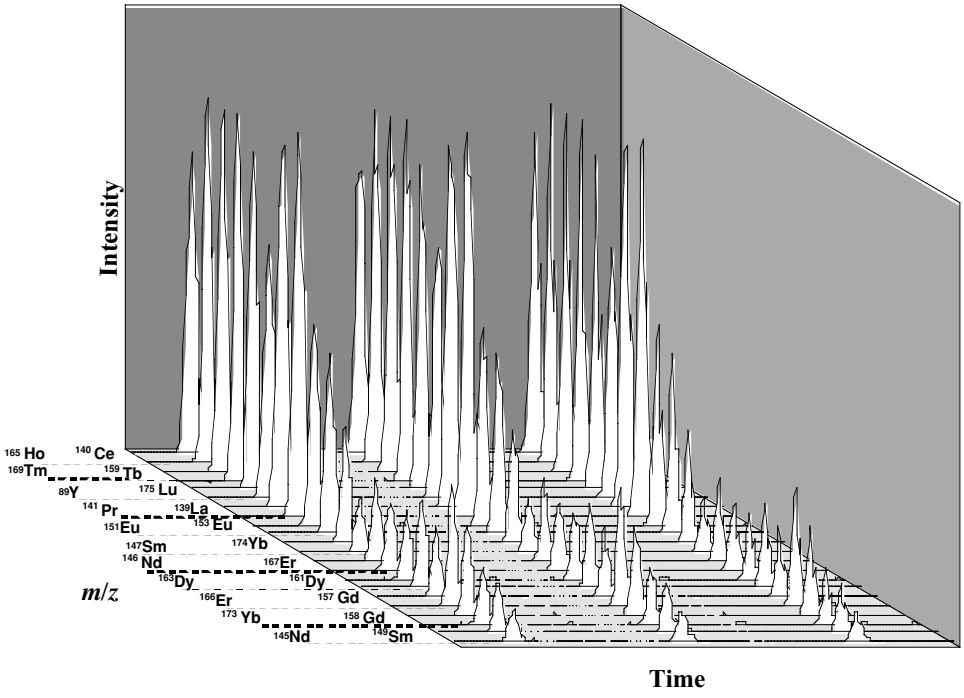

Figure 2.24 Performance of ICP-TOF-MS for the simultaneous determination of 22 isotopes of REEs in a FI peak.[35] Reproduced with permission from Elsevier Science

Effective pre-concentration and separation of REEs, from the major constituents of natural waters (alkali and alkaline earth elements), was achieved. Elution of the analytes with nitric acid and detection using USN-ICP-TOF-MS along with enhancement factors of 15–22 led to detection limits that ranged from 3 to 4 pg/L.

The performance optimisation of Pb isotope ratio measurements in FI signals by ICP-TOF-MS analysis of Pb aqueous standard solutions was evaluated by Carrión *et al*.[27] These authors demonstrated that the detection of high intensity transient signals (such as those achieved using USN)

produces isotope ratio data of high quality using ICP-TOF-MS. They reported typical precisions of about 1.0, 0.3 and 0.3% RSD for $^{204}Pb/^{206}Pb$, $^{207}Pb/^{206}Pb$ and $^{208}Pb/^{206}Pb$, respectively. However, these data were obtained from transient signals reaching a steady-state level in analog mode and relied on relatively long integration times. These conditions cannot be guaranteed for samples with low lead concentrations and high matrix content. More recently, Benkhedda *et al*.[28]demonstrated that the combination of ICP-TOF-MS with FI on-line pre-concentration provides a very useful technique for simultaneous determination of lead at trace levels and lead isotope ratios in natural water samples. The selectivity and sensitivity afforded by this method allowed accurate and precise (in the ranges 1.5–4.3% and 0.1–0.8% RSD for $^{204}Pb/^{206}Pb$ and $^{207}Pb/^{206}Pb$, $^{208}Pb/^{206}Pb$ ratios, respectively) transient isotope ratio analysis of water samples, with lead concentrations between 210 and 462 ng/L, to be achieved.

2.3.7.2 ICP-TOF-MS as a tool for speciation analysis

Hieftje and co-workers[56] have given an excellent overview of the applications of ICP-TOF-MS, as detector for chromatography and capillary electrophoresis (CE), for elemental speciation studies. For the interested reader, speciation using ICP-MS is covered in detail in Chapter 7 of this book.

Gas chromatography (GC) provides powerful separation of volatile species in terms of resolution and sensitivity. Its combination with ICP-TOF-MS detection leads to attractive figures of merit for the simultaneous determination of organocompounds of lead and tin, as illustrated by Leach and Hieftje.[38] The high acquisition speed of ICP-TOF-MS allowed the measurement of signals with peak widths of about 1 s with good precision and without spectral skew. Simultaneous extraction of all m/z provided the capability to perform isotopic analysis on GC peaks with a precision of 2.88% RSD, as calculated for the tetramethyltin peak. Developments over the past decade in the speciation analyses of organometals have led to the replacement of conventional capillary GC by multicapillary GC (MCGC) systems in some applications, thus achieving the resolution of complex mixtures of volatile thermally stable compounds at higher speed and using larger sample injection volumes without sacrificing efficiency. Recently, Jitaru *et al*.[46] demonstrated that ICP-TOF-MS is able to detect transient signals with a width down to 0.4 s (at half peak height) such as those produced by MCGC separation of methylmercury and inorganic mercury with ultra-trace sensitivity and high analytical precision. Excellent detection limits (16 and 257 fg/g for methylmercury (as Hg) and inorganic mercury, respectively) and precisions (RSD (%), $n = 10$, 10 pg Hg) of 1.2% for methylmercury and 4.1% for inorganic Hg were achieved using this approach. Adams and co-workers[45] demonstrated that the high data acquisition rate of ICP-TOF-MS (78 Hz) provides the required peak definition when combined with MCGC for speciation of organolead compounds. Figure 2.25 shows that operation at an integration time of 12.75 ms (equivalent to a data acquisition rate of 78 Hz) resulted in more than 35 measurement points being collected for a trimethyllead (TML) peak of FWHM of just 0.18 s.

The potential of LC-ICP-MS for trace metal speciation of non-volatile species has been widely discussed.[54,56] Of particular interest in the area of speciation analysis with LC-ICP-TOF-MS is the recent development of hyphenated isotope ratioing-based methods. The simultaneous extraction capability of ICP-TOF-MS makes it especially attractive for transient isotope ratios or isotope dilution measurements. Vázquez Peláez *et al*.[52] compared the characteristics of ICP-TOF-MS and quadrupole ICP-MS with respect to isotope ratio precision for elemental

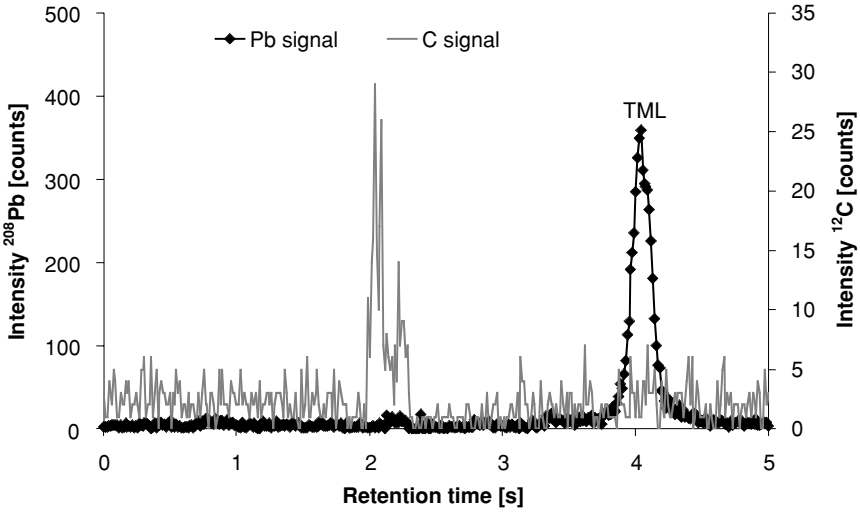

Figure 2.25 Shape of the TML peak obtained by multi-capillary GC-ICP-TOF-MS using an integration time of 12.75 ms.[45]

speciation measurements. The conclusion from this paper is that ICP-TOF-MS provides, not surprisingly, the better isotope ratio precision when many isotopes (more than 15) and isotope ratios are to be measured in the same rapid transient signal. Based on the advantages of ICP-TOF-MS for providing high-quality transient isotope ratio data, the combination of species-unspecific isotope dilution methods on-line with LC-ICP-TOF-MS has recently been exploited for Cd speciation in Sigma rabbit liver metallothionein isoforms[53] and for quantitative speciation of Cu, Zn and Cd in carp and eel cytosolic extracts.[43]

Recently, CE has gained widespread popularity as a powerful but simple technique for separation of a wide variety of compounds from large biomolecules to small metal species, because of its attractive features of high separation efficiency and minimal required sample volume (see Chapter 7 for further details about CE). Short transient peaks (with FWHM of 1–3 s or less) are becoming common in CE and very fast detectors are required to measure such very fast transients. Costa-Fernández *et al.*[41] demonstrated the suitability of ICP-TOF-MS for measurement of transient signals produced by CE separation of a mixture of several anionic species and negatively charged metal-cyanide complexes, with high precision (2–4% RSD) and good sensitivity (2–20 pg for 20 nL injection volume).

2.3.7.3 ETV sample introduction for ICP-TOF-MS

ETV, as a sample introduction method for ICP-MS elemental analysis, offers several advantages over conventional nebulisation systems. These advantages are related to higher analyte transmission efficiency, use of reduced sample volumes, achievement of very low detection limits and the ability to remove solvent and matrix components, which help in avoiding spectral and non-spectral interferences (see Chapter 3 for a detailed discussion of ETV-ICP-MS).

ETV devices generate a transient signal that has a typical duration of only a few seconds. Furthermore, elemental species with different volatilisation properties might be volatilised at different times within a fast transient profile. In such cases, the combination of an ETV sample introduction system with a detector capable of complete mass coverage and high temporal resolution, such as ICP-TOF-MS, can be employed for multi-elemental characterisation of individual ETV transients without spectral skew limitations. The performance of the coupling of ETV and ICP-TOF-MS for the quasi-simultaneous transient analysis of 34 elements was evaluated by Mahoney *et al*.[36] Isobaric overlaps were minimised by exploiting differences in the vaporisation characteristics of the elements. The dynamic range was found to be linear over a range of at least six orders of magnitude. Detection limits of 10–80 fg were obtained for Li, Mn, As, Ag, In, Au and Pb, based upon a 10 μL sample volume.

2.3.7.4 ICP-TOF-MS as detector for laser ablation

Considering the above-mentioned capabilities of ICP-TOF-MS for transient measurements in multi-elemental analysis, it can be concluded that ICP-TOF-MS is the detector of choice for laser ablation (LA), thanks to its simultaneous character. LA, as a sample introduction method for ICP-MS, offers the advantage of a simplified sample preparation technique without the need for sample decomposition prior to analysis. Although LA-ICP-MS has been increasingly used for the chemical analysis of solid materials over the last few years, a few research studies have been devoted to the area of direct LA of liquids. Bings[37] used the combination of direct LA with ICP-TOF-MS for rapid simultaneous multi-element determination of Na, Mg, Al, TI, Cr, Fe, Ni, Co, Cu, Ag and Pb in lubricant oil samples. As a consequence of the high data acquisition speed of the ICP-TOF-MS, an enormous amount of sample information could be collected within a short period of time from an oil sample volume of 300 μL (deposited in large sample vials to prevent most of the droplets formed from depositing on the walls of the ablation cell). Modification of the ablation cell (reduction of its volume by means of PTFE inserts) and elimination of the introduction of larger droplets into the transfer tubing (by placing a glass impactor behind the ablation cell) helped in the achievement of good detection limits (in the range of 0.5 ng/g (Pb) to 28 ng/g (Cr)), precisions (typically around 6% RSD) and accuracy (on the basis of the analysis of certified reference materials) with this method.

Leach and Hieftje[38] reported the use of single shot LA-ICP-TOF-MS as a powerful tool for the rapid identification of alloy samples. In this work, identification was based on the direct comparison of relative per cent composition values, measured for all elements simultaneously within a cloud of ablated particles, with certified concentrations. For the 18 standards used to validate the technique, samples were identified with a 93% success rate.

References

1. Leach, A. M., Heisterkamp, M., Adams, F. C., and Hieftje, G. M. (2000) Gas chromatography-inductively coupled plasma time-of-flight mass spectrometry for the speciation analysis of organometallic compounds. *J. Anal. At. Spectrom.*, **15**, 151.
2. Allen, L. A., Prang, H. M., Warren, A. R., and Houk, R. S. J. (1995) Simultaneous measurement of isotope ratios in solids by laser ablation with a twin quadrupole inductively coupled plasma mass spectrometer. *J. Anal. At. Spectrom.*, **10**, 267.

3. Allen, L. A., Warren, A. R., Prang, H. M., and Houk, R. S. J. (1997) Precise measurement of ion ratios in solid samples using laser ablation with a twin quadrupole inductively coupled plasma mass spectrometer. *J. Anal. At. Spectrom.*, **12**, 171.
4. Allen, L. A., Leach, J. J., and Houk, R. S. J. (1997) Spatial location of the space charge effect in individual ion clouds using monodisperse dried microparticulate injection with a twin quadrupole inductively coupled plasma mass spectrometer. *Anal. Chem.*, **69**, 2384.
5. Belshaw, N. S., Freedman, P. A., O'Nions, R. K., Frank, M., and Guo, Y. (1998) A new variable dispersion double-focusing plasma mass spectrometer with performance illustrated for Pb isotopes. *Int. J. Mass Spectrom.*, **181**, 51.
6. Walder, A. J. and Freedman, P. A. (1992) Isotopic ratio measurement using a double focusing magnetic sector mass analyzer with an inductively coupled plasma as an ion source. *J. Anal. At. Spectrom.*, **7**, 571.
7. Walder, A. J. and Furuta, N. (1993) High-precision lead isotope ratio measurement by inductively coupled plasma multiple collector mass spectrometry. *Anal. Sci.*, **9**, 675.
8. Heumann, K. G., Gallus, S. M., Rädlinger, G., and Vogl, J. (1998) Precision and accuracy in isotope ratio measurements by plasma source mass spectrometry. *J. Anal. At. Spectrom.*, **13**, 1001.
9. Halliday, A. N., Christensen, J. N., Lee, D. -C., Hall, C. M., Luo, X., and Rehkamper, M. (2000) Multiple-collector inductively coupled plasma mass spectrometry. In: *Inorganic Mass Spectrometry* (eds C. M. Barshick, D. C. Duckworth and D. H. Smith), Marcel Dekker, New York, p. 291.
10. Burgoyne, T. W., Hieftje, G. M., and Hites, R. A. (1997) Design and performance of a plasma-source mass spectrograph. *J. Am. Soc. Mass Spectrom.*, **8**, 307.
11. Hieftje, G. M., Myers, D. P., Li, G., Mahoney, P. P., Burgoyne, T. W., Ray, S. J., and Guzowski, J. P. (1997) Toward the next generation of atomic mass spectrometers. *J. Anal. At. Spectrom.*, **12**, 287.
12. Duckworth, D. C. and Barshick, C. M. (1998) Ion traps: what do they hold for elemental mass analysis? *Anal. Chem.*, **70**, 709.
13. Milgram, K. E., White, F. M., Goodner, K. L., Watson, C. H., Koppenaal, D. W., Barinaga, C. J., Smith, B. H., Winefordner, J. D., Marshall, A. G., Houk, R. S., and Eyler, J. R. (1997) High-resolution inductively coupled plasma Fourier transform ion cyclotron resonance mass spectrometry. *Anal. Chem.*, **69**, 3714.
14. Vanhaecke, F., Moens, L., Dams, R., Allen, L., and Georgitis, S. (1999) Evaluation of the isotope ratio performance of an axial time-of-flight ICP mass spectrometer. *Anal. Chem.*, **71**, 3297.
15. Emteborg, H., Tian, X., Ostermann, M., Berglund, M., and Adams, F. C. (2000) Isotope ratio and isotope dilution measurements using axial inductively coupled plasma time of flight mass spectrometry. *J. Anal. At. Spectrom.*, **15**, 239–46.
16. Myers, D. P., Mahoney, P. P., Li, G., and Hieftje, G. M. (1995) Isotope ratios and abundance sensitivity obtained with an inductively coupled plasma-time-of-flight mass spectrometer. *J. Am. Soc. Mass Spectrom.*, **6**, 920.
17. Sturgeon, R. E., Lam, J. W. H., and Saint, A. (2000) Analytical characteristics of commercial orthogonal acceleration time-of-flight ICP mass spectrometry. *J. Anal. At. Spectrom.*, **15**, 607.
18. Tian, X., Emteborg, H., and Adams, F. C. (1999) Analytical performance of axial inductively coupled plasma time of flight mass spectrometry. *J. Anal. At. Spectrom.*, **14**, 1807.
19. Ray, S. J. and Hieftje, G. M. (2001) Mass analysers for inductively coupled plasma time-of-flight mass spectrometry. *J. Anal. At. Spectrom.*, **16**, 1206.
20. Guilhaus, M. (2000) Essential elements of time-of-flight mass spectrometry in combination with the inductively coupled plasma ion source. *Spectrochim. Acta B*, **55**, 1511.

21. Myers, D. P. and Hieftje, G. M. (1993) Preliminary design considerations and characteristics of an inductively coupled plasma time-of-flight mass spectrometer. *Microchem. J.*, **48**, 259.
22. Myers, D. P., Li, G., Mahoney, P. P., and Hieftje, G. M. (1995) An inductively coupled plasma time-of-flight mass spectrometer for elemental analysis: part II. Direct current quadrupole lens system for improved analytical performance. *J. Am. Soc. Mass Spectrom.*, **6**, 400.
23. Myers, D. P., Li, G., Yang, P., and Hietfje, G. M. (1994) An inductively coupled plasma time-of-flight mass spectrometer for elemental analysis: part I. Optimisation and characteristics. *J. Am. Soc. Mass Spectrom.*, **5**, 1008.
24. Bandura D. and Peile, R. (1997) XXX Colloquium Spectroscopicum Internationale, Paper 227, Melbourne, Australia.
25. Davis, S., Bandura, D., Hoffman, A. D., and Makarov, A. A. (1998) WIPO Patent WO9840907A1.
26. Vlasak, P. R., Beussman, D. J., Davenport, M. R., and Enke, C. G. (1996) An interleaved comb ion deflection gate for m/z selection in time-of-flight mass spectrometry. *Rev. Sci. Instrum.*, **67**, 68.
27. Carrión, M. Castillo, Andrés, J. Reyes, Rubí, J. A. Martín, and Emteborg, H. (2003) Performance optimisation of isotope ratio measurements in transient signals by FI-ICP-TOFMS. *J. Anal. At. Spectrom.*, **18**, 437.
28. Benkhedda, K., Infante, H. G., and Adams, F. C. (2004) Determination of total lead and lead isotope ratios in natural waters by inductively coupled plasma time-of-flight mass spectrometry after flow injection on-line preconcentration. *Anal. Chim. Acta*, **506**, 137.
29. Willie, S. N. and Sturgeon, R. E. (2001) Determination of transition and rare earth elements in seawater by flow injection inductively coupled plasma time-of-flight mass spectrometry. *Spectrochim. Acta B*, **56**, 1707.
30. McClenathan, D. M., Ray, S. J., and Hieftje, G. M. (2001) Novel flow injection strategies for study and control of matrix interferences by inductively coupled plasma time-of-flight mass spectrometry. *J. Anal. At. Spectrom.*, **16**, 987.
31. Benkhedda, K., Infante, H. G., Ivanova, E., and Adams, F. C. (2001) Determination of sub-parts-per-trillion levels of rare earth elements in natural waters by inductively coupled plasma time-of-flight mass spectrometry after flow injection on-line preconcentration in a knotted reactor. *J. Anal. At. Spectrom.*, **16**, 995.
32. Benkhedda, K., Infante, H. G., Ivanova, E., and Adams, F. C. (2000) Trace metal analysis of natural waters and biological samples by axial inductively coupled plasma time-of-flight mass spectrometry (ICP-TOFMS) with flow injection on-line adsorption preconcentration using a knotted reactor. *J. Anal. At. Spectrom.*, **15**, 1349.
33. Centineo, G., Bayon, M. M., and Sanz-Medel, A. (2000) Flow injection analysis with inductively coupled plasma time-of-flight mass spectrometry for the simultaneous determination of elements forming hydrides and its application to urine. *J. Anal. At. Spectrom.*, **15**, 1357.
34. Benkhedda, K., Dimitrova, B., Infante, H. G., Ivanova E., and Adams, F. C. (2003) Simultaneous on-line preconcentration and determination of Pt, Rh and Pd in urine, serum and road dust by flow injection combined with inductively coupled plasma time-of-flight mass spectrometry. *J. Anal. At. Spectrom.*, **18**, 1019.
35. Benkhedda, K., Infante, H. G., Ivanova, E., and Adams, F. C. (2002) Inductively coupled plasma mass spectrometry for trace analysis using flow injection on-line preconcentration and time-of-flight mass analyser. *Trends Anal. Chem.*, **21**, 332.
36. Mahoney, P. P., Ray, S. J., Li, G., and Hieftje, G. M. (1999) Preliminary investigation of electrothermal vaporisation sample introduction for inductively coupled plasma time-of-flight mass spectrometry. *Anal. Chem.*, **71**, 1378.

37. Bings, N. H. (2002) Direct determination of metals in lubricating oils by laser ablation coupled to inductively coupled plasma time-of-flight mass spectrometry. *J. Anal. At. Spectrom.*, **17**, 759.
38. Leach, A. M. and Hieftje, G. M. (2002) Identification of alloys using single shot laser ablation inductively coupled plasma time-of-flight mass spectrometry. *J. Anal. At. Spectrom.*, **17**, 852.
39. Leach, A. M. and Hieftje, G. M. (2002) Factors affecting the production of fast transient signals in single shot laser ablation inductively coupled plasma mass spectrometry. *Appl. Spectrosc.*, **56**, 62.
40. Bleiner, D., Hametner, K., and Gunther, D. (2000) Optimisation of a laser ablation-inductively coupled plasma "time of flight" mass spectrometry system for short transient signal acquisition. *Fresenius' J. Anal. Chem.*, **368**, 37.
41. Costa-Fernández, J. M., Bings, N. H., Leach, A. M., and Hieftje, G. M. (2000) Rapid simultaneous multielemental speciation by capillary electrophoresis coupled to inductively coupled plasma time-of-flight mass spectrometry. *J. Anal. At. Spectrom.*, **15**, 1063.
42. Ferrarelo, C. N., de la Campa, Fernández, M. R., and Sanz-Medel, A. (2002) Multielement trace-element speciation in metal-biomolecules by chromatography coupled with ICP-MS. *Anal. Bioanal. Chem.*, **373**, 412.
43. Infante, H. Goenaga, Van Campenhout, K., Schaumlöffel, D., Blust, R., and Adams, F. C. (2003) Multi-element speciation of metalloproteins in fish tissue using size-exclusion chromatography coupled "on-line" with ICP-isotope dilution-time-of-flight mass spectrometry. *Analyst*, **128**, 651.
44. Infante, H. Goenaga, Van Campenhout, K., Blust, R., and Adams, F. C. (2002) Inductively coupled plasma time-of-flight mass spectrometry coupled to high-performance liquid chromatography for multi-elemental speciation analysis of metalloproteins in carp cytosols. *J. Anal. At. Spectrom.*, **17**, 79–87.
45. Infante, H. Goenaga, Heisterkamp, M., Benkhedda, K., Van Campenhout, K., Blust R., and Adams, F. C. (2001) ICP-TOF-MS for rapid simultaneous multi-element analysis in fast transient signals. *Spectra Anal.*, **220**, 23.
46. Jitaru, P., Infante, H. Goenaga, and Adams, F. C. (2003) Multicapillary gas chromatography coupled to inductively coupled plasma-time-of-flight mass spectrometry for rapid mercury speciation analysis. *Anal. Chim. Acta*, **489**, 45.
47. Heisterkamp, M. and Adams, F. C. (2001) Gas chromatography inductively coupled plasma time-of-flight mass spectrometry for the speciation analysis of organolead compounds in environmental water samples. *Fresenius' J. Anal. Chem.*, **370**, 597.
48. Bings, N. H., Costa-Fernández, J. M., Guzowski, J. P., Leach, A. M., and Hieftje, G. M. (2000) Time-of-flight mass spectrometry as a tool for speciation analysis. *Spectrochim. Acta B*, **55**, 767.
49. Infante, H. Goenaga, Heisterkamp, M., Van Campenhout, K., Tian, X., Blust, R., and Adams, F. (2001) *Plasma Source Mass Spectrometry: The New Millennium* (eds J. G. Holland and S. D. Tanner), The Royal Society of Chemistry, Cambridge, UK, p. 369.
50. Heisterkamp, M., Van De Velde, K., Ferrari, C., Boutron, C. F., and Adams, F. C. (1999) Present century record of organolead pollution in high altitude alpine snow. *Environ. Sci. Technol.*, **33**, 4416.
51. Baena, J. R., Gallego, M., Valcárcel, M., Leenaers, J., and Adams, F. C. (2001) Comparison of three coupled gas chromatographic detectors (MS, MIP-AES, ICP-TOFMS) for organolead speciation analysis. *Anal. Chem.*, **73**, 3927.
52. Vázquez Peláez, M., Costa -Fernández, J. M., and Sanz-Medel, A. (2002) Critical comparison between quadrupole and time-of-flight inductively coupled plasma mass spectrometers for isotope ratio measurements in elemental speciation. *J. Anal. At. Spectrom.*, **17**, 950.

53. Ferrarelo, C. N., Encinar, Ruiz, J., Centineo, G., Alonso, J. I. García, de la Campa, M. R. Fernández, and Sanz-Medel, A. (2002) Comparison of three different ICP-MS instruments in the study of cadmium speciation in rabbit liver metallothionein-1 using reversed-phase HPLC and post-column isotope dilution analysis. *J. Anal. At. Spectrom.*, **17**, 1024.
54. Infante, H. G. and Adams, F. C. (2001) Inductively coupled plasma ion source for LC-MS. LC GC Europe, Guide to LC-MS, p. 36.
55. Infante, H. G., Cuyckens, F., Van Campenhout, K., Blust, R., Claeys, M., Van Vaeck, L., and Adams, F. C. (2004) Characterisation of metal complexes with metallothioneins in the liver of the carp Cyprinus carpio by reversed-phase HPLC with ICP-MS and electrospray ionisation (ESI)-MS. *J. Anal. At. Spectrom.*, **19**, 159.
56. Leach, A. M., McClenathan, D. M., and Hieftje, G. M. (2003) Plasma source time- of-flight mass spectrometry: a powerful tool for elemental speciation *Handbook of Elemental Speciation: Techniques and Methodology* (eds R. Cornelis, J. Caruso, H. Crews, and K. Heumann), John Wiley & Sons, New York, Chap 5.4, p. 313.

2.4 ION TRAP MASS SPECTROMETRY

Gregory C. Eiden

2.4.1 Introduction

Over the past two decades, ICP-MS has matured to the point that most elements can be determined at part-per-trillion or lower concentrations.[1] Hallmarks of ICP-MS include high sensitivity, instrumental flexibility and the ability to measure most elements rapidly from a single scan. The inductively coupled plasma (ICP) ion source has been successfully interfaced to most conventional mass analysers, the linear quadrupole mass filter being the most common in commercial ICP-MS instruments. ICP ion sources have been coupled to magnetic sector field mass analysers[2] and, more recently, to time-of-flight (TOF) mass analysers[3,4]. In this chapter, the interfacing of the ICP to ion trap mass spectrometers of both the RF quadrupole ion trap type[5–18] and the Fourier transform ion cyclotron resonance (FTICR) ion trap design[19] is discussed. Most of the reported work on ICP ion trap MS has been based on the RF quadrupole ion trap, or Paul trap, and the design, operation and performance of these devices are the main focus of this chapter.

The chemistry, physics and engineering communities have employed RF (radiofrequency) and magnetic ion trap devices for measurement of atomic, molecular, physical and chemical properties for nearly 50 years. Most studies by chemists have dealt with molecular ions and their structural examination and reaction chemistry.[20–24] Of all the research conducted using ion traps, relatively little has focused on analytical atomic spectroscopy. Blades and co-workers reported the use of ion traps for *in situ* measurement of laser ablated ions in 1991 and later.[25,26] Experiments incorporating a glow discharge ion source with an ion trap were subsequently reported by the Oak Ridge research group.[27,28] Paul traps have also been utilized for storage and study of large, even macroscopic, particles. With large particles, the force of gravity cannot always be ignored (as is done in atomic/molecular mass spectrometry) and an electrostatic field is necessary to keep the particles suspended. For this reason, these traps are sometimes referred to as 'electrodynamic balances'.[29,30] Laser desorption of individual particles levitated in a trap followed by mass spectrometric detection of desorbed atomic ions has been reported by Ramsey and co-workers.[31] Investigators at Los Alamos National Laboratory have used resonant laser

ablation techniques to ablate and selectively ionize metallic constituents into an ion trap for detection and analysis.[32]

2.4.2 RF Quadrupole Ion Traps

2.4.2.1 Introduction and history

The RF quadrupole ion trap, or 'Paul' trap, has been known for a little over 50 years and applied in numerous fields of chemistry, physics and engineering. Detailed, authoritative descriptions of the RF quadrupole ion trap have appeared in two excellent books, by March and Hughes[21] and Todd.[33] A Paul trap is typically formed using cylindrically symmetrical electrodes whose 'trapping' surfaces are hyperboloids of revolution. There is a 'ring' electrode and two 'endcap' electrodes, as shown in Figure 2.26. The trapping field is typically formed by application of an RF potential to the 'ring' electrode. The endcaps are typically grounded with respect to this RF trapping potential (smaller RF potentials are often applied to the endcaps to affect various motions of the trapped ions). The goal is to form a quadrupolar field near the center of the trap. In such a field, ions execute simple harmonic motion due to a restoring force that is linear with displacement of the ion from the center of the trap. Higher order fields such as

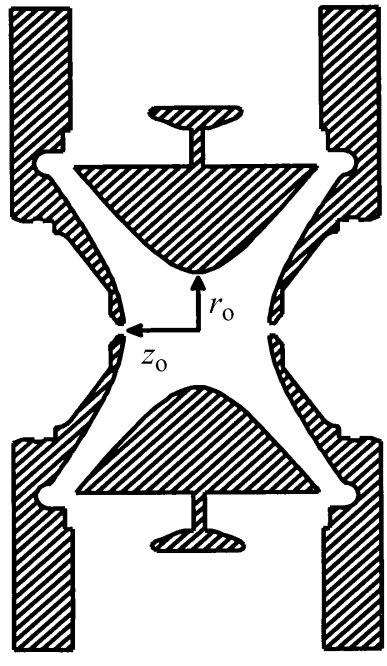

Figure 2.26 Ion trap electrodes. A cross-sectional view of the cylindrically symmetric electrodes from a Finnigan LCQ™ ion trap is shown. The symmetry axis coincides with the line labelled 'z_0'. In the ICP-MS ion trap instruments, ions are injected through a hole in the center of one endcap electrode (left side of figure) and ions are mass-selectively ejected from the opposite endcap electrode where they are detected

hexapolar or octopolar result in much more complex motions and the conditions leading to stable confinement are generally less obvious. The higher order fields can be tailored to produce advantageous effects such as improved mass resolution. Real trapping fields include components with all of these symmetries, and more; however, the dominant component in the Paul trap is quadrupolar.

Commercialization of the Paul trap was greatly aided by the pioneering work of George Stafford and co-workers at Finnigan Corporation, now Thermo Electron (San Jose, CA), who developed analytically useful methods to 'scan' ions out of the trap and generate high-quality mass spectra.[34] Recognition of the importance of these devices was reinforced in 1989 when the Nobel Prize in physics was awarded to Wolfgang Paul and Hans Dehmelt for their development of the RF quadrupole ion trap. The Pacific Northwest National Laboratory's (PNNL) use of ion trap technology began around 1991 with preliminary studies of how an ICP ion source might be coupled to a Paul trap. In the course of about 8 years, PNNL reported extensive results using three generations of prototype ICP-ion trap instruments.[5–16] All three instruments were built using slightly modified commercial ion trap mass spectrometers from Finnigan.

Before describing the theory behind ion traps and proceeding with the details of their operation, it is useful to consider how an ion trap is used in an ICP-MS instrument. Figure 2.27 shows PNNL's first and second generation plasma source ion trap (PSIT) instruments, PSIT-I and PSIT-II.

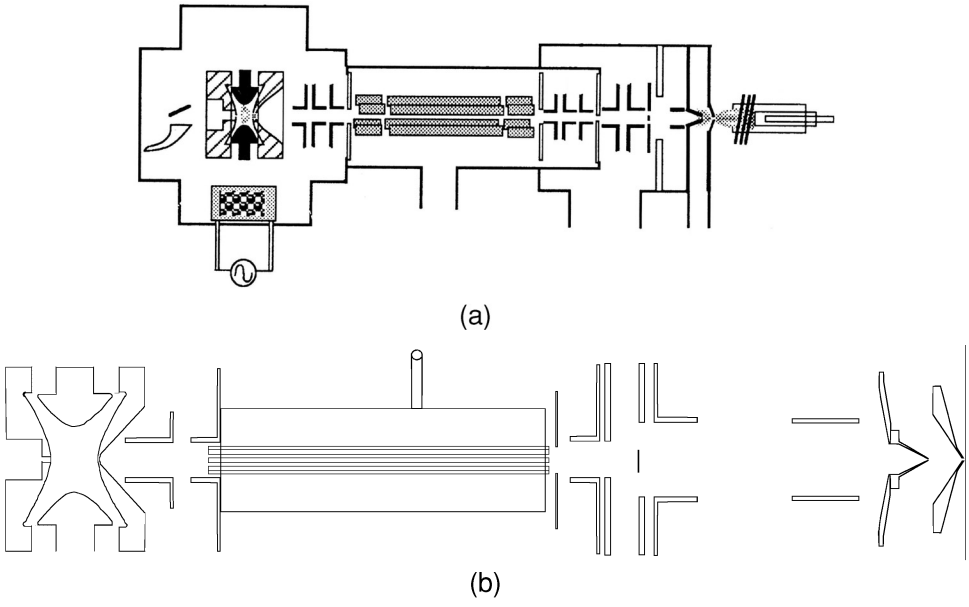

Figure 2.27 (a) Schematic diagram of the first generation plasma source ion trap instrument at PNNL (PSIT-I) showing the ICP interface, DC optics, quadrupole mass filter, gate optics and ion trap. (b) Schematic diagram of the second generation plasma source ion trap instrument at PNNL (PSIT-II) showing the ICP interface, DC optics, RF multipole ion guide/collision cell and ion trap.

Ions are transferred from the atmospheric pressure ICP into the high vacuum chamber of the mass spectrometer via a differential pumping interface. The ions are formed into a beam

by conventional ICP-MS ion optics and focused onto the center hole of one of the ion trap endcap electrodes. The timing of ion injection into the trap is controlled by gating the potential applied to the ion optics. Ions are typically injected for a long period of time (tens to hundreds of milliseconds) in order to allow accumulation of the less abundant ions, corresponding to the trace and ultratrace components of the sample, which are usually of analytical interest. Following ion injection, various ion isolation techniques may be applied in order to selectively remove unwanted ions from the trap prior to generating the mass spectrum. These selective ion trapping or ejection methods can also be applied during the ion accumulation step, thereby reducing space charge effects during the trapping stage. Once the ions of interest have been accumulated in the ion trap, the RF trapping potential is slowly ramped causing ion ejection in order of m/z. This sequence of events is known as a 'scan function' and a typical PSIT scan function is shown in Figure 2.28.

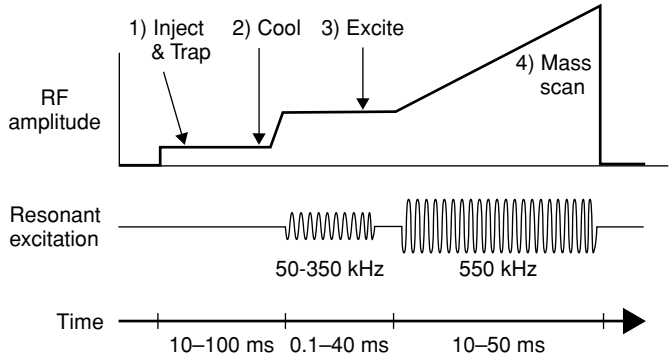

Figure 2.28 Ion trap scan function. The sequence of events used to generate a mass spectrum in a typical Paul trap is shown. This sequence is typically repeated many times with the individual spectra summed or averaged to produce the final spectrum. The generic parts of the scan function shown include: (1) ion injection and trapping, (2) ion relaxation/cooling, (3) auxiliary excitation for selective ejection/storage of desired ions and (4) mass-selective instability scan. The timing of the resonant excitation function is also indicated; two sine waves shown indicate a first pulse for selective excitation and a second pulse for enhancing the mass selective instability scan

Many variations on ion trap scan functions are known and utilized for all manner of ion manipulation and detection: collisionally induced dissociation (CID), selective ejection or trapping, high mass resolution, ion reaction, chemically selective excitation of motion via the 'mass shift', etc. The interested reader is referred to the significant ion trap literature already cited.

2.4.2.2 Equations of motion of trapped ions

The differential equations describing the forces acting on the trapped particles have been developed and discussed in detail. A summarized version of the derivation given by Todd[33] is presented here. The equations of motion are of the form

$$\frac{m}{e}\ddot{u} - 2(U - V\cos\Omega t)\frac{u}{r_0^2} = 0 \tag{2.4.1}$$

where m and e are the ion's mass and charge, respectively, U is the DC potential applied to the ring electrode, V and Ω are the amplitude and frequency, respectively, of the RF potential applied to the ring electrode, u is a spatial dimension (x, y or z), and r_0 is the radius of the ring electrode. This equation ignores gravitational forces and viscous drag forces due to any gas present in the trap. These forces cannot be ignored when large particles are considered[30]. Equation 2.4.1 is an example of the Mathieu equation, which has the general form:

$$\frac{d^2u}{d\xi^2} + (a_u + 2q_u \cos 2\xi)u = 0 \tag{2.4.2}$$

From the cylindrical symmetry of the ion trap, x and y are combined into a radial component r such that one Mathieu equation is obtained for r and one for the z direction of motion. The solutions to the Mathieu equation are parameterized by a and q; one such pair of parameters is obtained for z and one pair for r. The physical meaning of these parameters is important: their magnitude and sign determine whether an ion is stably trapped or not and if stably trapped, they quantify the energetics and dynamics of the trapped ion. The parameters are given by:

$$a_z = -2a_x = -2a_y = -2a_r = -\frac{16eU}{m\left(r_0^2 + 2z_0^2\right)\Omega^2} \tag{2.4.3}$$

$$q_z = -2q_x = -2q_y = -\frac{8eV}{m\left(r_0^2 + 2z_0^2\right)\Omega^2} \tag{2.4.4}$$

Equation (2.4.4) is typically rearranged to give a more useful form

$$\left(\frac{m}{e}\right)_{\max} = \frac{8eV_{\max}}{q_{\mathrm{ej}}\left(r_0^2 + 2z_0^2\right)\Omega^2} \tag{2.4.5}$$

These equations relate the experimental parameters (RF potential and frequency, trap radius and endcap spacing) to the Mathieu parameters, a and q. In equation (2.4.5), q_{ej} is the value of the q parameter at which ion ejection occurs, typically 0.908. For $a = 0$, this value of q corresponds to the right-hand edge of the stability region (Figure 2.29). The motion of trapped ions is such that only certain combinations of a and q result in stable trapping of ions. The (a, q) space has an infinite number of 'islands of stability'; however, only the stability regions closest to the origin are of practical interest. For the mass-to-charge ratios of interest in elemental/isotopic mass spectrometry, the other stability regions require inordinately large RF or DC potentials to be generated and applied to the electrodes. Figure 2.29 (adapted from[35]) shows the characteristic shape of the first stability region. Note that this same diagram also applies to linear quadrupole filters, a two-dimensional version of the Paul trap in which ion motion is governed by the same Mathieu equations.[36]

2.4.2.3 Useful formulas

The development of the RF quadrupole ion trap into a mass spectrometer has resulted in a great deal of detailed, practical operating knowledge. Thus, in addition to extensive literature on the fundamental physics of ion motion in such fields, significant knowledge has also been accumulated regarding the practical use of ion traps as mass selective ion reactors and mass

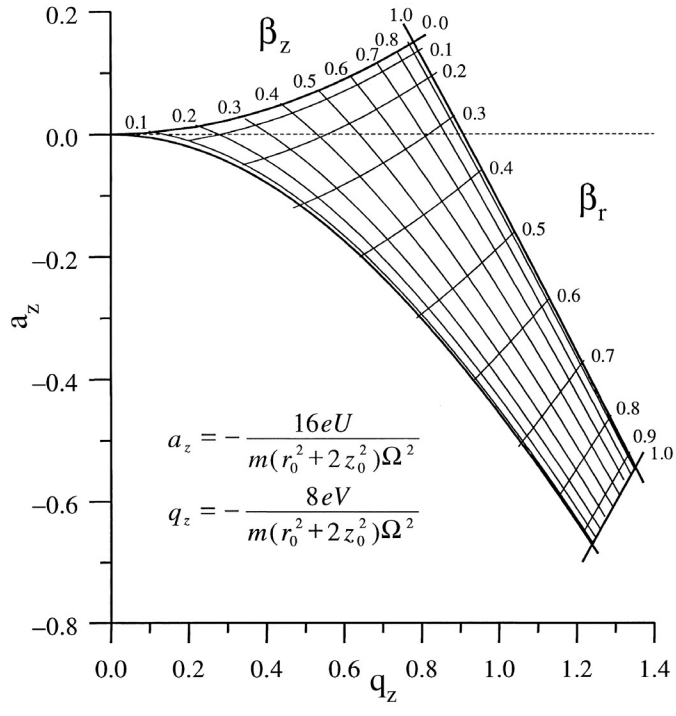

Figure 2.29 First stability region. (a, q) values inside the boundaries of the region shown correspond to stable trapping conditions. Note that for a given geometry and trapping field strength, different m/z ions will lie in different areas of the stability region due to the mass dependence of the a and q parameters. The motion and energy of trapped ions are strongly dependent on where they lie inside this stability region

spectrometers. A few equations are briefly summarized here; for greater detail and completeness, the interested reader is referred to the volumes by March and Todd and by March and Hughes.

Resonance excitation of trapped ions is used extensively (see below) and is possible because in a quadrupole field, the trapped ions behave as simple harmonic oscillators (SHO's), which can be 'driven' by suitable application of an RF field at a frequency related to the secular frequency of the oscillating ion. The approximate frequency of motion for such an oscillator is given by (see March and Hughes equation (3.2)):

$$\omega_0 = \beta\Omega/2 \ (r \text{ or } z) \tag{2.4.6a}$$

$$= \mathrm{q}\Omega/2\sqrt{2} \tag{2.4.6b}$$

where β is given to a good approximation by (see March and Hughes, equations (3.54) and (3.12)):

$$\beta = [q^2/(2-q^2) - (1/128)(7q^4 - (29/18)q^6)]^{1/2} \tag{2.4.7a}$$

$$+\text{higher order terms} \quad (\text{for } a = 0)$$

$$\sim [a + q^2/2]^{1/2} \tag{2.4.7b}$$

2.4.3 Features of RF quadrupole ion trap mass spectrometers

The basic features of an RF quadrupole ion trap mass spectrometer will now be listed briefly, following the outline of Prof. J. F. J. Todd in his excellent, three-volume monograph on 'practical aspects of ion trap mass spectrometry'.[33]

2.4.3.1 Mass-selective ion ejection

Prior to the development of practical means for mass selective ion ejection to generate mass spectra, ion traps were used as 'test tubes' for ions, storage devices for study of the trapped ions. A collection of trapped ions of various mass-to-charge ratios can be ejected in order of their m/z values by slowly ramping up the magnitude of the RF potential. This has the effect of increasing the q value for each trapped ion. As each ion's q value approaches the edge of the stability region (at $q = 0.908$, along the $a = 0$ axis in Figure 2.29), the ion becomes unstable. However, the instability of the ion's motion is not random, but rather, the ion begins to oscillate in the z-direction. As the RF potential is ramped up further and the q value reaches 0.908, the ion's z-direction motion causes the ion to leave the trapping field along the z-axis in both the positive and negative directions. Holes in the endcap electrode allow the ions to escape where they are typically detected using a conversion electrode (ions strike a surface that responds with the emission of secondary electrons) and electron multiplier to amplify the ion current.

2.4.3.2 Buffer gas

Early in the development of the ion trap mass spectrometer, an important application of the device was as a detector for gas chromatography. Through this work, it was discovered that unlike virtually all other mass separators, ion traps work better with a small amount of gas present, incidentally introduced by the GC carrier gas. In other mass analysers, the presence of residual gases leads to scattering of the ions away from their desired trajectories in the mass separator and to a degradation in mass spectrometer performance. In an ion trap, the presence of a small amount of low molecular weight gas causes this same scattering, but in concert with the trapping field, these scattering collisions cause the ions to slowly lose kinetic energy (ions typically have significant kinetic energy left over from the ion formation process) and the trapped ion cloud 'cools' toward the center of the ion trap. This lower energy ion cloud, located nearer to the center of the ion trap, can be excited or ejected with much higher m/z resolution.

2.4.3.3 Stretched geometry and axial modulation

Finnigan developed a novel 'stretched' geometry ion trap, which they kept as a trade secret for many years. In 1992, it was announced that Finnigan's ion traps were stretched 10.8% in the z-direction (10.8% greater endcap electrode separation than the purely quadrupolar value in which $r_0^2 = 2z_0^2$). This modification solved an early problem encountered with the ideal, quadrupolar geometry ion trap, namely, a mass shift: molecular ions with different structures, but the same nominal m/z, could be ejected at a slightly different q-value. The main effect of this stretching is to add a significant octopolar component to the otherwise quadrupolar trapping

field. Axial modulation refers to the application of a low-amplitude (typically 1–10 Vpp) RF potential to the endcap electrodes at a frequency of about half that of the main trapping RF potential. The effect of this field is to greatly sharpen the spectra by narrowing the range of trapping RF potential (q value) over which ions of a given m/z are ejected.

2.4.3.4 High resolution

It has been observed that by slowing down the rate at which the trapping RF field amplitude is ramped for ion ejection, the mass spectral resolution increases. In addition, if the endcap and ring RF potentials are phase synchronized (and synchronized with the main instrument 50–60 Hz AC power), truly remarkable mass resolution can be achieved.[37] It is noteworthy that this increase in resolution does not come at the expense of ion signal. In fact, signal intensity is dramatically increased at the same time that resolution is increased. For many of the polyatomic interferences encountered in ICP-MS, only modest resolution is required to separate the interfering ion species from the analyte ions of interest.

2.4.3.5 Ion injection

The most common ionization methods employed in ion trap mass spectrometry involve formation of the ions to be detected inside the ion trap. However, certain ion sources must be located outside of the ion trap electrode structure, e.g., plasma sources requiring supporting electrodes or gases such as the ICP. Other ion sources such as laser desorption/ionization sources have been located both internal (typically at one of the trapping electrode surfaces) to the trap and external. External generation of ions requires that ions be transferred efficiently into the ion trap in such a way that they become trapped. It is beyond the scope of this text to give any detail, but the essential considerations in efficiently transferring ions into a trap concern formation of the right beam shape, energy and, for pulsed ion sources, phase of the ion pulse with respect to the RF trapping field.

2.4.3.6 Space charge effects

Ion traps have an Achilles heel in that the mutual Coulombic repulsion of trapped ions greatly complicates their motion and typically degrades mass spectrometer performance. The main effect of a high net charge density in an ion trap mass spectrometer is a broadening of the spectral lines. Schwartz *et al.* have pointed out that, depending on one's criteria, various space charge limits for an ion trap can be defined.[38] The ultimate space charge limit occurs when the repulsive potential generated by the trapped ion cloud just matches the trapping field potential well depth. At this space charge limit, no additional ions can be trapped. For the early commercial ion traps, this limit is $\sim 1 \times 10^7$ ions. However, the ion trap ceases to function as a useful mass spectrometer at much lower space charge limits than this. Schwartz *et al.* describe space charge limits thus: 'storage', the ultimate limit just described; 'spectral', how many ions can be in the trap and still produce quality spectra (mass accuracy and resolution); 'isolation', how many ions can be in the trap and still effect efficient isolation of ions of interest; 'activation', how many ions can be in the trap and still produce representative product ion spectra.

2.4.4 Selective ion trapping methods

2.4.4.1 'Low mass cut-off' and other stability edges

The most straightforward method with which one achieves mass selective storage of ions in a Paul trap is to simply raise the trapping field potential high enough to exclude ions below the 'low-mass cut-off', as given in equation (2.4.5) above. Eiden *et al.* showed that by excluding Ar^+ ions from the ion trap in this way, chemical ionization background could be significantly suppressed[7,8,10]. In earlier work by the same group, it was shown that a quadrupole mass filter placed ahead of the ion trap could be used to 'notch filter' selected ions or groups of ions from the beam prior to their entering the ion trap.[5,16,39] In this way, deleterious effects of certain ions, e.g., chemical ionization by Ar^+ and other intense plasma ion beams, could be avoided.

Since the same equations of motion are involved, a Paul trap can be operated in a 'filter' mode in the same way as quadrupole mass filters are operated. This is done by adding a DC component to the RF trapping field. This brings the operating point of the trap closer to the upper apex of the first stability region (see Figure 2.29). If the DC is raised sufficiently, at the correct RF field, a given mass-to-charge-ratio ion can be brought very near to this apex such that it is the only m/z stably trapped. In a quadrupole mass filter, there is a special combination of RF and DC for each ion that results in only that ion being 'trapped' – actually, in the two-dimensional filter, the ions are not trapped, but are transmitted through the quadrupole, but only a single m/z can be transmitted if the operating point is appropriately near the stability diagram's apex. By moving away from this apex somewhat (lowering the DC portion of the trapping field), the width of this pass-band can be increased to an arbitrary magnitude. Thus, for example, one could transmit simultaneously (or trap simultaneously for the Paul device) all the isotopes of a given element and thereby limit detection, reaction or other processes only to those ions.

Other means of excluding ions of various m/z have been devised and the interested reader is referred to the text by March and Hughes.[21]

2.4.4.2 Resonance excitation of trapped ion motion

Trapped ions behave like oscillators and each unique m/z possesses unique resonances in its frequency of motion. The full details of the kinds of motions and resonances are beyond the scope of this text; the interested reader is referred to[40–43]. However, it is important to note a few features of this resonance behavior. First, resonances in ion motion can be strongly excited by supplementing the trapping RF field with a second RF field at the resonance frequency of a given ion. Resonance motion can be excited to such a degree that collisions between the ions and the background gas (buffer gas, reagent gas or impurity gases) can lead to dissociation of the trapped ions. Second, ions can be ejected from the trap via resonance excitation. Moreover, by applying an RF field with multiple frequency components, an arbitrary set of different specific ions can be simultaneously excited in their motion. This is a powerful method for removing any desired ion m/z or range of m/z from the ion trap prior to detection of the ions. Last, endothermic ion–molecule reactions can be driven by increasing the trapped ions' kinetic energy via resonant excitation. An example of this was shown by Eiden *et al.* using the $Ta^+ + O_2$ reaction.[15]

(a) Single frequency excitation

The quadrupolar field of the ion trap exerts a restoring force on ions near its center that is linear with respect to displacement from the trap's center. This results in simple harmonic motion.

Trapped ions possess a 'secular' oscillatory motion whose frequency is given approximately by the well-known SHO equation.[44] This same motion can be excited to larger amplitudes by application of an RF potential to the endcap electrodes at the harmonic frequency. By excitation of this motion, molecular ions can attain sufficient internal energy via collisions with the buffer gas to dissociate. Since the secular frequency of an ion depends on its mass-to-charge ratio, such excitations can also be used to eject specific m/z ions from the trap. An ion trapped without buffer gas is an undamped oscillator whose motion is described by the SHO equation. Addition of buffer gas dampens this motion somewhat. Addition of an RF potential at the secular frequency drives the ion motion. The result is that the ion can be described as a damped, driven, harmonic oscillator. Such behavior has been extensively studied in RF quadrupole ion traps.[10,42,45–48]

The dynamic range of the PSIT is limited by the large numbers of ions associated with the sample matrix and ICP plasma. These typically occur at m/z values such that they are efficiently ejected via broadband (or narrower passband) excitation without affecting the analyte ions of interest. If a single, intense ion peak is to be ejected, a single frequency excitation waveform (typically a sinewave) can be used. An example of a single intense 'background' ion being ejected selectively with respect to analyte ions of very similar mass was modeled by Eiden *et al.* using a solution of Sr, Y and Zr. The Y concentration is ~100-fold greater than that of Sr or Zr. As shown in Figure 2.30, the Y can be selectively ejected with minimal distortion of the adjacent peaks for the isotopes of Sr and Zr. If the charge in the trap is too great, the spectrum is distorted as shown in Figure 2.30.

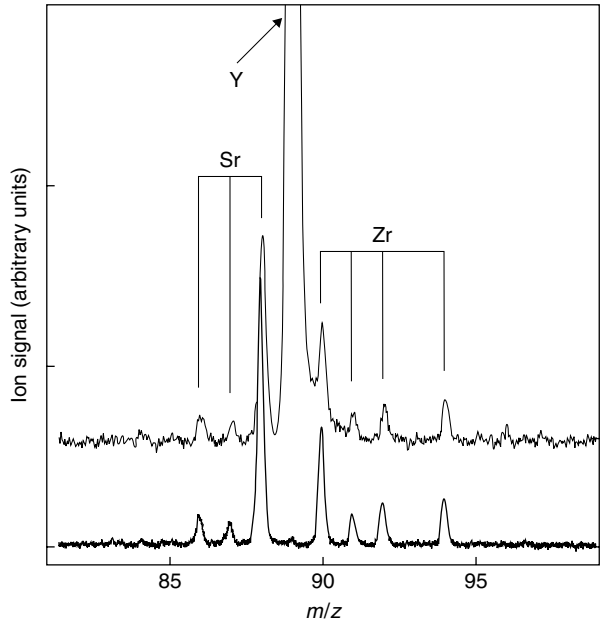

Figure 2.30 Selective ejection of an intense peak at a single m/z reduces the space charge distortion of the mass spectrum. Here, the high m/z selectivity of such resonant excitation is shown for $^{89}Y^+$ in the presence of Sr^+ and Zr^+. If $^{89}Y^+$ is not ejected prior to mass analysis (upper trace), the spectrum is space charge distorted. By ejecting the m/z 89 peak prior to mass analysis, an undistorted spectrum is obtained (lower trace; virtually identical to the spectrum of a solution containing only Sr and Zr). Comparison of the spectra shown with spectra of Sr and Zr solutions without Y shows that ejection of $^{89}Y^+$ is 50 000 times more efficient than ejection of either $^{88}Sr^+$ or $^{90}Zr^+$

(b) Broadband excitation

More than one m/z at a time can be excited via resonance excitation. By application of a waveform containing the secular frequency of different mass ions, multiple species can be simultaneously excited. Broadband methods have been borrowed from other fields, especially FTICR-MS[49,50], and applied to the RF quadrupole ion trap to effect such excitations.[51,52]

The data in Figure 2.31 are for various solutions containing Cd, the analyte of interest and an excess of Ag, which distorts some of the Cd peaks (Figure 2.31(a)). Using broadband resonant ejection of the Ag (Figure 2.31(b)), the undistorted Cd spectrum (Figure 2.31(c)) is recovered (the ^{110}Cd isotope peak remains somewhat distorted).

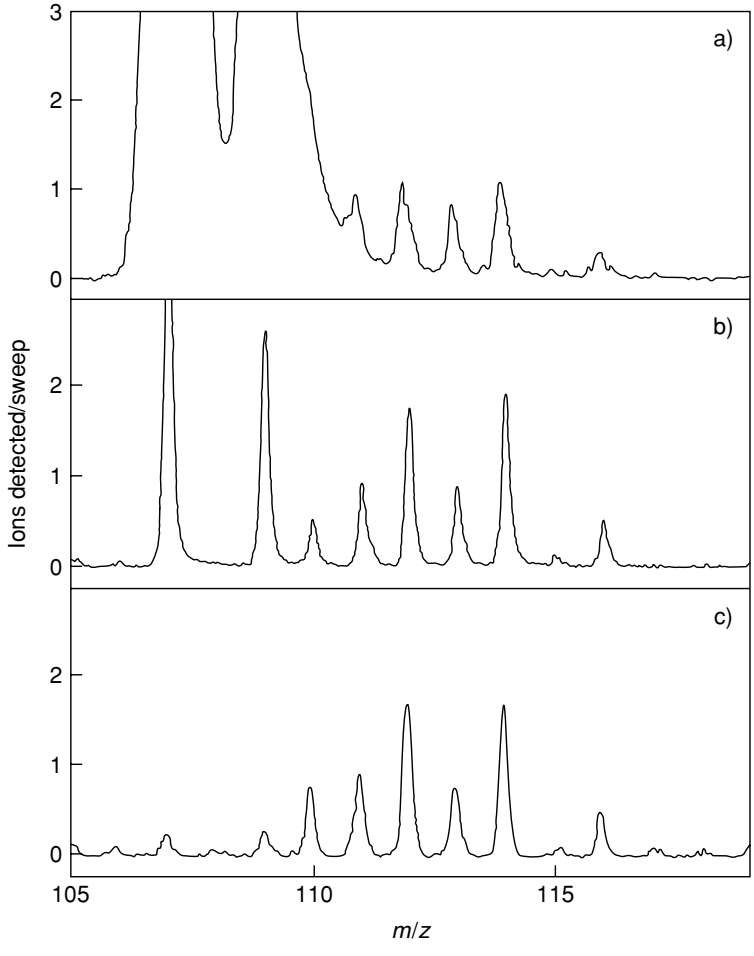

Figure 2.31 Mass spectra for solutions of Ag and Cd, showing the abundance sensitivity enhancement realized with broadband resonant ejection. (a) Mixture of 100 ppb Ag and 1 ppb Cd, no broadband excitation. (b) Same sample as (a), but excitation waveform applied. (c) 1 ppb Cd only, no broadband excitation

2.4.5 Inductively coupled plasma source ion trap mass spectrometers

2.4.5.1 Instruments

(a) The RF quadrupole ion trap ICP-MS

There are only a small number of groups worldwide that have developed or are working with RF quadrupole ion trap ICP-MS instruments. They are the group of Eiden, Barinaga, and Koppenaal at the U.S. Department of Energy's Pacific Northwest National Laboratory[5–16] and the Furuta group in Japan working with a Hitachi Corporation instrument.[53] Two other groups that have contributed significantly, but are no longer active in this field, are Professor John F. J. Todd's group at the University of Kent in UK[17] and Dr Cory I. Frum at the University of Nevada-Las Vegas.[18] A schematic of the Todd instrument is shown in Figure 2.32. Significant features of this instrument include the use of an offset geometry in which the axis of the ICP and vacuum interface optics are parallel to, but offset from, the axis of the ion guide and ion trap.

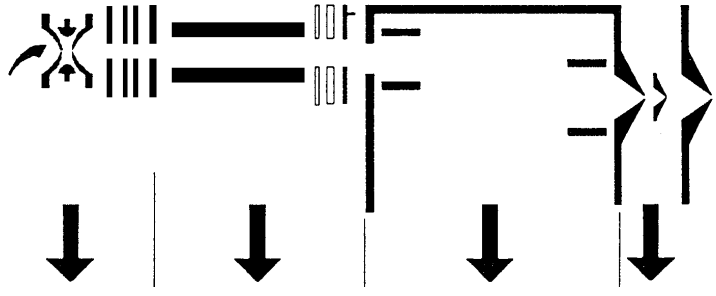

Figure 2.32 Schematic of 'ITEMS' (Todd) instrument

The majority of literature reports in this area are from the PNNL group and we will focus on that body of work in describing the design and performance of these instruments.

RF quadrupole ion trap mass spectrometers have been developed primarily for molecular mass spectrometry where the range of mass-to-charge ratio of interest is typically much greater than that required for elemental or isotopic mass spectrometry, often by an order of magnitude or more. This leads to compromises in design, which are not required for a spectrometer of more modest mass range. In PNNL's second generation PSIT (Figure 2.27(b)), we utilized a larger than standard electrode set as the simplest means to reduce the mass range of the ion trap (i.e., without modifying the main RF circuits). The electronics and software used were commercial-off-the-shelf and it was deemed beyond the scope of our development project to modify these. However, by simply machining a set of electrodes that were 1.44× larger than the standard ones, the mass range of the ion trap was reduced from the standard 650 Da of the Finnigan ITMS^{TM} to ∼300 Da. This can be better understood by reference to the trap size dependence shown in equations (2.4.3)–(2.4.5) above. Without changes to the electronics and software, this also had the effect of slowing down the mass scan rate, thereby increasing the mass resolution (*vide infra*).

The third generation PSIT built at PNNL was based on Finnigan's LCQ^{TM} ion trap. This ion trap MS technology represented advances of 10 years in electronics, data acquisition and RF

power systems over the ITMS^{TM} traps used in PSIT-I and PSIT-II. The goals for developing this third generation PSIT included evaluating performance with a much improved mass spectrometer electronics package and more modern software for instrument control and data acquisition. This third generation instrument was dubbed the PSQ, for 'plasma source QUISTOR' (an acronym within an acronym; 'QUISTOR' was Prof. Todd's term for the 'quadrupole ion store', an early linear trap used in studies of ion–molecule chemistry[54]); a schematic of the PSQ design is shown in Figure 2.33.

Significant features of this instrument include the use of several ion guides (a 2 inch long, enclosed octopole and a 6 inch long octopole). These ion guides can be pressurized with a first reagent or buffer gas while the ion trap is pressurized with a second gas. This affords great flexibility in the use of chemical resolution to eliminate spectral interferences.

(b) The Fourier transform ion cyclotron resonance ICP-MS

Milgram *et al.* have described initial results obtained by incorporation of an ICP ion source with an FTICR mass spectrometer.[19] Two instrumental configurations were used to conduct this work, one at the University of Florida and the other at the National High Magnetic Field Laboratory (NHMFL). The University of Florida instrument (Figure 2.34) uses a 2 T superconducting magnet. Challenges associated with the development of this instrument included efficient transfer of ions from the atmospheric pressure ICP into the ultrahigh vacuum (UHV) environment of the analyser cell of the FTICR/MS and shielding of the RF emissions of the ICP so as to minimize noise in the highly sensitive measurements of the image current signal in the FTICR experiment. The instrument consists of a commercial ICP ion source, differentially pumped vacuum interface and first ion optic ('extraction' lens). These are fitted to the two instruments via appropriate adaptor flanges and ion optics.

The FTICR/MS experiment for external ion sources has been described elsewhere.[55] Ions are injected into the analyser cell of the FTICR/MS and allowed to relax into a low-energy state. A mass spectrum is generated by applying an RF pulse to the 'excite' electrodes, which form two walls of the analyser cell. This pulse excites the trapped ions into large orbits where the ions pass close to a pair of detection electrodes, which also form two other walls of the cell. The periodic motion of the ions passing the detection electrodes induces a time varying image current in those electrodes. The Fourier transform of this image current yields the mass spectrum.

The spectra obtained demonstrate sub-mg/L detection limits and high mass resolution (mass resolving power, $m/\Delta m_{10\%V} = 7000$–$10\,000$). For example, a 1 mg/L solution of copper yields a S/N of 8 for ^{63}Cu (isotopic concentration 0.69 mg/L), clearly demonstrating sub-mg/L detection limits. The highest reported mass resolving power for an ICP-FTICR spectrum in this work is $m/\Delta m_{10\%V} = 88\,000$, obtained for $^{40}Ar^{+}$.

As shown in Figure 2.35, spectra were obtained with resolving power that was sufficient to separate some spectral interferences that cannot be separated with conventional ICP-MS instrumentation. At the 1–20 mg/L analyte concentrations used in this study, the potential dynamic range problems presented by an overabundance of argon ions relative to analyte ions were not as severe as many would have expected. Furthermore, the dynamic range of an ICP-FTICR instrument can be extended by selective ejection of unwanted ions, using methods similar to those described herein for the Paul trap. These initial experiments have also demonstrated the important role of RF shielding in ICP-FTICR/MS experiments.

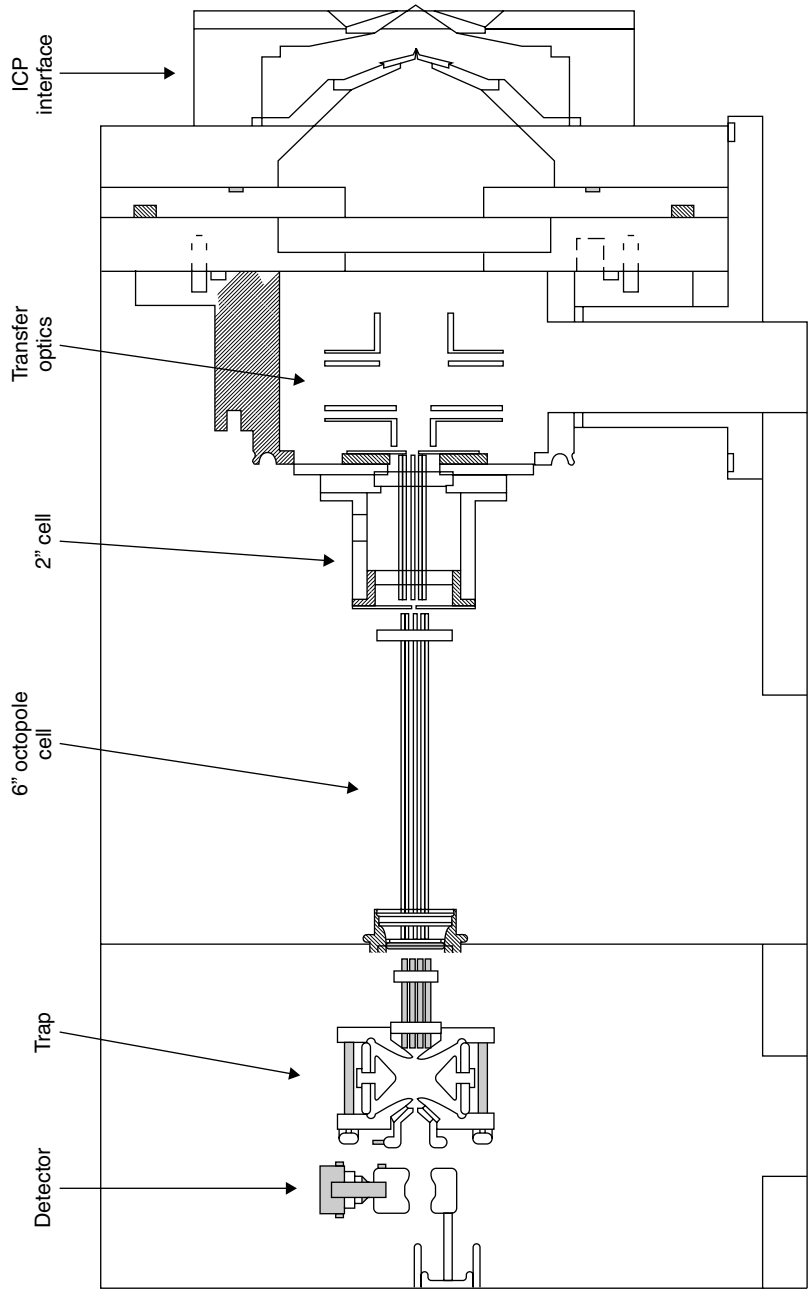

Figure 2.33 Plasma source quistor (PSQ). Schematic diagram of the vacuum interface, octopole ion guide/collision cell and the associated DC ion optics.

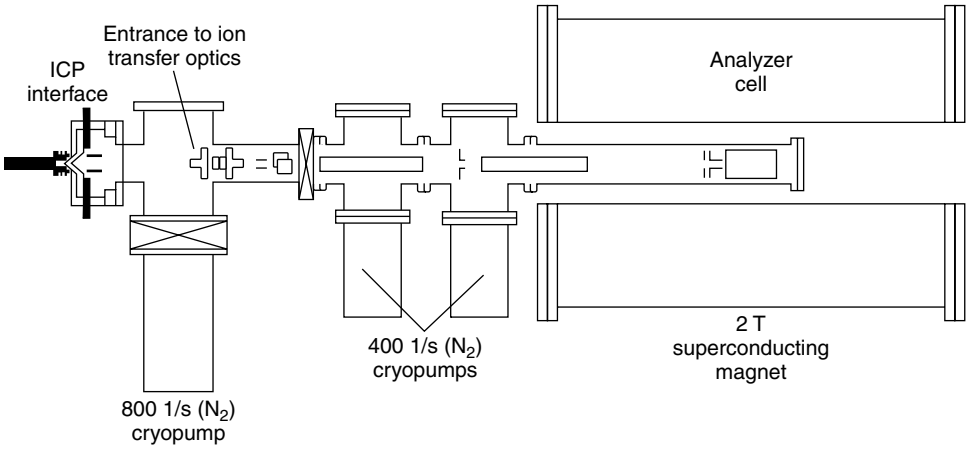

Figure 2.34 University of Florida ICP-FTICR/MS instrument. Ions are transported from the source region to the analyser region via a series of electrostatic lenses

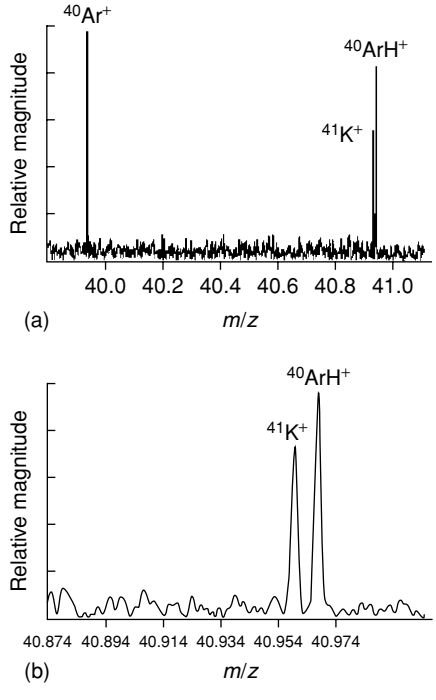

Figure 2.35 (a) High-resolution ($m/\Delta m$10%V ~10 000) ICP-FTICR/MS broad-band spectrum of a 22 mg/L potassium solution obtained with the NHMFL instrument, showing the region between Ar^+ and $^{40}Ar^1H^+$. (b) Expanded view of the mass region around m/z 41, showing baseline resolution of $^{41}K^+$ and $^{40}Ar^1H^+$

The mass resolving power obtained for analyte ions with the NHMFL instrument rivaled that which can be obtained with the best magnetic/electric-sector-based ICP-MS instruments for samples with comparable concentrations. The work here, in conjunction with typical FTICR performance characteristics, indicates that, with future improvements (i.e., more efficient ion transfer, additional differential pumping, and better RF shielding), ICP-FTICR/MS should be capable of yielding mass resolving powers in excess of 10^6 for samples with μg/L concentrations.

2.4.5.2 Interferences and methods for their elimination

Isobaric interferences are one of the most troublesome factors affecting accuracy and sensitivity in elemental MS. Molecular ion interferences arise from at least three sources: (1) the plasma support gas alone or in combination with the sample/solvent leading to formation of intense molecular ion peaks (ArH^+, ArC^+, ArN^+, ArO^+, Ar_2^+, etc.); (2) ions derived from the sample/solvent only (diatomic hydride cations, OH^+, ClO^+, NO^+, CaO^+, LaO^+, etc.) and (3) chemical ionization of vacuum system background gases (H_2^+, H_2O^+, H_3O^+, $C_xH_y^+$, etc.). A new and significant source of isobaric interference arises in collision cell equipped instruments in which unwanted reactions between either the reagent gas or other gases in the cell occur. In addition there are atomic isobars associated with the sample to contend with, especially with samples containing low levels of radioactive isotopes. The magnitude of these various interferences depends on the plasma operating and sampling conditions. Different molecular ions respond differently to changes in plasma operating conditions so that no single set of operating parameters can be found, which simultaneously minimizes all molecular ion interferences. Of course, plasma operating conditions also affect the intensities of analyte (atomic) ions. The intensity of each interferent ion also depends on the nature of the sample to be analyzed and on the method of sample volatilization and introduction to the ICP. Since many of the molecular ions are derived from the sample solvent, selective solvent removal from the sample aerosol prior to introduction into the ICP is an effective and widely used way to reduce the intensities of selected molecular ion interferences.[56]

The characteristics of the ICP can be dramatically altered by using a shielding electrode between the RF coil and the plasma. Such 'shield torches' have been used along with lowered RF power, (so-called cold plasma conditions), to achieve dramatic reductions in molecular and atomic ion interferences without comparable reductions in analyte ion response.[57] A significant drawback to the use of cold plasma conditions for ultratrace detection of selected analytes is that more than one ICP operating mode (RF power, aerosol flow rate) is typically used to analyze the full range of elements of interest.

The RF quadrupole ion trap enables collision induced dissociation (CID), a means for molecular ion discrimination that is nearly independent of m/z. This method of interference discrimination is also independent of the ICP operating conditions or the nature of the sample. This allows the ICP to be operated at 'normal' RF power, in a conventional 'hot' regime, where ionization efficiency is high for most elements. Of course, dissociation does depend on the strength of the bond to be broken, but even very strongly bound molecular ions can be dissociated efficiently with good recovery (trapping) of the bare atomic cation of interest (see below). Utilizing CID[5,16] and selective ion–molecule chemistry[9,12] we have previously shown that nearly all major plasma ion interferences can be dramatically reduced or even eliminated from the spectrum (i.e., below instrument noise level).

RF quadrupole ion traps are typically operated with a significant pressure (~1 mTorr) of a light gas (He) inside the ion trap.[21,33] This so-called buffer gas serves to dampen ion motion and enhances most key aspects of ion trap MS operation (trapping efficiency, mass resolution and ejection selectivity). Collisions between injected ions and the buffer gas are crucial for efficient trapping since the initial kinetic energy of injected ions must be dissipated in order for the ions to become stably trapped. The collisional processes necessary for efficient trapping also result in an increase in the internal energy of ions through translational-to-vibrational energy transfer processes. This internal ion heating can provide sufficient energy to easily dissociate weakly bound molecular ions (as many of the ICP-MS matrix and plasma-gas molecular ions are). Thus, for example, although Ar_2^+ is one of the more intense molecular ion interferences in ICP-MS, we were unable to observe Ar_2^+ in our early ion trap ICP-MS spectra since the collisions used to trap ions are more than sufficient to dissociate Ar_2^+ (bond dissociation energy ~1.2 eV). In more recent collision cell ICP-MS work, Ar_2^+ is observed, presumably due to gentler ion guiding and trapping conditions (lower energy collisions).

More strongly bound molecular ions can be selectively heated and dissociated using resonance excitation of trapped ion motion.[58] Duckworth *et al.* have shown that even quite strongly bound molecular cations can be dissociated in an RF quadrupole ion trap with very high recovery of the bare metal cation. Using a glow discharge ion source, they measured ~95% recovery of Ba^+ from dissociation of trapped $BaOH^+$ (bond dissociation energy (bde) ~130 kcal/mol or ~5.6 eV).[28] In more recent work, Duckworth *et al.* have shown a very respectable Ta^+ recovery of ~30% from dissociation of the very strongly bound TaO^+ (bde = 8.2 eV).[59]

Resonance excitation methods have been exploited in molecular MS to obtain daughter ion spectra, i.e., an MS/MS experiment (MS/MS is also known as MS^2, and MS^n experiments have been shown for n up to 10). In elemental and isotopic MS, the excitation energy used can be much higher since further dissociation of the 'daughter', i.e., an atomic cation, is not a concern. The use of such collisional dissociation techniques enables the removal and resolution of many polyatomic ion interferences. The approach thus provides a low-cost alternative to high resolution mass analysers. CID is less effective in linear quadrupole ion guides (the two-dimensional equivalent of a Paul trap; see[21,36]) than in ion traps because there is less interaction time between the ion and the collision gas. The transit time of an ion through a linear multipole ion guide is often on the order of 1 ms compared with residence times in ion traps that are of the order of 100 ms. Ion traps are thus able to achieve much greater energy deposition into the ion and thereby induce dissociation of more strongly bound ions, more extensive dissociation of complex polyatomics (not typically of great interest in ICP-based elemental or isotopic MS work) and dissociation of a greater fraction of a population of ions. Nevertheless, CID has been shown to be effective for weakly bound ions where just a few collisions are sufficient to induce dissociation. Examples include argides and other weakly bound dimer cations.

There is an important difference between CID in PSIT MS and in the earlier, organic, biological applications of this method. Our interest is in removing interferences whereas in this earlier work, the interest was typically in obtaining molecular structure information via the dissociation patterns observed (known as MS-MS spectrometry). That is, the daughter ions from the dissociative events were the analytes of interest whereas in our work, we do not wish to detect these ions. If one does not wish to retain and detect the daughter ions, then much more energetic CID conditions can be used and more strongly bound species can be dissociated.

2.4.5.3 Analytical performance

The principal motivation for seeking alternative mass analysers for ICP-MS is to improve analytical performance or overall instrument design and function (smaller, faster, cheaper). The primary limitations of linear quadrupole mass filters for use in ICP-MS are low duty cycle per isotope (typical of any scanning mass analyser coupled to a continuous ion source), low mass resolution coupled with the occurrence of numerous isobaric interferences and, traditionally, poor isotope ratio measurement precision (the latter has improved significantly in recent years). A low duty cycle degrades sensitivity since in a scanning instrument only one isotope signal can be recorded at any given instant in time, thus, other signals are ignored and lost. Both TOF and RF quadrupole ion trap MS instruments have the potential to overcome the duty cycle limitations. Instruments using electric/magnetic sectors for mass analysis provide more precise isotope ratio measurements and can be used to resolve many polyatomic isobaric interferences. These instruments also typically have very high transmission efficiency compared with the trapping/detection efficiency of ion traps or the transmission efficiency of TOF analysers. This incredible performance comes at a price, literally, with most multiple detector, sector field instruments costing US $ 1 000 000 compared with a quadrupole ICP-MS, which might be had for a little more than US $ 100 000. Also, quadrupole instruments have recently achieved isotope ratio precision as good as 0.05% (relative standard deviation),[60] much better than the ~1% level that these instruments have traditionally delivered. Ion trap and TOF mass analysers can be operated at moderately high resolution (1000–5000 at m/z 40–240) without the trade-off between sensitivity and resolution that typically occurs with magnetic sector or linear quadrupole MS instruments. Very high resolution can be attained using FTICR mass spectrometers. Eyler and co-workers at the University of Florida have reported[19] the successful coupling of an FT/ICR mass spectrometer to an ICP ion source (*vide supra*). The FTICR has the highest mass resolving power of any mass analyser previously used for ICP-MS. The Florida group has reported single analytical scan resolution of over 10^6.

Sample introduction has been accomplished using both conventional, pneumatic nebulizers (Meinhard type) and spray chambers as well as via ultrasonic nebulization coupled with desolvation (Cetac, Inc.; model U-5000). The ICP sources and vacuum interfaces we have incorporated into our PSIT and PSQ instruments were manufactured by VG Elemental (now Thermo Electron Corp). ICP operating conditions were 1250 W forward power, sampling distance ~10 mm, argon flow rates of 0.9, 1.2 and 13 L/min respectively for the nebulizer, auxiliary and cool gas channels. The ion traps used were ITMS™ or LCQ™ instruments manufactured by the Finnigan Corporation (San Jose, CA; now Thermo Electron Corp). The ICPs were coupled to the ion traps using custom built vacuum chambers and ion optical components as well as portions of the original VG Elemental ICP-MS vacuum interface. These and other experimental details have been published elsewhere.[5,9,10,12,14,16]

High mass resolution is achieved in the PSIT work using phase synchronization of the axial modulation waveform and the ring electrode trapping RF waveform.[37] The axial modulation frequency used was 450 kHz ($\beta_{z,\text{eject}} = 0.818$). The typical mass resolving power of the PSIT-II instrument is shown in Figure 2.39. The large ion trap is 'unstretched', that is, the separation of the endcaps is a factor of $\sqrt{2}$ smaller than the inside diameter of the ring electrode. Abundance sensitivity was enhanced by the use of selective ion ejection via resonance excitation as described in our earlier work (see Figure 2.30).[10]

Table 2.7 Analytical performance circa 1998[14]

Figure of merit	Performance
Detection limit*	0.3–5 ng/L
Dynamic range	$> 3 \times 10^5$
Isotope ratio precision	2–5% RSD at ng/mL (0.7% champion)
Mass resolution	Background organic ions partially resolved ΔM_{FWHM} ~0.03–0.04 Da at 1900 Da/s scan rate
Mass scale linearity	0.01% over a 200 amu range ($b_{eject} = 4/5$)
Abundance sensitivity	10^5–10^6
Collisional dissociation	Only atomic daughter ions of interest, therefore can use higher fluence (limited by trapping loss)
Ion–molecule reactions	Use to remove isobaric interferences React ions in collision cell before trapping Replaces some sample separations Fast separations: milliseconds not seconds or minutes

* Instrument LOD, taken as analyte response versus 3σ noise off peak.

(a) Detection limits

Analytical performance of the PNNL PSIT's is summarized in Table 2.7. Instrument limits of detection (LOD) for light elements, i.e., atomic mass ~100 or less, are in the low to sub-pg/mL range. It is noteworthy that for some of these element/matrix combinations, detection limits reported since this early work have not improved significantly. This is another indication that the collision cell ICP-MS method is far from mature. LOD were obtained in a single analytical scan for a wide range of elements; the scan time was 3 min or less. Compared with linear quadrupole ICP-MS performance, the sensitivity of the PSIT for classically interfered isotopes such as ^{39}K ($^{38}ArH^+$ interference), ^{40}Ca ($^{40}Ar^+$ interference) and ^{56}Fe (ArO^+ interference) is orders of magnitude better due to collisional dissociation and selective reactions of interferent ions in the ion trap. Low pg/mL LODs are also observed for other elements typically obscured by sample matrix or plasma ions. For example, there is a background signal in the spectrum of 1% HCl solutions at m/z 51 due to ClO^+. This interferent is reduced in the PSIT to less than 50 pg/mL ^{51}V equivalent. Similarly, we observe no interference with ^{75}As by $^{40}Ar^{35}Cl^+$. These diatomic cations have bonds, which are apparently strong enough for the molecular ion to survive transit through the RF and DC fringing fields of linear quadrupoles. In the RF quadrupole ion trap, efficient trapping is made possible by pressurizing the trap with a gas, which serves to reduce the kinetic energy of ions entering the trap leading to their capture in the trapping field. The collisions also lead to internal excitation and ultimate dissociation of weakly bound molecular ions (e.g., ArO^+, ClO^+, $ArCl^+$, Ar_2^+), allowing improved detection limits for isotopes normally obscured at these mass positions.

(b) Isotope ratio measurement precision

Isotope ratio precision should be better than scanning mass analysers since the ion trap monitors multiple isotopes simultaneously, but the precision observed to date in ion trap mass

spectrometers used for elemental/isotopic analysis is only ~1% relative standard deviation. A first, significant reason for this poor isotope ratio performance is that analog ion detection has been used, rather than ion counting. Also, hardware and software have not been optimized for the mass range of interest in elemental/isotopic MS. It should be noted that a trade-off for ion traps using pulse counting detection is that linear dynamic range will be affected. Ions of a given m/z are ejected from the trap and strike the detector over a narrow time window (typically tens of microseconds), leading to saturation, large deadtime corrections and/or detector fatigue. There are known methods of operating and scanning the ion trap that can be used to alleviate this problem, including the fact that ion detectors are now available that provide both pulse counting and analog outputs with claimed effective dynamic range of ~10.[8]

(c) Dynamic range

The linear dynamic range of the PSIT instruments was evaluated by measuring the response for selected elements in a solution containing 15 different elements. Aliquots of analytical stock solutions (National Inst. of Standards and Tech.; Inorganic Ventures) of Mg, Al, K, Ca, Sc through Cu, As and Sr were combined to produce a working solution containing 3.23 mg/L of each element in 1% HNO_3. This working solution was serially diluted in 1% HNO_3 to cover a concentration range down to 20 ng/L. The mass spectral intensities were measured by averaging multiple scans of the ITMS electron multiplier detector output (analog mode) using a digital storage oscilloscope. Intensities for the linear dynamic range data are based on peak areas. No internal standards were used in this work.

The dynamic range of an ion trap is limited by the amount of distortion in peak shapes that can be tolerated in a typical experiment. For our PSIT instruments, this limit was approximately 10^4 ions detected. However, the PSIT electronics enable accurate control over the ion injection time from a fraction of a millisecond up to several seconds. This intrinsic dynamic range can thus be increased by about three orders of magnitude by controlling the amount of ion injection time used. Ion trap electronics and software could in principle be developed that provide at least an additional order of magnitude by using very short ion injection times. If a single analytical scan must be used, the use of variable injection time is only useful for samples in which the isotopes of interest occur at abundances that do not differ by more than a few orders of magnitude. Figure 2.36 shows the linearity of the response versus concentration for the PSIT-II instrument. The data shown are for $^{59}Co^+$, but similar results have been obtained for other analytes including V, Fe, Sr, and In. The response is linear ($r^2 = 0.999$, $n = 28$) over nearly six orders of magnitude, from <20 ng/L to 3 mg/L. At the highest concentrations, an ion injection time of 1 ms was used. At lower concentrations, the injection time was varied between 10 and 500 ms. The intrinsic linear dynamic range of the ion trap would be best measured using a single element solution (as opposed to the multielement solutions actually used in this work), so that at the highest concentrations, the trapped ion cloud would consist primarily of the ion of interest.

It should be emphasized that this dynamic range has been measured using multielement solutions and as such represents performance intermediate between that expected for a single element solution and a solution with a high concentration of matrix ions. Linear dynamic range for multielement samples can be extended using selective ion monitoring. In this method, only the ions of interest are detected, other ions are ejected from the trap either during the ion injection step or between the ion injection and ion detection steps. This improves performance enormously since the spectral space charge limit is the effective (smallest) space charge limit.[38] The dynamic

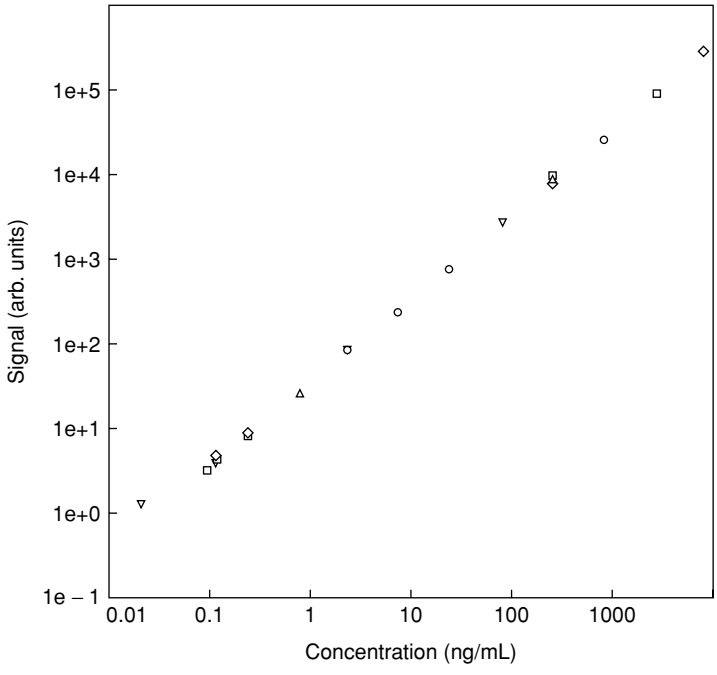

Figure 2.36 Plasma source ion trap-II dynamic range. The observed signal for various solutions is plotted against the analyte concentration (data for Co-59 are shown here). No internal corrections or normalizations have been applied. Different ion inejction times were used to control space charge effects (see text for details)

range indicated in Table 2.7 is representative of the performance observed over many months of operation using a variety of samples and operating conditions.

(d) Abundance sensitivity and mass resolution

The ion trap can be operated at higher mass resolution by synchronizing the AC and RF waveforms applied to the trap electrodes and by reducing the scan rate of the RF voltage.[37,61] Using larger than standard trap electrodes gives a lower mass range for a given RF trapping potential and thus a lower mass scan rate (~1900 amu/s in this work), thereby increasing the mass resolution. Comparable resolution has been demonstrated with standard size traps when scanned at similar rates.[47,62,63] It should be noted that by further reducing the scan rate by just a factor of 2 to ~1000 Da/s, many atomic/inorganic ion isobaric pairs, e.g., $^{56}Fe^{+}/ArO^{+}$, can be resolved while maintaining a reasonably high scan rate. We observe mass spectral peak widths in the large trap of ~0.05 Da (FWHM). This compares with 0.12 Da in a standard ion trap. The mass resolution at m/z 50 ($m/\Delta m$ ~1000) is thus sufficient to partially resolve most hydrocarbon peaks from elemental peaks, even at low m/z, e.g., ^{44}Ca, ^{51}V, ^{56}Fe, etc. This is illustrated in Figure 2.37. A further decrease in the RF scan rate by less than a factor of 2 will increase the mass resolution sufficiently such that most isobars of interest in elemental mass spectrometry can be resolved.[35] It is significant that this dramatic increase in resolution does *not* come at

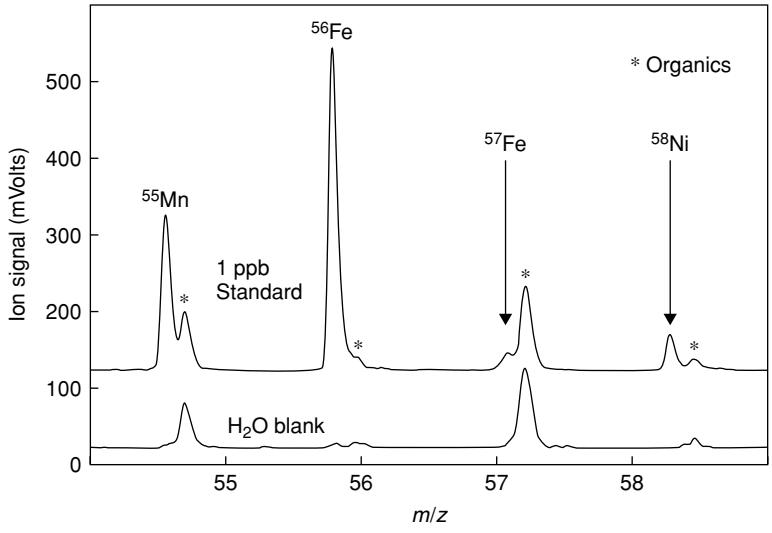

Figure 2.37 High mass resolution of Mn–Co region in the PSIT-II instrument's spectrum

the expense of ion signal. In conventional high resolution mass spectrometry, high resolution is achieved by closing the instrument slits down, resulting in 1–2 orders of magnitude of signal loss in going from nominal resolution of 300 to 10 000. In conclusion, the PSIT demonstrates orders of magnitude lower background for many classically interfered atomic ions and the prospects of higher mass resolution are excellent for making further background reductions.

Abundance sensitivity is 10^5–10^6 using selective ejection of the more abundant isotopes, as described in detail elsewhere.[10]

(e) Selective chemistry

Recently, selective ion molecule chemistry has been applied as an alternative approach to reducing or eliminating isobaric interferences in ICP-MS. This approach, 'chemical resolution' MS, has been developed into a viable analytical method, and its current status is described in detail in Chapter 8 of this book. This approach uses ion–molecule reactions inside the mass spectrometer to remove interferences from selected mass-to-charge ratio detection channels of interest. More than 200 peer-reviewed papers have been published on this subject, more than 500 conference presentations given and several review articles have now appeared. Our contributions in this area began with PSIT studies that we will describe below.

Ion/molecule reactions have been studied for a very long time, now approaching a century, primarily motivated by basic scientific interests. The chemistry of gas-phase ions provides a tractable starting point for both experiment and theory in understanding more complex, condensed phase systems. Our interest in ion–molecule chemistry is in how gas phase reactions can affect the ions inside a mass spectrometer and thereby affect an analytical measurement. Our focus is on elemental mass spectrometry but the ideas discussed below are equally applicable to molecular mass spectrometry. The idea of using gas-phase reactions to alter an ion population analyzed by mass spectrometry is not new;[64,65] however, it has not been extensively

exploited, presumably because of the high vacuum requirements for many mass spectrometric methods (note, linear quadrupole, magnetic/electric sector field, TOF, etc. are all degraded by collisions of the ions with background gas). The use of buffer gases in the RF quadrupole ion trap facilitates the use of reagent-gases for chemical resolution, as long as the reagent gas molecular weight is low compared to the ion masses of interest. Heavy gases will cause excessive scattering of lighter ions. The ion trap is both a highly efficient reaction vessel and a mass analyzing device. RF multipoles operated as ion guides can also tolerate high pressures,[66–68] although early applications focused on fundamental studies of ion/molecule chemistry under low-pressure, single-collision conditions.[69] Finally, the use of selective ion storage to pre-select an ion of interest in ion–molecule reaction studies is well documented in March and Hughes (and elsewhere); see especially, the historical review chapter by John Todd (pp. 24 ff.).

The first PSIT work at PNNL[5] showed how important such reactions can be. Adventitious water in the ion trap was shown to be responsible for rapid reaction of Ar^+ to form H_2O^+ and H_3O^+. With the 'low-mass cut-off' of the ion trap set to m/z 19 or more, H_3O^+ ions are ejected from the trap as they are formed, thereby interrupting the mechanism by which H_2O^+, and H_3O^+ chemically ionize background species. Unfortunately, H_2O also reacts with a wide variety of cations that are of great analytical interest, in particular, metal atomic cations. A more selective reagent gas is needed.

Chemical ionization by Ar^+ in the ion trap (of H_2O, O_2, N_2, pump oil, etc.) can produce background at nearly every elemental m/z. The intensity of the chemical ionization background spectrum in PNNL's early ion trap work was in the range <0.005 to 1 ppb BEC (background equivalent concentration) as shown by a comparison of the mass spectra in Figure 2.38. The background is nearly eliminated if the low mass cut-off of the ion trap is set above m/z 40 during

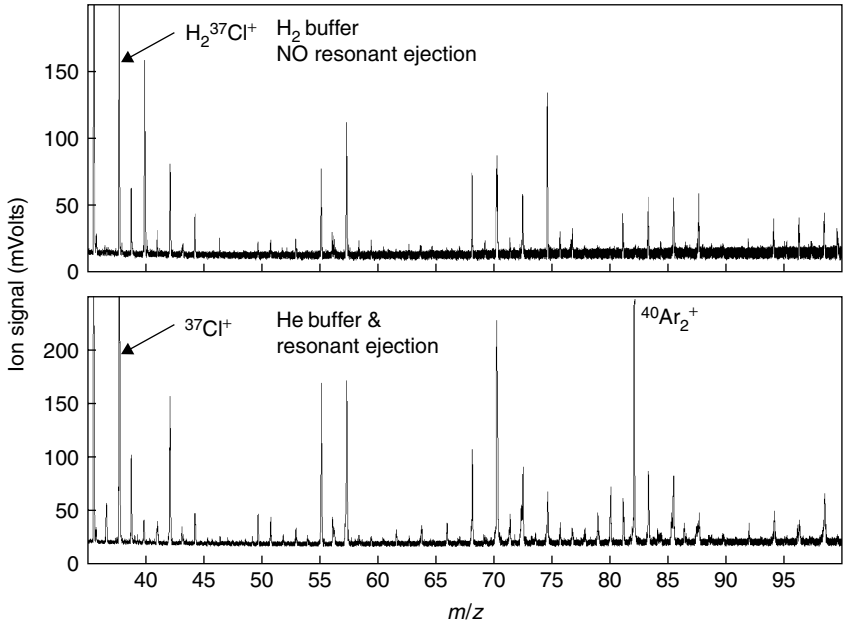

Figure 2.38 Comparison of H_2 'buffer gas' and resonance ejection (with He buffer gas)

ion injection, thereby preventing Ar^+ from interacting significantly with background gases in the trap, analogous to the suppression of H_2O^+ and H_3O^+ mentioned above. Trapping of low m/z ions (m/z ~20–60) requires a low mass cut-off that is too low to suppress trapping of Ar^+, so that Ar^+ must be removed by some other means. In this case, resonant ejection of Ar^+ during ion trapping has been the method of choice; it is very effective in reducing the background spectrum. An alternative approach to eliminating Ar^+ and related, chemical ionization interferences is the addition of H_2 to the buffer gas (normally pure He).[9,11,70]

Hydrogen neutralizes Ar^+ before significant chemical ionization occurs. Ar^+ and H_2 react by electron transfer and H atom transfer;[70] the latter reaction is significant under our trapping conditions, producing ArH^+, which reacts further with H_2 to form both $H_2{}^+$ and $H_3{}^+$. The charge on Ar^+ is thus rapidly migrated to $H_2{}^+$ and $H_3{}^+$, which are ejected from the trap virtually as soon as they form since the low mass cut-off is much greater than 3 amu. Reaction of H_2 with most analyte ions is undetectable.[9,12] This same mechanism can be utilized in a linear quadrupole ion guide or bandpass filter. Since the introduction of the H_2 'chemical resolution' method, other gases have been reported for dealing with various interferences. However, none of these other gases possess the extremely high reaction selectivity of H_2. Thus, these other gases must be used in combination with selective ion storage or transmission methods. The H_2 chemistry allows direct detection of $^{39}K^+$, $^{40}Ca^+$, $^{56}Fe^+$ and $^{80}Se^+$, ions normally obscured by intense plasma gas-ion peaks. Low PSIT background also allows direct detection of other problematic ICP-MS ions, e.g., $^{28}Si^+$, $^{31}P^+$, $^{32}S^+$, $^{51}V^+$ and $^{75}As^+$ using either resonance ejection or H_2 chemical resolution.

As shown in Figures 2.27 and 2.33, in the PSIT and PSQ instruments built at PNNL, an RF octopole ion guide/collision cell (hereafter called the collision cell) is interposed between the ICP interface and the ion trap.[9,11] By judicious choice of the reagent gas(es) added to the collision cell, undesirable ions in the ion beam sampled from the ICP can be selectively removed or shifted in mass-to-charge ratio prior to mass analysis, or, in this work, prior to injection into the ion trap. Thus, Ar^+ can be eliminated in the collision cell via chemical resolution with H_2, thereby preventing Ar^+ from entering the ion trap and causing chemical ionization of the background gases. The elimination of Ar^+ by reaction with H_2 in the collision cell can also enable increased analyte ion transmission efficiency since the space charge of a typical ICP-MS instrument's Ar^+ ion flux limits flow through the ion optics. Reactions in the ion trap due to reagent gas admitted into the collision cell are minimal, so that results reported here are equally applicable to a conventional (linear quadrupole-based) ICP-MS instrument incorporating a collision cell between the ion source and mass spectrometer.

In Figure 2.39, we show mass spectra obtained using neat H_2 as the buffer gas at a low mass cut-off of 25 amu. The upper trace shows the spectrum for a 1 ppb multielement solution in 1% HNO_3; the lower trace shows the spectrum for a H_2O blank. Using reactive removal of Ar^+ with H_2, many classically obscured ions ($^{28}Si^+$, $^{31}P^+$, $^{32}S^+$, $^{39}K^+$, $^{40}Ca^+$, $^{54}Fe^+$, $^{56}Fe^+$, $^{75}As^+$, and $^{80}Se^+$) can be directly analyzed, typically at sub-ppb levels. However, some ions react with H_2, e.g., Si^+, K^+, Cl^+, O^+. For analysis of such reactive ions, resonant ejection is superior to H_2 chemistry for the removal of Ar^+.

Figure 2.40 shows the mass spectra obtained for 0.1% HCl blank solutions using the PSIT and H_2 chemical resolution or a conventional ICP-MS (VG PlasmaQuad II+). The PSIT spectrum shows far lower background between m/z 28 and 42 (m/z 40, 41 were skipped in the PQ-II+ mass scan) and at m/z 54, 56, 80 and 84. In other m/z regions, e.g., m/z 47, 48, 65–74, 77, 79, the PQ-II+ shows lower background than the PSIT.

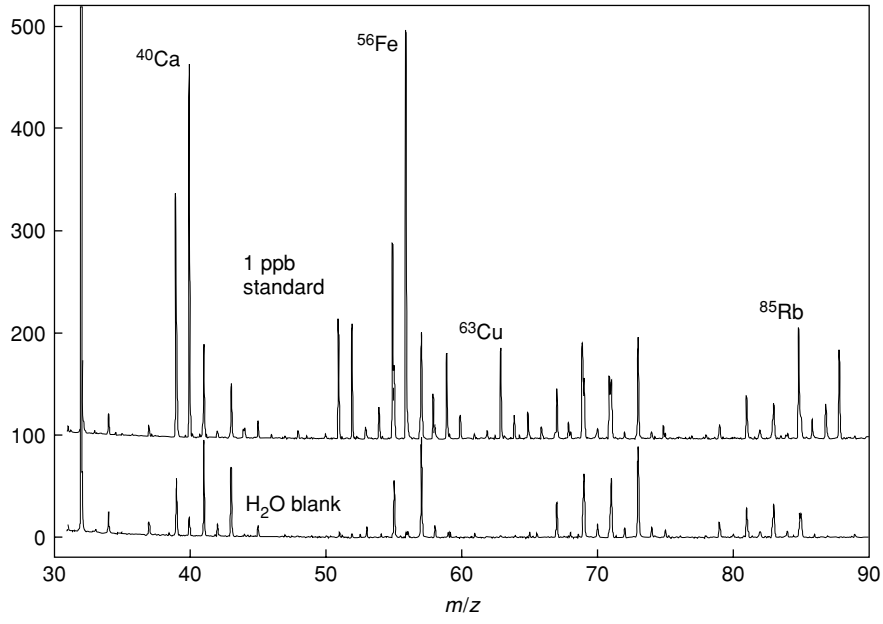

Figure 2.39 Spectrum of multielement solution in HNO_3 versus H_2O blank using hydrogen gas in the PSIT-II instrument

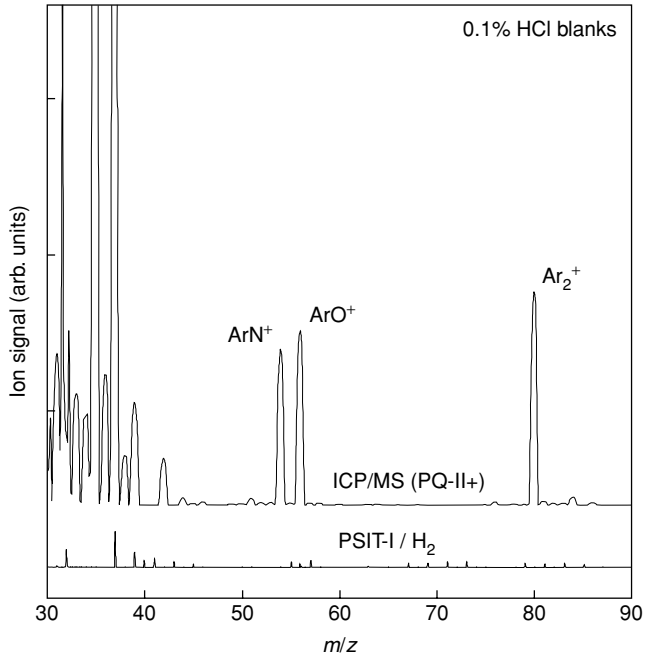

Figure 2.40 H_2 effect with HCl solution: PSIT-II versus conventional ICPMS (PQ-II). This figure shows spectra for 0.1% HCl blank solutions recorded with a conventional ICP-MS (top trace) and with the PSIT-I instrument. Note the orders of magnitude reduction in plasma related polyatomics (ArN^+, ArO^+, Ar_2^+) and matrix polyatomics (ClO^+). Note also the use of H_2 results in conversion of Cl^+ to H_2Cl^+. The spectra were each normalized to the $^{59}Co^+$ response, which at 10 ng/mL was about the intensity of the ArO^+ peak in the figure

For other isobaric interferences, specialized reaction gases can be used. In Figures 2.41–2.43, several examples of highly effective interference removal are illustrated. The chemical resolution studies performed in the PNNL PSIT instruments are summarized in Table 2.8.

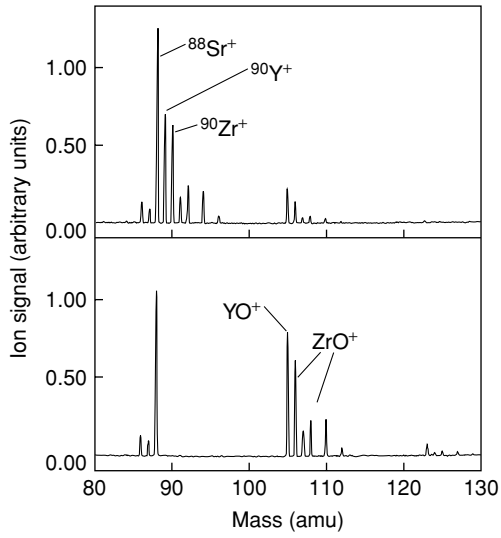

Figure 2.41 Separation of Zr^+ and Y^+ from Sr^+ by reaction with O_2. ^{90}Y and ^{90}Zr are isobaric with ^{90}Sr; they are resolved at mass resolutions of 150 000 and 30 000, respectively. Here, they are separated chemically *in situ*

The purity of the reagent gas(es) used in the ion trap is very important because of the very high efficiency of the ion trap as a reaction vessel. Part-per-million levels of impurities in the reagent gases or buffer gas can lead to significant side reactions and the formation of new interferences. Fortunately, methods for purifying many of the gases used in ion trap ICP-MS are available. The most straightforward gases to purify are the noble gases because of their inertness and low boiling points. These properties enable one to use chemical reactions to remove impurities or cryogenic trapping of higher boiling impurities. The need for extremely high purity gases in semiconductor manufacturing has driven the development of robust getters (note that a getter is a solid material that reacts selectively with impurities and not the gas of interest) for many of the gases used in 'chemical resolution' ICP-MS, e.g., noble gases and hydrogen can be gettered to produce point-of-use purities as high as '9-nines' (99.999 999 9%).

Hydrogen is unique among the common reaction gases in use with respect to the purity that can be achieved without specialized effort and using off-the-shelf technology. This is because the gettering mechanism results in the 'cracking' of hydrogen-containing polyatomic molecules (H_2O, CH_4, hydrocarbons and other organics) in which the hydrogen component is released as H_2 and all other constituents (C, O, N) are captured by irreversible reaction with the getter material to form a solid compound. Thus, the only impurities that are not reactive with the getter are rare gases, which in low abundance do not affect the operation of the reaction cell. All other impurities are completely trapped by the getter (output purities are claimed to be in excess of 99.999 999 9%) with the exception of the hydrogenic component of the impurities. But, of course, the release of a small amount of H_2 from the cracking of the impurities is irrelevant when

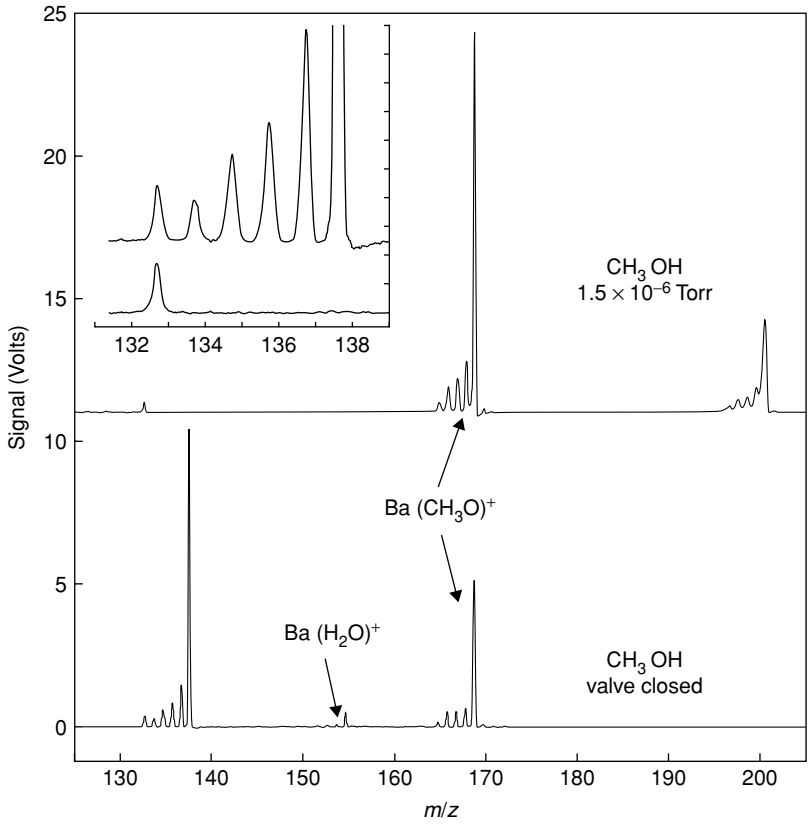

Figure 2.42 Separation of Cs^+ from Ba^+ by reaction with CH_3OH. Isotopes of natural barium are isobaric with ^{135}Cs and ^{137}Cs; these interferences are resolved at mass resolutions of ~600 000 and 110 000, respectively, beyond that of any conventional ICP-MS instrument (only FTICR instruments have sufficient resolution). Here, they are separated chemically *in situ*

the gas being purified *is* H_2. Purification by gettering of other gases such as CH_4, O_2 or NH_3 is more problematic.

One of the most persistent impurities in any collision cell will be water because of the difficulty of completely removing it from the interior walls of vacuum chambers and gas lines. Ultra-high vacuum (UHV) practices (use of appropriate materials of construction, extreme cleanliness, bake-out of the vacuum chamber, etc.) are essential for complete removal of water. Unfortunately, most commercial ICP-MS instruments are not constructed using UHV materials and methods of construction so that full system bake-out is not practical except at very modest temperatures, say 100°C or lower. However, internal bake-out heaters may be possible to use in some instrument designs, after modifications such as replacing plastic coated wires with ceramic insulation or bare wire.

Another intrinsic impurity in the reagent gases arises in a more subtle way. As described by Tanner,[71] the gases from the ICP ion source can enter a collision cell and lead to significant side reactions. While the bulk of this gas is argon, there is substantial water, oxygen, nitrogen, etc. from

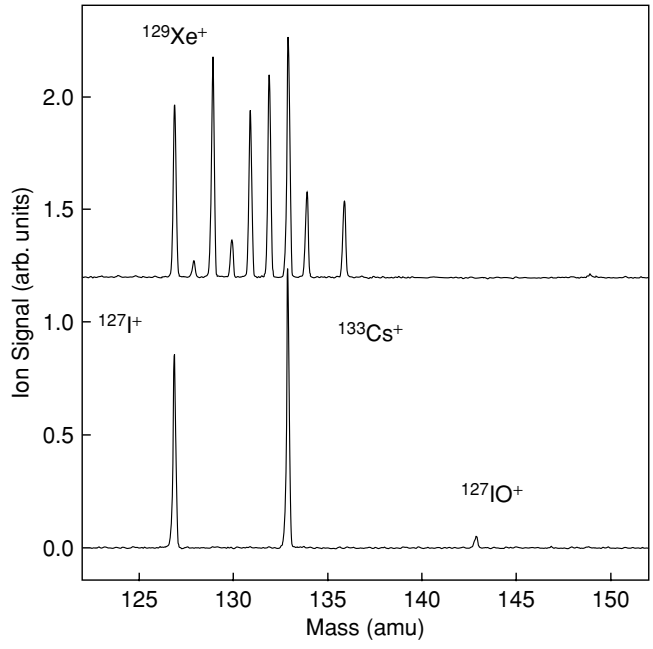

Figure 2.43 These spectra show that radioactive $^{129}I^+$ can be detected mass spectrometrically in the presence of interference by natural Xe^+. This isobaric interference is resolved at a mass resolution of ~600 000. Here, they are separated chemically *in situ* with a selectivity of $\sim 10^4$. The reduction in Xe^+ intensity is $\sim 10^4$ greater than loss of I^+

Table 2.8 Reactions used to address isobaric interferences in ion trap ICP-MS*

Gas	Interferences	Analytes	Comment
H_2	Ar^+	^{40}Ca, ^{40}K	
	ArH^+	^{39}K	
	ArN^+, ArO^+	$^{54,56}Fe$	Mechanism is reaction, CID or both
	$Ar_2{}^+$	$^{78,80}Se$	SeH^+ formation reported
O_2	^{129}Xe	^{129}I	$>10^5$-fold improvement
	^{90}Y, ^{90}Zr	^{90}Sr	^{88}Sr scattering tail is limiting
	O_2	^{32}S	Change analyte m/z, not interferent
CH_3OH	$^{135,137}Ba$	$^{135,137}Cs$	^{133}Cs tail limiting
NH_3	^{79}Br	^{79}Se	$SeH/Se < 1 \times 10^{-4}$
	^{87}Sr	^{87}Rb	
H_2O	Ar^+, ArN^+, ArO^+	^{39}K, ^{40}Ca, $^{54,56}Fe$	Poor selectivity with respect to most metal cations

* The research listed is from the PNNL group circa 1994–1999.

the sample matrix/solvent and from air that gets entrained in the ICP. The most straightforward solutions to this problem are to locate the collision cell or ion trap farther from the ICP (the gas jet intensity from the ICP decreases as the square of the distance between the ICP and cell) or to use an offset geometry such that the gas jet does not impinge on the entrance to the cell/trap. The latter solution is complex in that ion optics must be able to separate the ion beam from the gas jet under conditions of high collision rates and strong space charge forces and thus far no completely satisfying solution has been found.

2.4.6 Conclusion

The research described here shows the great potential of ion trap mass spectrometers for performing specialized and routine isotope ratio and elemental analyses. Early concerns over space charge and other performance limitations of ion traps for plasma source MS have been largely laid to rest. Thus far there have been no commercial instruments offered in which software and hardware have been optimized for the elemental and isotopic mass range and the specialized operating modes that these analyses require. There are also no such research instruments. However, it is the author's belief that the ion trap still has untapped potential for high precision isotope ratio MS measurements, but this will require investments to produce the right hardware and software combination. New ion trap products are appearing all the time, which offers encouragement that these mass analysers will yet find their place in the elemental/isotopic mass spectrometry fields.

This research has also borne important fruit in that our research into the reactive effects of hydrogen and other gases in ion trap ICP-MS instruments and other collision cell equipped instruments has revived interest in the utility of ion–molecule chemistry for interference reduction. Building on work by Douglas, Houk and others, this revived interest has resulted in hundreds of peer-reviewed publications, dozens of symposia at international meetings and a new generation of commercial ICP-MS instrumentation that incorporates collision cells (virtually every manufacturer of such instrumentation now offers a collision cell equipped ICP-MS instrument).

Acknowledgments

The author would like to acknowledge the contribution of many individuals at PNNL and elsewhere to the development of the ion trap ICP-MS method. First, at PNNL, the originators of the ICP-ion trap project, Dr Monty R. Smith (deceased), Dr Charles J. Barinaga and Dr David W. Koppenaal. They built the first generation PSIT and demonstrated the many advantages of ion trap ICP-MS. Their work refuted most, if not all, of the dire predictions of the conventional wisdom. The success of their work was evidenced by the acquisition of follow-on funding to develop second and third generation instruments. Dr Michael L. Alexander at PNNL also contributed to the early ion trap research through many stimulating discussions, reviews and independent, though related, research. Bruce Harrer has provided outstanding stewardship in the area of analytical method commercialization at PNNL and has been involved with us from the outset of patenting and commercialization efforts for the chemical resolution MS approach that arose out of some of the research described here. The collegiality of Dr Cory Frum and Prof. John Todd and their research colleagues, the only other ICP-ion trappers in the mid-1990s, was and is very much appreciated. During the Finnigan supported phases of this work, which were considerable, we benefited greatly from consultations with Dr Jae Schwartz, Dr Dan Wiederin, Dr Charles

Douthitt, and Dr Mike Senko. Last, the author would like to acknowledge the many other funding organizations that have supported development of this new technology and scientific method: PNNL's Laboratory Directed R&D program, the Battelle Memorial Institute through it's Internal R&D program, the US Department of Energy through its office of non-proliferation R&D (NA-22, formerly NN-20), and DOE/ER-LTA for CRADA support.

References

1. Houk, R. S., Fassel, V. A., Flesch, G. D., Svec, H. J., Gray, A. L., and Taylor, C. E. (1980) Inductively coupled argon plasma as an ion source for mass spectrometric determination of trace elements. *Anal. Chem.*, **52**(14), 2283–9.
2. Jakubowski, N., Moens, L., and Vanhaecke, F. (1998) Sector field mass spectrometers in ICP-MS. *Spectrochim. Acta B*, **53**, 1739–63.
3. Mahoney, P. P., Ray, S. J., Hieftje, G. M., and Li, G. Q. (1997) Continuum background reduction in orthogonal-acceleration time-of-flight mass-spectrometry with continuous ion sources. *J. Amer. Soc. Mass Spectrom.*, **8**(2), 125–31.
4. Myers, D. P. and Hieftje, G. M. (1993) Preliminary design considerations and characteristics of an inductively-coupled plasma-time-of-flight mass-spectrometer. *Microchem. J.*, **48**(3), 259–77.
5. Barinaga, C. J. and Koppenaal, D. W. (1994) Ion-trap mass-spectrometry with an inductively-coupled plasma source. *Rapid Commun. Mass Spectrom.*, **8**(1), 71–6.
6. Koppenaal, D. W., Eiden, G. C., and Barinaga, C. J. (2004) Collision and reaction cells in atomic mass spectrometry: development, status, and applications. *J. Anal. At. Spectrom.*, **19**(5), 561–70.
7. Eiden, G. C., Barinaga, C. J., and Koppenaal, D. W. (1995) Resonant excitation of injected atomic ions in an ion trap MS. In: *Proceedings of the 43rd ASMS Conference on Mass Spectrometry and Allied Topics*, Atlanta, GA.
8. Eiden, G. C., Barinaga, C. J., and Koppenaal, D. W. (1995) Selective ion accumulation in an ICP/ITMS using a filtered noise field. In: *Proceedings of the 43rd ASMS Conference on Mass Spectrometry and Allied Topics*, Atlanta, GA.
9. Eiden, G. C., Barinaga, C. J., and Koppenaal, D. W. (1996) Selective removal of plasma matrix ions in plasma source mass spectrometry. *J. Anal. At. Spectrom.*, **11**(4), 317–22.
10. Eiden, G. C., Barinaga, C. J., and Koppenaal, D. W. (1996) Plasma source ion trap mass spectrometry: enhanced abundance sensitivity by resonant ejection of atomic ions. *J. Am. Soc. Mass Spectrom.*, **7**(11), 1161–71.
11. Eiden, G. C., Barinaga, C. J., and Koppenaal, D. W. (1996) Argon ion and matrix polyatomic ion loss phenomena in ICP/MS and ICP/ITMS. *ICP Infor. Newslett.*, **21**, 179.
12. Eiden, G. C., Barinaga, C. J., and Koppenaal, D. W. (1997) Beneficial ion/molecule reactions in elemental mass spectrometry. *Rapid Commun. Mass Spectrom.*, **11**(1), 37–42.
13. Eiden, G. C., Barinaga, C. J., and Koppenaal, D. W. (1997) An improved plasma source ion trap MS incorporating an octopole collision cell. In: *45th ASMS Conference on Mass Spectrometry & Allied Topic*, Palm Springs, CA.
14. Eiden, G. C., Barinaga, C. J., and Koppenaal, D. W. (1999) Analytical performance of the plasma source RF quadrupole ion trap in elemental and isotopic MS. *J. Anal. At. Spectrom.*, **14**, 1129–32.
15. Eiden, G. C., Weir, D. G., Barinaga, C. J., and Koppenaal, D. W. (1999) Ion–molecule reactions for interference reduction in ICP/MS. In: *Federation of Analytical Chemistry and Spectroscopy Societies Meeting*. Vancouver, B.C.

16. Koppenaal, D. W., Barinaga, C. J., and Smith, M. R. (1994) Performance of an inductively coupled plasma source ion trap mass spectrometer. *J. Anal. At. Spectrom.*, **9**, 1053–8.
17. Franklin, T. M., Todd, J. F. J. Smith, R. D., and Schroeder, E. (1997) The ion trap elemental mass spectrometer (ITEMS): instrumentation and preliminary results. In: *The 45th ASMS Conference on Mass Spectrometry and Allied Topics*, Palm Springs, CA.
18. Frum, C. I. (1996) Elemental and isotopic analysis of geological and environmental samples by inductively coupled plasma quadrupole ion trap mass spectrometry (ICP-ITMS). In: *The 44th ASMS Conference on Mass Spectrometry and Allied Topics*, Portland, OR.
19. Milgram, K. E., White, F. M., Goodner, K. L., Watson, C. H., Koppenaal, D. W., Barinaga, C. J., Smith, B. H., Winefordner, J. D., Marshall, A. G., Houk, R. S., and Eyler, J. R. (1997) High-resolution inductively-coupled plasma fourier-transform ion-cyclotron resonance mass-spectrometry. *Anal. Chem.*, **69**(18), 3714–21.
20. Cooks, R. G., Glish, G. L., McLuckey, S. A., and Kaiser Jr, R. (1991) Ion trap mass spectrometry. *Chem. Engr. News.*, **69**, 26–41.
21. March, R. E. and Hughes, R. J. (1989) Quadrupole storage mass spectrometry. In: *Chemical Analysis* (ed. J. D. Winefordner). Vol. 102, John Wiley & Sons, New York, p. 196.
22. McLuckey, S. A., Vanberkel, G. J., Goeringer, D. E., and Glish, G. L. (1994) Ion-trap mass-spectrometry of externally generated ions. *Anal. Chem.*, **66**(13), A689–A696.
23. Doroshenko, V. M., Cornish, T. J., and Cotter, R. J. (1992) Matrix-assisted laser desorption ionization inside a quadrupole ion-trap detector cell. *Rapid Commun. Mass Spectrom.*, **6**(12), 753–7.
24. Vanberkel, G. J., Glish, G. L., and McLuckey, S. A. (1990) Electrospray ionization combined with ion trap mass-spectrometry. *Anal. Chem.*, **62**(13), 1284–95.
25. Gill, C. G. and Blades, M. W. (1993) Laser ablation ion-trap mass-spectrometry – atomic and molecular mass-spectrometry of metal, ceramic and polymer samples. *J. Anal. At. Spectrom.*, **8**(2), 261–7.
26. Gill, C. G., Daigle, B., and Blades, M. W. (1991) Atomic mass-spectrometry of solid samples using laser ablation-ion trap mass-spectrometry (Laitms). *Spectrochim. Acta B*, **46**(8), 1227–35.
27. Duckworth, D. C., Barshick, C. M., Smith, D. H., and McLuckey, S. A. (1994) Dynamic-range extension in glow-discharge quadrupole ion-trap mass-spectrometry. *Anal. Chem.*, **66**(1), 92–8.
28. McLuckey, S. A., Glish, G. L. Duckworth, D. C., and Marcus, R. K. (1992) Radiofrequency glow-discharge ion trap mass-spectrometry. *Anal. Chem.*, **64**(14), 1606–9.
29. Hartung, W. H. and Avedisian, C. T. (1992) On the electrodynamic balance. *Proc. R. Soc. London A*, **437**, 237–66.
30. Davis, E. J., Buehler, M. F., and Ward, T. L. (1990) The double-ring electrodynamic balance for microparticle characterization. *Rev. Sci. Instrum.*, **61**(4), 1281–8.
31. Yang, M., Dale, J. M., Whitten, W. B., and Ramsey, J. M. (1995) Laser-desorption mass-spectrometry of a levitated single microparticle in a quadrupole ion-trap. *Anal. Chem.*, **67**(6), 1021–25.
32. Garrett, A. W., Hemberger, P. H., and Nogar, N. S. (1995) Selective ionization for elemental analysis with an ion-trap mass-spectrometer. *Spectrochim. Acta B*, **50**(14), 1889–95.
33. Todd, J. F. J. (1995) Introduction to practical aspects of ion trap mass spectrometry. In: *Practical Aspects of Ion Trap Mass Spectrometry*, (eds R. E. March and J. F. J. Todd), CRC Press, Boca Raton, FL, pp. 3–24.
34. Syka, J. E. P. (1995) Commercialization of the quadrupole ion trap. In: *Practical Aspects of Ion Trap Mass Spectrometry*, (eds R. E. March and J. F. J. Todd), CRC Press, Boca Raton, FL, pp. 169–205.
35. Williams, J. D., Cox, K. A., Schwartz, J. C., and Cooks, R. G. (1995) High mass, high resolution mass spectrometry. In: *Practical Aspects of Ion Trap Mass Spectrometry,*

Vol. II – Ion Trap Instrumentation, (eds R. E. March and J. F. J. Todd), CRC Press, Boca Raton, FL, pp. 3–47.
36. Dawson, P. H., ed. (1976) *Quadrupole Mass Spectrometry and Its Applications*. Elsevier Publishing Company, Amsterdam.
37. Londry, F. A. and March, R. E. (1995) Systematic factors affecting high mass-resolution and accurate mass assignment in a quadrupole ion trap. *Int. J. Mass Spectrom. Ion Processes*, **144**, 87–103.
38. Schwartz, J. C. (1997) Do space charge effects limit LC quadrupole ion trap performance? In: *Sanibel Island Conference on Ion Traps*. American Society for Mass Spectrometry, Sanibel Island, FL.
39. Reinsfelder, R. E. and Denton, M. B. (1981) Theory and characterization of a separator analyzer mass-spectrometer. *Int. J. Mass Spectrom. Ion Processes*, **37**(2), 241–50.
40. Vedel, F. (1991) On the dynamics and energy of ion clouds stored in an rf quadrupole trap. *Int. J. Mass Spectrom. Ion Processes*, **106**, 33–61.
41. Vedel, F., Vedel, M., and March, R. E. (1991) A sensitive method for the detection of stored ions by resonant ejection using a wide-band signal. *Int. J. Mass Spectrom. Ion Processes*, **108**(2–3), R11–R20.
42. Vedel, F., Vedel, M., and March, R. E. (1990) New schemes for resonant ejection in r.f. quadrupolar ion traps. *Int. J. Mass Spectrom. Ion Processes*, **99**, 125–38.
43. Franzen, J., Gabling, R.-H., Schubert, M., and Wang, Y. (1995) Nonlinear ion traps. In: *Practical Aspects of Ion Trap Mass Spectrometry, Vol. I – Fundamentals of Ion Trap Mass Spectrometry*, (eds R. E. March and J. F. J. Todd), CRC Press, Boca Raton, FL. pp. 49–167.
44. Halliday, D. and Resnick, R. (1966) *Oscillations* in *Physics, Parts I and II*. John Wiley & Sons, Inc., New York, Chapter 15, pp. 345–375. See discussion of simple harmonic motion in Chapter 15.
45. Robb, D. B. and Blades, M. W. (1999) Optimum phase angle for laser desorption ion trap mass spectrometry is dependent on the number of ions produced. *Int. J. Mass Spectrom.*, **191**, 69–80.
46. Sugiyama, K. and Yoda, J. (1990) Anharmonic oscillation of ions trapped in a rf trap with light buffer gas. *Appl. Phys. B*, **51**, 146–52.
47. Makarov, A. A., (1996) Resonance ejection from the Paul trap – a theoretical treatment incorporating a weak octapole field. *Anal. Chem.*, **68**(23), 4257–63.
48. Fulford, J. E., Hoa, D.-N. Hughes, R. J. March, R. E. Bonner, R. F., and Wong, G. J. (1980) Radio-frequency mass selective excitation and resonant ejection of ions in a three-dimensional quadrupole ion trap. *J. Vac. Sci. Technol.*, **17**(4), 829–35.
49. Marshall, A. G., Wang, T. C. L., and Ricca, T. L. (1985) Tailored excitation for fourier-transform ion-cyclotron resonance mass-spectrometry. *J. Am. Chem. Soc.*, **107**(26), 7893–97.
50. Hanson, C. D., Castro, M. E., Kerley, E. L., and Russell, D. H. (1990) High-precision arbitrary wave-form generator for ion selection in fourier-transform ion-cyclotron resonance. *Anal. Chem.*, **62**(13), 1352–5.
51. Kenny, D. V., Callahan, P. J., Gordon, S. M., and Stiller, S. W. (1993) Simultaneous isolation of 2 different M/Z ions in an ion-trap mass-spectrometer and their tandem mass-spectra using filtered-noise fields. *Rapid Commun. Mass Spectrom.*, **7**(12), 1086–9.
52. Goeringer, D. E., Asano, K. G., McLuckey, S. A., Hoekman, D., and S. W. Stiller, (1994) Filtered noise field signals for mass-selective accumulation of externally formed ions in a quadrupole ion-trap. *Anal. Chem.*, **66**(3), 313–8.
53. Furuta, N., Takeda, A., and Zheng, J. (2001) Evaluation of inductively coupled plasma-ion trap mass spectrometry. In: *Plasma Source Mass Spectrometry: The New Millenium*. Royal Society of Chemistry, Durham.
54. Lawson, G. and Todd, J. F. J. (1971) *Mass Spectrometry Group Meeting*. Bristol, United Kingdom.

55. Barshick, C. M. and Eyler, J. R. (1993) An improved ion guide for external ion injection in glow discharge-Fourier transform ion cyclotron resonance mass spectrometry. *J. Am. Soc. Mass Spectrom.*, **4**(5), 387–92.
56. Alves, L. C., Minnich, M. G., Wiederin, D. R., and Houk, R. S. (1994) Removal of organic solvents by cryogenic desolvation in inductively coupled plasma mass spectrometry. Invited lecture. *J. Anal. At. Spectrom.*, **9**(3), 399–403.
57. Tanner, S. D., Paul, M., Beres, S. A., and Denoyer, E. R. (1995) The application of cold-plasma conditions for the determination of trace levels of Fe, Ca, K, Na, and Li by ICP-MS. *Atom. Spectrosc.*, **16**(1), 16–8.
58. March, R. E., Strife, R. J., and Creaser, C. S. (1995) Ion traps as tandem mass spectrometers. In: *Practical Aspects of Ion Trap Mass Spectrometry*, (eds R. E. March and J. F. J. Todd), Boca Raton, CRC Press, FL, pp. 27–88.
59. Duckworth, D. C., Smith, D. H., and McLuckey, S. A. (1998) Fundamental investigations of collisional processes in quadrupole ion traps and their utility in plasma source mass spectrometry. In: *1998 Winter Conference on Plasma Spectrochemistry*, Scottsdale, AZ.
60. Becker, J. S., (2002) State of the art in isotope ratio measurement by inductively coupled plasma mass spectrometry. *J. Anal. At. Spectrom.*, **17**, 1172–85.
61. Kaiser, R. E., Cooks, R. G., Stafford, G. C., Syka, J. E. P., and Hemberger, P. H. (1991) Operation of a quadrupole ion trap mass-spectrometer to achieve high mass charge ratios. *Int. J. Mass Spectrom. Ion Processes*, **106**(May), 79–115.
62. Arnold, N. S., Hars, G., and Meuzelaar, H. L. C. (1994) Extended theoretical considerations for mass resolution in the resonance ejection mode of quadrupole ion-trap mass-spectrometry. *J. Amer. Soc. Mass Spectrom.*, **5**(7), 676–88.
63. Williams, J. D., Cox, K. A., Cooks, R. G., Mcluckey, S. A., Hart, K. J., and Goeringer, D. E. (1994) Resonance ejection ion-trap mass-spectrometry and nonlinear field contributions – the effect of scan direction on mass resolution. *Anal. Chem.*, **66**(5), 725–9.
64. Douglas, D. J. (1989) Some current perspectives on ICP-MS. *Can. J. Spectrosc.*, **34**(2), 38–49.
65. Rowan, J. T. and Houk, R. S. (1989) Attenuation of polyatomic ion interferences in inductively coupled plasma mass-spectrometry by gas-phase collisions. *Appl. Spectrosc.*, **43**(6), 976–80.
66. Chernushevich, I. V., Tolmachev, A. V., Krutchinsky, A. N., Spicer, V. L., Ens, W., and Standing, K. G. (1996) Collisional focusing of ions in the electrospray TOF mass spectrometer. In: *The 44th ASMS Conference on Mass Spectrometry and Allied Topics*, Portland, Oregon.
67. Douglas, D. J. and French, J. B. (1991) Collisional focusing effects in radio frequency quadrupoles. *J. Amer. Soc. Mass Spectrom.*, **3**, 398–408.
68. Xu, H. J., Wada, M., Tanaka, J., Kawakami, H., Katayama, I., and Ohtani, S. (1993) A new cooling and focusing device for ion guide. *Nuc. Instrum. Methods Phys. Res. A*, **333**, 274–81.
69. Gerlich, D. (1992) Inhomogeneous RF fields: a versatile tool for the study of processes with slow ions. In: *State-Selected and State-to-State Ion–Molecule Reaction Dynamics* (eds C.-Y. Ng and M. Baer), John Wiley & Sons, Inc., New York, p. 176.
70. Liao, C.-L., Xu, R., Nourbakhsh, S., Glesch, G. D., Baer, M., and Ng, C. Y. (1990) Experimental and theoretical total state-selected and state-to-state absolute cross sections. II. The Ar+(2P3/2,1/2) + H2 reaction. *J. Chem. Phys.*, **93**(7), 4832–44.
71. Tanner, S. D., Baranov, V. I., and Bandura, D. R. (2002) Reaction cells and collision cells for ICP-MS: a tutorial review. *Spectrochim. Acta B*, **57**, 1361–452.

Chapter 3
Ion Detection

Kevin Hunter and Dick Stresau

3.1 Introduction

After mass analysis, an ion signal must be detected and amplified in order to determine its intensity. Inductively coupled plasma mass spectrometers generally incorporate one of two basic detection schemes: Faraday cup detectors, or electron multiplier detectors. Since a Faraday cup has unity gain, its sensitivity is limited by the capability of the electronics. Therefore, relatively large ion signals are required with this approach. Where there is sufficient signal to use Faraday cups, they offer high accuracy and long term stability suitable for applications such as precision isotope ratio measurement. In order to detect extremely small signals, the high amplification of an electron multiplier is necessary.

Electron multipliers used in mass spectrometers can detect minute ion currents, or even single ions, emerging from the mass filter. Because of their ability to reliably and quantitatively measure these small streams of ions, they have been used for ion detection in mass spectrometry for around 50 years.

The core process at the heart of all electron multipliers is secondary electron emission, first reported in 1902 by Austin and Starke.[1] They observed that when electrons of sufficient energy strike a target, more electrons are emitted from the surface than are incident. This discovery opened up the possibility of using this effect to amplify small electron currents and in 1919 the first patent proposing the use of secondary electron emission for this purpose was filed by Slepian.[2] This patent described the principle of electron multiplication using a single dynode device and in the following years discrete-dynode multipliers with multiple dynodes capable of much larger electron gains were developed by Daspence and Pericaud,[3] Jarvis and Blair[4] and others.[5–7]

An electron multiplier using a continuous resistive surface, instead of discrete dynodes, was first proposed by Farnsworth[8] in 1930 and later developed by Goodrich and Wiley[9] in 1962.

Today, commercial electron multipliers have sufficient gain to detect single ions and are capable of detecting ion currents ranging up to millions of ions per second with high signal-to-noise ratio and excellent linearity.

3.2 Electron multipliers

Historically, two types of electron multipliers have been incorporated in ICP-MS instruments: (1) discrete-dynode electron multipliers and (2) 'continuous dynode', or channel electron

Inductively Coupled Plasma Mass Spectrometry Handbook Edited by Simon M. Nelms
 ISBN: 978-1-405-10916-1

multipliers (CEMs). Earlier ICP-MS instruments used CEMs almost exclusively, as they were more stable in air than the BeCu discrete-dynode multipliers available at the time. However, with the development of suitable air-stable dynode materials, discrete-dynode multipliers became widely used during the 1990s due to their higher dynamic range capability.

There are many different multiplier configurations available that have been tailored for the specific requirements of each application, depending on the type of mass analyzer used and the method by which the signal is collected from the detector. In general, detectors fall into three main application types: pulse-counting, analog and time-of-flight (TOF). The requirements for the detector are very different in each case. The remainder of this section covers the performance aspects that are common to all three types of detector, and subsequent sections describe each type in detail.

3.2.1 Principles of operation

While the principles of operation are similar, the structures of discrete-dynode multipliers and CEMs are quite different. Figure 3.1 illustrates each type schematically.

Discrete-dynode multipliers consist of an array of separate dynodes with high secondary electron yield surfaces. CEMs consist of a lead–silicate glass tube processed to have a resistive inner surface with a suitably high secondary electron emission to multiply electrons. The following discussion is restricted to discrete-dynode detectors, which are the most common type used in ICP-MS. However most of the principles described can be readily applied to CEMs.

The basic principles of discrete-dynode electron multiplier operation are shown schematically in Figure 3.1. When an ion strikes the first dynode of a discrete-dynode electron multiplier (or conversion dynode) it liberates secondary electrons. The electron-optics of the dynodes then accelerates these electrons to the next dynode in the multiplier, which in turn produces a greater number of secondary electrons. This process is repeated at each subsequent dynode, generating a cascade of millions of electrons, which are finally captured (as an output 'pulse', hence the term pulse counting) at the multiplier output electrode. The gain of an electron multiplier can be defined as the average number of electrons collected at the multiplier's output electrode for each input ion that initiates an electron cascade. Similarly, it can be described as the current measured from the output divided by the input ion current. It should be noted that this second definition includes the ion detection efficiency of the multiplier.

The gain of each dynode depends on the dynode surface material and the energy of the electrons striking it. By adjusting the high voltage applied to the multiplier, the inter-dynode voltage (and consequently the electron impact energy) can be set to achieve the required gain. Figure 3.2 shows gain curves for typical electron multipliers for analog and pulse-counting applications.

The operating gain of an electron multiplier is typically set in the range of 10^4–10^6 for analog applications, and 10^6–10^8 for pulse-counting applications.

Each input ion generates a single pulse of electrons that are collected at the detector's output electrode. This pulse of electrical current, which is extracted via the output electrode (signal) lead, is typically 4–10 ns wide (FWHM) depending on the configuration of the detector used. Detectors for TOF mass spectrometry are designed to have a much narrower pulse width (see section 3.6).

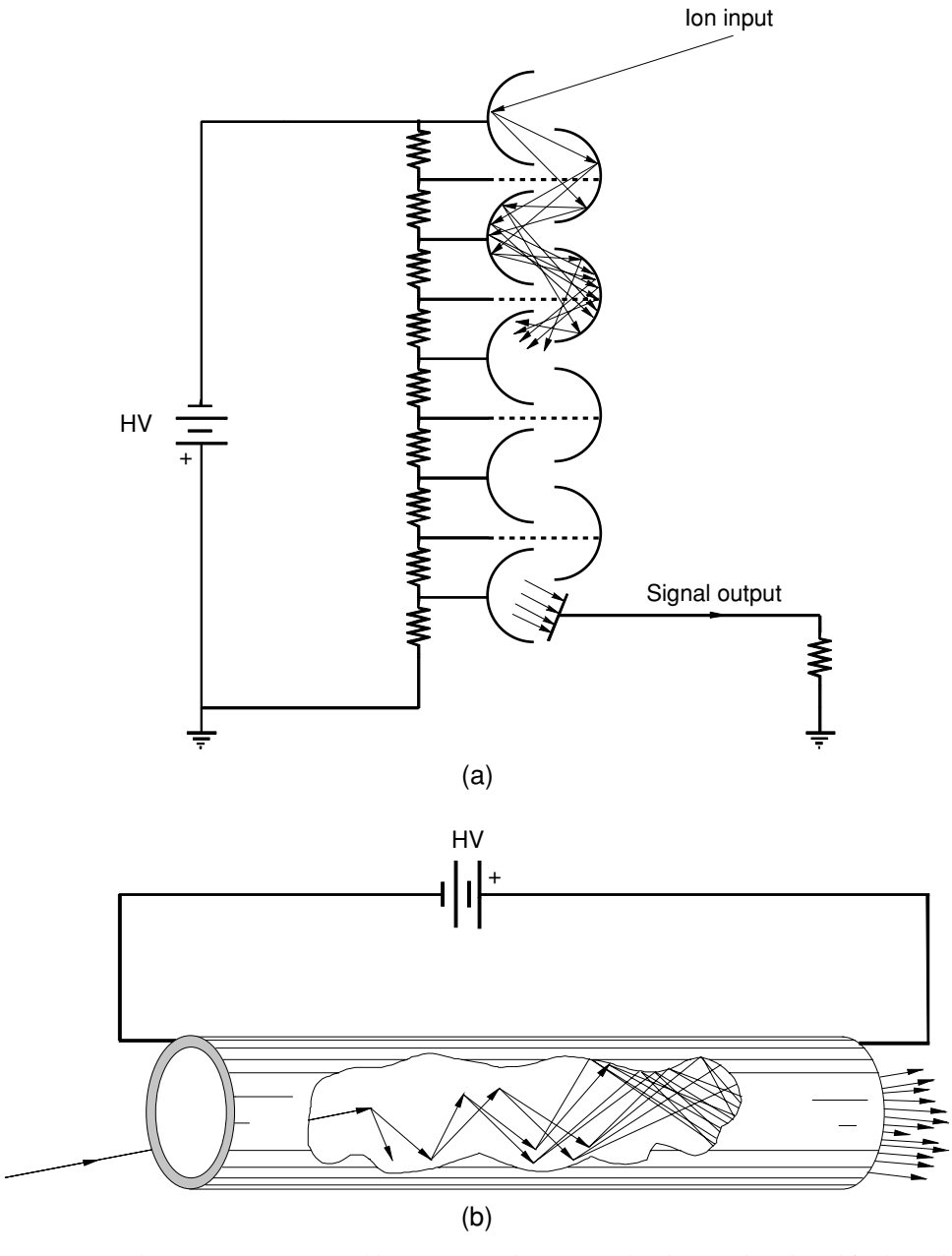

Figure 3.1 Schematic representation of the structure and operation of (a) discrete-dynode and (b) channel electron multipliers.

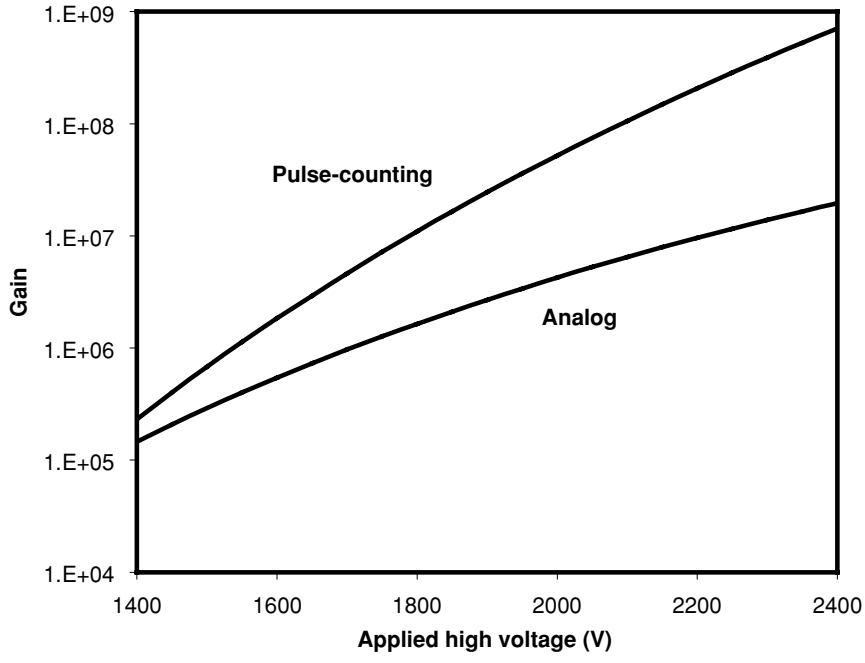

Figure 3.2 Typical gain curves for a 15-dynode analog electron multiplier and a 21-dynode pulse-counting electron multiplier.

3.2.2 Ion detection efficiency

When an ion strikes the first dynode of a detector, the average number of secondary electrons emitted depends upon the mass and energy of the incident ion. It should be noted that not every ion that strikes the first dynode of the detector produces at least one secondary electron, and therefore not every ion is detected by the electron multiplier.

The number of secondary electrons emitted due to an ion impact is governed by Poisson statistics. For example, if an ion strikes the first dynode and produces an average ion-to-electron conversion yield of 1.0, then for each individual ion the number of electrons produced will follow a distribution as shown in Figure 3.3(a). In this case 37% of ions produce no secondary electrons at all. Thus, the resultant detection efficiency is limited to around 63%, assuming there are no other losses in the detector and its associated electronics. If the average ion-to-electron conversion yield is higher, for example 3.0 as shown in Figure 3.3(b), then 95% of ions will produce secondary electrons and a detection efficiency of near 95% can be achieved.

To obtain high detection efficiency it is important to have a high ion-to-electron conversion yield at the first dynode of the detector. Figure 3.4 shows the relationship between the average ion-to-electron conversion yield and the maximum achievable detection efficiency.

As a rule of thumb, the ion-to-electron conversion yield at a given energy is proportional to $M^{-1/2}$, where M is the mass of the ion. This results in the gain of the detector having a mass dependence as shown in Figure 3.5.

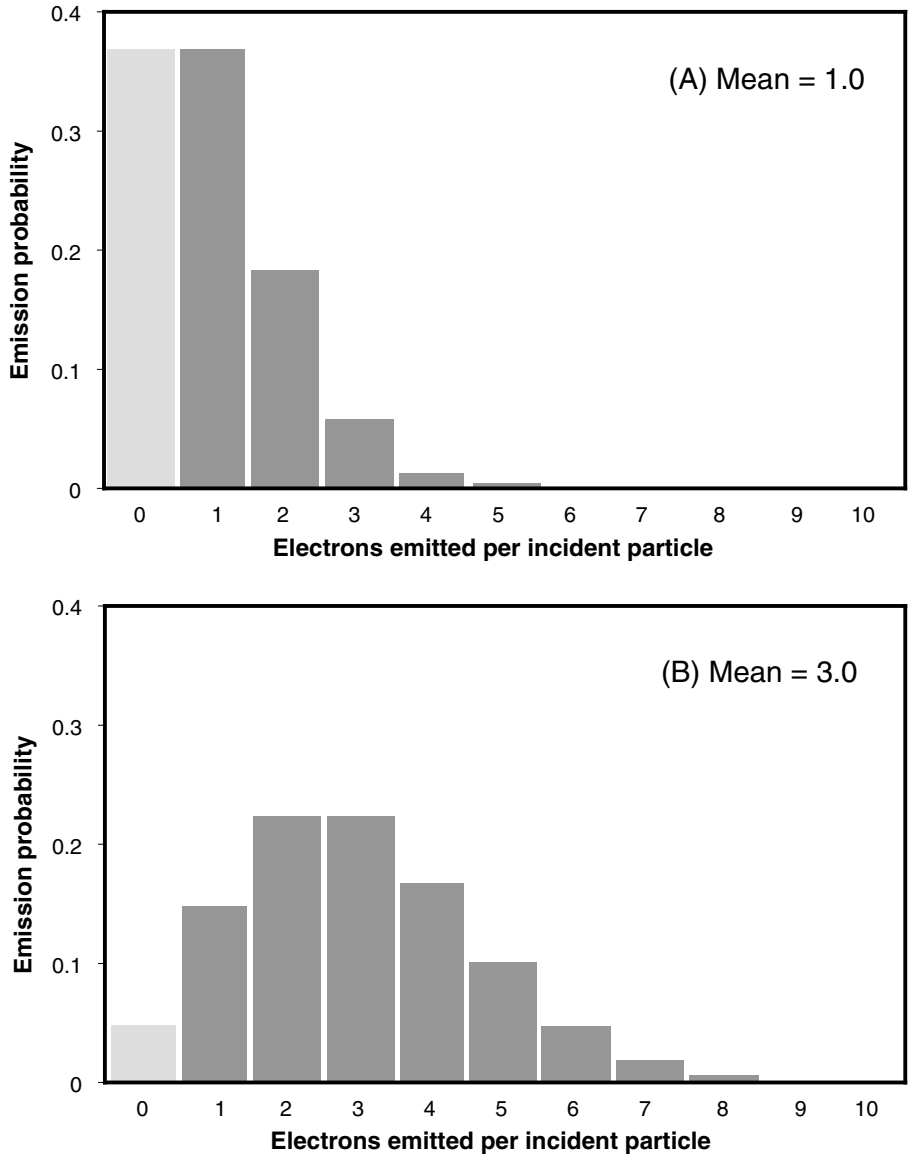

Figure 3.3 Probability distributions for the number of emitted secondary electrons per incident ion, according to Poisson statistics, for a mean secondary electron yield of (a) 1.0 and (b) 3.0.

In addition to the mass effect, the ion-to-electron conversion yield also varies with ion energy. Figure 3.6 shows some measurements from Inghram *et al.*[10] These relationships serve only as a guide and in practice ion sensitivity must be determined by calibration.

To achieve high detection efficiency for high ion masses, some applications use a special high voltage conversion dynode (typically operated at 10 kV) to increase the impact energy of the

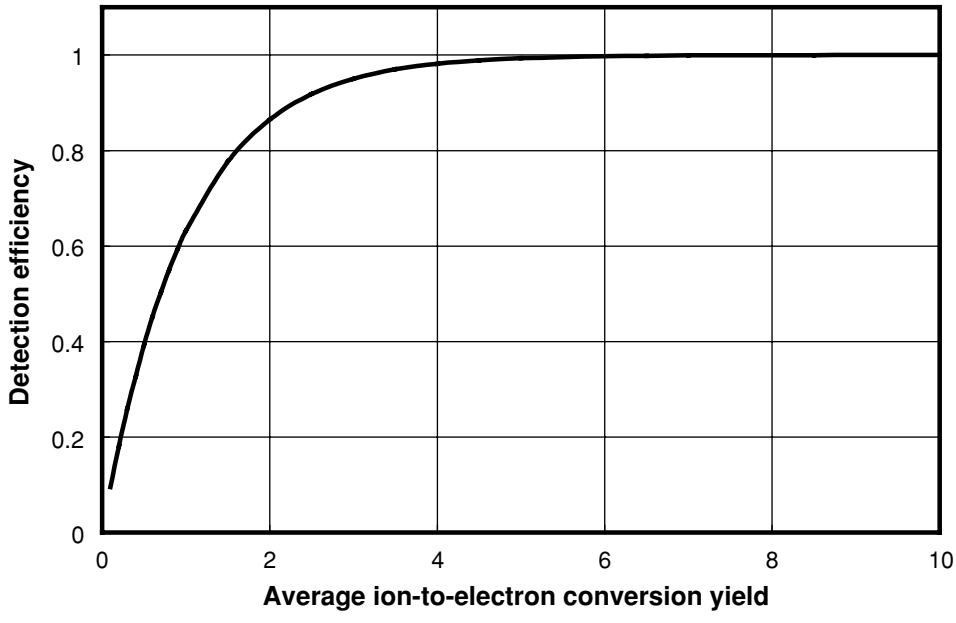

Figure 3.4 Maximum possible detection efficiency of the detector plotted as a function of the average ion-to-electron conversion yield.

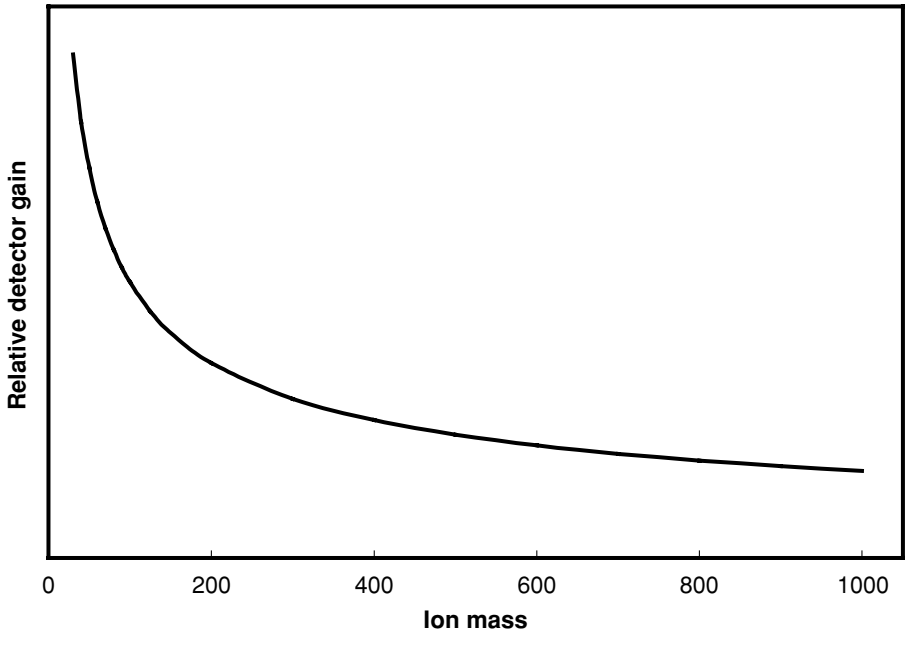

Figure 3.5 General form of the mass dependence of the detector gain.

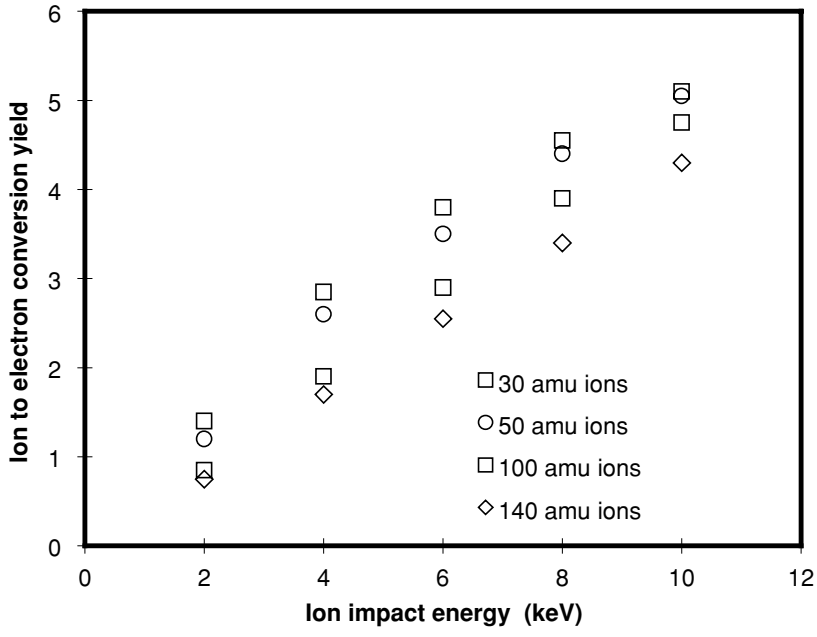

Figure 3.6 Ion energy dependence of the ion-to-electron conversion yield for some alkali metals. Data from Inghram *et al.*[10]

ion and consequently its ion-to-electron conversion yield. This approach is not generally used in ICP-MS (with the exception of the Element2 high resolution ICP-MS instrument), as good ion detection efficiency is achieved using the conventional approach over the limited mass range measured with this technique (from ~2–250 mass units).

3.2.3 Linearity and dynamic range

An important property of an electron multiplier is its ability to operate linearly over a wide range of output current. The signal current drawn from the output must be supplied by the bias current flowing through the voltage divider network. In a standard discrete-dynode multiplier, the voltage divider network consists of a chain of series resistors, as illustrated in Figure 3.1, which apply the appropriate voltages to each of the dynodes. Typically an electron multiplier can operate linearly for output currents up to ~15% of the bias current. Figure 3.7 shows the typical analog linearity for a 21-dynode multiplier.

It should be noted that when the output current is sufficiently large to cause nonlinear response, the detector will over-respond and at much higher output currents the gain begins to collapse. This is characteristic of discrete-dynode electron multipliers, which use a simple resistive voltage divider network.

To understand how this over-response can occur at high output currents, consider the currents flowing through each of the elements of the multiplier circuit shown in Figure 3.8(a).

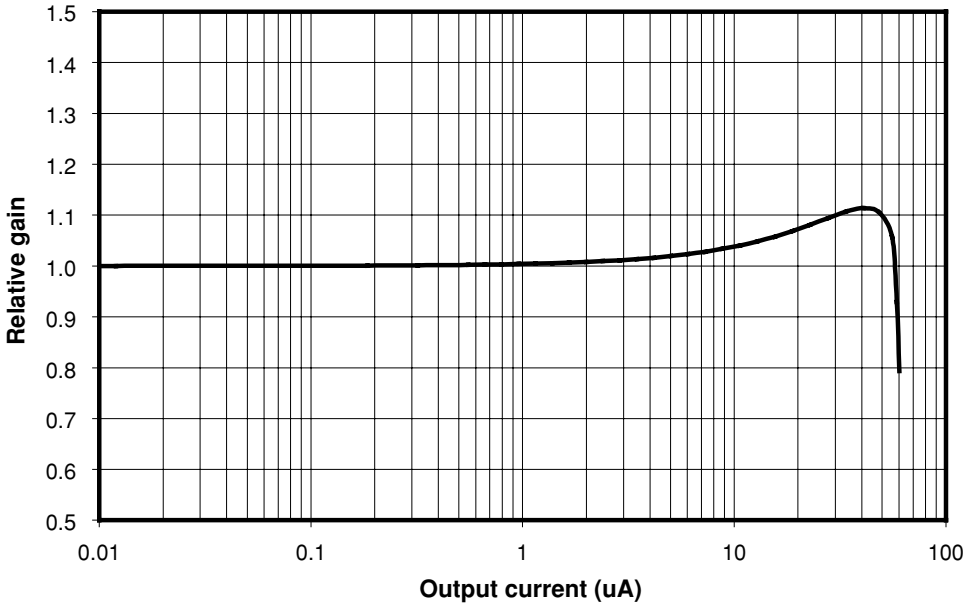

Figure 3.7 Typical analog gain linearity curve plotted as a function of the output current for a 21-dynode electron multiplier operated at a gain of 5×10^7. In this case the multiplier bias current is $\sim 70\,\mu$A.

When an electron current, I_{n-1}, from a dynode, D_{n-1}, is incident on the next dynode, D_n, which has a gain, δ, there is a net current, I_{D_n}, being drawn from the voltage divider chain at that dynode that is equal to:

$$I_{D_n} = \delta I_{n-1} - I_{n-1} = I_{n-1}(\delta - 1) \tag{3.1}$$

This net current, being extracted at dynode D_n, subtracts from the bias current flowing through the next resistor down the chain. This lowers the voltage developed across that resistor, resulting in the voltage between dynode D_n and the next dynode down the chain, D_{n+1}, being reduced.

When operating at high output currents, the net current being extracted from a dynode near the output can be a significant fraction of the multiplier bias current, causing the voltage developed across the next resistor down the chain to be significantly reduced as shown in Figure 3.8(b). Because the total voltage applied across all the resistors in the multiplier is constant, the voltages between dynodes nearer the input will be increased, resulting in the over-response at high output currents.

A number of methods have been employed to increase the linear output current limit of a detector. One method is simply to increase the bias current of the multiplier by using smaller resistor values in the voltage divider network connected to the dynodes. Special high-current multiplier models are in common use that have a total resistance across their dynodes of only 3 MΩ, giving a bias current of $> 600\,\mu$A. These multipliers have linear count rate limits of $\sim 20 \times 10^6$ cps (when operated at a gain of 10^7). Alternate approaches use a variety of specialized voltage divider networks to increase the linear limit of the detector. These networks incorporate zener diodes and additional capacitance to stabilize dynode voltages.[11,12]

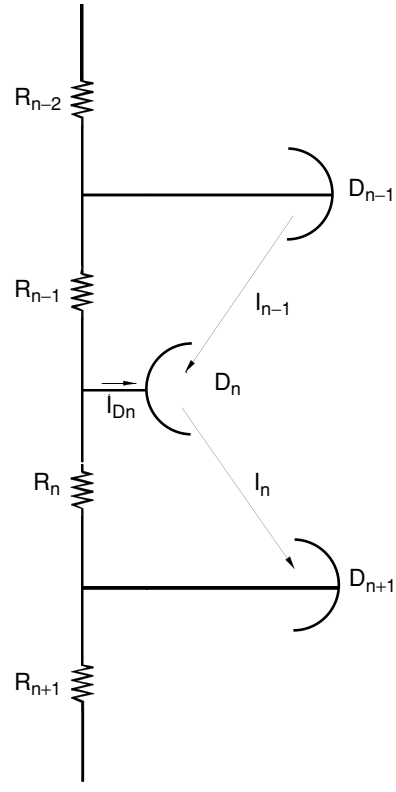

(a)

Figure 3.8(a) A current of electrons I_{n-1} emitted from dynode D_{n-1} and incident on the next dynode in the multiplier, D_n, will cause a current of electrons I_n to be emitted from that dynode. This will cause a net current to be drawn from the resistive voltage divider chain, I_{Dn}, reducing the current flowing through resistor R_n and causing the voltage across R_n to also be reduced.

The linear dynamic range of a detector is defined as the ratio of the largest signal that the multiplier can measure and still respond linearly, divided by the smallest signal that it can usefully measure. Dynamic range is usually stated in terms of orders of magnitude. The dynamic range of conventional multipliers is typically six orders and multipliers designed for extended dynamic range can give linear response over 10 orders of magnitude (refer to section 3.5).

3.2.4 Background noise

Background noise in electron multipliers, often called dark noise (a term borrowed from photomultipliers), is the measured output signal from the detector in the absence of any input ion signal. Under normal operating conditions the background noise of an electron multiplier is typically <0.05 cps for pulse-counting applications, or <1 pA of output current for analog applications. In most cases the detector contribution to background noise is insignificant, and the measured

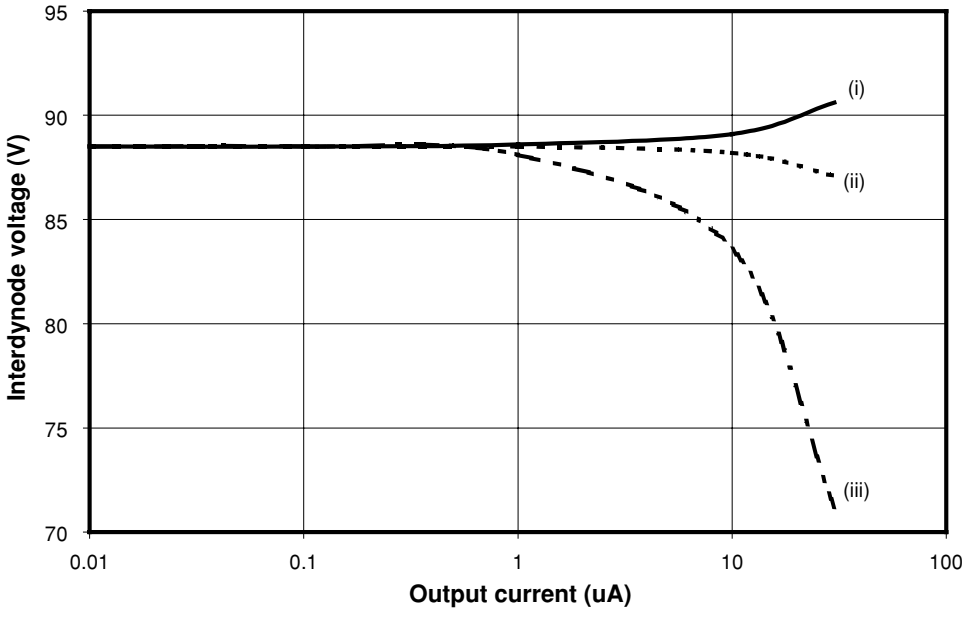

Figure 3.8(b) Effect on the voltages seen between selected dynodes of a 21-stage discrete-dynode electron multiplier plotted as a function of the output current. Curve (i) is the voltage between dynodes 15 and 16, (ii) is the voltage between dynodes 18 and 19 and curve (iii) is the voltage between dynodes 20 and 21.

background is a result of non-mass-correlated ions reaching the detector from the mass analyzer. This very low background noise contribution from the detector usually means that the noise measured on an ion signal is dominated by statistical noise of the ions, or by noise from the ion source.

3.2.5 Multiplier operating life

When an electron multiplier is in operation and is detecting and amplifying ion signals, its gain will slowly decay. This loss of gain is primarily due to the slow build-up of contaminants on the dynode surfaces.[13] In most commercial vacuum systems there are trace amounts of contaminants in the residual gas, which is partially composed of oil from the vacuum pumps. In the presence of the electron cascade in a multiplier, some of these contaminants may be bonded to the dynode surfaces, effectively burying the high secondary electron yield material beneath a thin layer of contamination. As a result, the applied high voltage of the electron multiplier must be periodically increased to restore its gain to the required level. The rate at which contamination builds up on dynode surfaces is largely determined by the level of usage it gets.

Multiplier usage is usually quantified in terms of accumulated charge from the multiplier output. Figure 3.9 shows a typical plot of the required high voltage as a function of multiplier usage for a pulse-counting electron multiplier to operate at a gain of 3×10^7.

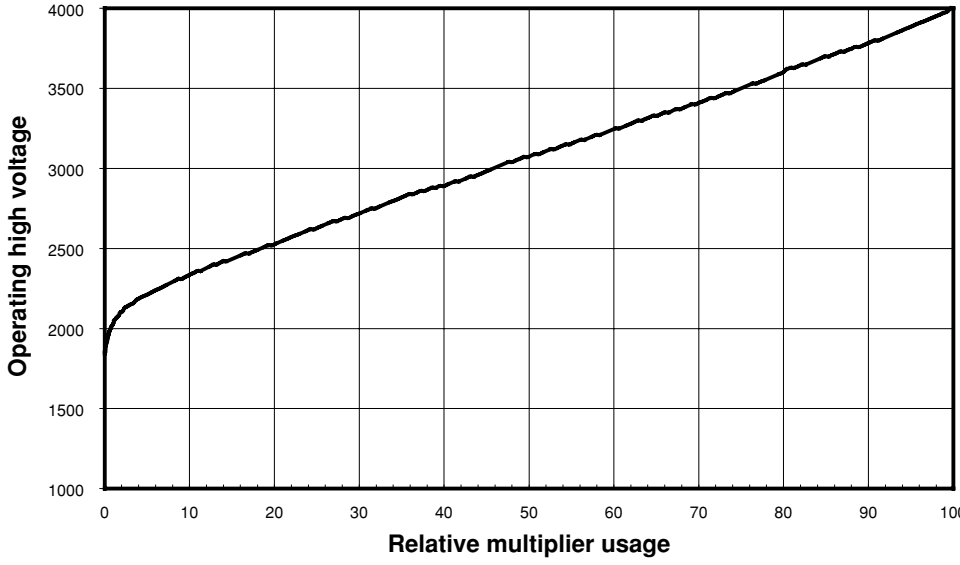

Figure 3.9 Required high voltage for a 21-stage pulse-counting electron multiplier to operate at a gain of 3×10^7 plotted as a function of relative multiplier usage (where a relative usage of 100 corresponds to the end of the multiplier's life). Multiplier usage is normally defined in terms of accumulated charge from the multiplier output.

The multiplier is considered to be at the end of its useful life when the high voltage necessary to achieve the required gain reaches the design maximum for the multiplier. This maximum high voltage limit varies for different multiplier models, but is typically around 4 kV. The operating life of an electron multiplier is also highly dependent on the vacuum system and the amount and composition of any corrosive components of the materials analyzed, and consequently it varies greatly from one application to another.

3.3 Pulse-counting detectors

Electron multipliers for pulse-counting applications are typically designed to operate at a gain of around 2×10^7, although this can be as low as 10^6 in some applications. Discrete-dynode detectors for pulse-counting applications have a relatively large number of dynodes (typically between 21 and 26) to provide good operating life at the high gains used in this mode of operation.

When a multiplier is set to a particular operating gain, say 10^7, it might be expected that it will generate output pulses all containing 10^7 electrons. However, the gain at which the multiplier is set refers only to the *average* gain. The number of electrons in each individual output pulse varies considerably and follows a distribution (see Figure 3.10) that is dominated by the *Poisson* statistics of the first few dynode interactions.

The reason for this variation in output pulse size resides in the statistical nature of the secondary electron emission process of each dynode interaction within the electron multiplier.

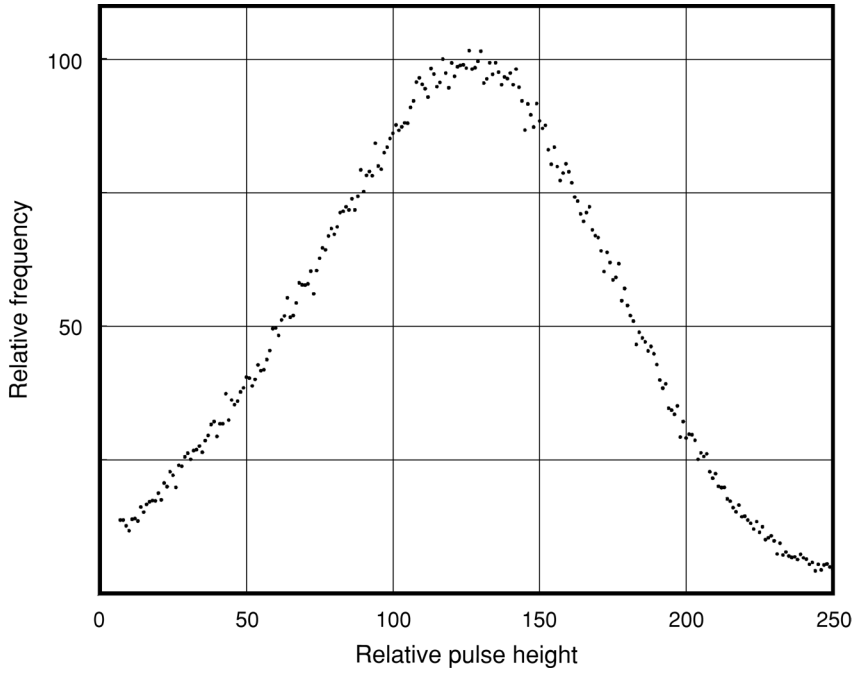

Figure 3.10 Distribution of output pulse heights for a pulse-counting electron multiplier.

A typical pulse-counting detection circuit connected to an electron multiplier signal output is shown schematically in Figure 3.11. In this case the short electrical pulses (typically 4–10 ns wide) extracted from the multiplier output are discharged through a load resistor, generating a negative voltage pulse. This pulse is fed into the detection electronics, which in general consists of a pre-amplifying stage followed by a discriminator/comparator and the data collection electronics.

The discriminator sets the threshold voltage that an output pulse must exceed before being counted by the detection electronics. The discriminator level is set to just above the system's electronic noise level (or line noise), so that only the signal pulses from the multiplier are counted.

3.3.1 Setting the multiplier operating voltage

The process of setting the applied high voltage of the detector for best pulse-counting operation is referred to as '*setting the operating point*'. The curve describing the relationship between the number of ions detected and the multiplier's applied high voltage is referred to as the pulse-counting *plateau curve*, which has the form shown in Figure 3.12.

In a mass spectrometer, a plateau curve is typically generated using the following method. The mass spectrometer is set to monitor a mid-mass-range elemental mass (in some cases several ion masses are used). A specially prepared sample solution which contains a suitable concentration of the selected element(s) is then input to the ion source, so that the detector sees an ion flux sufficiently large to obtain good counting statistics, but small enough to be well below the linear

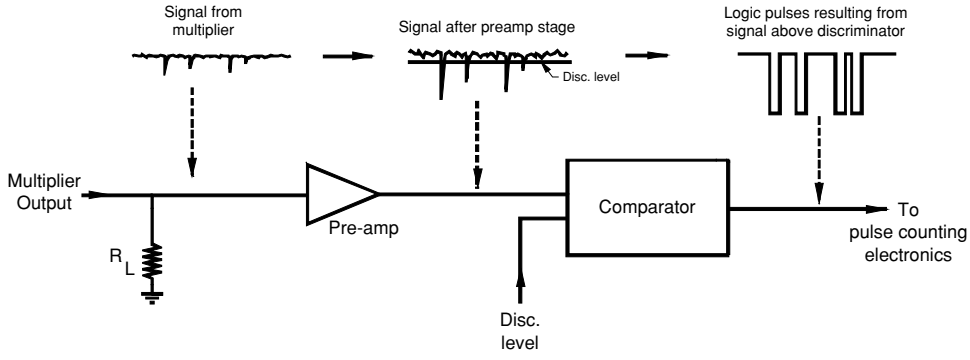

Figure 3.11 Schematic diagram of typical ion-counting detection electronics connected to the signal output of an electron multiplier. This circuit shows a pre-amplifier and a comparator with discriminator to separate multiplier pulses from noise. Note R_L can be a separate load resistor or the input impedance of the preamp.

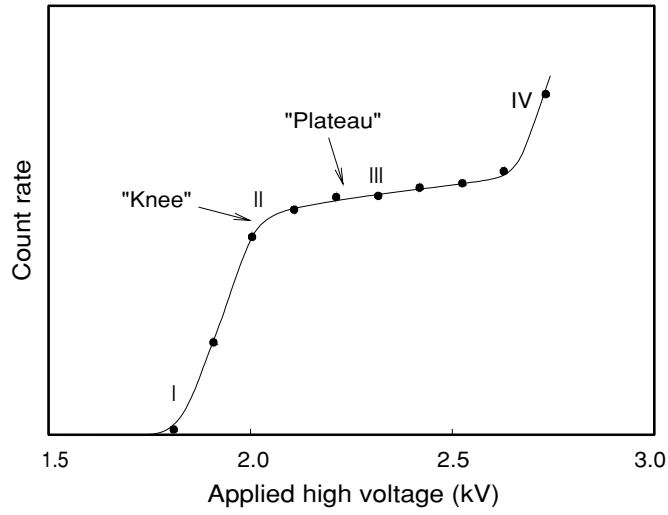

Figure 3.12 Ion-counting plateau curve for a typical pulse-counting multiplier. Region I: onset of ions crossing the discriminator threshold. Region II: *knee* of the ion-counting plateau curve. Region III: *plateau* region of the ion-counting plateau curve. Region IV: *multiple-pulsing* region where the nonlinear effects of *ion-feedback* and electronic *double-counting* are seen.

count rate limit of the instrument. An ion flux of $\sim 10^5$ ions/s measured at the knee of the plateau curve is a typical safe level for most instruments. The electron multiplier is initially set to a low applied voltage (and a correspondingly low gain), so that none of its output signal pulses are large enough to cross the threshold of the discriminator level, and no signal pulses are detected. As the multiplier operating voltage is increased, the gain of the multiplier also increases and the larger output pulses begin to cross the discriminator level to be counted by the electronics (region I of Figure 3.12).

When the high voltage is further increased a greater fraction of output pulses are counted. When the majority of multiplier output pulses are above the discriminator level (and are counted), the effect of increasing the applied high voltage on the measured count rate decreases. This results in the *knee* seen in region II of Figure 3.12. Further increasing the multiplier high voltage results in little change in the measured count rate as the vast majority of pulses from the multiplier are now already being counted. This region is called the *plateau* (region III of Figure 3.12).

Beyond the plateau, at very high electron multiplier voltages, the ion count rate again increases sharply (region IV of Figure 3.12). This sharp increase is due to the onset of multiple-pulsing effects, which fall into two broad categories: (1) ion-feedback in the electron multiplier and (2) electronic double-counting of pulses resulting from ringing effects. Ion-feedback is generated by ionization of residual gas molecules within the structure of the multiplier caused by interaction with the cascading electron pulse. These positively charged ions can be accelerated back up the multiplier and impact on a surface with sufficient energy to produce secondary electrons, which can initiate a second pulse from the multiplier output. Electronic double-counting is caused by an impedance mismatch between the signal output electrode of the multiplier and the detection electronics resulting in significant ringing on the output pulse. At very high gains a ring on the signal pulse can also cross the discriminator level and be counted along with the real signal pulse. It is important to note that in both cases the increased count rate seen is not due to a greater number of ions being detected, but rather to single ion events being counted more than once. Operating in this region of the plateau curve does not improve the sensitivity or the signal-to-noise of the instrument, and the elevated multiplier gains used in this region will cause shortened multiplier operating life and reduce the linearity limit of the detector.

For an electron multiplier to operate with the best ion detection sensitivity, linearity and stability, the applied high voltage should be set so that the measured ion count rate is just above the *knee* of the plateau curve. This represents the most efficient operating point for the multiplier, giving the best combination of ion detection sensitivity, gain stability, linearity and operating life.

Figure 3.13 illustrates how the choice of discriminator level setting influences the resulting plateau curve.

In this illustration, curve (i) corresponds to a discriminator level setting that is just sufficient to remove noise and curves (ii) and (iii) correspond to higher discriminator level settings. In the case of higher discriminator level settings, the operating point is shifted to a higher applied voltage on the detector, as the detector must have a higher operating gain to make the pulses large enough to cross the discriminator level and be counted. A higher gain for the detector means that for a given ion count rate, the average output current will be correspondingly higher. This results in the operating life of the detector being used up at an increased rate. Also the higher multiplier gain will reduce the ion count rate achievable before the detector's linear output current limit is reached, thus reducing the linear dynamic range. Consequently, setting the discriminator level to an appropriately low level is important to get the best operating life and linearity from the detector. Typically the discriminator level is set to around 1 mV as measured at the multiplier output (before the preamplifier).

3.3.2 Dead time

In pulse-counting detection systems there is a minimum time separation requirement between two signal pulses (which includes the detector and its associated electronics) for both pulses to

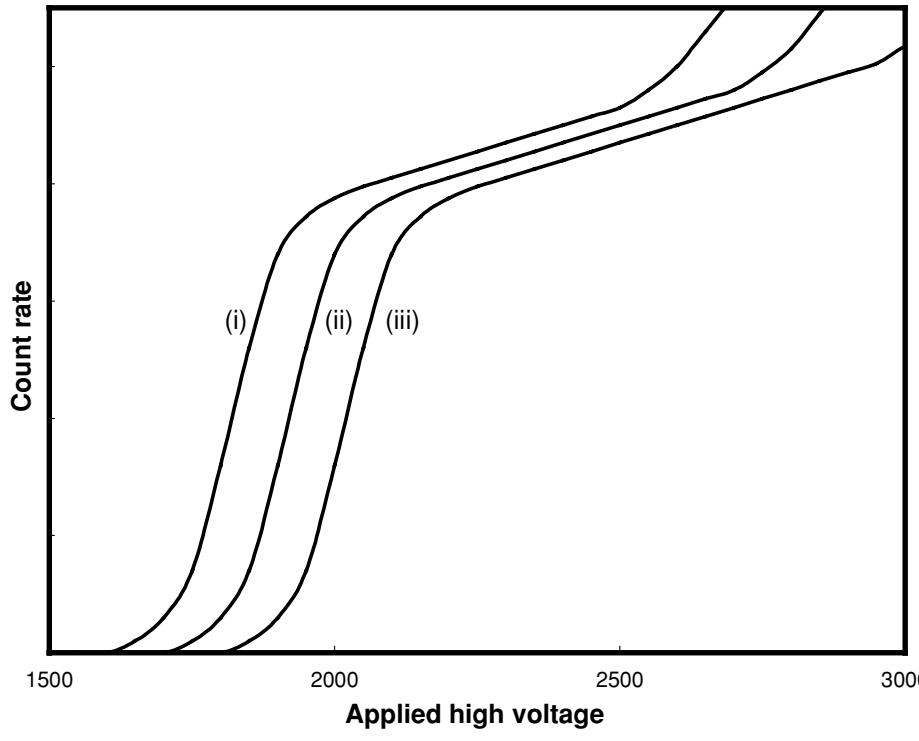

Figure 3.13 Effect of increasing discriminator level setting on plateau curve. Shown are discriminator threshold settings of (i) 1 mV, (ii) 3 mV and (iii) 9 mV.

be recorded. This minimum time interval is called the *dead time* (or *pulse-pair resolution*). The dead time of the system is influenced by two major factors: (i) the pulse width of the multiplier and (ii) the reset time of the pulse-counting electronics and data system. Ion counting detection systems can be classified as either paralyzable or nonparalyzable systems. In paralyzable systems an ion impacting during the dead time created by the impact of the previous ion is not counted but generates a dead time itself, thereby extending the observed dead time of the previous impact. In nonparalyzable systems the impact of an ion leads directly to a dead time during which an incoming ion is not detected and generates no associated dead time itself.[17]

In the detection circuit shown in Figure 3.11 the comparator will not reset until the pulse has fallen below the discriminator level. The time this takes can vary depending on the width of each individual pulse. Once the pulse has fallen below the discriminator level, the electronics and data system will require an amount of time to reset before being ready for the next pulse. This feature of the counting system extends the dead time above that of the detector itself.

To maintain detection linearity when measuring high count rate ion signals, it is important to take the dead time of the counting system into consideration and apply an appropriate correction. In ICP-MS applications, correction for detection dead time is performed by applying the following equation:[15–17]

$$I_t = \frac{I_o}{(1 - I_o\tau)} \tag{3.2}$$

where I_t is the true ion count rate corrected for dead time losses, I_o is the measured count rate obtained with no dead time correction applied and τ is the dead time of the detection system. The expression given in equation (3.2) above is, strictly speaking, only appropriate for the nonparalyzable model, but at ion count rates $\ll 1/\tau$, the paralyzable and nonparalyzable models approximate each other.

Details of methods for measuring system dead time are described in Knoll[14] and Nelms *et al.*[16] The latter reference describes methods of applying dead time correction specifically in ICP-MS applications.

Note that it is important to ensure that the electronics dead time is longer than the longest possible pulse width from the detector. This will minimize the influence of dead time variations resulting from the spread of times that pulses of different size are above the discriminator level and make the resulting total dead time correction more accurate.

3.3.3 Signal noise

At low signal levels the noise measured on the ion signal is usually dominated by statistical noise resulting from the random nature of ion arrival at the detector. This statistical noise follows *Poisson* statistics, which determines that the standard deviation in a set of measurements each containing an average of N ions is $N^{1/2}$. The *relative standard deviation* (RSD) of a set of measurements is defined as:

$$RSD = \frac{\text{std dev}}{\text{mean}} = \frac{N^{1/2}}{N} = N^{-1/2} \tag{3.3}$$

The solid line in Figure 3.14 shows the predicted RSD as a result of statistical noise for a set of measurements as a function of the number of ions in each measurement.

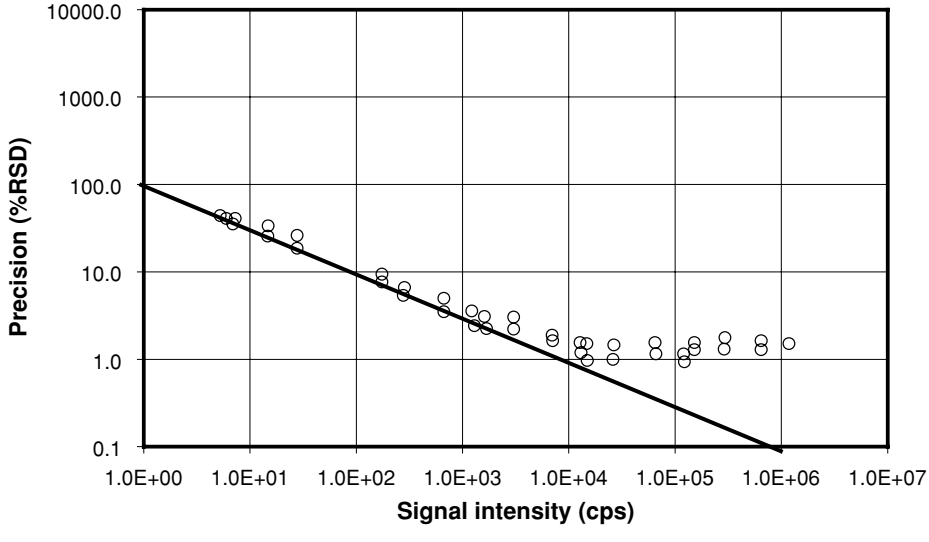

Figure 3.14 RSD of ion signal measurements of 1 plotted as a function of the signal intensity. Solid line is the predicted values for ion counting statistics alone. Data were taken on a Perkin-Elmer Sciex ELAN5000 ICP-MS.[18]

At higher signal levels, the contribution to signal noise of fluctuations in the sample introduction system or ion source begins to dominate. In practice, the RSD achievable will reach a limit where longer integration times to include more signal ions in the measurement will not improve the signal-to-noise of the measurement (see Figure 3.14).

3.4 Analog detectors

Analog detection alone is not widely used in commercial ICP-MS systems, but is most commonly used in conjunction with pulse-counting detection (see section 3.5).

In the case of analog applications, the detector is typically designed to operate at a gain between 10^4 and 10^6. Analog multipliers typically have fewer stages than pulse-counting multipliers. This limits the slope of their gain versus voltage curve (see Figure 3.2), making it easier to accurately adjust and set the gain.

A typical detection system for measuring currents from a multiplier operated in analog mode is shown in Figure 3.15.

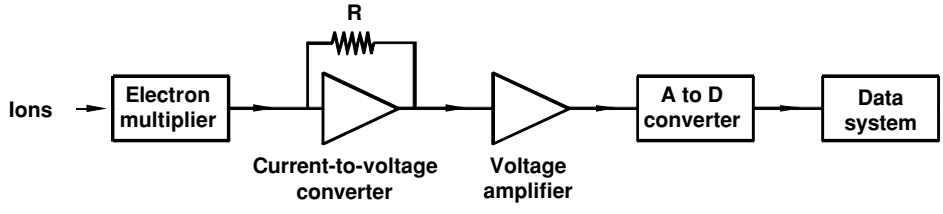

Figure 3.15 Schematic of a typical analog detection circuit. Output current from the electron multiplier is converted to a voltage and then to a digital signal for recording by the data system.

The ion beam is first detected and amplified by an electron multiplier. A current-to-voltage converter converts the output electron current from the multiplier to a voltage, which may be further amplified by a voltage amplifier before being converted to a digital signal and recorded by the data system.

In analog applications the electron multiplier is essentially used as a current amplifier and the individual output pulses from the multiplier are measured as a continuous current. In this case, the output pulses are effectively averaged over the time constant of the analog detection circuit (or electrometer), connected to the output of the detector.

3.4.1 Analog signal noise

As in the case of pulse-counting detection, there is a statistical noise associated with the random arrival of ions at the detector. This represents a fundamental limit on the signal-to-noise of any measurement.

If the average number of ions detected in a given time interval t is N, then the standard deviation, σ, for a set of measurements is $N^{1/2}$. As 95% of measurements are within $N \pm 2\sigma$, this is a useful definition of the noise in a given measurement. The signal-to-noise ratio for the

statistical noise on the signal, SNR_{STAT}, can then be given by:

$$SNR_{STAT} = \frac{N}{2N^{1/2}} = \frac{N^{1/2}}{2} \tag{3.4}$$

For an ion current I containing N ions in the measurement period t, we can write the following equation:

$$I = \frac{Ne}{t} \tag{3.5}$$

where e is the electronic charge (1.6×10^{-19} C). It has been shown by Harris *et al.*[19] that equation (3.5) can be expressed in terms of parameters more appropriate to continuous measurement by replacing the observation time t with 3τ, where τ is the time constant of the detection electronics. Therefore equation (3.5) becomes:

$$N = \frac{3\tau I}{e} \tag{3.6}$$

and equation (3.4) can now be written as:

$$SNR_{STAT} = \left\{\frac{3I\tau}{4e}\right\}^{1/2} = 0.87\left\{\frac{I\tau}{e}\right\}^{1/2} \tag{3.7}$$

However, this only takes account of the contribution to signal noise by the random arrival of ions. The electron multiplier will add an additional amount of statistical noise due to the *Poisson* statistics of the secondary electron emission process, which results in input ions generating electron pulses with a distribution of sizes at the output of the multiplier.

For an analog detector that has a near exponential distribution of output pulse heights, it has been shown that the contribution of the electron multiplier to the standard deviation of a given measurement is approximately the same as that of the random ion arrival[20] (this has been confirmed by the authors using computer simulation methods). The standard deviation due to ion statistical noise, σ_s, adds to the standard deviation due to the detector pulse size distribution, σ_d, according to:

$$\sigma = \sqrt{\sigma_S^2 + \sigma_d^2} \sim \sqrt{2\sigma_S^2} = 1.4\sigma_S \tag{3.8}$$

So the expression for the total signal-to-noise of an analog current becomes:

$$SNR_{TOT} = \frac{1}{1.4} SNR_{STAT} \sim 0.6\left\{\frac{I\tau}{e}\right\}^{1/2} \tag{3.9}$$

In general, this statistical noise becomes the practical limit on the SNR achievable by the detection system. However, there can be other influences on the measured noise from other parts of the mass spectrometer, such as the ion source, or thermal noise from the electronics.

3.4.2 Linearity

In analog applications the multiplier gain is in general much lower than that used for pulse counting. This allows higher ion signal levels to be measured while still remaining in the linear

operating range of the detector. For a given average input ion rate, n(ions/s), the output current from the multiplier is determined by:

$$I_o = enG \tag{3.10}$$

where e is the electronic charge (1.6×10^{-19} C), G is the gain of the multiplier and I_o is the measured output current. For example, if the linear limit output current of the detector is 10 μA and the operating gain is 10^5, then input ion rates of $\sim 10^9$ ions/s can be measured and still remain in the linear range of the detector.

It should be noted that with analog detection the preamplifier is always active and accepting signal, so, unlike pulse-counting detection, there is no associated dead time to be considered. There is another nonlinearity mechanism to be considered when the preamplifier output signal is near its maximum. This can occur even when the detector is responding linearly. As discussed in the previous section, an analog signal will always have a level of noise associated with it, and when the measured signal level is near the maximum output limit of the preamplifier the 'high-points' of the signal fluctuations can be limited, thereby reducing the measured average signal level. Consequently, it is good practice to keep measured signal levels well below the maximum output of the analog preamplifier.

3.5 Extended dynamic range detectors

In order to obtain extended dynamic range, the use of both analog and pulse-counting modes of operation in a single detector has become widespread.[21–23]

A few different approaches have been developed and the first to find commercial application involved switching the high voltage (and hence the multiplier gain) between two settings.[22] At the higher voltage setting the multiplier is used in pulse-counting mode (with a gain of $\sim 10^7$) and at the lower voltage setting the multiplier is used in analog mode (with a gain of $\sim 10^4$). In more recent times other methods have been used and have become standard in most commercial ICP-MS applications.

3.5.1 Simultaneous mode detector

Most ICP-MS instruments in current production incorporate detectors capable of operation in both pulse-counting and analog modes *simultaneously*. In these detectors, ion signal levels from a few counts per second (cps) up to $\sim 10^6$ cps are measured by ion counting, while larger signals, up to an equivalent count rate of 10^9 cps or more, are measured using the multiplier in analog mode.

The *simultaneous mode detector*[23] divides the electron multiplier into two separate amplifying sections, shown schematically in Figure 3.16.

The first section of the multiplier operates in analog mode and is typically operated at a gain of $\sim 1 \times 10^4$. Following this analog section a special *beam-splitting* dynode extracts part of the electron signal and directs it into a shielded Faraday cup from which the analog output signal is taken. The remaining electron signal continues on to the pulse-counting section of the multiplier to be further amplified to a level suitable for pulse-counting operation (typically 3×10^7 in total) before being collected at the pulse-counting output electrode.

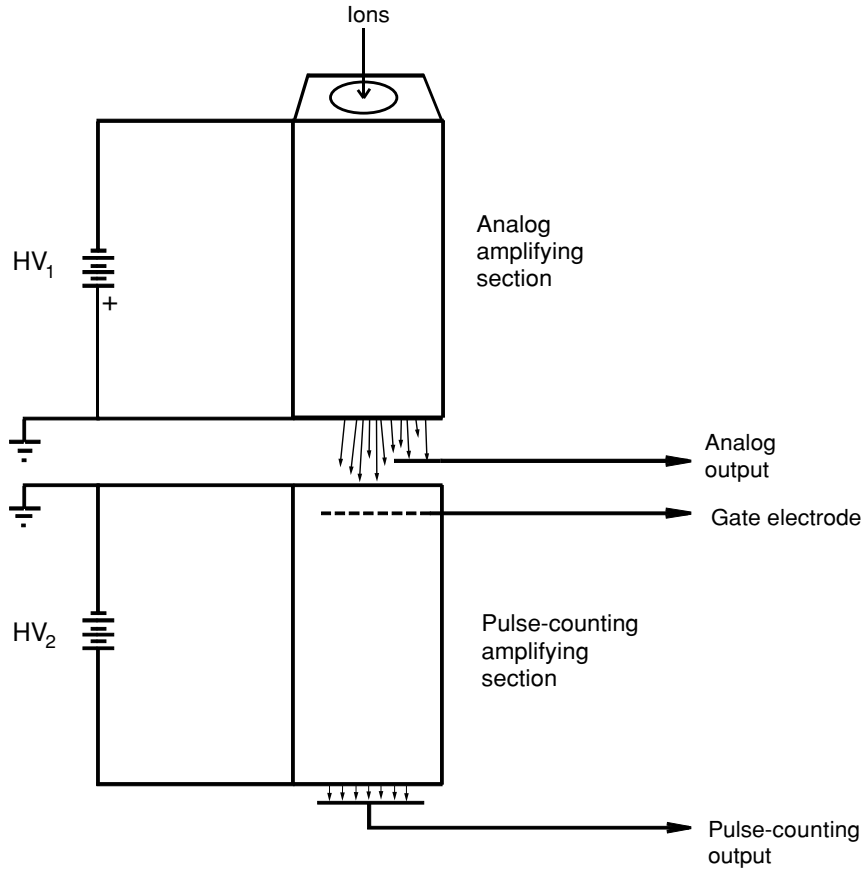

Figure 3.16 Schematic diagram showing the functional layout of a *simultaneous mode* discrete-dynode detector.

At 1×10^4 gain the correlation between the analog output current and input ion count rate is represented by curve (ii) in Figure 3.17.

The maximum linear output current for the analog output of the multiplier is $\sim 5\ \mu$A, so at a gain of 10^4, this limit corresponds to an equivalent input ion count rate of $\sim 10^9$ cps.

For operation in pulse-counting mode the gain of the second section of the multiplier is set so that the combined gain of both sections of the multiplier is $\sim 3 \times 10^7$. At this gain, the maximum linear count rate of the pulse-counting output of the multiplier (so that its output current is $< 15\ \mu$A) is $\sim 4 \times 10^6$ cps.

The correlation between output current and input ion count rate for the pulse-counting section of the multiplier is represented by curve (i) of Figure 3.17. From the two lines it can be readily seen that when the two modes of operation (analog and pulse-counting) are used in one detector, the overall linear dynamic range of the detection system would extend over nine orders of magnitude.

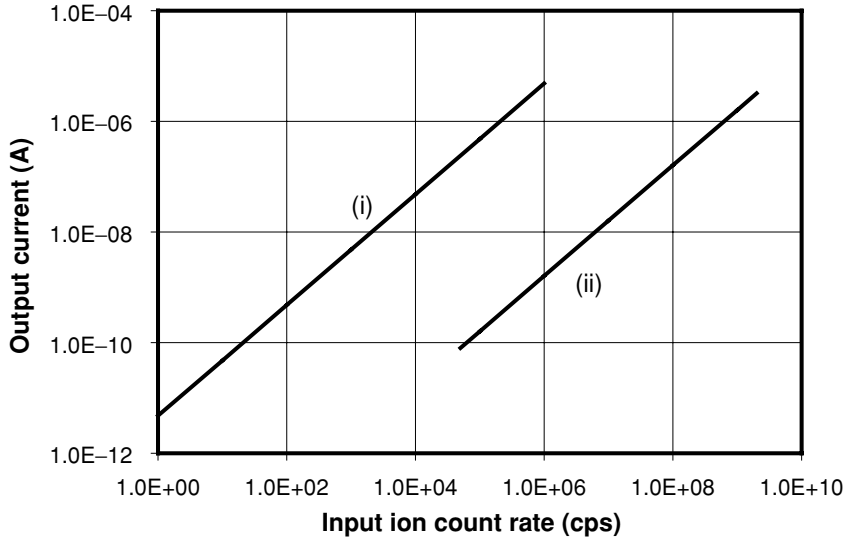

Figure 3.17 The current measured (i) at the pulse-counting output of a simultaneous mode multiplier operated with an overall gain of 3×10^7, and (ii) at the analog output of the multiplier operated at a gain of 1×10^4, plotted as a function of the input ion count rate.

The two sections of the multiplier are separated by a special gate electrode. In the presence of very high signal levels, the gate electrode can be activated to gate off the pulse-counting part of the detector to protect it from excessive signal levels and thus extend its operational life.

Figure 3.18 shows the effect of the voltage applied to the gate electrode on both the analog and pulse-counting outputs.

When the gate voltage is set to a specified voltage, the pulse-counting section is enabled and pulses from the input ions are seen from the pulse-counting output. At the same time the

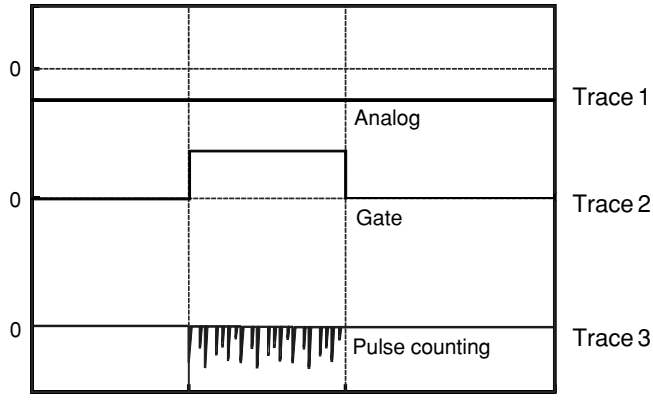

Figure 3.18 Effect of the gate electrode voltage (trace 2) on the analog (trace 1) and pulse-counting (trace 3) outputs.

analog output is also functioning. When the gate is set to ground (0 V) the pulse-counting section is disabled and there is no output from the pulse-counting section. The operation of the analog output is unaffected by the gate and is still functioning normally with the gate closed. Consequently, it monitors the ion signal at all times and can be used to select when the higher gain of the pulse-counting mode part of the detector is required.

In order to use the *simultaneous mode* detector across its full linear dynamic range, it is necessary to cross-calibrate the signals from the analog and pulse-counting outputs. From Figure 3.17 it can be seen that there is a region of input signal intensity where both analog and pulse-counting modes operate at the same time. Cross-calibration between the two detector outputs is obtained either by using a set of calibration samples prepared to attain ion signal intensities that are in this overlap intensity range or by aspirating a single, high-concentration solution and using the instrument hardware to vary the signal intensity across the overlap range. This allows a cross-calibration factor to be determined to convert the analog output current into an equivalent ion count rate. More information about analog signal detection and cross-calibration can be found in section 3.7 of this chapter.

3.5.2 Scaling pulse-counting detector

A very recent and novel development in pulse-counting detectors for ICP-MS is *the scaling pulse-counting detector*.[24] This discrete-dynode pulse-counting detector has been developed to measure input ion beam intensities in excess of 1×10^{10} cps while using conventional pulse-counting electronics. This new method extends the effective upper limit for accurate ion counting using the detector only in pulse-counting mode.

The scaling pulse-counting detector comprises three functionally distinct sections, as shown in Figure 3.19.

When ions enter the detector they strike an ion-to-electron conversion dynode and the resulting electrons then undergo a few stages of multiplication to ensure that there is complete separation of the ion input and the signal attenuation process. This is essential to minimize mass dependence effects.

In the following section (the control section) a voltage applied to a special electrode adjusts the transfer efficiency of the pulses to the amplifying section. This voltage can be adjusted dynamically to change the detector's effective ion detection efficiency from ~90% down to 0.01% (for intense ion fluxes). Figure 3.20 shows the measured attenuation of the output pulse rate of a scaling pulse detector with changes in the control voltage.

Even with this very large attenuation of the output count rate, the average height of the multiplier's output pulses is changed by less than a factor of 3. Those electron pulses that are passed by the attenuation section are then amplified in the final section of the multiplier, so that they have a pulse height that is typical for conventional pulse-counting electronics.

With the control section set to maximum attenuation, only a small fraction (<0.01%) of the incident particles produce an output pulse, and the detector's output pulse rate is correspondingly decreased. In this case, an input ion flux of 10^{10} ions/s will result in an output pulse rate of only around 10^6 cps, which is well within the counting capability of the conventional electronics used in most commercial ICP mass spectrometers.

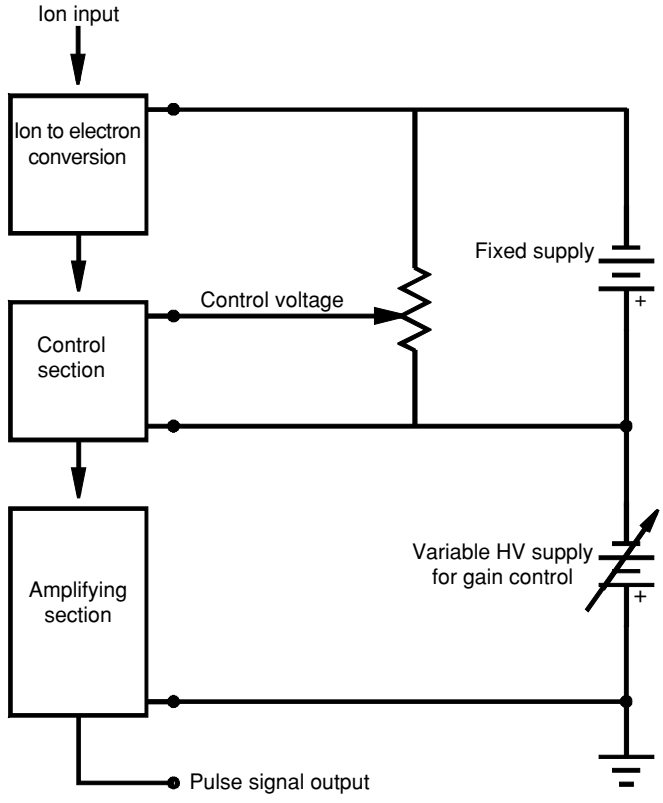

Figure 3.19 Schematic diagram of a *scaling pulse-counting* detector.

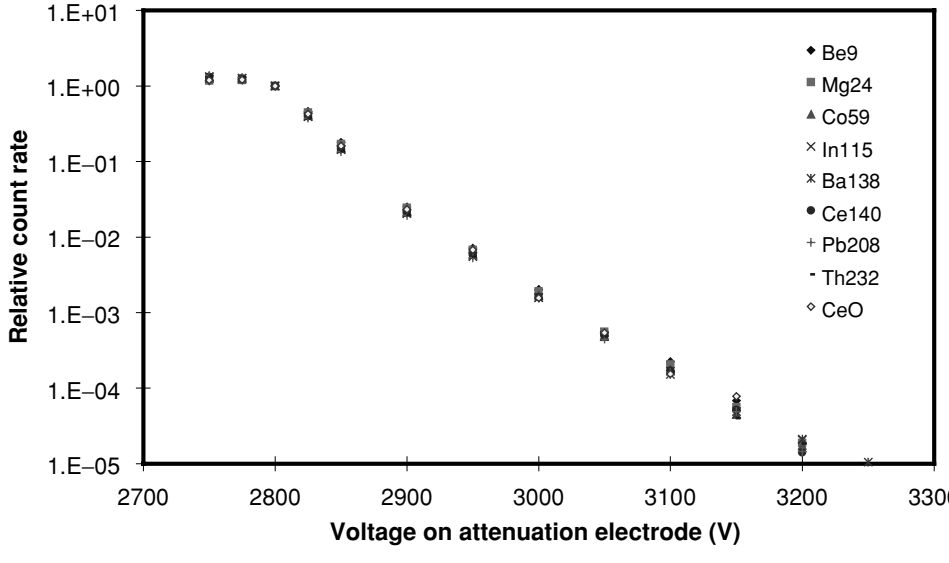

Figure 3.20 Attenuation of the measured output pulse rate of a scaling pulse-counting detector with changes in the control voltage. Measurements were taken with a Varian Ultramass700 ICP-MS and using an ETP model DM169B detector. Data courtesy of Varian Australia (2003).

3.6 Time-of-flight (TOF) detectors

At present, TOF mass analyzers are not widely used in ICP-MS. However, there are commercial systems available (as described in Chapter 2) and the following brief description of detectors used in TOF-MS applications is included for completeness. There are two main types of detectors used in TOF-MS applications: microchannel plates (MCPs) and fast discrete-dynode multipliers.

Due to their robustness, high pulse linearity and dynamic range, most commercial TOF ICP-MS systems use a fast discrete-dynode electron multiplier for ion detection. A discrete-dynode multiplier designed for TOF applications requires the first (conversion) dynode to be flat and perpendicular to the ion trajectories so that all the ions of a given mass peak arrive at this dynode at nearly the same time. Once the ions have been converted to electrons, which are much lighter and move far more quickly than ions, the electron signal can be transferred to the electron multiplying structure with only a small effect on the output pulse width of the detector. Typical pulse widths obtainable from a discrete-dynode multiplier for TOF applications are from 2 to 5 ns, depending on the model of detector used.

The linear response for large average output currents is similar to that of conventional analog or pulse-counting detectors, and high bias current models are linear for output currents up to $\sim 30\ \mu$A.[25] A multiplier can be driven to very high output currents by operation at high gain and with a high input ion current from high abundance samples, and care should be taken not to exceed the linear limit of the detector.

In TOF applications, an additional consideration is the *pulse linearity* of the detector, which is the *linear limit for an individual peak* in a single TOF spectrum. Discrete-dynode TOF multipliers will operate linearly with very large output pulses with up to 10^9electrons in a single pulse (or 1000 mV into 50 Ω with a 3 ns wide pulse). The size of a pulse is limited by the ability of the detector to deliver the necessary charge from the internal capacitance of the multiplier. To allow a discrete-dynode detector to store sufficient charge, specialized voltage divider networks are used that include capacitance elements. If an individual isotope peak exceeds the linear pulse limit of the detector it will be diminished, while smaller peaks will remain unaffected, thereby distorting the measured isotope abundance ratios.

The dynamic range of a TOF system depends on its signal handling electronics as well as the detector performance. Operation with lower multiplier gains will directly increase the system's upper pulse-linearity limit for the number of ions in a single input pulse. For example, if the maximum charge in an output pulse is 10^9 electrons, then operation at a gain of 10^6 will allow up to 1000 ions to be detected linearly in a single pulse, while a gain of 10^5 will enable linear detection of 10 000 ions.

An important parameter for a detector used in TOF-MS is its ability to recover quickly after a large signal pulse. Discrete-dynode detectors used in TOF-MS applications use voltage divider networks, that include distributed capacitance to supply the charge extracted by the electron cascade and reduce saturation effects, and lower resistance elements that allow a high bias current to quickly recharge the capacitors. Experimental measurements have shown no variation in detector response for two intense mass peaks <30 ns apart, indicating that the large-pulse recovery time for the discrete-dynode TOF detector is less than 30 ns.[25]

For applications where narrower output pulse widths are required from the detector, an MCP can be used. An MCP consists of an array of glass capillaries, with inner diameters of typically 5–10 μm, which have been formed into a thin plate. The front and back surfaces of the plate

are made conductive and a voltage is applied between them to bias the array of capillaries. The inner surfaces of the capillaries consist of a secondary electron emissive material so that when an ion strikes the surface, a cascade of electrons is initiated. Such devices can achieve output pulse widths of <1 ns.[26] More recent MCPs made with 2 μm bore size have reported pulse widths of less than 0.5 ns[27] for a detector incorporating two MCPs used in a Chevron arrangement.

Although MCPs can achieve very narrow pulse widths, they also have some significant limitations. The need to linearly detect signal pulses over a large pulse dynamic range, and to handle very high signal intensities for sustained periods, with fast recovery after intense bursts of ions, restricts their use in most ICP-MS applications.

3.7 Analog multiplier signal processing

3.7.1 Introduction

The multiplier analog current signal has to be digitized for use by the data system. This has historically been accomplished using an oscillator whose frequency is proportional to the signal current and then accumulating a count from this oscillator in a digital register, which can be conveniently read by the data system.

For a fast acquisition this technique is too slow, especially at low signal levels where long integration times are required to accumulate a significant count of the analog value.

More recently analog to digital converters have been used in conjunction with a current-to-voltage converter. This arrangement produces much faster acquisition, the speed of which is limited mainly by the response of the current-to-voltage converter.

3.7.2 Noise

At the sort of signal levels used by analog multipliers, the ion statistical noise is small compared to other noise sources and especially the ICP source. This means that fast analog data acquisition is likely to be noise limited by the ICP source noise.

For the minimum noise on the measured data, integration in software can be used with a speed penalty.

3.7.3 Current-to-voltage converter

Converting the multiplier current to a voltage is accomplished using an operational amplifier in the inverting configuration (See Figure 3.21).

To provide protection from discharges, a pair of back to back diodes (D1 and D2) with a current limiting resistor (R_{in}) is usually connected in the input circuit.

The output voltage V_{o} is given by:

$$V_{\text{o}} = I_{\text{in}} R_{\text{f}} \tag{3.11}$$

where I_{in} is the input current in ampere (A) and R_{f} is the feedback resistor value in ohm (Ω).

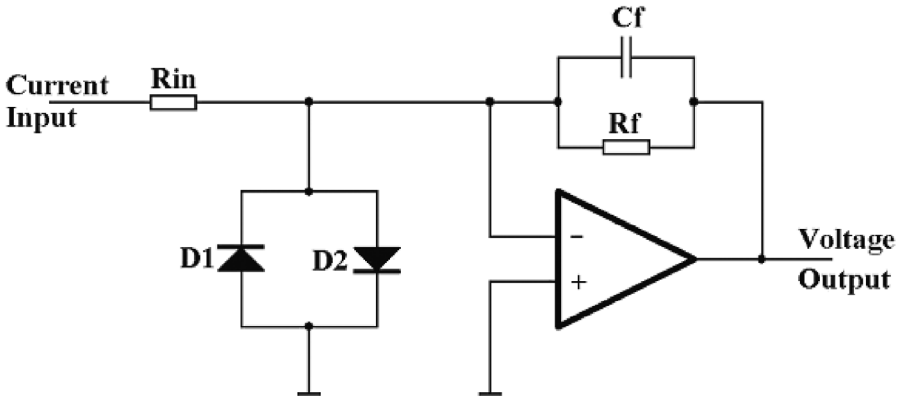

Figure 3.21 Current-to-voltage converter.

The feedback capacitor, C_f, determines the bandwidth/response of the converter and also ensures amplifier stability.

The step response of the circuit is equivalent to a single exponential function with a time constant of $C_f R_f$ seconds. Therefore the highest speed of data acquisition is determined by the choice of this time constant.

3.7.4 Analog-to-digital converter

This device converts analog voltages into digital values, which can be readily used by the data system. Today, cost effective converters capable of converting in a few tens of microseconds and offering 16 bits of resolution are readily available.

To gain the best use of the resolution of a converter it should be used in a monopolar configuration. This usually means a signal range of 0 to +10 V. Any signal that is negative cannot therefore be measured.

In a practical system this is not acceptable since there will be some zero drift in the measuring system and any signal noise that is bipolar in nature must be properly measured so that it can be integrated if required.

The solution to the problem is to add a small fixed positive DC offset to the signal to ensure that under all conditions the signal plus its noise and any zero drift will always be positive in value and therefore measurable. The value of this DC offset can be measured periodically and then used to correct measured values by applying a zero correction in the software.

3.7.5 Converting analog measurements to equivalent pulse counts

With a dual detector employing pulse counting and an analog multiplier, the operating conditions have to be established by some system measurements. These measurements rely on the assumption that the pulse-counting plateau characteristics represent the true signal ion count. The procedure involves first measuring the pulse count mode plateau characteristics and positioning

the operating point just above the plateau knee (to maintain the longest possible multiplier lifetime) as described earlier (section 3.3.1). Then the analog multiplier HT is adjusted to set the gain of the analog multiplier to the desired value specified by the multiplier manufacturer by comparing the measured values from a specific peak in pulse counting and analog mode. For a simultaneous detector this is a recursive process since changing the analog HT will also modify the pulse-counting plateau setting.

It is known that the analog signal sensitivity has a significant mass dependence (section 3.2.2) and observations have shown that this sensitivity is also determined by the particular species being measured. The factor used to convert the analog signal into equivalent counts is best determined by means of a mass/species versus pulse counting to analog signal ratio look-up table, which is maintained by a calibration procedure (as described earlier).

3.8 Data handling

This section discusses the basic control required to acquire data and how the detector outputs are converted into count rate data that can be used for further calculation.

3.8.1 Defining acquisitions

There are two methods of defining the regions of the usable mass range of the instrument where data are to be acquired. Using peak jump, the actual analytes to be measured are specified along with the number of data points, or channels, to be used for each analyte, the dwell to be used for each channel and the separation of the channels for each analyte. Using scan, regions of the mass range are specified as a start and end mass along with the number of channels per mass and the dwell to be used for each channel.

There are also two methods of defining how to acquire data. In continuous acquisition the number of sweeps of the defined regions is specified, and in TRA (time resolved acquisition) the number of sweeps of the defined regions is specified in terms of the number of time slices to store, each time slice being one sweep. The main difference in acquisition terms between continuous and TRA is how the acquired data are stored. In continuous acquisition the data are accumulated over the number of sweeps and then the accumulated data are stored. In TRA the data acquired for each sweep are stored separately.

3.8.2 Data acquisition

Low level data acquisition is the same for peak jump and scan and only differs for continuous and TRA in the handling of the per sweep data. The first step is to convert the acquisition regions, which have been specified in terms of mass, into terms that the acquisition electronics can handle. The mass value of each channel in the specified regions is converted to a digital value that the quadrupole electronics can handle by using a mass calibration equation. Once this conversion has been done, the acquisition electronics can acquire a sweep of data. At the end of this sweep the data handling differs depending upon whether this is a continuous acquisition or TRA.

If this is a continuous acquisition then the acquired data are added to an accumulation buffer and another sweep is then acquired. This is repeated until all of the sweeps have been acquired at which point the accumulation buffer is then stored.

If this is a TRA acquisition, then the acquired data are stored and another sweep is then acquired. This is repeated until all of the time slices have been acquired.

3.8.3 Raw data to count rate data

The acquired data consist of two numbers for each channel. One number is the pulse-counting data and the other is the analog data.

The pulse-counting data is the total number of pulses output from the detector during the acquisition time for that channel. To convert the pulse-counting data to a count rate in cps, the following equation is used:

$$cps = \frac{\text{counts} \times 10^{-6}}{\text{dwell}\,(\mu\text{s}) \times \text{sweeps}} \tag{3.12}$$

The result of this equation needs to be corrected for the dead time of the detector system, as discussed in section 3.3.2.

The analog data is representative of the analog output and depends upon the design of the detector electronics. For systems that use a voltage to frequency converter the same equation as the pulse-counting data is used. For systems that use an analog to digital converter the following equation is used.

$$cps = \frac{\text{counts} \times \text{sampling period}\,(\mu\text{s})}{\text{dwell}\,(\mu\text{s}) \times \text{sweeps}} \tag{3.13}$$

3.8.4 Converting analog count rates

Before the analog count rate data can be used in further calculations, they need to be converted into an equivalent pulse-counting count rate. This is done by using the following equation:

$$\text{equivalent PC cps} = (\text{analog cps} - \text{amplifier offset}) \times \text{factor} \tag{3.14}$$

In order to ensure that the analog detector electronics always produce a valid output, an offset signal is added to the detector's analog output signal (section 3.7.4). This offset signal needs to be subtracted before the analog count rate data can be converted. The factor indirectly represents the difference in gain between the pulse-counting and analog outputs of the detector. The actual value of the factor to be used depends upon the analyte being measured and is obtained from the instruments cross-calibration look-up table.

3.8.5 Integration

After the conversion of the analog count data to equivalent pulse count rates, the data can be integrated. The integration technique for peak jump is slightly different from that used for scan.

For peak jump data the integrated count rate for an analyte is the average count rate of all of the channels in the region defined for that analyte.

For scan data the integrated count rate for an analyte is the average count rate of a portion of the channels in the region whose mass range includes the analyte. The channels used depend upon the mass of the analyte and the size of the integration range to be used in the calculation.

3.8.6 Pulse count or analog?

Part of the calculation is to decide whether to use the integrated data generated by the analog data or the pulse count data for each analyte. In general, pulse-counting data are used, unless the detector electronics indicate that the pulse-counting detector protection circuitry (see section 3.5.1) has operated during the acquisition of data for the analyte; in this case the analog data are used.

Acknowledgments

The authors are greatly appreciative of the contribution and efforts of Wayne Sheils of ETP Electron Multipliers, Australia and John Gray of SGE Inc., USA.

Simon Nelms also wishes to thank Roger Fletcher and Dave Grindley of Thermo Electron Corporation, for their contributions to the analog signal processing and data handling sections of this chapter.

References

1. Austin, L. and Starke, H. (1902) *Ann. Phys.*, **9**, 271.
2. Slepian, J. (1919) US Patent No. 1450265.
3. Daspence and Pericaud (1923) French Patent No. 582428.
4. Jarvis and Blair (1926) US Patent No. 1903569.
5. Zworykin, V. K., Morton G. A., and Malter, L. (1936) *Proc. I. R. E.*, **24**, 351.
6. Rajchman, J. A. (1938) *Arch. Sci. Phys. Nat.*, **20**, 231.
7. Sommer, A. H. and Turk, W. E. (1950) *J. Sci. Instrum.*, **27**, 113.
8. Farnsworth, P. T. (1930) US Patent No. 1969399.
9. Goodrich, G. W. and Wiley, W. C. (1962) *Rev. Sci. Instrum.*, **33**, 761.
10. Inghram, M. G., Hayden, R. J., and Hess, D. C. (1953) Mass spectrometry in physics research. *Natl. Bur. Std.* (USA), *Circ.*, **522**, 257.
11. Hunter, K. L. Stresau, R. W., and Sheils, W. L. (2002) *Proc. ASMS Conference Mass Spectroscopy and Allied Topics*, Orlando, June 2–6.
12. 'Voltage Divider Design' (1982) Thorn EMI Electron Tubes.
13. Cutter, A. D., Hunter, K. L., Paterson, P. J. K., and Stresau, R. W. (1994) *Proc. ASMS Conference Mass Spectroscopy and Allied Topics*, Chicago, May 29–June 4.
14. Knoll, G. F. (1979) *Radiation Detection and Measurement*, John Wiley & Sons, New York.
15. Muller, J. W. (1973) *Nucl. Instrum. Methods*, **112**, 47.
16. Nelms, S. M., Quetel, C. R., Prohaska, T., Vogl, J., and Taylor, P. D. P. (2001) *J. Anal. At. Spectrom.*, **16**, 333.

17. Van Heuzen, A. A., Hoekstra, T., and van Wingerden, B. (1989) *J. Anal. At. Spectrom*., **4**, 483.
18. Denoyer, E. R. (1994) *At. Spectrosc*., **15**(1), 7–16.
19. Harris, F. M., Trott, G. W., Morgan, T. G., Brenton, A. G., Kingston, E. E., and Beyton, J. H. (1984) *Mass Spectrom. Reviews*, **3**, 209.
20. Kelly, P. C. and Horlick, G. (1973) *Anal. Chem*, **45**, 518.
21. Kristo, M. J. and Enke, C. G. (1988) *Rev. Sci. Instrum*., **59**, 438.
22. Hutton, R. C., Eaton, A. N., and Gosland, R. M. (1990) *Appl. Spectrosc*., **40**, 238.
23. Stresau, R. W. and Hunter, K. L. (1993) *Proc. ASMS Conference Mass Spectroscopy and Allied Topics*, San Francisco, May 31–June 4.
24. Stresau, R. W. and Hunter, K. L. (2001) *European Winter Conference on Plasma Spectrochemistry*, Lillehammer, Norway, Feb. 4–8.
25. Stresau, R. W., Hunter, K. L., and Gray, J. (1995) *Proc. ASMS Conference Mass Spectroscopy and Allied Topics*, Atlanta, May 22–26.
26. Wiza, J. L. (1979) *Nucl. Instrum. Methods*, **162**, 587–601.
27. Laprade, B. and Starcher, R. (2001) '2 Micron Bore MCP' data sheet, Burle Electro-Optics, Inc.

Chapter 4
Calibration Strategies and Quality Assurance

Jochen Vogl

4.1 Terminology

Certainly the generation of 'precise' and 'accurate' results represents the most important part of analytical chemistry. But what is meant by 'precise' and 'accurate' results? When talking about analytical topics, whether they are results, procedures or others, we need a common understanding of the terms used to avoid their misunderstanding or misuse. This is becoming increasingly important as further opening of international borders for trade and communication proceeds.

Several efforts have been made to harmonise terms in analytical chemistry. The most central publication is the 'International Vocabulary of Basic and General Terms in Metrology (VIM)',[1] which has been prepared by a joint working group of several international commissions (IUPAC, ISO, BIPM and others). The VIM is mainly focused on basic expressions in metrology. Analytical terms can also be found in several ISO guides. The most useful series of publications, however, is the 'Glossary of Analytical Terms (GAT)',[2–4] which is a project run by the EURACHEM Education and Training Working Group. GAT is an ongoing project, which translates analytical terms into more than 30 languages and publishes them together with their definitions. A list of defined terms and where they can be found is also given in references.[5–7] To avoid going beyond the scope of this book, only the most important terms are defined below.

Accuracy

Definition: The closeness of agreement between the result of a measurement and the true value of the measurand.[1]
Description: Accuracy is a measure that combines precision and trueness (i.e. the effects of random and systematic factors respectively). Suppose the results produced by the application of a method show zero or very low bias (i.e. are 'true'), their accuracy becomes equivalent to their precision.[2] Due to the worldwide concept of measurement uncertainty as expressed in ISO[8] and EURACHEM[9] documents, it is recommended to use the clearer and less ambiguous term 'uncertainty' instead of 'accuracy'.

Bias

Definition: The difference between the expectation of the test results and an accepted reference value.[10]
Description: Bias is the total systematic error of a test result (in contrast to random error).

Inductively Coupled Plasma Mass Spectrometry Handbook Edited by Simon M. Nelms
 ISBN: 978-1-405-10916-1

Conventional true value

Definition: Value attributed to a particular quantity and accepted, sometimes by convention, as having an uncertainty appropriate for a given purpose.[1]
Description: As the 'true value' is not accessible by definition, the best approach to it, the conventional true value, is used. The conventional true value should be realised only by the best available estimate of the value. This strategy is often applied for reference material certification, when a number of measurements of a quantity are used to establish the certified value, a conventional true value.

Error

Definition: The error of a measurement is the result of the measurement minus the true value of the measurand.[1] (In practice mostly conventional true values are used, as the true value cannot be determined.)
Description: Error is the sum of systematic and random error.

Limit of detection

Definition: The detection limit of an individual analytical procedure is the lowest amount of an analyte in a sample, which can be detected but not necessarily quantified as an exact value.
Description: The limit of detection, expressed as a concentration or a quantity, is derived from the smallest signal x_L , which can be detected with a reasonable certainty for a given analytical procedure: $x_L = x_{b1} + ks_{b1}$, where x_{b1} is the mean and s_{b1} the standard deviation of the blank measurements and k is a numerical factor chosen according to the level of confidence required. For many purposes the limit of detection is taken to be $3s_{b1}$.[3]

Limit of determination

Definition: The determination limit of an individual analytical procedure, although not officially defined, is widely recognised as being the lowest amount of an analyte in a sample, which can be determined as an exact value.
Description: The limit of determination, expressed as a concentration or a quantity, is derived from the smallest signal x_L, which can be determined with a reasonable certainty for a given analytical procedure: $x_L = x_{b1} + ks_{b1}$, where x_{b1} is the mean and s_{b1} the standard deviation of the blank measurements and k is a numerical factor chosen according to the level of confidence required. It is widely agreed that the limit of determination, often referred as limit of quantitation, is taken to be $6s_{b1}$.[3]

Precision

Definition: The closeness of agreement between independent test results obtained under stipulated conditions.[10]
Description: The precision of a set of results, which have been obtained under stated experimental conditions, can be quantified as standard deviation.[3] Precision is normally differentiated as repeatability and reproducibility.

Repeatability

Definition: The closeness of agreement between the results of successive measurements of the same measurand carried out under the same conditions of measurement.[1]
Description: Repeatability may be expressed in terms of dispersion characteristics of the result (e.g. standard deviation) and is often referred to as 'internal' standard deviation. Repeatability conditions are constant conditions and require the same measurement procedure, the same observer, the same instruments used under the same conditions at the same location and repetition over a short period of time.[1]

Reproducibility

Definition: The closeness of agreement between the results of measurements of the same measurand carried out under changed conditions of measurement.[1]
Description: Reproducibility may also be expressed in terms of dispersion characteristics of the result (e.g. standard deviation) and is often referred to as 'external' standard deviation. As soon as measurement conditions have been changed it is a matter of reproducibility and not any more of repeatability. This is valid for the same individual sample measured under altered conditions (e.g. another day, another calibration) as well as the measurement of different sub-samples under the same or under varying conditions.

Sensitivity

Definition: Change in the response of a measuring instrument divided by the corresponding change in the stimulus.[1]
Description: The sensitivity can give information about measurement range and detection power of an instrument. In ICP-MS sensitivity usually is expressed as the measured intensity of a standard solution divided by the concentration (mass fraction, in this case) and extrapolated to a mass fraction of 1 mg/kg.

Trueness

Definition: The closeness of agreement between the average value obtained from a large series of test results and an accepted reference value.[1] ('Accepted reference value' is assumed to be equivalent to 'conventional true value.')
Description: A true result is a result with little or ideally no bias. Perfect trueness cannot be achieved, so trueness in its analytical meaning is always trueness within certain limits. It is important to keep the difference to accuracy in mind. Accuracy is the closeness of agreement between a single test result and the conventional true value.[2]

True value

Definition: The value that characterises a quantity perfectly defined in the conditions, which exist when that quantity is considered.[2] This value is consistent with the definition of a given particular quantity.[1]
Description: The true value is a theoretical concept and would be obtained by a perfect measurement. In reality it is indeterminate and not accessible, as all measurements are biased.

Traceability

Definition: The property of a result of a measurement or the value of a standard whereby it can be related to stated references, usually national or international standards, through an unbroken chain of comparisons, all having stated uncertainties.[1]
Description: For each analytical measurement it should be possible to relate the result to an international standard or unit through an unbroken chain of comparisons. In terms of mass this is the kilogram in Paris, for amount of substance it is the mole. Traceability enables comparability of measurement results.

Trackability

Definition: The property of a result of a measurement whereby the result can be uniquely related to the sample.[2]
Description: Each step of an analytical procedure has to be documented, so that the result of a measurement can be linked unambiguously to the sample.[2]

Uncertainty

Definition: A parameter, associated with the result of a measurement, that characterises the dispersion of the values that could reasonably be attributed to the measurand.[1]
Description: Uncertainty sets the limits within which a result is regarded as accurate, i.e. precise and true.

4.2 Practical considerations

The most important aspect to consider before performing an analysis is the properties of the sample to be measured. For ICP-MS this leads to a number of questions. The most important ones are listed below:

(1) Is the sample available in solid, gaseous or liquid form?
(2) For a liquid sample, is it a slurry, a suspension, an emulsion or a solution?
(3) What are the analytes? Which elements, isotopes, isotope ratios or species are to be measured?
(4) What is the concentration range of the selected analytes?
(5) What is the concentration of total dissolved solids in the sample?
(6) How much sample volume is available?
(7) What acids have been used to prepare the sample?
(8) What are the main matrix components?
(9) How small is the required uncertainty?

To answer all these questions, more background information is necessary. Assistance will be given in the following section of this chapter for a better understanding of these questions and to facilitate a proper selection of the technical and analytical possibilities for ICP-MS measurements.

1. Solid samples can be analysed by direct solid sampling (Chapter 6) or by dissolving the solid sample. Dissolution and decomposition processes are described in Chapter 9 and can also be found in the literature.[11,12] Gaseous samples are usually analysed by coupling gas chromatography with ICP-MS (Chapter 7), although for certain applications, such as measurement

Figure 4.1 Concentrated solution of digested, freeze-dried plant material (~120 mg in ~23 mL of 2% nitric acid) leads to blockage of the cooler skimmer cone (right) while the hotter sample cone shows no deposits (left).

of semiconductor grade gases, customised sample introduction manifolds have been developed (see semiconductor applications in Chapter 9). For liquid samples we proceed with question 2.

2. For slurries, suspensions and emulsions, a sample digestion or decomposition is generally recommended, but in some special cases, direct sample introduction of emulsions,[13,14] suspensions or slurries[15] is possible. Here robust, easy to clean nebulisers such as V-groove, Burgener parallel-path or cross-flow devices are used (see Chapter 5). For solutions in which the concentration of organic compounds exceeds a certain limit (dependent on the organic material present, the instrumental set-up and the analytical conditions used), sample digestion can become necessary. Organic compounds can lead to interferences, cone blockage (Figure 4.1), plasma stability problems and strong matrix effects.

3. It should be clearly stated what the analytes are. The number of isotopes to be measured sets the total measurement time. When transient signals are to be recorded the peak width, or more specifically the equivalent peak duration, limits the number of measurable isotopes, as at least 10–15 points per isotope are required to properly characterise the transient signal. Isotope ratio measurements require other conditions and calibration strategies than quantitative analysis. Also, for speciation different aspects have to be considered (Chapter 7). Additionally, characteristics of the analyte have to be considered. Some elements tend to stick on surfaces of the sample introduction system and therefore lead to an increased analyte signal after each sample measurement. This so-called memory effect can lead to biased results. A good example of an element that is well known to suffer from severe memory effects is Hg. This element tends to adsorb to glass and Teflon surfaces, particularly when it is in its atomic form (as Hg^0). Fortunately, addition of certain oxidising (e.g. Au^{3+}) or chelating substances (e.g. cysteine) to the sample can reduce this memory effect. Addition of Au^{3+} functions by oxidising any Hg^0 present to Hg^{2+} (with corresponding reduction of Au^{3+} to Au^+), thereby reducing Hg adsorption. Addition of Au^{3+} does not work through amalgamation of Au with Hg as is often suggested, since the latter process only occurs when Au and Hg are both present as base metals.[16] The wash-out behaviour of Hg using different set-ups can be seen in Figure 4.2. Au^{3+} leads to good wash-out behaviour of Hg, which is

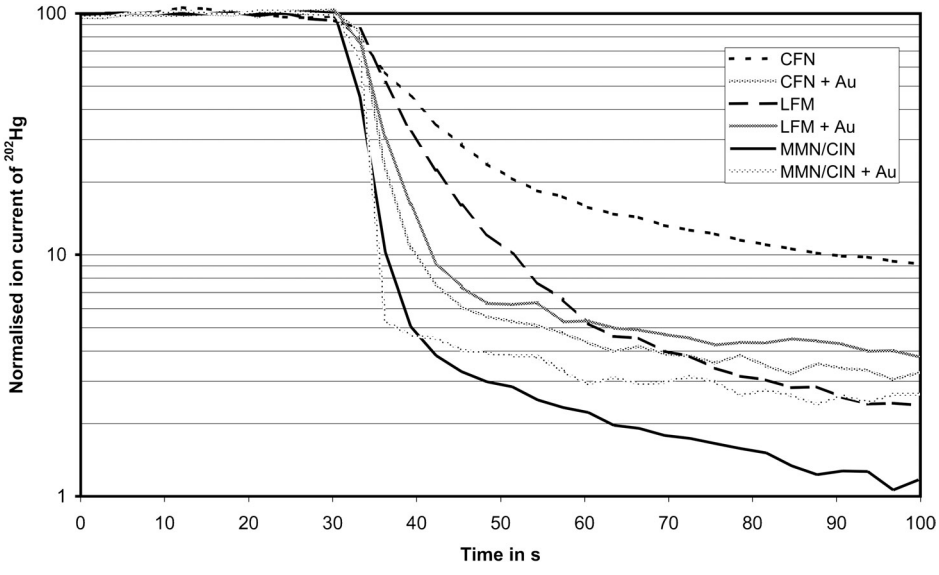

Figure 4.2 Wash-out experiments of a Hg standard (10 μg/kg) demonstrated for different nebuliser/spray chamber set-ups: Cross Flow neb./Scott-type double pass (CFN ~1 mL/min, Perkin Elmer Sciex, Ontario, Canada), low flow Meinhard neb./Scott-type double pass (LFM ~200 μL/min, Glass Expansion, Australia/Perkin Elmer Sciex, Ontario, Canada), MicroMist neb./Cinnabar (MMN/CIN ~100 μL/min, Glass Expansion, Australia); each set-up was tested with and without addition of Au (100 μg/kg).

quite similar for different nebuliser/spray chamber combinations. The best results were achieved with a combination of a MicroMist nebuliser (Glass Expansion, Australia) and a Cinnabar spray chamber (also Glass Expansion), which offered the lowest sample consumption and smallest spray chamber inner surface in this comparison and thus the least possibility for adsorption.

4. The analyte's concentration ranges are important to identify, in consideration of the sensitivity of the instrument, to establish whether or not a dilution or enrichment step is necessary. In good analytical practice, the calibration range should cover the analyte concentration present in each sample. Additionally further decisions in terms of equipment have to be made. For working in the mg/kg range, conventional glassware for nebuliser and spray chamber can be used, but to go down to the μg/kg or ng/kg level requires the sample introduction system to be made from quartz or PFA (**perfluoroalkoxy** polymer) to minimise blank contribution, memory effects and cross contamination.

5. High concentrations of total dissolved solids (TDS) results in clogging of the nebuliser, the injector tube, the sampler cone and especially the skimmer cone. Clogging is a time dependent process and results in dramatic sensitivity drifts before the system is completely blocked, which is due to decreasing sampler and skimmer orifice (Figure 4.1). The limit of TDS (1–10 g/L) that can be tolerated strongly depends on the instrument type, the nebuliser used (cross-flow > concentric), the inner diameter of the injector tube (larger diameters (2–3 mm) offer greater tolerance) and the orifice of the cones (smaller ones reduce contamination of ion optics but block faster). To avoid strong drift and matrix effects as well as clogging, the concentration of TDS should be controlled. Usually 1–2 g/L(i.e. 0.1–0.2% m/v) is taken as the practical upper limit of TDS concentration.

6. The sample volume available for analysis is directly linked to the analyte concentration (can the sample be diluted and the analyte still be detected?) and mainly results from the sample preparation procedure. For this purpose, a variety of nebulisers with different sample uptake rates is available ranging from some 20 μL/min (microconcentric nebuliser) to 2 mL/min (ultrasonic nebuliser). For more details on nebulisers see Chapter 5.

7. The acids used for sample digestion and preparation can cause certain limitations in ICP-MS. In particular, acids generate specific spectral interferences, often referred to simply as interferences. These interferences have the same nominal mass as the target analyte and are caused by molecular (polyatomic) or atomic (isobaric) species produced by reactions between the sample matrix and plasma gases or by overlap of isotopes of different elements (e.g. ^{40}Ca and ^{40}Ar, ^{87}Rb and ^{87}Sr). Perhaps the most well-known example of an acid derived polyatomic interference is $^{40}Ar^{35}Cl$, produced from HCl, which interferes with ^{75}As. In addition, some acids, such as hydrofluoric acid (HF), require special handling precautions. Nitric acid (HNO_3) is the least problematic and therefore most widely used acid, mainly due to its ease of handling and the fact that it does not generally create significantly increased interferences above those already generated by H, N and O from the air and water introduced into the plasma with the sample. In contrast, sulfuric acid (H_2SO_4) and phosphoric acid (H_3PO_4) are among the least favoured acids to use because of the large number of interferences they create in the plasma. If significant levels of HF are present in the sample, the whole sample introduction system has to be made from HF-resistant material (e.g. PFA) to avoid damage. Methods for eliminating or correcting for these interferences form a major part of ICP-MS method and instrumentation development and are covered extensively later in this book.

8. The sample matrix can bias the analyte signal through spectral (see above and later chapters) and non-spectral interference effects. Non-spectral interferences, or matrix effects as they are often known are characterised by changes in signal intensity that are matrix-induced and not related to spectral overlap. Matrix effects mainly lead to signal suppression, although under certain conditions signal enhancements have also been observed.[17] An important issue in ICP-MS is that matrix effects depend on the absolute matrix concentration, not on the relative concentration of matrix to analyte. Matrix effects can be reduced by simply diluting the sample (if permitted by analyte concentration) or corrected for by using internal standardisation. The most effective way, however, to correct for matrix effects is isotope dilution mass spectrometry (IDMS). More details on matrix effects can be found in the literature.[18,19]

9. The required measurement uncertainty determines the analytical procedure to be applied, as the measurement uncertainty describes the range within which the measured value covers the 'true value'. For a rough estimation of the sample composition semi-quantitative measurements are adequate. Decreasing uncertainties can be reached in the order of external calibration $>$ standard addition $\approx$ internal standardisation $>$ IDMS, with this last method offering the possibility to reach the smallest uncertainties. For a given measurement, it is not necessarily always a question of reaching the smallest uncertainty, but rather of the analysis being fit for purpose.

4.3 Spectral interference correction

The best way to avoid spectral interferences is to separate interfering elements before the measurement (see Chapter 5), to separate the interfering species by high resolution (HR) capabilities (Chapter 2) or to remove the interference by collision/reaction cell technology (Chapter 8).

Quite often these possibilities are not available or not applicable, either due to a lack of appropriate technology or financial or personnel constraints. The following section covers how isobaric and molecular interferences can be corrected for under these circumstances.

4.3.1 Isobaric interferences

In ICP-MS measurements, interferences caused by an isobaric overlap of another element β are corrected by the following equation:

$$I_{\alpha 1}^{\text{cor}} = I_{\alpha 1+\beta 1}^{\text{meas}} - I_{\beta 2} R_{\beta 1/\beta 2} \tag{4.1}$$

In this equation the index α1 represents the interfered isotope of the element α while the index β1 represents the interfering isotope of element β. $R_{\beta 1/\beta 2}$ represents the measured isotope amount ratio β1/β2, where β2 is a non-interfered isotope of element β. Since the interference is present, this ratio cannot be accurately measured in the sample and therefore has to be replaced with a value derived from an alternative source. Most ICP-MS instruments simply replace the ratio $R_{\beta 1/\beta 2}$ by the reported IUPAC ratio value.[20] They do not consider mass discrimination effects, despite the fact that equation (4.1) only deals with measured intensities, which are intrinsically affected by mass discrimination. For measurements requiring higher accuracy, especially isotope ratio measurements, this fact has to be taken into account and the interference correction has to be modified accordingly.

The ratio $R_{\beta 1/\beta 2}$ is now replaced by the IUPAC value divided by the mass discrimination correction factor, or K-factor, where $K = R^{\text{'true'}}/R^{\text{observed}}$ as shown in equation (4.2). The K-factor however has to be calculated from the mass bias per mass unit, ε (equation (4.3)), as the ratio $R_{\beta 1/\beta 2}$ cannot be measured directly, due to interference (as mentioned earlier). The mass bias per mass unit mainly depends on the relative mass difference of the two isotopes β1 and β2 such that, for example, the mass bias for the $^{6}Li/^{7}Li$ ratio is larger than that for the $^{206}Pb/^{207}Pb$ ratio. Within a small mass range the mass bias per mass unit is in first approximation equal for different isotope ratios of a given element. Following this the K-factor can be calculated from a different isotope ratio of element β or approximately even α. It should be emphasised that this approximation is only valid for relatively small mass ranges ($\Delta m < 10$) in the medium and high mass region. This approximation is applicable for quadrupole ICP-MS (Q-ICP-MS) measurements only. For more accurate measurements with the intention of gaining smaller uncertainties equation (4.3) should be replaced by the power law (equation (4.10)) or exponential law (equation (4.11)) as described. This should be applied especially for HR and multi-collector (MC) ICP-MS measurements.

$$R_{\beta 1/\beta 2} = \frac{R_{\beta 1/\beta 2}^{\text{IUPAC}}}{K_{\beta 1/\beta 2}} \tag{4.2}$$

$$\varepsilon = (K - 1)\frac{1}{\Delta m} \tag{4.3}$$

Replacing $R_{\beta 1/\beta 2}$ in equation (4.1) by equation (4.2) leads to equation (4.4):

$$I_{\alpha 1}^{\text{cor}} = I_{\alpha 1+\beta 1}^{\text{meas}} - I_{\beta 2}\frac{R_{\beta 1/\beta 2}^{\text{IUPAC}}}{K_{\beta 1/\beta 2}} \tag{4.4}$$

For IDMS determinations and other isotope ratio measurements, this equation can be transformed into the following equation:

$$R^{\text{cor}}_{\alpha 1/\alpha 3} = R^{\text{uncor}}_{\alpha 1/\alpha 3} - R_{\beta 2/\alpha 3}\frac{R^{\text{IUPAC}}_{\beta 1/\beta 2}}{K_{\beta 1/\beta 2}} \tag{4.5}$$

Applying equation (4.5), an uncertainty budget for the interference corrected isotope amount ratios can be calculated by using the method of propagation of uncertainties according to ISO[8] and EURACHEM[9] guidelines. The mass bias corrected equation for the interference correction equation (4.5) only uses ratios and therefore reduces the total uncertainty, as isotope ratios can be measured more precisely than intensities. The additional correction of the mass bias on the interference correction becomes more important the higher the interfering signal is, relative to the analyte signal.

4.3.2 Molecular (polyatomic) interferences

Molecular (polyatomic) interferences are more difficult to correct for, as they depend on the abundance of at least two isotopes and the interference formation rate, which often is strongly matrix dependent. In some cases, the interference can be measured at another, non-interfered mass. When only one interference affects the target isotope, the same equations as for isobaric interferences apply. An example for this is the $^{40}Ar^{35}Cl$ interference on ^{75}As, which can be corrected for via $^{40}Ar^{37}Cl$ (in the absence of ^{77}Se). In the case of polyatomic interferences from two or more species on a particular mass, the correction factors have to be calculated using the natural isotope abundances of the atoms from which the interference is formed. As a first approximation, the molecular abundance is the product of the single isotopic abundances, when neglecting isotopic effects in the formation process of the molecule. The isotopic composition of a molecular ion built from two or three atoms follows equation (4.6), where a_i^{α} is the abundance of isotope i in element α and n_{α} is the number of atoms of element α in the molecular ion:

$$\textit{Isotopic composition} = \left(\sum_i a_i^{\alpha}\right)^{n_{\alpha}}\left(\sum_j a_j^{\beta}\right)^{n_{\beta}}\left(\sum_k a_k^{\gamma}\right)^{n_{\gamma}} \tag{4.6}$$

An example is the $^{94}Mo^{17}O$ and $^{95}Mo^{16}O$ interferences on ^{111}Cd. These interferences can be corrected via $^{97}Mo^{18}O$ on the Cd-free mass, 115. The total correction factor can then be calculated from the natural isotopic abundances of ^{94}Mo (0.0925), ^{95}Mo (0.1592), ^{97}Mo (0.0955), ^{16}O (0.997 57), ^{17}O (0.000 38) and ^{18}O (0.0025) where (1.00) means the isotope is 100% abundant.[20] For $^{95}Mo^{16}O$ the molecular abundance is the abundance of ^{16}O multiplied with the abundance of ^{95}Mo:

$$(0.997\,57 \times 0.1592) = 0.158\,81$$

Further application of this calculation process results in corresponding molecular abundances of 0.000 04 for $^{94}Mo^{17}O$ and 0.000 20 for $^{97}Mo^{18}O$. As $^{94}Mo^{17}O$ and $^{95}Mo^{16}O$ interfere with ^{111}Cd, both molecular abundances have to be added and divided by the molecular abundance of $^{97}Mo^{18}O$ to give the correction factor:

$$(0.000\,04 + 0.158\,81)/0.000\,20 = 794.25$$

The intensity of $^{97}Mo^{18}O$ at mass 115 (in absence of ^{115}In) is multiplied with the correction factor of 794.25 (and mass bias corrected if necessary) and gives the sum of the intensities of $^{94}Mo^{17}O$ and $^{95}Mo^{16}O$ interfering with ^{111}Cd. Such high correction factors should only be used for high analyte intensities (here ^{111}Cd). Moreover the intensity of the interfering species used for correction should be sufficiently high above the background (here $^{97}Mo^{18}O$), otherwise over-correction errors will arise.

Another way to correct for molecular interferences is to empirically determine their formation rates. Usually this is carried out in a 2% (v/v) HNO_3 solution containing the element generating the interference. A good example is again the $^{94}Mo^{17}O$ and $^{95}Mo^{16}O$ interference on ^{111}Cd. The oxide formation rate can be determined in a Mo standard solution by measuring the Mo intensity at $m/z = 100$ and the MoO intensity at $m/z = 116$. This formation rate is then used to correct the intensity on $m/z = 111$ for MoO contributions in the sample of interest by subtracting the intensity of ^{95}Mo multiplied by the oxide formation rate (the contribution of $^{94}Mo^{17}O$ is negligible). More accurate results will be achieved when a matrix-matched solution is used for the determination of the oxide formation rate.

For the interested reader, a practical but more complex example for correcting molecular interferences when analysing rare earth elements has been reported by Dulski.[21]

4.4 Semi-quantitative calibration

Semi-quantitative analysis facilitates fast and simple multi-element measurements with limited precision. ICP-MS offers excellent semi-quantitative capabilities, as a result of the high ionisation efficiencies achieved for the majority of elements and the simplicity of the resulting mass spectra. Semi-quantitative determinations are mostly based on a comparison of response tables and the actual count rates of the sample. The response (intensity I in counts/s) of an analyte ion depends on the concentration of the analyte element, the isotopic abundance of the observed isotope, the ionisation efficiency, the atomic mass and the efficiencies of nebulisation, ion transmission and ion detection in the mass spectrometer. In most ICP-MS instruments a plot of the atomic response, R_a, versus atomic mass yields a smooth response curve, which is fitted best by a third order polynomial (Figure 4.3).[22] The atomic response is defined by equation (4.7) and is equivalent to the molar response divided by the Avogadro constant, N_A.

$$R_a = \frac{IM_{el}}{c_{el} f_{iso} IEN_A} \tag{4.7}$$

where M_{el} is the molar mass of the element, c_{el} is the mass content of the element in solution, f_{iso} is the isotopic abundance and IE is the ionisation efficiency.

Default settings of response tables are available in nearly all ICP-MS instruments and can be updated by analysing a multi-element standard (>three elements) before sample analysis. On the basis of the updated response factors the analyte concentration is calculated from the measured intensity. Most ICP-MS instruments include software for semi-quantitative applications, which often offers algorithms for interference corrections in addition. To reduce uncertainty due to fluctuations in instrument sensitivity, in most cases an internal standard is added to the sample and to the multi-element standard used to update the response factors.

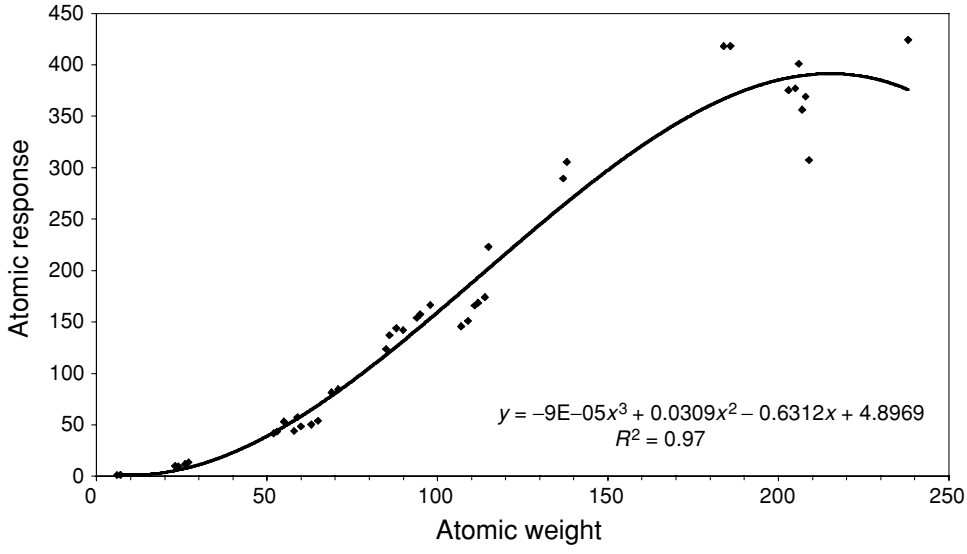

Figure 4.3 Third order polynomial fit for the atomic response of an Elan 5000 ICP-MS instrument based on measured data of 40 elements (^{6}Li to ^{238}U); the unit of the displayed atomic response is 10^{-11} counts/s atoms g solution.

Uncertainties in semi-quantitative applications are generally around 30–50% for non-interfered analytes. For carefully developed semi-quantitative procedures, lower uncertainties can be reached, but only for certain elements. Strongly interfered or blank dominated elements (e.g. Cl, Si, S) result in higher uncertainties, sometimes of the order of several hundred per cent. Semi-quantitative calibration therefore is suited for sample screening and preliminary tests, when only a rough estimate of the sample composition is required. More details on the applications of semi-quantitative calibration can be found in the literature.[13,22–25]

4.5 External calibration

Quantitative analysis in ICP-MS[26,27] can be achieved by several calibration strategies, which are described in the following chapters. External calibration assesses the analyte concentration via a calibration curve established by analysis of separately measured standards. The intensities of the calibration standards are then plotted versus their concentrations and a linear regression line is calculated. Applying the corresponding linear equation (of the form $y = ax+b$, where $a =$ the calibration slope and $b =$ the y-axis intercept) the analyte concentration in the sample (x) can be calculated from the analyte intensity (y) via the equation $x = (y - b)/a$.

Conventional external calibration uses pure standard solutions (single- or multi-element) and is therefore unable to compensate for matrix effects, fluctuations or drifts in sensitivity. To some extent drifts can be compensated for by regularly repeating the calibration or by repeated measurement of one standard, which allows a mathematical drift correction to be applied. Matrix effects can be compensated for by using matrix-matched calibration solutions, which means

adjusting the matrix of the calibration standards to match that of the sample. The degree of compensation depends on the completeness of the matrix adjustment. In practice conventional external calibration by itself is rarely used due to the missing compensation for matrix and drift effects. Generally, a combination of external calibration and internal standardisation or matrix-matched calibration and internal standardisation is applied.

A good example of applying external calibration with matrix-matched standards is the following recovery experiment. When analysing Sb in a Si chip,[28] the sample is usually dissolved by a HF/HNO_3 mixture and the Si matrix is removed by evaporation to dryness. The residue is then redissolved prior to analysis. As Sb can be lost at high temperatures, the recovery has to be checked for the evaporation step at 60°C. A high purity silicon chip (about 800 mg) was decomposed with a HF/HNO_3 mixture (20 mL). Three sub-samples (1 mL) of the resulting solution were spiked with 5.3 µg natural antimony and evaporated to dryness at 60°C. The solid residues were dissolved again as described above and filled up to 10 mL total. These solutions served as the samples. Another three sub-samples (1 mL) of the matrix solution were prepared. After evaporation to dryness these sub-samples were spiked with 3.2 µg, 5.3 µg and 8.5 µg antimony and filled up to 10 mL total. These sub-samples served as matrix-matched calibration standards. Additionally a matrix-free blank was prepared. The calibration curves for ^{121}Sb and ^{123}Sb, which are displayed in Figure 4.4 together with their linear equations, show a good linearity (correlation coefficient >0.99). On the basis of the linear equations and the measurement results the mass of the spiked Sb has been calculated and found to agree very well with the gravimetric value. The recovery results were $99.2 \pm 5.0\%$. The combined standard uncertainty of 5% includes spiking (1%), measurement (1.2%), calibration (1.5%) and drift (1.2%). The

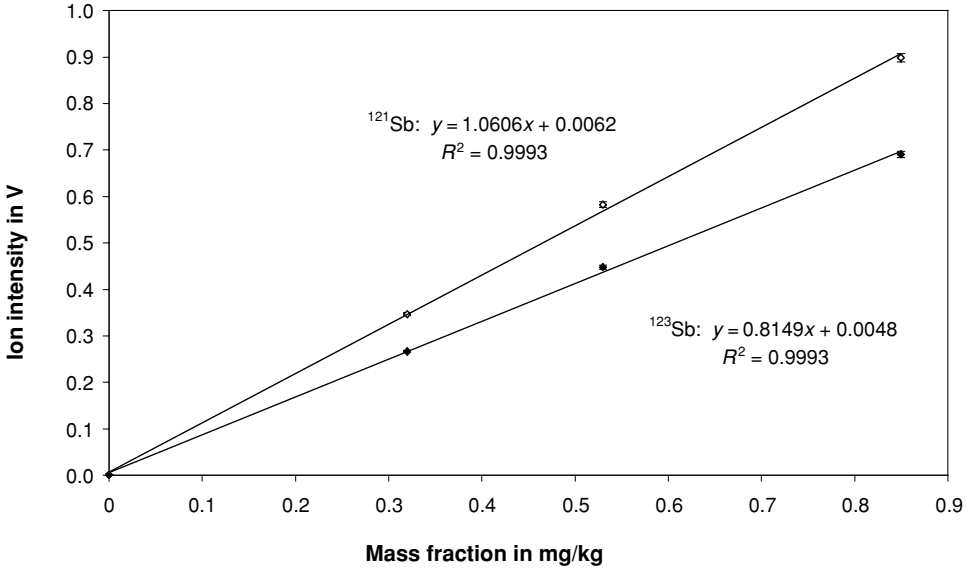

Figure 4.4 Calibration data with regression lines and linear equations for matrix-matched Sb standards as used for the recovery experiment described above, MC-ICP-MS instrument IsoProbe equipped with Faraday cups.

good quality of these results demonstrates the advantage of matrix-matched external calibration. External calibration without matrix-matching would have suffered from signal depression of 15% or more, which would directly give a measurement result biased by the same amount.

4.6 Standard addition

Standard addition calibration is performed by dividing the sample into n sub-samples (at least 2) and adding a known and increasing amount of analyte (the spike) to $(n - 1)$ sub-samples. From experience, two or three sub-samples should be spiked to reach optimum conditions, each with an increasing multiple of the estimated analyte amount in the sample. Practically the added spike solution should have a much higher (>100 times) concentration than the analyte concentration in the sample, so that when the spike is added the total sample volume does not increase significantly and the dilution effect of the addition is negligible. If larger volumes of less concentrated spike solutions are used, dilution effects on the sample become important and should be corrected for. A more accurate way is to add the same volume to all sub-samples, using spike solutions with different concentrations, plus a blank solution for the unspiked sample. This added volume has to be corrected for in the calculation of the analyte concentration. The prepared sub-samples (including the blank) are then measured and the resulting intensities are plotted versus the concentrations of the added spikes. The calculated regression line gives the analyte concentration as the intercept of the x-axis, which also can be calculated via the equation of the linear regression line (Figure 4.5). If necessary, dilution corrections for the added spike volume are then applied to this result.

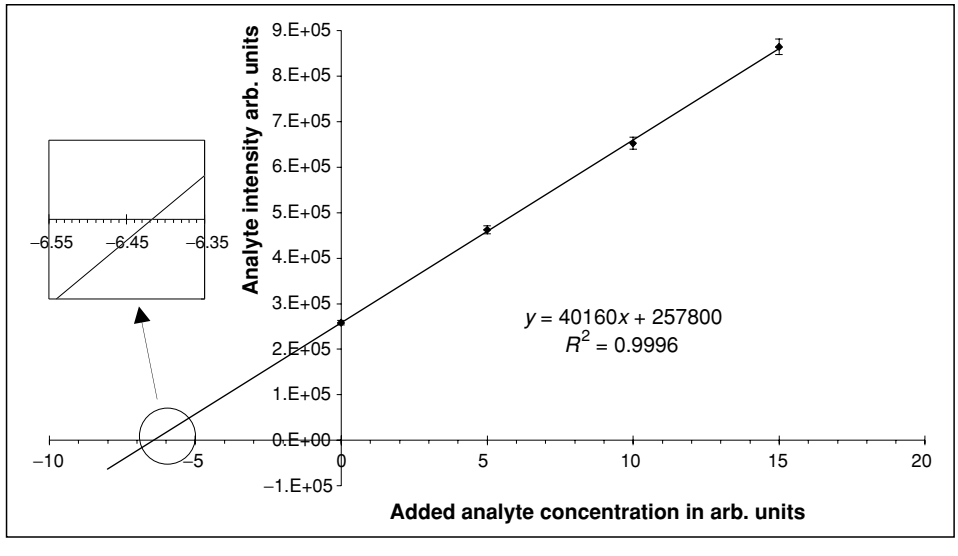

Figure 4.5 Schematic diagram of a standard addition calibration with the x-axis intercept giving the analyte concentration in the unspiked sample; this can also be calculated with the equation of the regression line.

Standard addition calibration is more robust and reliable than conventional external calibration, but is more time consuming and costly if it is applied separately for every sample. It is however possible to utilise the calibration generated from only one sample to quantify analytes in subsequent samples of the same type. For example, Pb in blood is often measured in this way in high throughput clinical laboratories, using a known, low Pb level blood sample as the calibration matrix. Successive analyses of the unspiked blood sample in this case can also serve as one mechanism by which to validate the method.

If matrix-matched standards cannot be prepared due to the matrix being too complex to practically match against (e.g. environmental samples) and less expensive calibration schemes are judged inappropriate, standard addition is a valuable methodology. A major advantage of standard addition is the correction of multiplicative matrix effects like alteration of nebulisation efficiency. The intensities of all samples (and spiked samples) change by the same factor, which leads to an altered calibration slope. The intercept of the x-axis however stays constant. However, for additive effects, like interferences caused by the matrix, the calibration line is shifted parallel and the intercept changes, which results in biased analyte concentrations. In some cases, this bias can be avoided (or indeed identified) by choosing another isotope and comparing the results for each. A good example is using ^{65}Cu together with (or in place of) ^{63}Cu, to avoid the bias caused by the $^{40}Ar^{23}Na$ interference in samples containing high levels of sodium.

A recent study demonstrated that using just a single spiked sample was sufficient for ICP-MS and that a bracketing approach (i.e. unknown sample – spike sample – unknown sample) was helpful for drift reduction.[29] More details on standard addition in general can be found in the literature.[30–32]

4.7 Internal standardisation

Quantitative analysis applying internal standardisation is the most popular calibration strategy used in ICP-MS. The principle is rather simple. To all standards, samples and blanks the same amount (amount of substance, mole) of an internal standard is added, preferably an equal amount to the analyte amount in order to achieve an optimum ratio of ~1, since ratios of the order of 1 can be measured with the smallest uncertainties (see isotope ratios). First of all, however, the signal intensity of the internal standard should be within the optimum measurement range of the instrument (generally 5×10^3 to 5×10^5 counts/s). The analyte signal is recorded as intensity and then expressed either as a ratio of the analyte intensity to the internal standard intensity or as actual data corrected for internal standard suppression or enhancement. Accordingly the calibration curve is set up. The internal standard at best is an element, which is similar to the analyte element in mass, ionisation potential and chemical behaviour. The internal standard must not be present in the sample, otherwise erroneous results will be achieved, as the signal is biased without being considered in the calculation. In practice however these requirements cannot be met in full and therefore in most cases a compromise has to be found. The only way to fulfil all requirements is to apply IDMS, which is the ideal case of internal standardisation. A carefully selected internal standard can compensate for drift and noise effects. Moreover it is possible to use internal standardisation to reduce or correct matrix effects in ICP-MS.[18] be checked carefully for a given analysis as it is not a general rule. A good example of the importance of selecting the correct internal standard has been described in the literature.[33] The analysis of Cd and Tl in pure zinc metal was carried out by four different IDMS procedures and one calibration procedure

using internal standardisation. The matrix content (in this case Zn) was ~1000 mg/kg in all sample solutions. For Tl, using Bi as the internal standard works quite well. All five procedures agreed well within their stated uncertainties. For Cd, the IDMS results agree well within <0.5%, but the result obtained using internal standardisation (with Pd as the internal standard) was ~5% off, which was not even approximately covered by the uncertainty. The assumed reason is an incomplete correction of matrix and drift effects by the internal standard. Further applications of internal standardisation can be found in numerous papers.[34–39]

4.8 Calibration with certified reference materials

Certified reference materials (CRMs)[40] can be used in different ways to calibrate analytical procedures. The first and simplest way is to directly use CRMs for setting up calibration curves of the instrument. This is often applied in solid sampling techniques but can also be used in techniques requiring the sample in liquid form (e.g. after digestion). For this approach however CRMs of different analyte concentrations are necessary to establish a reliable calibration curve covering the sample concentration. Moreover the consumption of CRMs as a result of using this approach is rather high, which contributes significantly to the measurement costs.

To avoid this high consumption of CRMs and so reduce the measurement costs, the CRM approach can be replaced by an indirect method based on the use of in-house prepared calibration samples, whose contents are determined using the original CRMs. When proper uncertainty estimation has been carried out, traceability can even be established in this case. However, the chain of comparisons is enlarged and thus the number of parameters being charged with a distinct uncertainty increases. This in turn increases the overall uncertainty compared to the direct CRM method. Moreover the determination of the content of the calibration samples has to be carried out under the best possible conditions, as the resulting values will become the basis of all succeeding analyses. Also, the homogeneity of the whole batch of calibration samples must be proven.

The most economic way of using CRMs for calibration purposes is to validate[41] a procedure for routine analysis. The analytical procedure is carried out with the CRMs analysed as samples. With the results achieved, all relevant analytical parameters can be determined, e.g. uncertainty, recovery, reproducibility, selectivity, linearity, etc. The procedure is then well known for the specific sample type and the specific analytes for which it is validated and can be applied routinely for this analytical problem, with a few regular reviews of the analytical performance. CRMs in this case are not used for calibration but rather for validation of the procedure and regular review of the method performance.

4.9 Isotope ratio measurements

The determination of isotope ratios is a unique tool for the tracing and clarification of transport processes in the area of geology.[42–44] Application of tracer experiments using stable isotopes is also becoming increasingly important in biology and medicine to clarify metabolic processes.[45] Other applications include archaeology[46,47] and spent reactor fuel analysis.[48,49] Another important field of application of isotope ratio measurement is in IDMS. Before the advent of ICP-MS, most isotope ratio work was carried out using thermal ionisation mass spectrometry (TIMS).[50]

This is still considered today as the reference isotope ratio measurement method, as the processes are nearly completely understood. However, due to the ease of use and accessibility of most of the elements, ICP-MS is now preferably applied and the number of projects based on isotope ratio measurements is clearly on the increase.

When performing isotope ratio measurements, especially with ICP-MS, the following points have to be considered:

- Precision required
- Interferences
- Mass discrimination effects
- Dead time effects for pulse counting detectors
- Low and high frequency noise and fluctuations from the instrument
- Contamination risk
- Abundance sensitivity
- Isotopic abundance and molar mass

A brief description of these topics providing basic information only is given within this chapter. For detailed and specialised information please refer to the cited literature.

4.9.1 Precision required

The first consideration is on the precision the experiments require, because this will lead you to the instrument you need. In this context there are three major differences between the available ICP-MS instrument designs (for details on the different designs see Chapter 2).

Quadrupole (Q) ICP-MS is easy to use, robust and relatively inexpensive. Due to their fast scanning capabilities these instruments enable short measurement times and therefore multi-elemental analysis while measuring transient signals.[51] This is most important for coupling with other techniques such as laser ablation (see Chapter 6), HPLC and GC (for both see Chapter 7). In general, quadrupole instruments enable a good precision on isotope ratio measurements. Typical values for internal standard deviations range from 0.1 to 0.5%.[52] The essentially single mass unit transmission at any instant of time offered by quadrupole technology, coupled with the fact that only a single detector is used in such systems, means that each isotope signal has to be measured sequentially (albeit relatively quickly) and thus isotope ratio measurements with these instruments are subject to ion beam fluctuations deriving from plasma oscillations and variations in sample introduction, nebulisation, ionisation and extraction efficiencies. In addition the rounded peak shape of quadrupoles renders obtaining reproducible signals from a given mass as the quadrupole jumps from one isotope to the next and back again difficult. These properties limit the achievable precision of Q-ICP-MS instruments to values less than that statistically predicted.

High resolution (HR) instruments are based on double-focusing and single detector technologies. The major advantage here is the unequivocal identification and quantification of measured mass peaks. The scanning speed of current instruments is close to that of quadrupoles, thereby also enabling multi-elemental analysis in transient signals. The use of a single detector means that the limitations of sequential measurement technique apply here as well. However, the energy focusing ability of double-focusing HR-ICP-MS systems facilitates the generation of ‘flat top’ peaks, which lead to improvements in the achievable isotope ratio precision compared to

quadrupole instruments, mainly as a result of reproducible recovery of the peak maximum. Internal standard deviations in terms of isotope ratio measurements for single detector HR-ICP-MS instruments hence typically range from 0.05 to 0.2%.[52]

The ions in a multi-collector (MC) ICP-MS are first energy-focused (using either an electrostatic field or a collision cell) and then separated in a magnetic field. This enables a simultaneous detection of several isotopes by multiple analog or digital detectors (usually between 9 and 17). Ion beam fluctuations in these systems do not influence isotope ratio precision because the isotopes of interest are measured simultaneously. Typical internal standard deviations for analog detectors (such as Faraday cups) are 0.005 to 0.02%.[52] Digital detectors are limited by counting statistics, but precision can be achieved provided that sufficiently large signals are measured. This high performance in terms of isotope ratio measurements is also applicable to transient signals as for example in laser ablation ICP-MS.[53–55] Due to the limited number of detectors available, MC-ICP-MS systems do not easily offer multi-element analysis capability. The precision data given above apply to non-interfered isotope ratios.[52] A current overview on Fe isotope ratio measurements comparing the capabilities of the different types of ICP-MS instrumentation is given in the literature.[56]

4.9.2 Interferences

For isotope ratio measurements, at least two ideally non-interfered isotopes of an element are required. The same techniques and technologies (see Chapter 2) as well as correction strategies apply for these measurements as for standard ICP-MS measurements.

4.9.3 Mass discrimination effects

Ideally the transmission efficiency of ions through a mass spectrometer is independent of their mass-to-charge ratio. Unfortunately, in the real (and not ideal) world, this type of mass spectrometer does not exist. Ions of different mass-to-charge ratios are transmitted with different efficiencies, a characteristic referred to as mass discrimination. This effect sums up throughout all compartments of the mass spectrometer, as there are ionisation, ion optic, mass separation and ion detection contributions to it. Conventional ion counting[57] and dual mode detection systems suffer from mass discrimination, which can be reduced by introducing conversion dynodes.[58,59] For ions of the same energy, lighter mass ions will produce more secondary electrons when striking the first electrode of an electron multiplier detector than heavier mass ions. This leads to an increase in the multiplier gain for the lighter mass ions, thus discriminating against heavier mass ions.[60] Faraday detectors show no mass discrimination. While magnetic field mass separators show no mass discrimination, quadrupole mass separators do. The heavier the ion the longer the time it spends in the quadrupole fringing fields and the greater the dispersion. Heavier ions tend to transmit less efficiently, and are therefore discriminated against.[61] In ICP-MS however these effects are small compared to those occurring in the interface region and ion optics. Moreover this mass discrimination of the heavier isotopes is in the opposite direction to that of the so-called space charge effects, which dominate mass discrimination in ICP-MS. Space charge effects affect the ion beam in the interface and ion optics region (see Chapter 1 for

a more detailed discussion). Charge diffusion and electrostatic effects cause charge separation within the ion beam and the net charge becomes substantially positive. The plasma flow through the sampler and skimmer cones is largely neutral. The ion number density is balanced by the electron number density, thus the net charge flow is small. Distinct space charge effects are not expected as long as the interface allows an undisturbed beam flow through the skimmer. Behind the skimmer the low mass and high thermal energy of electrons lead to them having higher mobility compared to ions. This induces diffusion of the electrons from the beam and the formation of an electron sheath at the inside of the skimmer. This again induces concomitant diffusion of positive ions to retain plasma neutrality. Positive charge flow is delayed and so a positive net charge density remains on axis. The radial electric field caused by the net charge imbalance, the space charge, is significant compared to the external electrostatic field and leads to radial expansion or defocusing of the ion beam. The constantly defocusing space charge field is dominated by Ar^+ (in the case of Ar ICPs), but not significantly influenced by trace levels of analyte ions. Ions of high kinetic energy are transmitted more efficiently through the space charge field. Heavier ions have a higher initial kinetic energy, which derives from the supersonic expansion. Thus heavier ions are favoured and lighter ions are discriminated against. A more detailed description can be found in the literature,[62] together with a clear illustration in a paper by Allen *et. al.*[63] The overall mass discrimination is often called mass bias. In contrast to TIMS, mass discrimination in ICP-MS is independent of time, as the sample is introduced continuously in the plasma.

Accurate isotope ratio measurements require corrections for mass discrimination. The basis for all corrections is equation (4.8) describing the correction for a certain isotope ratio:

$$K = \frac{R_{\text{'true'}}}{R_{\text{obs}}} \tag{4.8}$$

K is the correction factor for mass discrimination, (the so-called K-factor). $R_{\text{'true'}}$ is the so-called true isotope ratio, which practically is replaced by a certified isotope ratio of an isotope reference material, as 'true' values commonly are not known. R_{obs} is the measured isotope ratio including the bias caused by mass discrimination. The three most commonly used strategies for mass discrimination corrections are external correction, internal correction and so-called absolute or calibrated measurements.

External correction is the most practical and most frequently used method that offers sufficient accuracy. In this case the K-factor is determined for an isotope reference material or for a standard solution using the certified or IUPAC values[20] respectively, by applying equation (4.8). This K-factor is then used for the mass discrimination correction of the equivalent isotope ratio in the sample by again applying equation (4.8). Usually an average K-factor is determined for the reference material, based on measurements taken before and after the sample measurement (referred to as 'bracketing'), to correct for any drift that may have occurred throughout the measurement cycle.

Internal correction has the advantage of simultaneous (MC instruments) or quasi-simultaneous (single-collector instruments) correction, but in this case obviously the measured isotope ratio cannot be corrected by using the same isotope ratio. In ICP-MS the mass discrimination for a limited mass range (<10 mass units) only depends on the mass difference. Other dependencies have not yet been observed. Thus the mass discrimination for a certain isotope ratio in the first approximation can be calculated from a different isotope ratio close to the target one. In practice another isotope ratio of the same element with a constant universal value is used or the sample

is doped with a neighbouring element of known isotope ratios. The latter approach is quite often applied for Pb isotope ratio measurements by doping Tl into the samples.[64] In geology, internal correction by doping another element is sometimes denoted as external, which is misleading. The authors of this chapter understand internal as being within the sample, e.g. internal standard, and external as being outside the sample, e.g. external calibration. The mathematical calculations for internal mass discrimination correction are based on the following equations:

$$K_{\text{lin}} = 1 + (\Delta m \varepsilon_{\text{lin}}) \tag{4.9}$$

$$K_{\text{pow}} = \left(1 + \varepsilon_{\text{pow}}\right)^{\Delta m} \tag{4.10}$$

$$K_{\text{exp}} = \exp\left(\Delta m \varepsilon_{\text{exp}}\right) \tag{4.11}$$

where Δm is the mass difference of the two isotopes and ε_{lin}, ε_{pow} and ε_{exp} are the mass discriminations per mass unit for the linear (equation (4.9)), power law (equation (4.10)) and exponential (equation (4.11)) models. Several MC-ICP-MS studies have shown the exponential and power law models to be superior to the linear model in terms of accuracy.[65,66] A recent paper describes a new approach to the estimation and correction of mass bias based on modelling the instrument's response curve.[67] The linear model however is sufficiently accurate for quadrupole applications. The relative mass discrimination for different isotope ratios and different instruments is given in Table 4.1 The per cent deviation of the measured isotope ratio relative to the mass difference gives the relative mass discrimination, which for the linear model is $\varepsilon_{\text{lin}} \times 100\%$. There is no great difference in terms of the order of magnitude of the listed mass bias between quadrupoles, magnetic sectors, collision cells, instruments using different acceleration voltages or others. The only common parts are the plasma torch and the interface, so it can be deduced that the main origin of mass discrimination is located in these parts and that space charge effects play a major role.

The most rarely used strategy for mass discrimination is the absolute or calibrated measurement approach.[75] For this purpose synthetic mixtures of purified and highly enriched isotopes

Table 4.1 Relative mass discrimination of different ICP-MS instruments

Isotope ratio	ICP-MS type	ICP-MS name	$\varepsilon_{\text{lin}} \times 100\%$	Reference
$^{6}Li/^{7}Li$	Q-ICP-MS	ELAN 5000	Up to 46	68
$^{6}Li/^{7}Li$	Q-ICP-MS	ELAN 5000	9.5	69
$^{63}Cu/^{65}Cu$	HR-ICP-MS	Element	3	70
$^{63}Cu/^{65}Cu$	Q-ICP-MS	ELAN 5000	3.9	69
$^{63}Cu/^{65}Cu$	HEX-ICP-MS	Platform ICP	5.7	71
$^{90}Zr/^{91}Zr$	Q-ICP-MS	ELAN 5000	2.2–5.0	72
$^{90}Zr/^{91}Zr$	Q-ICP-MS	ELAN 5000	2.3	69
$^{97}Mo/^{98}Mo$	Q-ICP-MS	ELAN 5000	1.6	73
$^{97}Mo/^{98}Mo$	Q-ICP-MS	ELAN 5000	1.9	69
$^{95}Mo/^{96}Mo$	HEX-ICP-MS	Platform ICP	1.67	71
$^{203}Tl/^{205}Tl$	MC-ICP-MS	Plasma 54	0.4	74
$^{203}Tl/^{205}Tl$	Q-ICP-MS	ELAN 5000	0.25	69
$^{203}Tl/^{205}Tl$	HEX-ICP-MS	Platform ICP	0.11	71
$^{235}U/^{238}U$	MC-ICP-MS	Plasma 54	0.9	75
$^{235}U/^{238}U$	Q-ICP-MS	ELAN 5000	0.9	69

are prepared under full gravimetric control. The resulting synthetic isotope mixtures with gravimetrically defined isotope ratios are used to calibrate the mass spectrometer. This correction is highly laborious and is therefore only used for isotope ratio measurements of the highest metrological quality, such as refining the determination of the atomic weight of an element.

4.9.4 Dead time effects for pulse counting detectors

Dead time effects only occur for ion counting detectors, not for analog detectors. The detector dead time is the time after the impact of an ion for which the ion counting system is 'blind' to further incoming ions. The detector dead time is a property of the whole ion counting system and arises from both the detector and the ion counting electronics. In ICP-MS detector dead time is corrected for by applying equation (4.12).[76,77]

$$I_t = \frac{I_0}{(1 - I_0\tau)} \tag{4.12}$$

where I_t is the count rate corrected for dead time losses, I_0 is the count rate obtained with no dead time correction applied and τ is the apparent dead time of the detection system. Typical dead times are in the range of some 10–60 ns and therefore difficult to detect accurately and precisely. According to equation (4.12) dead times of 10^{-7}–10^{-8} s lead to significant biases in the measured ion intensity at count rates above 10^4–10^5 ions per second. In external calibration work this is not that much of an issue, as the calibration standards are affected in the same way as the samples. For isotope ratio measurements however it is very important, because it leads to biased isotope ratios, which cannot be corrected by standard measurements such as those shown for mass bias correction. The effect of the detector dead time becomes increasingly stronger as the isotope count rate increases. Thus the higher the count rate and the larger the measured isotope ratio is, the greater dead time effects will be. Only for isotope ratios close, or equal, to 1 (for example, natural $^{107}Ag/^{109}Ag$) do dead time effects become unimportant, as they are cancelled out in the ratio calculation because in these cases, the count rates of both isotopes are approximately, or exactly, equal (see equation (4.13)):

$$R_{obs} = \frac{I_t^a}{I_t^b} = \frac{\frac{I_0^a}{(1-I_0^a\tau)}}{\frac{I_0^b}{(1-I_0^b\tau)}} \tag{4.13}$$

In ICP-MS several methods for the determination of detector dead time have been applied and a comparison of the four most commonly used methods has been described.[78] A short description of the most practical method for producing clear and unambiguous values for the dead time and allowing a systematic approach for uncertainty evaluation is given in the following section. In this method, $^{204}Pb/^{208}Pb$ isotope ratios have to be measured at different the Pb concentrations ranging from 10 to 90% of the detector full scale for ^{208}Pb without dead time correction. The measured ^{204}Pb and ^{208}Pb intensities are recalculated for different dead times and the resulting $^{204}Pb/^{208}Pb$ isotope ratios are corrected for mass bias. Preferably SRM 982 is used as the Pb standard, because the mass bias can be corrected internally as the certified $^{206}Pb/^{208}Pb$ ratio is approximately 1 (exactly 0.999 84).[79] Otherwise the mass bias has to be corrected externally. The obtained, corrected $^{204}Pb/^{208}Pb$ isotope ratios are plotted versus the Pb concentration (Figure 4.6). The optimum dead time is determined by plotting linear regression lines through the data

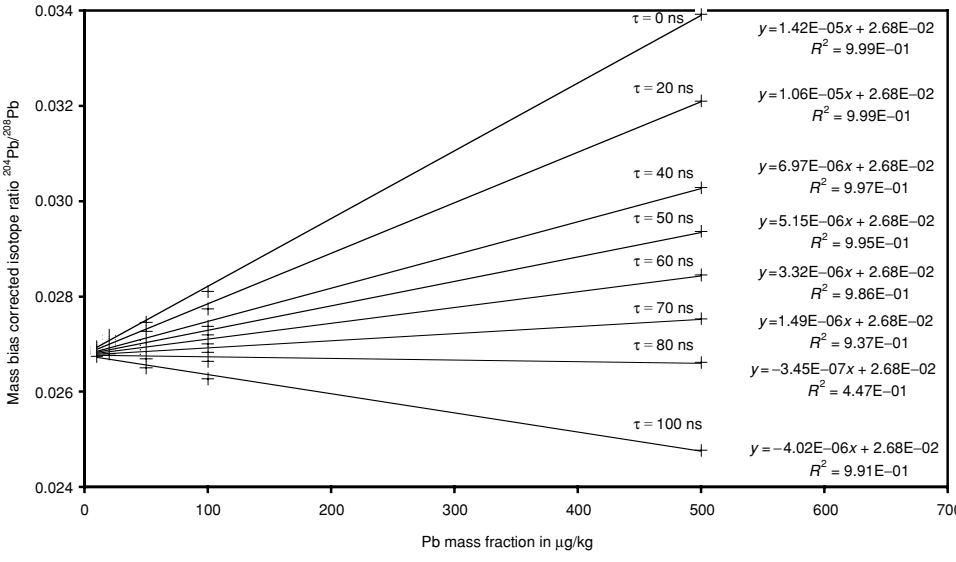

Figure 4.6 $^{204}Pb/^{208}Pb$ isotope ratio versus Pb mass content in the solution for different dead time settings displayed together with the corresponding equations of the linear regression lines.

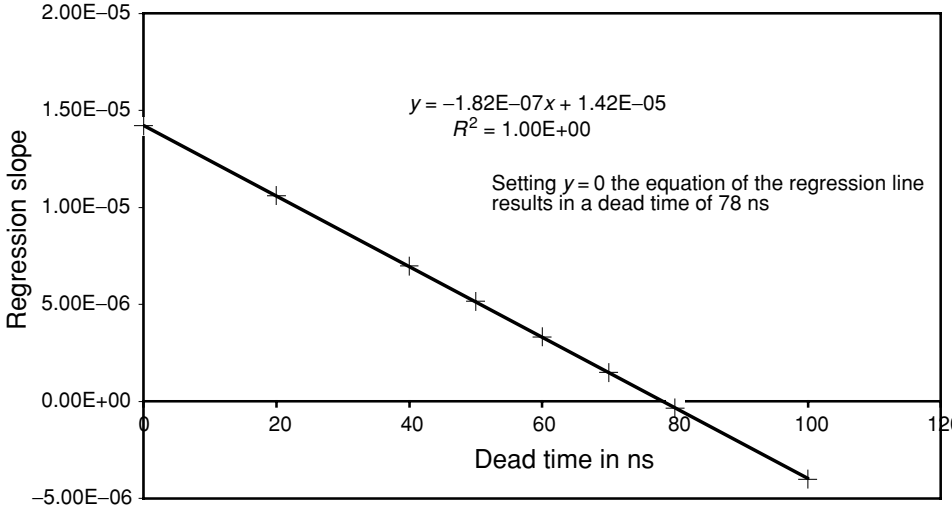

Figure 4.7 Regression slopes from Figure 4.6 versus dead time; the proper dead time is determined by the intercept of the *x*-axis or by setting $y = 0$ in the equation of the linear regression line.

for each dead time and selecting the data set with a slope of zero. This data set reflects the dead time for which the isotope ratio is independent of concentration and thus identifies the optimum value for dead time correction. This value can be evaluated in a clearer and unambiguous way by plotting the slopes of the linear regression lines versus the dead time (Figure 4.7). The resulting near linear curve allows the direct calculation of the optimum dead time at zero regression

slope. Based on this a realistic uncertainty can be calculated, which clearly reflects the fact that worse measurement repeatability leads to a larger dead time uncertainty. For more details on this method the interested reader is directed to the literature.[78] Further information on the dead time determination by an electronic method is given in reference,[80] and other dead time related topics can also be found in the literature.[81–83]

4.9.5 Low and high frequency noise and fluctuations from the instrument

Low frequency noise is below 10 Hz and is largely generated by the sample introduction system (peristaltic pumps, nebulisation).[18] High frequency noise is above 10 Hz and is related to the gas dynamics of the ICP and desolvation in and before the plasma[84] or to interference noise from the AC line voltage. White noise represents the background in a noise amplitude spectrum and occurs for all possible frequencies. A noise amplitude spectrum shows the frequency composition of the noise for the entire spectrometric system (noise amplitude versus frequency). Other fluctuations can be drift effects, which affect sensitivity and mass discrimination.

Pulse-free pumps (gas displacement or dual-piston pumps) or the self-aspirating mode of some nebulisers (e.g. Meinhard-type nebuliser) can clearly reduce the low frequency noise. Cooled spray chambers can reduce white noise; certain types (e.g. Scott-type double pass spray chamber) can even further reduce white and low frequency noise. Flared and extended torches can reduce the magnitude of noise caused by the gas dynamics of the ICP. Choosing signal integration times of less than f^{-1} (where f is the noise frequency) can reduce all noise effects. In practice, for Q-ICP-MS for example, this means using short quadrupole settling times (down to 0.2 ms), isotope integration times of around 10 or 20 ms and restricting the measurement to only a few isotopes. For optimum results an optimisation for each instrument is recommended. This primarily affects quadrupole and single-collector instruments. MC instruments are not as susceptible to noise in terms of isotope ratio determination as they measure the target ion signals simultaneously.

Drifts in sensitivity do not affect isotope ratio measurements unless they become very large. Blank subtraction can become an issue in cases where the blank drifts upwards or downwards throughout the analysis. Any drift in mass discrimination has to be monitored and considered, because this directly biases the measured isotope ratio. As discussed earlier, this drift can be corrected for either internally or by using the bracketing approach.

4.9.6 Contamination risk

Contamination affects isotope ratio measurements in a particularly negative way, when working with enriched isotopes or samples having a non-natural isotopic composition. In these cases, the contaminant always has a different isotope ratio than the sample and contamination causes the sample isotope ratio to change dramatically. In particular, ubiquitous elements such as boron and iron are highly susceptible to contamination and great care has to be taken to avoid this when such elements are measured.

4.9.7 Abundance sensitivity

Not only interferences at the same m/z value can bias the intensity of a certain isotope but also the contribution of a neighbouring isotope. Due to the initial energy distribution and collisions with residual gas molecules, ions of the same mass show a mass-to-charge distribution with tailing at the high and low mass sides. The amplitude of this tailing is named 'abundance sensitivity' and accounts for the fraction of the peak intensity contributing to the neighbouring mass ($m \pm 1$). Typical values for the abundance sensitivity are in the magnitude of 10^{-7}–10^{-6}. An abundance sensitivity of 10^{-6} means a contribution, for example, of 1 counts/s to the neighbouring mass ($m \pm 1$) when the main peak (m) intensity is 10^6 counts/s.

Abundance sensitivity becomes critical when measuring extreme isotope ratios (>100 000) or when neighbouring elements are present in the sample at high concentrations. In ICP-MS this occurs for isotope ratio measurements of elements such as U and Th (extreme ratios) or boron isotope ratio measurements in the presence of high carbon contents (tailing of ^{12}C onto ^{11}B). Specially designed filters (electrostatic filter, quadrupole lenses) can increase the abundance sensitivity up to 2×10^{-8} (see Chapter 2, section 2.2.1 for further details). In the case of boron, a simple matrix separation can help. In the majority of isotope ratio measurements however abundance sensitivity effects are negligible.

4.9.8 Isotopic abundance and molar mass

When measuring isotope ratios, often the isotopic abundance of an isotope or the molar mass of the analyte element in the sample is desired. Both can be calculated from the isotope ratios of the analyte element (equations (4.14) and (4.15)). It is noteworthy that all isotope ratios of the element are needed, even if only one isotope abundance is required.

$$a_i = \frac{K_{i,b} R_{i,b}}{\sum K_{j,b} R_{j,b}} \tag{4.14}$$

$$M = \sum (a_i M_i) \tag{4.15}$$

Here a_i is the required abundance of isotope i of the requested element. $K_{j,b}$ are all K-factors and $R_{j,b}$ are all isotope ratios related to isotope b (also including the ratio $b/b = 1$). M is the atomic weight (molar mass) of the requested element, a_i are the isotopic abundances and M_i the atomic weights (molar masses) of the isotopes.

4.10 Isotope dilution mass spectrometry

Based on its proven record especially in reference material certification, IDMS is considered as one of the most powerful and most accurate methods for determining amounts of substance. Contrary to other calibration approaches, IDMS does not directly suffer from long-time changes or drifts in instrument sensitivity. Moreover, provided isotopic exchange between the sample and spike is ensured, losses of analyte do not affect the analytical result. Both advantages are

based on the fact that IDMS only requires isotope ratio measurements and isotope ratios are largely unaffected by instrumental drift, set-up or by matrix, unless an isobaric interference is present.

The Consultative Committee for Amount of Substance (CCQM),[85] the world's highest institution for metrology in chemistry, considers IDMS as the most important 'primary method of measurement' for amount determination. The total combined uncertainty, according to ISO[8] and EURACHEM[9] guidelines, can easily be calculated via the IDMS equations. Applying it correctly, IDMS has the potential to be a primary method of measurement yielding SI traceable values in the most direct way with combined uncertainties significantly smaller than obtainable by other methods.

The principle of IDMS is surprisingly simple. A sample with known isotopic composition but unknown element content is mixed with an accurately known amount of spike. This spike contains the analyte element in a non-natural isotopic composition; the ideal is to use a spike that has an enrichment of the rarest natural isotope. After complete mixing of the sample and spike the so-called isotope diluted sample (blend) has a new isotope ratio, which lies between the isotope ratio of the sample and the isotope ratio of the spike. This is demonstrated in Figure 4.8 for the example of copper. The sample shows the natural isotopic composition of copper, which is 69.17% of ^{63}Cu and 30.83% of ^{65}Cu. The spike is enriched in ^{65}Cu (91.90%); the abundance of ^{63}Cu is 8.10%. After complete mixing, the isotope diluted sample (blend) shows a new isotope ratio ^{65}Cu/^{63}Cu, which directly reflects the analyte concentration in the sample.

A short derivation of the IDMS equation system is given in the following section. The compatibility to equations used elsewhere[86,87] is given on the same basis, which is the definition of the blend isotope ratio, R_{xy}. This quantity is the ratio of the total number of atoms of isotope a to the total number of atoms of isotope b in the blend, with b being the most abundant spike

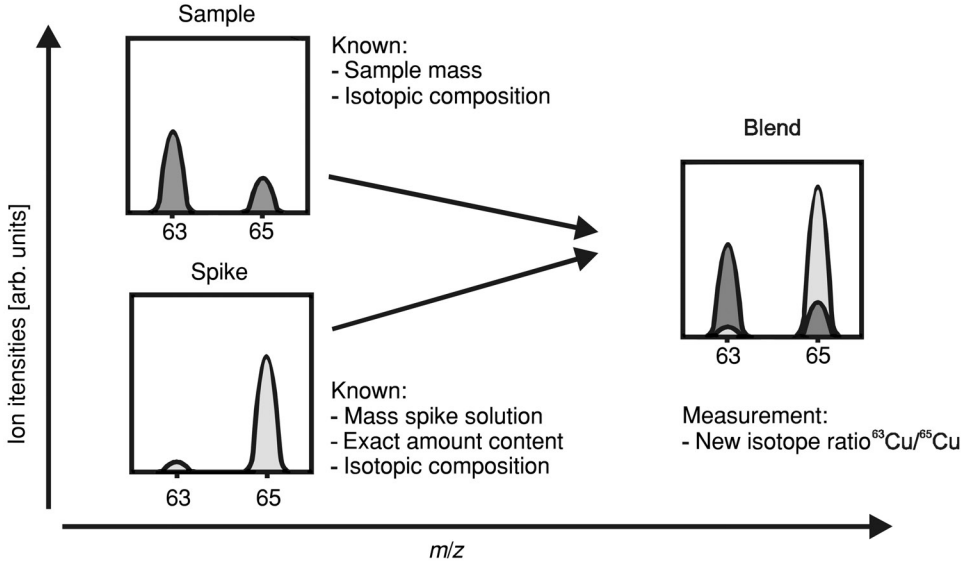

Figure 4.8 Schematic diagram/principle of IDMS as demonstrated for copper.

Table 4.2 Abbreviations and quantities in the IDMS equation system

Symbol	Unit	Explanation
N_x, N_y	–	Number of atoms in the sample (x) and the spike (y)
$a_{x,a}$, $a_{y,a}$, $a_{z,a}$	–	Abundance of isotope a in the sample, the spike and the back-spike
$a_{x,b}$, $a_{y,b}$, $a_{z,b}$	–	Abundance of isotope b in the sample, the spike and the back-spike
R_{xy}, R_{yz}, R_{Blk}	–	Isotope amount ratio (isotope a/b) in blend 1 (sample-spike), blend 2 (spike-back-spike) and blend 3 (blank-spike)
R_x, R_y, R_z	–	Isotope amount ratio (isotope a/b) in sample, spike and back-spike
N_{A}	mol^{-1}	Avogadro constant
C_x, C_z, C_{Blk}	mg/kg	Amount content of the element in the sample, the back-spike and the procedure blank
$C_{y,b}$	mg/kg	Amount content of isotope b in the spike
m_x, m_y, m'_y, m_z, $m_{y,\mathrm{Blk}}$	kg	Weight of sample, spike solution added to the sample, spike solution used for spike characterisation, back-spike solution used for spike characterisation and spike solution used for blank determination
M_x, M_z, M_b	g/mol	Molar mass of the element in the sample (x), the back-spike (z) and of isotope b

isotope, and can be expressed by a simple equation (equation (4.16)). In the case of copper, a represents ^{63}Cu and b represents ^{65}Cu. All quantities and corresponding units are summarised in Table 4.2:

$$R_{xy} = \frac{N_x a_{x,a} + N_y a_{y,a}}{N_x a_{x,b} + N_y a_{y,b}} \tag{4.16}$$

with $R_x = \frac{a_{x,a}}{a_{x,b}}$ and $R_y = \frac{a_{y,a}}{a_{y,b}}$ follows:

$$N_x = N_y \left(\frac{R_y - R_{xy}}{R_{xy} - R_x} \right) \frac{a_{y,b}}{a_{x,a}} \tag{4.17}$$

Using

$$N_x = \frac{N_A C_x m_x \times 10^{-3}}{M_x} \qquad \text{and} \qquad N_y = \frac{N_A C_{y,b} m_y \times 10^{-3}}{M_b a_{y,b}}$$

gives

$$C_x = \frac{M_x m_y}{a_{x,b} M_b m_x} C_{y,b} \left(\frac{R_y - R_{xy}}{R_{xy} - R_x} \right) \tag{4.18}$$

Isotope ratios measured by mass spectrometry have to be corrected for mass discrimination and mass fractionation effects by the K-factors. In the case of equation (4.18) this correction is not necessary when the four isotope ratios are measured under the same conditions, because the correction K-factors are then cancelled out. This approach is only valid as long as there are no

drift effects of the K-factor and it can be assumed that it is constant for the isotope ratio range under investigation, which means that it is independent of the value of the isotope ratio. This has already been proved for varying values of U isotope ratios measured by MC-ICP-MS.[75]

The above presented IDMS equation (equation (4.18)) can only be applied if an appropriate certified spike is available. But in many cases an adequate spike is not commercially available. Reasons for this may be that the materials that are available have uncertainties that are too large to be of use or are too expensive. It may also be that there is simply a lack of commercial spike solutions for the requested element/isotope. In this case, a spike solution has to be prepared from enriched isotopes in solid form. As these materials are not certified for chemical purity and isotopic composition, the produced spike solution has to be characterised. This can be done by inverting the IDMS principle and analysing the spike by a well-characterised standard solution of the same element, the so-called back-spike or assay material. This often is referred to as reverse IDMS. The proper term however is double IDMS, which describes the characterisation of the sample by the spike and the characterisation of the spike by the back-spike. The spike characterisation by the back-spike or assay material is expressed by equation (4.19):

$$C_{y,b} = \frac{a_{z,b} M_b m_z}{M_z m_{y'}} C_z \left(\frac{R_{yz} - R_z}{R_y - R_{yz}} \right) \tag{4.19}$$

Now $C_{y,b}$ in equation (4.18) can be replaced by equation (4.19), which leads to equation (4.20):

$$C_x = \frac{M_x m_y}{a_{x,b} M_b m_x} \frac{a_{z,b} M_b m_z}{M_z m_{y'}} C_z \left(\frac{R_y - R_{xy}}{R_{xy} - R_x} \right) \left(\frac{R_{yz} - R_z}{R_y - R_{yz}} \right) \tag{4.20}$$

If sample and back-spike show identical isotopic composition of the analyte element, M_x, M_z, $a_{x,b}$ and $a_{z,b}$ cancel out. This can be checked by measuring R_z and R_x and verifying $R_x = R_z$ for all isotope ratios. The resulting equation (equation (4.21)) directly shows the major advantages of double spiking, when all measurements are carried out under the same conditions. Correction K-factors for mass discrimination and mass fractionation effects are all cancelled out, as are the IUPAC isotopic compositions and molar masses[20,88] if sample and back-spike show identical isotopic composition of the analyte element. In cases where isotopic variations occur equation (4.20) has to be applied:

$$C_x = C_z \frac{m_y m_z}{m_x m_{y'}} \left(\frac{R_y - R_{xy}}{R_{xy} - R_x} \right) \left(\frac{R_{yz} - R_z}{R_y - R_{yz}} \right) \tag{4.21}$$

The blank of the complete analytical procedure is spiked as well. The IDMS determination of this procedure blank is described by equation (4.22):

$$C_{\mathrm{Blk}} m_x = C_{y,b} \frac{M_z m_{\mathrm{y,Blk}}}{a_{z,b} M_{\mathrm{b}}} \left(\frac{R_y - R_{\mathrm{Blk}}}{R_{\mathrm{Blk}} - R_z} \right) \tag{4.22}$$

As described above IDMS is based on measurements of masses (sample, spike, back-spike) and isotope ratios only. The advantages compared to other methods therefore are quite clear:

- Losses of analyte do not affect the accuracy of the analytical result because the measurand, the isotope ratio of the blend, is equal in all sub-samples of the blend.
- IDMS is largely unaffected by matrix suppression or enhancement effects, as only isotope ratios have to be measured and both isotopes will be affected in the same way.

- Multi-element IDMS is available when using ICP-MS. For transient signals, however, the multi-element capability is reduced as two isotopes have to be measured for each element.
- In principle all elements of the periodic system having two natural isotopes can be analysed by IDMS as long as mass spectrometric methods for isotope ratio determinations are available. Moreover even mono-isotopic elements can be determined, if they also have a long-lived radionuclide isotope such as iodine-129.
- IDMS enables high accuracy and small measurement uncertainties, when applied properly.
- A full uncertainty budget can easily be calculated.

However, there are also some disadvantages. IDMS is an expensive and destructive method. In order to use it, two isotopes ideally completely free from any isobaric or polyatomic interference must be available. The most important issue however is the isotopic exchange between sample and spike isotopes. Most commonly this is ensured using a digestion step, when determining element content. For species analysis/speciation the spike must be added in the same species form as the analyte to enable isotopic equilibrium (see Chapter 7).

The outstanding performance of IDMS in terms of accuracy and smallest uncertainties is demonstrated by some applications. One example explained already describes the analysis of Cd and Tl in pure zinc metal[33] by IDMS and internal standardisation. For Tl all procedures agree well within their stated uncertainties. For Cd, however, the different IDMS results agree well within $<0.5\%$, but the internal standard result is $\sim 5\%$ off, which is due to an incomplete correction of matrix and drift effects by the internal standard. Another example is the certification of trace elements in polyethylene resulting in the certified reference material BCR 680.[89] The results of this certification campaign for Hg are displayed in ascending order and are labelled according to the methods used (Figure 4.9). Polyethylene causes particular problems with difficulties in achieving complete digestion and strong matrix effects. IDMS applied to ICP-MS (ID-ICP-MS)

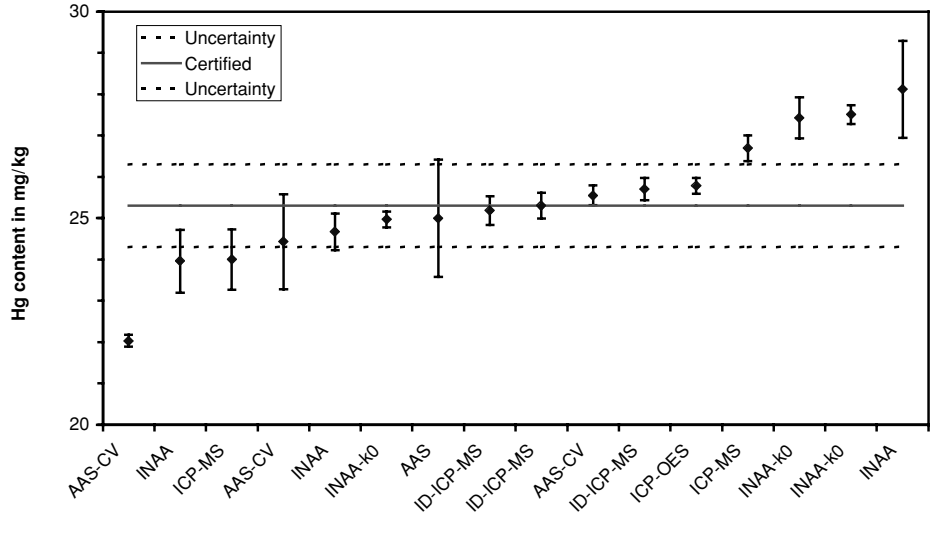

Figure 4.9 Individual results for the certification of Hg in polyethylene in ascending order together with the resulting certified value and its expanded uncertainty ($k = 2$), individual results represent laboratory means with their standard deviation (data from certification report[89]).

managed these problems in the best way and gained the best results in terms of accurate and reproducible values.

Whenever results of highest reliability and accuracy and smallest measurement uncertainty are required IDMS is applied as far as possible. In the past the main fields of application therefore have been certification[90–92] or reference[93,94] measurements and nuclear measurements.[95] Nowadays, with ICP-MS becoming a routine technique, IDMS is being applied to an expanding number of analytical applications, such as serum analysis,[96] human tissues[97] and others.[98–100]

One particular breakthrough has been the development of the on-line IDMS technique in 1994,[101,102] which enables the application of IDMS to chromatographic systems coupled to ICP-MS. This technique accelerated the development of speciation especially for non-synthesisable or labile species. Speciation by on-line IDMS is still a growing field. More details on IDMS in general are given elsewhere.[103,104]

4.11 Measurement uncertainty

Within the scope of this book only the idea and the basic concept of measurement uncertainty can be described. Although given, the definition of measurement uncertainty will be repeated here to make the reader more familiar with it:

> Uncertainy is that parameter, associated with the result of a measurement, which characterises the dispersion of the values that could reasonably be attributed to the measurand.

The measurement uncertainty therefore is not an optional extra, but a fundamental property of each measurement result. All measurement results consist of a value and the accompanying uncertainty, which in general comprises many components. The well-defined but negative sounding term 'uncertainty' replaces the positive term 'accuracy', which reflects the illusion of exactness but in reality is somewhat vague. When talking about the property of a measurement 'accurate' and 'precise' are still in use, but for describing the property of a measurement, especially in numerical form and manner, only uncertainty should be used.

How to calculate or set up an uncertainty budget is best described in the ISO[8] and EURACHEM[9] guidelines, where assistance is given by means of practical examples as well. The most important facts will be summarised in the following section. The single components of the measurement uncertainty may be assessed by statistical distribution of a series of measurements and may be expressed by the standard deviation. These single components derive from all influencing parameters, correction factors, tabulated quantities etc., which all have uncertainties themselves and thus have to be considered in the total uncertainty budget. Generally, there are two main directions for uncertainty calculation. When the analytical result can be directly calculated from the instrument response via a clear and unambiguous equation (e.g. IDMS), the uncertainty in turn can be calculated using the symbolic or numerical differentiation of this equation. For other calibration strategies (e.g. external, internal calibration) all uncertainty contributions have to be identified and charged in the uncertainty budget applying a model specific for these procedures. More details as well as some applications are given in the literature.[105–107] Helpful tools are also available, including software packages for numeric differentiation[108] and articles providing specific models.[109]

4.12 Quality assurance

Due to overregulation[110] and contradictory effects such as unacceptable results from accredited laboratories, quality assurance in analytical chemistry is constantly under discussion and exposed to criticism. Certainly quality assurance (QA) will not improve analytical work and its quality, which is at present very high in routine analysis as well as in research and development.[111] Documenting all important processes, however, will make results trackable and possibilities for improvements (errors, quality, costs etc.) will be made visible. Therewith QA leads to better transparency and thus improves comparability. Proving properties of the applied analytical procedure like bias, uncertainty, reproducibility etc., which is often viewed as a key objective of QA, is actually the bread-and-butter work in analytical chemistry and should be self-evident for every reliable analyst.

In environmental analysis, clinical chemistry and pharmaceutical measurements, for example, QA is mandatory, because of obvious safety reasons and corresponding regulations. Also in analytical chemistry QA is becoming increasingly obligatory due to specific regulations but also due to customer requirements, e.g. government contracts.

In analytical chemistry QA often is used for and understood as 'good quality analytical work', which means to check all analytical parameters and keep them under control. A good example for this is the use of 'QA samples' in ICP-MS analysis applying external calibration. These QA samples are regularly measured materials, similar in composition to the samples routinely analysed, except that the analyte content is known, and so serve as proof of the absence of drift effects. Should the bias between measured and known analyte content exceed a certain level, the calibration has to be repeated. The control of the calibration's validity however should be checked regularly even if no QA system is installed.

Being a topic by itself, QA is well summarised in reference 112. The definition as well as a description of QA is given in the literature,[3] and some applications are presented in a number of articles.[113–115] Applications of QA in the environmental field in particular are covered in detail in Chapter 9 of this book.

References

1. International Standards Organization (1993) International Vocabulary of Basic and General Terms in Metrology (BIPM, IEC, IFCC, ISO, IUPAC, IUPAP, OIML); 2nd edn ISO, Geneva, ISBN 92-67-01075-1.
2. Fleming, J., Neidhart, B., Tausch, C., and Wegscheider, W. (1996) Glossary of analytical terms (II to VI). *Accred. Qual. Assur.*, **1**, 41–3, 87–8, 135, 190–1, 233–4, 277.
3. Fleming, J., Neidhart, B., Tausch, C., and Wegscheider, W. (1997) Glossary of analytical terms (VII to IX). *Accred. Qual. Assur.*, **2**, 51–2, 160–1, 348–9.
4. Fleming, J., Neidhart, B., Tausch, C., and Wegscheider, W. (1998) Glossary of analytical terms X. *Accred. Qual. Assur.*, **3**, 171–3.
5. Holcombe, D. (1999) Alphabetical index of defined terms and where they can be found, Part I: A-F. *Accred. Qual. Assur.*, **4**, 525–30.
6. Holcombe, D. (2000) Alphabetical index of defined terms and where they can be found, Part II: G-Q. *Accred. Qual. Assur.*, **5**, 77–82.

7. Holcombe, D. (2000) Alphabetical index of defined terms and where they can be found, Part III: R-Z. *Accred. Qual. Assur.*, **5**, 159–64.
8. International Standards Organization (1995) Guide to expression of Uncertainty in Measurement, ISO, Geneva.
9. EURACHEM (1995) Quantifying Uncertainty in Analytical Measurement, LGC, Teddington, UK.
10. International Standards Organization (1993) Geneva, ISO 3534-1.
11. Šulcek, Z. and Povondra, P. (1989) *Methods of Decomposition in Inorganic Analysis*, CRC Press, Boca Raton.
12. Kingston, H. M. and Haswell, S. J. (eds) (1997) *Microwave-Enhanced Chemistry*, American Chemical Society, Washington, DC.
13. Castillo, J. R., Jiménez, M. S., and Ebdon, L. (1999) Semiquantitative simultaneous determination of metals in olive oil using direct emulsion nebulization. *J. Anal. At. Spectrom.*, **14**, 1515–8.
14. Kumar, S. J. and Gangadharan, S. (1999) Determination of trace elements in naphtha by inductively coupled plasma mass spectrometry using water-in-oil emulsions. *J. Anal. At. Spectrom.*, **14**, 967–71.
15. Ebdon, L., Foulkes, M., and Sutton, K. (1997) Slurry nebulisation in plasmas. *J. Anal. At. Spectrom.*, **12**, 213–29.
16. Sturman, B. T. (2000) Comment on determination of mercury in potable water by ICP-MS using gold as a stabilising agent. *J. Anal. At. Spectrom.* **15**, 1512.
17. Larsen, E. H. and Stürup, S. (1994) Carbon-enhanced inductively coupled plasma mass spectrometric detection of arsenic and selenium and its application to arsenic speciation. *J. Anal. At. Spectrom.*, **9**, 1099–105.
18. Horlick, G. and Montaser, A. (1998) Analytical characteristics of ICPMS. In: *Inductively Coupled Plasma Mass Spectrometry* (ed. A. Montaser), Wiley-VCH, New York, pp. 503–613.
19. Evans, E. H. and Giglio, J. J. (1993) Interferences in inductively coupled plasma mass spectrometry. *J. Anal. At. Spectrom.*, **8**, 1–18.
20. Rosman, K. J. R. and Taylor, P. D. P. (1998) Isotopic composition of the elements. *Pure Appl. Chem.*, **70**, 217–35.
21. Dulski, P. (1994) Interferences of oxide, hydroxide and chloride analyte species in the determination of rare earth elements in geological samples by inductively coupled plasma mass spectrometry. *Fresenius' J. Anal. Chem.*, **350**, 194–203.
22. Montes Bayón, M., García Alonso, J. I., and Sanz Medel, A. (1998) Enhanced semiquantitative multi-analysis of trace elements in environmental samples using inductively coupled plasma mass spectrometry. *J. Anal. At. Spectrom.*, **13**, 277–82.
23. Soldevila, J., El Himri, M., Pastor, A., and de la Guardia, M. (1998) Evaluation of operational parameters affecting semiquantitative multi-elemental analysis by inductively coupled plasma mass spectrometry. *J. Anal. At. Spectrom.*, **13**, 803–7.
24. Laborda, F., Medrano, J., and Castillo, J. R. (2001) Quality of quantitative and semiquantitative results in inductively coupled plasma mass spectrometry. *J. Anal. At. Spectrom.*, **16**, 732–8.
25. García Alonso, J. I., Montes Bayón, M., and Sanz Medel, A. (1999) Environmental applications using ICP-MS: semiquantitative analysis. In: *Plasma Source Mass Spectrometry – New Developments and Applications* (eds G. Holland and S. D. Tanner), Royal Society of Chemistry, Cambridge, UK, pp. 95–107.
26. Woods, G. D. and McCurdy, E. (1999) Implementation of ICP-MS as a single technique for the multielement analysis of environmental samples. In: *Plasma Source Mass Spectrometry – New Developments and Applications* (eds G. Holland and S. D Tanner), Royal Society of Chemistry, Cambridge, UK, pp. 108–19.

27. Taylor, H. E., Huff, R. A., and Montaser, A. (1998) Novel applications of ICP-MS. In: *Inductively Coupled Plasma Mass Spectrometry* (ed. A. Montaser), Wiley-VCH, New York, pp. 9681–808.
28. Pritzkow, W., Vogl, J., Berger, A., Ecker, K., Grötzschel, R., Klingbeil, P., Persson, L., Riebe, G., and Wätjen, U. (2001) Contribution of ICP-IDMS to the certification of antimony implanted in a silicon wafer – comparison with RBS and INAA results. *Fresenius J. Anal. Chem.*, **371**, 867–73.
29. Abbyad, P., Trump, J., Lam, J., and Salin, E. (2001) Optimization of the technique of standard additions for inductively coupled plasma mass spectrometry. *J. Anal. At. Spectrom.*, **16**, 464–9.
30. Cheatham, M. M., Sangrey, W. F., and White, W. M. (1993) Sources of error in external calibration ICP-MS analysis of geological samples and improved non-linear drift correction procedure. *Spectrochim. Acta*, **48B**, E487–E506.
31. Ratzlaff, K. L. (1979) Optimizing precision in standard addition measurement. *Anal. Chem.*, **51**, 232–5.
32. Kemp, G. J. (1985) The susceptibility of calibration methods to errors in the analytical signal. *Anal. Chim. Acta*, **176**, 229–47.
33. Klingbeil, P., Vogl, J., Pritzkow, W., Riebe, G., and Müller, J. (2001) Comparative studies on the certification of reference materials by ICPMS and TIMS using isotope dilution procedures. *Anal. Chem.*, **73**, 1881–8.
34. Vasileyeva, I. E., Shabanova, V., Sokolnikova, Y. V., Proydakova, O. A., and Lozhkin, V. I. (1999) Selection of internal standard for determination of boron and phosphorous by ICP-MS in silicon photovoltaic materials. *J. Anal. At. Spectrom.*, **14**, 1519–21.
35. Gammelgaard, B., and Jøns, O. (1999) Determination of selenium in urine by inductively coupled plasma mass spectrometry: interferences and optimization. *J. Anal. At. Spectrom.*, **14**, 867–74.
36. Arslan, Z., Ertas, N., Tyson, J. F., Uden, P. C., and Denoyer, E. R. (2000) Determination of trace elements in marine plankton by inductively coupled plasma mass spectrometry (ICP-MS). *Fresenius' J. Anal. Chem.*, **366**, 273–82.
37. Tibi, M. and Heumann, K. G. (2001) Determination of trace elements in quartz glass by use of LINA-Spark-ICP-MS as a new method for bulk analysis of solid samples. *Fresenius' J. Anal. Chem.*, **370**, 521–6.
38. Hu, J. and Wang, H. (2001) Determination of trace elements in super alloy by ICP-MS. *Mikrochim. Acta*, **137**, 149–55.
39. Riondato, J., Vanhaecke, F., Moens, L., and Dams, R. (2000) Fast and reliable determination of (ultra) trace and/or spectrally interfered elements in water by sector field ICP-MS. *J. Anal. At. Spectrom.*, **15**, 341–5.
40. Zschunke, A. (2000) (ed.), *Reference Materials in Analytical Chemistry – A Guide for Selection and Use*, Springer-Verlag, Berlin.
41. International Standards Organization (1999), Geneva, DIN EN ISO/IEC 17025.
42. Maréchal, C. N., Télouk, P., and Albarède, F. (1999) Precise analysis of copper and zinc isotopic compositions by plasma-source mass spectrometry. *Chem. Geol.*, **156**, 251–73.
43. Tirez, K., Seuntjens, P., and de Brucker, N. (1999) Full uncertainty calculation on quantitative determination of tracer (^{111}Cd) cadmium and natural cadmium in soil column effluents with ICP-MS. *J. Anal. At. Spectrom.*, **14**, 1475–84.
44. Hulbert, L. J. and Grégoire, D. C. (1993) Re-Os isotope systematics of the rankin inlet Ni ores: an example of the application of ICP-MS to investigate Ni-Cu-PGE mineralization and the potential use of Os isotopes in mineral exploration. *Canadian Mineralogist*, **31**, 861–76.

45. Walczyk, T. and von Blanckenburg, F. (2002) Natural iron isotope variations in human blood. *Science*, **295**(5562), 2065–6.
46. Prohaska, T., Latkoczy, C., Schultheis, G., Teschler-Nicola, M., and Stingeder, G. (2002) Investigation of Sr isotope ratios in prehistoric human bones and teeth using laser ablation ICP-MS and ICP-MS after Rb/Sr separation. *J. Anal. At. Spectrom.*, **17**, 887–91.
47. De Wannemaker, G., Vanhaecke, F., Moens, L., Van Mele, A., and Thoen, H. (2000) Lead isotopic and elemental analysis of copper statuettew by double focusing sectro field ICP mass spectrometry. *J. Anal. At. Spectrom.*, **15**, 323–7.
48. Becker, J. S., and Dietze, H.-J. (1999) Precise isotope ratio measurements for uranium, thorium and plutonium by quadrupole-based inductively coupled plasma mass spectrometry. *Fresenius' J. Anal. Chem.*, **364**, 482–8.
49. Boulyga, S. F., Becker, J. S., Matusevitch, J. L., and Dietze, H.-J. (2000) Isotope ratio measurements of spent reactor uranium in environmental samples by using inductively coupled plasma mass spectrometry. *Int. J. Mass Spectrom.*, **203**, 143–54.
50. Platzner, I. T. (1997) (ed.), *Modern Isotope Ratio Mass Spectrometry*, John Wiley & Sons, Chichester, UK.
51. Vogl, J. and Heumann, K. G. (1997) Determination of heavy metal complexes with humic substances by HPLC/ICP-MS coupling using on-line isotope dilution technique. *Fresenius, J. Anal. Chem.*, **359**, 438–41.
52. Heumann, K. G., Gallus, S. M., Rädlinger, G., and Vogl, J. (1998) Precision and accuracy in isotope ratio measurements by plasma source mass spectrometry. *J. Anal. At. Spectrom.*, **13**, 1001–8.
53. Jackson, S. E. and Günther, D. (2003) The nature and sources of laser induced isotopic fractionation in laser ablation-multicollector-inductively coupled plasma-mass spectrometry. *J. Anal. At. Spectrom.*, **18**, 205–12.
54. Hirata, T. and Yamaguchi, T. (1999) Isotopic analysis of zirconium using enhanced sensitivity-laser-ablation-multiple collector-inductively coupled plasma mass spectrometry. *J. Anal. At. Spectrom.*, **14**, 1455–9.
55. Halliday, A. N., Lee, D.-C., Christensen, J. N., Walder, A. J., Freedman, P. A., Jones, C. E., Hall, C. M., Yi, W., and Teagle, D. (1995) Recent developments in inductively coupled plasma magnetic sector multiple collector mass spectrometry. *Int. J. Mass Spectrom. Ion Proc.*, **146/147**, 21–33.
56. Vogl, J., Klingbeil, P., Pritzkow, W., and Riebe, G. (2003) High accuracy measurements of Fe isotopes using hexapole collision cell MC-ICP-MS and isotope dilution for certification of reference materials. *J. Anal. At. Spectrom.*, **18**, 1125–32.
57. Hunter, K. L. and Gray, J. W. (1993) *Ion Detection in Mass Spectrometry using the Ion Counting Technique*. Technical Publication, ETP Scientific Inc., Auburn, MA, USA.
58. Turner, P. J., Mills, D. J., Schröder, E., Lapitajs, G., Jung, G., Iacone, L. A., Haydar, D. A., and Montaser, A. (1998) Instrumentation for low- and high-resolution ICP-MS. In: *Inductively Coupled Plasma Mass Spectrometry* (ed. A. Montaser), Wiley-VCH, New York, pp. 421–501.
59. Habfast, K. (1997) Advanced isotope ratio mass spectrometry I: magnetic isotope ratio mass spectrometers. In: *Modern Isotope Ratio Mass Spectrometry* (ed. I. T. Platzner), John Wiley & Sons, Chichester, UK, pp. 11–82.
60. ETP Scientific Inc. (1992) *Active Film Multipliers – Handbook for Mass Spectrometry Applications*, Auburn, MA, USA.
61. Dawson, P. H. (ed.) (1976) *Quadrupole Mass Spectrometry and its Applications*, Elsevier, Amsterdam, p. 143.

62. Douglas, D. J. and Tanner, S. D. (1998) Fundamental considerations in ICP-MS. In: *Inductively Coupled Plasma Mass Spectrometry* (ed. A. Montaser), Wiley-VCH, New York, pp. 421–501.
63. Allen, L. A., Leach, J. J., and Houk, R. S. (1997) Spatial location of the space charge effect in individual ion clouds using monodisperse dried microparticulate injection with a twin quadrupole inductively coupled plasma mass spectrometer. *Anal. Chem.*, **69**, 2384–91.
64. Belshaw, N. S., Freedman, P. A., O'Nions, R. K., Franks, M., and Guo, Y. (1998) A new dispersion double-focusing plasma mass spectrometer with performance illustrated for Pb isotopes. *Int. J. Mass Spectrom.*, **181**, 51–8.
65. Rehkämper, M. and Halliday, A. N. (1998) Accuracy and long-term reproducibility of lead isotopic measurements by multiple-collector inductively coupled plasma mass spectrometry using an external method for correction of mass discrimination. *Int. J. Mass Spectrom.*, **181**, 123–33.
66. Walder, A. J. (1997) Advanced isotope ratio mass spectrometry II: isotope ratio measurement by multiple collector inductively coupled plasma mass spectrometers. In: *Modern Isotope Ratio Mass Spectrometry* (ed. I. T. Platzner), John Wiley & Sons, Chichester, UK, pp. 11–82.
67. Ingle, C. P., Sharp, B. L., Horstwood, M. S. A., Parrish, R. R., and Lewis, D. J. (2003) Instrument response functions, mass bias and matrix effects in isotope ratio measurements and semi-quantitative analysis by single and multi-collector ICP-MS. *J. Anal. At. Spectrom.*, **18**, 219–29.
68. Gregoire, D. C., Acheson, B. M., and Taylor, R. P. (1996) Measurement of lithium isotope ratios by inductively coupled plasma mass spectrometry: application to geological materials. *J. Anal. At. Spectrom.*, **11**, 765–72.
69. Vogl, J. (1997) Charakterisierung und Quantifizierung von Schwermetall/Huminstoff-Species durch HPLC/ICP-MS, Ph.D. Thesis, University of Regensburg.
70. Vanhaecke, F., Moens, L., Dams, R., Papadakis, I., and Taylor, P. (1997) Applicability of high-resolution ICP-mass spectrometry for isotope ratio measurements. *Anal. Chem.*, **69**, 268–73.
71. Xie, Q. and Kerich, R. (2002) Isotope ratio measurement by hexapole ICP-MS: mass bias effect, precision and accuracy. *J. Anal. At. Spectrom.*, **17**, 69–74.
72. Xie, Q., and Kerich, R. (1995) Optimization of operating conditions for improved precision of zirconium and hafnium isotope ratio measurement by inductively coupled plasma mass spectrometry (ICP-MS). *J. Anal. At. Spectrom.*, **10**, 99–103.
73. Alonso, J. I. G., Sena, F., Arbore, P., Betti, M., and Koch, L. (1995) Determination of fission products and actinides in spent nuclear fuels by isotope dilution ion chromatography inductively coupled plasma mass spectrometry. *J. Anal. At. Spectrom.*, **10**, 381–93.
74. Hirata, T. (1996) Lead isotopic analysis of NIST standard reference materials using multiple collector inductively coupled plasma mass spectrometry coupled with a modified external correction method for mass discrimination effect. *Analyst*, **121**, 1407–11.
75. Taylor, P. D. P., De Bievre, P., Walder, A. J., and Entwistle, A. (1995) Validation of the analytical linearity and mass discrimination correction model exhibited by a multiple collector inductively coupled plasma mass spectrometer by means of a set of synthetic uranium isotope mixtures. *J. Anal. At. Spectrom.*, **10**, 395–8.
76. Müller, J. W. (1973) Dead time problems. *Nucl. Instrum. Methods*, **112**, 47–57.
77. Knoll, G. F. (2000) *Radiation Detection and Measurement*, John Wiley & Sons, Chichester, Ch. 4, pp. 119–28.
78. Nelms, S. M., Quétel, C. R., Prohaska, T., Vogl, J., and Taylor, P. D. P. (2001) Evaluation of detector dead time calculation models for ICP-MS. *J. Anal. At. Spectrom.*, **16**, 333–8.

79. Webpage of the National Institute for Standards and Technology NIST, Gaithersburg, MD, USA, http://www.nist.gov/
80. Ramebäck, H., Berglund, M., Vendelbo, D., Wellum, R., and Taylor, P. D. P. (2001) On the determination of the true dead-time of a pulse-counting system in isotope ratio mass spectrometry. *J. Anal. At. Spectrom.*, **16**, 1271–4.
81. Hayes, J. M. and Schoeller, D. A. (1977) High precision pulse counting: limitations and optimal conditions. *Anal. Chem.*, **49**, 306–11.
82. Appelblad, P. K. and Baxter, D. C. (2000) A model for calculating dead time and mass discrimination correction factors from inductively coupled plasma mass spectrometry calibration curves. *J. Anal. At. Spectrom.*, **15**, 557–60.
83. Adriaens, A. G., Kelly, W. R., and Adams, F. C. (1993) Propagation of uncertainties in isotope dilution mass spectrometry using pulse counting detection. *Anal. Chem.*, **65**, 660–3.
84. Montaser, A., Minnich, M. G., and Liu, H. (1998) Fundamental aspects of sample introduction in ICP spectrometry. In: *Inductively Coupled Plasma Mass Spectrometry* (ed. A. Montaser), Wiley-VCH, New York, pp. 335–419.
85. Webpage of the Consultative Committee for Amount of Substance, Bureau International des Poids et Mesures, Paris, France, http://www.bipm.fr/enus/2_Committees/CCQM.shtml
86. De Bièvre, P. (1994) Isotope dilution mass spectrometry (IDMS). In: *Isotope Dilution Mass Spectrometry (IDMS)* (eds R. F. Herber and M. Stoeppler), Elsevier, Amsterdam, pp. 169–83.
87. Heumann, K. G. (1992) Isotope dilution mass spectrometry (IDMS) of the elements. *Mass Spectrom. Rev.*, **11**, 41–67.
88. Coplen, T. B. (1996) Atomic weights of the elements. *Pure Appl. Chem.*, **68**, 2339–59.
89. Lamberty, A., Van Borm, W., and Quevauviller, Ph. (2001) The certification of mass fraction of As, Br, Cl, Cr, Hg, Pb and S in two polyethylene CRMs – BCR-680 and BCR-681. In: *European Commission 2001*.
90. Murphy, K. E., Beary, E. S., Rearick, M. S., and Vocke, R. D. (2000) Isotope dilution inductively coupled plasma mass spectrometry (ID ICP-MS) for the certification of lead and cadmium in environmental standard reference materials. *Fresenius' J. Anal. Chem.*, **368**, 362–70.
91. Diemer, J. and Heumann, K. G. (2000) Development of an ICP-IDMS method for accurate routine analyses of toxic heavy metals in polyolefins and comparison with results by TI-IDMS. *Fresenius' J. Anal. Chem.*, **368**, 103–8.
92. Diemer, J., Vogl, J., Quétel, C. R., Linsinger, T., Taylor, P. D. P., Lamberty, A., and Pauwels, J. (2001) SI-traceable certification of the amount content of cadmium below the ng g^{-1} level in blood samples by isotope dilution ICP-MS applied as a primary method of measurement. *Fresenius' J. Anal. Chem.*, **370**, 492–8.
93. Vogl, J., Quétel, C. R., Ostermann, M., Papadakis, I., Van Nevel, L., and Taylor, P. D. P. (2000) Contribution to the certification of B, Cd, Mg, Pb, Rb Sr and U in a natural water sample for the international measurement evaluation programme round 9 (IMEP-9) using ID-ICP-MS. *Accred. Qual. Assur.*, **5**, 272–9.
94. Horn, M. and Heumann, K. G. (1994) Comparison of heavy metal analyses in hydrofluoric acid used in microelectronic industry by ICP-MS and thermal ionization isotope dilution mass spectrometry. *Fresenius' J. Anal. Chem.*, **350**, 286–92.
95. Alonso, J. I. G. (1995) Determination of fission products and actinides by inductively coupled plasma-mass spectrometry using isotope dilution analysis: a study of random and systematic errors. *Anal. Chim. Acta*, **312**, 57–78.
96. Muñiz, C. S., Gayón, J. M. M., Alonso, J. I. G., and Sanz-Medel, A. (1999) Accurate determination of iron, copper and zinc in human serum by isotope dilution analysis using double focusing ICP-MS. *J. Anal. At. Spectrom.*, **14**, 1505–10.

97. Klemens, P. and Heumann, K. G., Development of an ICP-HRIDMS method for accurate determination of traces of silicon in biological and clinical samples. *Fresenius' J. Anal. Chem.*, **371**, 758–63.
98. Park, C. J., Cho, K. H., Suh, J. K., and Han, M. S. (2000) Determination of cadmium in sediment reference materials by isotope dilution by inductively coupled plasma mass spectrometry with correction of tin isobaric interference using mass bias equations. *J. Anal. At. Spectrom.*, **15**, 567–70.
99. Gäbler, H.-E., Bahr, A., and Mieke, B. (1999) Determination of the interchangeable heavy-metal fraction in soils by isotope dilution mass spectrometry. *Fresenius' J. Anal. Chem.*, **365**, 409–14.
100. Vogl, J. and Heumann, K. G. (1998) Development of an ICP-IDMS method for dissolved organic carbon determinations and its application to chromatographic fractions of heavy metal complexes with humic substances. *Anal. Chem.*, **70**, 2038–43.
101. Rottmann, L. and Heumann, K. G. (1994) Development of an on-line isotope dilution technique with HPLC/ICP-MS for the accurate determination of elemental species. *Fresenius' J. Anal. Chem.*, **350**, 221–7.
102. Heumann, K. G., Rottman, L., and Vogl, J. (1994) Elemental speciation with liquid chromatography-inductively coupled plasma isotope dilution mass spectrometry. *J. Anal. At. Spectrom.*, **9**, 1351–5.
103. Heumann, K. G. (1988) Isotope dilution mass spectrometry. In: *Inorganic Mass Spectrometry* (eds F. Adams, R. Gÿbels and R. Van Grieken), Wiley & Sons, New York, pp. 301–76.
104. De Bièvre, P. (1993) Isotope dilution mass spectrometry as a primary method of analysis. *Anal. Proc.*, **30**, 328–33.
105. King, B. (2001) Meeting the measurement uncertainty and traceability requirements of ISO/IEC standard 17025 in chemical analysis. *Fresenius' J. Anal. Chem.* **371**, 714–20.
106. Brüggemann, L. and Wennrich, R. (2002) Evaluation of measurement uncertainty for analytical procedures using a linear calibration function. *Accred. Qual. Assur.*, **7**, 269–73.
107. Mazej, D. and Stibilj, V. (2003) Measurement uncertainty of selenium determination in the reference material seronorm trace elements serum by hydride generation atomic fluorescence spectrometry. *Accred. Qual. Assur.*, **8**, 117–23.
108. GUM workbench, Metrodata GmbH, Germany, http://www.metrodata.de/
109. Achermann, E. (2002) MUSAC – A Tool for Evaluating Measurement Uncertainty, Verlag Dr Kovac, Hamburg, Germany.
110. Hey, H. (2001) Analytical quality assurance: obscure, overregulated. *Accred. Qual. Assur.*, **6**, 223–25.
111. Cammann, K. and Kleiböhmer, W. (1997) The need for quality assurance in analytical research and development. *Accred. Qual. Assur.*, **2**, 262–3.
112. Güzler, H. (1996) *Accreditation and Quality Assurance in Analytical Chemistry*, Springer Verlag, Berlin.
113. Senoner, M., Unger, W., and Reiners, G. (2003) Quality assurance in nano-scale analysis. *Appl. Phys.*, A **76**, 919–21.
114. Erber, D., Roth, J., and Cammann, K. (1997) Quality assurance system for a decomposition method as demonstrated for the Wickbold combustion technique. *Accred. Qual. Assur.*, **2**, 332–7.
115. Trancoso, M. A., Correia dos Santos, M. M., and Simões Gonçalves, M. L. (2003) Quality assurance program for the chemical characterization of soils. *Accred. Qual. Assur.*, **8**, 323–33.

Chapter 5

Liquid Sample Introduction and Electrothermal Vaporisation for ICP-MS: Fundamentals and Applications

José L Todoli and Frank Vanhaecke

5.1 NEBULISERS, SPRAY CHAMBERS AND DESOLVATION SYSTEMS – OVERVIEW

José L Todoli

5.1.1 Standard liquid sample introduction system – Main drawbacks

One of the most common ways of performing direct liquid sample analysis with ICP-MS involves the generation of an aerosol followed by further filtering of the coarsest droplets, thus preventing them from being introduced into the plasma. Due to the characteristics and requirements of the ICP-MS spectrometer, the design and efficiency of the sample introduction system is a key point that imposes the quality of the analytical results.[1] Several comprehensive books have appeared that deal with this subject.[2–4] In the following section, attention has been paid to the recent advances in this field.

Generally, a liquid sample introduction system suitable for ICP-MS consists of two main components: (i) a nebuliser that turns the liquid bulk into an aerosol and (ii) a spray chamber that selects the maximum drop size that will be introduced into the plasma. The most often used nebuliser–spray chamber combination for ICP-MS is depicted in Figure 5.1. It consists of a pneumatic concentric nebuliser coupled to a double pass spray chamber.

Pneumatic concentric nebuliser. This device has a narrow capillary centred in and fixed to a cylindrical main body, usually both made from glass. Pneumatic concentric nebulisers can also be made of polymeric materials such as PFA. Disassembled nebulisers have been described as well.[5] In concentric nebulisers, a gas stream emerges at high velocity through the annulus left between the inner capillary and the external body. Simultaneously, the liquid is passed through the capillary. The resulting aerosol is called the *primary aerosol*. Pneumatically generated primary aerosols are coarse, having droplets with diameters even higher than 100 μm; they are polydisperse in terms of drop diameters, and they move at high velocities and have a high degree of turbulence.

Double pass spray chamber. This device consists of two concentric tubes (Figure 5.1). The aerosol is passed through the inner tube and then forced to change its path by 180°. The aerosol leaving the chamber (i.e. the *tertiary* aerosol) is introduced into the plasma base by means of the torch injector. The main processes taking place inside the spray chamber (Figure 5.1), called aerosol transport phenomena[6], are: (i) solvent evaporation from the aerosol droplets; (ii) droplet

Inductively Coupled Plasma Mass Spectrometry Handbook Edited by Simon M. Nelms
 ISBN: 978-1-405-10916-1

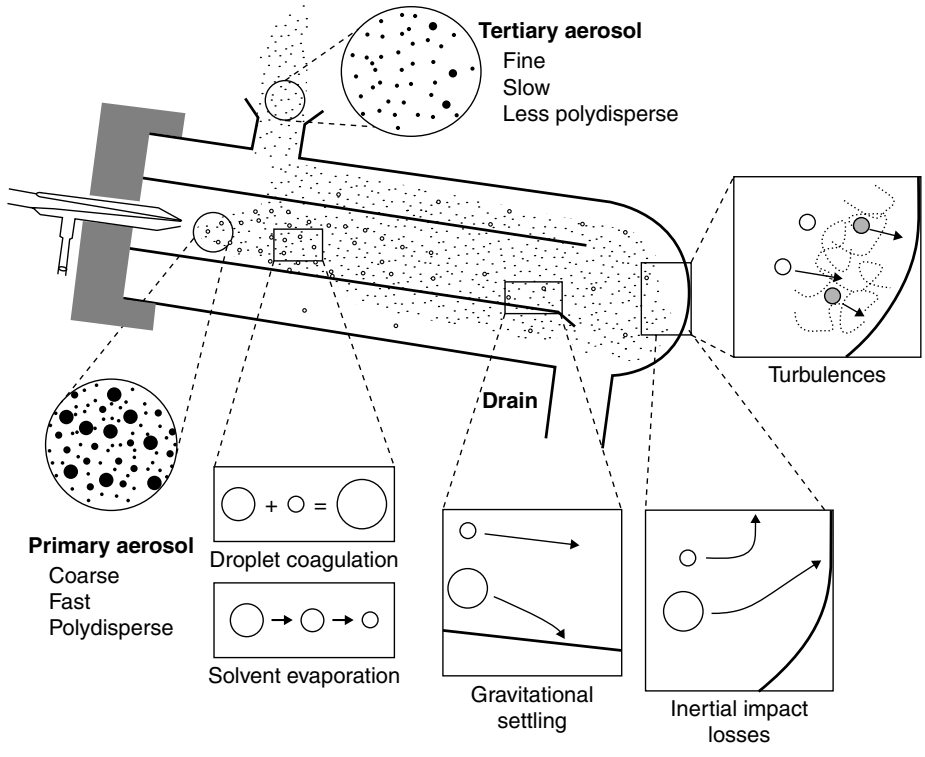

Figure 5.1 Conventional liquid sample introduction system for ICP-MS and aerosol transport processes taking place inside the spray chamber.

inertial losses; (iii) droplet coagulation or coalescence; (iv) gravitational settling and (v) turbulent impact losses. Other events including the aerosol thermal equilibration, droplet break-up and re-nebulisation also take place inside the spray chamber. Tertiary aerosols are finer, less polydisperse, the drop velocities are lower and the droplet number density is also lower than for primary ones.

The sample introduction system depicted in Figure 5.1 shows some drawbacks for use in ICP-MS:

(1) The analyte transport efficiency is very low (i.e. only 0.5–2% of the analyte contained in primary aerosols reaches the plasma).
(2) The nebuliser suffers from tip blocking when high salt content solutions or slurries are analysed.
(3) Memory effects are high and wash-out times are long.
(4) There are serious limitations for the analysis of very low liquid sample volumes (i.e. <1 mL).
(5) The solvent plasma load is too high for performing some particular determinations.
(6) Matrix effects deteriorate the accuracy of the results.

These drawbacks have driven research into and development of new nebuliser/spray chamber systems, as described in the following section.

5.1.1.1 Alternative nebulisers

In order to overcome drawback 1 several nebulisers and spray chambers have been developed. In this field, considerable effort has been dedicated to the design of new pneumatic devices able to efficiently take advantage of the gas kinetic energy. To solve drawback 2, two general choices are available: (i) pneumatic concentric nebulisers with modified critical dimensions and (ii) pneumatic nebulisers in which the geometry of the liquid and gas interaction is not concentric. Other non–pneumatic nebulisers have also been designed that overcome either or both of these drawbacks.

(a) Additional pneumatic nebulisers

The dimensions of pneumatic concentric nebulisers play a very important role in terms of their applicability to the analysis of complex samples.[7] Figure 5.2 shows several different concentric nebulisers with varying performance properties. While nebuliser (a) suffers from tip blocking when introducing high salt content solutions and slurries, nebuliser (b) is able to work with 20% sodium chloride solutions. Nebuliser (c) works properly with slurries having solid particles

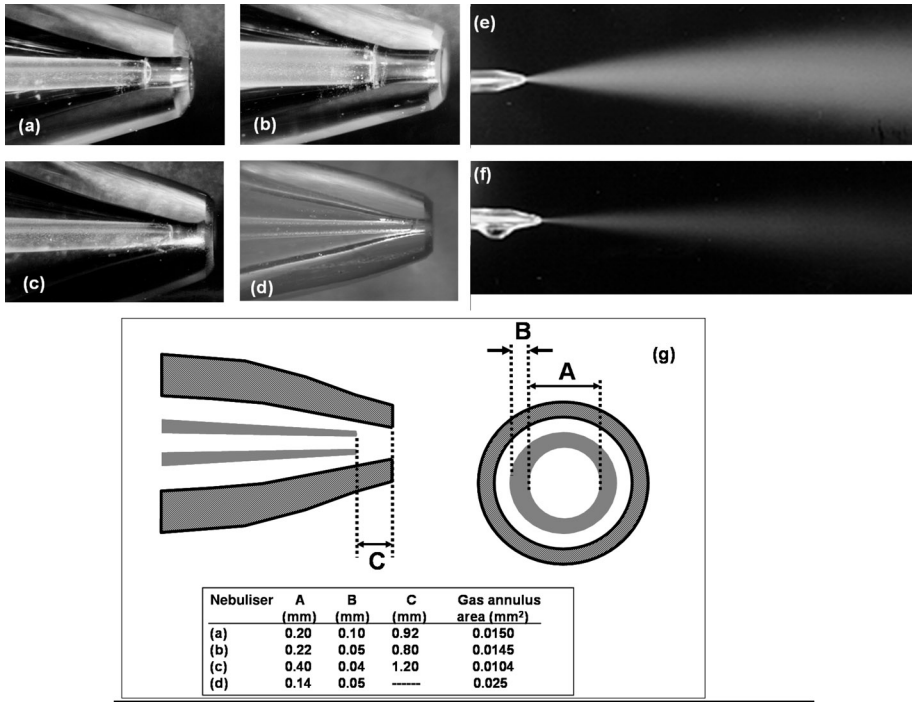

Nebuliser	A (mm)	B (mm)	C (mm)	Gas annulus area (mm²)
(a)	0.20	0.10	0.92	0.0150
(b)	0.22	0.05	0.80	0.0145
(c)	0.40	0.04	1.20	0.0104
(d)	0.14	0.05	------	0.025

Figure 5.2 Pictures of several glass pneumatic concentric nebulisers. (a) Conventional nebuliser; (b) nebuliser suitable for the analysis of high salt content solutions; (c) nebuliser suitable for the analysis of slurries; (d) nebuliser used for the introduction of very small samples; (e) nebuliser (b) operated with deionised water; (f) nebuliser (c) operated with deionised water; and (g) main dimensions of each nebuliser.

with sizes as large as 120 μm. Finally, the device labelled as (d) is able to work efficiently at liquid flow rates of the order of several (approximately 1–10) microlitres per minute as well as at conventional values of this parameter (approximately 1–2 mL/min). It is also worth mentioning that for nebuliser (c), the aerosol generation yield is lower than 100%. As can be seen from Figure 5.2(f), a portion of the sample accumulates at the tip of nebuliser (c) without being transformed into an aerosol. This is not observed in the case of nebuliser (b) (Figure 5.2(e)).

Other pneumatic nebulisers have also been developed that enhance the analyte transport efficiency with respect to the concentric one. Included within this category are the glass frit nebuliser, the capillary array nebuliser and the cross flow MAK nebuliser.[3] Nebuliser tip blocking is virtually avoided for devices such as the so-called Babington, V-groove and Conespray devices. Parallel path nebulisers have also been developed (by Burgener Research Inc.) to introduce liquid samples for plasma spectrometry.[8] With this nebuliser design, the liquid and gas streams are aligned with each other (Figure 5.3). According to the manufacturer, this nebuliser does not suffer from blocking when working with high salt content solutions or slurries. A modified Burgener nebuliser has been recently used for the generation of volatile species, with subsequent detection using ICP-MS.[9,10]

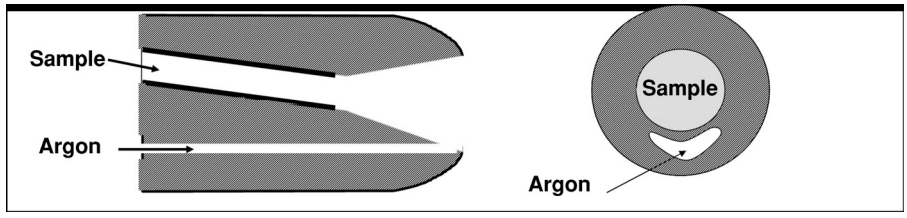

Figure 5.3 Drawing of the Burgener parallel path nebuliser (adapted from http://burgenerresearch.com).

(b) Other nebulisers

With ultrasonic nebulisers (USNs), the acoustic energy provided by a transducer made of a piezoelectric crystal is transferred to the sample. All the aerosol liquid volume is transformed into droplets whose diameters are lower than 10 μm. This fact makes the solvent plasma load very high, which means that it is compulsory to include a system for solvent removal prior to entry to the plasma with this nebuliser type. With this coupling, the analyte transport efficiency is as high as 30%, thus giving rise to extremely high sensitivities and low limits of detection. USNs have been used for applications such as ICP-MS speciation,[11] analysis of crude oil[12] and analysis of water samples, after a preconcentration step.[13] The main drawbacks of USNs are their long memory effects and wash-out times, the high sample volume required (>1 mL/min), although micro-USN devices have also been developed (see Section 5.1.2.1), and their high cost.

Thermal, *or thermospray*, *nebulisers* also improve sensitivity.[14] With these nebulisers, the sample goes through a narrow, heated capillary. A fraction of the solvent evaporates and the aerosol is generated as the vapour expands at the exit of the capillary. The thermospray device provides similar analytical figures of merit as the ultrasonic nebuliser and it also requires a system for solvent removal.[15] Furthermore, the capillary is easily blocked, so the tolerance of this nebuliser design to dissolved solids is limited.

The hydraulic high pressure nebuliser (HHPN)[3] utilizes the kinetic energy of a high velocity liquid stream emerging through a nozzle with a 5–30 μm id bore for aerosol generation. The aerosol is formed as the liquid vein impacts against a glass bead. The detection limits reached with the HHPN are about one order of magnitude lower than those reported for pneumatic nebulisers, but it also requires the use of a desolvation system. With the HHPN, the solution must be free from any solid particles and a filter is always placed before the nozzle.

5.1.1.2 Alternative spray chambers

As regards spray chambers, simplified designs imposing a rather simple aerosol path towards the plasma are able to achieve higher sensitivities and shorter wash-out times than the double pass type. Figure 5.4 shows several spray chambers used in ICP-MS.

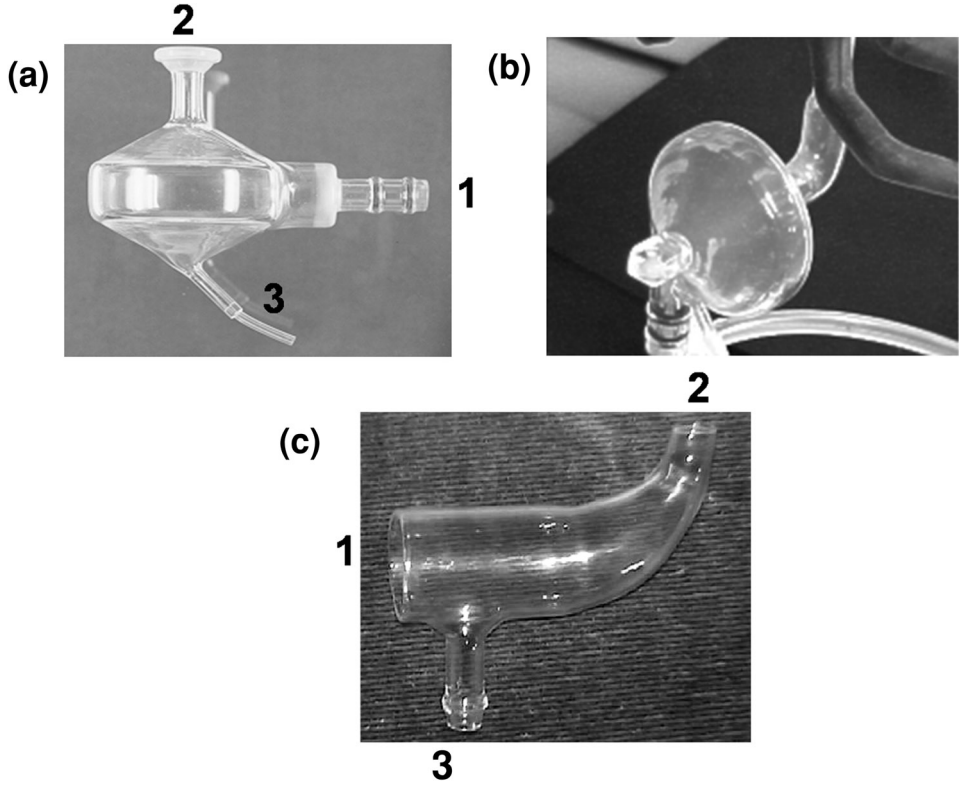

Figure 5.4 Pictures of different spray chambers used in ICP-MS. (a) cyclonic; (b) vertical cyclonic; (c) single pass spray chamber. 1, nebuliser; 2 tertiary aerosol exit; 3, drain.

(a) Cyclonic spray chambers

Cyclonic chambers (Figure 5.4) exhibit better analytical performance than double pass spray chambers. The nebuliser is tangentially connected to the spray chamber body. In the early

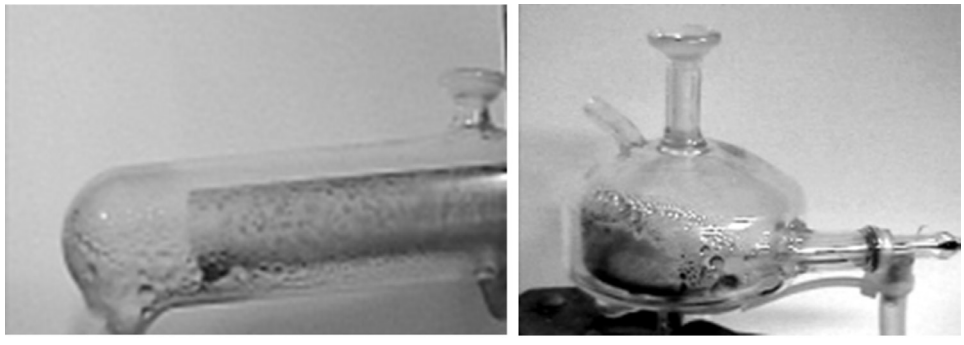

(a) (b)

Figure 5.5 Pictures of two spray chambers operated with a solution containing methylene blue. (a) Double pass spray chamber and (b) cyclonic spray chamber.

studies, it was thought that the aerosol followed a double spiral concentric path. However, in recent studies based on computer simulation it has been concluded that the chamber behaves primarily as an impactor, rather than as a cyclone of the type used in technical areas.[16] Figure 5.5 shows the pictures corresponding to the evaluation of the behaviour of a cyclonic and a double pass spray chamber.[17] The dark zones correspond to the areas of drop impacts. It can be seen that in the case of the double pass spray chamber, droplets are mainly lost as they impact against the inner walls of the central tube and the front wall of the external tube. Meanwhile, the wall in front of the nebuliser is indeed responsible for the removal of droplets in the case of the cyclonic spray chamber. Since cyclonic spray chambers have rapid wash-out characteristics, they have been found to be particularly beneficial for coupling liquid chromatography[18] and capillary electrophoresis[19] (CE) with ICP-MS.

(b) Single pass barrel-type spray chambers

These chambers are used when the primary aerosols are sufficiently fine (i.e. have droplet sizes <10 μm) and do not need further filtering. The aerosol leaving single pass spray chambers is coarser than the tertiary aerosols generated when using double pass spray chambers. In addition, the former device affords higher ICP-MS sensitivities than the latter one.[20] When using conventional pneumatic nebulisers, single pass spray chambers can be equipped with an impact bead or baffles[21] inside them. With this impact surface a fraction of the primary aerosols' coarsest droplets are removed as they adhere to the surface, whereas some droplets are dispersed into smaller ones as they impact against the bead.

The main advantage of single pass spray chambers is that they are easily rinsed and therefore the wash-out time is significantly shortened. This characteristic makes the single pass spray chamber design very interesting for HPLC–ICP-MS coupling.

5.1.2 Low sample consumption systems

Due to the high sensitivity offered by ICP-MS, there has been an increasing interest in using this technique for applications in which the available sample volume is very low.[22]

The reasons for this interest can be summarized as follows: (i) in some fields, (e.g forensic, biological and clinical analysis), the sample size is a limiting factor; (ii) the development of new coupling techniques such as CE-ICP-MS[23] requires working at very low sample delivery rates; (iii) the presence of organic solvents and complex inorganic matrices in some sample types gives rise to serious spectral as well as non-spectral interferences and (iv) the management of waste (particularly radioactive waste) is less complicated when using apparatus that consumes very low sample volumes. The effort made in this field has resulted in the development of micronebulisers able to generate stable and fine aerosols at liquid flow rates as low as 1 μL/min.

5.1.2.1 Micronebulisers

Many of the pneumatic micronebulisers have their precursors in conventional ones. Although conventional pneumatic concentric nebulisers are able to work at low liquid flow rates, the aerosol generation process is unstable and coarse droplets are formed. In addition, the nebuliser dead volume is too high and memory effects are severe. *Pneumatic concentric micronebulisers*[24] are popular under these conditions. Three different designs are commercially available: (i) the high efficiency nebuliser (HEN); (ii) the MicroMist (MM) and (iii) the microconcentric nebuliser (MCN). The former two are made of glass, although plastic (PFA) pneumatic concentric micronebulisers are also available.[25] The main modifications made to these nebulisers (Figure 5.2(d)) compared to conventional concentric devices are a reduction in the capillary dimensions (i.e. inner diameter and wall thickness) or the gas annulus area. As a result, the liquid and gas interaction takes place more efficiently than with conventional nebulisers and finer primary aerosols are generated. In the case of the HEN, the gas exit cross sectional area is much smaller than for the other nebulisers and therefore it is necessary to apply a higher pressure to the gas line. This leads to higher kinetic energy being available for aerosol generation, which in turn leads to finer primary aerosols being produced than for MCN or MM nebulisers.[26] All three of these nebulisers have been successfully used for the analysis of liquid samples by ICP-MS as well as effectively employed in HPLC-ICP-MS[27] and CE–ICP-MS interfaces.[28,29]

A *pneumatic cross-flow micronebuliser* has been described for use in ICP-MS.[30] The high efficiency cross-flow micronebuliser (HECFMN) has a narrow capillary placed inside the conventional sample capillary. The inner diameter of the nebuliser gas nozzle is reduced with respect to the conventional cross-flow design. Due to the characteristics of this device, the free liquid uptake rate (i.e. about 9 μL/min) is lower than that found for either a conventional cross-flow nebuliser (i.e. 1900 μL/min) or concentric pneumatic micronebulisers (i.e. from about 30 to 100 μL/min). This fact makes the HECFMN attractive for CE ICP-MS interfaces.[31]

The *sonic spray nebuliser* (SSN) is a pneumatic nebuliser, which consists of a chamber with a 250 μm inner diameter orifice (Figure 5.6(a)). The end of a 150 μm outer diameter, 50 μm inner diameter silica capillary is placed in the middle of this orifice. Compared with a conventional pneumatic concentric nebuliser, the SSN gives rise to lower limits of detection by working at liquid flow rates of the order of seven times lower.[32] In the *multimicrospray nebuliser* (MMSN), the sample solution is divided into three streams (Figure 5.6(b)).[33] Each one of these streams emerges through three nozzles, giving three separate concentric nebulisers with a single source of liquid solution and nebuliser gas. In this way, the gas energy is more efficiently employed in the aerosol generation. This is probably the main reason why the analyte transport efficiencies and

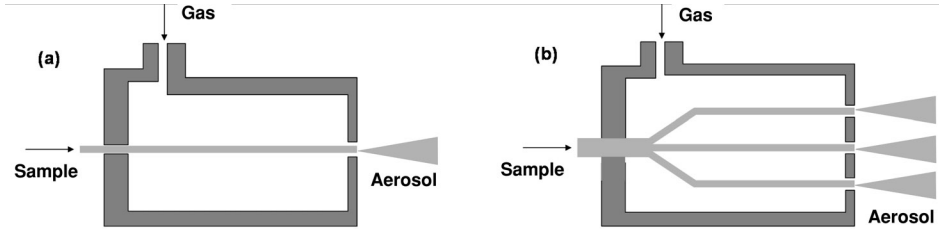

Figure 5.6 Schematic drawing of the SSN (a), adapted from reference 32, and the multi-microspray nebuliser, MMSN, adapted from reference 33.

sensitivities reached by the MMSN are higher than those provided by a conventional pneumatic concentric nebuliser or a SSN.

Direct injection nebulisers. The so-called direct injection nebuliser (DIN), or total sample consumption nebuliser, has been used as a system for sample introduction in ICP-MS for more than 10 years.[34] The DIN generates the aerosol at the plasma base, so a spray chamber is not required. As a result, analyte transport efficiency is virtually 100%, which provides the advantage of improved sensitivity with respect to conventional nebuliser – spray chamber combinations. However, there are several problems that must be overcome because the DIN is extremely fragile, expensive and is rather complicated to use. The concentric capillary is easily blocked so solutions should be filtered prior to their introduction into the DIN. In addition, the solvent loading of the plasma is higher with the DIN than with conventional systems, so oxide generation and other related matrix effects are more significant with this device. The DIN is a very good choice for the analysis of very low liquid sample volumes and for elements that give severe memory effects in conventional nebuliser–spray chamber configurations (such as Hg) because it drastically reduces the wash-out time, which explains its use in CE–ICP-MS interfaces.[35,36]

More recently, Montaser and co-workers have developed a new low cost DIN called the direct injection high efficiency nebuliser (DIHEN).[37] The DIHEN is entirely made of glass and is similar in construction to a HEN, but it is longer. The main advantages provided by the DIHEN with respect to other conventional liquid sample introduction systems for ICP-MS are higher sensitivities, better signal stability and lower limits of detection. The dead volume of the DIHEN can be made lower than 10 nL, which significantly reduces the wash-out times for elements such as iodine, mercury and boron.[38] As a result, this nebuliser has also proven to be suitable as an interface between separation techniques and ICP-MS.[39,40] Note that in these later studies, with a modified low dead volume DIHEN, the liquid flow rate can be lowered down to 0.5 μL/min.

As regards the drawbacks of the DIHEN, it is important to indicate that, depending on the nebulisation conditions, droplets with diameters higher than 10–20 μm can be introduced into the plasma.[41] Moreover, the ICP-MS interferences caused by inorganic acids are similar to or even more severe than those for a MCN coupled to a spray chamber.[42] Besides this, despite the large analyte transport rate enhancement compared to a conventional system (i.e. 5–10), the ICP-MS ion signals are improved by only a factor of about 2.[43] The reason for these findings is likely to be due to changes in the spatial analyte distribution.[42] Due to the somewhat coarse aerosols and the high solvent plasma load, the RF power must be increased up to about 1.5 kW to obtain optimum analytical performance.[37]

Finally, another disadvantage of the DIHEN is that it is prone to tip blocking because of the narrow capillary used. In order to overcome this drawback, a new version of the DIHEN has

been developed called the large bore direct injection nebuliser (LB-DIHEN).[38,44] In this new design, the sample capillary has been enlarged. Unfortunately, the precision reached with the LB-DIHEN is worse than that achieved with a conventional system.[44]

The *oscillating capillary nebuliser* (OCN)[45] is composed of two concentric silica capillaries. Samples pass along the central capillary whereas the nebuliser gas flows through the area between the two capillaries. Because the OCN sample capillary is longer than the nebuliser body, the gas stream induces capillary oscillations. A longitudinal standing wave appears along this capillary that is thought to be responsible for the fine aerosol generation. By comparison with micronebulisers, it was initially found that the OCN gave higher ICP-MS limits of detection than a HEN when both systems were used for HPLC-ICP-MS analysis.[46] However, recent modifications in the OCN liquid capillary dimensions have enhanced the performance of this nebuliser for ICP-MS.[20]

The results provided by other low sample consumption nebulisers such as the glass frit nebuliser, microultrasonic nebuliser (μUSN), the monodisperse dried microparticulate injector and the electrospray nebuliser for sample introduction in ICP spectrometry are described elsewhere.[3]

5.1.2.2 Low inner volume spray chambers

When an aerosol is generated at liquid flow rates of the order of several microlitres to tens of microlitres per minute, the relative significance of the aerosol transport phenomena is different with respect to that at liquid flow rates in the mL/min range. Solvent evaporation becomes much more pronounced and droplet coalescence is much less significant under the former nebulisation conditions. Both effects combine to increase the analyte transport efficiency.

A negative effect found when working at low liquid flow rates is an increase in wash-out times, leading to a subsequent drop in sample throughput. In order to mitigate this problem, new low inner volume spray chambers have been developed and their performance has been tested in ICP-MS. For a mini cyclonic spray chamber, called the *Cinnabar*, wash-out times were found to be significantly shortened with respect to a double pass spray chamber for the analysis of iodine species.[47] Due to its simplicity and the small dispersion provided by this spray chamber, it has also been successfully applied as part of a CE-ICP-MS interface.[48] Low inner volume *single pass spray chambers* have also been used in various ways as aerosol transport devices for ICP-MS, namely with the nebuliser directly connected to them,[46] with an impact surface (i.e. bead) inside them and as part of a CE-ICP-MS interface.[49]

5.1.3 Desolvation systems

In ICP-MS, the desolvation of an aerosol can be beneficial in several cases: (i) when using efficient nebulisers such as ultrasonic nebulisers or thermospray devices, (ii) when analysing samples containing organic solvents, (iii) when an increase in the sensitivity is required and (iv) when trying to remove polyatomic interferences.

The most simple desolvation system that can be used is a thermostated spray chamber. With this device the extent of the aerosol solvent evaporation is reduced by working at low temperatures. As a result, the plasma vapour solvent load decreases. A drawback of the thermostated chambers is that the analyte transport efficiency decreases, which can lead to a reduction in the sensitivity. Two-step desolvation systems can also be used to improve the sensitivity and remove

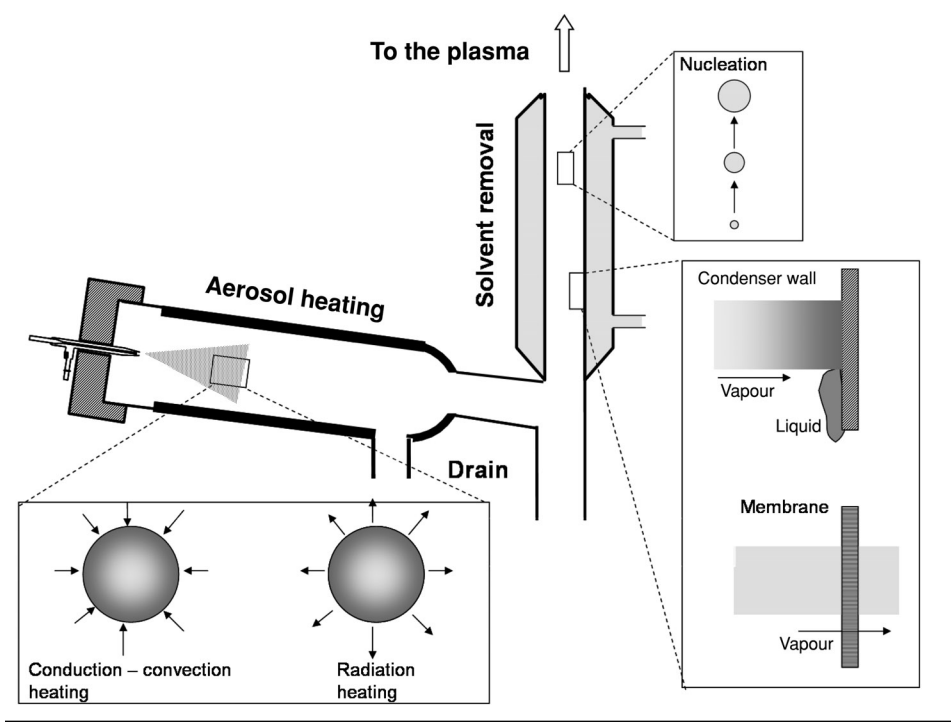

Figure 5.7 Two-step desolvation system.

interferences. Figure 5.7 shows a schematic of a basic desolvation system used for ICP-MS. In this case, the aerosol is first heated and then the vapour generated is removed from the stream.

The aerosol heating promotes solvent evaporation and analyte transport efficiency at the end of this step can be made close to 100%. The aerosol heating can be performed either by conductive–convective means or by a radiative mechanism. In the conduction–convection systems, a single pass spray chamber is heated by means of a tape wound around it. In this way, droplets are heated as a result of the energy transfer from the chamber walls (Figure 5.7). The use of these systems can result in a deterioration of signal stability because of the sudden evaporation of the droplets as they impact against the hot inner walls of the chamber. In radiative based heating systems, the aerosol is heated by direct absorption of radiation.

As regards solvent vapour removal, two main devices have been proposed in the literature (Figure 5.7): (i) a condenser and (ii) a membrane. In the first case, the hot aerosol is passed into a low temperature region and a fraction of the vapour generated in the previous step is removed, as it condenses on the cold walls and is drained away. This way of eliminating vapour solvent has one main drawback, namely, solvent nucleation. This phenomenon consists of droplet growth, produced as a fraction of the solvent vapour condenses on the aerosol particles instead of on the condenser walls. Nucleation causes the total solvent plasma load to increase again, thus decreasing the efficiency of the desolvation system. In order to avoid this process, a heated porous membrane can be used after the aerosol heating system. These membranes typically have 70% porosity with a maximum pore size of about 3 μm. As the working temperature of the membrane

is relatively high (typically around 160 °C), solvent nucleation is almost negligible. A problem found when using a PTFE membrane is the loss of a fraction of volatile analytes (e.g. Hg, B).[50]

A desolvation system equipped with a membrane has been used for the analysis of very low liquid sample volumes. In the so-called high efficiency sample introduction system (HESIS),[51,52] a HEN is operated at a gas flow rate of about 0.3 L/min and coupled to a heated single pass spray chamber. A 0.7 L/min argon stream is introduced longitudinally to the spray chamber. Since this gas is heated as it enters the spray chamber, aerosol solvent evaporation is enhanced and analyte transport efficiencies close to 100% are obtained. Following this step, a membrane dryer is used. With the HESIS the ICP-MS signals are enhanced 20 times with respect to those achieved by a conventional sample introduction system. The use of a micronebuliser coupled to a membrane based desolvation system reduces the wash-in and wash-out times with respect to those found for a conventional system.[53] With a double membrane desolvation system, a decrease in solvent-derived interferences has been found when analysing organic samples using ICP-MS.[54]

Concluding this section, it has been shown that analytical problems with the conventional sample introduction systems have promoted the development of new systems and techniques in order to solve or mitigate these problems. The drawback of low sensitivity for some applications can be overcome by using specially developed nebulisers, spray chambers and desolvation systems. Some devices are also able to handle high salt content solutions without tip blocking. The work with low sample consumption nebulisers and low inner volume spray chambers has facilitated efficient analysis of samples for which volumes of only 1 mL or less are available. Finally, by using a desolvation system, the plasma solvent load is significantly reduced with respect to a conventional sample introduction apparatus, leading to reduced solvent interferences and enhanced sensitivity. However, when switching from the conventional nebuliser–spray chamber combination to another special device in order to solve a given problem, additional drawbacks can be found. For example, the benefit of reduced interferences offered by desolvation systems is countered by an increase in wash-out times, as well as the system becoming more expensive and more difficult to use. Another example is the DIN. These devices provide higher sensitivities and shorter wash-out times than conventional systems, but interferences can be even more pronounced and the DIN can be seriously damaged if attention is not paid to its tip position with respect to the plasma. It is therefore the task of the analyst to evaluate the best sample introduction system for a particular application.

References

1. Bings, N. H., Boegaerts, A., and Broekaert, J. A. C. (2002) Atomic spectroscopy. *Anal. Chem.*, **74**, 2691–712.
2. Sneddon, J. (1990) *Sample Introduction in Atomic Spectroscopy*, Elsevier, New York.
3. Montaser, A. (ed.) (1998) *Inductively Coupled Plasma Mass Spectrometry*, Wiley-VCH, New York.
4. Hill, S. J. (ed.) (1999) *Inductively Coupled Plasma Spectrometry and its Applications*, Shefield Academic Press, Shefield.
5. Ketterer, M. E. and Hudson, D. D. (2000) Preliminary characterization of a laboratory-constructed, easily disassembled concentric pneumatic nebulizer for inductively coupled plasma mass spectrometry. *J. Anal. At. Spectrom.*, **15**, 1547–77.
6. Sharp, B. L. (1998) Pneumatic nebulisers and spray chambers for inductively coupled plasma spectrometry. A review. Part 2: Spray chambers. *J. Anal. At. Spectrom.* **3**, 939–63.

7. Cano, J. M., Todolí, J. L., Hernandis, V., and Mora, J. (2002) The role of the nebulizer on the sodium interferent effects in inductively coupled plasma atomic emission spectrometry. *J. Anal. At. Spectrom*, **17**, 57–63.
8. Burgener, J. A. (1995) Parallel path induction pneumatic nebuliser. U.S. Patent # 5,411,208.
9. Feng, Y. L., Lam, J. W., and Sturgeon, R. E. (2001) Expanding the scope of chemical vapor generation for noble and transition metals. *Analyst*, **126**, 1833–7.
10. Feng, Y. L., Sturgeon, R. E., and Lam, J. W. (2003) Generation of atomic and molecular cadmium species from aqueous media. *Anal. Chem.*, **75**, 635–40.
11. Gammelgaard, B. and Jons, O. (2000) Comparison of an ultrasonic nebulizer with a cross-flow nebulizer for selenium speciation by ion-chromatography and inductively coupled plasma mass spectrometry. *J. Anal. At. Spectrom.*, **15**, 499–505.
12. Duyck, C., Miekeley, N., Porto da Silveira, C. L., and Szatmari, P. (2002) Trace element determination in crude oil and its factions by inductively coupled plasma mass spectrometry using ultrasonic nebulization of toluene solutions. *Spectrochim. Acta* B, **57**, 1979–90.
13. Mesquita da Silva, M. A., Frescura, V. L. A., and Curtius, A. J. (2000) Determination of trace elements in water samples by ultrasonic nebulization inductively coupled plasma mass spectrometry after cloud point extraction. *Spectrochim. Acta* B, **55**, 803–13.
14. Zhang, X., Chen, D., Marquart, R., and Koropchak, J. A. (2000) Thermospray sample introduction to atomic spectrometry. *Microchem. J.*, **66**, 17–53.
15. Vanhoe, H., Saverwijns, S., Parent, M., Moens, L., and Dams, R. (1995) Analytical characteristics of an inductively coupled plasma mass spectrometer coupled with a thermospray nebulization system. *J. Anal. At. Spectrom.*, **10**, 575–81.
16. Schaldach, G., Berger, L., Raylov, I., and Berndt, H. (2002) Characterization of a cyclone spray chamber for ICP spectrometry by computer simulation. *J. Anal. At. Spectrom.*, **17**, 334–44.
17. Maestre, S. E. (2002) Influence of the spray chamber on the matrix effect caused by inorganic species in ICP-AES. *Ph.D.*, Alicante.
18. Svantesson, E., Capala, J., Markides, K. E., and Pettersson, J. (2002) Determination of boron-containing compounds in unrine and blood plasma from boron neutron capture therapy patients. The importance of using coupled techniques. *Anal. Chem.*, **74**, 5358–63.
19. Taylor, K. A., Sharp, B. L., Lewis, D. J., and Crews, H. M. (1998) Design and characterisation of a microconcentric nebuliser interface for capillary electrophoresis – inductively coupled plasma mass spectrometry. *J. Anal. At. Spectrom.*, **13**, 1095–100.
20. Hoang, T. T., May, S. W., and Browner, R. F. (2002) Developments with the oscillating capillary nebulizer – effects of spray chamber design, droplet size and turbulence on analytical signals and analyte transport efficiency of selected biochemically important organoselenium compounds. *J. Anal. At. Spectrom.*, **17**, 1575–81.
21. Koropchak, J. A., Sadain, S., and Szostek, B. (1996) Dispersion of discrete signals within aerosol spray chambers: preliminary investigations. *Spectrochim. Acta* B, **51**, 1733–45.
22. Beauchemin, D. (2002) Inductively coupled plasma mass spectrometry. *Anal. Chem.*, **74**, 2873–94.
23. Kannamkumarath, S. S., Wrobel, K., Wrobel, K., B'Hymer, C., and Caruso, J. A. (2002) Capillary electrophoresis-inductively coupled plasma – mass spectrometry: an attractive complementary technique for elemental speciation analysis. *J. Chromatogr.* A, **975**, 245–66.
24. McLean, J. A., Minnich, M. G., Iacone, L. A., Liu, H., and Montaser, A. (1998) Nebulizer diagnostics: fundamental parameters, challenges, and techniques on the horizon. *J. Anal. At. Spectrom.*, **13**, 829–42.
25. Wind, M., Wesch, H., and Lehman, W. D. (2001) Protein phosphorylation degree: determination by capillary liquid chromatography and inductively coupled plasma mass spectrometry. *Anal. Chem.*, **73**, 3006–10.

26. Todolí, J. L., Hernandis, V., Canals, A., and Mermet, J. M. (1999) Comparison of characteristics and limits of detection of pneumatic micro-nebulizers and a conventional nebulizer operating at low uptake rates in ICP-AES. *J. Anal. At. Spectrom.*, **14**, 1289–95.
27. Woller, A., Garraud, H., Boisson, J., Dorthe, A. M., Fodor, P., and Donard, O. F. X. (1998) Simultaneous speciation of redox species of arsenic and selenium using an anion-exchange microbore column coupled with a microconcentric nebulizer and an inductively coupled plasma mass spectrometer as detector. *J. Anal. At. Spectrom.*, **13**, 141–9.
28. Tangen A. and Lund, W. (2000) Capillary electrophoresis-inductively coupled plasma mass spectrometry interface with minimised dead volume for high separation efficiency. *J. Chromatogr.* A, **891**, 129–38.
29. Casiot, C., Donard, O. F. X., and Potin-Gautier, M. (2002) Optimization of the hyphenation between capillary zone electrophoresis and inductively coupled plasma mass spectrometry for the measurement of As-, Sb-, Se- and Te-species, applicable to soil extracts. *Spectrochim. Acta* B, **57**, 173–87.
30. Li, J., Umemura, T., Odake, T., and Tsunoda, K. (2001) A high-efficiency cross-flow nebulizer for inductively coupled mass spectrometry. *Anal. Chem.*, **73**, 1416–24.
31. Li, J., Umemura, T., Odake, T., and Tsunoda, K. (2001) A high-efficiency cross-flow micronebulizer interface for capillary electrophoresis and inductively coupled plasma mass spectrometry. *Anal. Chem.*, **73**, 5992–9.
32. Huang, M., Shirasaki, A., Hirabayashi, T., and Koizuma, H. (1999) Microliter sample introduction technique for microwave-induced plasma mass spectrometry. *Anal. Chem.,* **71**, 427–32.
33. Huang, M., Hirabayashi, A., Shirasaki, T., and Koizumi, H. (2000) A multimicrospray nebulizer for microwave-induced mass spectrometry. *Anal. Chem.*, **72**, 2463–7.
34. Wiederin, D. R., Smith, F. G., and Houk, R. S. (1991) Direct injection nebulization for inductively coupled plasma mass spectrometry. *Anal. Chem.*, **63**, 219–25.
35. Polec, K., Szpunar, J., Palacios, O., González-Duarte, P., Atrian, S., and Lobinski, R. (2001) Investigation of metal binding by recombinant and native metallothioneins by capillary zone electrophoresis (CZE) coupled with inductively coupled plasma mass spectrometry (ICP-MS) via a self-aspirating total consumption micronebulizer. *J. Anal. At. Spectrom.*, **16**, 567–74.
36. Mounicou, S., McSheehy, S., Szpunar, J., Potin-Gautier, M., and Lobinski, R. (2002) Analysis of selenized yeast for selenium speciation by size-exclusion chromatography and capillary zone electrophoresis with inductively coupled plasma mass spectrometric detection (SEC-CZE-ICP-MS). *J. Anal. At. Spectrom.*, **17**, 15–20.
37. McLean, J. A., Zhang, H., and Montaser, A. (1998) A direct injection high efficiency nebulizer for inductively coupled plasma mass spectrometry. *Anal. Chem*., **70**, 1012–20.
38. O'-Brien, S. E., McLean, J. A., Acon, B. W., Eshelman, B. J., Bauer, W. F., and Montaser, A. (2002) Determination of memory-prone elements using direct injection high efficiency nebulizer inductively coupled plasma mass spectrometry. *Appl. Spectrosc.*, **56**, 1006–12.
39. Majidi, V., Qvarnstrom, J., Tu, Q., Frech, W., and Thomassen, Y. (1999) Improving sensitivity for CE-ICP-MS using multicapillary parallel separation. *J. Anal. At. Spectrom.*, **14**, 1933–6.
40. Wind, M., Eisenmenger, A., and Lehmann, W. D. (2002) Modified direct injection high efficiency nebulizer with minimized dead volume for the analysis of biological samples by micro- and nano-LC-ICP-MS. *J. Anal. At. Spectrom.*, **17**, 21–6.
41. Todolí, J. L. and Mermet, J. M. (2001) Evaluation of a direct injection high-efficiency nebulizer (DIHEN) by comparison with a high-efficiency nebulizer (HEN) coupled to a cyclonic spray chamber as a liquid sample introduction system for ICP-AES. *J. Anal. At. Spectrom.*, **16**, 514–20.
42. Björn, E. and Frech, W. (2001) Non-spectral interference effects in inductively coupled plasma mass spectrometry using direct injection high efficiency and microconcentric nebulization. *J. Anal. At. Spectrom.*, **16**, 4–11.

43. Westphal, C. S., McLean, J. A., Acon, B. W., Allen, L. A., and Montaser, A. (2002) Axial inductively coupled plasma time-of-flight mass spectrometry using direct liquid sample introduction. *J. Anal. At. Spectom.*, **17**, 669–75.
44. Acon, B. W., McLean, J. A., and Montaser, A. (2000) A large bore-direct injection high efficiency nebulizer for inductively coupled plasma spectrometry. *Anal. Chem.*, **72**, 1885–93.
45. Wang, L., May, S. W., Browner, R. F., and Pollock, S. H. (1996) Low-flow interface for liquid chromatography – inductively coupled plasma mass spectrometry speciation using oscillating capillary nebulizer. *J. Anal. At. Spectrom.*, **11**, 1137–46.
46. B'Hymer, C., Sutton, K. L., and Caruso, J. A. (1998) Comparison of four nebulizer-spray chamber interfaces for the high-performance liquid chromatographic separation of arsenic compounds using inductively coupled plasma mass spectrometric detection. *J. Anal. At. Spectrom.*, **13**, 855–8.
47. Haldiman, M., Eastgate, A., and Zimmerli, B. (2000) Improved measurement of iodine in food samples using inductively coupled plasma isotope dilution mass spectrometry. *Analyst*, **125**, 1977–82.
48. Day, J. A., Caruso, J. A., Becker, J. S., and Dietze, H. J. (2000) Application of capillary electrophoresis interfaced to double focusing sector field ICP-MS for nuclide abundance determination of lanthanides produced via spallation reactions in an irradiated tantalum target. *J. Anal. At. Spectrom.*, **15**, 1343–8.
49. Wang, Z. and Prange, A. (2002) Use of surface-modified capillaries in the separation and characterization of metallothionein isoforms by capillary electrophoresis inductively coupled plasma mass spectrometry. *Anal. Chem.*, **74**, 626–31.
50. Gray, D. J., LeBlanc, C., Chan, W., and Denis, B. (2001) USN-ICP-MS: a poor man's high resolution. In: *Plasma Source Mass Spectrometry* (eds G. Holland and S. D. Tanner), Royal Society of Chemistry, Cambrigde, pp. 3–16.
51. Debrah, E. and Légère, G. (1999) Design and performance of a novel high efficiency sample introduction system for plasma source spectrometry. In: *Plasma Source Mass Spectrometry* (eds J. G. Holland and S. D. Tanner), Royal Society of Chemistry, Cambrigde, pp. 20–6.
52. Olesik, J. W., Hensman, C., Rabb, S., and Rago, D. (2001) Sample introduction, plasma – sample interactions, ion transport and ion–molecule reactions: fundamental understanding and practical improvements in ICP-MS. In: *Plasma Source Mass Spectrometry* (eds G. Holland and S.D. Tanner), Royal Society of Chemistry, Cambrigde, pp. 3–16.
53. Ma, R., Bellis, D., and McLeod, C. W. (2000) Isotopic analysis of uranium in tree bark by ICP mass spectrometry: a strategy for assessment of airborne contamination. *Anal. Chem.*, **72**, 4878–81.
54. Sung, Y. and Lim, H. B. (2000) Double membrana desolvator for direct anályis of isopropyl alcohol in inductively coupled plasma atomic emission spectrometry (ICP-AES) and inductively coupled plasma mass spectrometry (ICP-MS). *Microchem. J.*, **64**, 51–7.

5.2 FLOW INJECTION SAMPLE INTRODUCTION FOR ICP-MS

José L Todoli

5.2.1 Introduction

In the past 5 years, great interest has been paid to the application and development of flow injection (FI) techniques using ICP-MS as the detection system. The majority of the studies devoted to this subject (i.e. about 70% of the published articles) have appeared since 1999

(source: SciFinder Scholar 2002, ACS). This growing interest is undoubtedly due to the unique characteristics and advantages offered by the combination of the extremely sensitive ICP-MS technique with the FI analytical concept.

Some of the well known advantages of FI over continuous systems are:[1,2] (i) the sample and/or reagent consumed volumes are reduced by several orders of magnitude; (ii) automation is easier; (iii) the precision of the method is better; (iv) the sample throughput is higher; (v) matrix effects can be eliminated, although some studies have indicated that the interferences caused by nitric acid can be more severe in FI than in continuous mode[3] and (vi) the sensitivity and limits of detection are in some cases better. FI-based methods are also interesting for the analysis of hazardous samples and the minimization of waste.

When a sample is injected into a carrier stream, a concentration gradient between the sample and the carrier is established. Therefore, it is possible to study the effect of the matrix concentration on the ion signal intensity from a single sample injection.[3] If high salt content solutions are continuously introduced into the spectrometer, a progressive loss in sensitivity is observed as a consequence of salt deposition on the sampler and skimmer cones. One of the most accepted and studied solutions to this inconvenience is on-line matrix removal. Organic solvents also cause deterioration of the ICP-MS operation, as carbon becomes deposited in the torch injector, on the interface cones and to some degree on the ion lenses. These effects can be circumvented by injecting small sample volumes into the plasma[4,5] or by on-line generation of emulsions.[6] Finally, it is also worth noting that FI facilitates reproducible sample introduction in capillary electrophoresis – ICP-MS.[7] The present section describes some of the latest progress and applications of FI (in) ICP-MS.

5.2.2 Data acquisition of transient signals in ICP-MS

In FI techniques a transient signal, typically only a few seconds in width, is obtained. A fast readout system must therefore be used. The ICP-TOF (time of flight) MS (see Chapter 2, section 2.3) is able to produce more than 20 000 full mass spectra per second, which makes it suitable for the recording of fast transient signals. Furthermore, it can be considered as nearly simultaneous because the detected ions are simultaneously extracted from the plasma.[8] The characteristics of ICP-TOF-MS make it possible to monitor more than 100 isotopes in a single transient signal without any loss in sensitivity.[9] In contrast, although quadrupole ICP-MS instruments, which acquire signals sequentially, give rise to better limits of detection, there are several difficulties encountered when monitoring transient signals for different isotopes with these systems. The sequential nature of quadrupoles means that only one m/z ratio can be monitored at a time (albeit relatively quickly; a minimum quadrupole settle time of around 0.2 ms between isotopes is achievable). Another key point to be considered is the transient signal distortion (or peak skew) that results from the measurement of different isotopes at different times within the transient signal. As a result, errors in the determined analyte concentration may arise as a function of where in the transient signal the data for the analyte were collected.

No single general criterion about the number of points required across the complete transient signal peak for obtaining good precision on transient signals exists, although for quadrupole ICP-MS this variable restricts the maximum number of isotopes that can be satisfactorily measured.[10] Transient signal peak shape differences between standards and samples, for example when interferences are present, can affect the precision of the calibration procedure.[11] As a consequence,

when working with peaks of differing shapes, the peak should be monitored accurately and in order to obtain a precision within the 0.2–0.4% range, at least 10 points across the peak signal are required. In contrast, when obtaining peaks having identical shapes, the number of points required falls to 3,[10] and, therefore, the number of isotopes that can be determined with quadrupole ICP-MS is high (up to 71). As a conclusion, in order to select the optimum number of points per peak, several factors, such as the injected sample volume, the dwell time (i.e. the time devoted to counting ions per channel), the peak shape and the number of isotopes to be measured, must be controlled.

Interestingly, in some instances it is better to monitor a part of the transient signal rather than the total signal. For example, it has been reported[9] that when an ICP-TOFMS is used for isotope dilution (ID) procedures, with its detector operated in the analog mode, more precise results are obtained when calculating the ratio from at least five points at the peak apex than if the whole peak is considered.

Additional factors to take into consideration such as the blank characteristics, working with either peak height or area and the working mode of the spectrometer are discussed in reference 2 of this section.

5.2.3 Flow injection modes

Since the first FI publication in 1975, huge progress in the instrumentation and application of this analytical concept has been made.[13] FI has evolved through four principle steps:[13] (i) FI; (ii) sequential injection (SI); (iii) bead injection (BI); and (iv) laboratory-on-valve (LOV).

Flow injection. With this technique, a carrier stream is pumped into the detector, usually via a peristaltic pump. A discrete volume of sample, of the order of 0.1–1 mL, is then injected into this stream manually or automatically using a valve. The carrier stream can simply contain a transporting solution, such as dilute nitric acid, or it can be composed of chemical reagents for on-line reaction with the injected sample (Figure 5.8(a)). A zone in which a concentration gradient is established is carried toward the detector, leading to the generation of a transient signal or peak.

Normally in FI methods, the sample consumption is very low, but they present several drawbacks: (i) due to its mode of operation the amount of reagent required for the analysis is often excessive. (ii) In addition, the liquid flow rate supplied by peristaltic pumps can alter over time as the pump tubing ages, a problem that becomes more significant at very low liquid flow rates; (iii) procedures such as extraction and back-extraction using organic solvents can be achieved using FI, but these procedures pose several manipulation problems derived from the fact that organic solvents and complex systems are used[14]; and, more importantly (iv) a different manifold is required for each analytical method.

Sequential injection. These methods overcome some of the FI drawbacks. In SI,[15] the sample and reagents are sequentially transported by means of a syringe pump (that, unlike peristaltic pumps, has zero inertia and elasticity) and a multiposition valve (able to connect solutions from different reservoirs) and they are loaded into a coil (Figure 5.8(b)). First, the pump delivers controlled volumes of different solutions. The different segments are partially mixed and reaction takes place during transportation toward the detector. Alternatively, the pump can be stopped to improve sample–reagent mixing and reaction, if required. Despite their limitations (i.e. poor long term stability), peristaltic pumps can be used in SI in order to increase analysis throughput, because there is no need to aspirate a wash solution.

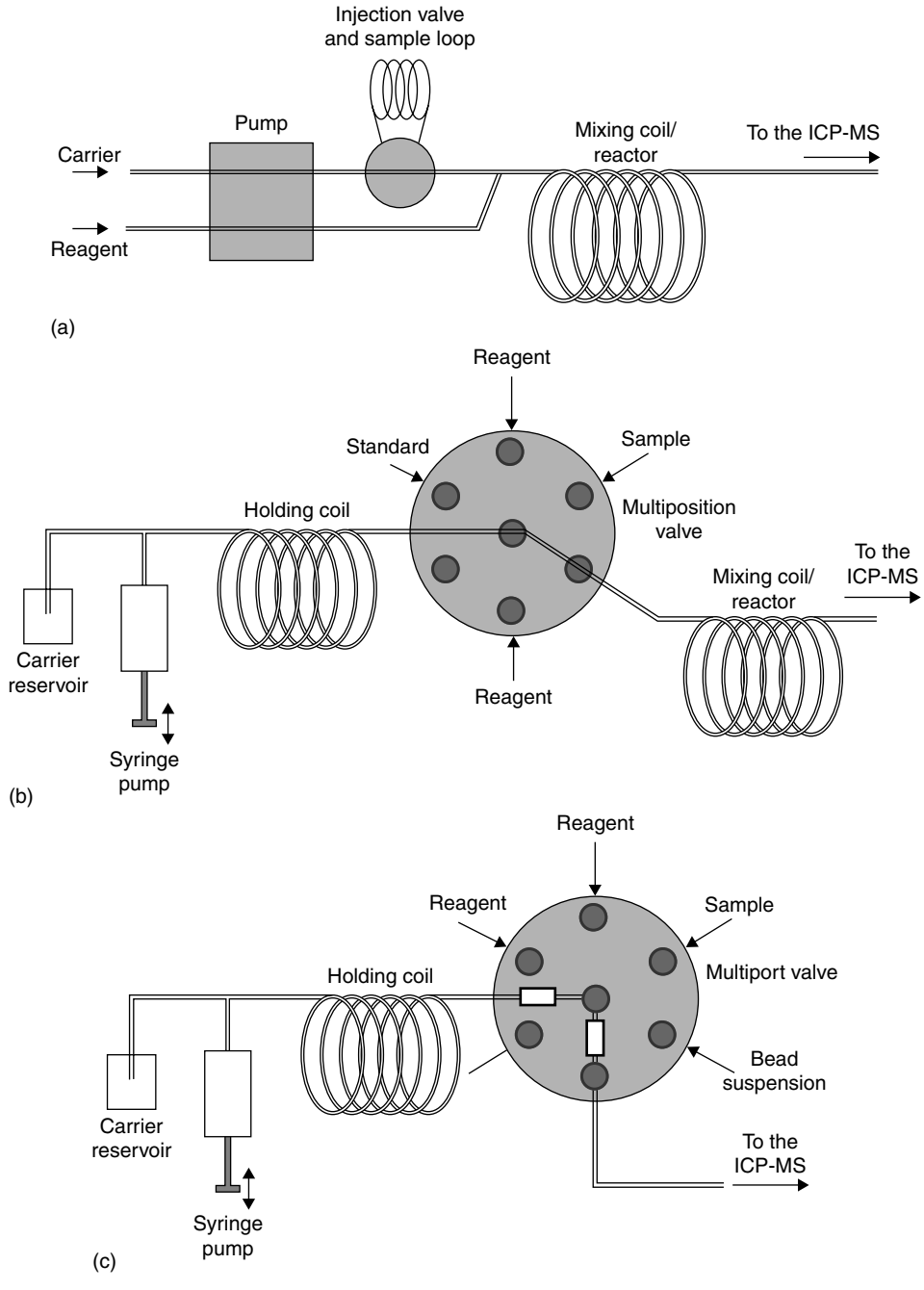

Figure 5.8 Scheme of FI (a), SI (b) and LOV (c) setups (adapted from reference 17).

Bead injection. The methods described previously show several disadvantages. For preconcentration and separation purposes using FI, a packed column is permanently placed in the line. The presence of the column in the line significantly affects the efficiency of the system. The lower the particle size of the stationary phase in the column, the more efficient the separation and preconcentration. However, flow resistance is created by the presence of the column in the line, which can lead to leaks, restriction or stopping of the solution flow (due to a build up of back pressure in the line) and the maximum flow rate through the column being limited, which in turn increases analysis time. Other factors that should be considered are the deactivation of the surface of the stationary phase over time caused by column contamination and degradation in performance caused by the loss of functional groups on the stationary phase.

BI emerges as an alternative to alleviate the aforementioned problems.[16] In this case, a uniform suspension of surface active beads (e.g. coated with a chelating or ion-exchange material), with diameters in the 10–150 μm range is injected into a flow cell, where the beads are trapped and exposed to the analyte. The analytes of interest are retained on the surface of the beads while unwanted matrix ions, such as Na, are not retained and flow to waste. The beads are then eluted using, for example, dilute nitric acid, and the eluted analytes are carried to the detector. The stationary phase is then rejected, which ensures complete renewal of the resin beads before analysis of the next sample. Additional advantages of BI include improved sensitivity and limits of detection, because the analyte concentration in the (small) eluent volume is usually somewhat larger than in the original sample.

Two aspects that are important in BI are the reproducibility of the bead packing and the stability of the reagent layer. In order to uniformly trap the beads, special cells must be used, such as the so-called jet ring cell (Figure 5.9(a)).[16] In this case, a capillary is placed in front of a flat surface. The capillary–surface gap allows the liquid stream to escape whereas the beads are trapped inside the cell. The processes for cell packing and unpacking are schematically shown in Figure 5.9(a). If the capillary–flat surface distance is increased, the cell is emptied. An additional cell design is shown in Figure 5.9(b). In this case, a nozzle is placed inside a conduit so that the liquid can go through whereas the beads are retained. Once the analyte elution has been completed, the flow is either reversed or increased to unpack the beads (see Section 5.2.4.2(a)).

Laboratory-on-valve. In some instances (e.g. analysis of limited sample volumes or hazardous materials) FI and SI present some limitations. A new way of carrying out these analyses has been proposed; the so called lab-on-valve (LOV) technology.[14,17,18] In LOV, a multi-port valve is used (Figure 5.8(c)), which has a central flow-through channel and a set of working channels that can be used for instance to add reagents to the sample or to carry out in-valve sample dilutions. So far, this system has been applied as a method for BI separation and preconcentration.[19] Miniaturization is easily performed and the system is able to handle sample volumes in the sub-microliter range.

5.2.4 Applications of FI in ICP-MS

In FI, the process of injecting the small sample volume into the carrier stream generates a concentration gradient as a result of dilution of the sample plug into the carrier stream as the plug is transported to the detector. This dilution effect is called *dispersion* and is the primary feature of the basic FI technique. Dispersion (D) can be calculated as follows:

$$D = \frac{C_0}{C_{\max}} \tag{5.2.1}$$

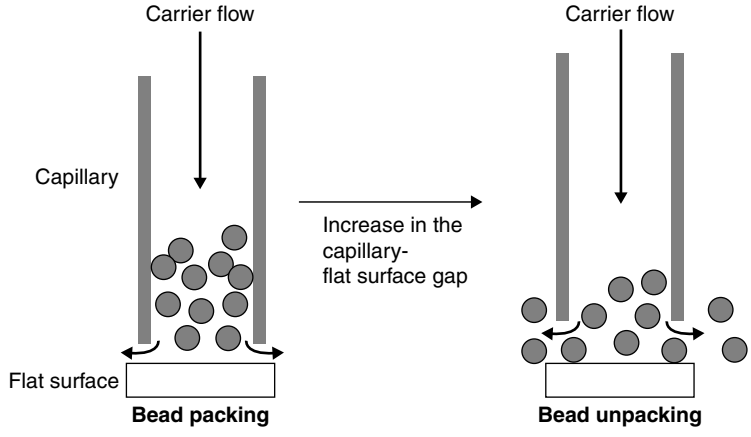

(a)

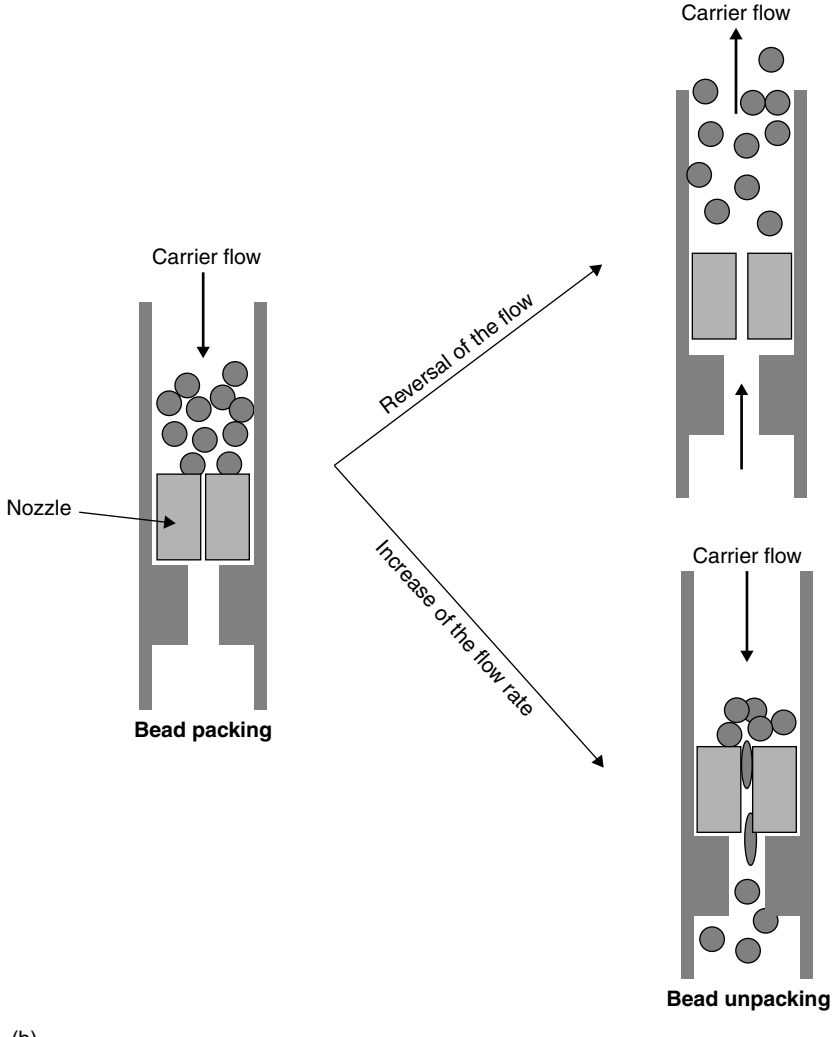

(b)

Figure 5.9 Bead packing and unpacking procedures for a jet ring cell (a) and a cell based on the insertion of a nozzle inside the tubing (b).

where C_0 is the analyte concentration before the sample injection and C_{max} is the maximum analyte concentration within the injected sample plug. All the components of the system (peristaltic pump, tubing, injection loop, connections, nebulizer and spray chamber) contribute to the total dispersion. Under a given set of system parameters, such as carrier stream flow rate, injected sample volume and tubing length, the dispersion will be fixed and reproducible for successive injections. It is dispersion that generates the characteristic transient FI peak shape, allows concentrated, low volume samples to be directly injected and facilitates reaction between the injected sample and the carrier stream (if required). In general, the smaller the injected sample volume and the longer the distance between the injection valve and the detector, the greater the dispersion will be. More turbulent carrier flow or on-line mixing of the injected sample plug with another reagent stream will also usually increase the dispersion. Setting the required dispersion for a particular application is a major part of developing a FI method.

Table 5.1 summarizes a classification of the FI applications as a function of the D value.[2] In some FI applications, the analyte is preconcentrated and D becomes lower than 1. Meanwhile, in other cases, larger values of D are produced, as a result of small sample volume injection or as a consequence of efficient on-line sample–reagent mixing, as described earlier.

Table 5.1 FI applications as a function of the dispersion range (see reference 2)

D range	Dispersion degree	Application
<1	Reduced. Analyte concentration in the plug is higher than in the sample	Preconcentration
1–3	Limited. The center of the sample plug does not merge with the external carrier	Calibration (IS, standard addition, isotopic dilution)
3–10	Medium	Calibration (gradient calibration, standard addition, isotopic dilution)
>10	Large	Sample dilution, kinetic studies

5.2.4.1 Calibration with FI

Calibration with FI reduces the risk of sample contamination and in some cases improves the precision of the analysis. The throughput of the standard addition method is significantly enhanced by on-line mixing of the standards with the sample. This method has proven to be particularly effective for the analysis of seawater samples.[20] More recently, a human serum sample has been successfully analyzed by ICP-MS[21] using a method consisting of injection of the sample into two streams: a dilute nitric acid one and another one of a standard solution having the same acid concentration.[2] With this method, sample contamination is minimized because no sample pretreatment is needed. The flexibility of FI also permits combination of internal standardization (to correct for signal fluctuation) with standard addition, providing good results for urine samples.[22]

When dealing with transient signals, calibration with internal standard (IS) involves calculation of the ratio of the peak heights or areas obtained for the analytes and internal standards. In other instances, the ratios are calculated for each data point acquired across the whole peak.[3,23] Isotope dilution (ID) can be carried using FI methodology, such that various additions can be performed from a single enriched solution.[2,24,25] Compared to conventional ID methods, on-line ID provides

higher sample throughput without compromising the precision of the results.[26] As expected, for fast transient signals (i.e. faster than 8 s, at half the peak width) and when many isotopes (i.e. more than 15) must be measured, ICP-TOFMS instruments are better suited for ID than quadrupole ICP-MS.[27] A reverse flow ID FI method has been described.[28] A volume (approximately 100–250 μL) of an isotopically enriched standard is injected in both the sample and standard solution streams. As a result, a positive peak is obtained for the enriched isotope and a negative one for the reference isotope. The isotopic ratio is calculated point-by-point across the peaks. This method shows important advantages over the off-line method and the on-line ID method: (i) a preliminary analysis of the sample is not required, provided that the method affords isotopic ratios from much greater than unity to much smaller than unity. As a consequence, the best ratio for a particular analysis can be selected; (ii) it is not time consuming and higher sample throughputs are obtained; (iii) the analysis is carried out in a closed system and the contamination risks are therefore reduced; (iv) isotopic carryover is minimized, since the sample itself acts as a washing solution and (v) only one isotope free of spectroscopic interferences is required. The present method yielded good results for the determination of Ni in river water and Mo in saline water.[28]

5.2.4.2 Solid phase and solvent extraction matrix separation and preconcentration FI techniques

(a) Ion-exchange/complexation/sorbent extraction

Although sample matrix effects such as ionization suppression and drift can be alleviated to some extent by on-line sample dilution,[3,22] this is not an appropriate approach when the target analyte concentrations are very low. In these cases, solid phase extraction[29] is often used as a means for on-line separation and preconcentration of analytes in ICP-MS. This is especially useful for the analysis of samples such as seawater, estuarine waters or sediments. Figure 5.10 shows the principle of FI analyte preconcentration and matrix separation. In this mode, a given sample volume is mixed with a buffer solution (usually ammonium acetate), either on- or off-line and

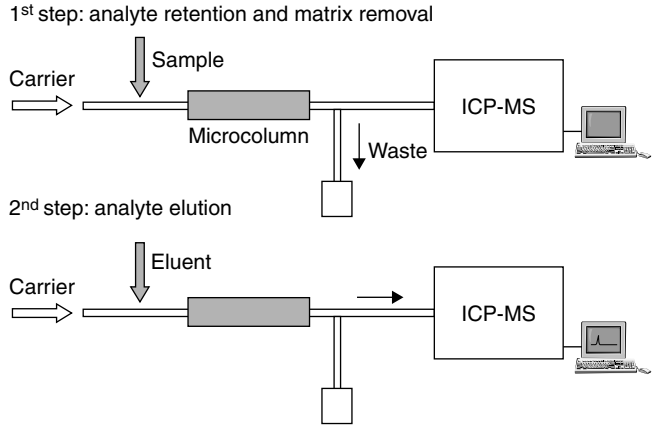

Figure 5.10 Scheme of the system for preconcentration and matrix elimination through a solid stationary phase in ICP-MS and the involved steps.

pH adjusted (typically to around pH 6), then injected (or simply carried, if on-line buffering has been used) into the system and passed through a column filled with a surface active material composed of particles of sizes in the 40–150 μm range, depending on the working liquid flow rate (first step). The analyte is retained on these particles, whereas the sample matrix goes through the column to waste. The column is then typically rinsed with water. An eluting solution such as dilute nitric acid then passes through the column, thus releasing the analytes that are carried toward the spectrometer (second step). Alternatively, the sample plug can be presented to the instrument either by air[30] or aqueous[19] segmentation. The first choice has the advantage of generating lower sample dispersion with the subsequent increase in sensitivity.

Several choices for the surface active materials required for analyte preconcentration and matrix separation in ICP-MS have been investigated, such as ion exchangers[31–33] or chelating agents.[34–38] The two most widely used chelating resins are based on iminodiacetate and 8-hydroxyquinoline functional groups. These resins have a high selectivity for transition metal ions without significantly retaining alkali and alkaline earth metals. The level of alkali/alkaline earth metals that are retained during the sample loading step can be minimized by careful selection of the sample/buffer pH and by the buffer concentration.[34] The problem of high blank levels (and hence degraded detection limits) caused by impurities in the reagents can be overcome by using additional resin columns in the buffer and rinse carrier tubing to scavenge the metals contaminating these streams.[39] Another problem emerges when analyzing samples containing a high level of organic matter, such as some natural waters, because a non-negligible fraction of certain analytes in these samples is complexed with natural chelating species, such as humic materials. In these cases, sample digestion by UV irradiation prior to sample analysis is recommended.[39]

The combination of solid phase extraction with SI[40] gives rise to a reduction in both the analysis time and the required sample volume. It has been found that when applying this methodology to the determination of Pu isotopes in sea water, the volume of sample required is reduced from 60 L (in the case of using α-spectrometry) to only 5 L. More importantly, the analysis time is shortened from 2 days to 15 min.[41]

Recently, matrix separation and analyte preconcentration have been carried out for the analysis of biological and environmental samples using SI-BI-LOV.[19] In this case, two channels are used as microcolumns: one for trapping approximately 2 mg of the resin beads and another one for preventing the beads from escaping during the analysis step. The analyte/matrix separation, analyte preconcentration and elution are carried out automatically by using the different valve ports. Once the analyte has been introduced into the ICP-MS spectrometer, the column is discarded simply by increasing the flow rate. This is possible because the beads, made of Sephadex and coated with an ion exchanger, are perfectly spherical at low liquid flow rates (i.e. at about 70 μL/min), whereas at higher liquid flows (i.e. above 600 μL/min) they become squeezed and can then pass through the system tubing. The studies carried out show that SI-BI-LOV compares favorably against conventional FI methodology in terms of precision and achievable limit of detection.

Sorbent extraction consists of on-line transformation of the analyte to a neutral complex by reaction with a suitable ligand (e.g. diethyldithiocarbamate, DDTC), followed by retention of this complex on a C-18 column. The complex is then subsequently eluted with either an organic solvent (e.g. methanol) or an inorganic acid (e.g. nitric acid). Compared to retention on resins, this procedure exhibits better selectivity. Note that with this methodology, the complexation and retention steps can be optimized separately.

So-called knotted reactors (KR) have also been used to preconcentrate analytes.[30] With this method, a chelating agent is passed through the reactor in order to create a layer on its inner walls. The analytes of interest react with the chelating agent (e.g. ammonium pyrrolidine dithiocarbamate, APDC,[30] 1-phenyl-3-methyl-4-benzolpyrazol-5-one, PMBP[42]) thus forming complexes that are immobilized on the walls of the reactor. Thereafter the reactor is rinsed in order to remove any residual matrix without releasing the retained analyte complexes. Following this step the analytes are eluted in a small volume. The most important variables affecting the behavior of the system are: pH of the solution containing the KR coating agent, pH of the sample solution, concentration of chelating agent, sample and reagent solutions flow rates, KR coating and analyte complexation times, KR length, rinsing time and eluent volume.

The virtually unlimited lifetime of the KR makes it a reliable and stable preconcentration system. Comparative studies have demonstrated that with KR the preconcentration efficiencies are higher than for serpentine 8-shaped reactors (SR) (i.e. from 4 to 36 and from 3 to 12, for the KR and SR, respectively).[43] Nonetheless, this method has limitations, including blank problems and errors induced as a result of different complexation efficiencies for analytes present in different chemical forms (e.g. oxidation states).[2]

Elution with organic matrices, such as methanol, has been made possible by employing sample introduction systems able to remove the solvent from the aerosol stream (i.e. desolvation systems)[30] or through electrothermal vaporization (ETV).[44] In the latter case it has been confirmed that the ETV technique is preferable to using a cross-flow nebulizer–double pass spray chamber combination in terms of sensitivity and limits of detection. Desolvation systems also eliminate some polyatomic interferences caused by inorganic eluents (e.g. nitric acid, hydrochloric acid).[41]

(b) Precipitation/co-precipitation

In this approach, the sample is initially mixed with a reagent and the analyte precipitates as an insoluble salt. The precipitate is accumulated, washed and then dissolved for introduction into the ICP-MS apparatus. Analytes are precipitated as either hydroxides[45] or with organic reagents[46] (e.g. ammonium pyrrolidinedithiocarbamate, APDC, sodium diethyldithiocarbamate, NaDDTC). A common problem of the precipitation and co-precipitation methods is that analytes are not quantitatively separated from the matrix.

One of the most efficient ways of carrying out these procedures is through the use of KR.[45] Figure 5.11 shows a scheme of the steps followed with these reactors for analyte preconcentration by precipitation. KR can be used with[47] or without[45] a filter placed downstream. The basic separation principle consists of the deposition of the precipitate particles on the inner walls of the reactor as a result of the secondary flows induced by the reactor geometry. Recent studies demonstrate that the temperature of the KR plays an important role in terms of analyte–matrix separation. Thus for the analysis of estuarine water samples,[47] it has been found that heating the reactor at about 70 °C enhances analyte precipitation with DDTC. At the same temperature, after washing the precipitate with distilled water, it is easily dissolved with a concentrated (i.e., 4 mol/L) nitric acid solution. Nonetheless, problems due to inhomogeneous sample heating are a source of imprecision, because this leads to the precipitate becoming irregularly distributed along the KR. The use of more efficient heating means (e.g. microwave radiation) is expected to improve the precision of this method.[47] When trying to optimize the FI conditions using the

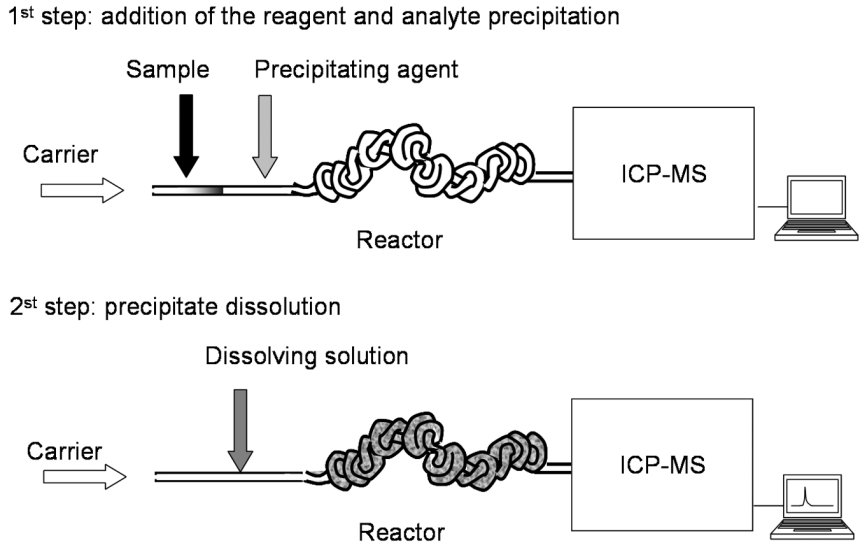

Figure 5.11 Steps followed for analyte preconcentration by precipitation with a knotted reactor in ICP-MS.

precipitation–co-precipitation approach, attention must be paid to the length of the reactor, the concentration of the dissolving agent and the temperature of the system.

(c) Solvent extraction

This method is based on complex formation between the analyte (in aqueous solution) and a complexing agent dissolved in an organic solvent. The sample is merged with the extractant through a segmenter. The two phases are then allowed to reach equilibrium inside a coil after which they are separated using (generally) a porous membrane. The organic phase is then passed on to the ICP-MS.[2] A simpler alternative has also been developed, based on SI. In this case, the organic phase (containing the chelating reagent) is pumped and the aqueous one (initially containing the analyte) is propelled through it. Afterwards the flow direction is reversed and the aqueous phase is passed through the organic one again. The analytes are extracted into the organic phase, and the aqueous phase is discarded. This method takes advantage of the different migration velocity of the two phases due to their different interactions with the pump tubing capillary.[2]

The use of KR is also beneficial for FI solvent extraction methods because they increase the area of the liquid–liquid interface thereby enhancing the separation of the two phases. Since organic solvents give rise to serious interferences in ICP-MS, the analyte complexes can be back-extracted into an aqueous stream prior to transport into the ICP-MS. Figure 5.12 shows the steps applied in this operating mode. If a judicious choice of the sample–extractant volume ratio (it should be high) and that of the aqueous eluent–organic phase (it should be low) is made for these solvent extraction methods, high enrichment analyte factors can be achieved.

Cloud point extraction is also of great interest for preconcentration and matrix elimination procedures. In this method, a non-ionic surfactant is mixed with an aqueous solution containing the analyte. Above a given temperature (the cloud point temperature), the aqueous–surfactant

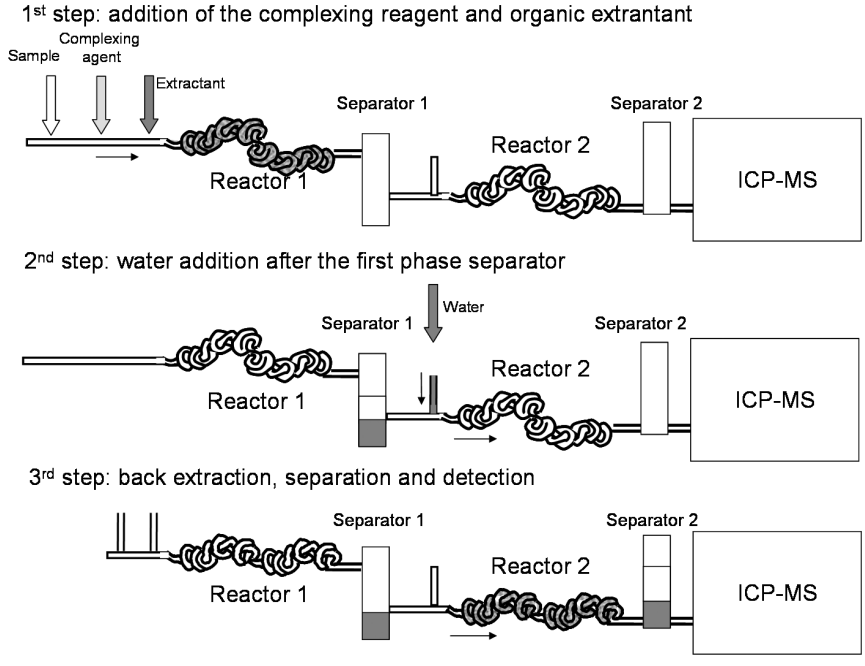

Figure 5.12 Solvent extraction and back-extraction procedure using knotted reactors.

mixture separates into two phases, one rich in surfactant (with a very low volume) and the other in which the surfactant concentration approaches its critical micelle concentration. If an analyte can be dissolved in the hydrophobic core of the micelles, it will become concentrated.[48] A FI method that utilizes this approach has been used for the introduction of metal complexes extracted with Triton X-114 into an ICP-MS using an ultrasonic nebulizer.[49]

Table 5.2 shows a comparison of the efficiency of the different preconcentration methods described so far. In general, with any of these methods, sensitivity is improved by around one order of magnitude. From Table 5.2 it emerges that by combining a chelating resin with an ETV system (both of which are able to preconcentrate analytes; for the ETV, this is achieved by loading successive samples into the furnace and raising the temperature sufficiently to remove the solvent, but not enough to atomize the analyte), the concentration of some elements can be increased by more than two orders of magnitude.

5.2.4.3 Hydride generation

In hydride generation (HG) methods, the sample is mixed with an acid stream and then with a suitable reducing agent (e.g. sodium borohydride). The analyte is transformed into its gaseous hydride, whereas the remaining sample matrix components stay in the liquid phase. A gas–liquid phase separation is performed on-line and, by using a carrier argon stream, the hydrides are carried toward the plasma. Gas–liquid separation can be achieved either via the nebulizer/spray chamber arrangement, whereby the gas–liquid separation takes place inside the spray chamber, or using an on-line separator, followed by introduction of the hydride gases directly into the

Table 5.2 Comparison of the different preconcentration/matrix separation methods in ICP-MS

Method	Analysis throughput (samples/h) and detection method	Isotope and preconcentration factor	Isotope and limits of detection(ng/L)	Sample consumed volume (mL)	Reference
Solid phase extraction with chelating resins	20, Pneumatic nebulizer/double pass spray chamber/ICP–QMS	^{63}Cu: 22 ^{75}As: 27 ^{77}Se: 61 ^{107}Ag: 33 ^{111}Cd: 19 ^{208}Pb: 22	^{63}Cu: 33 ^{75}As: 5 ^{77}Se: 7 ^{107}Ag: 0.8 ^{111}Cd: 7 ^{208}Pb: 4.5	2.3	44
Solid phase extraction with chelating resins	20, ETV/ICP–QMS	^{63}Cu: 52 ^{75}As: 166 ^{77}Se: 70 ^{107}Ag: 153 ^{111}Cd: 45 ^{208}Pb: 280	^{63}Cu: 5 ^{75}As: 8 ^{77}Se: 5 ^{107}Ag: 0.15 ^{111}Cd: 0.2 ^{208}Pb: 0.3	2.3	44
On-line adsorption with KR	~30, Ultrasonic nebulizer/ICP-TOFMS	^{63}Cu: 14 ^{107}Ag: 10 ^{114}Cd: 5 ^{208}Pb: 15	^{63}Cu: 5 ^{107}Ag: 5 ^{114}Cd: 17 ^{208}Pb: 26	5.2	30
Cloud point extraction	Ultrasonic nebulizer/ICP-QMS	^{63}Cu: 17 ^{75}As: 42 ^{77}Se: 37 ^{107}Ag: 20 ^{114}Cd: 29 ^{208}Pb: 25	^{63}Cu: 30 ^{75}As: 6 ^{77}Se: 20 ^{107}Ag: 4 ^{114}Cd: 6 ^{208}Pb: 4	40	49

injector tube of the plasma torch. With this methodology, besides achieving complete analyte–matrix separation, the hydride transport efficiency is virtually 100%, leading to enhanced limits of detection (typically one order of magnitude lower) with respect to conventional liquid sample introduction. In some instances, the hydrides can be electrochemically generated, thereby avoiding problems associated with the instability of the sodium borohydride reagent.[50] Elements such as Ge, Sn, As, Bi, Sb, Se and Te can be determined through FI-HG-ICP-MS with good results. Mercury, in turn, has been determined through cold vapour (CV) ICP-MS. HG (or CV) has also been used in speciation studies.[51,52] In these cases, a vapour generation unit is placed after the column used to separate the different species (Figure 5.13).

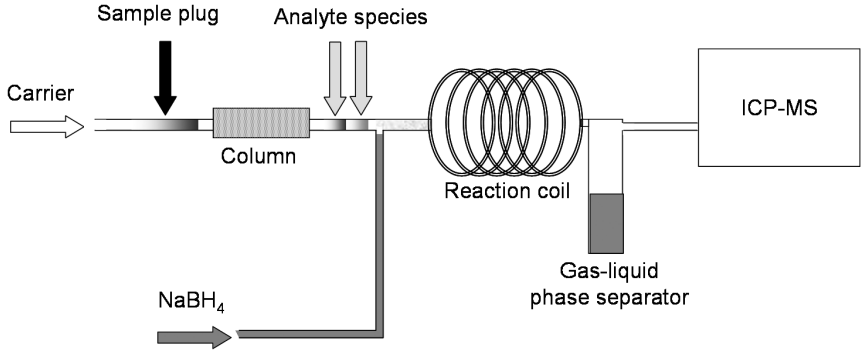

Figure 5.13 Speciation through ICP-MS by using liquid chromatography and post-column hydride/cold vapour generation.

One of the problems encountered with HG arises when analyzing difficult samples. Poor recoveries have been reported for complex matrices, as a result of chemical processes, such as catalytic decomposition of hydrides by transition metals. The use of masking agents (e.g. thiourea, L-cysteine, ascorbic acid, citric acid, and iodide) suppresses hydride decomposition when transition metals are present.[53,54] An internal standard (e.g. Ge) can also be used in order to compensate for matrix interferences in samples such as urine.[55]

An advantage of FI-HG (or CV)-ICP-MS is that the long wash out times found for some elements (e.g. Hg) are significantly shortened, as they are transported toward the plasma as vapour compounds. The application of FI HG-ICP-quadrupole MS to the analysis of sediments demonstrated that similar recoveries are found as with direct analysis using sector field high resolution ICP-MS, which demonstrates the efficiency of HG for alleviating interferences.[56] The parameters that must be optimized for HG are: the carrier argon gas flow rate and variables influencing the extent of the reaction, such as the choice of reducing agent and its concentration, the liquid flow rates, the pH and the masking agent concentration and type. The main limitation of hydride generation is that there are only a few elements that readily form hydrides, so the range of application of this approach is restricted.

5.2.4.4 Anodic stripping voltammetry

This approach to on-line matrix separation/preconcentration is based on passing an electrolyte stream through an anodic stripping voltammetry (ASV) cell and injecting the sample into this stream. When the ASV cell is set at an appropriate potential, the analyte is preferentially deposited

and accumulated on the working electrode while the matrix goes to waste. At a given moment, the potential is changed to rapidly release the analyte back into the carrier stream to transport it into the ICP-MS.[57] Thin layer ASV cells are preferred over flow-through cells with porous electrodes, for coupling with ICP-MS because of their higher preconcentration factors, sample throughputs, lower sample consumption and simplicity.[58] ASV-ICP-MS has several interesting features such as matrix removal and excellent analytical figures of merit (elements present in sub-ppt or even ppq levels can be determined). Furthermore, due to the extremely high sensitivity of the detection system, it is possible to monitor electrode reactions involving trace amounts of metals.[59]

The most important variables for ASV-ICP-MS are the injected sample volume, the flow rate, pH and the choice of carrier electrolyte. Finally, those variables involving the analyte accumulation and release processes (i.e. the potential variation speed and the material of the working electrode) must also be considered.

Another electrochemical way to separate the analyte from the matrix that has been described is electrolytic deposition of the matrix elements on a mercury cathode in the presence of low sulfuric acid concentrations.[60] Once the matrix is separated, the solution is carried to the spectrometer and elements are determined. This procedure is especially useful for the analysis of alloys, because elements such as rare earth elements can be easily separated from iron, chromium, nickel, copper, etc. For the analysis of steel samples, this method provides limits of quantification 10 times better than direct analysis, without the need for matrix matching. Recently, an FI electrolytic dissolution procedure has been reported for the treatment of metallic (i.e. high-purity copper) samples, the specimen acting as the anode of an electrodissolution cell.[61]

5.2.5 Future studies

In the field of hydride generation, the use of membranes for gas–liquid separation has proved to be effective. An alternative to membranes are the pervaporation systems. Analytical pervaporation is defined as the integration of evaporation and gas diffusion into a single module.[62] The volatile species present in a heated phase (donor) evaporate through a porous membrane and the vapour condenses on the surface of a cool stream (acceptor) on the other side of the membrane. The use of pervaporation devices may be more promising than membranes because the sample solution does not contact the membrane. This is possible because there exists an air volume separation between the sample and the membrane (Figure 5.14).

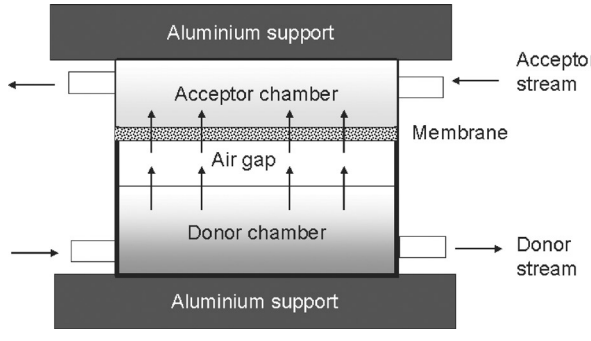

Figure 5.14 Schematic of a pervaporation system.

Surprisingly, FI on-line microwave digestion of solid samples coupled to an ICP-MS spectrometer has not been explored as much with ICP-MS as with optical emission. The complex, high dissolved solids matrix resulting from the sample digestion may be one of the reasons, as it is difficult to subject the sample on-line to the subsequent treatment processes (e.g. dilution, pH adjustment, matrix separation) required to enable the sample to be transported into the ICP-MS. Nonetheless, as has been shown throughout this section, there are FI methods for efficient matrix removal, so there are opportunities for future developments in this area.

Miniaturization is a global trend in analytical chemistry that has been extended to FI. Several μFI systems have been developed and coupled to ICP-MS. This has accompanied the development of nano-injection systems.[63] The use of low-sample-consumption micronebulizers is expected to increase the number of applications dealing with micro-flow systems.[24,64] By injecting sample volumes as low as 0.2 μL into the plasma in a precise fashion, the problems associated with analysis of organic samples using ICP-MS are mitigated.[65] The development of low inner volume spray chambers reduces transient signal dispersion, thereby facilitating the use of more efficient μFI systems. Recently, a direct injection high efficiency nebulizer has been used as a sample introduction system for the analysis of petroleum samples[66] and highly volatile organic solvents[67] by quadrupole ICP-MS.

Due to its unique characteristics, SI-BI-LOV (Figure 5.15) methods can be applied to virtually any kind of solid liquid interaction (i.e. precipitation/co-precipitation separation/preconcentration) and it is likely that more attention will be focused on these methods.

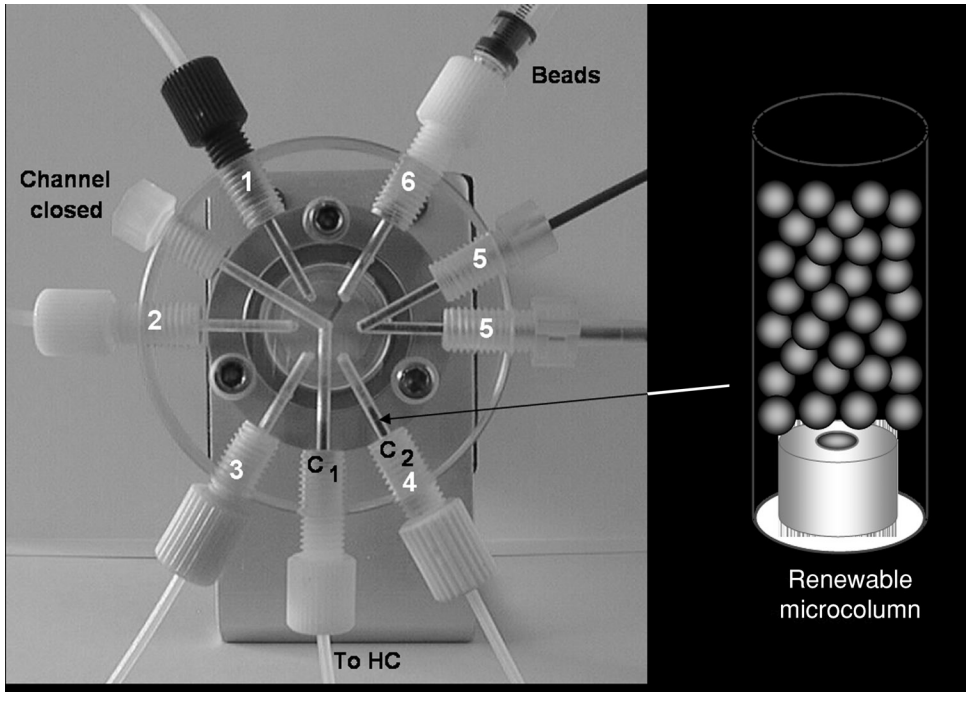

Figure 5.15 Picture of the SI-BI-LOV system used in ICP-MS. HC, holding coil; C_1 and C_2, microcolumn positions (taken from reference 18 with permission).

LOV technology is also expected to grow in combination with existing procedures for sample treatment in order to develop more reliable, sensitive and selective methods.

References

1. Sanz-Medel, A. (ed.) (1999) *Flow Analysis with atomic spectrometric detectors*. Elsevier, Amsterdam.
2. Beauchemin, D. (2000) Flow injection techniques. In: Discrete Sample Introduction Techniques for Inductively Coupled Plasma Mass Spectrometry (ed. D. Barceló) Elsevier, Amsterdam.
3. McClenathan, D. M., Ray, S. J., and Hieftje, G.M. (2001) New flow injection strategies for study and control of matrix interferences by inductively coupled plasma time-of-flight mass spectrometry. *J. Anal. At. Spectrom.*, **16**, 987–90.
4. Dressler, V. L., Pozebon, D., and Curtius, A. J. (1999) Introduction of alcohols in inductively coupled plasma mass spectrometry by a flow injection system. *Anal. Chim. Acta*, **379**, 175–83.
5. Dressler, V. L., Pozebon, D., and Curtius, A. J. (1998) Determination of heavy metals by inductively coupled plasma mass spectrometry after on-line separation and preconcentration. *Spectrochim. Acta*, B, **53**, 1527–39.
6. Jiménez, M. S., Velarte, R., and Castillo, J. R. (2003) On-line emulsions of olive oil samples and ICP-MS multi-elemental determination. *J. Anal. At. Spectrom.*, **18**.
7. Giné, M. F., Gervasio, A. P. G., Lavorante, A. F., Miranda, C. E. S., and Carrilho, E. (2002) Interfacing flow injection with capillary electrophoresis and inductively coupled plasma mass spectrometry for Cr speciation in water samples. *J. Anal. At. Spectrom.*, **17**, 736–8.
8. Hieftje, G. M., Myers, D. P., Li, G., Mahoney, P. P., Burgoyne, S. J., Ray S. J., and Guzowski, J. P. (1997) Toward the next generation of atomic mass spectrometers. *J. Anal. At. Spectrom.*, **12**, 287–92.
9. Castillo-Carrión, M., Reyes Andrés, J., Rubí, J. A., and Emteborg, H. (2003) Performance optimization of isotope ratio measurements in transient signals by FI-ICP-TOFMS. *J. Anal. At. Spectrom.*, **18**, 437–43.
10. Laborda, F., Medrano, J., and Castillo, J. R. (2000) Data acquisition of transient signals in inductively coupled plasma mass spectrometry. *Anal. Chim. Acta*, **407**, 301–9.
11. Björn, E., Baxter, D. C., and Frech, W. (2002) Calibration errors due to variation in peak characteristics in the measurement of transient signals by inductively coupled plasma-scanning mass spectrometry. *J. Anal. At. Spectrom.*, **17**, 1582–8.
12. Ruzicka, J. and Hansen, E. H. (2000) Flow injection: from beaker to microfluidics. *Anal. Chem.*, **72**, 212A–217A.
13. http://www.flowinjection.com/method2.html
14. Hansen, E. H. and Wang, J. (2002) Implementation of suitable flow injection/sequential injection-sample separation/preconcentration schemes for determination of trace metal concentrations using detection by electrothermal atomic absorption spectrometry and inductively coupled plasma mass spectrometry. *Anal. Chim. Acta*, **467**, 3–12.
15. Lenehan, C. E., Barnett, N. W., and Lewis, S. W. (2002) Sequential injection analysis. *Analyst*, **127**, 997–1020.
16. Ruzicka, J. and Scampavia, L. (1999) From flow injection to bead injection. *Anal. Chem.*, **71**, 257A–263A.
17. Ruzicka, J. (2000) Lab-on-valve: universal microflow analyzer based on sequential and bead injection. *Analyst*, **125**, 1053–60.
18. Wang, J. and Hansen, E. H. (2003) Sequential injection lab-on-valve: the third generation of flow injection analysis. *Trends Anal. Chem.*, **22**, 225–31.

19. Wang, J. and Hansen, E. H. (2001) Interfacing sequential injection on-line preconcentration using a renewable micro-column incorporated in a 'lab-on-valve' system with direct injection nebulization inductively coupled plasma mass spectrometry. *J. Anal. At. Spectrom.*, **16**, 1349–55.
20. Beauchemin, D. (1995) On-line standard addition method with ICPMS using flow injection. *Anal. Chem.*, **67**, 1553–7.
21. Huang, C. and Beauchemin, D. (2003) Direct multielemental analysis of human serum by ICP-MS with on-line standard addition using flow injection. *J. Anal. At. Spectrom.*, **18**, 951–2.
22. Wang, J., Hansen, E. H., and Gammelgaard, B. (2001) Flow injection on-line dilution for multi-element determination in human urine with detection by inductively coupled plasma mass spectrometry. *Talanta*, **55**, 117–26.
23. Specht, A. A. and Beauchemin, D. (1998) Automated on-line isotope dilution analysis with ICP-MS using sandwich flow injection. *Anal. Chem.*, **70**, 1036–40.
24. Packer, A. P., Giné, M. F., dos Reis, B. F., and Menegário, A. A. (2001) Micro flow system to perform programmable isotope dilution for inductively coupled plasma-mass spectrometry. *Anal. Chim. Acta*, **438**, 267–72.
25. Vanhaecke, F., Moens, L., Dams, R., Allen, L., and Georgitis, S. (1999) Evaluation of the isotope ratio performance of an axial time-of-flight ICP mass spectrometer. *Anal. Chem.*, **71**, 3297–303.
26. Valles-Mota, J. P., Fernández de la Campa, M. R., García-Alonso, J. I., and Sanz-Medel, A. (1999) Determination of cadmium in biological and environmental materials by isotope dilution inductively coupled plasma mass spectrometry: effect of flow sample introduction methods. *J. Anal. At.. Spectrom.*, **14**, 113–20.
27. Vázquez-Peláez, M., Costa-Fernández, J. M., and Sanz-Medel, A. (2002) Critical comparison between quadrupole and time-of-flight inductively coupled plasma mass spectrometers for isotope ratio measurements in elemental speciation. *J. Anal. At.. Spectrom.*, **17**, 950–7.
28. Beauchemin, D. and Specht, A. A. (1997) On-line isotope dilution analysis with ICPMS using reverse flow injection. *Anal. Chem.*, **69**, 3183–7.
29. Camel, V. (2003) Solid phase extraction of trace elements. *Spectrochim. Acta* B, **58**, 1177–233.
30. Benkhedda, K., Infante, H. G., Ivanova, E., and Adams, F. C. (2000) Trace metal analysis of natural waters and biological samples by axial inductively coupled plasma time of flight mass spectrometry (ICP-TOFMS) with flow injection on-line adsorption preconcentration using a knotted reactor. *J. Anal. At. Spectrom.*, **15**, 1349–56.
31. Coedo, A.-G., Dorado, M. T., and Padilla, I. (2002) On-line ion-exchange matrix separation and inductively coupled plasma mass spectrometric determination of trace impurities in high-purity aluminium. *J. Anal. At. Spectrom.*, **17**, 502–6.
32. Elwaer, A. R., McLeod, C. W., and Thompson, K. C. (2000) On-line separation and determination of bromate in drinking water using flow injection ICP mass spectrometry. *Anal. Chem.*, **72**, 5725–30.
33. Yang, L. and Sturgeon, R. E. (2002) On-line determination of silver in sea-water and marine sediment by inductively coupled plasma mass spectrometry. *J. Anal. At. Spectrom.*, **17**, 88–93.
34. Nelms, S. M., Greenway, G. M., and Koller, D. (1996) Evaluation of controlled-pore glass immobilized iminodiacetate as a reagent for automated on-line matrix separation for inductively coupled plasma mass spectrometry. *J. Anal. At. Spectrom.*, **11**, 907–13.
35. Lee, K. H., Oshima, M., and Motozima, S. (2002) Inductively coupled plasma mass spectrometric determination of heavy metals in sea-water samples after pre-treatment with a chelating resin disk by an on-line flow injection method. *Analyst*, **127**, 769–74.
36. Nicolai, N., Rosin, C., Tousset, N., and Nicolai, Y. (1999) Trace metals analysis in estuarine and seawater by ICP-MS using on line preconcentration and matrix elimination with chelating resin. *Talanta*, **50**, 433–44.

37. Willie, S. N., Lam, J. W. H., Yang, L., and Tao, G. (2001) On-line removal of Ca, Na and Mg from iminodiacetate resin for the determination of trace elements in seawater and fish otoliths by flow injection ICP-MS. *Anal. Chim. Acta*, **447**, 143–52.
38. Beck, N. G., Franks, R. P., and Bruland, K. W. (2002) Analysis for Cd, Cu, Ni, Zn and Mn in estuarine water by inductively coupled plasma mass spectrometry coupled with an automated flow injection system. *Anal. Chim. Acta*, **455**, 11–22.
39. Ndung'u, K., Franks, R. P., Bruland, K. W., and Flegal, A. R. (2003) Organic complexation and total dissolved metal analysis in estuarine waters: comparison of solvent-extraction graphite furnace atomic absorption spectrometric and chelating resin flow injection inductively coupled plasma mass spectrometry analysis. *Anal. Chim. Acta*, **481**, 127–38.
40. Jiménez, M. S., Velarte R., and Castillo, J. R. (2002) Performance of different preconcentration columns used in sequential injection analysis and inductively coupled plasma-mass spectrometry for multielemental determination in seawater. *Spectrochim. Acta* B, **57**, 391–402.
41. Kim, C.-S. and Kim, C.-K. (2002) Determination of Pu isotopes in seawater by an on-line sequential injection technique with sector field inductively coupled plasma mass spectrometry. *Anal. Chem.*, **74**, 3824–32.
42. Benkhedda, K., Infante, H. G., Ivanova, E., and Adams, F. C. (2001) Determination of sub-parts-per-trillion levels of rare earth elements in natural waters by inductively coupled plasma time-of-flight mass spectrometry after flow injection on-line sorption preconcentration in a knotted reactor. *J. Anal. At. Spectrom.*, **16**, 995–1001.
43. Liawruangrath, S., Som-aum, W., and Townshend, A. (2002) A comparison of enrichment factor of knotted and serpentine reactors using flow injection sorption and preconcentration for the off-line determination of some trace elements by inductively coupled plasma mass spectrometry. *Talanta*, **58**, 1177–84.
44. Pozebon, D., Dressler, V. L., and Curtius, A. J. (2001) Comparison of the performance of FI-ICP-MS and FI-ETV-ICP-MS systems for the determination of trace elements in sea water. *Anal. Chim. Acta*, **438**, 215–25.
45. Yan, X.-P., Kerrich, R., and Hendry, M. J. (1999) Flow injection on-line group preconcentration and separation of (ultra)trace rare earth elements in environmental and geological samples by precipitation using a knotted reactor as a filterless collector for inductively coupled plasma mass spectrometric determination. *J. Anal. At. Spectrom.*, **14**, 215–21.
46. Hengwu, C., Jincao, J., and Yufeng, W. (1997) Flow injection on-line coprecipitation-preconcentration system using copper(II) diethyldithiocarbamate as carrier for flame atomic absorption spectrometric determination of cadmium, lead and nickel in environmental samples. *Anal. Chim. Acta*, **353**, 181–8.
47. Chen, H. H. and Beauchemin, D. (2001) Determination of trace metals in saline water using flow injection on-line precipitation coupled with inductively coupled plasma mass spectrometry. *J. Anal. At. Spectrom.*, **16**, 1356–63.
48. Ortega, C., Gómez, M. R., Olsina, R. A., Silva, M. F., and Martínez, L. D. (2002) On-line cloud point preconcentration and determination of gadolinium in urine using flow injection inductively coupled plasma optical emission spectrometry. *J. Anal. At. Spectrom.*, **17**, 530–3.
49. Mesquita da Silva, M. A. and Frescura, V. L. A. (2000) Determination of trace elements in water samples by ultrasonic nebulization inductively coupled plasma mass spectrometry alter cloud point extraction. *Spectrochim. Acta* B, **55**, 803–13.
50. Bings, N. H., Stefanka, Z., and Rodríguez Mallada, S. (2003) Flow injection electrochemical hydride generation inductively coupled plasma time-of-flight mass spectrometry for the simultaneous determination of hydride forming elements and its application to the analysis of fresh water samples. *Anal. Chim. Acta*, **479**, 203–14.

51. Tu, Q., Johnson, W. Jr., and Buckley, B. (2003) Mercury speciation analysis in soil samples by ion chromatography, post-column cold vapor generation and inductively coupled plasma mass spectrometry. *J. Anal. At. Spectrom.*, **18**, 696–701.
52. Chatterjee, A., Shibata, Y., Tanaka, A., and Morita, M. (2001) Determination of selenoethionine by flow injection-hydride generation-atomic absorption spectrometry/high-performance liquid chromatography-hydride generation-high power nitrogen microwave-induced plasma mass spectrometry, *Anal. Chim. Acta*, **436**, 253–63.
53. Danadurai, K. S. K., Hsu, Y.-L., and Jiang, S.-J. (2002) Determination of selenium in nickel-based alloys by flow injection hydride generation reaction cell inductively coupled plasma mass spectrometry. *J. Anal. At. Spectrom.*, **17**, 552–5.
54. Chen, Y. L. and Jiang, S. J. (2000) Determination of tellurium in a nickel-based alloy by flow injection vapor generation inductively coupled plasma mass spectrometry. *J. Anal. At. Spectrom.*, **15**, 1578–82.
55. Centineo, G., Montes Bayón, M., and Sanz-Medel, A. (2000) Flow injection analysis with inductively coupled plasma time-of-flight mass spectrometry for the simultaneous determination of elements forming hydrides and its application to urine. *J. Anal. At. Spectrom.*, **15**, 1357–62.
56. Moor, C. and Kobler, J. (2001) Determination of selenium in sediments by inductively coupled plasma-mass spectrometry: high resolution versus hydride generation. *J. Anal. At. Spectrom.*, **16**, 285–8.
57. Pretty, J. R., Duckworth, D. C., and Van Berkel, G. J. (1997) Anodic stripping voltammetry coupled on-line with inductively coupled plasma mass spectrometry: optimization of a thin-layer flow cell system for analyte signal enhancement. *Anal. Chem.*, **69**, 3544–51.
58. Pretty, J. R., Duckworth, D. C., and Van Berkel, G. J. (1998) Electrochemical sample pretreatment coupled on-line with ICP-MS: analysis of uranium using an anodically conditioned glassy carbon working electrode. *Anal. Chem.*, **70**, 1141–8.
59. Baca, A. J., de la Ree, A. B., Zhou, F., and Masson, A. Z. (2003) Anodic stripping voltammetry combined on-line with inductively coupled plasma-MS via a direct-injection high-efficiency nebulizer. *Anal. Chem.*, **75**, 2507–11.
60. Coedo, A. G., Padilla, I., Dorado, T., and Alguacil, F. J. (1999) A micro-scale mercury cathode electrolysis procedure for on-line flow injection inductively coupled plasma mass spectrometry trace elements analysis in steel samples. *Anal. Chim. Acta*, **389**, 247–255.
61. Packer, A. P., Gervasio, A. P. G., Miranda, C. E. S., Reis, B. F., Menegário, A. A., and Giné, M. F. (2003) On-line electrolytic dissolution for lead determination in high-purity copper by isotope dilution inductively coupled plasma mass spectrometry. *Anal. Chim. Acta*, **485**, 145–53.
62. Luque de Castro, M. D. and Papaefstathiou, I. (1998) Analytical pervaporation: a new separation technique. *Trends Anal. Chem.*, **17**, 41–9.
63. Gorbounov, V., Kuban, P., Dasgupta, P. K., and Temkin, H. (2003) A nanoinjector for microanalysis. *Anal. Chem.*, **75**, 3919–23.
64. Pergantis, S. A., Heithmar, E. M., and Hinners, T. A. (1995) Microscale flow injection and microbore high-performance liquid chromatography coupled with inductively coupled plasma mass spectrometry via a high-efficiency nebulizer. *Anal. Chem.*, **67**, 4530–5.
65. Wangkarn, S. and Pergantis, S. A. (1999) Determination of arsenic in organic solvents and wines using microscale flow injection inductively coupled plasma mass spectrometry. *J. Anal. At. Spectrom.*, **14**, 657–62.
66. Kahen, K., Strubinger, A., Chirinos, J. R., and Montaser, A. (2003) Direct injection high efficiency nebulizer-inductively coupled plasma mass spectrometry for analysis of petroleum samples. *Spectrochim. Acta*, B, **58**, 397–413.
67. Björn, E. and Frech, W. (2003) Introduction of high carbon content solvents into inductively coupled plasma mass spectrometry by a direct injection high efficiency nebulizer. *Anal. Bioanal. Chem.*, **376**, 274–8.

5.3 ELECTROTHERMAL VAPORISATION AS A MEANS OF SAMPLE INTRODUCTION IN ICP-MS

Frank Vanhaecke

5.3.1 Introduction

Very shortly after the commercial introduction of ICP-MS in 1983, the analytical community became aware of the drawbacks of pneumatic nebulisation (PN) as a means of sample introduction. The combination of a concentric or cross-flow pneumatic nebuliser with a spray chamber only provides an analyte introduction efficiency of 1–2%.[1,2] Additionally, relatively large amounts ($\geq$1 mL) of sample solution are required and the simultaneous introduction of analyte element(s), matrix components and solvent(s) into the ICP gives rise to both spectral (overlap of the signals of the analyte ion(s) and those of atomic or molecular ions showing the same nominal mass-to-charge ratio) and non-spectral (matrix-induced signal suppression or enhancement) interferences. These disadvantages served as strong incentives for the development of improved sample introduction systems and in this context, electrothermal vaporisation (ETV) was suggested as an interesting alternative. In fact, already in 1983 this combination of ETV and ICP-MS was described by Gray and Date.[3]

In ETV-ICP-MS, an aliquot of sample solution (typically 5–40 μL) is introduced into a small graphite furnace, very similar to that used in electrothermal atomic absorption spectrometry (ETAAS), also known as graphite furnace atomic absorption spectrometry (GFAAS). By resistive heating of the graphite tube, the sample solution is subjected to a multi-step temperature programme[4] (Figure 5.16). During the first step, gentle drying of the sample solution is

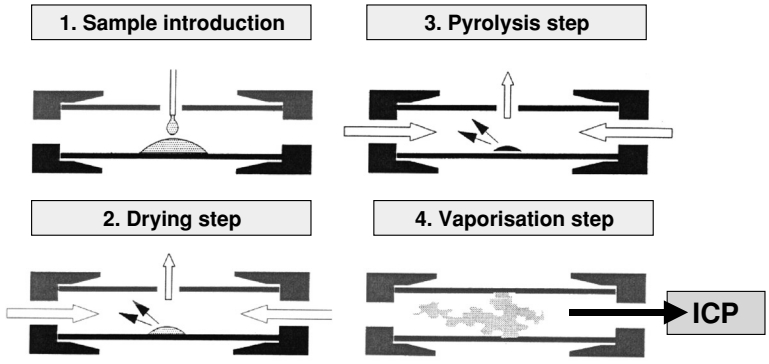

Figure 5.16 Subsequent steps in sample introduction by means of electrothermal vaporisation (ETV) from a graphite furnace: (1) liquid sample introduction into the graphite furnace using a micropipette or autosampler, (2) gentle drying at a temperature slightly higher than 100 °C, (3) pyrolysis, aiming at efficient removal of the matrix components and (4) analyte vaporisation. During steps (2) and (3) the dosing hole may be left open to vent the vapours generated, during step (4), the analyte vapours are transported into the ICP using an Ar carrier gas. The furnace can be subsequently cleaned by heating it to the highest temperature attainable (not depicted).[4] With the most advanced ETV devices, temperature, duration and ramp (~heating rate or time elapsed to reach the desired end temperature) can be selected for each step. Subjecting the furnace (and sample) to an entire heating cycle typically takes a couple of minutes.

accomplished at a temperature slightly higher than 100 °C. Subsequently, the sample undergoes pyrolysis at a higher temperature. This thermal pre-treatment aims at removal (as complete as possible) of the matrix components, while premature analyte losses have to be avoided at all cost. After pyrolysis, the temperature is rapidly increased, such that the target analytes are vaporised and transported into the ICP by means of an Ar carrier gas. Finally, the furnace is cleaned via heating to the highest temperature attainable. In rare cases, the analytes are more volatile than (most of) the matrix components. Under these conditions, vaporisation of the target element(s) is accomplished at a relatively low temperature at which (most of) the matrix remains in the furnace.[5,6] It is worthwhile to point out that while in AAS, atomisation in the furnace is required, in ETV-ICP-MS volatilisation suffices as in the high temperature ICP, efficient atomisation and subsequent ionisation are guaranteed. In addition to these more 'traditional' graphite furnaces, other ETV devices whereby the analytes are vaporised from a metal (e.g. W or Ta) coil or filament have also been developed.[7] Alternatively, metal foil inserts can also be used in a graphite furnace to modify the surface from which the analyte elements are vaporised.[8] The vast majority of real-life applications reported on in the literature, however, have been carried out using 'standard' graphite furnaces.

For analysis of sample solutions, ETV-ICP-MS seemed promising as the analyte transport efficiency is considerably higher ($\geq$10%)[9,10] than that offered by PN, only μL- amounts of sample solution are required for analysis, and since the volatilisation of solvent(s), matrix components and analyte element(s) can be separated in time, both spectral and non-spectral interferences can be alleviated. On the other hand, when using ETV for sample introduction, transient signals, with a typical duration of a few seconds only, are obtained instead of stable continuous signals (see Figures 5.17[11] and 5.18[12]). This limits the multi-element capabilities of ICP-MS (*vide infra*)

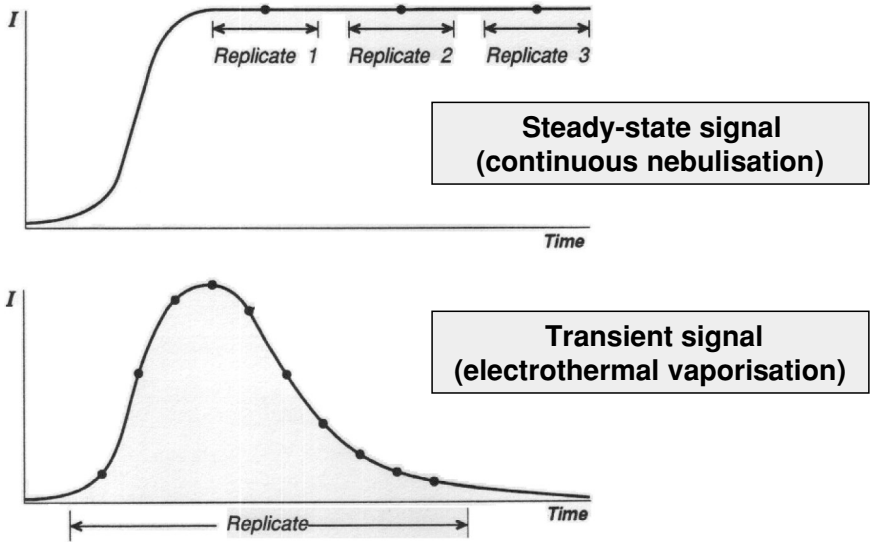

Figure 5.17 Steady-state signal, as obtained when using continuous nebulisation for sample introduction, versus transient signal, as obtained when using ETV. While with a steady-state signal replicate measurements can be carried out easily, each replicate measurement with ETV-ICP-MS requires introduction of a new sample aliquot into the furnace.[11]

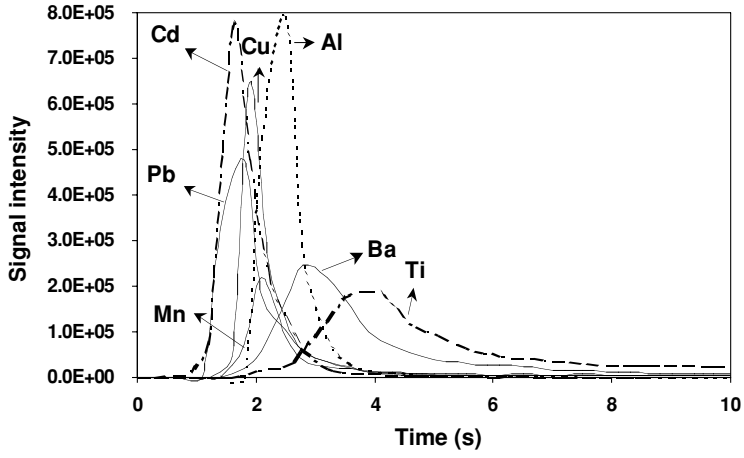

Figure 5.18 Transient signals as obtained in a real-life application (multi-element trace analysis of polyethylene).[12] More volatile elements (e.g., Cd or Pb) are volatilised more rapidly and show a narrower peak profile than more refractory elements (e.g., Ba or Ti).

and results in a deteriorated precision (from 1–2% RSD with PN to typically 5–10% with ETV). Successful use of ETV-ICP-MS also requires greater operator skills than does PN-ICP-MS.

Since the late 1980s, great improvements have been made in sample introduction techniques and some of the features that could be considered as unique for ETV at one time are now also offered by other, more practicable techniques. Miniaturised nebulisers offer stable sample introduction into the ICP at μL/min flow rates at an improved analyte introduction efficiency[13–15] and when combined with a (membrane) aerosol desolvation unit,[16] the occurrence of O- and Cl-based molecular ions can be strongly reduced. Compared to traditional pneumatic nebulisation, ultrasonic nebulisation,[2,17] for example, provides a 10-fold (or more) improved analyte introduction efficiency. While coping (at least to some extent) with the original disadvantages of PN, the multi-element capabilities and typical precision of ICP-MS are preserved completely as a result of the continuous sample introduction with these devices. But despite the success of, among others, these miniaturised and ultrasonic nebulisers, there is still interest in ETV-ICP-MS, mainly because this approach permits successful analysis of very demanding samples, such as organics, slurries and even dry solid materials. It can be stated that while ETV has failed in becoming a 'standard' sample introduction strategy, it is extremely useful in niche applications.

5.3.2 Analyte/matrix separation

With the standard sample introduction system, consisting of a pneumatic nebuliser and spray chamber, only droplets <10 μm in diameter are permitted to reach the ICP. This selection results in an analyte introduction efficiency of only 1–2%, but is required to maintain plasma stability and ensure efficient desolvation, atomisation and ionisation in the ICP. Additionally, the total concentration of dissolved solids is usually limited to a maximum of 2 g/L only, to prevent clogging of the nebuliser, torch injector tube and/or sampling cone and skimmer orifices, and also to limit signal suppression and long-lasting memory effects. Of course, when using ETV for sample

introduction, maintenance of the plasma stability is also of importance. A first prerequisite in accomplishing this goal is separation of the vaporisation of the solvent(s) and sample matrix from that of the analyte elements. In the easiest cases, this can be realised by optimisation of the temperature programme the sample is subjected to (temperature and duration of subsequent steps). It is preferable (or even mandatory) that the vapours originating during drying and pyrolysis are not directed into the ICP. With the HGA-600 MS (an ETV unit formerly available from Perkin-Elmer), for example, this is accomplished by using opposing flows of Ar that remove the vapours through the dosing hole during the drying, pyrolysis and high-temperature cleaning steps of the programme (Figure 5.19).[18] Immediately before the vaporisation commences, a graphite probe automatically seals the dosing hole and the vapours formed during this step are transported into the ICP by means of an Ar carrier gas (Figure 5.18). In other set-ups, a three-way valve is sometimes used to vent the vapours generated during the drying, pyrolysis and high-temperature cleaning steps.[19]

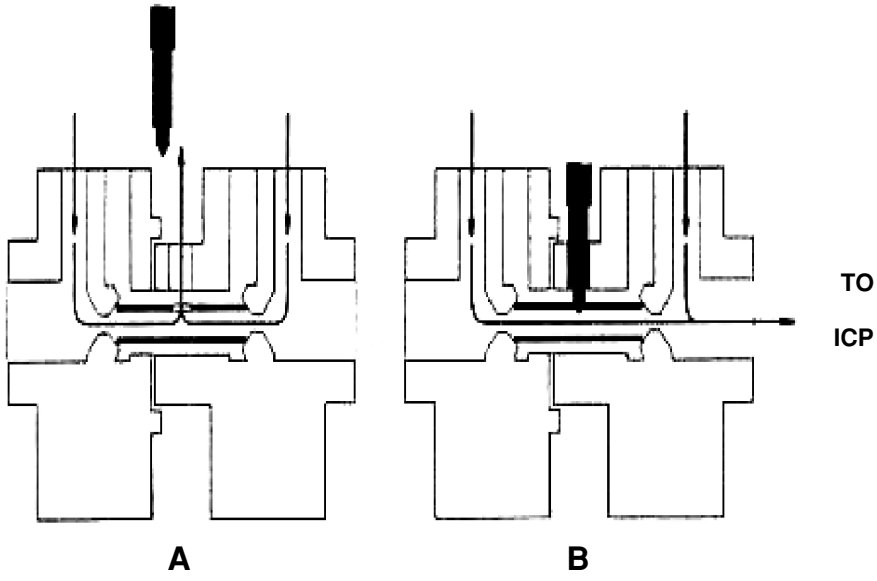

Figure 5.19 Schematic representation of the HGA-600 MS ETV-unit from Perkin-Elmer. Opposing flows of Ar remove the vapours through the dosing hole during drying, pyrolysis and cleaning steps. Immediately before vaporisation, a graphite probe automatically seals the dosing hole. During the vaporisation stage, the analyte vapours are transported into the ICP by means of an Ar carrier gas.[18]

In more demanding applications, optimisation of the multi-step temperature programme often does not suffice to separate the vaporisation of the analyte elements from that of dominant matrix components in time. In this instance, the use of a chemical modifier may offer a solution. The most classical example is palladium, which is capable, once in reduced form, of stabilising a variety of analyte elements, thereby permitting a significantly higher pyrolysis temperature without resulting in analyte losses.[20] Additionally, it has also been reported that the use of palladium improves the analyte transport efficiency by providing 'nuclei' on which the analyte vapour can readily condense.[21] Often, the application of such a modifier has even been reported as being mandatory for obtaining linear calibration curves. Of course, not only palladium is used in this

context. Zirconium, for example, was used in the context of the determination of trace amounts of phosphorus in high purity iron.[22] Phosphorus affects the chemical and physical properties of cast iron and steel. The bulk of the iron matrix was removed by means of solvent extraction. The remaining Fe could be selectively removed during the pyrolysis step on condition that phosphorus was thermally stabilised by using zirconium as a chemical modifier. Other modifiers aim at enhancing the volatility of the matrix components, thereby stimulating their removal at a lower pyrolysis temperature. In the analysis of geological samples, for example, the selective removal of silica can be promoted by addition of an aliquot of HF into the graphite furnace.[23] Finally, a modifier can also be added with the purpose of facilitating analyte vaporisation. For example, by addition of trifluoromethane[24] or PTFE,[25] the vaporisation of rare earth elements (REE) was promoted, facilitating their determination by means of ETV-ICP-MS in body fluids and tissues and in high purity Y_2O_3, respectively.

5.3.3 ETV-ICP-MS for analysis of sample solutions

Of course, ETV-ICP-MS is applicable to the analysis of all aqueous sample solutions that are amenable to analysis via PN-ICP-MS. However, as a result of the transient nature of the signals, the precision attainable is typically limited to between 5 and 10% RSD, while the multi-element capabilities are reduced. Therefore, only for those sample types for which analysis with PN-ICP-MS is problematic or at least not self-evident does the use of ETV-ICP-MS become preferable. Bettinelli *et al.*[26] used ETV-ICP-MS for trace element analysis of bee honey, used as an indicator of environmental pollution. Due to the rather complex composition of this viscous product and the typically very low trace element concentrations, an appropriate sample preparation procedure for PN-ICP-MS is not self-evident. With ETV-ICP-MS, however, the sample preparation was limited to simple dilution with water. Eighteen target elements – divided into two groups – were determined using this approach. Huang and Jiang analysed edible oils by means of ETV-ICP-MS.[27] In this instance, the sample preparation consisted of emulsification with a mixture of H_2O, H_2O_2, HNO_3 and a detergent (Triton X-100). Also for the analysis of lubricating oil[28] and gasoline,[29] ETV was reported to offer important advantages over PN for sample introduction. In this context, O_2 is sometimes added into the furnace to facilitate removal of organic matrix components during the thermal pre-treatment,[30] albeit at the cost of more rapid tube deterioration.

As a result of the difficult nature of the samples typically subjected to analysis via ETV-ICP-MS, external calibration versus an aqueous standard solution is only applicable in a minority of applications. Most often, single standard addition or isotope dilution is used for quantification purposes. Of course, when the ETV unit is equipped with an autosampler, the addition of aliquots of modifier, standard or isotopic spike solution into the graphite furnace is facilitated.

The loss of multi-element capabilities has often been mentioned as one of the most important disadvantages of ETV-ICP-MS with a quadrupole-based instrument. Since with time-of-flight (TOF)-ICP-MS[31] thousands of complete mass spectra can be obtained per second, it should be the mass analyser of choice for ETV-ICP-MS applications.[32] However, Resano *et al.*[33] systematically studied the multi-element capabilities of ETV-ICP-MS with a quadrupole-based instrument and came to the conclusion that for signals with a duration of 1.5–2 s, up to 20 signals could be monitored without significant losses in detection power or precision. Basically, there is no deterioration of the figures of merit as long as at least 3 to 4 data points are available for description of the signal profile. If necessary, a further extension of the multi-element capabilities

can be accomplished, for example, by promoting peak broadening[34] by using longer tubing, a lower carrier gas flow rate or an expansion chamber.[35] All of these approaches however lead to a lower signal-to-background ratio. In a more recent approach, the analyte vapours coming from the furnace were trapped in a cylindrical container, the content of which was subsequently transported into the ICP in a controlled way, i.e. by using a moving piston to evacuate the cylinder.[36] This approach results in the generation of a square wave signal profile, enabling the use of the signal height instead of the integrated signal intensity for quantitative analysis and thus enhancing the multi-element capabilities of ETV-ICP-MS considerably. Alternatively, further optimisation of the temperature programme may result in the separation of the vaporisation of the target elements in time.[33] Hence, it seems that nowadays, the characteristics of the mass spectrometric device should no longer seriously limit the multi-element characteristics of ETV-ICP-MS. Finding a furnace temperature programme suited for all target elements on the other hand may constitute a bigger challenge.

5.3.4 ETV-ICP-MS for analysis of solid samples

It was indicated before that in the case of demanding applications, the advantages of using ETV for sample introduction become obvious. In fact, ETV even opens the possibility for direct analysis of solid samples, introduced into the furnace either as slurries (slurry sampling) or as 'dry' material (solid sampling).

Complete sample dissolution is not always readily achievable. Some materials cannot, or only with great difficulty, be brought into solution. In such instances, slurry or solid sampling may constitute an attractive alternative. In the case of slurry sampling, the material is ground to a particle size that is sufficiently small and the particles thus obtained are transferred into a solvent. Although this grinding brings about a risk of contamination, it improves the sample homogeneity, aids (partial) extraction of the analyte(s) into the solvent and helps in avoiding errors as a result of sedimentation. Gravitational settling of the particles can be further counteracted by sonication. Compared to 'true' solid sampling, working with slurries shows some practical advantages, since automation is much easier as a traditional autosampler can be used, and unlike solids, slurries can be diluted to bring the analyte concentration to within the detector range.

Both Mierzwa and Yang[37] and Wende and Broekaert[38] described the use of slurry sampling–ETV-ICP-MS for the trace analysis of Al_2O_3 ceramic powders. Al_2O_3 is a basic component in the production of many advanced ceramic materials, the properties of which strongly depend on the concentration of the trace elements present either as dopants or as contaminants. Since dissolution of Al_2O_3 – especially of the corundum variety – is not easily achievable, both groups preferred analysis of Al_2O_3 slurries instead. From the literature, it is clear that practically all types of solid samples (e.g. plant material, animal tissue, dust, coal, soil) can be converted into slurries that can then be analysed via ETV-ICP-MS.

The direct analysis of 'dry' solid samples (solid sampling) is even more straightforward than that of slurries and it also constitutes an excellent approach for sample materials that are hard to dissolve. Even for materials that are not so difficult to take into solution, solid sampling offers advantages. Obviously, the necessary amount of sample pre-treatment is decreased, such that the speed of analysis is increased and the risk of contamination and/or analyte losses is reduced. Since the sample is not diluted, lower limits of detection are attainable. Sample manipulation,

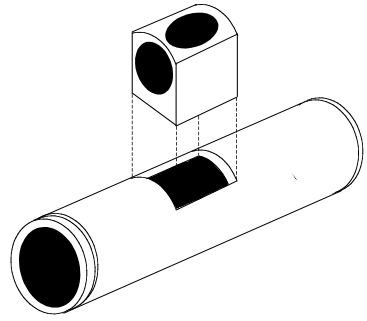

Figure 5.20 Cup-in-tube technique for solid sampling ETV-ICP-MS. Solid material is introduced into the cup, which is subsequently inserted into the graphite cylinder.

however, is somewhat more complex and cannot be easily automated. Sample dilution is not possible, or at least extremely difficult, and the results obtained are characterised by a larger uncertainty (poorer precision). The capabilities and limitations of solid sampling ETV-ICP-MS and a description of the circumstances under which this approach is really useful – basically, whenever high analysis speed is more important than obtaining an excellent precision – have been discussed by Belarra *et al*.[39] Vanhaecke *et al*.[40] reported on the use of solid sampling ETV-ICP-MS for various real-life applications. In the applications reported on, introduction of solid samples was enabled by either using the cup-in-tube (Figure 5.20) technique or by loading the solid material onto a graphite holder ('boat'), subsequently inserted into the graphite cylinder. The latter approach was preferred for powdered materials. The rapid determination of dopants, catalyst residues and unwanted contaminants in various types of plastics was shown to be often more rapid, straightforward and practicable than with other techniques, while limits of detection of approximately 1 ng/g were typical. In all cases, either external calibration or single standard addition (both using an aqueous standard solution) was used. One of the more challenging analyses reported on was the determination of Si in polyamide,[41] where the pitfalls typical of PN (i.e. contamination and/or analyte loss during sample digestion and spectral interferences at all of the mass-to-charge ratios of interest) could be circumvented by opting for ETV as the means of sample introduction.

As a result of the possibility of analysing micro-samples (5–40 μL of slurries or ∼mg amounts of solid samples), both slurry sampling[42] and solid sampling ETV-ICP-MS[43] have been used to assess the homogeneity of the distribution of trace elements in certified reference materials. It was shown that very often, materials can be considered as being homogeneous at much lower sample amounts than that specified as the minimum required in the corresponding certificates.

5.3.5 Overcoming spectral overlap

Whether aqueous solutions, slurries or dry solid samples are analysed, spectral interferences can often be avoided by using the graphite furnace as a thermochemical reactor. Basically, by using an appropriate temperature programme, if necessary in combination with a carefully selected chemical modifier, vaporisation (and therefore removal) of parent elements that give rise to

molecular ions that interfere with the analyte element(s), can be achieved prior to that of the target elements.

Marshall and Franks[44] were among the first to point out the improved limits of detection attainable for elements such as P ($^{31}P^+/^{14}N^{16}O^1H^+$), V ($^{51}V^+/^{35}Cl^{16}O^+$) and Ti ($^{48}Ti^+/^{32}S^{16}O^+$) as a result of the possibility of interference removal (or at least reduction) offered by ETV. Whittaker and co-workers[45] aimed at obtaining insight into the uptake of Fe from nutrition by carrying out stable isotopic tracer experiments. In this study, $^{54}Fe/^{56}Fe$ and $^{57}Fe/^{56}Fe$ isotope ratios had to be determined in blood serum collected at various intervals after administration of ^{54}Fe (oral) and ^{57}Fe (intravenous) tracers. PN was discarded as a means of sample introduction in this study, because under these conditions, the occurrence of Ar-containing (e.g. ArO^+, ArN^+ and $ArOH^+$) and other (e.g. CaO^+, $CaOH^+$ and $ClOH^+$) molecular ions prevented accurate results from being obtained. Owing to the 'dry' plasma conditions with ETV, the signal intensity for these molecular ions was reduced to such an extent that accurate isotope ratio determination was enabled. The possibility of analysing small sample sizes presented an important additional advantage. Yu *et al.*[46] used ETV-ICP-MS for the determination of S in fossil fuels, the primary contribution to atmospheric S contamination. The use of isotope dilution for calibration necessitated monitoring of the signals of both ^{32}S and ^{34}S. With PN-ICP-MS, both of these signals are subject to severe spectral interference as a result of the occurrence of O-containing molecular ions, primarily the notorious oxygen dimer signals, O_2^+). When using ETV for sample introduction however, a water-free sample aerosol is generated and introduced into the ICP, which leads to a dramatic reduction in the level of the oxygen-based interferences. This dry plasma also has a higher temperature, which leads to enhanced ionization (and hence greater sensitivity) of high ionization potential elements like sulfur. The occurrence of oxygen in the ICP was further reduced by adding N_2 as an oxygen scavenger into the Ar supply for the ICP. Song *et al.*[47] even succeeded in overcoming the spectral overlap of isobaric nuclides, an achievement which, considering the high mass resolution required, is far beyond the capabilities of present-day sector field ICP-MS.[48] The determination of radionuclides in environmental samples is of great importance, especially since the Chernobyl accident. Various authors have demonstrated that for long-lived radionuclides, ICP-MS offers lower limits of detection than radiometric methods. In many instances however, the sample pre-treatment requires the application of chemical separation techniques to avoid isobaric overlap. Song *et al.* aimed at the determination of radiocaesium in environmental matrices. The orders of magnitude more abundant Ba in the samples could be selectively removed during the pyrolysis step by adding KSCN as a chemical modifier, such that the radionuclides of interest, ^{135}Cs and ^{137}Cs, could be measured interference-free with sub-ng/L limits of detection. Also the use of solid sampling ETV-ICP-MS for the determination of platinum group elements (PGEs), originating from car exhaust catalysts, in various environmental samples (grass, tunnel dust and atmospheric aerosol) has been described.[49] Due to the low concentration of the elements of interest with respect to more abundant elements in the samples, such as Cu, Hf, Pb, Rb, Sr, Y, Zn and Zr, polyatomic ions (for example, argides such as $ArCu^+$ and oxides such as HfO^+) and doubly charged ions (e.g. Pb^{2+}) interfere with the determination when using PN-ICP-MS. Not all of these interferences can be resolved by applying a higher mass resolution in a sector field ICP-MS instrument. Therefore, chemical separation techniques are often used to isolate the target elements from the 'parent' elements of the interfering ions. With ETV-ICP-MS, the aforementioned parent elements could be removed by thermal pre-treatment, enabling rapid and accurate PGE determination with sub-ng/g limits of detection.

A review of applications wherein the graphite furnace has been used as a thermochemical reactor to solve more complicated analytical problems has been published by Sturgeon and Lam.[50]

5.3.6 ETV-ICP-MS in elemental speciation

Elemental speciation aims at the separation, identification and quantification of the chemical forms in which the (trace) elements of interest are present. This can be accomplished by coupling a chromatographic (e.g. HPLC or GC) or electrophoretic separation technique on-line to an ICP-MS instrument. In this context, ETV is of little use as it is a 'discrete' sample introduction system that does not permit the continuous introduction of sample into the ICP.

Chery *et al.* however reported on the use of the combination of polyacrylamide gel electrophoresis (PAGE) and ETV-ICP-MS for investigating the Se-containing proteins present in selenised yeast extract.[51] After the separation procedure, the protein spots in the electrophoresis gel were revealed by silver staining and ETV-ICP-MS was applied for Se quantification. For this purpose, the gel obtained was cut into fragments that were individually analysed using ETV-ICP-MS. Quantification was accomplished via external calibration versus an aqueous standard solution added onto a blank gel. The latter provided matrix matching and was obtained by soaking a gel in an albumin solution, followed by silver staining. Te was used as an internal standard to correct for variations in matrix effects and in vaporisation and transport efficiencies. By using a glutathione peroxidase standard, complete recovery could be demonstrated, while the chromatographic resolution obtained exceeded that offered by size exclusion chromatography (HPLC)-ICP-MS.

Willie *et al.*[52] used ETV-ICP-MS to determine the content of inorganic mercury and methylmercury (MM) in fish tissue using an approach based on the different volatilities of the target compounds. In the first measurement, Hg was vaporised from the samples of interest, solubilised using TMAH, and introduced into the ICP, so that the total content of this element could be determined. For the second measurement, iodoacetic acid, sodium thiosulfate and acetic acid were added to the sample. During the drying step of the temperature programme, MM iodide is already removed from the furnace, such that during the vaporisation step, only the inorganic fraction of the Hg is introduced into the ICP and measured. Gelaude *et al.*[53] developed an even more elegant method for Hg speciation in fish tissue based on ETV-ICP-MS. By submitting freeze-dried fish tissue to a multi-step heating programme, the vaporisation of methylmercury (~150–200 °C) and inorganic Hg (~400–700 °C) could be separated from one another in time (Figure 5.21). Species-unspecific isotope dilution[54] was enabled by directing a gaseous Hg flow, isotopically enriched in ^{200}Hg, through the furnace while the sample was subjected to the multi-step heating programme. Limits of detection in the low ng/g range made the method fit-for-purpose and accurate results were obtained for the *Lobster Hepatopancreas* certified reference material TORT-2 (National Research Council of Canada).

5.3.6 Conclusions

ETV has failed to become a 'standard' sample introduction technique, but there is ample evidence in the current literature for its unmatched capabilities for handling difficult sample types.

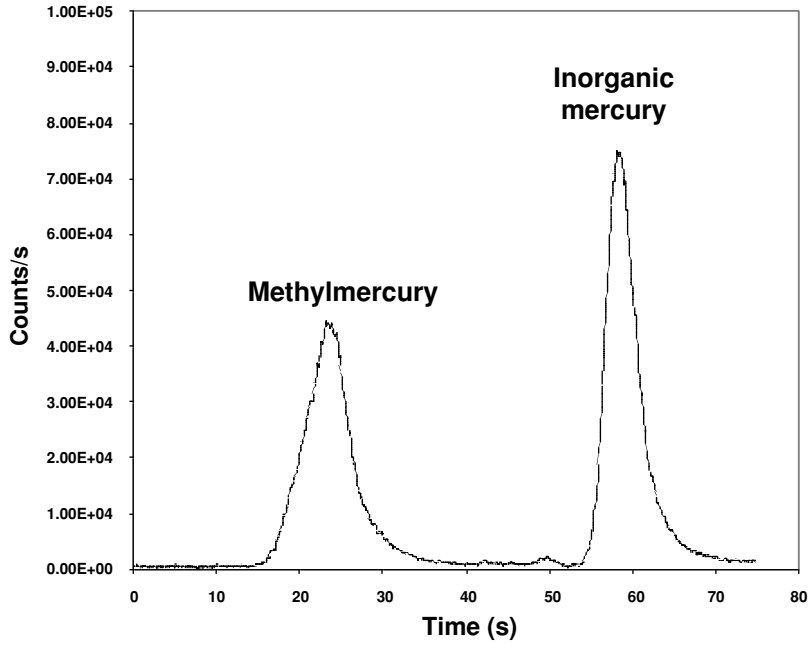

Figure 5.21 Elemental speciation with ETV-ICP-MS.[53] Separation of the vaporisation of methylmercury (~150–200 °C) from that of inorganic mercury (~400–700 °C) by furnace temperature optimisation.

Therefore the present lack of interest of instrument manufacturers for developing, optimising and selling these devices is unfortunate.

References

1. Browner, R. F. and Boorn, A. W. (1984) Sample introduction – the Achilles heel of atomic spectroscopy. *Anal. Chem.*, **56**, A786–A798.
2. Koropchak, J. A. (1993) Liquid sample introduction to ICP spectrometries. *Spectroscopy*, **8**, 21–30.
3. Gray, A. L. and Date, A. R. (1983) Inductively coupled plasma source-mass spectrometry using continuum flow ion extraction. *Analyst*, **108**, 1033–50.
4. Ebdon, L., Evans, E. H., Fisher, A., and Hill, S. J. (1998) *An Introduction to Analytical Atomic Spectrometry*, Wiley, Chichester.
5. Hinds, M. W., Gregoire, D. C., and Ozaki, E. A. (1997) Direct determination of volatile elements in nickel alloys by electrothermal vaporization inductively coupled plasma mass spectrometry. *J. Anal. At. Spectrom.*, **12**, 131–5.
6. Vanhaecke, F., Gelaude, L., Moens, L., and Dams, R. (1999) Solid sampling electrothermal vaporization inductively coupled plasma mass spectrometry for the direct determination of Hg in sludge samples. *Anal. Chim. Acta*, **383**, 253–61.
7. Tsukahara, R. and Kubota, M. (1990) Some characteristics of inductively coupled plasma mass spectrometry with sample introduction by tungsten furnace electrothermal vaporization. *Spectrochim. Acta* B, **45**, 779–87.

8. Goltz, D. M., Gregoire, D. C., and Chakrabarti, C. L. (1996) Characterization and evaluation of Mo, Ta, Re and W metal vaporization surfaces for electrothermal vaporization ICP mass spectrometry. *Can. J. App. Spectrosc.*, **41**, 70–6.
9. Gregoire, D. C. and Sturgeon, R. E. (1999) Analyte transport efficiency with electrothermal vaporization inductively coupled plasma mass spectrometry. *Spectrochim. Acta* B, **54**, 773–86.
10. Friese, K. C., Watjen, U., and Grobecker, K. H. (2001) Analyte transport efficiencies in electrothermal vaporization for inductively coupled plasma mass spectrometry. *Fresenius' J. Anal. Chem.*, **370**, 843–9.
11. (1992) Elan5000 User's Manual, 0993-8429, May Rev. B.
12. Vanhaecke, F., Resano, M., Verstraete, M., Moens, L., and Dams, R. (2000) Multielement analysis of polyethylene using solid sampling electrothermal vaporization ICP mass spectrometry. *Anal. Chem.*, **72**, 4310–6.
13. Nam, S. H., Lim, J. S., and Montaser, A. (1994) High-efficiency nebulizer for argon inductively coupled plasma mass spectrometry. *J. Anal. At. Spectrom.*, **9**, 1357–62.
14. Vanhaecke, F., Van Holderbeke, M., Moens, L., and Dams, R. (1996) Evaluation of a commercially available microconcentric nebulizer for inductively coupled plasma mass spectrometry. *J. Anal. At. Spectrom.*, **11**, 543–8.
15. Lofthouse, S. D., Greenway, G. M., and Stephen, S. C. (1997) Microconcentric nebulizer for the analysis of small sample volumes by inductively coupled plasma mass spectrometry. *J. Anal. At. Spectrom.*, **12**, 1373–6.
16. Minnich, M. G. and Houk, R. S. (1998) Comparison of cryogenic and membrane desolvation for attenuation of oxide, hydride and hydroxide ions and ions containing chlorine in inductively coupled plasma mass spectrometry. *J. Anal. At. Spectrom.*, **13**, 167–74.
17. Fassel, V. A. and Bear, B. R. (1986) Ultrasonic nebulization of liquids for analytical inductively coupled plasma atomic spectroscopy – an update. *Spectrochim. Acta* B, **41**, 1089–113.
18. (1995/96) PE Atomic Spectroscopy Supplies Catalog.
19. Vanhaecke, F., Boonen, S., Moens, L., and Dams, R. (1995) Solid sampling electrothermal vaporization inductively coupled plasma mass spectrometry for the determination of arsenic in standard reference materials of plant-origin. *J. Anal. At. Spectrom.*, **10**, 81–7.
20. Volynsky, A., Tikhomirov, S., and Elagin, A. (1991) Proposed mechanism for the action of palladium and nickel modifiers in electrothermal atomic absorption spectrometry. *Analyst*, **116**, 145–8.
21. Ediger, R. D. and Beres, S. A. (1992) The role of chemical modifiers in analyte transport loss interferences with electrothermal vaporization ICP mass spectrometry. *Spectrochim. Acta* B, **47**, 907–22.
22. Hughes, D. M., Gregoire, D. C., Naka, H., and Chakrabarti, C. L. (1998) Determination of trace amounts of phosphorus in high purity iron by electrothermal vaporization inductively coupled plasma mass spectrometry. *Spectrochim. Acta* B, **53**, 1079–85.
23. Ben Younes, M. E., Gregoire, D. C., and Chakrabarti, C. L. (1999) Vaporization and removal of silica for the direct analysis of geological materials by slurry sampling electrothermal vaporization inductively coupled plasma mass spectrometry. *J. Anal. At. Spectrom.*, **14**, 1703–8.
24. Buseth, E., Wibetoe, G., and Martinsen, I. (1998) Determination of endogenous concentrations of the lanthanides in body fluids and tissues using electrothermal vaporization inductively coupled plasma mass spectrometry. *J. Anal. At. Spectrom.*, **13**, 1039–49.
25. Cai, B., Hu, B., and Jiang, Z. C. (2000) Direct determination of trace rare earth elements in high purity Y_2O_3 using fluorination assisted electrothermal vaporization inductively coupled plasma atomic emission spectrometry with slurry sampling. *Fresenius' J. Anal. Chem.*, **367**, 259–63.

26. Bettinelli, M., Baroni, U., Spezia, S., and Terni, C. (2000) Determination of trace elements in honey using ETV-ICP-MS. *At. Spectrosc.*, **21**, 195–204.
27. Huang, S. J. and Jiang, S. J. (2001) Determination of Zn, Cd and Pb in vegetable oil by inductively coupled plasma mass spectrometry. *J. Anal. At. Spectrom.*, **16**, 664–8.
28. Escobar, M. P., Smith, B. W., and Winefordner, J. D. (1996) Determination of metallo-organic species in lubricating oil by electrothermal vaporization inductively coupled plasma mass spectrometry. *Anal. Chim. Acta*, **320**, 11–7.
29. Saint'Pierre, T. D., Dias, L. F., Pozebon, D., Aucelio, R. Q., Curtius, A. J., and Welz, B. (2002) Determination of Cu, Mn, Ni and Sn in gasoline by electrothermal vaporization inductively coupled plasma mass spectrometry and emulsion sample introduction. *Spectrochim. Acta* B, **57**, 1991–2001.
30. Fonseca, R. W., Miller-Ihli, N. J., Sparks, C., Holcombe, J. A., and Shaver, B. (1997) Effect of oxygen ashing on analyte transport efficiency using ETV-ICP-MS. *Appl. Spectrosc.*, **51**, 1800–6.
31. Mahoney, P. P., Ray, S. J., and Hieftje, G. M. (1997) Time-of-flight mass spectrometry for elemental analysis, *Appl. Spectrosc.*, **51**, A16–A28.
32. Mahoney, P. P., Ray, S. J., Li, G. Q., and Hieftje, G. M. (1999) Preliminary investigation of electrothermal vaporization sample introduction for inductively coupled plasma time-of-flight mass spectrometry. *Anal. Chem.*, **71**, 1378–83.
33. Resano, M., Verstraete, M., Vanhaecke, F., and Moens, L. (2001) Evaluation of the multi-element capabilities of electrothermal vaporization quadrupole based ICP mass spectrometry. *J. Anal. At. Spectrom.*, **16**, 1018–27.
34. Venable, J. and Holcombe, J. A. (2001) Peak broadening from an electrothermal vaporization sample introduction source into an inductively coupled plasma. *Spectrochim. Acta* B, **56**, 1431–40.
35. Langer, D. and Holcombe, J. A. (1999) Simple transient extension chamber to permit full scans with electrothermal inductively coupled plasma mass spectrometry. *Appl. Spectrosc.*, **53**, 1244–50.
36. Balsanek, W. J., Venable, J. D., and Holcombe, J. A. (2003) Generation of a square wave inductively coupled plasma scanning mass spectrometry signal using electrothermal vaporization sample introduction. *J. Anal. At. Spectrom.*, **18**, 59–64.
37. Mierzwa, J. and Yang, M. H. (1998) Electrothermal vaporization inductively coupled plasma mass spectrometry for determination of metal impurities in slurries of aluminium oxide. *J. Anal. At. Spectrom.*, **13**, 667–71.
38. Wende, M. C. and Broekaert, J. A. C. (2001) Investigations on the use of chemical modifiers for the direct determination of trace impurities in Al_2O_3 ceramic powders by slurry electrothermal evaporation coupled with inductively coupled plasma mass spectrometry (ETV-ICP-MS). *Fresenius' J. Anal. Chem.*, **370**, 513–20.
39. Belarra, M. A., Resano, M., Vanhaecke, F., and Moens, L. (2002) Direct solid sampling with electrothermal vaporization/atomisation: what for and how? *Trends Anal. Chem.*, **21**, 828–39.
40. Vanhaecke, F., Resano, M., and Moens, L. (2002) Electrothermal vaporisation ICP-mass spectrometry (ETV-ICP-MS) for the determination and speciation of trace elements in solid samples – a review of real-life applications from the author's lab. *Anal. Bioanal. Chem.*, **374**, 188–95.
41. Resano, M., Verstraete, M., Vanhaecke, F., and Moens, L. (2002) Direct determination of trace amounts of silicon in polyamides by means of solid sampling electrothermal vaporization inductively coupled plasma mass spectrometry. *J. Anal. At. Spectrom.*, **17**, 897–903.
42. Miller-Ihli, N. J. and Baker, S. A. (2001) Microhomogeneity assessments using ultrasonic slurry sampling coupled with electrothermal vaporization isotope dilution inductively coupled plasma mass spectrometry. *Spectrochim. Acta* B, **56**, 1673–86.

43. Friese, K. C., Grobecker, K. H., and Watjen, U. (2001) Development of an electrothermal vaporization ICP-MS method and assessment of its applicability to studies of the homogeneity of reference materials. *Fresenius' J. Anal. Chem.*, **370**, 499–507.
44. Marshall, J. and Franks, J. (1990) Multi-element analysis and reduction of spectral interferences using electrothermal vaporization inductively coupled plasma mass spectrometry. *At. Spectrosc.*, **11**, 177–86.
45. Whittaker, P. G., Lind, T., Williams, J. G., and Gray, A. L. (1989) Inductively coupled plasma mass spectrometric determination of the absorption of iron in normal women. *Analyst*, **114**, 675–8.
46. Yu, L. L., Kelly, W. R., Fassett, J. D., and Vocke, R. D. (2001) Determination of sulfur in fossil fuels by isotope dilution electrothermal vaporization inductively coupled plasma mass spectrometry. *J. Anal. At. Spectrom.*, **16**, 140–5.
47. Song, M., Probst, T. U., and Berryman, N. G. (2001) Rapid and sensitive determination of radiocesium (Cs-135, Cs-137) in the presence of excess barium by electrothermal vaporization-inductively coupled plasma-mass spectrometry (ETV-ICP-MS) with potassium thiocyanate as modifier. *Fresenius' J. Anal. Chem.*, **370**, 744–51.
48. Jakubowski, N., Moens, L., and Vanhaecke, F. (1998) Sector field mass spectrometers in ICP-MS. *Spectrochim. Acta* B, **53**, 1739–63.
49. Vanhaecke, F., Resano, M., Pruneda-Lopez, M., and Moens, L. (2002) Determination of platinum and rhodium in environmental matrixes by solid sampling-electrothermal vaporization-inductively coupled plasma mass spectrometry. *Anal. Chem.*, **74**, 6040–8.
50. Sturgeon, R. E. and Lam, J. W. (1999) The ETV as a thermochemical reactor for ICP-MS sample introduction. *J. Anal. At. Spectrom.*, **14**, 785–91.
51. Chery, C. C., Chassaigne, H., Verbeeck, L., Cornelis, R., Vanhaecke, F., and Moens, L. (2002) Detection and quantification of selenium in proteins by means of gel electrophoresis and electrothermal vaporization ICP-MS. *J. Anal. At. Spectrom.*, **17**, 576–80.
52. Willie, S. N., Gregoire, D. C., and Sturgeon, R. E. (1997) Determination of inorganic and total mercury in biological tissues by electrothermal vaporization inductively coupled plasma mass spectrometry. *Analyst*, **122**, 751–4.
53. Gelaude, I., Dams, R., Resano, M., Vanhaecke, F., and Moens, L. (2002) Direct determination of methylmercury and inorganic mercury in biological materials by solid sampling-electrothermal vaporization-inductively coupled plasma-isotope dilution-mass spectrometry. *Anal. Chem.*, **74**, 3833–42.
54. Rottmann, L. and Heumann, K. G. (1994) Development of an online isotope-dilution technique with HPLC ICP-MS for the accurate determination of elemental species. *Fresenius' J. Anal. Chem.*, **350**, 221–7.

Chapter 6

Laser Ablation ICP-MS

Carla Vogt and Christopher Latkoczy

6.1 Introduction

Laser ablation ICP-MS is used for direct analysis of the elemental and isotopic composition of solid samples. Photons from the laser system are focused into a high peak power energy pulse that interacts with the sample. As a result of this interaction, small particles, atoms and ions are removed from the topmost atomic layers forming a laser-induced aerosol above the sample surface. The aerosol is then transported by an inert gas stream to the ICP-MS. After vaporization, atomization and ionization of the particles in the ICP, quadrupole, magnetic sector field or time-of-flight mass filters are used for mass separation. Because of the properties of the laser systems available today, bulk analysis with low spatial resolution (>100 μm) as well as local analysis with high spatial resolution (<20 μm) are possible. Since only small sample amounts are ablated per laser shot, a high sensitivity analytical detection system is a prerequisite for trace and ultratrace analysis.

In the following sections, the physical background of laser systems, the ablation process, important details of the technique, and applications and limitations of LA-ICP-MS are discussed in detail.

6.2 Lasers

6.2.1 Physical background

The word *laser* is an acronym for 'light amplification by stimulated emission of radiation', which summarily describes the controlled process by which photons are released from energized atoms in these devices. The emitted light of a laser is monochromatic, coherent and directional, which makes it well suited for directed interaction with samples.

To obtain these three properties, stimulated emission in the laser medium under conditions of population inversion is necessary. The achievement of a significant population inversion in atomic or molecular energy states is a precondition for laser action. A population inversion is characterized by a higher number of electrons in a specific high-energy state relative to the low-energy state. Electrons will normally reside in the lowest available energy state. They can be elevated to excited states by absorption, but no significant collection of electrons can be accumulated by absorption alone since both spontaneous emission and stimulated emission will bring them back down. To maintain the necessary population inversion, a pumping mechanism

Inductively Coupled Plasma Mass Spectrometry Handbook Edited by Simon M. Nelms
 ISBN: 978-1-405-10916-1

is used to elevate the electrons to a metastable state. Typically, very intense flashes of light or electrical discharges are used for this purpose.

In stimulated emission, a first photon can stimulate or induce atomic emission such that the subsequent emitted photon from a second atom vibrates with the same frequency and direction as the incoming photon. The rate of stimulated emission is proportional to the difference in the number of atoms in the excited state and the ground state, which in turn is affected by the average lifetime of the excited state and the average lifetime of the emission in the laser cavity.

The lasing medium is positioned between a pair of mirrors, one at each end. These cavity mirrors have to meet stringent wavelength-dependent specifications in order to cause amplification at a certain wavelength, while suppressing others. When a resonator structure is generated by the mirrors, photons that are emitted along the axis of the cavity can be reflected multiple times between the mirrors. These reflecting photons can interact with other excited atoms (same excitation level) and cause them to emit light (stimulated emission), ending up with a light amplification each time the photons pass through the amplifying lasing medium, and owing to the cascade effect many photons of the same wavelength and phase are released. One of the mirrors, called the total reflector, reflects almost all of the light, and the other mirror reflects between 20 and 98% of the incident light, depending upon the type of laser (Figure 6.1). The transmitted portion constitutes the output beam of the laser. Diameter, bandwidth and polarization quality are determined by the properties of the resonator mirrors and other optical components that lie along the axis of the optical resonator. The cavity ensures that the divergence of the beam is small. Only light that travels in a direction closely parallel to the axis of the cavity can undergo multiple reflections at the mirrors. Only certain frequencies of the radiation will set up standing waves within the cavity. These allowed frequencies of oscillation are referred to as axial or longitudinal modes of the cavity.

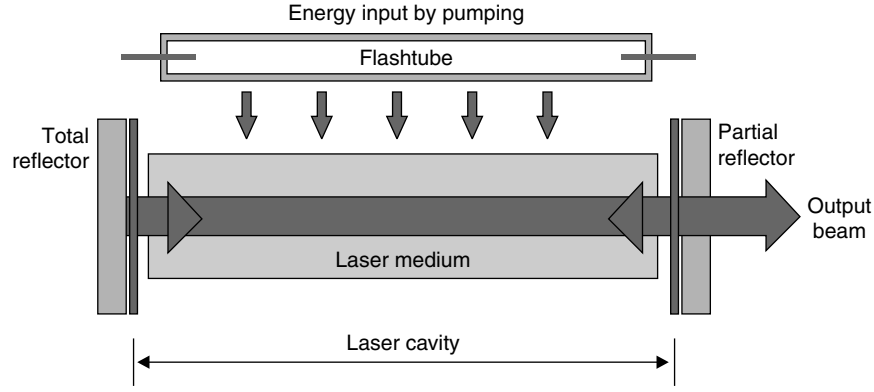

Figure 6.1 Laser principle.

6.2.2 Laser types used for analytical purposes

Several criteria have been used for classification; the most common is the laser material. Accordingly, lasers can be grouped as solid-state, gas, dye and semiconductor lasers.[1]

(a) Solid-state lasers

These are characterized as follows:

- The lasing material is distributed in a solid matrix, usually a transparent crystal or glass doped with small amounts of trivalent metal ions (Cr^{3+}, Nd^{3+})
- Excited by discharge lamps or lasers
- Ruby or Nd:YAG lasers
- Nd:YAG lasers
  - Nd-doped yttrium aluminum garnet, Nd-$Y_3Al_5O_{15}$
  - Four-level laser systems: by optical pumping, Nd ions are excited to a higher energy level (pump level), followed by a decay to a metastable level (laser level); generation of population inversion between upper and lower laser levels is the basic step for the laser process shown in Figure 6.2
  - Because of splitting of initial and final states for lasing action into several crystal field levels, several lasing wavelengths are possible (most powerful at 1064 nm)
  - Wavelengths in the UV region are obtained by harmonic generation (532, 355, 266, 213 nm)
- Tunable solid-state lasers use a lasing transition from a thermally excited electron in a broad continuum of high-level states to one of many vibronic levels
  - Ti:sapphire, Ti:Al_2O_3, output range 670–1070 nm

(b) Gas lasers

These are characterized as follows:

- Four groups: He–Ne lasers, ion lasers (noble gas ions), molecular-gas lasers (CO, CO_2), excimer lasers (F_2, ArF, KrCl, KrF, XeCl, XeF)
- Usually excited by a high-voltage glow discharge

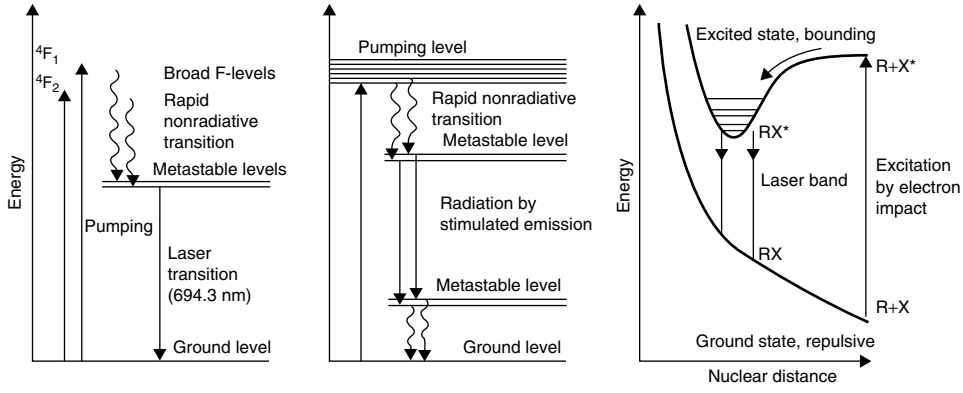

(a) Three energy level diagram Cr^{3+} ions in a ruby laser

(b) Four energy level diagram Nd^{3+} ions in a Nd:YAG laser

(c) Excimer energy level diagram for a diatomic molecule RX

Figure 6.2 Energy level diagrams for (a) ruby, (b) Nd:YAG and (c) excimer lasers. (a) Lasing occurs between the metastable energy levels and the ground level; (b) lasing occurs between the metastable levels; (c) lasing occurs between the upper bound state and the lower free electronic state of a molecule.

- Excimer lasers
  - Mixture of reactive gases (Cl_2, F_2) and inert gases (Ar, Kr or Xe)
  - Name derived from the terms *excited* and *dimers – excimers* are molecules that are formed and exist only in electronically excited states
- When electrically stimulated by a discharge, the produced pseudo molecule (dimer) is excited to a higher excited state with a potential energy minimum where population inversion can take place; when lasing, the dimer produces light in the UV range (Figure 6.2)
- With the following reactions for the ArF laser (193 nm) the mechanism of light production can be described, where He acts as the buffer gas:

Ionization	$Ar + e^- \rightarrow Ar^+ + 2e^-$
	$F_2 + e^- \rightarrow F^- + F$
Complex formation	$F^- + Ar^+ + He \rightarrow (ArF)^* + He$
Lasing process	$(ArF)^* \rightarrow Ar + F + h\nu$
Reformation process	$F + F \rightarrow F_2$

  - Maintenance costs are high, since expensive high-purity gases have to be changed periodically
  - Advantages are the wide output energy range, emitted UV wavelengths and flat-top beam profile

(c) Dye lasers

These are characterized as follows:

- Use fluorescent transition in complex organic dyes (e.g. Rhodamine 6G) dissolved in liquid solution or suspension
- Broadband emission is caused by the interaction of vibrational and electronic states of the dye molecule; with wavelength-selective cavity optics the laser output can be tuned to the desired frequency (tunable over a broad range of wavelengths: approx. 340 nm to 1 μm)
- Usually excited by lamps or lasers

(d) Semiconductor lasers

These are characterized as follows:

- Sometimes called diode lasers
- Electronic devices, generally very small, that use low power
- Made from materials from the III–V group (e.g. GaAs) and the IV–VI group (e.g. PbSeTe)
- Excited optically, by electron beams or by passage of an electrical current through a p-n junction
- Lasing process based on electron crossing between conduction and valence bands, leading to radiation emission by electron–hole recombinations

For laser ablation as a method of sample introduction for ICP-MS, solid-state lasers are preferred, because for these systems an acceptable compromise between output laser parameters and system costs is obtained. Nevertheless, excimer lasers are also becoming more popular regardless of the high maintenance demands, since the outstanding beam profile characteristics and high-energy output they offer are attractive features for several analytical applications. In

Table 6.1 Characteristic parameters of selected lasers used for laser ablation ICP-MS

Laser type	Wavelength (nm)	Pulse duration	Energy (mJ)	Comments
Excimer				
ArF	193	13 ns	200	High maintenance, higher pulse energy, better crater profile
KrF	248	20 ns	200–500	
XeCl	308	25 ns	200	
Solid state				
Ruby (Cr-Al_2O_3)	694	ns to μs	1000	
Nd:YAG	213	5–10 ns	2	Low maintenance, compact size, relatively easy handling
Nd:YAG	266	5–10 ns	4	
Nd:YAG	1064	10–15 ns	200–500	
Ti:sapphire	775	150 fs	0.5	

general, laser systems can be selected based on the desired emission wavelength, power required, pulse duration, spatial resolution, repetition rate and beam profile (Table 6.1).

6.2.3 Laser beam properties

The properties of the laser and the laser instrumentation which make the system suitable for the ablation process required for sample introduction for elemental analysis are the laser wavelength, power density, pulse-to-pulse stability, pulse frequency, pulse duration, laser beam profile and ablation spot size.

(a) Laser wavelength

The wavelength of the applied laser system has a significant influence on the ablation process, ablation rate, fractionation processes and the materials that can be ablated. Generally, lower laser wavelengths in the ultra-voilet (UV) region are preferred, owing to less restrictions on the materials that can be analyzed. For example, glass materials can be efficiently ablated using UV wavelength lasers, whereas the same materials are simply melted or fractured by infra-red (IR) wavelength lasers. Therefore, laser systems with wavelengths in the IR or visible (Vis) region are submitted to wavelength/frequency conversion. In this way, the frequency of the fundamental wavelength is quadrupled or quintupled by harmonic generators through nonlinear interactions of the laser light with crystal materials. Nonlinear optical materials are materials in which the intensity of light input, including its frequency, is not related to the intensity of the light output by a simple proportionality constant. Light beams are electromagnetic waves made up of electric and magnetic fields that are locked to each other and oscillate together at the frequency of the light. When such an oscillating field interacts with an atom, the outermost electrons can redistribute themselves in step with the electric field and the atom becomes charge polarized. This means that positive and negative parts separate slightly to form a small electric dipole with a dipole moment pointing in the direction of the impressed field. The magnitude of the induced

charge polarization depends on the magnitude of the applied electric field. A rapidly oscillating electric field of $10^{14} - 10^{15}$ Hz (optical frequencies) will induce two types of oscillating charge polarization, one with frequency ω and another with frequency 2ω. The effects of the induced charge polarization and subsequent re-radiation, which are important here, are a decrease in the speed of light in the medium and the re-radiation of energy at a frequency 2ω, which is twice the frequency of the incident radiation. This doubling of frequency is known as second harmonic generation or frequency doubling. Combinations of several crystals can be used to quadruple or quintuple frequencies. The polarization effect strongly depends on the direction of the electric field used for generation. Thus, most effective charge polarization occurs in crystals with no internal symmetry. Although only about 10% of the crystals found in nature fall in this category, a wide variety of crystals are available, among them KH_2PO_4 (KDP).

Although the frequency conversion efficiency is normally low (5–10%), the energy output is still above the limit that is required for ablation of most materials (>1 mJ).

(b) Pulse energy

At high power density (i.e. radiant flux incident per unit area of surface) a measurable amount of light can pass through an optically dense medium, such as a solid sample, to a greater depth, leading to high absorbance of the energy in the sample. Therefore, laser pulse energy is an important parameter for the ablation process since ablation rates at given pulse energies vary with the composition of the material. Generally, pulse energy can be controlled and adjusted by apertures, filters, or variable optical attenuators as well as by the flashlamp voltage.

For a rapid change of the quality of the laser pulse, Q-switching is applied. The term 'Q' is used to describe the quality of the resonant cavity, especially how much light from the gain medium of the laser is fed back into itself by the resonator. Q-switching involves the application of an optical switch to concentrate the output energy into pulses of a few nanoseconds duration. In this way, the coupling of the photon energy with the sample is greatly improved. To produce a Q-switched pulse, either a shutter is placed into the cavity or one of the end mirrors of the cavity is made to rotate at a tilted angle, so that the two mirrors are not parallel. When the laser is strongly pumped with a flashlamp near the end of the pump pulse, a large population inversion builds up in the laser material while actual laser action is prevented (i.e. system not under resonance conditions, mirrors not parallel). At this point the shutter is removed or the rotating mirror is stopped parallel to the fixed mirror. Owing to the large population inversion obtained during the off-cycle, the gain and the available stored energy in the laser rod are very high, and the round trip gain in the laser cavity is much greater than that obtained for a one-way traverse of the cavity. Consequently, the laser oscillation builds up more rapidly than in normal operation and will rise very rapidly to a peak power level high above normal. Thus, a very short, very high power pulse is produced. Q-switching is applicable for laser materials with long-lived excited states, such as Nd:YAG lasers (Figure 6.3).

For a laser with one mirror reflecting 100% and the output mirror reflecting R, the Q-factor is given by

$$Q = \frac{2L}{\lambda(1 - R)}$$

with L being the length of the cavity (distance between the mirrors) and λ the wavelength.

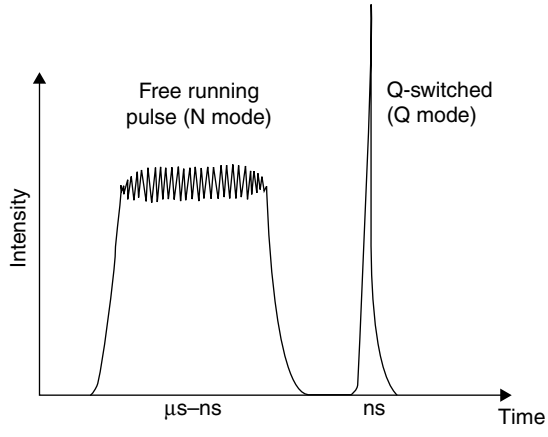

Figure 6.3 Comparison of free running and Q-switched pulses.

(c) Pulse frequency

Pulse repetition rates vary widely with the lasing medium. This parameter shows great influence on the ablation process, because plasma shielding can take place at high pulse frequency which alters the ablation rate of the sample. Plasma shielding could be described as absorption or reflection of the incident laser beam by a plasma formed close to the sample surface as a result of the previous laser shot.

(d) Pulse duration

The pulse duration also has significant influence on the ablation process. With laser pulses of nanoseconds duration, the ablation mechanism is highly dominated by thermal effects. Materials with lower melting points, e.g. many metals, are melted during the interaction of the laser shot with the material and part of the ablated material is evaporated from the melt after modifications (changes of physicochemical properties) and mixing of the sample material, thus leading to a deterioration of the local spatial and/or depth resolution. With laser pulses of much shorter duration (femtoseconds) the melting effects are reduced dramatically, because the deposition of the laser energy is so fast that the thermal diffusion length is drastically reduced (about 100 nm compared to approximately 1 µm with nanosecond pulses).[2] Less thermal diffusion provides better lateral and depth resolution. Investigation of femtosecond-laser systems or so-called 'cold' laser systems for ablation purposes is still in its infancy, but will gain more importance in the near future.

(e) Laser beam profile

The energy profile of the laser beam affects the geometry of the resultant ablation crater. Most lasers applied for ablation possess a Gaussian profile. In this case, the intensity of the laser light is at its peak at the center of the beam and drops off gradually toward the edges. The intensity profile measured across the center of the beam has a Gaussian distribution. For bulk analysis, the beam profile has no great influence on the results obtainable. In contrast, for performing

analysis with high demands on spatial or depth resolution, a flat-top beam profile is desirable as this enables higher resolution to be achieved. With appropriate imaging optics, the generation of flat-top profiles from Gaussian profiles is possible. So-called beam homogenizing optics are used for the production of more uniform energy distribution in the laser beam.

(f) Spot size

The lateral resolution obtainable during the analysis is linked to the spot size. To a smaller degree, signal generation at the ICP-MS also depends on spot size, since the dimensions of the crater diameter together with the applied power density influence the amount of ablated material. The aspect ratio of the ablation crater formed (quotient of crater depth to crater diameter) has an influence on the transport of ablated material. The higher this aspect ratio, the lower the amount of material transferred from the crater bottom to the ICP-MS.

For Nd:YAG lasers, the spot size is controlled by adjusting the laser focus and incident energy in combination. In excimer lasers, an aperture imaging system is used, defining the spot size by the size of the focused image of an aperture placed at an appropriate position in the optical path. With such lasers, change of spot size with change of aperture size can be achieved with constant energy density on the surface. The range of commonly used spot sizes is between 10 and 400 μm.

6.2.4 Laser sampling processes and corresponding elemental response

One of the limitations in LA-ICP-MS is that the signal intensities observed sometimes do not reflect the stoichiometric sample composition, which makes an accurate determination of the concentration of elements rather difficult. This phenomenon is called elemental fractionation and can occur during the laser ablation process, the aerosol transport process and the vaporization, atomization and ionization processes in the ICP.[3] Various parameters, such as the laser energy and wavelength, the pulse duration and the beam profile, influence the amount of elemental fractionation.[4] Recent studies have proved that the particle size distribution of laser-induced particles obtained during the ablation process plays a major role in elemental fractionation occurring within the ICP.[5] The particle size distribution itself is a function of the laser wavelength and the absorption of the material, and is reduced with lower laser wavelengths.[6,7] In addition, the particle size distribution is also dependent on the carrier gas used.[8] The efficiency of vaporization, atomization and ionization processes in the ICP is dependent on the particle size of laser-induced particles and therefore directly affects the degree of elemental fractionation.[9] The operating parameters of the ICP have to be selected very carefully so as not to increase such effects. Optimization and tuning procedures should be selected differently compared to solution-based determinations to minimize elemental fractionation.[10] In conclusion, it can be stated that fundamental research in the last few years has shed light on the different sources of uncertainties using laser ablation coupled to ICP-MS and is still part of ongoing studies for better understanding and description of the different processes involved. Laser ablation ICP-MS has proved, and continues to prove, to be a reliable, accurate and precise method for the quantitative determination of major, minor and trace elements in solid samples. Routine methods in many different fields have been established and the area of new applications is growing fast. A selection of important applications is given at the end of this chapter.

6.2.5 Safety considerations

Aside from their design classifications (i.e. solid state, gas, etc.), lasers are also classified into four groups depending on their potential for causing biological damage:

- Class I: emit laser radiation below known hazard levels
- Class II: low-power visible lasers that emit above Class I levels but at a radiant power not above 1 mW
- Class IIIA: intermediate-power lasers (around 1–5 mW), which are hazardous only for intrabeam viewing
- Class IIIB: moderate-power lasers
- Class IV: high-power lasers (around 500 mW), hazardous to view the laser light under any condition (either directly or diffusely scattered), potential fire hazard (causes heating of the sample and can cause ignition) and skin hazard (causes irritation, reddening or burning). Significant controls are required for Class IV laser facilities.

Nowadays, many lasers used for LA-ICP-MS are available as Class I lasers, since manufacturers have taken safety requirements into account by locking and shielding the dangerous parts of the laser system from direct access.

6.3 Laser ablation sample cells

6.3.1 Introduction

The volume of the laser ablation sample cell, the geometry, the type of carrier gas and its flow pattern, and the tubing properties of the transfer line to transport the aerosol into the ICP are all together important factors that contribute to the total transport process and the transient signal structure. The transport efficiency of laser-induced particles therefore restricts the detection capabilities for laser ablation microanalysis. Any enhancement in the transport process will make it possible to decrease the laser spot size and still detect a signal from the ablated mass, and therefore will lead to an increase of the spatial resolution that can be successfully used for laser ablation.

The sample cell consists of a gas inlet and a gas outlet, a laser cell window which is transparent for the laser wavelength used, and optical arrangements for illuminating the sample with either transmitted or reflected light, respectively. The laser beam itself is deflected and transmitted through the cell window onto the sample and focused via objective lenses onto the surface. The imaging focal point is aligned together with the laser focal point to ensure optimum ablation as long as the sample surface stays in focus. Sample observation is performed by CCD cameras often together with a microscope.[11] The number of gas inlets and their arrangement is often modified to decrease any possible dead volume inside the cell to improve the sample transport efficiency for the analytical needs. The cell can be equipped with a computer software controlled x–y–z stage to follow specific patterns on the sample, such as line scans or individually shaped patterns. Such an arrangement is very helpful for reproducible and controlled sampling and can be automated to analyze different features of interest within one run. A schematic view of a typical sample cell used for laser ablation is given in Figure 6.4. There are various designs available that differ in their geometry and total volume, but as a general classification, the cells can be divided into closed and open cell designs. In the closed design, the samples are completely inside the

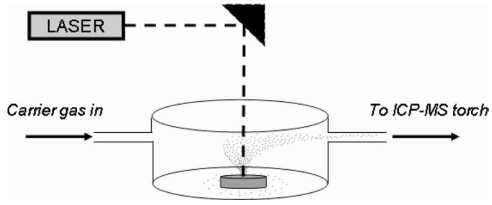

Figure 6.4 Schematic of a standard laser ablation cell. (*Source*: Simon Nelms, Thermo Electron Corporation.)

cell. Therefore, the volume of the cell restricts the sample size and the amount of samples that can be used at any one time. Using an open design, the cells are attached to the sample and sealed to their surface. Such cells are independent of the sample size and the only restriction is that the samples have to be polished to ensure proper sealing. Such laser ablation cells are very attractive for large and valuable samples, like art objects, where the sample must not be segmented.

6.3.2 Transport efficiency

The overall transport efficiency in laser ablation is reported to be around only 10% of the total amount of material ablated. Therefore, further investigations of the transport process will result in better understanding of the aerosol transport behaviour, the transport efficiency and the possibilities available to influence the signal structure. Laser ablation cells can be characterized by their volume variation, which can range from 0.25 to 60 cm^3 and occasionally even larger (see Figure 6.5). To avoid cross-contamination of different samples, gun-barrel cells were developed to have reduced free volume and to have multisample capabilities. The carrier gas is introduced into the sample cell via an inlet nozzle, which can vary in its inner diameter and which influences the geometry of the gas injection zone and therefore the flush-out properties of a specific sample cell. Within the field of this injection zone is a high transportation efficiency area, whereas outside a 'dead-volume' zone can be observed. A visualization of the gas flow dynamics and

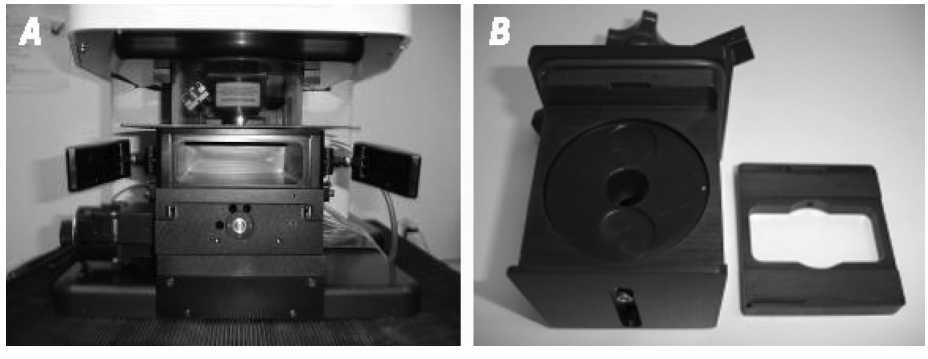

Figure 6.5 Laser ablation cells of different volumes. *A*: Large format ablation cell. *B*: SuperCell(TM). (*Source*: New Wave Research, Inc.)

its dependence on the particle size of different materials is shown in Figure 6.6. This example shows gas flow dynamics for MgO (particle size < 10 μm) and SiO_2 (particle size < 60 μm).[12] The gas inlet angle is dependent on the inner diameter of the nozzle and the flow rate of the gas used for ablation. The turbulent flow outside the gas inlet zone leads to different aerosol transport efficiencies and therefore to non-uniform signal intensities for different sampling positions within the cell. As shown in Figure 6.7, this variation is also dependent on the gas used and can vary by up to 35% for argon, suggesting that a helium laser ablation atmosphere provides more uniform transportation. Therefore, more gas inlets are recommended to create a higher efficiency zone with a more uniform gas flow pattern inside the cell and to decrease any possible dead zones. Using cells of larger volume, gas circulation within the cell significantly influences the transport time and increases signal dispersion. Since the aerosol density decreases with increasing sample cell volume, the flush-out time of laser-induced particles increases using large volume cells due to recirculation of the aerosol within the cell. This leads to a linear increase of time dispersion of the signal, making the transient ablation signals much broader using large volume cells. In contrast, reduction of the cell volume results in significant deposition of particles on the

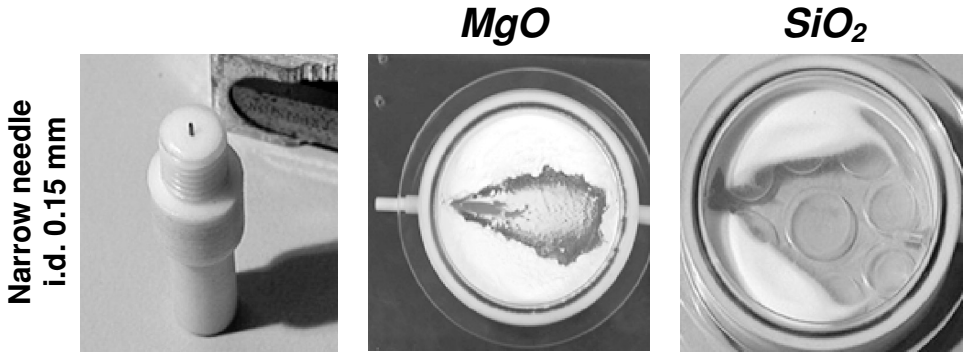

Figure 6.6 Visualization of gas flow dynamics in the ablation cell using materials of different particle size diameter. (Reproduced from reference 12, with permission of The Royal Society of Chemistry.)

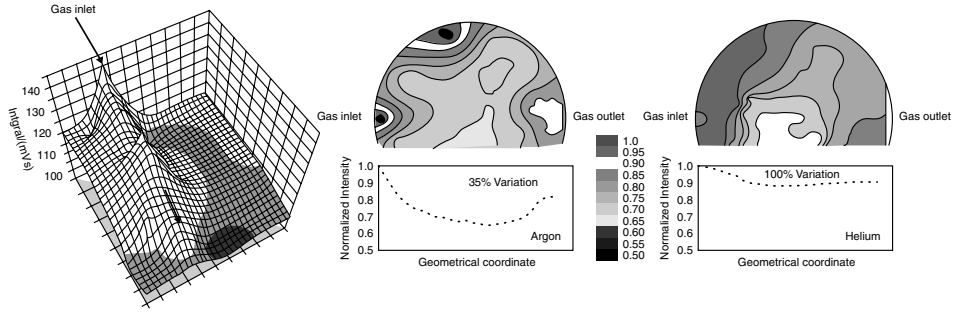

Figure 6.7 Signal variations within the ablation cell for different sampling positions and the variation in different gas atmospheres (argon, helium). (Reproduced from reference 12, with permission of The Royal Society of Chemistry.)

ablation cell walls with pronounced aerosol–wall interactions leading to a partial loss of aerosol. However, reduction of the cell volume gives sharper single-shot signals. Therefore, such low-volume cells are favorable for any analysis which is restricted by the need for fast transient data acquisition, e.g. depth profiling to gain high depth-resolved elemental information and composition of elements. The total transport efficiency of laser-induced particles, based on the total integral of the transient signals obtained, is actually not significantly different for laser ablation cells of different volumes. The diameter and the volume of the transfer tube have no influence on the total amount of transported material, but do affect the signal structure and the time it takes the particles to reach the ICP. The gas velocity of the carrier gas in the transfer line linearly increases with smaller inner diameters, with an experimental optimum signal-to-noise ratio for an inner diameter of 4 mm. Again, the longer the transfer line, the higher the signal dispersion for transient signals. Taking these observations into account, transfer lines should be as short as possible to reduce transport time, dispersion and flush-out time.

6.3.3 Carrier gases used for laser ablation

Different authors have reported that using different gas mixtures for the laser ablation carrier gas alters the signal intensities and background levels obtained. Argon gas is most commonly used for this application. The advantage of using argon for the carrier gas stream within the laser cell is that it can be passed directly into the ICP (via the injector tube of the ICP torch) without the need to add any other gases and therefore does not induce any changes in the plasma conditions. Different plasma conditions, such as the plasma temperature, would result in changing ionization efficiencies within the ICP and could lead to non-stoichiometric signal responses. Addition of nitrogen (N_2) to the carrier gas flow has been shown to lead to increased signal intensities for high-mass elements,[13,14] but at the same time to increased polyatomic ion formation, such as $^{14}N^{14}N^{1}H$ and $^{14}N^{14}N^{14}N$, which interfere with isotopes in the low-mass region, that are important as internal standards, like ^{29}Si and ^{42}Ca.

In recent years, several groups have reported enhanced signal-to-noise ratios when using helium as the laser ablation gas and mixing argon to the gas stream after the ablation cell.[15,16] There are several explanations to this phenomenon, but a very obvious one is that particle deposition around the ablation spot is reduced when using helium.[15] Since both gases have very different thermal conductivity properties and form different laser-induced microplasmas on the sample surface, smaller particles (<200 nm) are preserved in the helium laser plume compared to the larger argon laser induced microplasma, leading to less condensation and enhanced transport efficiency of smaller particles.[8] This results in less particle deposition using helium as the laser ablation gas. As an example, the ablation of a silicate glass sample with a 193 nm ArF laser system using both gases (Ar, then He) is shown in Figure 6.8. Other setups have been developed and tested, such as using moistened argon gas which is then mixed with the helium ablation carrier gas or a high-pressure helium setup for improved sample cell flush-out.[16] Some of these requirements are difficult to control reproducibly (e.g. the degree of moistening of argon) and lead to additional polyatomic interferences in the low-mass region. Still, the results are encouraging since the limits of detection for heavy elements were improved by almost one order of magnitude. The high-pressure setup led to the generation of very reproducible helium aerosol/dry argon mixtures, resulting in stable transport to the plasma. In addition, the

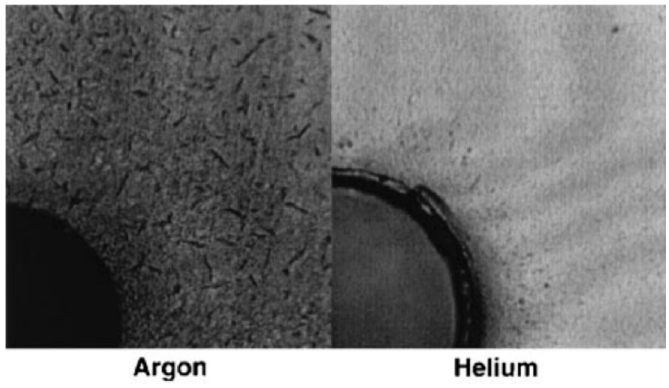

Figure 6.8 Comparison of particle deposition around the laser crater of silicate glass matrix (NIST SRM 612) using a 193 nm laser system in argon and helium, respectively. (Reproduced from reference 16, with permission of the Royal Society of Chemistry.)

high-pressure approach shows no increase in dispersion and maintains the ablation-related signal structure, which is very important for single-spot analysis or fluid inclusion studies. As a further instrumental modification, the introduction of different amounts of helium requires installation of an additional rotary pump in the interface region of the ICP-MS to maintain the vacuum under these gas conditions. Often, different sample and skimmer cone orifices are used for laser ablation experiments (reduced sampler cone orifice diameter, increased skimmer cone orifice) if helium is the main carrier gas, as this has proved to increase the signal-to-noise ratios even further.[17] This can be explained by the different shapes of the Mach disk under helium conditions, resulting in less post-ionization of material deposited on the lenses and lower background levels. Together with lower on- and off-peak background signals, an increase in signal sensitivity can be experimentally observed. Therefore, the portion of ions passing through the interface region is directly influenced by the skimmer geometry and by its pressure conditions.

In conclusion, comparing different sample introduction systems using helium as the ablation gas, a significant reduction of the limits of detection was observed for 193 nm laser systems applying all instrumental modifications in contrast to the 'conventional' setup using argon as the carrier gas (see Figure 6.9).[18] Improvement factors of up to 2–3 orders of magnitude for nearly all elements covering the whole mass range were achieved. The increase was not as pronounced for other laser systems using higher wavelengths, which can be explained by the larger particle sizes produced during the ablation process by the longer laser wavelengths and the corresponding lower transport efficiency of the larger laser-induced particles to the plasma and their different excitation processes in the ICP.

6.3.4 Alternative sample cells for in situ analysis

To analyze trace elements using laser ablation ICP-MS in materials such as biological samples or frozen samples, one has to ensure that these samples are either freeze dried or kept frozen, even during the laser ablation. Therefore, different groups have developed cryogenically cooled ablation cells that enable direct analysis of thin biological sample sections and ice core samples

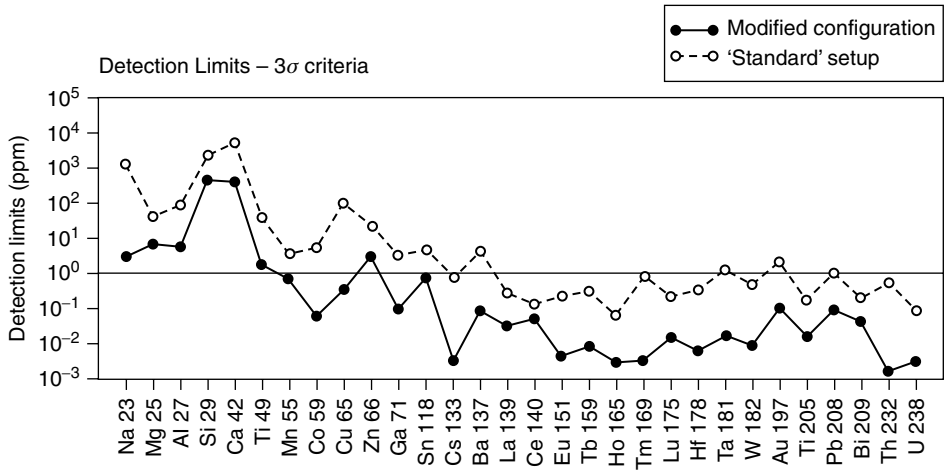

Figure 6.9 Improvement for the limits of detection for a 193 nm laser system using helium as carrier gas and instrumental modifications. (Reproduced from reference 18, with permission of The Royal Society of Chemistry.)

at a temperature below −60°C.[19,20] For a schematic of such a cell together with all control units, see Figure 6.10. These groups achieved reproducibilities of about 2–6% using this technique. Their work demonstrates that the development of such cooled cells could be used in the future for mapping samples for the 2D distribution of trace elements in fresh tissues by rastering a

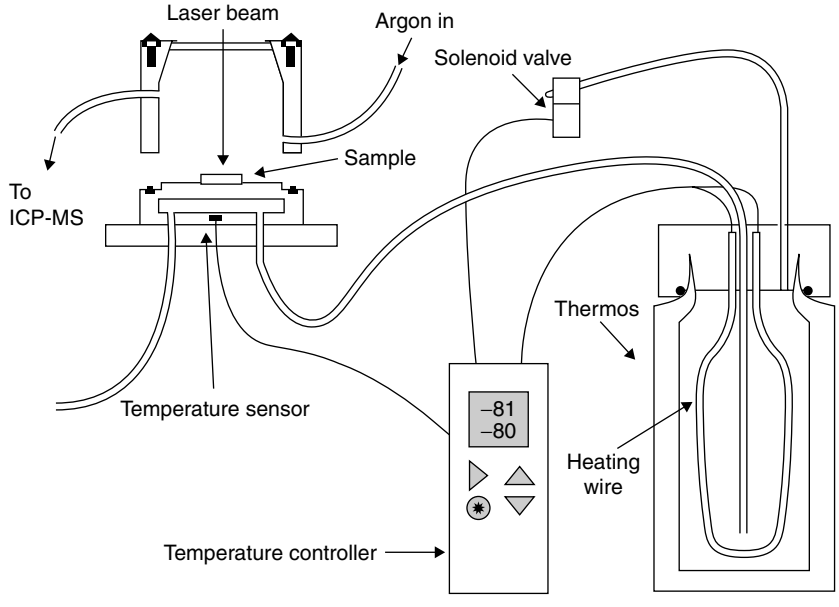

Figure 6.10 Schematic of a cryogenically cooled ablation cell. (Reproduced from reference 20, with permission of The Royal Society of Chemistry.)

grid or scanning individual lines over the frozen sample. Cryogenic ablation cells are therefore potentially an excellent tool for histologists and molecular cell biologists to correlate elemental patterns with certain features in tissues to study the role of, or distribution of, these elements in the tissue feature under study. Using such alternative cells, together with high sensitivity ICP-MS instruments, may in future be very useful to enhance spatial resolution near the cellular level to perform single cell analysis or at least to study the accumulation of trace elements in tissue features below the 0.05 mm range.

6.3.5 Conclusion

In summary, the following results for the aerosol transport can be formulated. The gas inlet geometry and pressure both influence the flushing time of the aerosol out of the ablation cell. The ablation cell has no influence on the total amount of transported material, but rather on the signal dispersion and washout only. The transport tube has a small influence on signal dispersion, since the volume of the tube is, under normal conditions, rather negligible compared to the volume of the cell. The overall transport efficiency is still only 5–10% of the ablated material. This means that there is still an improvement of more than 1 order of magnitude possible by developing different sample cell designs that result in enhanced or complete transport efficiency for laser-induced particles to the ICP.

6.4 Quantification procedures for laser ablation ICP-MS

6.4.1 Introduction

To fulfill the objectives of quantitative trace element determination in solid materials, different calibration strategies have been established to accurately and precisely describe a relationship between the signal response and the elemental concentration by LA-ICP-MS. There are three main criteria that, in principle, have to be met for a successful absolute quantification of trace elements in solid samples. These are:

(1) That the exact amount of sample transported to the ICP is known.
(2) That the composition of the laser-induced aerosol represents the stoichiometry of the original sample.
(3) That the particles transported to the ICP are fully atomized and ionized within the plasma.

Since these criteria are rarely completely fulfilled, it has been necessary to develop relative calibration techniques to achieve the best possible results. Different calibration techniques using various approaches have been established, including external calibration using solid standard reference materials with matrix-matched composition and internal standardization, on-line solution-based calibration techniques by nebulization of standard solutions through desolvation units, absolute quantification procedures collecting the total spectra and all components of the sample at once, and non-matrix-matched calibration methods using silicate glasses to quantify different geological or biological materials. Let us compare the different approaches in a little more detail.

6.4.2 Calibration using matrix-matched external standards

Calibration techniques where the matrix of the standards used closely matches that of the sample, both chemically as well as physically, are called 'matrix-matched' calibration methods. To correct for differences in laser ablation yields, signal drifts and matrix effects, the signal responses are normalized to a known major element (as an internal standard) within both the standards and the samples.[21] Previous work has indicated that use of this internal standard is a prerequisite in order to correct for differences in ablation efficiency from one analytical site to another, and to compensate for differences in physical and chemical properties. The concentration of this element has to be determined prior to LA-ICP-MS analysis with complementary techniques, like XRF. For the analysis of high-purity materials, the concentration of the internal standard element can be sufficiently well estimated from the stoichiometry and purity of the material. This procedure works extremely well where elements being determined and the internal reference element being used share similar ablation behaviour; i.e., they do not progressively fractionate during the ablation and transport processes. Different elements have been studied to establish whether they are suitable for internal standardization (Si, Ca, Ti, In, etc.), but as a general rule, it has been reported that elements homogeneously distributed in the sample showing similar laser ablation behaviour as the elements of interest give the best results. The most natural choice is to use elements that are matrix elements whose (high) concentration can be easily assessed using other solid mass spectrometric methods. By comparing the signal response (i.e. the signal intensity of a specific isotope normalized to the internal standard signal intensity) for both the standard of known elemental concentration and the unknown sample, the concentration of the trace elements of interest can be calculated. The procedure for acquisition and calculation of transient analyte signals can be derived from Longerich et al.,[22] employing the factory-supplied time-resolved software and transferring the raw data to a spreadsheet program for evaluation and quantification. The two commonly used commercial software programs that are currently available for laser ablation ICP-MS analysis are LAMTRACE (developed by Simon Jackson, Department of Earth and Planetary Sciences, Macquarie University, Sydney, NSW, Australia) and GLITTER (developed by William Griffin at the ARC National Key Centre for Geochemical Evolution and Metallogeny of Continents (GEMOC), Macquarie University, NSW 2109, Australia).

Another widely used approach that can be applied for semi-quantitative determination in LA-ICP-MS is to use the relative sensitivity factors (RSFs) of the elements under consideration. RSFs are defined as the ratio of the experimentally measured and certified elemental concentrations in a given sample matrix, and are based on factors such as isotope ionization efficiency. Default RSF values for all the measurable elements in the Periodic Table are usually stored in a database in the instruments' software, and on some instruments, can be adjusted by the user within a particular experiment. By using a certified reference material of similar matrix to the sample, containing known concentrations of a set of elements across the mass range, the RSFs allow a response curve (in counts per second per μg/g (for example) versus isotope mass) to be generated. The concentrations of non-certified elements can then be calculated by first deriving the interpolated response of the isotope from the curve and then ratioing this to the RSF corrected signal for the isotope in the sample. By adjusting the RSF values within the experiment, the response curve can be 'fine-tuned' to yield semiquantitative results that are close to fully quantitative data. This method of concentration measurement is explained in more detail in Chapter 4, Section 4.4.

For many applications in LA-ICP-MS, a variety of different suitable geological and solid standard reference materials (SRMs) are commercially available from national institutions that specialize in preparing standard materials, such as the National Institute for Standards and Technology (NIST, Gaithersburg, USA) and the United States Geological Survey (USGS, Denver, USA), or in metal analysis, such as the Swedish Institute for Metals Research (SIMR, Stockholm, Sweden).[23–25] If such SRMs are not available, synthetic laboratory standards can be produced in-house and used further for quantification. They are prepared from compounds of the matrix elements, doped with trace elements at given concentrations.[26–29] The fact that a large number of natural minerals are oxides permits the possibility that reference materials used for other microtechniques can be prepared entirely synthetically by fusion of high-purity oxides doped with trace elements. Recent studies by Tibi and Heumann[30] show the possibility of adding isotopically enriched spike solutions to solid base materials prior to laser analysis. By using such a sample preparation procedure, it has been possible to determine bulk elemental concentrations for selected elements with very high accuracy in finely powdered sample materials pressed into pellets. In general, measurement of concentrations of homogeneous materials was accomplished with better than 10% accuracy and a precision of 2–5%, using this procedure.

6.4.3 Non-matrix-matched calibration method

Previous studies have shown that employing silicate glass standards for the quantitative analysis of a suite of elements in a wide variety of matrices, including titanites, zircons, apatites, uraninites and garnets, using major-element internal standards provides good accuracy and precision (between 10 and 20% RSD).[31] Since the matrix of the standards and the sample materials are very different, this technique is referred to as the non-matrix-matched calibration method. Calcium and silicon have been used as internal standard elements, but Ca is preferred because of its more similar chemical behaviour to the elements of interest, such as the rare earth elements. Other studies using lithium tetraborate fused glass disks, using reference glass materials as external standards and Si or Li as internal standard elements, proved that non-matrix-matched calibration procedures also result in accurate and precise results on different geological samples.[32] However, Craig and co-workers[33] showed some systematic negative bias (up to 30%) in calculated concentrations, when a geological reference material was analyzed using non-matrix-matched standards for calibration. They explained the deviation to be due to different mineralogical features (crystalline versus cryptocrystalline) of both samples, resulting in varying ablation efficiencies along grain boundaries during ablation using a 266 nm laser system. Recent studies show very good agreement of measured concentrations compared to the concentration of doped elements in synthetic standard materials, like CaF_2 (calcium concentration of 51.3% m/m) using a 193 nm laser system, even for concentrations as low as 100 ng/g.[35] Element concentrations were determined using a silicate glass reference material, NIST SRM 612 (calcium concentration of 8.2% m/m) for external calibration, using ^{42}Ca as the internal standard. As an example, the calibration curve obtained for yttrium in this work is shown in Figure 6.11. In summary, non-matrix-matched calibration is an effective approach if the laser ablation process is not, or at least only slightly, matrix dependent. The criteria are that the absorption of the laser wavelength is constant for different samples and is independent of the optical properties of such materials, as shown by Horn *et al*. in their work using a 193 nm laser wavelength.[7] The elemental response for a given element normalized to the internal standard signal intensity in different materials

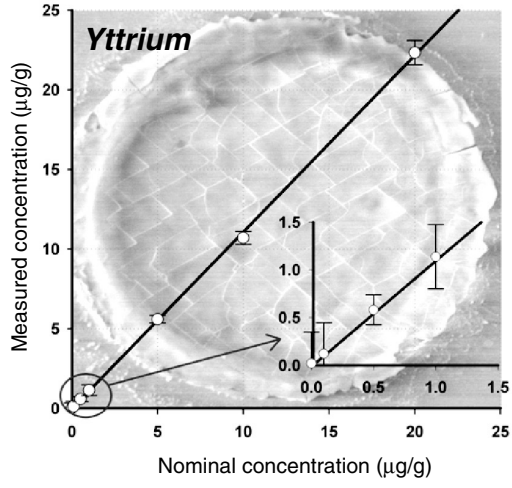

Figure 6.11 Non-matrix-matched calibration of synthetic CaF_2 material doped with increasing concentrations of trace elements. As an example, the calibration curve for yttrium is given (*Source*: Reference 35.)

should also be the same. All these criteria have been met using the 193 nm laser wavelength, making non-matrix-matched calibration a promising calibration method for such laser systems.

6.4.4 Absolute quantification procedures

Standardless measurement of the elemental composition of metal samples has been developed from single laser ablation pulses. This method directly compares elemental signals to the total mass signal to produce relative composition information. By measuring the ratio of the individual analyte signal to the total ion signal, it has been demonstrated that laser mass spectrometry can produce accurate element concentrations without the use of standards.[34] In Figure 6.12, the transient signal is plotted as the analyte signal (S_d) for each element as a function of the integrated signal produced by all ablated elements ($\sum S_d$). In this format, the slope for each analyte determined from a linear regression directly gives that element's fractional composition in the sample. This technique is largely immune to sample matrix related signal variations normally observed in LA-ICP-MS. Such procedures require the simultaneous measurement of concentrations of all elements from a transient signal and assume that the sum of all elements should equal the total mass ablated. Laser ablation TOF-ICP-MS investigations have been shown to provide accurate composition information for elements present at concentrations ranging from 0.02 to 100% m/m for a variety of metal samples after adjustment of the analyte signals to account for instrumental bias.[34,36] The accuracy is found to be largely dependent on the sample element concentration and ranges between 3 and 4% for concentrations between 10 and 100% m/m and deteriorates to 20% for lower concentrations. Unfortunately, if the material contains, for example, oxide, carbonate or nitrogenous components as major parts of the sample matrix, these will not be detected in the ICP. In these cases, this calibration technique cannot yet be successfully applied.

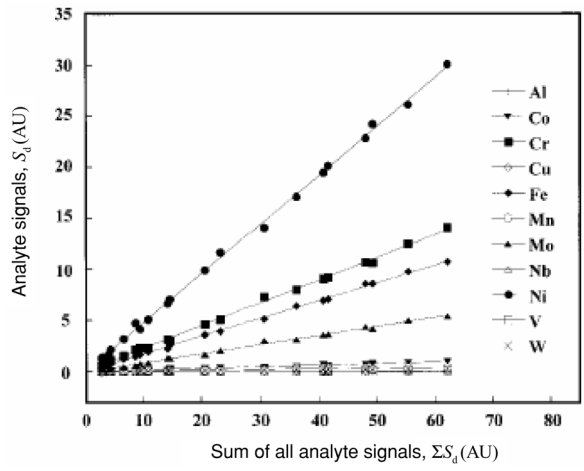

Figure 6.12 Calibration curves for selected elements using the ratio of the analyte signal to the sum of all analyte signals. The slope gives the elemental fraction in the sample. (Reproduced from reference 34, with permission of The American Chemical Society.)

6.4.5 On-line solution-based calibration procedures

Multi-element trace analysis by LA-ICP-MS of high-purity metals, semiconductors and insulators (e.g. ceramics) is often limited by the lack of suitable SRMs of the same matrix composition. In addition, a significant number of trace element concentrations are not certified in the specific commercially available SRMs.

Several other alternative calibration methods using aqueous standard solutions have been applied in the case that appropriate standard reference materials are not available.[37–40] On-line solution-based calibration utilizes the introduction of mixed laser-ablated sample material together with nebulized standard solutions through desolvation units to the ICP. Two setups are in use, based on adding the solutions either before (the so-called single gas flow system) or after (known as the dual gas flow system) the laser cell (see Figure 6.13).[37,40] Using such a procedure, one can use either external standardization,[41,42] analyte standard addition,[38,43] or even isotope dilution techniques for small sample sizes.[44,45]

External calibration is performed by nebulization of standard solutions through a membrane desolvation unit, followed by mixing with the laser-induced signal of a blank (i.e. lowest available concentration) target. In order to achieve matrix matching, the blank matrix is ablated while simultaneously aspirating the calibration solutions. The advantage is that any combination of elements in different concentrations can be analyzed since preparation of external calibration laboratory standard solutions is straightforward. Another advantage is that both gas flow settings can be individually optimized, and therefore, tuning of the lens settings, ion optics settings, mass calibration, and dual detector calibration is less time-consuming. This method has been successfully applied to analyze high-purity materials[40] and geological samples fused with lithium borate.[39]

If no blank solid target exists, a standard addition method, very well known from solution-based analysis, can be applied to the analysis of solid material with LA-ICP-MS. Here, the standard solutions containing different concentrations of analytes are again introduced via a membrane

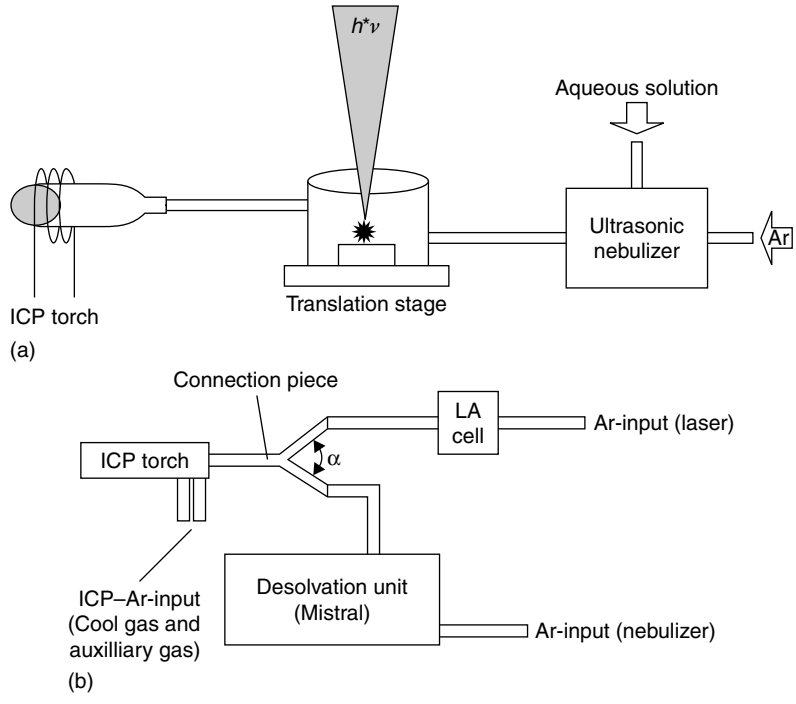

Figure 6.13 Schematic diagram of simultaneous 'dried' aerosol and laser-induced aerosol introduction systems, single flow and dual flow systems, respectively. (a) Single flow system. (Reproduced from reference 40, with permission of The Royal Society of Chemistry.) (b) Dual flow system. (Reproduced from reference 37, with permission of The Royal Society of Chemistry.)

desolvation unit, but this time the sample is continuously ablated and the laser-induced particles are mixed with the standards. By way of example, for the laser ablation analysis of a steel sample using in this case flow injections of cobalt standards with increasing concentrations, see Figure 6.14.[38] The concentrations of the trace elements can then be readily determined from the established calibration curves.

Relative standard deviations for trace element determination of between 2 and 10% have been reported by external calibration and standard addition using the described solution-based calibration methods.

In an on-line isotope dilution technique used with LA-ICP-MS, an isotope-enriched spike solution, which can be a multielement solution containing all the spikes of interest, was nebulized using a low-flow nebulizer and introduced through a membrane desolvation unit in front of the sample cell. The isotope ratio of the spike solution was measured (spike ratio), and after a distinct time, the laser was turned on and the isotope ratio of both the sample and the spike solution (blend ratio) was measured. After turning the laser off, the spike solution was replaced by blank solution and the isotope ratio of the blank was used for any blank correction. Using this setup, very accurate determination of trace impurities in small sample sizes was successfully performed.[44]

A drawback of all these solution-based techniques are the different excitation processes between wet and dry plasma conditions occurring in the ICP, resulting in different signal responses

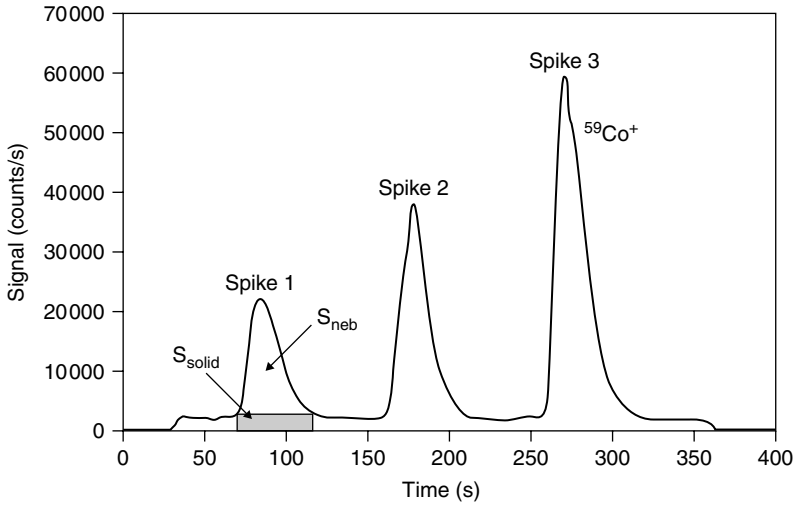

Figure 6.14 Cobalt solution standards added via flow injection during continuous laser ablation of a steel sample, NIST 1263a. (Reproduced from reference 38, with permission of The American Chemical Society.)

(elemental sensitivities) for wet droplets and dry particles, respectively. Even with the desolvation strategies employed, nebulized solutions will still produce aerosols that are wetter than laser ablation aerosols. Therefore, to take these signal variations into account, correction factors via internal standard elements, present in both the solution and the solid material, have to be established first by comparing the elemental signal responses from both the solution and the laser signal.

6.4.6 Conclusion

Selecting and successfully applying the optimum quantification procedure for LA-ICP-MS is often not an easy task. The most effective procedure of using matrix-matched standards is not always straightforward if suitable standards are not available. For improved quantification possibilities, new certified reference materials have to be established and fully characterized. Using lower laser wavelengths for ablation, matrix-independent calibration procedures using external reference materials together with the correct choice of internal standards have become increasingly popular in recent years and will continue to advance in the future. Applying isotope dilution calibration techniques to LA-ICP-MS will improve the accuracy of this method and, in conjunction with highly sensitive ICP-MS instruments, opens an exciting new field in the analysis of very small sample sizes, for precise, interference-free isotope ratio measurements in solid samples.

6.5 Applications

Until recently, the dominating field of application for LA-ICP-MS was bulk analysis, with a focus on geological and metallic samples. The considerable developments and improvements in

the laser technique during the last 5 years, namely enhanced wavelength flexibility, increased energy range and spot size variation, improved beam profile properties, especially homogenization, improved knowledge about the fundamentals of ablation processes, and more user-friendly software for laser control and data handling, have been of great significance in extending the analytical applications of these systems. New fields of applications have become attractive; among them are geological analysis in microscale dimensions, isotope ratio measurements, measurement of heterogeneity and element distribution in modern materials, forensic fingerprinting, analysis of layer systems, and elemental determination in biological and clinical samples. An overview with papers published in the last 10 years is given in Table 6.2.

For the analysis of geological samples, LA-ICP-MS shows several advantages. In many cases direct solid sampling is preferred in comparison to time-consuming and often troublesome digestion procedures. In addition, the capability of the technique to obtain information about microstructures together with major, minor and trace element concentrations is increasingly used. Considerable progress has been reported for the analysis of fluid inclusions, where very small craters with diameters below 50 μm are used to obtain elemental and isotopic composition information from a limited ablated mass of just a few femtograms. Trace element analysis has been performed in silicates, calcites, sediments, meteorites and other geologically important samples. Advantage has also been taken of the significant improvements that have been made in the achievable precision of isotope ratio measurements using ICP-MS. With double-focusing magnetic sector instruments coupled to UV lasers, precision of isotope ratios of 0.01% has been reported. With LA-ICP-MS, remarkable results have been reported for the isotope ratios of $^{87}Sr/^{86}Sr$, $^{96}Zr/^{90}Zr$, $^{92}Zr/^{90}Zr$, $^{206}Pb/^{238}U$, $^{207}Pb/^{206}Pb$, $^{204}Pb/^{206}Pb$, $^{230}Th/^{232}Th$, $^{235}U/^{238}U$ and isotopes of Fe, Cr, Ti, Mo, W, Hf, Nd and Sm, measured for geochronological dating purposes.

In materials analysis, laser ablation has been applied to almost all fields of modern materials. For glasses, high-purity optical materials (e.g. CaF_2), ceramics, semi- and superconductors, polymers, high-purity metals and alloys, the heterogeneity of the material, trace element concentrations and elemental distributions have been measured. In addition, this method has been used for the investigation of trace element composition of concrete, radioactive waste and radioactive materials, the characterization of steel inclusions and the determination of the composition and thickness of layered systems.

Fingerprint analysis in forensic science has been used to source the provenance of metals and cannabis crops as well as parts of weapons, housebreaking tools and safes. In many crime cases there is often no need for full quantification, as semiquantitative results are sufficient for reliable comparison of the results with archived multielement data (or spectra) from other samples.

In environmental analysis, tree components, road sediments and dust, domestic waste and calcareous biological structures have been investigated to obtain information about changes in ecosystems.

Recently, the first applications of LA-ICP-MS for analysis of biological and clinical samples have been reported. In dental analysis, calcium, silver and mercury have been measured in low concentrations to identify nano-leakages of teeth restorations. A newly developed cryogenically cooled laser cell (cryocell) for ablation allows the determination of trace elements in frozen tissues, making time-consuming digestions unnecessary in many cases. In proteins separated by gel electrophoresis, selenium and phosphorus concentrations have been determined using standards for quantification separated under the same electrophoretic conditions.

More applications of LA-ICP-MS in all of the mentioned fields are given in the references and reviews summarized in Table 6.2.

Table 6.2 An overview of different LA-ICP-MS applications

Field of application/samples	Laser system	References
Analysis of geological samples		
Trace elements in minerals	Excimer ArF 193 nm	11, 45–47
Isotope ratios	Nd:YAG 1064 nm, 266 nm, 213 nm	48–53
Fluid inclusions and fluids in minerals	Excimer ArF 193 nm	54, 55
	Nd:YAG 266 nm	56
Calcites	Nd:YAG 1064 nm	32, 57
Silicates	Nd:YAG 1064 nm	11, 45, 58
	Excimer ArF 193 nm	59
Meteorites	Nd:YAG 266 nm	60
Sediments	Nd:YAG 266 nm	61
Determination of rare earth elements	Nd:YAG 266 nm	62, 63
Platinum group elements	Nd:YAG 266 nm	60, 64, 65
Materials analysis		
Steel	Nd:YAG 1064 nm	66
Glasses	Nd:YAG 1064 nm, 532 nm, 266 nm	7, 67–70
	Excimer ArF 193 nm	7, 69
Metals and alloys	Nd:YAG 1064 nm, 532 nm, 266 nm	66, 69, 71, 72
	Excimer ArF 193 nm, KrF 248 nm	69, 72
Calcium fluoride	Nd:YAG 266 nm	7, 73
	Excimer ArF 193 nm	7, 73
High-purity materials	Nd:YAG 1064 nm, 266 nm	39, 74–76
Coatings and layers	Excimer ArF 193 nm	77
	Nd:YAG 266 nm	78, 79
Semiconductors	Nd:YAG 1064 nm, 266 nm	80, 81
Ceramics	Nd:YAG 266 nm	82, 83
Superconductors	Excimer XeCl 308 nm	84
Concrete	Nd:YAG 266 nm	85
Radioactive materials and waste	Excimer XeCl, 308 nm	86
	Nd:YAG 266 nm	87, 88
Polymers and organics	Nd:YAG 266 nm	89–91
	Nd:YAG 1064 nm	92
Amorphous materials	Nd:YAG 266 nm	93
Analysis of biological and clinical samples		
Dental analysis	Nd:YAG 266 nm, 213 nm	94, 95
	Nd:YAG 1064 nm	96
Tissue	Nd:YAG 266 nm, 213 nm	20, 97, 98
	Nd:YAG 1064 nm	99
Proteins	Nd:YAG 213 nm	100, 101
Forensics		
Fingerprinting scene of crime evidence	Nd:YAG 1064 nm	102, 103
Archeology		
Iron samples	Nd:YAG 532 nm	104
Environmental analysis		
Tree components	Nd:YAG 1064 nm, 266 nm	105–109
Road sediments and dust	Nd:YAG 1064 nm, 266 nm	110, 111
Domestic waste	Nd:YAG 266 nm	112
Calcareous biological structures	Nd:YAG 266 nm	97, 113–115
Reviews		116–120

References

1. Sneddon, J. and Lee, Y. I. (1997) Lasers in analytical atomic spectrometry – an overview. *Spectrosc. Lett.*, **30**, 1417–27.
2. Margetic, V., Pakulev, A., Stockhaus, A., Bolshov, M., Niemax, K., and Hergenroder, R. (2000) A comparison of nanosecond and femtosecond laser-induced plasma spectroscopy of brass samples. *Spectrochim. Acta B*, **55**, 1771–85.
3. Fryer, B. J., Jackson, S. E., and Longerich, H. P. (1995) Design, operation and role of the laser ablation micrprobe coupled with an inductively coupled plasma mass spectrometer (LAM-ICP-MS) in the earth sciences. *Can. Mineral*., **33**, 303–12.
4. Russo, R. E., Mao, X. L., Borisov, O. V., and Liu, H. C. (2000) Influence of wavelength on fractionation in laser ablation ICP-MS. *J. Anal. At. Spectrom*., **15**, 1115–20.
5. Guillong, M., Kuhn, H. R., and Günther, D. (2003) Application of a particle separation device to reduce inductively coupled plasma-enhanced elemental fractionation in laser ablation-inductively coupled plasma-mass spectrometry. *Spectrochim. Acta B*, **58**, 211–20.
6. Guillong, M. and Günther, D. (2002) Effect of particle size distribution on ICP-induced elemental fractionation in laser ablation-inductively coupled plasma-mass spectrometry. *J. Anal. At. Spectrom*., **17**, 831–7.
7. Horn, I., Guillong, M., and Günther, D. (2001) Wavelength dependant ablation rates for metals and silicate glasses using homogenized laser beam profiles – implications for LA-ICP-MS. *Appl. Surf. Sci*., **182**, 91–102.
8. Horn, I. and Günther, D. (2003) The influence of ablation carrier gasses Ar, He and Ne on the particle size distribution and transport efficiencies of laser ablation-induced aerosols: implications for LA-ICP-MS. *Appl. Surf. Sci*., **207**, 144–57.
9. Rodushkin, I., Axelsson, M. D., Malinovsky, D., and Baxter, D. C. (2002) Analyte- and matrix-dependent elemental response variations in laser ablation inductively coupled plasma mass spectrometry, Part 1: The roles of plasma and ion sampling conditions. *J. Anal. At. Spectrom*., **17**, 1223–30.
10. Rodushkin, I., Axelsson, M. D., Malinovsky, D., and Baxter, D.C. (2002) Analyte- and matrix-dependent elemental response variations in laser ablation inductively coupled plasma mass spectrometry, Part 2: Implications for multielement analyses. *J. Anal. At. Spectrom*., **17**, 1231–9.
11. Günther, D., Frischknecht, R., Heinrich, C. A., and Kahlert, H. J. (1997) Capabilities of an argon fluoride 193 nm excimer laser for laser ablation inductively coupled plasma mass spectrometry microanalysis of geological materials. *J. Anal. At. Spectrom*., **12**, 939–44.
12. Bleiner, D. and Günther, D. (2001) Theoretical description and experimental observation of aerosol transport processes in laser ablation inductively coupled plasma mass spectrometry. *J. Anal. At. Spectrom*., **16**, 449–56.
13. Durrant, S. F. (1992) Multi-elemental analysis of environmental matrices by laser ablation inductively coupled plasma mass spectrometry. *Analyst*, **117**, 1585–92.
14. Hirata, T. and Nesbitt, R. W. (1995) U/Pb isotope geochronology of zircon: evaluation of the laser probe inductively coupled plasma mass spectrometry technique. *Geochim. Cosmochim. Acta*, **59**, 2491–500.
15. Eggins, S. M., Kinsley, L. P. J., and Shelley, J. M. G. (1998) Deposition and element fractionation processes during atmospheric pressure laser sampling for analysis by ICP-MS. *Appl. Surf. Sci*., **129**, 278–86.
16. Günther, D. and Heinrich, C. A. (1999) Enhanced sensitivity in laser ablation-ICP mass spectrometry using helium–argon mixtures as aerosol carrier: Plenary Lecture. *J. Anal. At. Spectrom*., **14**, 1363–8.

17. Günther, D., Longerich, H. P., Jackson, S. E., and Forsythe, L. (1996) Effect of sampler orifice diameter on dry plasma inductively coupled plasma mass spectrometry (ICP MS). Backgrounds, sensitivities, and limits of detection using laser ablation sample introduction. *Fresenius' J. Anal. Chem*., **355**, 771–3.
18. Latkoczy, C. and Günther, D. (2002) Enhanced sensitivity in inductively coupled plasma sector field mass spectrometry for direct solid analysis using laser ablation (LA-ICP-SFMS). *J. Anal. At. Spectrom*., **17**, 1264–70.
19. Reinhardt, H., Kriews, M., Miller, H., Schrems, O., Ludke, C., Hoffmann, E., and Skole, J. (2001) Laser ablation inductively coupled plasma mass spectrometry: a new tool for trace element analysis in ice cores. *Fresenius' J. Anal. Chem*., **370**, 629–36.
20. Feldmann, J., Kindness, A., and Ek, P. (2002) Laser ablation of soft tissue using a cryogenically cooled ablation cell. *J. Anal. At. Spectrom*., **17**, 813–8.
21. Longerich, H. P., Günther, D., and Jackson, S. E. (1996) Elemental fractionation in laser ablation inductively coupled plasma mass spectrometry. *Fresenius' J. Anal. Chem*., **355**, 538–42.
22. Longerich, H. P., Jackson, S. E., and Günther, D. (1996) Laser ablation inductively coupled plasma mass spectrometric transient signal data acquisition and analyte concentration calculation. *J. Anal. At. Spectrom*., **11**, 899–904.
23. Wilson, S. A., Briggs, P. H., Mee, J. S., and Siems, D. F. (1994) Determination of thirty-two major and trace elements in three NIST soil SRMs using ICP-AES and WDXRF. *Geostand. Newsl*., **18**, 85–9.
24. Jochum, K. P., Dingwell, D. B., Rocholl, A., Stoll, B., Hofmann, A. W., Becker, S., Besmehn, A., Bessette, D., Dietze, H. J., Dulski, P., Erzinger, J., Hellebrand, E., Hoppe, P., Horn, I., Janssens, K., Jenner, G. A., Klein, M., Mcdonough, W. F., Maetz, M., Mezger, K., Munker, C., Nikogosian, I. K., Pickhardt. C., Raczek, I., Rhede, D., Seufert, H. M., Simakin, S. G., Sobolev, A. V., Spettel, B., Straub, S., Vincze, L., Wallianos, A., Weckwerth, G., Weyer, S., Wolf, D., and Zimmer, M. (2000) The preparation and preliminary characterisation of eight geological MPI-DING reference glasses for in-site microanalysis. *Geostand. Newsl*., **24**, 87–133.
25. Wilson, S. A., Ridley, W. I., and Koenig, A. E. (2002) Development of sulfide calibration standards for the laser ablation inductively-coupled plasma mass spectrometry technique. *J. Anal. At. Spectrom*., **17**, 406–9.
26. Westheide, J. T., Becker, J. S., Jager, R., Dietze, H. J., and Broekaert, J. A. C. (1996) Analysis of ceramic layers for solid oxide fuel cells by laser ablation inductively coupled plasma mass spectroscopy. *J. Anal. At. Spectrom*., **11**, 661–6.
27. Odegard, M. (1999) Preparation of synthetic calibration materials for use in the microanalysis of oxide minerals by direct fusion in high-purity graphite electrodes: preliminary results for quartz and rutile. *Geostand. Newsl*., **23**, 173–86.
28. Pickhardt, C. and Becker, J. S. (2001) Trace analysis of high-purity graphite by LA-ICP-MS. *Fresenius' J. Anal. Chem*., **370**, 534–40.
29. Odegard, M., Mansfeld, J., and Dundas, S. H. (2001) Preparation of calibration materials for microanalysis of Ti minerals by direct fusion of synthetic and natural materials: experience with LA-ICP-MS analysis of some important minor and trace elements in ilmenite and rutile. *Fresenius' J. Anal. Chem*., **370**, 819–27.
30. Tibi, M. and Heumann, K. G. (2003) Isotope dilution mass spectrometry as a calibration method for the analysis of trace elements in powder samples by LA-ICP-MS. *J. Anal. At. Spectrom*., **18**, 1076–81.
31. Jackson, S. E., Longerich, H. P., Dunning, G. R., and Freyer, B. J. (1992) The application of laser-ablation microprobe; inductively coupled plasma-mass spectrometry (LAM-ICP-MS) to in situ trace-element determinations in minerals. *Can. Mineral*., **30**(Pt 4), 1049–64.

32. Günther, D., Von Quadt, A., Wirz, R., Cousin, H., and Dietrich, V. J. (2001) Elemental analyses using laser ablation-inductively coupled plasma-mass spectrometry (LA-ICP-MS) of geological samples fused with $Li_2B_4O_7$ and calibrated without matrix-matched standards. *Mikrochim. Acta*, **136**, 101–7.
33. Craig, C. A., Jarvis, K. E., and Clarke, L. J. (2000) An assessment of calibration strategies for the quantitative and semi-quantitative analysis of calcium carbonate matrices by laser ablation-inductively coupled plasma-mass spectrometry (LA-ICP-MS). *J. Anal. At. Spectrom.*, **15**, 1001–8.
34. Leach, A. M. and Hieftje, G. M. (2001) Standardless semi-quantitative analysis of metals using single-shot laser ablation inductively coupled plasma time-of-flight mass spectrometry. *Anal. Chem.*, **73**, 2959–67.
35. Latkoczy, C., Günther, D., and Odegard, M. (2003) Poster presentation at *European Winter Conference 2003*, Garmisch-Partenkirchen, Germany.
36. Leach, A. M. and Hieftje, G. M. (2002) Identification of alloys using single shot laser ablation inductively coupled plasma time-of-flight mass spectrometry. *J. Anal. At. Spectrom.*, **17**, 852–7.
37. Günther, D., Cousin, H., Magyar, B., and Leopold, I. (1997) Calibration studies on dried aerosols for laser ablation inductively coupled plasma mass spectrometry. *J. Anal. At. Spectrom.*, **12**, 165–70.
38. Leach, J. J., Allen, L. A., Aeschliman, D. B., and Houk, R. S. (1999) Calibration of laser ablation inductively coupled plasma mass spectrometry using standard additions with dried solution aerosols. *Anal. Chem.*, **71**, 440–5.
39. Pickhardt, C., Becker, J. S., and Dietze, H. J. (2000) A new strategy of solution calibration in laser ablation inductively coupled plasma mass spectrometry for multielement trace analysis of geological samples. *Fresenius' J. Anal. Chem.*, **368**, 173–81.
40. Becker, J. S., Pickhardt, C., and Dietze, H. J. (2001) Determination of trace elements in high-purity platinum by laser ablation inductively coupled plasma mass spectrometry using solution calibration. *J. Anal. At. Spectrom.*, **16**, 603–6.
41. Falk, H. F., Hattendorf, B., Krengelrothensee, K., Wieberneit, N., and Dannen, S. L. (1998) Calibration of laser-ablation ICP-MS. Can we use synthetic standards with pneumatic nebulization? *Fresenius' J. Anal. Chem.*, **362**, 468–72.
42. Boue-Bigne, F., Masters, B. J., Crighton, J. S., and Sharp, B. L. (1999) A calibration strategy for LA-ICP-MS analysis employing aqueous standards having modified absorption coefficients. *J. Anal. At. Spectrom.*, **14**, 1665–72.
43. Baldwin, D. P., Zamzow, D. S., and Dsilva, A. P. (1994) Aerosol mass measurement and solution based standard additions for quantitation in laser ablation inductively coupled plasma atomic emission spectrometry. *Anal. Chem.*, **66**, 1911–7.
44. Becker, J. S. (2002) Applications of inductively coupled plasma mass spectrometry and laser ablation inductively coupled plasma mass spectrometry in materials science. *Spectrochim. Acta B*, **57**, 1805–20.
45. Boulyga, S. F., Desideri, D., Meli, M. A., Testa, C., and Becker, J. S. (2003) Plutonium and americium determination in mosses by laser ablation ICP-MS combined with isotope dilution technique. *Int. J. Mass Spectrom.*, **226**, 329–39.
46. Perkins, W. T., Pearce, N.-J. G., and Jeffries, T. E. (1993) Laser ablation inductively coupled plasma mass spectrometry: a new technique for the determination of trace and ultra-trace elements in silicates. *Geochim. Cosmochim. Acta*, **57**, 475–82.
47. Sylvester, P. J. and Ghaderi, M. (1997) Trace element analysis of scheelite by excimer laser ablation inductively coupled plasma mass spectrometry (ELA-ICP-MS) using a synthetic silicate glass standard. *Chem. Geol.*, **141**, 49–65.

48. Guillong, M. and Günther, D. (2001) Quasi 'non-destructive' laser ablation-inductively coupled plasma-mass spectrometry fingerprinting of sapphires. *Spectrochim. Acta B*, **56**, 1219–31.
49. Christensen, J. N., Halliday, Alex N., Lee, Der Chuen, Hall, and Chris M. (1995) In situ Sr isotopic analysis by laser ablation. *Earth Planet. Sci. Lett*. **136**, 79–85.
50. Hirata, T., Hattori, Michinari; Tanaka, and Tsuyoshi (1998) In-situ osmium isotope ratio analyses of iridosmines by laser ablation-multiple collector-inductively coupled plasma mass spectrometry. *Chem. Geol*., **144**, 269–80.
51. Li, X. H., Liang, X. R., Sun, M., Guan, H., and Malpas, J. G. (2001) Precise Pb-206/U-238 age determination on zircons by laser ablation microprobe-inductively coupled plasma-mass spectrometry using continuous linear ablation. *Chem. Geol*., **175**, 209–19.
52. Becker, J. S. (2002) State-of-the-art and progress in precise and accurate isotope ratio measurements by ICP-MS and LA-ICP-MS: Plenary Lecture. *J. Anal. At. Spectrom*., **17**, 1172–85.
53. Hirata, T. (2002) In-situ precise isotopic analysis of tungsten using laser ablation multicollector inductively coupled plasma mass spectrometry (LA-MC-ICP-MS) with time resolved data acquisition. *J. Anal. At. Spectrom*., **17**, 204–10.
54. Prohaska, T., Latkoczy, C., Schultheis, G., Teschler-Nicola, M., and Stingeder, G. (2002) Investigation of Sr isotope ratios in prehistoric human bones and teeth using laser ablation ICP-MS and ICP-MS after Rb/Sr separation. *J. Anal. At. Spectrom*., **17**, 887–91.
55. Audetat, A., Günther, D., and Heinrich, C. A. (1998) Formation of a magmatic-hydrothermal ore deposit: insights with LA-ICP-MS analysis of fluid inclusions. *Science*, **279**, 2091–4.
56. Günther, D., Audetat, A., Frischknecht, R., and Heinrich, C. A. (1998) Quantitative analysis of major, minor and trace elements in fluid inclusions using laser ablation inductively coupled plasma mass spectrometry. *J. Anal. At. Spectrom*., **13**, 263–70.
57. Stalder, R., Foley, S. F., Brey, G. P., and Horn, I. (1998) Mineral aqueous fluid partitioning of trace elements at 900–1200°C and 3.0–5.7 GPa: new experimental data for garnet, clinopyroxene, and rutile, and implications for mantle metasomatism. *Geochim. Cosmochim. Acta*, **62**, 1781–801.
58. Vander Putten, E., Dehairs, F., Andre, L., and Baeyens, W. (1999) Quantitative in situ microanalysis of minor and trace elements in biogenic calcite using infrared laser ablation-inductively coupled plasma mass spectrometry: a critical evaluation. *Anal. Chim. Acta*, **378**, 261–72.
59. Becker, J. S., Pickhardt, C., and Dietze, H. J. (2000) Laser ablation inductively coupled plasma mass spectrometry for determination of trace elements in geological glasses. *Mikrochim. Acta*, **135**, 71–80.
60. Eggins, S. M., Rudnick, R. L., and Mcdonough, W. F. (1998) The composition of peridotites and their minerals: a laser-ablation ICP-MS study. *Earth Planet. Sci. Lett*., **154**, 53–71.
61. Campbell, A. J. and Humayun, M. (1999) Trace element microanalysis in iron meteorites by laser ablation ICP-MS. *Anal. Chem*., **71**, 939–46.
62. Tao, G.H., Fujikawa, Y., Mitsui, M., and Yamada, R. (2002) Determination of mercury in sediment samples by laser ablation inductively coupled plasma mass spectrometry. *J. Anal. At. Spectrom*., **17**, 560–2.
63. Odegard, M., Dundas, S. H., Flem, B., and Grimstvedt, A. (1998) Application of a double-focusing magnetic sector inductively coupled plasma mass spectrometer with laser ablation for the bulk analysis of rare earth elements in rocks fused with $Li_2B_4O_7$. *Fresenius' J. Anal. Chem*., **362**, 477–82.
64. Lee, S. H. and Son, B. M. (2001) Determination of rare earth elements in geological samples by laser ablation inductively coupled plasma mass spectrometry. *Anal. Sci*., **17**, a239–42.

65. Hirata, T. and Nesbitt, R. W. (1997) Distribution of platinum group elements and rhenium between metallic phases of iron meteorites. *Earth Planet. Sci. Lett*., **147**, 11–24.
66. Shibuya, E. K., Sarkis, J. E. S., Enzweiler, J., Jorge, A. P. S., and Figueiredo, A. M. G. (1998) Determination of platinum group elements and gold in geological materials using an ultraviolet laser ablation high-resolution inductively coupled plasma mass spectrometric technique. *J. Anal. At. Spectrom*., **13**, 941–4.
67. Allen, L., Georgitis, S., Myers, D. P., and Brushwyler, K. (1998) Trace elemental analysis of metals by laser ablation inductively coupled plasma time-of-flight mass spectrometry. *Phys. Status Solidi a*, **167**, 357–64.
68. Moenke, B. L., Schumann, T., Günther, D., Kuss, H. M., and Paul, M. (1992) Quantitative-analysis of glass using inductively coupled plasma atomic emission and mass-spectrometry, laser microanalysis inductively coupled plasma atomic emission-spectrometry and laser ablation inductively coupled plasma mass-spectrometry. *J. Anal. At. Spectrom*., **7**, 251–4.
69. Figg, D. and Kahr, M. S. (1997) Elemental fractionation of glass using laser ablation inductively coupled plasma mass spectrometry. *Appl. Spectrosc*., **51**, 1185–92.
70. Mason, P. R. D. and Mank, A. J. G. (2001) Depth-resolved analysis in multi-layered glass and metal materials using laser ablation inductively coupled plasma mass spectrometry (LA-ICP-MS). *J. Anal. At. Spectrom*., **16**, 1381–8.
71. Becker, J. S., Pickhardt, C., Hoffmann, N., and Hocker, H. (2002) Multielement analysis of alkaline-resistant glass and basalt glass fibers using laser ablation ICP-MS: a useful tool in technical textile quality control. *At. Spectrosc*., **23**, 1–6.
72. Yuzefovsky, A. I. and Miser, D. E. (1998) Analysis of discolored aluminum foil by laser ablation inductively coupled plasma mass spectrometry and scanning electron microscopy. *Appl. Spectrosc*., **52**, 629–37.
73. Borisov, O. V., Mao, X. L., Fernandez, A., Caetano, M., and Russo, R. E. (1999) Inductively coupled plasma mass spectrometric study of non-linear calibration behavior during laser ablation of binary Cu–Zn alloys. *Spectrochim. Acta B*, **54**, 1351–65.
74. Koch, J., Feldmann, I., Hattendorf, B., Günther, D., Engel, U., Jakubowski, N., Bolshov, M., Niemax, K., and Hergenroder, R. (2002) Trace element analysis of synthetic mono- and poly-crystalline CaF_2 by ultraviolet laser ablation inductively coupled plasma mass spectrometry at 266 and 193 nm. *Spectrochim. Acta B*, **57**, 1057–70.
75. Becker, J. S., Soman, R. S., Becker, T., Panday, V. K., and Dietze, H. J. (1998) Trace and ultratrace analysis of gallium arsenide by different mass spectrometric techniques. *J. Anal. At. Spectrom*., **13**, 983–7.
76. Hoffmann, E., Ludke, C., Skole, J., Stephanowitz, H., and Wagner, G. (1999) Studies on the quantitative analysis of trace elements in single SiC crystals using laser ablation-ICP-MS. *J. Anal. At. Spectrom*., **14**, 1679–84.
77. Pattberg, S. and Matschat, R. (1999) Determination of trace impurities in high purity copper using sector-field ICP-MS: continuous nebulization, flow injection analysis and laser ablation. *Fresenius' J. Anal. Chem*., **364**, 410–6.
78. Bleiner, D., Plotnikov, A., Vogt, C., Wetzig, K., and Günther, D. (2000) Depth profile analysis of various titanium based coatings on steel and tungsten carbide using laser ablation inductively coupled plasma–'time of flight' mass spectrometry. *Fresenius' J. Anal. Chem*., **368**, 221–6.
79. Bi, M., Ruiz, A. M., Gornushkin, I., Smith, B. W., and Winefordner, J. D. (2000) Profiling of patterned metal layers by laser ablation inductively coupled plasma mass spectrometry (LA-ICP-MS). *Appl. Surf. Sci*., **158**, 197–204.
80. Plotnikov, A., Vogt, C., Hoffmann, V., Taschner, C., and Wetzig, K. (2001) Application of laser ablation inductively coupled plasma quadrupole mass spectrometry (LA-ICP-QMS) for depth profile analysis. *J. Anal. At. Spectrom*., **16**, 1290–5.

81. Buldini, P. L., Mevoli, A., and Sharma, J. L. (1998) LA-ICP-MS, IC and DPASV-DPCSV determination of metallic impurities in solar-grade silicon. *Talanta*, **47**, 203–12.
82. Schroeder, E., Hamester, M., and Kaiser, M. (1998) Properties and characteristics of a laser ablation ICP-MS system for the quantitative elemental analysis of glasses. *Appl. Surf. Sci*., **129**, 292–8.
83. Baker, S. A., Dellavecchia, M. J., Smith, B. W., and Winefordner, J. D. (1997) Analysis of silicon nitride bearings with laser ablation inductively coupled plasma mass spectrometry. *Anal. Chim. Acta*, **355**, 113–9.
84. Becker, J. S., Westheide, J., Saprykin, A. I., Holzbrecher, H., Breuer, U., and Dietze, H. J. (1997) Mass spectrometric analysis of ceramic components for solid oxide fuel cells. *Mikrochim. Acta*, **125**, 153–60.
85. Giapintzakis, J., Sfounis, A., and Velegrakis, M. (1999) A comparative mass spectroscopic study between infrared and ultraviolet laser ablation of a superconducting $YBa_2Cu_3O_{7-x}$ target. *Int. J. Mass Spectrom., Ion Processes*, **189**, 1–7.
86. Gastel, M., Becker, J. S., Kuppers, G., and Dietze, H. J. (1997) Determination of long-lived radionuclides in concrete matrix by laser ablation inductively coupled plasma mass spectrometry. *Spectrochim. Acta B*, **52**, 2051–9.
87. Leloup, C., Marty, P., Dallava, D., and Perdereau, M. (1997) Quantitative analysis for impurities in uranium by laser ablation inductively coupled plasma mass spectrometry: Improvements in the experimental setup. *J. Anal. At. Spectrom*., **12**, 945–50.
88. Becker, J. S., Pickhardt, C., and Dietze, H. J. (2000) Laser ablation inductively coupled plasma mass spectrometry for the trace, ultratrace and isotope analysis of long-lived radionuclides in solid samples. *Int. J. Mass Spectrom. Ion Processes*, **202**, 283–97.
89. Becker, J. S. and Dietze, H. J. (2000) Inorganic mass spectrometric methods for trace, ultratrace, isotope, and surface analysis. *Int. J. Mass Spectrom. Ion Processes*, **197**, 1–35.
90. Wolf, R. E., Thomas, C., and Bohlke, A. (1998) Analytical determination of metals in industrial polymers by laser ablation ICP-MS. *Appl. Surf. Sci*., **129**, 299–303.
91. Dobney, A. M., Mank, A. J. G., Grobecker, K. H., Conneely, P., and de Koster, C. G. (2000) Laser ablation inductively coupled plasma mass spectrometry as a tool for studying heterogeneity within polymers. *Anal. Chim. Acta*, **423**, 9–19.
92. Bings, N. H. (2002) Direct determination of metals in lubricating oils by laser ablation coupled to inductively coupled plasma time-of-flight mass spectrometry. *J. Anal. At. Spectrom*., **17**, 759–67.
93. Chi, P. H., Ko, F. H., Hsu, C. T., Chen, H. L., Yang, C. K., Sun, Y. C., and Yang, M. H. (2002) Direct impurity analysis of semiconductor photoresist samples with laser ablation ICP-MS. *J. Anal. At. Spectrom*., **17**, 358–65.
94. Rings, S., Sievers, R., and Jansen, M. (1999) Analysis of the spatial distribution of the constituting elements in amorphous solids: laser ablation with ICP spectrometry. *Fresenius' J. Anal. Chem*., **363**, 165–73.
95. Ghazi, A. M., Shuttleworth, S., Angulo, S. J., and Pashley, D. H. (2000) Gallium diffusion in human root dentin: quantitative measurements by pulsed Nd:YAG laser ablation combined with an inductively coupled plasma mass spectrometer. *J. Clin. Laser Med. Surg*., **18**, 173–83.
96. Ghazi, A. M., Shuttleworth, S., Simmons, R., Paul, S. J., and Pashley, D. H. (2002) Nanoleakage at the dentin adhesive interface: a new application for laser ablation-sector field-ICPMS. *J. Anal. At. Spectrom*., **17**, 682–7.
97. Hoffmann, E., Stephanowitz, H., Ullrich, E., Skole, J., Ludke, C., and Hoffmann, B. (2000) Investigation of mercury migration in human teeth using spatially resolved analysis by laser ablation-ICP-MS. *J. Anal. At. Spectrom*., **15**, 663–7.

98. Raith, A., Perkins, W. T., Pearce, N. J. G., and Jeffries, T. E. (1996) Environmental monitoring on shellfish using uv laser ablation icp ms. *Fresenius' J. Anal. Chem.*, **355**, 789–92.
99. Ghazi, A. M., Wataha, J. C., O'Dell, N. L., Singh, B. B., Simmons, R., and Shuttleworth, S. (2002) Quantitative concentration profiling of nickel in tissues around metal implants: a new biomedical application of laser ablation sector field ICP-MS. *J. Anal. At. Spectrom.*, **17**, 1295–9.
100. Wang, S., Brown, R., and Gray, D. J. (1994) Application of laser ablation ICP-MS to the spatially resolved micro-analysis of biological tissue. *Appl. Spectrosc.*, **48**, 1321–5.
101. Fan, T. W. M., Pruszkowski, E., and Shuttleworth, S. (2002) Speciation of selenoproteins in Se-contaminated wildlife by gel electrophoresis and laser ablation-ICP-MS. *J. Anal. At. Spectrom.*, **17**, 1621–3.
102. Marshall, P., Heudi, O., Bains, S., Freeman, H. N., Abou-Shakra, F., and Reardon, K. (2002) The determination of protein phosphorylation on electrophoresis gel blots by laser ablation inductively coupled plasma-mass spectrometry. *Analyst*, **127**, 459–61.
103. Watling, R. J., Lynch, B. F., and Herring, D. (1997) Use of laser ablation inductively coupled plasma mass spectrometry for fingerprinting scene of crime evidence. *J. Anal. At. Spectrom.*, **12**, 195–203.
104. Watling, R. J. (1998) Sourcing the provenance of cannabis crops using inter-element association patterns 'fingerprinting' and laser ablation inductively coupled plasma mass spectrometry. *J. Anal. At. Spectrom.*, **13**, 917–26.
105. Wanner, B., Moor, C., Richner, P., Bronnimann, R., and Magyar, B. (1999) Laser ablation inductively coupled plasma mass spectrometry (LA-ICP-MS) for spatially resolved trace element determination of solids using an autofocus system. *Spectrochim. Acta B*, **54**, 289–98.
106. Hoffmann, E., Stephanowitz, H., and Skole, J. (1996) Investigations of the migration of elements in tree rings by laser ICP-MS. *Fresenius' J. Anal. Chem.*, **355**, 690–3.
107. Scholze, H., Hoffmann, E., Ludke, C., and Platalla, A. (1996) Analysis of leaves by using the laser ICP MS with isotope dissolution method. *Fresenius' J. Anal. Chem.*, **355**, 892–4.
108. Watmough, S. A., Hutchinson, T. C., and Evans, R. D. (1997) Application of laser ablation inductively coupled plasma mass spectrometry in dendrochemical analysis. *Environ. Sci. Technol.*, **31**, 114–8.
109. Prohaska, T., Stadlbauer, C., Wimmer, R., Stingeder, G., Latkoczy, C., Hoffmann, E., and Stephanowitz, H. (1998) Investigation of element variability in tree rings of young Norway spruce by laser-ablation-ICP-MS. *Sci. Total Environ.*, **219**, 29–39.
110. Narewski, U., Werner, G., Schulz, H., and Vogt, C. (2000) Application of laser ablation inductively coupled mass spectrometry (LA-ICP-MS) for the determination of major, minor, and trace elements in bark samples. *Fresenius' J. Anal. Chem.*, **366**, 167–70.
111. Wang, C. F., Jeng, S. L., and Shieh, F. J. (1997) Determination of arsenic in airborne particulate matter by inductively coupled plasma mass spectrometry. *J. Anal. At. Spectrom.*, **12**, 61–7.
112. Motelica-Heino, M., Rauch, S., Morrison, G. M., and Donard, O. F. X. (2001) Determination of palladium, platinum and rhodium concentrations in urban road sediments by laser ablation-ICP-MS. *Anal. Chim. Acta*, **436**, 233–44.
113. Motelica-Heino, M., Le Coustumer, P., Thomassin, J. H., Gauthier, A., and Donard, O. F. X. (1998). Macro and microchemistry of trace metals in vitrified domestic wastes by laser ablation ICP-MS and scanning electron microprobe X-ray energy dispersive spectroscopy. *Talanta*, **46**, 407–22.
114. Bellotto, V. R. and Miekeley, N. (2000) Improvements in calibration procedures for the quantitative determination of trace elements in carbonate material (mussel shells) by laser ablation ICP-MS. *Fresenius' J. Anal. Chem.*, **367**, 635–40.

115. Thorrold, S. R. and Shuttleworth, S. (2000) In situ analysis of trace elements and isotope ratios in fish otoliths using laser ablation sector field inductively coupled plasma mass spectrometry. *Can. J. Fish. Aquat. Sci*., **57**, 1232–42.
116. Thorrold, S. R., Latkoczy, C., Swart, P. K., and Jones, C. M. (2001) Natal homing in a marine fish metapopulation. *Science*, **291**, 297–9.
117. Balaram, V. (1996) Recent trends in the instrumental analysis of rare earth elements in geological and industrial materials. *TrAC Trends Anal. Chem*., **15**, 475–486.
118. Durrant, S. F. (1999) Laser ablation inductively coupled plasma mass spectrometry: achievements, problems, prospects. *J. Anal. At. Spectrom*., **14**, 1385–403.
119. Günther, D., Jackson, S. E., and Longerich, H. P. (1999) Laser ablation and arc/spark solid sample introduction into inductively coupled plasma mass spectrometers [Review]. *Spectrochim. Acta B*, **54**, 381–409.
120. Watling, R. J. (1999) Novel application of laser ablation inductively coupled plasma mass spectrometry (LA-ICP-MS). in the field of forensic science and forensic archaeology. *Spectroscopy*, **14** (6), 16–34.
121. Günther, D., Horn, I., and Hattendorf, B. (2000) Recent trends and developments in laser ablation-ICP-mass spectrometry. *Fresenius' J. Anal. Chem*., **368**, 4–14.

Chapter 7

Trace Metal Speciation with ICP-MS Detection

Eva Krupp, Fabienne Seby, Rosa Rodríguez Martín-Doimeadios, Alison Holliday, Mariella Moldován, Gunda Köllensperger, Stephan Hann and Olivier F X Donard

7.1 Introduction

The IUPAC (International Union for Pure and Applied Chemistry) recommends the following definitions for the terms 'chemical species', 'speciation analysis' and 'speciation'[1]:

A 'chemical species' is the specific form of an element as defined by its isotopic composition, electronic or oxidation state and/or complex or molecular structure. 'Speciation analysis' describes the identification and quantification of individual 'chemical species' in a sample, and 'speciation' is the distribution of a given element species in a system.

Speciation analysis has become an important field in analytical chemistry in the recent years, and is still growing. It is well accepted in the scientific community that only the information on the species in which an element occurs, i.e. the chemical form, can provide necessary knowledge about its environmental or health impact. The numerous reviews and the rising number of papers published in peer reviewed journals stress this trend.

Since the Minamata disaster in the 1950s, when hundreds of people were poisoned and several died because their fish diet was highly loaded with methylmercury, element species information has become of public interest. With the movie 'Erin Brokovich', a true story about a young woman who discovered chromium(VI) contamination of drinking water, speciation even made it into the cinema.[2]

The importance of species information rather than total element concentration becomes clear when looking at environmental cycling processes.

The biogeochemical cycling of an element is governed by the transformation of this element into different species. Each species has different physico-chemical properties and behaves according to them; e.g. volatile species being released into the atmosphere, or compounds prone to biomagnification, such as methylmercury, being taken up by fish or other living organisms.[3,4]

If we look at the aquatic mercury cycle as an example, we find ourselves in an extremely complicated network of reactions, each one of them depending on the respective environmental conditions in the respective compartment, where the mercury is present.

The mercury cycle reproduced in Figure 7.1 does in fact describe only a part of all the reactions taking place in reality. The cycle of biomethylation, volatilisation, subsequent washout and reintroduction into the water body gives us the feeling that we can literally observe a single

Inductively Coupled Plasma Mass Spectrometry Handbook Edited by Simon M. Nelms
 ISBN: 978-1-405-10916-1

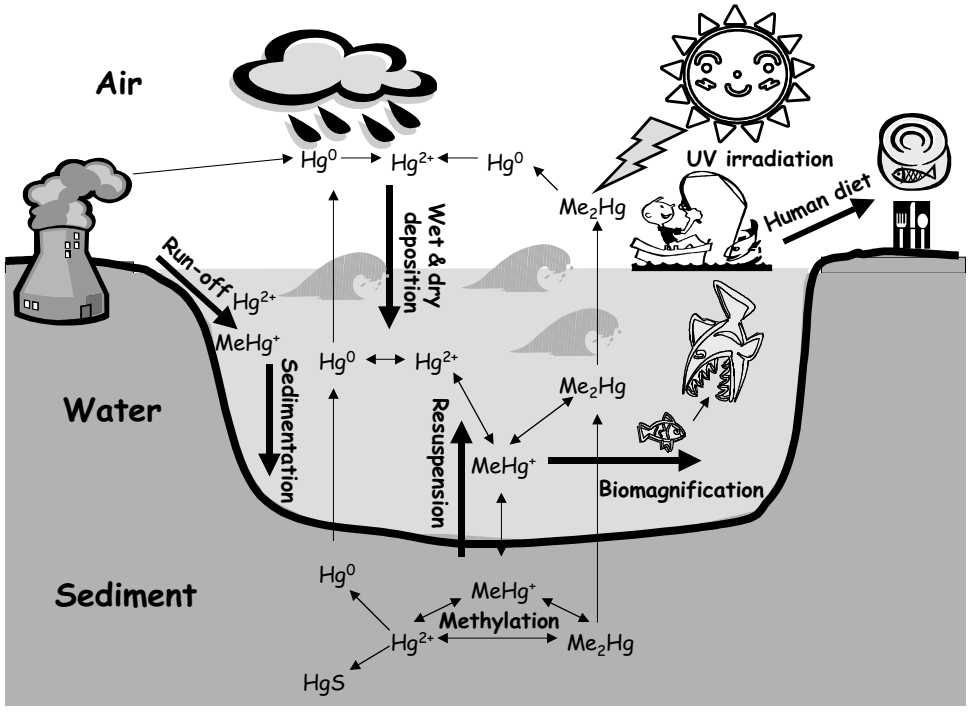

Figure 7.1 The aquatic mercury cycle.

mercury atom cycling around the globe in an eternal loop. Of special interest in speciation studies is monomethylmercury ($HgMe^+$), derived, e.g., from anaerobic biomethylation. This compound is prone to biomagnification via the food chain in higher marine organisms like tuna fish, and enters the human diet through this pathway.

This has lately led to concern about fish and shellfish consumption, and in March 2004 the US Food and Drug Administration (FDA) together with the US Environmental Protection Agency (EPA) launched a campaign of recommendation for pregnant women, nursing women and young children to reduce fish consumption to low-level-mercury specimens, and to limit seafood consumption to 2 meals per week.[6] A similar, but not as strict, recommendation has been released by the French Food Agency (AFSSA).[7]

In all parts of element cycling, important questions are arising: Where are the sinks and sources of the element in question, what is the anthropogenic impact compared to the natural background, which species introduced by anthropogenic activity are available for biomethylation, will, e.g., climate changes have an impact on the species distribution and thus the bioavailability, and which sinks may turn into sources and vice versa?

To address all these questions, speciation analysis has to be performed in all types of matrices usually at trace or ultratrace concentrations. Several analytical techniques have been developed for speciation analysis, usually consisting of a chromatographic step for the species separation [liquid chromatography (LC), capillary electrophoresis (CE) or gas chromatography (GC)], followed by detection using an element selective detector, for example atomic

fluorescence (AFS), atomic emission spectroscopy (MIP-OES, ICP-OES) and, to an increasing extent, ICP-MS.

The use of ICP-MS as an element selective detector has unique advantages, and this chapter exclusively focuses on speciation employing ICP-MS.

ICP-MS offers not only unequalled sensitivity and selectivity for a majority of elements in the Periodic Table, but is also a robust detector that can (more or less easily) be coupled to any of the aforementioned chromatographic separation techniques.[8,9] Moreover, the multi-element and multi-isotope abilities offer invaluable potential for environmental studies. For example, for mercury, isotopically labelled tracers have been introduced into the environment or used in laboratory experiments, which has shed light on extremely complex reaction pathways.[10,11]

The development of species-specific isotope dilution analysis, i.e. using a spike with isotopically labelled species, has led to more precision and accuracy in the quantitative results, because with this technique, species loss, transformation or degradation during storage and sample preparation steps can be recognised and corrected for.[12,13] Therefore, isotope dilution techniques for speciation are also discussed.

As is the case for all analytical methods, the sampling, sample storage, sample preparation steps and subsequent measurement parameters are of prime importance in order to yield correct, i.e. accurate and precise, results. Many of the species we look at are prone to oxidation under normal atmospheric conditions and destruction by UV radiation or water vapour, and especially redox species [Cr(III)/Cr(VI), As(III)/As(V) or Fe(II)/Fe(III)] tend to undergo interconversion reactions. It is thus imperative to carefully preserve the species distribution until the final measurement. Here, the introduction of isotope dilution into speciation analysis, as mentioned above, has been a huge step forward.

During the recent years, special protocols have been developed according to the species, the matrix and the analytical requirements concerned, and will be highlighted later on in this chapter.

As speciation analysis slowly enters authority's regulations (already the case for chromium, organotin and methylmercury species) and routine analysis becomes required, precise and accurate quantitative species determination, as well as access to certified reference materials, is becoming imperative.

Finally, recent trends and developments in speciation analysis using collision and reaction cell ICP-MS and multicollector-ICP-MS (MC-ICP-MS) will be discussed. This new instrumentation opens up more possibilities in speciation analysis, be it for the measurement of elements traditionally not attempted with ICP-MS or for element isotopes traditionally ruled out due to molecular interference, like ^{56}Fe or ^{80}Se, as well as opening up new opportunities in the determination of precise isotope ratios in species.

7.2 Sampling and storage for speciation analysis

In speciation analysis, the sampling step must always be considered as the most important part on the way to obtaining accurate and meaningful results at the end of the overall analytical procedure. Errors produced during the collection of samples, be it due to contamination, non-quantitative or non-homogeneous sampling, can never be retrieved, no matter how powerful or precise the final analytical measurement may be. While this statement is true for any kind of sample and analyte, it is even more pronounced when performing speciation analysis. Here, the procedures chosen must additionally provide species preservation, namely avoiding species

loss due to, e.g., volatilisation, species decomposition or transformation, but also irreversible adsorption on container walls or sorbent material. The requirements for sampling and storage mainly depend on the physico-chemical properties of the species of interest, but also on its concentration, the sample matrix and the analytical method envisaged.

In the following sections, we will discuss and introduce a number of sampling and storing strategies applied prior to speciation analysis. For the interested reader, comprehensive information on sample preparation strategies in speciation analysis can also be found elsewhere.[15,16]

7.2.1 Gaseous samples

The first point to be considered in gaseous material sampling is to determine whether samples can be collected in a controlled environment. Sewage gas can be sampled directly from a continuously processed fermentation tank; thus the gas composition will not vary for several hours or even days. Landfill gas sampled from a gas drainage system will also maintain a similar composition on the long term. When sampling is performed from closed 'batch' systems, e.g. in bacterial fermentation experiments, care has to be taken about the amount of gas removed. In small batches, the gas pressure change may induce changes in the reaction behaviour and thus falsify the results. When sampling hot gases, e.g. from a stack, gas should be sampled isothermally in order to avoid condensation or chemical reaction during the transport of the species into the sampling device. Special care must be taken when sampling in the open field. Wind, rain, sun; basically all kinds of weather conditions must be taken into account. Sampling of diffuse sources has often been attempted using so-called flux chambers. These are most often boxes made from Plexiglas or other inert materials that keep out wind and rain. Soil gas sampling is performed through perforated plastic tubes inserted vertically into the ground. The upper connection to the ground must be carefully tightened with clay in order to avoid sampling of ambient air instead of soil gas.

The main problems encountered with sampling, storage and subsequent transfer into the ICP-MS for analysis are related to humidity, gaseous matrix compounds and the usually low analyte concentration, which necessitates analyte preconcentration.

One sampling technique for gaseous mercury compounds has been described, based on species-specific adsorption using a chain of different traps where the gas was pumped through. This technique implies that the species selective adsorption is ensured for all kinds of sample matrix and species concentration, which is a difficult task. Other authors employ trapping of organolead species on a mixture of the sorbents Tenax and Porapak[17,18] or trapping of $SbMe_3$.[19] While organolead species seem to be stable for at least 45 days when stored at 4°C, $SbMe_3$ is less stable.

The technique most often used for sampling and storage is cryofocusing on a solid support. A typical sampling chain as shown in Figure 7.2 consists of a filter for separation from particulate matter, a drying device, the actual trap emerged in liquid nitrogen or a cooling mixture at a certain temperature, a suction pump and a gas meter in line. The pump will draw the gas through the whole system, which must be connected gas-tight with inert (preferably Teflon) tubing. In general, a few litres of gas are collected, and the gaseous species are preconcentrated in the trap on an inert support. After sampling, this trap is disconnected from the system, closed with Teflon stoppers to avoid loss or air contact, and stored cryogenically at −196°C until measurement.

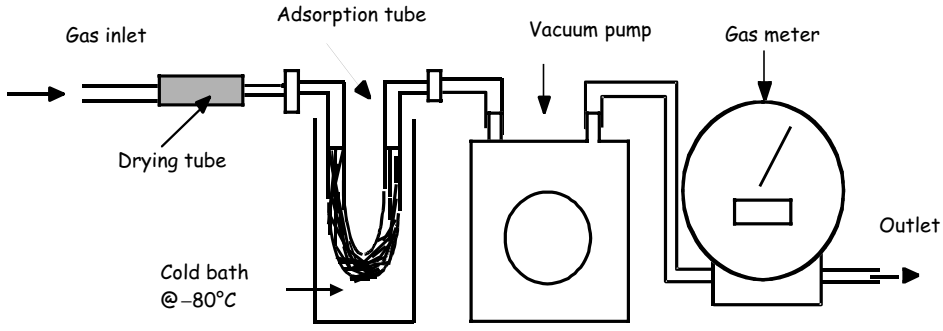

Figure 7.2 Schematic of a simple cryofocusing apparatus for the collection of volatile organometallic compounds in gases.

Storage under cryogenic conditions not only ensures that samples are in an inert atmosphere, in the dark, but also kinetically inhibits any reactions.

Sampling in Tedlar® bags has been employed when gas samples were taken in remote areas. Different volatile metal compounds (VMCs) of arsenic, tin and antimony were shown to be stable for at least a few days, provided they were stored in the dark to prevent UV-mediated decomposition.[20–22]

The advantage of cryogenic sampling is that the technique is non-specific, which means a range of species with similar physico-chemical properties can be trapped simultaneously. The inert support provides easy and quantitative thermodesorption, which can be performed directly in a gas chromatographic device connected to the ICP-MS. Also, the sample is preconcentrated and, more or less, matrix separated. The main constraints are due to gas humidity and co-trapped matrix gases.

For gas drying, either chemical (drying tubes filled with $CaCl_2$ or $MgClO_4$)[23–25] or physical (Nafion membrane, cold trap)[26,27] methods were used. A review on the different strategies for gas drying has been published by Namiesnik and Wardencki.[28]

The problem of high concentration in matrix gases mostly concerns measurements in anaerobic environments or combustion processes. Here, the gas is charged with methane, CO_2 and/or SO_2. As non-specific sampling is performed, based on physical adsorption, the determining factor for sampling is the species' boiling point. This means that matrix gases with boiling points similar to those of the analytes are trapped as well. Thus, cryotraps may be blocked before the desired amount of gas is collected, or the comparably huge amount of matrix gas eluting during the analysis step may drastically disturb the chromatographic and analytical conditions.

To overcome co-trapping of matrix gases like CO_2 or SO_2, trapping temperatures higher than that of liquid nitrogen are used.[29] For sewage and landfill gas sampling for example, the gas was trapped at $-80^{\circ}C$. The disadvantage of this method is that very low boiling species, like hydrides, are not quantitatively trapped. CO_2 may also be removed by the use of a cartridge filled with NaOH, but this is feasible for very volatile species only. An overview on cryofocusing for VMCs has recently been published, which highlights the problems of quantitative sampling and gas matrix compounds.[30]

Despite these problems, cryotrapping is the most often and most successfully applied technique for sampling and storage of VMCs.

7.2.2 Water (aqueous) samples

Organometallic compounds dissolved in water are mostly ionic species, i.e. partly alkylated metal atoms with at least one free valence bond. These ionic species are most likely present as hydrate complexes, but may also be coordinated with a counterion.

Gaseous organometallic species like $HgMe_2$, Hg^0 or methylated selenium may be dissolved in the water phase, and are usually determined after purging from the water phase into a cryogenic sampling and detection system as described for the determination of VMCs. This step should be performed as soon as possible, ideally on-site or soon after the arrival of the sample in the laboratory.

Organometallic species in the water phase are subject to adsorption on the container surface, the extent of adsorption depending on the lipophilic character of the species: the least polar species will be adsorbed most efficiently, which in turn can provoke species decomposition. The same effect is observed on particles or colloids present in the water sample; therefore, in case of high amounts of suspended matter, filtration is necessary prior to sampling. The sampling should always be performed ensuring as little air contact as possible, e.g. filling and closing sample containers under water, as many organometallic species are prone to oxidation.

Organotin species stability in environmental waters has been investigated. Filtration is necessary especially for tributyltin (TBT), which tends to adsorb to particles. Tributyltin (TBT), dibutyltin (DBT) and monobutyltin (MBT) in filtered, acidified seawater stored in the dark at 4°C were stable for a period of 4 months,[31] and TBT was shown to be stable in Pyrex glass at 4°C for 4–5 months.[31] On the contrary, phenyltins degraded during the first month of storage.[32]

The most efficient way is to store the samples deep-frozen immediately after sampling, using polyethylene or polycarbonate containers. Under this condition, TBT was shown to be stable for 2–3 months.[33] Polytetrafluoroethylene (PTFE) as the container material was shown to cause species loss, most probably owing to the porosity of this material.[34–36] Poly(vinyl chloride) (PVC) bottles must be ruled out as container material, because PVC contains TBT for UV stabilisation which has been found to leach out of PVC containers[37] and also from PVC tubes used for water supply.[38] Several reviews on this topic can be found.[39–43]

Ionic lead species were stable in water stored in the dark at 4°C for up to 3 months, while tetraalkylated lead was less stable.[44]

For the preservation of mercury species, some authors recommend acidification of the water sample with HNO_3.[45] Hintelmann[46] reports that MeHg in water samples is stable for at least 6 months when acidified to 1% HCl, or when deep-frozen immediately after sampling and storing in the dark. No special container material was recommended, but in an earlier publication[47] it was stated that Teflon and glass are appropriate, while plastics like polypropylene and polyethylene cause loss due to adsorption on the container walls.

No common statement can be given for the stability of arsenic compounds in water samples. Many different arsenic compounds have to be considered, such as the redox pair As(III)/As(V), the methylated compounds MMA (monomethylarsenic) and DMA (dimethylarsenic) (in either 3- or 5-valent forms), and arsenobetaine (AsB), arsenocholine (AsC) and the larger arsenosugars, which require different storage conditions.[48] For example, the arsenic species As(III), As(V), MMA and DMA were found to be stable in water samples without any preservation, when analysis was carried out during the following 24 h. Urine and water containing As(V), MMA, DMA, AsB and AsC were stable when stored at −20°C.[49]

Sampling and storage conditions must thus be adapted to the species present in the respective sample, and to the species intended to be analysed. Usually, only the inorganic arsenic and the small, methylated arsenic compounds are determined by GC methods, e.g. by using hydride-generation GC-ICP-MS. A complementary method must be used for the determination of, e.g., AsB or AsC. Although non-conclusive and not in agreement with other experiments, the degradation of AsB to DMA has been described.[48–50] This would misrepresent results on DMA analysis, when carried out after long-term storage.

In the case of Cr or Se speciation in waters, it is generally recommended to freeze samples immediately after filtration. If only redox species have to be determined and freezing is not possible, storage has to be done in an inert atmosphere.[51,52]

In any case, the stability of species during storage depends greatly on the matrix in which they are incorporated. As many of the stability experiments are performed with high concentration standards, no conclusion can be drawn on the stability of the same species, present at low concentration in a complex matrix. The aim should thus always be to store samples in cold and dark conditions and to perform the measurements with the shortest possible delay.

This topic has been reviewed by Quevauviller[42] and Gomez-Ariza.[43]

7.2.3 Solid samples

In comparison to aqueous samples, the handling of solid samples poses additional problems in terms of sample homogeneity. Solid samples may be soil or sediments, but also include sludge or faeces, which are much more complicated matrices. Organic matter may be abundant, and thus microbial activity high. Humic substance tends to bind lipophilic species, ionic species may be bound to clay surfaces, and pore water or general high humidity may be present. In addition, samples may be completely inhomogeneous, containing stones, wood pieces, or rubbish like plastic bags or old shoes. Great problems may be encountered when, e.g., sampling harbour sediments for TBT analysis. This compound is used in anti-fouling paints, which is the main route of sediment and seawater contamination with butyltins. A piece of dry paint scratched off from a boat surface and sampled with the sediment will give enormous concentrations of TBT in this sample, but will of course not reflect the overall sediment or water contamination.

In order to perform representative sampling of solid matter, the amount of sample should be generally large. For partitioning of aliquots, the sample must be free of large pieces, homogenised, and, if possible, dry. All these treatment steps involve intensive sample handling and may induce species conversion or loss.

In the literature, general discussions concerning the stability of CRMs can be found.[43,53] In the following paragraphs, we highlight storage conditions for organotin species and methylmercury in sediments, which are environmentally the most important species investigated in such samples.

For organotin species in sediments, storage under wet and dry conditions has been investigated at temperatures between -20 and $+40^{\circ}$C.[31,32,54] A degradation of MBT, DBT and TBT was found when samples were stored above 4°C, but stability for up to 1 year storage time was found when storing samples at -20°C.[32,54] The long-term storage of sediments at 4°C has proven to lead to significant degradation of organotins,[31] as demonstrated with the reference material BCR 462.[55] This coastal sediment had to be re-certified for its organotin content after 2 years of

storage at 4°C. Evidently, freeze-drying and storing at −20°C is a preferred means of preserving organotin species in sediment samples.[32]

For methylmercury in sediments, the main reason for loss is due to bacterial activity, leading to either demethylation or loss due to volatilisation, when methylmercury is converted to the volatile dimethylmercury.[55,57] γ-Radiation was proposed for the stabilisation of methylmercury, as the compound itself is not affected, but bacteria and microbes are effectively eliminated.[58]

Hintelmann recommends to immediately freeze the samples in order to suppress microbial activity. He also states that no statistical difference could be detected between wet, air-dried and oven-dried sediments, but that dry sediments provide more precise results, simply because a wet sediment slurry cannot be divided into subsamples as precisely.[46]

In the case of soil or sediment samples where As, Cr and Se speciation is required, conventional handling of solid environmental samples, including drying by lyophilisation and storage at −18°C, is generally used.[48,51,52]

Chromium speciation is very often performed in workplace air and a careful selection of the filter medium used for collecting dusts is of paramount importance. Cellulosic filters and glass fibre filters containing binders are ordinarily unsuitable, as these filter types can lead to significant reduction of Cr(VI). Filter materials acceptable for sampling of airborne Cr(VI) include PVC, PVF, PTFE or quartz fibre filters.[52,59]

7.2.4 Biological tissues

The range of biological tissues investigated for speciation issues is broad, although in most cases, measurement of a particular tissue is associated with determination of a particular species.

Methylmercury determination is dedicated to fish analysis, where methylmercury is found in relatively high amounts because of biomagnification.

Butyltins are mainly investigated in bivalve or mollusc tissues, e.g. oysters, because of the anthropogenic contamination of water with anti-fouling paints. Harbour or estuarine areas are of main concern, as the major contamination stems from boat hull painting, and estuaries are common grounds for oyster or shellfish farming.

Arsenic species are mainly determined in shellfish, but also in plants and algae, amongst others. One common point for sampling and storage is that these kinds of samples should be immediately frozen in order to suppress any enzymatic activity, proteolysis or autolysis.

For butyltin in biota, freeze-drying and storage at −20°C or better at −70°C will provide long-term stability over years, while phenyltins are at least stable over months.[60] For methylmercury, samples should also be stored freeze-dried and frozen.[46] MMA, DMA, AsB and AsC have been shown to be stable when spiked into fish samples at different temperatures.[50]

7.3 Speciation with CE-ICP-MS

7.3.1 Introduction

The importance of capillary electrophoresis (CE) in separation science has increased dramatically over the last 10 years. The complementarity of CE to other separation techniques, especially high-performance liquid chromatography (HPLC), has made its presence essential in a modern

analytical laboratory. The extraordinary resolution power of up to 500 000 or even 1 000 000 theoretical plates and the capability to separate anionic, cationic and neutral molecules in a single run are the obvious advantages of the technique. Several authors have suggested the possibility of monitoring complex chemical systems without influencing them, since separation is based on the movement of ions under the effect of the electric field rather than chemical interaction. The method is versatile and as such applicable to a diverse range of target analytes. While initially separation schemes were mainly developed focusing on investigation of macromolecules, the method can also be used for efficient separation of low-molecular-weight cations and anions. Hyphenation of CE to the sensitive and element-selective ICP-MS significantly increased the potential of the method, accelerating its use in speciation analysis. However, since 1995 when CE-ICP-MS was first introduced,[61] the technical difficulties of connecting the CE with the sample introduction system of the ICP-MS became evident.[62] Hence, the first years of CE-ICP-MS research were primarily focused on interface development.

7.3.2 Capillary electrophoresis

In CE, separation of charged species is based on their different migration properties along a capillary tube in a constant electric field. The capillary is filled with suitable conducting buffer and both ends of the capillary are immersed in buffer vials (see Figure 7.3). The electric field is established by applying a voltage gradient (10–30 kV) via Pt electrodes at both ends of the flexible CE capillary. The capillaries are made of fused silica, containing surface silanol groups (SiOH). Typically, capillary dimensions are an internal diameter of 20–100 μm, an external diameter of 150–520 μm and a length of 20–100 cm. Injection volumes range from 2 to 20 nL, depending

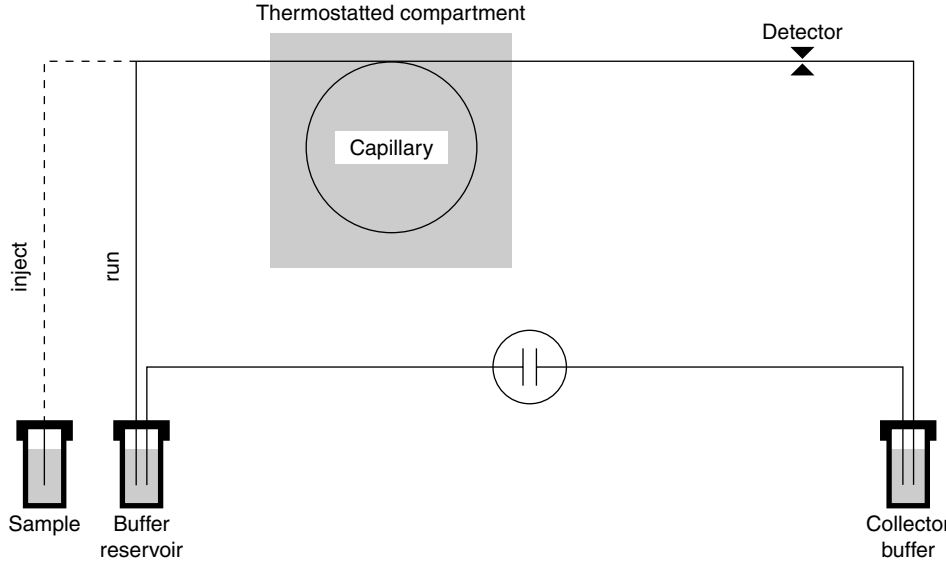

Figure 7.3 Capillary electrophoresis.

on capillary dimension and mode of injection (electrokinetic, hydrostatic and hydrodynamic injections).

The migration of ions in the capillary upon application of the electric field is controlled by two phenomena, the electrophoretic mobility and the electro-osmotic flow (EOF), which is a fundamental constituent of the CE operation. The electrophoretic mobility of an analyte depends on its charge, size and shape. The EOF is the bulk flow of a liquid in the capillary. Its occurrence is a consequence of the surface charge of the inner capillary wall. A unique feature of EOF is its flat profile, resulting in excellent resolution. In contrast, pressure-driven or laminar flows show a parabolic profile. By optimising the EOF and the applied voltage, the combined effects of the two forces, electrophoretic and electro-osmotic mobility, can improve the resolution of analytes. Buffer pH, concentration and composition are fundamental parameters affecting the separation. Generally, the EOF becomes significant only at pH >4, where the silanol groups are increasingly de-protonated. Since the electro-osmotic velocity is directly linked to the size of the zeta potential developed across the capillary/water interface, alteration or elimination of EOF can be performed by derivatisation of the capillary wall with silating reagents or by producing polymeric coatings.[63–66]

7.3.3 Coupling CE to ICP-MS

The key to successful post-column detection in CE-ICP-MS is to establish efficient transport of nanolitre amounts of sample, without affecting the separation process. The first hyphenation of CE to ICP-MS was accomplished using a conventional concentric nebuliser in combination with a conical spray chamber.[61] It was evident from this first publication that interface development was challenging. The fundamental requirements for hyphenation of CE to ICP-MS can be summarised as follows:

(1) The interface must adapt to the low flow rate (nL/min) in CE by use of a make-up liquid, as most nebulisers for ICP-MS are designed to operate at flow rates in the μL/min to mL/min range.
(2) The electric circuit must be achieved by grounding the CE capillary exit end. Stable electric current is crucial for reproducible separations.
(3) The interface must prevent induction of laminar flow in the capillary.
(4) The dead volume of the interface, which causes peak broadening must be minimised.

During the last few years, several interfaces for coupling CE with ICP-MS have been developed. The constructions are mostly based on Meinhard,[67,68] microconcentric[69–71] or ultrasonic nebulisers,[72] but also interfaces based on cross-flow,[69] high efficiency[73] or direct injection nebulisers[74] have been developed. Typically, low-dead-volume spray chambers, e.g. cyclonic or conical types, are employed to reduce memory effects and peak broadening. Schaumlöffel and Prange introduced an interface based on a modified microconcentric nebuliser and a low-dead-volume spray chamber, which is currently the only commercially available interface.[75,76]

The majority of developed interfaces implement the functional make-up flow interface design adapting the CE flow rate (<150 nL/min) to the flow rate of the nebuliser by a coaxial sheath flow. Figure 7.4 shows a representative scheme of such a CE-ICP-MS interface. A crosspiece allows connection of the CE capillary to a nebuliser, mixing the CE flow with a coaxial sheath flow. The make-up solution is transported by self-aspiration of the nebuliser and is mixed with

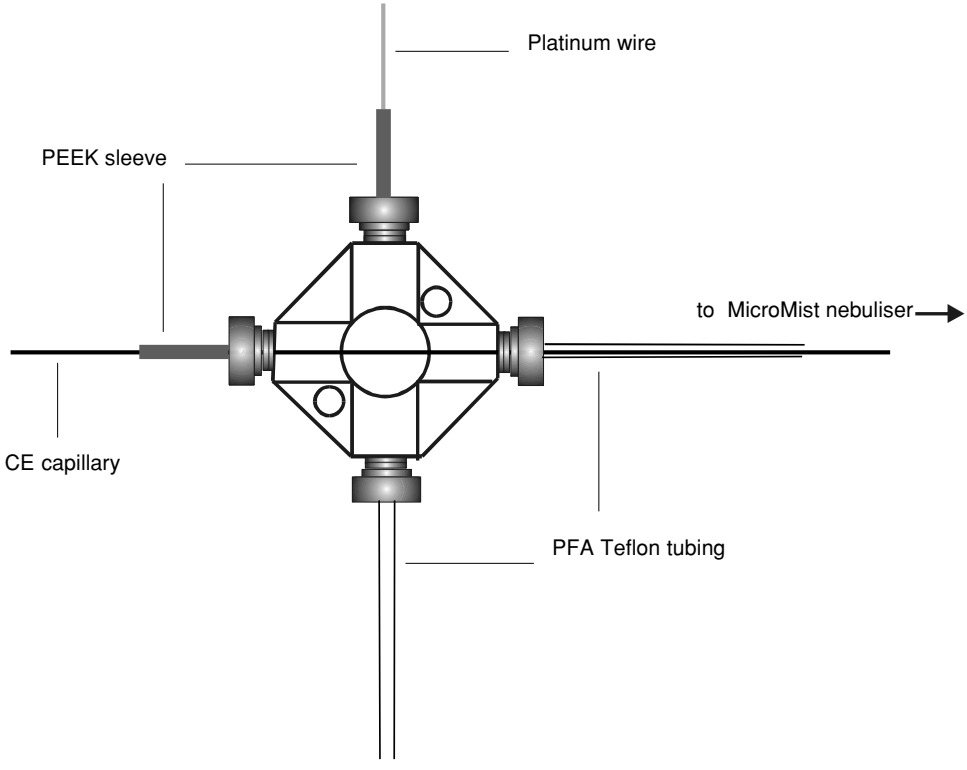

Figure 7.4 Scheme of CE-ICP-MS interface.

the CE buffer at the end of the CE capillary.[77] Moreover, the make-up flow serves for establishing an electrical connection (typically ground) to the end of the CE capillary. Dilution of the CE flow with a sheath flow reduces the sweep-out time through the nebuliser dead volume and eliminates laminar flow in the capillary as a result of nebuliser suction.

Sensitivity and detection limits of ICP-MS are governed by the absolute amount of analytes introduced to the plasma per time unit. Hence, sample transport efficiency of the ICP-MS introduction system will critically affect detection limits in CE-ICP-MS. A general drawback of CE is that concentration-based detection limits are limited by the small sample injection volumes and the electrophoretic peak width. Interfaces employing nebulisers in combination with spray chambers yield analyte transport efficiencies of $<100\%$, depending on the nebuliser and solution flow rate. Consequently, the sensitivity of CE-ICP-MS can be improved by using introduction systems with 100% aerosol transport efficiency, such as the direct injection nebuliser[74] and the direct injection high-efficiency nebuliser.[78]

7.3.4 Quantification in CE-ICP-MS

Owing to the general lack of standards and certified reference materials of elemental species in specific matrices, application of species-unspecific quantification strategies employing

ICP-MS detection have gained importance.[79–82] Several CE-ICP-MS studies employed species-unspecific isotope dilution MS for quantification of species in complex biological systems. The aim was the assessment of elemental ratios to characterise unknown species. Species-unspecific 'isotope dilution MS' is advantageous in situations where irreproducible capillary wall–sample interactions due to chemical interaction or trapping in the electrical double layer mitigate accurate external calibration by inorganic standards. Therefore, this section details the procedure of species-unspecific on-line 'isotope dilution MS'. Generally, the method delivers results with a lower expanded uncertainty than do methods using external calibration or standard addition for quantification. Isotopically enriched, inorganic reference standards added on-line after the separation of the analytes can be used for quantification of unknown species, provided that (1) complete and reproducible mixing of the spike flow and the flow of the separation method is achieved, (2) ionisation in the plasma is generic, i.e. gives the same response per atom for a certain element regardless of the species structure and oxidation state, and (3) the isotope ratio is measured over the whole chromatographic peak because it varies with time.

The principle of isotope dilution MS is that an unknown amount of atoms $N_x = c_x m_x N_A$ in the sample is blended with a known amount of atoms $N_y = c_y m_y N_A$ of an enriched spike (c_x, c_y are the concentrations of the investigated element in the sample and in the spike in mol/g, m_x is the mass of the sample, m_y is the mass of the spike, N_A is Avogadro's number). In its basic form 'isotope dilution MS' requires measurements of the isotope ratios in the sample (R_{ix}), in the enriched spike (R_{iy}), and in a blend of the two (R_b); If only two isotopes are measured, the equation can be written as

$$c_x m_x = c_y m_y \frac{R_y - R_b}{R_b - R_x} \frac{f_{iy}}{f_{ix}} \tag{7.1a}$$

where f_{ix}, *and* f_{iy} represent the isotopic abundance of the reference isotope in the sample (X) and in the spike (Y), respectively:

$$f_i = \frac{R_i}{\Sigma R_i} \tag{7.1b}$$

For transient signals, the m_x (mass of sample) and m_y (mass of spike) are replaced by the flow rate (mass per time unit) of the sample and the spike. Hence, equation 7.1a is transformed into equation 7.2, where $M_x(t)$ and $M_y(t)$ represent the analyte mass flow and the spike mass flow in moles per time unit.

$$M_x(t) = M_y(t) \frac{R_y - R_b(t)}{R_b(t) - R_x} \frac{f_{iy}}{f_{ix}} \tag{7.2}$$

When performing isotope dilution in the on-line mode, the blend ratio R_b is determined for every data pair of the chromatogram by calculating the intensity ratio of the two selected isotopes. If the isotopic composition of the investigated element does not vary, the value of R_x is taken from IUPAC tables.[83] R_y is listed in the certificate of the spike. If the isotopic composition of the sample or spike is variable or unknown, R_x and R_y can be determined by direct ICP-MS measurement. In analogy to isotope dilution MS, appropriate mass bias correction factors have to be applied to all the measured ratios. Detector dead time correction is imperative if transient signals are measured. Most manufacturers provide software with built-in dead time correction, provided that dead time has been accurately determined by the user, according to the well-known procedures.[84]

Determination of the spike mass flow is the most crucial point in on-line isotope dilution MS. Biased mass flow values will have the most influence on the expanded uncertainty of the final result. Two methods of mass flow assessment have been described in the literature. The first method determines the mass flow gravimetrically. The make-up flow f_{sp} can be supplied by a pump able to deliver a precise and accurate flow (micro-HPLC pump, syringe pump) or by self-aspiration of the nebuliser. f_{sp} is assessed gravimetrically by repeated measurement. The spike mass flow $M_y(t)$ is calculated as follows:

$$M_y(t) = f_{sp} c_{sp} \tag{7.3}$$

If the spike flow is not assessed gravimetrically, the mass flow of the spike flow has to be calibrated by a reverse isotope dilution technique. A standard solution of natural isotopic composition with the concentration c_{st}, is injected into the separation system. The spike flow $M_y(t)$ is calculated using equation 7.4a:

$$M_y(t) = M_{std} \frac{(R_x - R_{b\_average})}{(R_{b\_average} - R_y)} \frac{f_{ix}}{f_{iy}} \tag{7.4a}$$

where $R_{b\_average}$ is the average isotopic ratio of the chromatographic peak. M_{std}, the mass flow of the standard, is approximated by a constant average mass flow as given in equation 7.4-b, i.e. calculated from the base peak width w_{peak}, the injection volume V_{inj} and the concentration of the standard c_{st}.

$$M_{std} = \frac{c_{st} V_{inj}}{w_{peak}} = c_{peak} f_{HPLC} \tag{7.4b}$$

$$c_{peak} = \frac{c_{st} V_{inj}}{w_{peak} f_{HPLC}} \tag{7.4c}$$

f_{HPLC} is the flow supplied by the separation system and c_{peak} is the peak concentration of the injected standard. The described inverse calibration procedure is mostly used in applications of CE-ICP-MS, where the make-up flow is supplied by self-aspiration of the pneumatic nebuliser. However, it has been shown that this procedure delivers biased results associated with high uncertainties.[85] Hence, gravimetrical spike flow determination is a prerequisite to obtain accurate results.

Once the accurate value for $M_y(t)$ has been determined, the analyte mass flow M_{xj} at any point j of the transient profile can be calculated by equation 7.2. As a next step an analyte mass flow $M_x$versus time diagram is established. Figures 7.5(a) and 7.5(b) illustrate the principle of species-unspecific quantification via on-line isotope dilution MS.

Integration of the peaks in Figure 7.5(b) results in the absolute amount of the species injected onto the separation column. The species concentration c can be calculated by dividing the absolute amount of the species by the injection volume (V_{inj}). t_1 and t_2 represent the peak start and end times, respectively.

$$c = \frac{\int_{t_1}^{t_2} M_{xj}}{V_{inj}} \tag{7.5}$$

It is noteworthy that the number of data points (ratios/s) defining the peak significantly influences the combined uncertainty of the result obtained. The final combined uncertainty of the

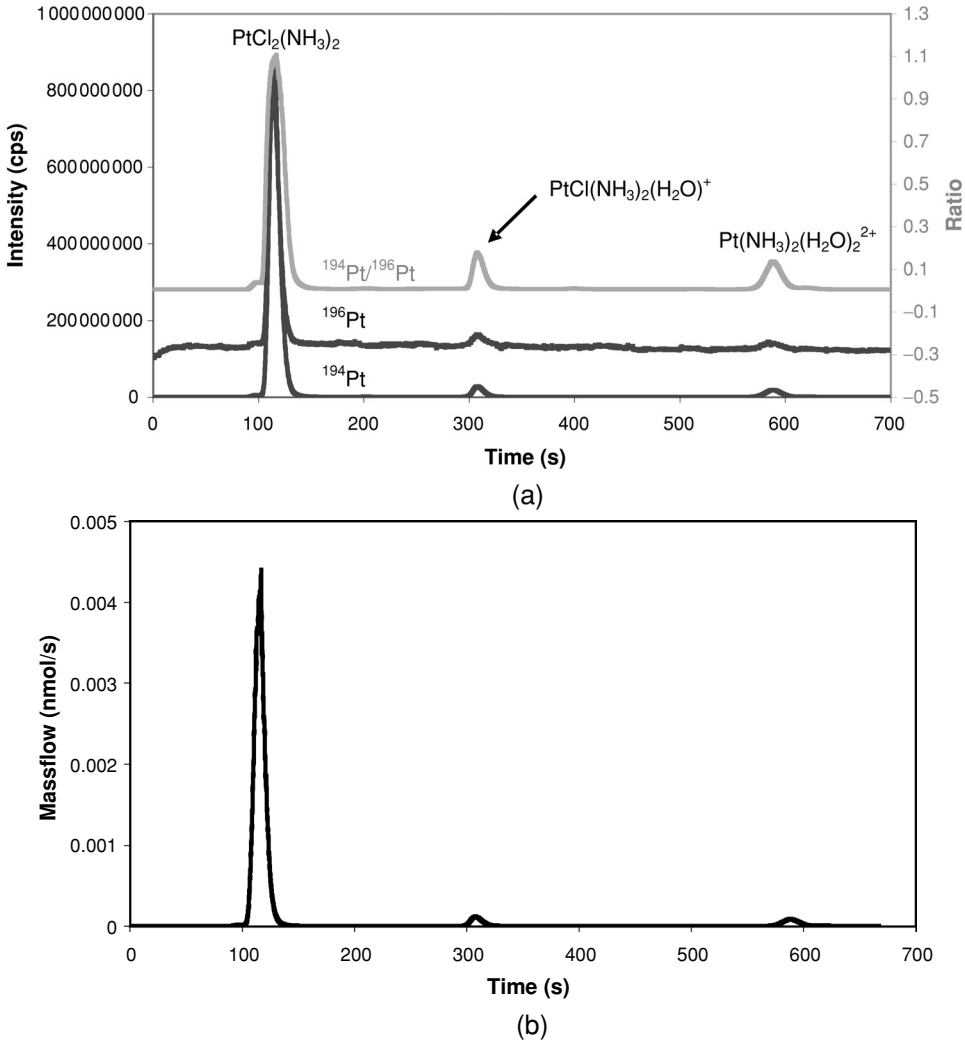

Figure 7.5 (a) Speciation of platinum in an aqueous sample of cisplatin. The black lines are the signals obtained for ^{194}Pt and ^{196}Pt, respectively. The ^{196}Pt spike was added post-column using a high-precision micro-HPLC pump. The grey line is the ratio chromatogram of ^{194}Pt/^{196}Pt. ([85] – Reproduced by permission of the Royal Society of Chemistry.) (b) Mass flow versus time diagram obtained by application of Equation 7.2 to every single ratio of the ratio chromatogram in Figure 5(a).

analytical result increases as the number of considered ratios (data points/peak) decreases. As a consequence, on-line isotope dilution MS in CE characterised by extremely short peak widths (a few seconds, typically 10–20 data points/peak) will produce results associated with higher relative uncertainties than HPLC (typically 120–200 data points/peak).[85]

7.3.5 Applications

As mentioned earlier, numerous publications on CE-ICP-MS have focused on interface design and thus it will not be discussed in this section. So far, the application of CE-ICP-MS to real samples is reported only in a few papers. Van Holderbeke *et al.*,[70] Prange and Schaumlöffel[86] and Köllensperger *et al.*[87] have applied CE-ICP-MS to arsenic speciation. Prange and Schaumlöffel investigated arsenic speciation in mineral water, soil leachate and urine samples in addition to standard solutions, in which detection limits of 1–2 μg/L for different arsenic species were reported. Köllensperger *et al*. compared HPIC-ICP-SFMS and CE-ICP-SFMS for speciation of arsenic in soil solutions and water extracts. The detection limits of HPIC-ICP-SFMS were in the range of 0.04 – 0.08 μg/L. The detection limits of CE-ICP-SFMS were found to be 2 orders of magnitude higher. Soil solutions and soil water extracts obtained by rhizobox experiments of the hyperaccumulating plant *Pteris vittata* were investigated. The measurements showed only As(V) ranging at concentration levels of 0.1–0.3 μg/g and 0.3–0.5 μg/g in soil solutions and water extracts, respectively.

In addition to arsenic, CE-ICP-MS has been successfully applied to chromium speciation. In the aquatic environment, Cr is usually present in either the trivalent, Cr(III), or the hexavalent, Cr(VI), oxidation state. Since Cr(III) is an essential nutrient and Cr(VI) is considered a toxin and a carcinogen, it is important to distinguish between the two oxidation states of Cr. Gine *et al.*[88] designed a combined flow injection/CE-ICP-MS system for Cr speciation in water samples in a working range of 50–200 μg/L. Sequential sample introduction by flow injection led to a robust system, with no interruption of the applied voltage during sample replacement or column conditioning.

The feasibility of a simple microchip CE-ICP-MS system was demonstrated by the separation of Cr(III)/Cr(VI).[89] The system provided baseline separation of the two species within 30 s using an 8 cm long channel of 100 μm width and 20 μm depth. The limits of detection were in the low μg/L range.

Selenium speciation has become a popular investigation area in speciation analysis. Selenium is either an essential or a toxic element for human health, depending on its chemical form and concentration. Therefore, it is essential to determine not only the concentration of selenium but also the chemical species and their concentrations to evaluate the effects on human health.

Michalke and Schramel have investigated selenium speciation in body fluids like human milk and serum.[90,91] The concentrations in milk samples were below the method detection limits, and the sample had to be preconcentrated. Serum samples contained several selenium species, which could not be identified. In order to enhance the information on species structure and identity, the same authors exploited the hyphenation of CE to electrospray ionisation MS.[92]

As a constituent of selenoproteins, selenium has structural and enzymatic roles, e.g. as an antioxidant or catalyst. In addition to these enzymatic functions, selenium has some important health effects in relation to immune response and cancer prevention. There is growing evidence that selenium intakes higher than the dietary reference intake of 55 μg/day[93] in combination with other antioxidants are associated with reduced cancer risk.[94] CE coupled to ICP-MS has been applied to investigate selenium speciation, particularly selenoamino acids, which are the principal dietary form of selenium.[78,90,95–97] Today, there are several commercial nutritional selenium supplements available. Mounicou *et al.* have investigated selenium speciation in selenium-containing nutritional supplements by CE-ICP-MS, especially in selenium-enriched yeast

materials. Selenium compounds could partly be determined in the water extracts, but the recovery of selenium species was reported to be significantly higher in proteolytic digested samples.

As a matter of fact, amino acids are a very important class of chiral compounds. In biological organisms, interaction between biomolecules is often controlled by enantiomeric specificity. Hence, only L-forms of amino acids are incorporated into proteins of living organisms, whereas D-forms or racemic mixtures may have harmful effects. Therefore, chiral speciation of D- and L-selenomethionine by CE-ICP-MS has been investigated by the groups of J. A. Caruso[98] and A. Sanz-Medel[99] using chiral derivatisation with 1-fluoro-2,4-dinitrophenyl-5-L-alanine amide (Marfey's reagent) prior to separation[98] and direct enantiomer separation with a chiral selector.[99] With both methods, excellent separation of the two enantiomers could be achieved. Figure 7.6 shows an electropherogram of selenised yeast containing selenite, L-selenomethionine and several unidentified compounds.

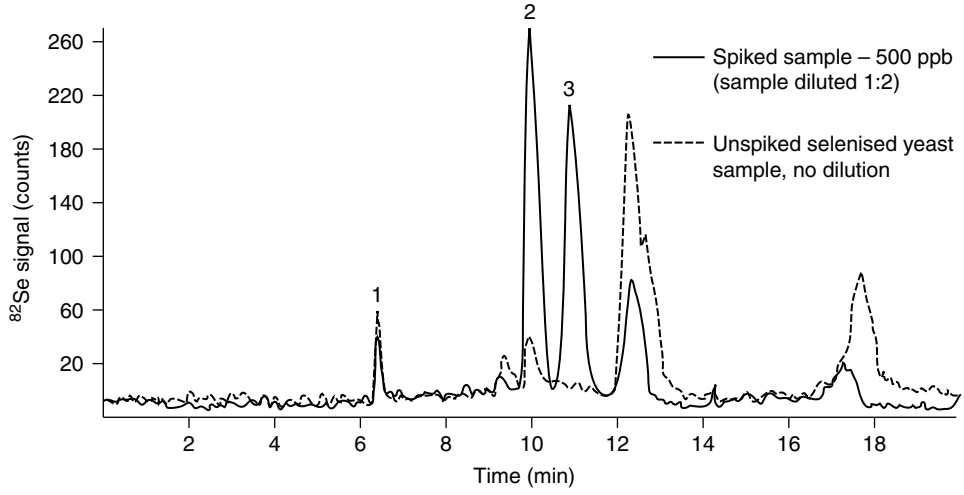

Figure 7.6 Overlaid CE-ICP-MS electropherogram of selenised yeast sample. 1, selenite; 2, L-selenomethionine; and 3, D-selenomethionine. Conditions: 30 mM $(NH_4)_2HPO_4$, pH 3.3 and 225 kV.[98] (Reproduced by permission of the Royal Society of Chemistry.)

Metallothioneins, a group of metal-binding proteins with a low molecular mass, have been a topical research theme in medicine and biology during the last decades. As a result of progress in new interface technologies, characterisation of metallothioneins by CE-ICP-MS has become a popular research area. Metallothioneins have multifunctional physiological behaviour in connection with the transport, storage and detoxification of metals or with protection from metal toxicity. They are believed to play a key role in connection with Alzheimer's disease. Metallothionein isoforms may differ only in few amino acids and therefore their separation requires a high-resolution technique that is able to separate compounds with minor differences.[100] CE-ICP-MS is an ideal technique for the determination of biological materials, because often only a small amount of sample is available. There are several papers published on metallothionein characterisation by CE-ICP-MS.[101–103] Sulfur-to-metal ratios were determined in order to support identification of metallothionein isoforms (MT-1, MT-2 and MT-3). Schaumlöffel *et al.*[104] introduced an on-line isotope dilution technique, using CE to separate the species and sector field ICP-MS operated

at medium resolution for the detection. Copper, zinc, cadmium and sulfur were detected simultaneously, and the stoichiometric compositions of metalloprotein complexes were characterized by determination of their sulfur-to-metal ratios. In a recent paper, Wang and Prange showed an improved CE separation of metallothionein isoforms.[105] Using capillaries whose surfaces had been modified with poly(2-acrylamido-2-methyl−1-propanesulfonic acid), nine metallothionein complexes in a commercial preparation of rat liver were separated (see Figure 7.7).

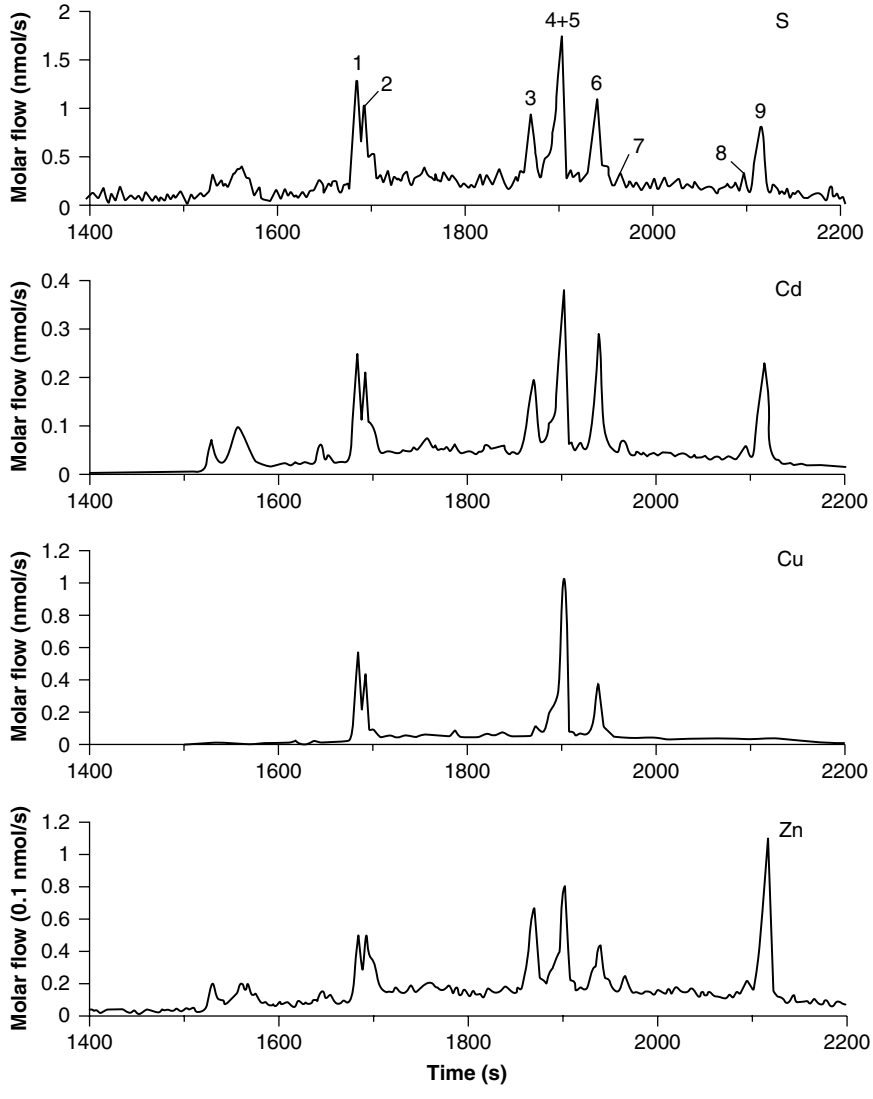

Figure 7.7 Derived molar flow electropherograms of metallothionein preparation from isotope dilution analysis on an anionic polymer-coated column, prepared by immobilising poly (2-acrylamido-2-methyl-1-propanesulfonic acid) on the fused-silica surface via a linking agent.[105] (Reprinted with permission. Copyright (1991), American Chemical Society.)

Moreover, species-unspecific isotope dilution MS indicated the stoichiometric ratio of S/Cu/Zn/Cd, allowing a suggestion of the normalised molar ratios of these elements.

7.3.6 Outlook

CE-ICP-MS is a valuable separation technique for the determination of high-molecular-weight analytes as well as low-molecular-weight analytes of different ionic character. Since the method utilises gentle and versatile separation schemes, the complementary application of HPLC and CE is promising for characterisation of complex, unknown systems. Presently, as a drawback, the technique is limited by its relatively high limits of detection and the robustness of the interface. This is reflected by the high proportion of CE-ICP-MS publications focusing primarily on interface design.

7.4 Speciation with HPLC-ICP-MS

7.4.1 Introduction

The combination of HPLC with ICP-MS provides a powerful and sensitive technique for on-line elemental speciation analysis because of its simplicity, its robustness, and its high reliability and reproducibility. Contrary to GC separation, which needs long and complex steps to form volatile derivatives, HPLC can very often be used with a minimum of sample preparation. HPLC also has the advantage to work at ambient temperature, and thus the method is not limited by thermal stability of the analytes. Furthermore, because of the variety of available separation mechanisms, HPLC-ICP-MS can be used for the analysis of very different compounds such as redox species, organometallic compounds, biomolecules, metabolites of xenobiotics, etc. This wide variety enables its use in domains as different as the environment, industrial hygiene, food and drug industries, medicine or toxicology. Moreover, completely automated HPLC-ICP-MS systems working in both isocratic and gradient elution modes are now available on the market, allowing this method to be used on a routine basis. In this chapter, different chromatographic separation principles are described that have been used in combination with ICP-MS detection. Advantages and disadvantages of the different methods are discussed for various species, and finally some environmentally important examples of application are described in detail.

7.4.2 Theory of HPLC

Liquid chromatography (LC) relies on various different interactions between a stationary and a mobile phase. Sample components are carried by a mobile phase through a bed of stationary phase, where individual species are retained by certain types of interactions. Mobile phases generally consist of mixtures of organic solvents, salts in buffer solution and/or ion pairing reagents.

A great variety of LC techniques using ICP-MS detection have already been applied, such as reversed phase with or without ion pairing, ion exchange and size exclusion. The relative polarity,

Table 7.1 Chromatographic modes used in HPLC-ICP-MS

Mechanism	Stationary phase	Mobile phase	Analytes
Reversed phase Reversed phase with ion pairing	Graft silica alkyl groups: • Octyl (C_8, MOS, RP8, etc.) • Octadecyl (C_{18}, ODS, RP18, BDS, etc.) Styrene–divinylbenzene copolymer (PS–DVB, PRP1)	Polar solvent: water, methanol, acetonitrile, etc. Polar solvent + counterion: • anionic ($R-SO_3^-$, $R-SO_4^-$, etc.) • cationic ($R-NH_3^+$, $R-N(CH_3)_3^+$, etc.)	Non-polar molecules Ionic and non-ionic molecules
Ion exchange	Silica or polymer grafted with: • anionic groups ($-SO_3^-$,$-CO_2^-$, etc.) • cationic groups ($-NH_3^+$,$-N(CH_3)_3^+$, etc.)	Water and ionic salt: • anionic (phosphates, acetate, borate, formate, carbonates, etc.) • cationic (hydronium, pyridinium, ammonium, etc.)	Organic and inorganic ions
Size exclusion or gel permeation	Organic gel (PS–DVB, polydextrane, etc.) Graft silica	Water or organic solvent	Macromolecules (M > 2000 Da)

solubility and molecular weight of the species of interest determine the type of separation used for a specific application. The principles of these separation modes are given in Table 7.1.

In general, two different elution modes can be applied; isocratic or gradient elution. Isocratic elution is the simpler concept; here, the concentration and nature of the eluent stay constant during the whole chromatographic run. Gradient elution involves a more complex HPLC system. During gradient elution, the concentration and/or nature of the eluent is changed, usually gradually. This principle demands a sophisticated mixing system, normally accommodating up to four different solvents. Gradient elution is often preferred to isocratic elution, mainly to speed up the chromatography at the end of the run to expedite elution of strongly retained species. However, with ICP-MS detection the user must bear in mind that the change in matrix may influence plasma conditions and lead to signal drift.

The overall mechanisms have already been described in detail in numerous reviews.[106–111] As a consequence, only a very brief description is given here.

(a) Reversed phase chromatography

Reversed phase (RP) chromatography is one of the most commonly used separation mechanisms in LC, and consists of a non-polar stationary phase and a polar mobile phase. Analytes are partitioned between the stationary and mobile phases: the more strongly retained species have a greater affinity for the stationary phase, compared to the mobile phase. Selectivity can be enhanced by modifying the type and quantity of organic solvent in the mobile phase. Different mixtures of solvents diluted in water or gradient elution with increasing organic solvent concentrations in the mobile phase may be used. Retention is also influenced by the pH of the

eluent, which controls the degree of dissociation of the analyte between the stationary and mobile phases.

Advantages of RP chromatography are the simplicity of the technique, its good resolution and high reproducibility. However, its main disadvantage is the limited compatibility of organic solvents with ICP-MS. Moreover, as organic solvents and acids are used, labile or reactive species may be converted during separation owing to reactions with the eluent constituents.

(b) Ion pairing reversed phase chromatography

As RP chromatography separates only non-polar and non-charged analytes, ion pairing can be applied to analyse charged, polar species. An ion pair is formed between the analyte ion and an appropriate ion of opposite charge added to the mobile phase. The resulting ion pair is hydrophobic and is partitioned between the mobile and the non-polar stationary phases under conditions similar to those used for RP chromatography. The separation efficiency depends on the choice of the counter-ion, the functional group of the stationary phase, the nature and the pH of the mobile phase, which also influence species dissociation. The principal consideration when selecting a counter-ion is the charge compatibility. It should be univalent, soluble in the mobile phase, aprotic and non-destructive to the chromatographic system and the analytes. In addition, pH changes can affect the separation; it is therefore important to buffer the mobile phase.

The advantages are similar to those of RP chromatography, but ion pairing reversed phase chromatography offers higher flexibility and versatility. However, changes in the speciation of analytes are more probable when a counter-ion is added to the mobile phase.

(c) Ion-exchange chromatography

Ion-exchange chromatography (IEC) is a commonly used separation mode for the analysis of ionic or ionisable compounds with HPLC-ICP-MS. With this mechanism, ionic species are retained on the ionic sites of the stationary phase having opposite charges. When positively charged analytes interact with negatively charged sites in the column, the process is referred to as cation exchange. When negatively charged analytes interact with positively charged sites, the process is called anion exchange.

Eluents for IEC are usually aqueous, salt-buffered solutions, and the separation process for the species of interest is mainly controlled by a change in the concentration and/or the nature of the buffer. Organic solvents such as methanol are often added to the mobile phase for control of the selectivity or to change solvent strength, retention times or column efficiency.

However, the addition of such solvents can cause problems during the ICP-MS detection. Most separations carried out using ion exchange involve the use of gradients to increase ionic strength, i.e. elution power, during the chromatographic run. The use of gradients allows the separation of complex mixtures but its use is time-consuming and the changes in the composition of the mobile phase during the analysis may lead to changes in the background or sensitivity. Moreover, high salt concentrations often present in the mobile phases used in ion exchange are not always compatible with detection by ICP-MS. Advantages of ion exchange include good resolution, high reproducibility and repeatability.

IEC is generally used for the separation of redox species such as Cr(III)/Cr(VI) or Sb(III)/Sb(V)/methyl Sb. Another frequent application is the analysis of Se species [Se(IV), Se(VI), Se-amino acids, etc.] or As species [As(III), As(V), MMA, DMA, arsenosugars, etc.].

(d) Size exclusion chromatography

Size exclusion chromatography is used to separate molecules according to their effective size: molecules larger than the pore size of the stationary phase are not retained on the column. On the contrary, molecules that are smaller than the pore size of the stationary phase are retained for a certain period of time. As separation is mainly affected by physical interactions, the mobile phase does not play a critical role in the separation of the species. Eluents commonly used are buffer solutions. If the chromatography system is suitably calibrated, it may be possible to identify the approximate molecular masses of the separated compounds. The correlation of retention time with molecular size makes it possible to estimate the molecular mass of an unknown substance. Compared to other separation techniques, the species interactions in size exclusion are the weakest; thus, species integrity is best preserved. However, several disadvantages are associated with this technique, such as its inability to resolve compounds with similar size distributions and also its limited peak capacity. Furthermore, retention of compounds such as ions with a high charge-to-mass ratio (by adsorption, diffusion or partition) can complicate the separation process because of secondary mechanisms.

This technique is especially useful for the separation of large proteins and polypeptides. For example, size exclusion chromatography has been used frequently to separate and identify biological macromolecules using hydrophilic column packings and aqueous mobile phases.

The different strategies available in liquid separation make HPLC-ICP-MS the method of choice for the analysis of non-volatile metal species. The selection of the separation mechanism will depend on the physico-chemical properties of the compounds that have to be determined. However, it is often recommended to verify the selected technique with other techniques and separation mechanisms, particularly when a chromatographic separation with a relatively poor resolution, such as size exclusion, is used.[112]

Other separation modes using LC are available, such as adsorption chromatography or chiral chromatography. However, these separation techniques are not frequently used with detection by ICP-MS.[106–111]

7.4.3 Instrumentation for HPLC-ICP-MS

Among the different separation methods that can be hyphenated to ICP-MS for speciation analysis, LC is the easiest to implement because of the simplicity of the interface. As illustrated in Figure 7.8, the coupling is performed by connecting the outlet of the chromatographic column directly to the inlet of the nebuliser by using an inert polymeric tubing. This is possible because of the compatibility of the chromatographic effluent flow rate and the flow rate of the pneumatic nebulisers commonly used for ICP-MS. The length of the tubing should be kept as short as possible in order to minimise dead volume of the transfer line and subsequent peak broadening.

Another advantage of coupling HPLC with ICP-MS is the possibility to separate spectral interferences from the analyte of interest. This advantage is well illustrated in Figure 7.9, where a chromatogram of a standard solution containing four species of arsenic [As(III), As(V), MMA and DMA] in the presence of chloride ions is presented.[113]

The ICP-MS analysis of arsenic is strongly interfered by chloride ions because of the spectral interference of $^{40}Ar^{35}Cl^{+}$ (m/z 75), with the monoisotopic arsenic also at m/z 75. The chromatogram shown in Figure 7.9 clearly illustrates the effective separation of chloride species

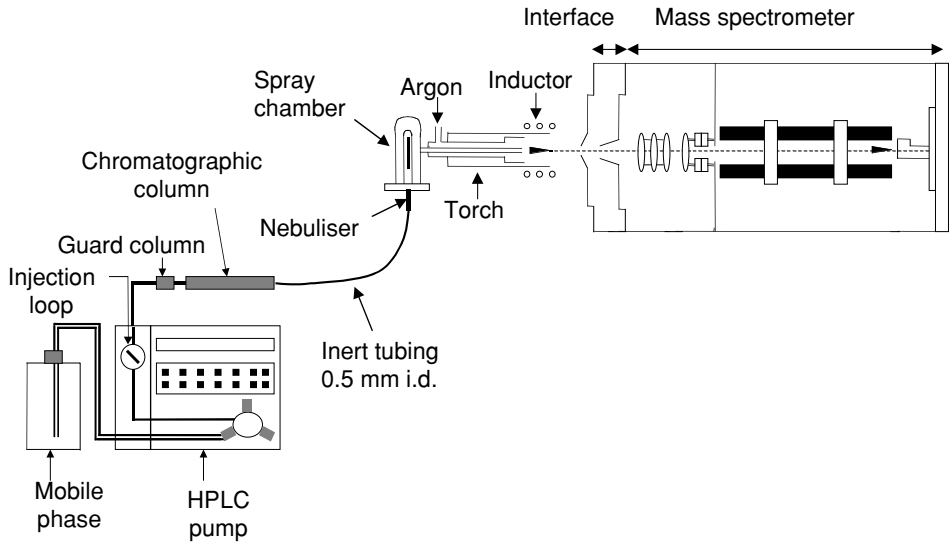

Figure 7.8 Experimental set-up of HPLC-ICP-MS.

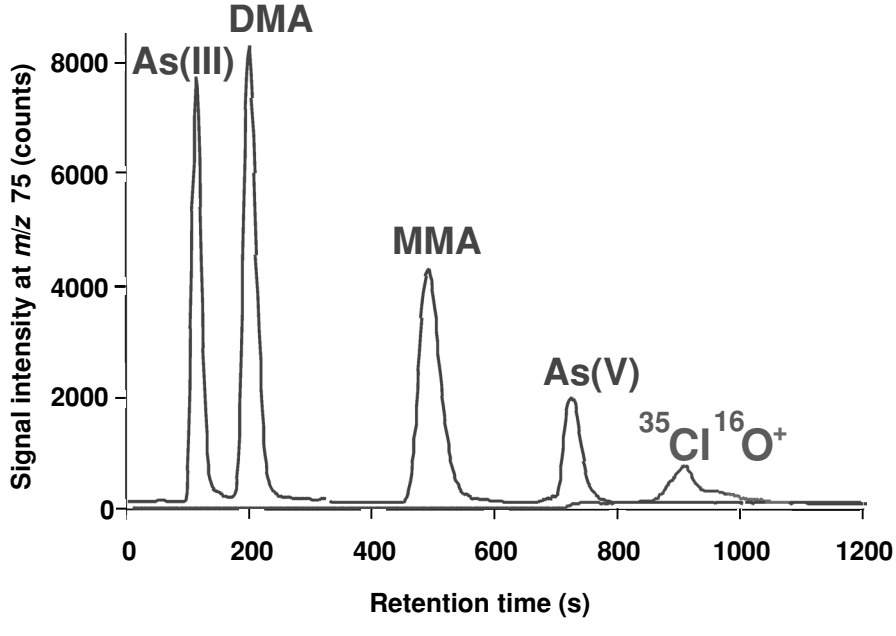

Figure 7.9 Chromatogram of a standard solution containing As(III), As(V), MMA, DMA and chloride ions. Separation with an anion-echange column [PRPX 100 (4.6 × 250)] and an elution gradient [6.25 mmol/L $NH_4H_2PO_4$, pH 5.5, from 0 to 9 min; then 25 mmol/L $(NH_4)_2HPO_4$ pH 11, from 10 to 20 min].

from arsenic species (here monitored via m/z 51, representing the $^{35}Cl^{16}O^{+}$ molecular ion), thus allowing, at least in many cases, interference-free detection of the arsenic peaks. A major drawback when coupling HPLC with ICP-MS is due to the introduction of HPLC effluents into the ICP-MS.[106,107] Mobile phases generally contain salts in buffer solution, organic solvents and/or ion-pairing reagents at elevated concentrations, which can lead to cone blockage.

IEC often needs buffers with an increased salt concentration for analyte elution. However, a high salt load leads to clogging and erosion of the nebuliser, the torch injector and the cones.[106–111,114] This ultimately affects the sensitivity and precision of the analysis as well as the long-term stability of the instrument. To avoid these problems, it is recommended to regularly clean the system with 1% HNO_3 and to keep the quantity of dissolved salts below 2%.[113] An alternative solution is to use organic compounds instead of inorganic salts for the mobile phase.[115] Organic compounds are volatilised in the plasma, thus avoiding clogging of the cones. The addition of small quantities of organic solvent also has the advantage of increasing analyte signals for metalloids like As, Se, Sb and Te, as shown in Figure 7.10.[113]

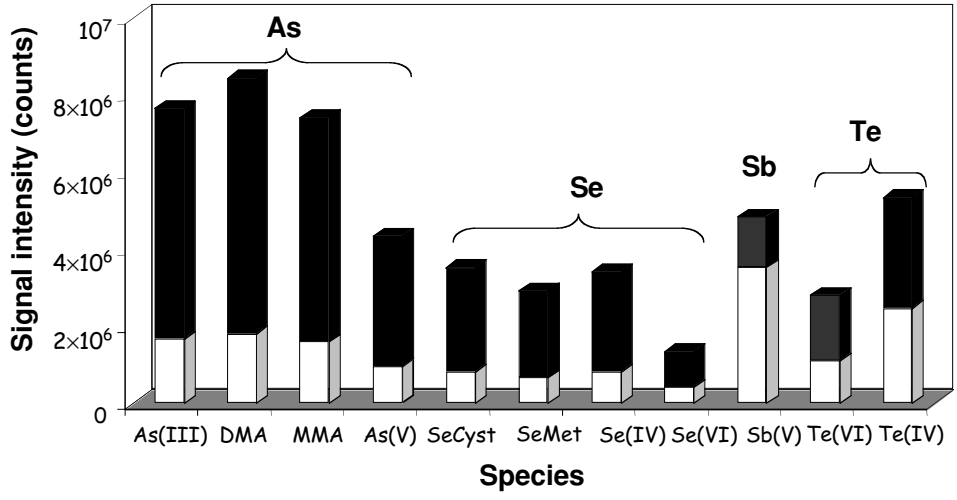

Figure 7.10 Intensity of the signal of different species with (■) or without (□) addition of 3% methanol in the mobile phase. Separation with an anion-exchange column (PRPX 100 (4.6 × 250)) and an elution gradient [6.25 mmol/L $NH_4H_2PO_4$, pH 5.5, from 0 to 9 min; then 25 mmol/L $(NH_4)_2HPO_4$, pH 11, from 10 to 20 min].[113]

Organic solvents are frequently used in mobile phases to achieve separation with reversed phase HPLC.[116] However, their presence has a number of detrimental effects during detection by ICP-MS.[117,118] High amounts of organic solvents in the mobile phase decrease the sensitivity, and the deposition of carbon on the cones can cause blocking of the sampler and skimmer orifice. Additionally, introduction of organic solvents may extinguish the plasma or cause plasma instability. Therefore, HPLC separation conditions must be adapted to ICP-MS capabilities, which implies that only very small amounts of organic solvents and modifiers (1–3%) can be mixed to the mobile phase.[106–111] Water-cooled spray chambers and introduction systems equipped with a desolvation unit are often used to overcome this problem. Adding a small amount of oxygen to the nebuliser gas flow and operating the plasma at higher powers can also help.[117]

7.4.4 Microbore columns for liquid chromatography

Compared to traditional HPLC columns, microbore columns certainly present the future in liquid separation techniques since the trend towards miniaturisation of analytical systems is evident. Moreover, microbore LC provides the advantage over conventional LC separation techniques, that significantly less undesired organic material and salt buffers are introduced into the detector.[119] The internal diameter of microbore columns is in the range of 0.5–2 mm and these columns can be used for all different types of species (positive, negative or neutral) by simply changing the stationary and/or mobile phase. Another advantage of microbore columns is the enhanced resolution power due to reduced transverse diffusion of the analytes.[120,121] Compared to traditional HPLC columns, the advantages of small LC columns are

- increased mass sensitivity, leading to enhanced resolution;
- smaller sample volumes, leading to avoidance of sample dilution;
- less solvent consumption, leading to decreased operation costs.

One important advantage of using microbore columns is the potential mass sensitivity. Indeed, sensitivity is demanded even more since the injected sample amount is reduced appreciably. Sample volumes of 5–10 μL are normally used along with low eluent flow rates.[119,122–126] The use of microbore columns requires the overall system to have low dispersion to limit the band broadening and minimise the dead volume.

A crucial point when coupling microbore columns with ICP-MS is the sample introduction. Different nebulisers have been evaluated for their ability to closely control the efficiency of the entire system.[127–129] Pneumatic nebulisers in combination with a spray chamber are traditionally used in classical ICP-MS applications. However, these devices suffer from low analyte transport efficiencies (<5%) and require sample uptake rates of 1–2 mL/min. This is well suited for normal bore HPLC coupling, but is problematic when small sample volumes and low eluent flow rates are used like those in microbore HPLC. Another disadvantage of classical nebulisation with low sample flow rates is that strong turbulence is introduced into the sample transport system. Several different low-flow nebulisers have been employed to provide finer primary aerosols and higher solution transport rates, thus improving the sensitivity at low sample uptake rates.[130]

The direct injection nebuliser (DIN) has so far the most popularity according to the publications on microscale trace element speciation.[119,122–125,131,132] Absolute detection limits are reported to be one order of magnitude better when compared to those of conventional nebulisers. This improvement in absolute detection limits can be explained by the complete nebulisation of the sample into the plasma, and so no loss of analyte occurs.

Another low-flow nebuliser used for coupling ICP-MS to chromatographic columns is the high-efficiency nebuliser (HEN). This device has a small capillary and is used with a spray chamber. Compared to pneumatic nebulisers, the HEN operates more efficiently at very low solution uptake rates. Micro-HPLC-HEN-ICP-MS coupling was applied to the speciation of five arsenic compounds.[125] The HEN operated most efficiently at sample uptake rates of 40 μL/min and was shown to have excellent absolute detection limits. A possible drawback of the HEN, as for all low-flow nebulisers, is the poor tolerance in nebulising highly concentrated solutions.

The microconcentric nebuliser (MCN) is another low-flow concentric pneumatic nebuliser designed to analyse low-volume samples. In contrast to the DIN and the HEN, the MCN is capable of nebulising samples containing high concentrations of mineral acids (e.g. hydrofluoric

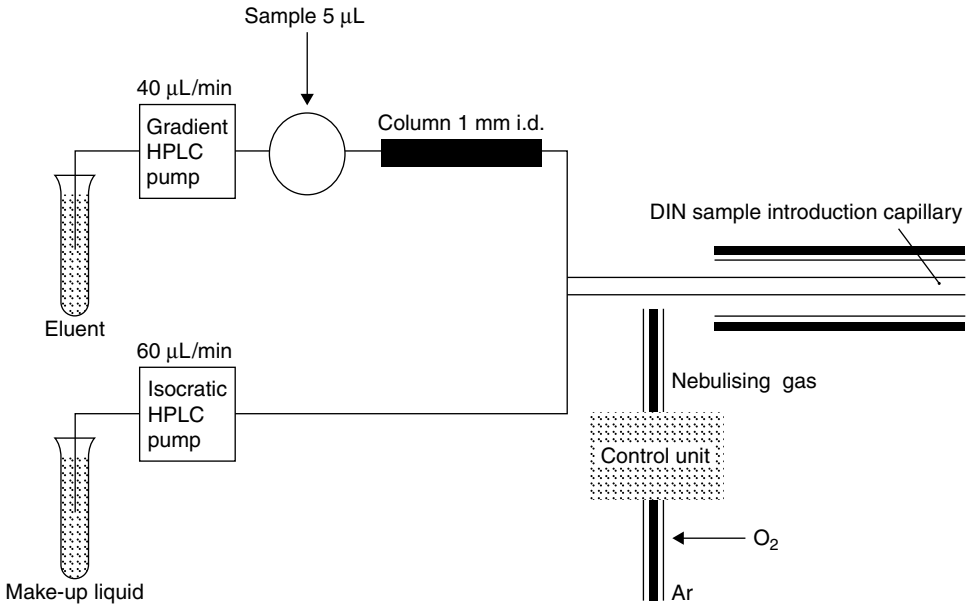

Figure 7.11 DIN-based interface for the coupling of HPLC to ICP-MS.[133] (Reproduced by permission of the Royal Society of Chemistry.)

acid) and high levels of dissolved solids. Performance of the MCN is similar to that of the HEN in terms of operating flow rate, detection limits, stability and robustness.[123] As an illustrative example, Figure 7.11 shows the experimental set-up of an interface between an RP separation and an ICP-MS, based on a microbore column with post-column dilution and DIN injection.[133] For further information on low-flow nebulisers for ICP-MS, see Chapter 5 of this book.

7.4.5 Selected applications

As several reviews are available for the speciation of biomolecules by HPLC-ICP-MS,[112,134] the applications given here illustrate the importance of HPLC-ICP-MS in the environment, industry and industrial hygiene, with a review of developments in HPLC-ICP-MS for mercury and chromium speciation.

(a) Mercury speciation in environmental samples

The core techniques developed for mercury speciation take advantage of gaseous species separation after an initial derivatisation step. However GC may lead to some problems and there is increasing motivation to use LC separation methods, for which the derivatisation step and all implications connected with it, like species transformation, etc., is avoided. With LC, inorganic mercury and methylmercury compounds can be determined, but it is also possible to analyse less volatile or non-volatile species such as mersalic acid or aromatic mercury compounds, which are not accessible for GC separation.

Mercury species have been separated by ion pairing reversed phase chromatography. The mobile phase usually contains 2-mercaptoethanol as the counter-ion,[135,138] but other ion pair forming or complexing agents like N,N-disubstituted dithiocarbamates[135,137,139–141] or L-cysteine,[142] have also been used.

Nine organic mercury species (alkyl- and arylmercury compounds and compounds with a carboxyl group) can be separated within 20 min by RP chromatography by applying gradient elution with methanol/water mixtures (30:70 to 50:50), buffered with sodium acetate to pH 5 and modified with 2-mercaptoethanol (0.1 M). The elution of benzoic mercury is strongly pH dependent, and retention times increase with decreasing pH.[142] Using a mobile phase of 30% methanol in water at pH 5, benzoic mercury is well separated from the other mercury species.

Inorganic mercury elutes prior to organic mercury species and close to methylmercury. Because of the usually high inorganic mercury-to-methylmercury ratios (10^2–10^3) in soils and sediments, a pre-separation between organic and inorganic mercury is needed, which can be achieved by a chloroform/water extraction. Acceptable RP separations can also be obtained by using N,N-disubstituted dithiocarbamates as complexing agents. When pyrrolidinedithiocarbamate is used as a complexing agent, five mercury species including inorganic mercury can be separated within 10 min.[141] Methyl, ethyl and inorganic mercury were also separated by reversed phase HPLC within 6 min using 0.5% L-cysteine at pH 5.[142]

As the use of organic solvents normally applied in RP chromatography can cause problems with ICP-MS detection, the separation conditions must usually be adapted, to allow only small amounts of organic solvents (1–3%) into the ICP-MS. Under these chromatographic conditions, mercury species are strongly retained, which in turn leads to prolonged analysis times.

To overcome these problems, alternative mobile phases such as 5% organic solvent with dodecyldimethylammonium bromide vesicles (0.2 nM) have been suggested.[138] With this type of mobile phase, it is possible to separate inorganic mercury from methylmercury in 8 min. Without organic modifiers, retention times increase to approximately 17 min, so for a fast separation of more than two mercury species, this is not recommended.

For detection by ICP-MS, absolute detection limits for mercury species are between 25 and 75 pg, which enables the use of HPLC-ICP-MS for mercury speciation in environmental samples.[135,136] When post-column oxidation/volatilisation is applied, absolute detection limits for Hg species can be as low as 10–20 pg.[137] Another advantage of post-column oxidation is that in this case there is no need to limit the concentration of organic solvents in the mobile phase, and so optimum separation conditions can be applied. The use of an *in situ* nebuliser/vapour generation sample introduction system for ICP-MS has been described.[142] In this system, the column effluent (containing no organic modifier) was mixed with a sodium borohydride solution just before introduction into a pneumatic nebuliser. This approach results in highly effective sample introduction and delivered excellent sensitivity. Detection limits obtained for inorganic, methylmercury and ethylmercury were in the range of 3–11 pg.

(b) Inorganic chromium speciation with HPLC-ICP-MS

Chromium compounds have various industrial applications including chromium plating, dye and pigment manufacturing, leather and wood preservation, and treatment of cooling tower water. This wide use results in dumping of large quantities of this element in the environment. Chromium can then be available to humans, and its toxicity depends greatly on its chemical form.

Cr(III) and Cr(VI) are the most common forms found in the environment, and it is generally accepted that Cr(III) is a trace element essential for human health, whereas Cr(VI) is a strong poison and carcinogen to humans and other animals.[2,143]

It is therefore obvious that speciation analysis is necessary to obtain adequate knowledge of the behaviour of chromium in the environment and its toxicity. As a result, several methods for inorganic chromium speciation have been described in the literature.[52,144] Among them, HPLC-ICP-MS is the technique that has received most attention in recent years for chromium speciation because of its high sensitivity. However, chromium detection by ICP-MS is often associated with polyatomic interferences generated by the presence of carbon, chlorine or sulfur that may disturb the measurement of the two most abundant chromium isotopes, $^{52}Cr^{+}$ (83.8%) and $^{53}Cr^{+}$ (9.50 %). The advantage of a chromatographic separation before detection by ICP-MS is the possibility to isolate interferences from the signals of Cr(III) and Cr(VI). Different HPLC separation mechanisms have been proposed for chromium speciation, such as RP chromatography or IEC. Lintschinger *et al.*[145] and Posta et al.[146] have associated reversed phase chromatography with ion pairing between Cr(VI) and tetraethylammonium or tetrabutylammonium salts. This ion pair is retained on the column whereas Cr(III) is eluted in the void volume. Andrle *et al.*[147] have preferred to complex both Cr(III) and Cr(VI) with ammonium-pyrrolidinedithioate before separation on a C18 column and elution with a water/acetonitrile mixture. In all these studies, the high levels of organic carbon in the mobile phases made use of the $^{52}Cr^{+}$ isotope difficult because of the resulting high baseline signal. Despite the use of devices decreasing carbon introduction into the plasma such as a high-pressure nebulisation system including desolvation equipment and addition of oxygen to the gas flow, only the less abundant $^{50}Cr^{+}$ isotope can be used.[147] When RP chromatography is used, elimination of spectroscopic inteferences has however be obtained with an ICP-MS detector equipped with a dynamic reaction cell.[148]

Because of the opposite charges of the two redox chromium species and the possibility to use an eluent without carbon, IEC is often preferred before detection by ICP-MS. Byrdy *et al.*[149] have used an anion-exchange column that allows the retention of both Cr(VI) and Cr(III) after transformation of this last form into an anionic complex with EDTA. However, the ammonium sulfate mobile phase did not allow the analysis of $^{52}Cr^{+}$ because this isotope is interfered by $^{36}S^{16}O^{+}$. Although the presence of chloride ions did not disturb the detection of $^{53}Cr^{+}$, the signal of ^{53}Cr(III) was affected by carbon from EDTA. The analysis of $^{52}Cr^{+}$ was also found to be difficult in a study by Zoorob *et al.*[122] where Cr(III) was complexed with 2, 6-pyridinedicarboxylic acid (PDCA) before separation on a cation–anion mixed-mode column and elution with a mobile phase containing both PDCA and lithium hydroxide. From these studies, it seems that complexation of Cr(III) and the use of a mobile phase with a high salt concentration have to be avoided for Cr speciation by HPLC-ICP-MS. The use of a microbore anion-exchange column with a nitric acid eluent allowing the retention of Cr(VI) and elution of Cr(III) in the void volume is also described in the literature.[124,150,151] However, although good results were obtained with pure solutions, it was shown that hydrogencarbonate ions co-eluted with Cr(VI) and interfered on both $^{52}Cr^{+}$ and $^{53}Cr^{+}$. Moreover, chloride ions co-eluted with Cr(III), disturbing the analysis of $^{53}Cr^{+}$. One solution to overcome the spectral interference from carbon is to work with cool plasma conditions. However, these conditions do not overcome interference generated by chloride ions. Interferences can only be completely resolved by increasing the mass resolution.[152]

A more promising approach for chromium speciation by HPLC-ICP-MS seems to be the use of a column having both anion- and cation-exchange capabilities,[151] or the on-line association of an anion- and a cation-exchange column.[153–155] Good results have been obtained with a CG5A-CS5A column set (DIONEX) containing both anionic and cationic groups to retain Cr(VI) and Cr(III), respectively, using nitric acid elution.[156] After optimisation, detection limits lower than 0.5 μg/L were obtained for both Cr species. This method is free from sulfate, chloride and organic or inorganic carbon interferences on the two most abundant chromium isotopes ($^{52}Cr^+$ and $^{53}Cr^+$). It should be noted however that an additional interference of $^{36}Ar^{16}O^+$ is also present on ^{52}Cr, providing a constant elevated baseline signal. A modification of the chemistry of Cr(III) was however observed in the presence of hydrogencarbonate ions. In this medium, for trivalent chromium, three peaks instead of one are present on the chromatograms. This modification was attributed to the hydrolysis of Cr(III) that occurs at a pH higher than 4.

7.4.6 Isotope dilution in speciation with HPLC-ICP-MS

Species-specific isotope dilution using HPLC-ICP-MS has not yet been applied extensively, but is a growing technique. The first description of species-specific isotope dilution employed selenium speciation with HPLC-ICP-MS.[80]

This technique has been used for a variety of element species, such as trimethyl- and triethyl-lead, organotins, iodine, methylmercury, and chromium. With HPLC, isotope dilution has been performed with species-specific as well as species-unspecific methods.

In species-unspecific isotope dilution techniques, an isotopically enriched standard solution is added post-column, and the data evaluation is performed as described in Section 7.3.4 for CE coupling. Species-unspecific isotope dilution for HPLC coupling has been described for the determination of Cd, Cu and Zn in metallothioneins extracted from eel liver,[157] while Fe, Cu and Zn were determined in proteins separated from human serum.[158] This technique has also been applied to iodine determination in humic substances,[159] as well as selenium speciation in human serum.[160] Species-specific isotope dilution using HPLC-ICP-MS has been described for selenium analysis,[80] the analysis of organotin species in sediments,[161,162] methylmercury in fish tissue,[163] trimethyllead in water,[164] and chromium speciation.[13] Overviews to this topic have been published, e.g. by Heumann[81] and Hill.[165]

The data evaluation for species-specific isotope dilution is achieved by peak area determination of the respective isotope peaks. A detailed description of the data evaluation in species-specific isotope dilution methods with ICP-MS detection can be found in Section 7.5.5. In species-specific isotope dilution procedures, isotopically labelled species are required, and the preparation of isotopically labelled methylmercury and butylated tin species is also described in detail in Section 7.5.5.

7.5 GC-ICP-MS

7.5.1 Theory of gas chromatography

GC is based on the distribution of a volatile (gaseous) analyte between a gaseous mobile phase and a liquid stationary phase present on a solid support. The analyte mixture must be volatilised

prior to introduction into the chromatographic column; most often, a mixture of analytes present in an organic solvent is injected into a heated injector tube at the column head. Depending on the analytes volatility and intensity of interchange with the liquid phase, analytes are more or less strongly retained on the stationary phase. An analyte mixture that passes through a GC system is separated into distinct analyte peaks as a result of these physical processes. The GC separation is usually driven by application of a temperature ramp, necessary to accelerate the distribution of analytes between the gaseous and the liquid phase. Several reviews and books have been published on the theory of GC, which will not be treated here in its entirety.[166,167]

In GC, we distinguish between separation on packed columns and on capillary columns. Briefly, packed columns have a large inner diameter (2–6 mm) and are filled with an inert support coated with the liquid stationary phase, while capillary columns are open tubes with small inner diameter, the liquid stationary phase coating the inner wall.

Packed columns are usually quite short (20 cm to 5 m), are run with relatively high carrier gas flow (e.g. 100 mL/min He) and provide low chromatographic resolution of typically around 1000 theoretical plates (for a packed column of 1 m length and 2 mm i.d.). In speciation analysis, packed columns are most often used for the separation of low volatility analytes (after cryotrapping) and/or analytes that interact strongly with the liquid phase. The columns used in these applications are often very short and wide with around 20 cm length and 4–6 mm i.d. Analyte peaks obtained by packed columns are usually broad being in the range of several (5–60) seconds.

Capillary columns can be obtained with different inner diameters (0.1–0.53 mm), with the liquid coating varying in thickness (0.1–5 μm) and with a column length up to 70 m (with 10–30 m being most often applied). Carrier gas flow is low, depending on the column inner diameter, but usually in the range of a few (1–5) mL/min He. The chromatographic resolution power is high; 100 000 theoretical plates can be achieved with a 0.53 mm column of 30 m length. Analyte peaks can be shorter than one second duration, with usual peak widths in the range of 1–5 s, depending on the column and separation conditions.[168]

Krupp[169] compared chromatographic parameters obtained for cryotrap-packed column chromatography-ICP-MS,[170] with those obtained for cryo-focusing capillary column chromatography-ICP-MS. As(III), MMA, DMA and TMAO (trimethylarsenic oxide) were submitted to hydride generation, and the resulting gaseous hydride species purged from the reaction vessel into cryotraps and submitted to either of the analytical systems.

Regarding the species pair $AsMe_2H$ and $AsMe_3$, the packed column system does not allow baseline separation between these two species [Figure 7.12(a)]. The superior resolution power of the capillary column system clearly allows baseline separation of the two species [Figure 7.12(b)]. Additionally, the analysis time is significantly reduced, and superior detection limits are obtained because of sharper peaks.

For speciation analysis using GC coupled to ICP-MS, it is imperative that the species in question is volatile or can be volatilised without degradation or destruction. Only a few species are directly accessible for GC-ICP-MS analysis, e.g. peralkylated organometallic compounds, element hydrides or carbonyls. Many of the species of interest are partly alkylated molecules, present in ionic form either in the water phase or in soil, sediments and biological materials. These compounds must be derivatised prior to GC-ICP-MS analysis, which usually necessitates an extraction step from the matrix, with subsequent derivatisation to the volatile compound and a final extraction into an adequate medium for GC injection.

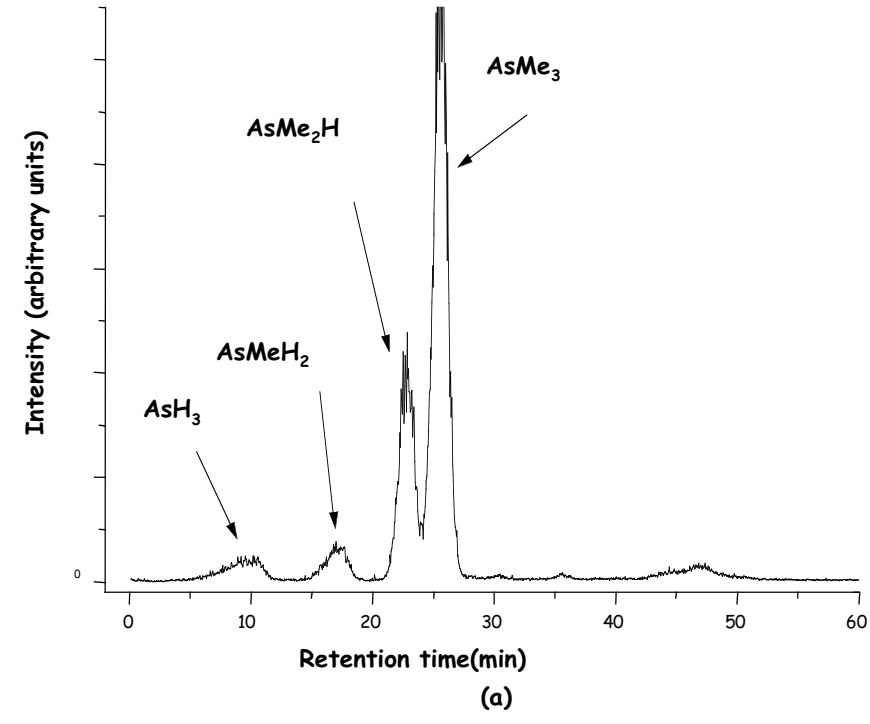

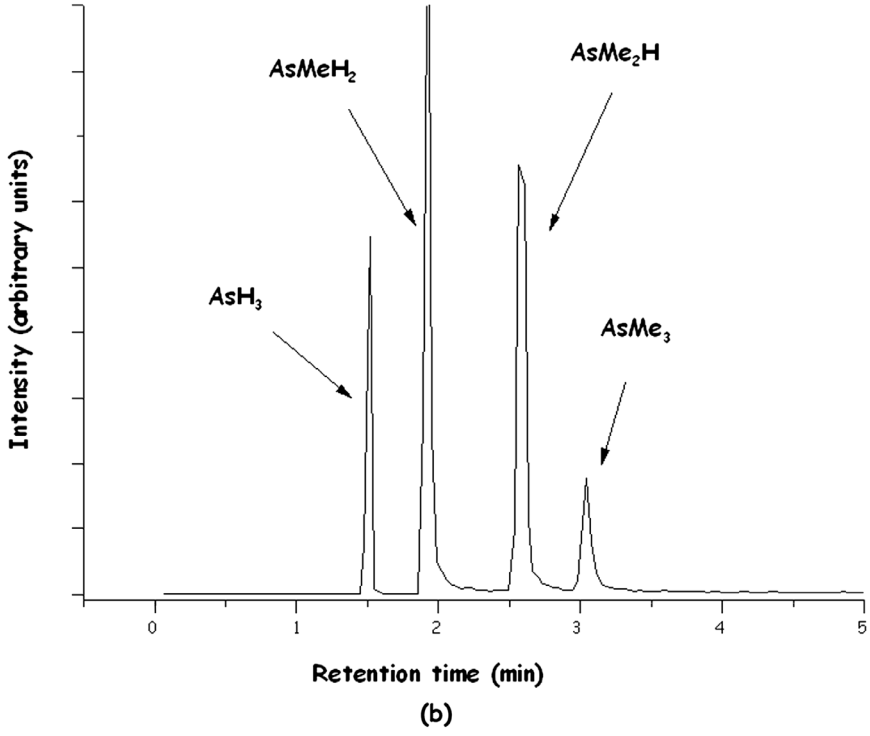

Figure 7.12 (a) Packed-column GC-ICP-MS chromatogram for the determination of inorganic and methylated arsenic species after hydride generation and cryotrapping. (b) Capillary column GC-ICP-MS chromatogram for the determination of inorganic and methylated arsenic species after hydride generation and cryotrapping.

7.5.2 Instrumentation for GC-ICP-MS coupling

In principle, the connection of a GC to an ICP-MS is straightforward – the outlet of the GC column is connected to the torch injector, either directly or via a transfer line. In reality, this simple approach bears several constraints:

(1) The analytes separated on the column must be transported into the ICP torch without loss, decomposition or deterioration of the GC separation.
(2) Optimisation of the ICP-MS parameters must be achieved with the GC connected.
(3) The GC carrier gas flow is too low to penetrate the plasma, and thus an additional 'sheathing' gas flow must be enabled.
(4) Connection and disconnection of the GC outlet to the ICP torch should be simple and fast.
(5) The construction should be flexible in order to facilitate handling and enable torch movement.
(6) All surfaces in contact with the analytes should be deactivated or coated in order to prevent decomposition or absorption.
(7) In many cases, oxygen must be added to prevent carbon build-up on the cones.

This listing is not exhaustive, but immediately brings up the question, why couple GC to ICP-MS when it may give so much trouble? This is simply because ICP-MS is definitely the ideal detector for a wide range of environmentally relevant elements. ICP-MS delivers highly selective multi-element and multi-isotope analysis combined with excellent sensitivity, while GC delivers the analytes to the plasma quasi matrix-free in a 'concentrated' peak and, moreover, in a gaseous form, which ensures 100% transport efficiency. The narrow peaks delivered by capillary GC result in excellent signal-to-background ratios, and detection limits have been reported in the lower or even sub-fg levels (related to the element being measured and the absolute amount injected).

The GC itself is a versatile tool, enabling, e.g., injection via thermodesorption of species preconcentrated on a solid phase microextraction (SPME) fibre, or the use of cold injection systems for volatile species, and of course is applicable to a wide range of species just by choosing appropriate columns and separation conditions.

(a) Interfacing GC with ICP-MS

The unequalled performance and versatility of GC-ICP-MS has made this detection system extremely attractive, and several interface constructions have been proposed in recent years. Most of these couplings are laboratory made, designed to fit the requirements of the respective application. Briefly, GC-ICP-MS instrumentation can be divided into low-temperature applications (e.g. volatile, gaseous species at ambient temperature) and high-temperature applications (e.g. derivatised organometals with low volatility). Another distinction can be made between interfaces using dry plasma conditions by coupling the GC directly to the torch body after removing the spray chamber, and interfaces using the simultaneous aspiration of an aerosol for optimisation and internal standardisation.

Volatile, gaseous organometallic species are often determined after cryotrapping and packed column GC. The high volatility of these species does not require excessive heating of the transfer line, if at all. Pecheyran *et al.* developed an interface connecting packed column cryo-GC with an Elan 6000 ICP-MS for the measurement of volatile species, sampled by cryotrapping and

refocused on the head of the packed column.[26,171,172] A 1 m Teflon tube (1 mm i.d.) was inserted into a 4 mm copper tubing and heated resistively to about 120°C. The Teflon tubing was connected to the packed column (a support-filled, 8 mm o.d. U-shaped glass tube) with Teflon unions. The connection to the torch was realized with a special Teflon adapter after removal of the spray chamber. In this adapter piece, the GC carrier gas (approx. 100 mL/min He), argon (nebuliser gas, approx. 900 mL/min), oxygen (15 mL/min, to avoid carbon deposition on the cones) and a mixture of 50 μg/mL xenon in argon (2.5 mL/min for ICP-MS optimisation and as the internal standard) were mixed prior to introduction into the torch injector. The GC effluent could be vented during the installation of a new sample trap.

This set-up was used for the determination of a variety of species, e.g. organolead in urban air,[26] volatile metal species in stack gas[171] and fuel burning processes,[172] or volatile selenium and mercury species purged and trapped from seawater.[173,174]

Another set-up was used for the determination of butyltin hydrides thermodesorbed from a packed column GC, giving satisfactory peak shape for MBT and DBT, but considerable peak tailing for the least volatile species, TBT. The problem was resolved by inserting a heated block at 250°C at the outlet of the column, and adding argon as make-up gas to the GC carrier.[175] An improved set-up of this principle was used by the same group for the measurement of ethylated butyltins, mercury species and lead compounds separated on a capillary column. The make-up gas (argon) in combination with the heated block at the very beginning of the transfer line enabled the transport of the species into the ICP torch via a 1.5 mm o.d. PTFE tube at 250°C.[176,177]

Interfacing multicapillary GC with ICP-MS for the determination of ethylated mercury compounds by purging and cryotrapping on a capillary with a non-heated transfer line proved suitable for the determination of species not heavier than Et_2Hg.[178,179]

An interface for the coupling of low-temperature GC on a packed column with ICP-MS was developed by Feldmann,[180] where the GC effluent was mixed with an the aerosol coming from a standard spray chamber right before the torch injector. The transfer line was a non-heated Teflon tube with 0.8 mm i.d., connected to the U-shaped glass tube filled with chromatographic support material and to the T-piece connector with the torch by means of nylon Swagelok unions. This principle allowed routine ICP-MS parameter optimisation as well as a semi-quantification of volatile species using a cross-calibration approach. Further advantages of these wet plasma conditions over dry plasma conditions are that oxygen mixing is not necessary because of abundant H_2O in the plasma, and that the plasma is apparently more stable towards eluting co-trapped matrix gases like CO_2. Detection limits are comparable to those obtained in dry plasma conditions, thus disproving the opinion that dry plasma conditions are advantageous in GC-ICP-MS because no energy is consumed in the process of aerosol drying. On the contrary, the presence of water introduces hydrogen and an excess of electrons into the plasma, thus promoting ionisation kinetics.

The same approach was further developed for low-temperature capillary GC coupling[169,181] and different packed column chromatographic set-ups.[182,183]

An interesting approach was realized in the early 1990s by Peters and Beauchemin.[184,185] They developed a GC interface to an Elan 500 ICP-MS, which enabled switching from standard aerosol introduction to GC introduction by just turning a valve. The interface was constructed to stay in place for all applications, which greatly reduced the time for changing from standard to GC operations. The transfer line was heated to 120°C, and the core of the interface was a heated sheathing device, which prevented aerosol condensation in the tubing and enhanced the overall sensitivity. With this design, GC measurements were performed in dry

plasma conditions. Despite its suitability and versatility, this coupling principle was never further developed.

An interface coupling capillary GC with ICP-MS and enabling the injection of large solvent amounts (up to 20 μL) has been developed by Glindemann *et al.*[186] The transfer line possesses a valve system for venting the solvent peak in order to avoid carbon deposition on the cones and plasma perturbation due to the arrival of large amounts of organic solvent. The transfer line itself is heated to only 140°C, but nevertheless the elution of compounds with very high boiling points up to that of tetraphenyltin was shown without significant peak broadening. This result was attributed to the fact that the GC effluent was mixed with a high nebuliser argon flow before entering the transfer line, which greatly reduces the species' condensation temperature.

The chromatographic separation of high boiling species is traditionally achieved with capillary GC, and for coupling to ICP-MS, heated interfaces have been designed in order to improve species transport.

DeSmaele[187] used a steel tube, resistively heated to 250°C. Before the arrival of the transfer capillary in the ICP torch, a heated, self-constructed T-joint was used to add pre-heated argon as the nebuliser gas, flowing around the transfer capillary. The interface was flexible, allowing easy connection and disconnection, and species as heavy as pentylated TBT (Bu_3SnPe) could be eluted, even though significant peak broadening occurred. A similar interface was used by Prange,[188] employing a quartz transfer capillary heated to 250°C.

A non-flexible interface has been constructed, where the transfer line could be heated up to 350°C.[189] The transfer capillary was inserted into a stainless steel tube, together with a second capillary, where a gaseous standard (arsine in argon) could be injected for ICP-MS optimisation. The ICP nebuliser gas flowed through a length of tubing inside the GC oven, and this pre-heated gas then flowed through the stainless steel tube, surrounding the transfer capillary. This design was applied to species with boiling points up to that of ethylated TBT, and did not reveal significant peak tailing. In another set-up, a non-flexible transfer line was introduced, using a heated aluminium rod with a longitudinal slit where the transfer line was inserted, to determine mercury chloride and alkyllead species.[190–192] Pretorius *et al.* modified this transfer line for the detection of metalloporphyrins, by adding pre-heated argon into the injector tube, and maintaining the temperature of the interface up to the torch at 400°C.[193]

Other interfaces employ heating of the transfer line right into the torch, thus demanding a more complicated construction and the insertion of metal into the torch box. Care must be taken in such interfaces to avoid RF leaking from the Faraday cage, which is usually achieved by grounding the metal parts with the torch box. The use of Teflon-coated NiCr wire for resistive heating of a transfer capillary right into the torch injector body has been described. This set-up was intended to be useable for any ICP, and the temperature applicable was only restricted by the Teflon which allowed a maximum temperature of 260°C (above 260°C, Teflon melts).[194]

A flexible, heated transfer line was constructed by Krupp[195] using the concept of simultaneous introduction of aerosol for ICP-MS parameter optimisation and addition of internal standards. Although only the transfer line was heated (to about 200°C, using Teflon-coated NiCr wire) without extending the heating into the torch, high boiling triphenyltin was eluted without significant peak broadening. This effect was ascribed to the influence of argon mixing with the GC effluent. The concept described here has been successfully used in combination with different ICP-MS the heating systems for the determination of methylmercury and butyltin compounds using species-specific isotope dilution methods. Continuously aspired internal standard solution was used to correct for instrumental mass bias during the GC measurements, employing a

continuous thallium signal for mercury measurements and a continuous antimony signal for tin measurements.[196–198]

(b) Commercial GC-ICP-MS systems

To date, two commercial GC-ICP-MS systems are available on the market. One is supplied by Agilent Technologies, coupling the HP 6890 GC with the 7500 series ICP-MS. The transfer line is flexible, in order to enable torch positioning, and is fitted into a specially designed torch. The GC transfer line injector replaces the spray chamber. The transfer line is heated up to 5 cm before the tip of the metal injector and can maintain temperatures up to 300°C. This system is operated in dry plasma conditions, and ICP-MS optimisation is achieved by feeding xenon gas into the GC column during the optimisation process. Oxygen can be added in order to avoid carbon deposition on the cones. A detailed description of the pre-commercial interface version has been published.[199,200]

A different GC-ICP-MS coupling principle, based on the simultaneous introduction of GC effluent and liquid from a standard spray chamber has been commercialised by Thermo Electron Corp. Here, the GC is coupled to the ICP-MS via a flexible line, using a modified torch, where GC and standard liquid sample introduction are connected simultaneously (Figure 7.13). While the transfer line can be heated to 400°C to elute high boiling compounds, the ICP-MS optimisation can be performed with a liquid standard solution of choice. Thus, routine optimisation parameters like oxide ratio, doubly charged ion ratios, etc., can be optimised during a standard autotune or manual optimisation procedure with a multi-element solution. During GC runs, an internal standard of choice can be introduced via the spray chamber. This continuous signal can be used for sensitivity drift correction in quantitative speciation studies.[201,202]

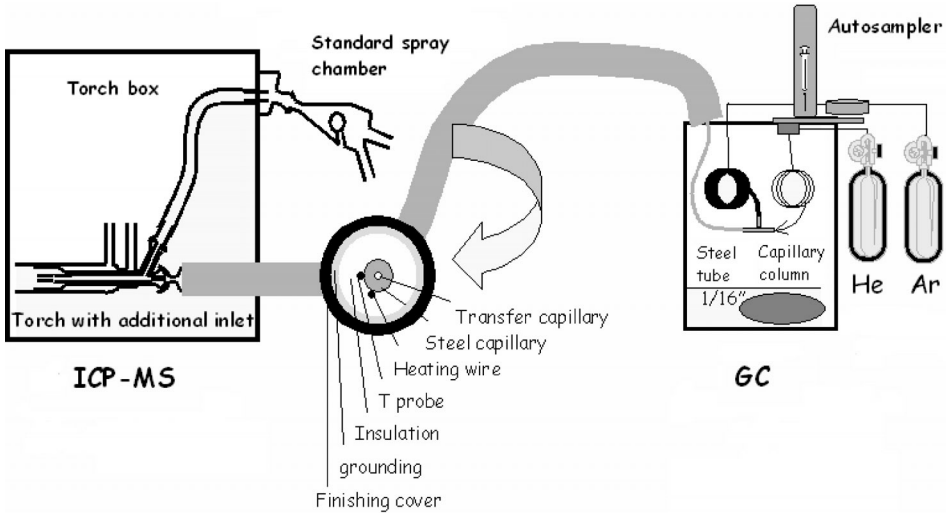

Figure 7.13 Coupling of GC to ICP-MS via a flexible, heated transfer line for the analysis of organometallic species with simultaneous introduction of liquid internal standard (prototype of a commercial system recently introduced by Thermo Electron Corp.).

The continuously aspirated aqueous standard of choice may also be used for simultaneous mass bias correction in species-specific isotope dilution analysis, e.g. by aspirating thallium

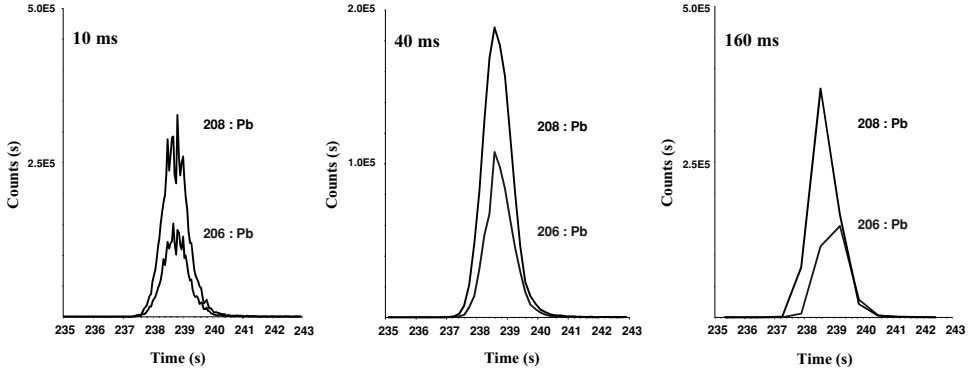

Figure 7.14 Peak definition for different dwell time settings.[203] (Reproduced by permission of the Royal Society of Chemistry.)

solution for mass bias correction of methylmercury, or by aspirating antimony solution for organotin analysis.[196–198]

(c) Parameter optimisation for GC-ICP-MS

The sequential detection of ICP-MS with quadrupole mass analysers poses a potential problem when dealing with very short transient signals as obtained from capillary GC separations. In order to avoid so-called spectral skew, which describes the peak shape deterioration and apparent shift on different isotopes,[203] as illustrated in Figure 7.14, the number of isotopes measured, the dwell time per isotope and the chromatographic separation conditions have to be carefully balanced. Long dwell times provide the advantage of improved signal-to-noise ratios, but will induce poorer peak definition, while very short dwell times provide good peak definition, but suffer from higher signal noise.

As a rule, a GC peak should be defined by at least 15 points to offer good peak definition. Thus, in a GC peak of 3 s base width, each isotope should be measured in an interval of a maximum of 200 ms. Provided that three different isotopes are measured, a maximum dwell time of 66 ms per isotope should be applied. Consequently, for narrower peaks and/or more isotopes to be measured, dwell times must be reduced. Thus, in GC-ICP-MS, GC parameter optimisation should not aim for extremely narrow peaks.

This balancing of GC and ICP-MS acquisition parameters is especially important when isotope dilution techniques are applied. Here, the determining factor is the precision on the isotope ratio, which is determined on integrated peak areas of the respective element isotopes. Precise peak integration can only be accomplished on well-defined symmetrical peaks.

7.5.3 Sample preparation for GC-ICP-MS

The sample preparation procedure applied for organometallic speciation depends on the matrix in which the respective species is present, and the state in which the species exists. Volatile organometallics that have been sampled by cryofocusing or adsorption methods can more or less

directly be submitted to GC-ICP-MS measurement by injection via desorption. Ionic species in water, solid or biological matrices are subject to at least two steps of sample preparation. Firstly, the species must be separated from the matrix, by either extraction or sample digestion and secondly, the ionic species must be derivatised to obtain volatile and thermally stable species, which are accessible to GC separation. Derivatisation and extraction can be performed relatively easily. A variety of sample preparation procedures has been developed, dedicated to the respective species, the matrix and the analytical method concerned. Two principal procedures can be distinguished: either extraction of the species from the sample matrix and subsequent derivatisation, or *in situ* derivatisation with extraction of the derivatised species in the same set-up. Additional preconcentration steps may be inserted into the procedure when ultratrace analysis is required, or additional extraction steps may be included for 'cleaning-up' difficult matrices, usually prior to derivatisation.

In the following sections, the most important procedures applied prior to GC-ICP-MS detection are highlighted.

(a) Volatile metal compounds (VMCs)

Cryotrapping is by far the most often applied method prior to the determination of VMCs. This technique serves as a sampling step as described above, as well as a means to transport and possibly refocus the species onto the GC-column head. The refocusing step serves for a more uniform 'injection' upon heating, as the species are concentrated in a few millimetres at the top of the chromatographic column.[26,204–207]

Direct thermodesorption into a packed column chromatography system has also been employed.[20,23,24,170,208] Refocusing onto a capillary column loop immersed in liquid nitrogen prior to flash thermodesorption into a capillary column has been shown to dramatically enhance the chromatographic resolution and improve detection limits compared to packed column GC.[169,181]

Sewage and landfill gas samples taken in Tedlar bags can be directly injected into a cryo-GC system cooled with liquid nitrogen at –196°C using a gastight syringe. Usually only a few (10–100) millilitres of gas are necessary for detection. A cartridge filled with NaOH pellets efficiently removes CO_2 in order to prevent the cold trap from clogging. This method is suited for very volatile hydride species (AsH_3, SnH_4), while semivolatile species are efficiently trapped at higher temperatures (−78°C), thus avoiding the trapping of large amounts of CO_2 and eliminating the need for a NaOH cartridge.[209]

Recently, SPME (solid-phase microextraction) has been applied for the adsorption–thermodesorption of methylmercury by headspace extraction. The advantage of this method is that no cryogenic trapping is involved, but the disadvantage is that it is limited to relatively clean samples, as high-abundant volatile organometallic compounds will compete with the adsorption reactions on the SPME fibre.[210,211]

Adsorption methods on Tenax or Porapak material have successfully been applied for the enrichment of organolead compounds from urban air. The organolead was subsequently extracted from the solid support by hexane.[17]

(b) Aqueous sample preparation

Purge-and-trap method for dissolved volatile species Dissolved VMCs in the water phase may be purged with the help of an inert gas (N_2, Ar, He) into a cryotrap system. When

trapping is performed with liquid nitrogen, helium must imperatively be used as the purge gas, as Ar and N_2 will also condense in the trap. This purge-and-trap technique has, for example, been successfully employed for the determination of selenium (Me_2Se, Me_2Se_2), mercury (Hg^0, Me_2Hg), tin (Me_4Sn, Me_3BuSn, Me_2Bu_2Sn, $MeBu_3Sn$) and lead (Me_4Pb–Et_4Pb and mixed ethyl–methyl lead) compounds in natural waters.[173,174] The trapped VMCs are then submitted to GC-ICP-MS as described in Section 7.2.1 for gaseous samples.

Volatilisation by derivatisation – purge-and-trap methods Ionic species need to be converted into volatile compounds prior to purging and trapping. The classical method is hydride generation in the original sample using $NaBH_4$, followed by cryotrapping. This approach is mainly used for As, Sn, Ge, Sb and their methylated dissolved species.[212–215] Ethylation using $NaBEt_4$ has been applied for derivatisation of mercury, lead, tin and selenium species prior to purging and trapping, and this technique overcomes some of the problems due to matrix interference and species instability encountered with hydride generation.[216,217]

As with gas sampling or purging of volatile species, effective moisture removal has to be performed before cryotrapping and releasing of the species onto a packed or capillary column. Application of these methods is generally limited to methyl and ethyl species, as less volatile compounds like butyltin or phenyltin hydrides are prone to condensation, leading to non-quantitative recovery.

Liquid–liquid extraction from the water phase Non-polar organometallic species, or those with predominantly covalent character, present in aqueous samples can be directly extracted into an organic solvent, as is the case for, e.g., tetraalkyllead, triethyllead or triphenyltin. Other compounds with more ionic character may be solvent extracted as chelate complexes formed with diethyldithiocarbamate or tropolone.[218–223] Derivatisation to non-polar compounds followed by solvent extraction has been performed using hydride generation,[224,225] and ethylation with $NaBEt_4$,[226,227] $NaBPr_4$,[11,228] or $NaPh_4$.[227,229] These methods are mainly used for organotin and organolead species, as well as for methylmercury.

For methylmercury, solvent extraction into dichloromethane or toluene after acidification has also been applied, in conjunction with ethylation.[230,231] Modified sulfhydryl cotton fibre can be used for the extraction of methylmercury from water, although this method has recently been suggested to generate artefact methylmercury.[46,232,233]

Steam distillation Vacuum or steam distillation is a technique feasible for methylmercury extraction because of the relative volatility of methylmercury hydrides.[234] The strong point of this technique is that efficient matrix separation is achieved, which is particularly important when analysing waters rich in organic matter. A detailed description of steam distillation for methylmercury analysis was published by Horvat,[235,236] and recently an improved apparatus was introduced by Hintelmann.[46]

Solid phase microextraction SPME is based on the sorption of non-polar organometallic species onto a fibre coated with a chromatographic phase. Sorption efficiency is governed by the species distribution coefficients between the two corresponding phases, which in most cases is the system aqueous solution – organic phase, e.g. a polydimethylsiloxane (PDMS) coating.[237,238] Sorption on the fibre can also be achieved from the headspace. The fibre charged with organometallic species is then transferred into the GC injector, where the species are

thermally desorbed and submitted to the GC. A special needle system, in which the microfibre is housed, is used to mechanically protect the fibre. A review on SPME for trace element speciation has been published by Mester *et al.*[210]

Preconcentration of organometallic species from the water phase onto a PDMS-coated microfibre has been applied to organomercury, organolead and organotin species. Peralkylated compounds like tetraethyllead can be adsorbed directly,[239] while ionic species were derivatised with $NaBEt_4$ beforehand.[240] It must be noted that adsorption equilibria depend on the respective species, which result in considerable differences for the detection limits obtained.[241,242] An interesting approach is sorption on a stir bar. Here, more organic phase is available, which greatly enhances the sorption efficiency. The stir bar is then subjected to thermodesorption in a commercial system (TDS, Gerstel, Germany) and species are injected into the GC by means of a cold injection system.[243]

(c) Soil and sediment

The principal goal of soil and sediment sample preparation is to liberate bound organometallics quantitatively, without provoking destruction, decomposition or transformation of the original species.[244] This prerequisite rules out harsh, quantitative digestion methods involving strong, oxidising reagents as applied for total element analysis. It is hoped that a quantitative digestion is not necessarily required, as organometallic species present in soil and sediments are considered to be bound by adsorption or absorption to the particle surface. Processes to liberate organometallics thus involve leaching or extraction processes, rather than complete sample digestion.

Species of main interest are butyl- and phenyltins and methylmercury, as well as organolead compounds.[245] Extraction methods for organotin species concerning environmental samples have been reviewed several times.[223,246–249] Acid leaching processes as well as methanolic extraction involving the use of complexing agents like tropolone have been widely used.[60] Extractions were performed using prolonged stirring, shaking or sonication as well as extraction into organic solvents,[250] but these procedures are long and cumbersome, and were shown to give unsatisfactory recovery and reproducibility, especially for the most polar species, monobutyltin. Recent developments in extraction procedures involving accelerated solvent extraction[251–253] supercritical fluid extraction,[254–257] and especially microwave-assisted extraction[222,258] have drastically reduced extraction time while providing excellent reproducibility and recovery. Open-focused microwave digestion was shown to give excellent results with an effective extraction time of 3 min only, compared to 12 or more hours for mechanical agitation methods.[198,259]

Traditional methods for the extraction of methylmercury from soil and sediment involve water vapour or vacuum distillation[234,235,236,260] besides acid leaching procedures, that were introduced in the late 1960s.[261–263] Here, microwave-assisted extraction has also been very successful; methylmercury is extracted from sediments using acetic acid in less than 3 min.[264–266]

The procedures of methylmercury extraction and derivatisation have lately been subject to doubt, as some traditionally used methods have proven to induce artificial methylation of inorganic mercury, with the consequence that a workshop and a complete journal issue of *Chemosphere* were dedicated to this subject.[267] Artefact methylmercury production has not only been shown to occur during extraction, but also during derivatisation, and has been studied using isotopically labelled Hg^{2+}.[268]

A more detailed discussion on this topic can be found in Section 7.5.5(e) on the use of isotopically labelled species for the determination of artefact formation or species degradation during extraction and derivatisation reactions.

(d) Biological tissues

Several approaches have been realized for the digestion of biological tissue for speciation analysis. For methylmercury analysis in fish tissue, alkaline digestion with TMAH (tetramethyl ammonium hydroxide) or a NaOH or KOH/methanol mixture is most often applied.[196,269,270] Acidic digestion using diluted HNO_3 has also been employed, and was found to more completely destroy the organic matrix, which in turn had a positive effect on derivatisation efficiency.[46] For organotin species in biological tissue, an alkaline digestion with TMAH can be applied, as well as extraction with acetic acid.[197,198]

(e) Derivatisation methods

The majority of species present in aqueous or solid samples will be ionic, and must be derivatised to non-polar, volatile compounds, accessible for GC analysis. Extraction and derivatisation can be accomplished simultaneously or sequentially, as described in the following sections. The derivatisation techniques most often applied are hydride generation with $NaBH_4$, ethylation with $NaBEt_4$ or Grignard alkylation,[271] and were recently reviewed by Morabito *et al.*[272]

An old, yet still very popular method is hydride generation[213] using $NaBH_4$ solution and simultaneous purging and cryotrapping of the volatilised compounds. This method can be applied to a wide range of elements (As, Ge, Se, Cd, Sn, Sb, Te, Hg, Pb, Bi), and has often been employed for the determination of methylated species of arsenic, germanium, tin and antimony.[169,183,214,215,273] Although hydride generation is a very useful and versatile derivatisation technique, there are several drawbacks when applied for trace metal speciation:

(1) Optimal pH conditions are different for different elements and element species, and so multi-element analysis is hampered,[212] though may be overcome by applying a pH gradient during derivatisation.[274]
(2) The hydride generation process is prone to matrix interference, e.g. by the presence of transition metals or organic matter.
(3) Hydrides are rather reactive and may decompose during chromatography.
(4) The applicability to heavier species, like butyltins, is hampered because of the low volatility of the derivatised species.
(5) Significant blank levels for a range of elements have been reported, stemming from the $NaBH_4$ reagent.[182,183]

Hydride generation has nevertheless often been used for simultaneous speciation of methylated and butylated tin species.[175,183,275]

Regarding the inorganic forms of the elements arsenic, selenium and antimony, only the reduced species [As(III), Se(II), Sb(III)] are readily hydrogenated. The higher oxidation state species [As(V), Se(IV), Sb(V)] must be reduced beforehand. In the end, the same hydride species are generated (AsH_3, SeH_2, SbH_3), so simultaneous speciation is not possible with hydride generation-GC-ICP-MS, and LC is preferred for the simultaneous determination of these redox species. Nevertheless, this behaviour enables the sequential speciation of the redox pairs, by performing hydride generation of the reduced element species prior to a subsequent reduction step and hydride generation of the originally oxidised element forms. This procedure requires exact control of the pH before and during hydride generation.[212]

Methyl- and dimethyl arsenic and antimony species are converted to $AsMeH_2$/$AsMe_2H$ and $SbMeH_2$/$SbMe_2H$, respectively, while the trimethylated species present in the aqueous phase

are reduced to the volatile trivalent species $AsMe_3$ and $SbMe_3$. Here also, special care must be taken over the hydride generation conditions, as demethylation reactions occur depending on the pH conditions applied.[276,277]

The applicability of hydride generation to mercury speciation is limited because of the thermal instability of MeHgH, and the fact that inorganic mercury will be reduced to elemental mercury (Hg^0).[278]

Aqueous alkylation with tetraalkylborates Since the first introduction of aqueous alkylation with $NaBEt_4$,[216] this method has, to a great extent, replaced the hydride generation technique. Alkyl derivatives are in general more stable than their respective hydrides, and the *in situ* derivatisation procedure is less affected by matrix effects. The derivatives are non-polar and can thus be extracted into an organic solvent to be directly injected into capillary GC, although for species sufficiently volatile (MeHg, methyltins), purge-and-trap methods can also be applied.[278,279]

Methyl-, butyl- and phenyltin species can be ethylated, and form thermally stable species suited for capillary GC separation. Methyltins are volatile enough to be treated in a purge-and-trap approach, while heavier species must be extracted into an organic solvent, like, for example, isooctane (2,2,4-trimethylpentane). Rapsomanikis[226] has reviewed the use of $NaBEt_4$ for speciation analysis.

A drawback when using ethylation for derivatisation is the fact that ethylated species originally present in the sample cannot be distinguished. Tetraethyllead, for example, is formed from inorganic lead as well as all partly ethylated lead species, and ethylation is thus not appropriate in this case. To overcome this, propylation with $NaBPr_4$ or phenylation with $NaBPh_4$ can be applied.[227,280] Propylation has also been shown to be favourable for methylmercury derivatisation, as ethylation using $NaBEt_4$ was shown to incidentally demethylate MeHg to form Hg^0.[281]

Grignard alkylation Grignard reagents were introduced by Victor Grignard in 1901, for which he received the Nobel prize in 1913. The use of Grignard reagents for the alkylation of metals is based on the reaction of alkylmagnesium halides for the carbanionic transfer of an alkyl group to form a covalent bond with the respective metal. This derivatisation technique must be carried out under strictly water-free conditions, thus necessitating the extraction of organometallic species into an organic, water-free medium. Different Grignard reagents have successfully been applied to the derivatisation of organotin compounds, including methyl-, ethyl-, propyl-, butyl- and pentylmagnesium halides,[250] but this technique has lost its importance with the introduction of alkylborate reagents directly applicable in aqueous solution. Nevertheless, Grignard alkylation is still being used for organolead speciation,[203,282] and is also applied to the derivatisation of organic mercury in petroleum products.[283,284] The derivatisation of methylmercury and inorganic mercury with different Grignard reagents has been evaluated.[285]

7.5.4 Applications of GC-ICP-MS

(a) Multispecies–multi-element analysis of gaseous and aqueous samples

Volatile metal species (VMCs) have been investigated in the natural atmosphere,[20,205] special environments like landfill or sewage gases,[169,170] in flue gas from combustion processes[171,172] and in workplace air.[26] Which VMCs are of interest mainly depends on the environment analysed. In urban air, methylated and ethylated lead species have been shown to be present as a

result of their use as anti-knocking agents in gasoline.[205] Industrial hygiene demands investigation of VMCs used in fumigation processes or as precursors (e.g. $GaMe_3$, $InMe_3$, AsH_3) for fabrication of semiconductors.[286] From estuarines, volatile selenium and mercury species ($SeMe_2$, Se_2Me_2, $HgMe_2$) as well as mixed methylated–butylated organotins are emitted, stemming from biological volatilisation of the dissolved metal or organometal precursors. Volatile compounds of phosphorus, arsenic, sulfur, selenium, tin, lead and mercury are formed in the marine environment.[287] An interesting cocktail of VMCs can be found in gas produced from anaerobic fermentation of sewage sludge or in landfill gas. In these sample types, more than 20 different volatile, mainly methylated, compounds of the elements arsenic, selenium, tin, antimony, mercury, lead and bismuth have been detected in the range of a few ng/m^3 to several $\mu g/m^3$.[23,170] Hexacarbonyls of tungsten [$W(CO)_6$] and molybdenum [$Mo(Co)_6$] as well as $Ni(CO)_4$ and $Fe(CO)_5$ have been identified in landfill gas in the range of a few ng/m^3,[206,207] while volatile siloxanes are quite abundant in sewage gas and have been detected in amounts up to the mg/m^3 range.[169]

Volatile organometallic species can be purged directly from the water sample. This purge-and-trap technique has, for example, been successfully employed for the determination of selenium (Me_2Se, Me_2Se_2), mercury (Hg^0, Me_2Hg), tin (Me_4Sn, Me_3BuSn, Me_2Bu_2Sn, $MeBu_3Sn$) and lead (Me_4Pb–Et_4Pb and mixed ethyl–methyl lead) compounds in natural waters.[173,174]

Ionic species must be derivatised into volatile compounds. These may be purged from the water phase into a cryogenic trap, an approach which is mainly applied after hydride generation for methylated species of As, Sn, Ge and Sb in urine, landfill condensates, seawater or geothermal waters.[20,173,182,182] Ethylation using $NaBEt_4$ has, for example, been shown for the derivatisation of mercury[281] and germanium[216] species prior to purging and trapping, and is favourable over derivatisation with hydride generation.

(b) Organotin speciation in solid samples

TBT, being an organotin compound, is of particular importance for sediment samples, as this species is the main component in anti-fouling paints for boats, and thus can be found in substantial amounts in harbour and estuarine sediments.[55] Organotin compounds also accumulate in mussels, and organotin speciation can be carried out using similar methods for both types of samples.[198]

After leaching or extraction from the solid, organotin species can be readily derivatised with $NaBEt_4$ and extracted into an organic solvent for GC-ICP-MS injection.[60,197,198,270,271] Detection limits in the lower fg level (absolute) are obtained.

The versatility of $NaBPr_4$ and $NaBEt_4$ as derivatisation reagents has been demonstrated by multi-element speciation in one set-up. Organolead, organomercury and organotin species can readily be derivatised and extracted in one run, although care must be taken, because the derivatisation yields for the different species are not equal. Nevertheless, sediment reference material (PACS-1) was analysed with satisfactory results using propylation.[228] SPME has been performed for the headspace extraction of ethylated organomercury, -lead and -tin compounds. High reproducibility and accuracy for organotin species demonstrated the effectiveness of the method.[242]

7.5.5 The use of stable isotopes in speciation with GC-ICP-MS

The application of isotopically labelled elemental compounds for species-specific isotope dilution analysis has greatly advanced during recent years. Species-specific isotope dilution has

been used to study and/or correct for problems arising from sample preparation issues (incomplete recovery, species decomposition, loss or rearrangement, etc.) since isotope dilution is an 'absolute method', it provides the most accurate and precise quantitative results. Heumann and co-workers were the first to introduce isotope dilution for speciation purposes,[288] and described the first use of isotope dilution for volatile selenium species determination using GC-ICP-MS.[289]

The principle of species-specific isotope dilution has recently begun experiencing growing interest for environmentally important species like butyltin compounds (with the focus on TBT), as well as inorganic mercury and methylmercury. Accurate and precise analysis of these compounds in different matrices (salt waters, sediments, soil, biological tissues) still poses a challenge to the analytical chemist, and species-specific isotope dilution is a promising tool for overcoming, at least partly, problems such as species loss, non-quantitative recovery, species transformation or artefact formation. Not only is precise and accurate species determination possible using this methodology, but species transformation or artefact formation can be recognized, and corrected for, thus helping to establish reliable analytical techniques. This section focuses on organotin species and methylmercury, as these compounds are of principal environmental interest and have been the subject of intense studies.

(a) Synthesis and characterisation of isotopically labelled organotin species and methylmercury

The prerequisite for performing species-specific isotope dilution analysis is the availability of a pure species-specific standard, highly enriched in one element isotope, with known isotopic abundance and concentration. To date, only one isotopic MeHg standard is available: a reference material provided by the Institute for Reference Materials and Measurements (IRMM, Geel, Belgium) under the name ERM-AE 670, certified for isotopic abundance and concentration. This reference material contains MeHg highly enriched in ^{200}Hg and comes as a 34.5 mg/L solution with the concentration certified for at least 2 years when stored at -20°C. Recently, the high-yield synthesis of ^{198}Hg-labelled MeHg has also been realised.[290] DBT and TBT enriched in ^{117}Sn have been produced by the Laboratory of the Government Chemist (LGC, UK), but are not yet available on the market.

Mostly, isotopically enriched standards are fabricated in-house. Because of the high costs for the enriched isotope starting material, microscale synthesis methods have been developed. The synthesis and purification of ^{201}MeHg as well as ^{199}MeHg has been successfully accomplished using methylation via methylcobalamine.[291,292] Ruiz-Encinar[293] described the synthesis of ^{118}Sn-labelled DBT as well as the synthesis of a mixed spike containing ^{119}Sn-labelled MBT, DBT and TBT. Another small-scale synthetic route for isotopically labelled butyl- and phenyltins has been described by Sutton.[294]

With the exception of the certified standard ERM-AE 670, which can be directly used for spiking, isotopically labelled species must be characterised in terms of isotopic abundance and concentration before use. Isotopic abundance is usually determined using repeated GC-ICP-MS measurements of the isotopically labelled species solution after following the same derivatisation process as envisaged for the sample. Procedure blanks must be measured repeatedly in order to perform blank corrections, if necessary, on the spike material. Data evaluation is performed using integrated peak areas of all element isotopes.

The concentration of the spike solution must be determined using reversed species-specific isotope dilution. This is achieved by using a standard solution of natural isotopic composition

with exact known concentration (fabricated gravimetrically) as the 'spike' in the normal species-specific isotope dilution equation (as explained below), while the enriched species solution is treated as the 'sample'.

(b) GC-ICP-MS parameter optimisation

As in all GC-ICP-MS analyses, the ICP-MS acquisition parameters have to be balanced with the chromatographic separation conditions. Parameters such as the number of points per mass unit, number of isotopes monitored and integration time per isotope need to be evaluated for the determination of precise isotope ratios in fast chromatographic peaks. Compromise conditions for data acquisition parameters have to be selected, owing to the opposite influence of integration time on sensitivity and peak profiles. Fast (1–3 s) transient chromatographic peaks are well defined at very short integration times. However, under these conditions the noise on the signal will increase. On the other hand, using very long integration times, peak definition worsens dramatically, spectral skew (as illustrated in Figure 7.14) is observed and peak areas exhibit poor reproducibility. Good results have been obtained in isotope dilution analysis when measuring only the three tin isotopes ^{118}Sn, ^{119}Sn and ^{120}Sn each using 66 ms integration time.[295] For the simultaneous determination of methylmercury and butyltin species with thallium and antimony as continuously nebulised standards for mass bias correction, 30 ms integration time was chosen for ^{202}Hg, ^{200}Hg, ^{120}Sn and ^{117}Sn respectively, while the internal standard isotopes ^{123}Sb, ^{121}Sb, ^{203}Tl and ^{205}Tl were monitored for 5 ms only. Thus, peaks were defined by at least 20 points.[197]

In species-specific isotope dilution, the chromatographic peak shape is also very important, and symmetrical peaks without tailing are desirable. Isotope ratios are usually calculated on the respective isotope peaks, integrated over the whole peak width. Uncertainty in peak integration will directly translate into uncertainty in the result, and must therefore be minimised.

Other ICP-MS derived parameters of concern are the detector dead time and the mass bias. Detector dead time is an instrumental parameter observed for electron multipliers working in pulse counting mode. Briefly, there is a finite time after each impact of an ion on the detector surface, during which the detector cannot measure another incoming ion; that means a certain part of the ions arriving at the detector is not measured. This effect is non-linearly amplified with a rising number of impacts, inducing a change in isotope ratios with increasing element concentration. Modern ICP-MS instruments have an implemented detector dead time correction, but the correct value must be experimentally determined, as it changes with each detector and also during the detector lifetime.

The effect of the detector dead time τ on the measured count rate can be expressed as

$$I_{\text{real}} = I_{\text{exp}}/(1 - \tau I_{\text{exp}}) \tag{7.6}$$

with I_{real} being the real count rate and I_{exp} the measured count rate.

For accurate isotope ratio measurements, the detector dead time is determined for the isotope pair of interest, usually by measuring different concentrations of element standard solutions,[296] for example by using the method proposed by Nelms *et al.* The isotope ratios for a chosen isotope pair are calculated for various values of detector dead time (normally in the range of 20–60 ns), and are then plotted against the element concentration. For each dead time value, a linear regression is calculated. The correct dead time value should result in a slope of 0; i.e., the isotope ratios are constant over the entire concentration range. In order to calculate the correct dead time rather than trying different dead time values, the slopes for each of the chosen dead

time values obtained can be plotted against the respective detector dead time values. The intercept with the x-axis will correspond to the correct detector dead time, which should be chosen for all subsequent measurements. Modern ICP-MS software provides the possibility to set detector dead time values for a given set of measurements, and to recalculate the results. This feature simplifies the determination of the detector dead time, and if, for any reason, detector dead time measurements are performed after GC-ICP-MS measurements, all integration and isotope ratio results can be easily recalculated.

Mass bias is another ICP-MS parameter that induces differences between measured isotope ratios and their true values. Mass bias in ICP-MS is mainly due to effects in the extraction region of the ICP-MS, which suppress transmission of lighter isotopes relative to heavier ones into the mass analyser. Mass bias cannot be solved instrumentally, but must be determined by measuring standard solutions with known isotopic composition. In species-specific isotope dilution, generally a simple linear approach is applied[297]:

$$R_{\text{true}} = \frac{R_{\text{exp}}}{1 + an} \tag{7.7}$$

where R_{true} is the corrected isotope ratio, R_{exp} the measured isotope ratio, a the bias per mass unit and n the mass difference between the isotopes in the respective isotope ratio.

The calculated mass bias factor a is then applied to the actual measurements and used for correction of the isotope ratio value. Simultaneous methods have been developed by determination of the mass bias factor on a different element, for example thallium for the mass bias correction of lead and mercury.[298,299] This principle has been adopted for species-specific isotope dilution measurements with GC-ICP-MS, with a system enabling the simultaneous aspiration of a standard solution during GC introduction. The simultaneous method was compared with mass bias correction using additionally measured standards, and showed satisfactory accuracy. Thallium was used for mass bias correction of lead and mercury species[300,301] while antimony has been used for correcting tin species isotope ratios.[198]

(c) Isotope dilution analysis procedure

In general, the procedure for speciation analysis can be derived from all kinds of sample preparation methods. The only difference is that the sample must be spiked with a solution containing the labelled species at the very beginning of the procedure. Ideally, the amount of spike species added will result in a spike isotope to reference isotope ratio of about 1. The achievement of complete equilibrium of the enriched spike and the sample is critical for the accuracy of the results. If the sample is a liquid, gentle mixing will ensure that a homogeneous mixture is obtained. For solid samples (soil, sediment or biological tissue), an equilibration time of at least 24 h is advisable before attempting any extraction process, to avoid preferential extraction of the spiked species over the analyte species. After spiking and stabilisation of the sample, extraction and chromatographic analysis is performed following the routine sample preparation steps. For GC, derivatisation to yield volatile species is necessary. ICP-MS analysis provides a chromatogram for each isotope, with peaks corresponding to individual analyte species. The area under each peak is determined for the spike and the reference isotope, and the isotope ratio is calculated. Recently, it has been shown that the precision obtained on isotope ratio determinations can be improved either by applying the determination of ratios on single points in the

peak in a 'steady state' approach,[163] or by defining a limited integration zone on the basis of the isotope ratio evolution during peak elution.[302]

The concentration of the species in the samples is calculated by applying the isotope dilution equation[303]:

$$c = \frac{c' w' A_r [R(X/Y)Y' - X']}{w A'_r [X - R(X/Y)Y]} \tag{7.8}$$

For the sample: c is the concentration of sample solution (m/m); w the mass of sample solution; A_r the relative atomic mass of the element being determined; X the isotope abundance (atom%) of isotope 1; Y the isotope abundance (atom%) of isotope 2.

For the spike: c' is the concentration of the spike solution; w' the mass of the spike solution; A'_r the relative atomic mass of the element in the spike; X' the isotope abundance (atom%) of isotope 1; Y' the isotope abundance (atom%) of isotope 2.

The only parameter to be measured and inserted into this equation is the isotope ratio $R(X/Y)$. Apart from R, the other parameters are all known quantities (constants masses and the concentration of the spike solution). Thus, the concentration in the unknown sample is ultimately determined simply by measurement of the isotope ratio R.

(d) Application of isotope dilution for speciation analysis with GC-ICP-MS

Accurate and precise isotope dilution speciation methods have been proposed for several compounds and materials. For MeHg determination in biological sample reference materials (DORM-1 and CRM 463) by capillary GC-ICP-MS, a method was developed using fast microwave-assisted extraction with TMAH followed by ethylation.[198] Optimum conditions for the measurements of isotope ratios on the fast transient chromatographic peak were determined. Mass bias was corrected by using the simultaneously measured thallium signals ^{205}Tl and ^{203}Tl.

For mercury species determination in natural gas condensate, isotopically enriched Me_2Hg, MeHgCl and $HgCl_2$ were prepared and used for species-specific isotope dilution and method assurance tests.[304] This method gave excellent detection limits and improved matrix tolerance compared with other speciation approaches for samples in an organic matrix.

Ruiz-Encinar *et al.* determined DBT in sediments by species-specific isotope dilution using an in-house synthesised ^{118}Sn-enriched DBT spike.[293] The different organotin compounds were separated by GC after aqueous ethylation using $NaBEt_4$ and extraction into hexane. The spike was added directly to the solid sample and extracted with a methanol/acetic acid mixture. The method was applied to the determination of DBT in sediment reference materials with satisfactory results. The same group applied a mixed ^{119}Sn-enriched spike for the simultaneous analysis of MBT, DBT and TBT in the certified reference sediments PACS-2 and CRM 646.[293] Sample pretreatment simply consisted of spiking the dry sediment with the spike solution and extracting the organotin species with a methanol/acetic acid mixture.

A modification of this method was developed for the simultaneous determination of MBT, DBT and TBT in coastal seawater samples,[305] based on the application of species-specific isotope dilution with a ^{119}Sn-enriched spike of the three butyltin compounds of interest.

Yang *et al*. described a method for the accurate and precise determination of TBT using SPME and GC-ICP-MS detection.[306] Butyltin compounds were ethylated in aqueous solution, and the headspace sampled via a PDMS-coated fused silica SPME fibre. The application of

species-specific isotope dilution in this method greatly improved the precision of TBT measurements as compared to standard addition procedures.

Recently, a method has been developed for simultaneous MeHg and TBT determination in biological samples.[197] The integrated simultaneous sample preparation for mercury and tin species included open-focused microwave-assisted extraction and derivatisation by ethylation. The determination was carried out by GC-ICP-MS. The first biological reference material certified for multielement speciation (CRM 710, IRMM, oyster tissue, in preparation) was analysed with satisfactory precision (uncertainty range between 0.7 and 13.7%) and accuracy. Figure 7.15 illustrates a chromatogram obtained for the simultaneous detection of methylmercury, inorganic mercury, MBT, DBT and TBT. It should be noted that this approach may only be successful when species recovery is quantitative during the extraction step.

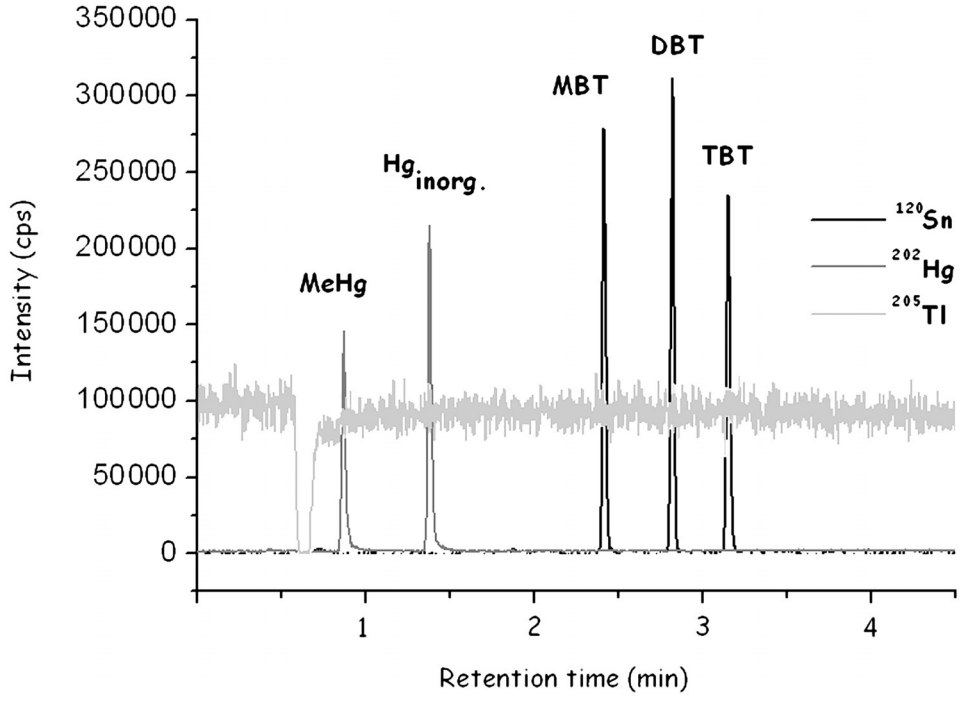

Figure 7.15 GC-ICP-MS chromatogram for the simultaneous determination of mercury and tin species in an oyster sample after derivatisation and ethylation. MeHg: Methylmercury, Hg_{inorg}: inorganic mercury (Hg^{2+}), MBT: monobutyltin, DBT: dibutyltin, TBT: tributyltin. Tl: thallium as continuously aspirated internal standard.

(e) Species transformation studies

Isotopic labelling provides an important diagnostic tool for the development of new analytical methods in terms of using isotopes as tracers. Matrix- or reagent-dependent rearrangement reactions between the different species, taking place during sample preparation and/or derivatisation, can be revealed by measuring the isotope ratios in the non-spiked species. Species isotope ratios measured with GC-ICP-MS have helped a great deal to unravel artificial formation of methylmercury.

The provenance of elemental mercury (Hg^0) as a breakdown product of Et_2Hg and MeEtHg during the derivatisation step has been observed for biological samples. The mechanism could not be completely described, but seems to be significantly affected by the combined effects of variables such as pH, buffer and $NaBEt_4$ concentration.

Isotopically labelled MeHg was used to investigate artefact formation in water samples during derivatisation with $NaBEt_4$. Halide ions were found to induce different transformation processes. While chloride and bromide converted MeHg into Hg^0, iodide hindered the ethylation of methylmercury.[281] The effect was shown to occur only during the derivatisation step, and in contrast to ethylation, propylation with $NaBPr_4$ did not cause any transformation.

Hintelmann *et al*. found that substantial amounts of methylmercury can be formed from inorganic labelled mercury ions ($^{199}Hg^{2+}$), when water vapour distillation is used as the extraction method.[307] This finding raised doubts about the accuracy of methylmercury determination in sediments.[308] Critical comments concerning certified MeHg value in reference materials were made,[309,310] and a workshop was held about this topic.[267]

In sediment samples, methylmercury levels are typically only a few percent or less of the inorganic mercury level and even minor artificial methylmercury formation during sample preparation will result in significant overestimation of the actual methylmercury content. A correction can be carried out with a single measurement, when stable Hg isotopes are used, by measuring different isotopes to determine the artefact formation factor.

Different methods have been described to distinguish and correct for the amount of artefact MeHg (mainly for sediment samples[268,311]) as well as for the degree of methylation of inorganic mercury and demethylation of methylmercury.[312]

Systematic experiments have been carried out to localise the sources of unintentional abiotic methylmercury formation during analysis by capillary GC-ICP-MS after open-focused microwave-assisted acid extraction.[266] Different spiking and derivatisation (ethylation, propylation and Grignard) procedures were tested. Artefact formation does not take place during spiking and extraction, but occurs during the final derivatisation, with the inorganic mercury amount in the derivatised solution being the determining factor. Solvent extraction with CH_2Cl_2 prior to ethylation allows adequate control of the artefact formation. A critical analysis of the results obtained revealed that artefact MeHg formation also depends on organic carbon and sulfur levels in the sediments investigated.

Sequential degradation reactions from TBT to DBT, from DBT to MBT and from MBT to inorganic tin during extraction from PACS-2 and BCR 646 certified reference materials have been studied. Different liquid–solid extraction techniques, including room temperature leaching with mechanical shaking, ultrasonic and microwave-assisted extractions, have been evaluated by Ruiz-Encinar *et al.*, employing a methanol/acetic acid mixture for extraction in all cases. Samples were spiked with a solution containing ^{119}Sn-enriched MBT, ^{118}Sn-enriched DBT and ^{119}Sn-enriched TBT. After extraction using the different methods, sample solutions were derivatised with sodium tetraethylborate and extracted into hexane. The isotope ratios $^{120}Sn/^{118}Sn$ and $^{120}Sn/^{119}Sn$ were determined as peak area ratios for all butyltin species, and a mathematical treatment allowed the determination of the correct species concentrations and the decomposition factor for each of the transformation reactions. Negligible degradation reactions were observed for ultrasonic extraction and mechanical shaking, while for microwave-assisted extractions, degradation factors of up to 7% (TBT to DBT) and 16% (DBT to MBT) were obtained for both the reference materials, when high microwave energy was applied. MBT seems to be strongly bound to the solid matrix, and for quantitative recovery, a harsher extraction technique and a longer extraction time are required. The same authors also investigated accelerated solvent

extraction using the same triple-spike technique for the determination of MBT, DBT and TBT degradation and conversion factors in PACS-2.[253]

7.6 Speciation using ICP-MS with reaction/collision cell technology

In general, ICP-MS is a sensitive and selective detector for speciation analysis; however, spectroscopic interferences can cause problems for quantitative determination of an analyte, as well as for species identification based on the analyte's isotopic pattern. Spectroscopic interferences by another element (isobaric interferences) can often be corrected for using equations involving the known natural isotopic distribution of the interferent and the analyte. Polyatomic interferences, on the other hand, are less easily evaluated and compensated for. The source of these interferences is often the plasma (e.g. Ar_2^+) or a combination of the plasma and the sample or separation medium (e.g. $ArCl^+$). Both the collision cell (CC) and the dynamic reaction cell (DRC) are designed to reduce the effect of spectroscopic interferences on the determination of the elements of interest.

The principles of CC and DRC have been highlighted in Chapter 8 of this book and will not be detailed here. Instead, the application of CC or DRC for speciation analysis only will be focused on here. To date, this has mainly been performed with HPLC coupling.

Many of the matrix interference problems found in total element determinations are eliminated because of the chromatographic step. Thus, important interferences in speciation studies originate either from Ar-based molecular ions like $^{40}Ar_2$ or $^{40}Ar^{16}O$, or matrix-based ions, like $^{16}O_2$.

Relatively few authors have reported the use of this instrumentation for detection in speciation analysis so far. Only five elements (Se, S, Cr, V, As) have been the focus of research papers, and of these, selenium has received the most attention. Very recently, attempts have been undertaken to establish iron speciation with ICP-CC-MS detection.[324]

A list of selected analytes for which speciation analysis detection has been accomplished using ICP-CC/DRC-MS, along with their interfering polyatomic species, can be found in Table 7.2.

Table 7.2 Analyte ions and their polyatomic spectroscopic interferences

Analyte	Main spectroscopic interference(s)
$^{32}S^+$	$^{16}O_2^+$, $^{14}N^{18}O^+$, $^{15}N^{16}OH^+$
$^{51}V^+$	$^{35}Cl^{16}O^+$, $^{34}S^{16}OH^+$
$^{52}Cr^+$	$^{40}Ar^{12}C^+$, $^{35}Cl^{16}OH^+$, $^{34}S^{18}O^+$, $^{36}Ar^{16}O^+$
$^{56}Fe^+$	$^{40}Ar^{16}O^+$, $^{40}Ca^{16}O^+$
$^{75}As^+$	$^{40}Ar^{35}Cl^+$, $^{38}Ar^{37}Cl^+$, $^{40}Ca^{35}Cl^+$
$^{80}Se^+$	$^{40}Ar_2^+$, $^{79}BrH^+$

Sloth and Larsen[314] explored the use of methane as a reaction gas in the DRC for the determination of Se. All selenium isotopes, m/z 74, 76, 77, 78, 80 and 82, were detected in steady-state (continuous nebulisation) mode. Under optimised DRC conditions (Table 7.3), the argon dimer

Table 7.3 Published parameters for ICP-CC-MS and ICP-DRC-MS for speciation analysis

Analyte	Species	Separation technique	CC/DRC	Gas flows (mL/min)	Other parameters	Reference
^{80}Se	Selenoamino acids, selenonium ions and inorganic selenium: yeast and algae	Cation and anion exchange	DRC	CH_4, 0.8	Rpa = 0 Rpq = 0.5	315
^{80}Se	Inorganic selenium	Porous graphite stationary phase	Hexapole CC	H_2, 3	Q bias: −7 V Hex bias: −4.7 V	318
^{76}Se, ^{77}Se, ^{78}Se, ^{82}Se	Cod muscle extracts	Reversed phase and size exclusion	Octopole CC	H_2, 4	Q bias: −12 V Oct bias: −13 V	321
^{77}Se, ^{80}Se	Yeast	Cation exchange	DRC	CH_4, 0.8	Rpa = 0 Rpq = 0.6	316
Se	Red blood cells and yeast	PAGE	DRC	CO, 0.28*	Rpa = 0 Rpq = 0.45	317
^{80}Se	Selenoamino acids	Cation exchange	DRC	CH_4, 0.8	Rpa = 0 Rpq = 0.5	314
^{78}Se, ^{80}Se	Nutritional supplements and Chinese tea	Reversed phase and ion pair	Hexapole CC	He, 1.0 H_2, 5.0–8.0†	Hex bias: −2 V	319
^{80}Se	Urine	Reversed phase and ion pair	Hexapole CC	He, 1.0 H_2, 5.0–8.0†	Hex bias: −2 V	320
^{32}S	Metallothioneins	Capillary electrophoresis	Octopole CC	Xe, 0.2	Q bias: −3 V Oct bias: −4 V	322
^{32}S, ^{56}Fe, ^{55}Mn	Metalloproteins	Size exclusion	DRC	O_2, 0.6	Rpa = 0 Rpq = 0.3	323
^{56}Fe	Water	Cation exchange Anion–cation ion exchange	Hexapole CC	He, 1 H_2, 1	Q bias: −1 V Hex bias: − 6.5 V	324

Continued

Table 7.3 Published parameters for ICP-CC-MS and ICP-DRC-MS for speciation analysis (*Continued*)

Analyte	Species	Separation technique	CC/DRC	Gas flows (mL/min)	Other parameters	Reference
^{52}Cr	Cr(VI) in air	Silica gel column	DRC	NH_3, 0.4	Rpa = 0 Rpq = 0.6	325
^{52}Cr	Cr(III) and Cr(VI) in water	Reversed phase (C_8)	DRC	NH_3, 0.65	Rpa = 0 Rpq = 0.6	326
^{51}V	Serum	Size exclusion	DRC	NH_3, 0.22*	Rpa = 0 Rpq = 0.65	327
^{51}V	Water	Reversed phase and ion pair	DRC	NH_3, 0.4	Rpa = 0 Rpq = 0.6	328
^{75}As	Water	Multi-mode ion exchange	Hexapole CC	He, 5.6 H_2, 2.8	Not stated	329
^{75}As	Water: As(III) and As(V)	Ion exchange	Hexapole CC	He, not stated H_2, 3.0	Not stated	330

* This is the absolute flow rate.

† Depends on the nebuliser used.

Note: Rpa, Rpq: DRC parameter settings; Q bias: quadrupole bias setting; Hex bias, Oct bias: collision cell parameter settings.

interference on ^{80}Se was greatly reduced. However, the authors also noted the presence of a signal at $m/z + 1$ for each of the isotopes of Se. These peaks were identified as SeH. The use of deuterated methane in the DRC did not alter the signal pattern, and thus the source of hydrogen must have arisen prior to the DRC cell. This finding is important, as the Se isotope counts then had to be corrected to account for the formation of this hydride species. ^{80}Se could then be monitored for the detection of selenoamino acids separated by cation-exchange LC. Larsen *et al.*[315] then used the same DRC parameters for the detection of low-molecular-weight selenium species in yeast and *Chlorella* algae. Anion-exchange LC was used for the separation of the free inorganic selenium species Se(IV) and Se(VI), and gradient elution cation-exchange LC was chosen for the separation of the selenoamino acids and selenonium ions. ESI-MS spectra allowed the identification of the selenium species. The same group later used a similar cation-exchange separation and similar DRC conditions for the determination of selenium species in enzymatic extracts of ^{77}Se-enriched yeast samples.[316]

For the determination of selenoproteins in red blood cells and yeast, two-dimensional gel electrophoresis followed by laser ablation ICP-DRC-MS has been used.[317] Methane, carbon monoxide, ammonia, oxygen and a combination of argon and hydrogen were tried as DRC gases. Carbon monoxide gave the best detection limits for ^{80}Se and ^{82}Se and good detection limits for ^{77}Se.

The hexapole collision cell has also been used for selenium determination. With N_2O (reaction gas) and He (collision gas) in the cell, selenium reacted to form selenium oxide.[318] Despite this, lower detection limits were still obtained for ^{80}Se than for ^{80}Se^{16}O because of a concurrent reduction in the argon dimer. However, owing to problems with irreproducible collision cell conditions when using N_2O/He, H_2 was finally used in the ICP-CC-MS detection of inorganic selenium [Se(IV) and Se(VI)]. A porous graphite carbon stationary phase and a formic acid mobile phase were used in this separation. Marchante-Gayón *et al.*[319] reported on the use of H_2 (reaction gas) and He (collision gas) in a hexapole collision cell for the detection of Se species with ICP-CC-MS. Different nebulisers and chromatographic techniques were compared for the analysis of nutritional supplements, Chinese tea,[319] and urine.[320] Additional spectroscopic interferences on ^{80}Se were attributed to organic ions ($C_6H_8^+$, $C_5H_4O^+$) produced from methanol present in both eluents and ^{79}Br^{1}H from trace amounts of Br in the eluent.

Using an octopole CC containing H_2, Huerta *et al.*[321] analysed Se species in cod muscle using both size exclusion chromatography and reversed phase HPLC. Multiple isotopes were measured to enable quantification by post-column isotope dilution. However, the most abundant isotope, ^{80}Se, was not measured because of possible interference from ^{79}Br^{1}H.

Two papers have been published on the speciation of sulfur using ICP-DRC/CC-MS as a detector.[322,323] ICP-MS with an octopole collision cell was used for the detection of a CE separation of metallothionein-like proteins.[322] The collision gas (Xe) and cell conditions were selected to reduce oxygen interference ($^{16}O_2^+$) on the main sulfur isotope ^{32}S. A completely different approach was taken by Hann *et al.*,[323] who introduced O_2 as the reaction gas in the collision cell, and measured the reaction product ^{32}S^{16}O. As obtaining metal-to-sulfur ratios in proteins was the aim of the study, the selected DRC conditions had to allow multi-element determination. Fe and Mn did not react significantly with the oxygen, and the ^{40}Ar^{16}O interference on ^{56}Fe was even reduced at low O_2 gas flow. However, the presence of more than 0.6 mL/min oxygen led to the competitive formation of more ArO.

In recent work, Holliday *et al.*[324] introduced speciation of iron using ICP-CC-MS. A hexapole collision cell containing He (collision gas) and H_2 (reaction gas) was used for the detection of free iron, Fe(II) and Fe(III), after cation-exchange separation, as well as for the mixed-mode (anion/cation) ion exchange separation of iron complexes.

For chromium speciation with ICP-DRC-MS analysis, ammonia was selected as the reaction gas. Airborne Cr(VI) was separated from Cr(III) using a silica gel; determination of ultratrace quantities of Cr(VI) was possible using preconcentration via complexation and ICP-DRC-MS.[325] For aqueous samples, ion pair reversed phase HPLC was applied.[326]

In cases where the sample is the source of chlorine-based ions, the major spectroscopic interferences on arsenic and vanadium can be removed as part of the separation step in the analysis. However, in some cases, this separation is not possible or desirable. In the case of speciation analysis of vanadium in serum, Chéry *et al.*[327] wanted to maintain near-physiological conditions during the size exclusion separation. As a result, 0.15 M NaCl was present in the eluent itself; a DRC with ammonia as the reaction gas was used to reduce the resulting spectroscopic interferences. The authors did consider a variety of other reaction gases (methane, carbon monoxide, oxygen and a mixture of hydrogen in argon), but they calculated and then experimentally confirmed that charge transfer with ammonia was the only energetically favourable reaction. Ammonia was also used as the DRC reaction gas for the detection of vanadium species in aqueous solution.[328] In this case, however, the use of the DRC did not appear to be as essential, as ClO^+ (as a product of Cl elution) eluted at a different retention time than the vanadium species of interest. However, improved detection limits were seen for vanadium when ammonia was present in the DRC.

In the separation of aqueous arsenic species by multimode (gel/cation) ion exchange, chloride co-elutes with As(V) and MMA.[329] Thus, a hexapole collision cell was employed for the reduction of the ArCl interferences, and quantification of five arsenic species using external calibration was possible. Helium (collision gas) and hydrogen (reaction gas) were used in the collision cell. Polya *et al.*[330] also used helium and hydrogen in a hexapole collision cell for the detection of the chromatographic separation of As(III) and As(V). However, this paper focused on different approaches for preserving As species, and thus did not contain much information about the separation or collision cell conditions. Table 7.3 gives a summary of the parameters used for speciation with ICP-CC-MS and ICP-DRC-MS.

7.7 Speciation using high resolution and MC-ICP-MS

High-resolution sector-field ICP-MS (SF-ICP-MS), be it double or single focusing, offers superior detection limits, and more precise quantitative and isotope ratio results when measurements are performed in low-resolution mode due to the flat-top spectral peaks. Use of higher mass resolution (up to 10 000) results in sharper spectral peaks and resolves polyatomic interferences from the target element signals. The result is improved detection capability for certain elements compared to quadrupole ICP-MS. Prominent examples of elements where measurements with SF-ICP-MS are beneficial are Fe, V, Cr, As and Se.[331]

7.7.1 SF-ICP-MS coupling

Matrix interference in speciation analysis is generally reduced because of the sample preparation step and the chromatographic separation employed. Nevertheless, there are cases in

which the elements to be determined are prone to argon-, reagent-, or sample-based spectral interferences, like Fe, As or Se.[296] Many of these interferences are easily overcome by using SF-ICP-MS.[331] In the early days, the use of these instruments as detectors in on-line coupled speciation was limited. Scanning speed was rather slow, and so speciation with on-line coupled chromatography was restricted to very few, or only one, isotope. Another drawback was the lack of suitable transient-signal handling software. This has changed in recent years, and SF-ICP-MS now offers the instrumental means to be hyphenated to both liquid and gaseous separation techniques.

(a) Liquid chromatography (HPLC and CE) coupled to SF-ICP-MS

Rottmann and Heumann were the first to publish high-resolution ICP-MS as detector for LC in 1994.[79] This work highlighted the potential of size exclusion chromatography using an SF-ICP-MS (Element, Thermo Electron Corp., Bremen, Germany) for on-line speciation of Fe complexes in humic substances. Iron can now readily be measured using collision or reaction cell technology,[332] but SF-ICP-MS still offers the advantage of real spectral resolution from the interfering $^{40}Ar^{16}O^+$ on $^{56}Fe^+$ at medium resolution power (R=3000).

The uptake and fate of platinum-group elements (PGE) by plants has been investigated.[333] Size exclusion chromatography was used for the separation of the species, and selected elements co-eluting with Pt (C, S, Ca, Pb) were measured. Medium mass resolution was applied for the detection of S and Ca, using a double-focusing ICP-MS (Element prototype, Thermo Electron Corp., Bremen, Germany) in order to overcome spectral interferences on $^{32}S^+$ ($^{16}O_2^+$) and $^{44}Ca^+$ ($^{12}C\ ^{16}O_2^+$). In another study investigating bioavailability, metabolism and kinetics of water-soluble PGE, size exclusion chromatography was coupled to the Element2 instrument.[334]

Feldmann *et al*. described the improvement for speciation of organic selenium compounds by coupling HPLC to SF-ICP-MS using hydraulic high-pressure nebulisation as the sample introduction system.[335] Selenocysteine, selenocystamine, selenomethionine and selenoethionine were separated by reversed phase chromatography. Medium mass resolution ($R = 1400$) resolved methanol-induced spectral interferences on ^{82}Se, and additionally improved the method detection limits by a factor of 4. This method was then applied to the speciation of Se compounds in herring gull eggs within the German Environmental Specimen Bank programme.[336,337]

Köllensperger *et al*. undertook arsenic speciation of six arsenic species [As(III), As(V), MMA, DMA, AB and AC] using ion chromatography or CE coupled with SF-ICP-MS in soil pore water and soil water extracts.[87] Low mass resolution (R= 300) was applied, and the major advance of the technique was the improvement of detection limits by factor of 1000 compared to quadrupole ICP-MS.

Arsenic speciation in water, sediments and plants of the Moira watershed (Ontario, Canada)[338] and in freshwater fish from an arsenic-rich lake[339] was performed using HPLC coupled to the Element2. Anion-exchange chromatography was employed for As(III), DMA, MMA and As(V) separation, while cationic arsenic compounds were separated on a cation-exchange column with pyridine as the mobile phase. The speciation of water samples revealed the presence of As(III) and As(V). Organoarsenic compounds (MMA, DMA, TMAO and tetramethylarsonium ion) were detected in emergent and submergent freshwater plants, as well as in all fish samples investigated.

Mercury speciation with CE coupled to quadrupole ICP-MS and SF-ICP-MS was performed by Silva da Rocha *et al*.[340] for the separation and determination of mercury species (as Hg-cysteine complexes) and detection limits were significantly improved when using SF-ICP-MS.

(b) GC coupled with SF-ICP-MS

Capillary GC has been coupled to SF-ICP-MS for the simultaneous speciation of organometallic compounds in a synthetic sample. Transient signals of Sn, Hg and Pb were monitored together with Xe as the internal standard. In this first approach of multielement determination on transient signals, the magnetic field was scanned either between ^{120}Sn and ^{126}Xe, or between ^{202}Hg and ^{208}Pb.[341]

Yang *et al.*[342] described the development of a sensitive method for the accurate and precise quantitative determination of TBT and DBT in sediments by species-specific isotope dilution ICP-MS. Using GC for sample introduction and analyte separation, detection with quadrupole ICP-MS and sector-field ICP-MS were compared. A more than two-fold improvement in precision of calculated ^{120}Sn/^{117}Sn ratios was obtained for both TBT and DBT in standards using GC-ICP-SF-MS as compared to GC coupled with quadrupole ICP-MS. Superior limits of detection were obtained for SF-ICP-MS coupling because of the improved signal-to-background ratio.

7.7.2 Trace metal speciation and MC-ICP-MS

MC-ICP-MS is a relatively recent technique for measuring isotope compositions with high precision and accuracy, achieved by the combination of the ICP ion source with a magnetic sector mass spectrometer employing multiple detectors (originally developed with thermal ionisation mass spectrometer instruments).[343]

The multicollector device enables real simultaneous detection of isotopes, thus eliminating classical sources of uncertainty in quadrupole-based ICP-MS isotope ratio measurements due to their sequential scanning mode of operation, and plasma flicker noise. For measurement of transient signals, the problem of so-called spectral skew, as described earlier for quadrupole ICP-MS instruments, is eliminated.

The high ionisation efficiency of the plasma source allows the measurement of a wide range of elements, including those that are not accessible to thermal ionisation sources. A good example is mercury, with its high first ionisation potential of 10.4 eV. Here, MC-ICP-MS opens a new field for environmental applications.[344,345]

A main obstacle in accurate isotope ratio determination using MC-ICP-MS is correction for instrumental mass bias, which becomes particularly important because of the excellent precision achieved on isotope ratios achieved with this technique. The mass bias observed is usually in the percent range (per amu), and can drift over time. This may be due to spectroscopic interference effects, or matrix-derived differences in the mass bias produced during the measurement of a sample compared to the measurement of the isotopic standard used for mass bias correction.[346]

So far, only a handful of papers have been published using MC-ICP-MS as detector for coupling techniques in speciation analysis in order to benefit from the superior isotope ratio precision. Several factors have to be taken into account when using MC-ICP-MS instrumentation:

(1) the isotope ratio calculation method used;
(2) the mass bias correction method applied;
(3) the effect of possibly co-eluting matrix compounds;

(4) the fact that chromatography can induce fractionation due to different retention of the same species incorporating different isotopes;
(5) the fact that the instrumental mass bias itself may be prone to drift during the elution of a peak, as a result of the analyte arriving in the plasma and ion extraction region.

Another issue of concern is the sample preparation. As soon as matrix separation, digestion, extraction, derivatisation or even simple sample dilution are necessary, the original isotope ratio in the sample might be affected. Contamination is one well-known problem, as well as non-quantitative reactions; e.g., reactions during matrix separation that provoke changes in the isotope ratio of interest.

As in any hyphenated technique, an important parameter is the duration of measurement for one point in the eluted chromatographic peak. In some cases, the MC-ICP-MS software may be the limiting factor, when the dwell time applicable has a certain minimum value. In any case, with MC-ICP-MS, the longest possible dwell time, which still results in a sufficient number of points per peak, is usually chosen.

The few papers published to date in an attempt to obtain precise and accurate isotope ratios on element species describe GC or HPLC coupled to MC-ICP-MS. Krupp *et al*. were the first to couple GC to an Axiom[347] and an Isoprobe[348] MC-ICP-MS, respectively. In both approaches, it was shown that highly precise isotope ratio determination (0.02–0.07% RSD for high abundant isotopes) is possible using a transient signal of 3.5 s peak base width obtained by the repeated injection of $PbEt_4$. No sign of chromatographic fractionation of isotopically different $PbEt_4$ was detectable, but careful observation of the single isotope ratio point evolution during peak elution, as illustrated in Figure 7.16, revealed a slight drift (E. M. Krupp, unpublished data). Mass bias was corrected for, by using the $^{203}Tl/^{205}Tl$ isotope ratio simultaneously monitored during the GC run.

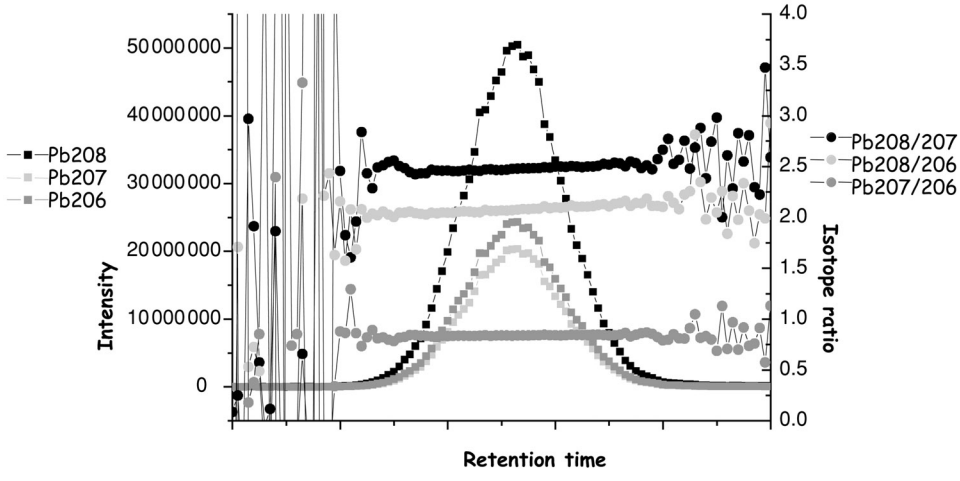

Figure 7.16 Lead isotope signals and lead isotope ratio evolution during peak elution for $PbEt_4$ measured by GC-MC-ICP-MS.

GC coupled to the Isoprobe MC-ICP-MS (GV Instruments, Wythenshawe, UK), with a hexapole collision cell, was also employed for the determination of sulfur isotope ratios in a volatile sulfur species, SF_6.[302] The SF_6 used was a pure isotopic gas standard (PIGS 2010,

IRMM, Geel, Belgium), certified for its sulfur isotope composition. The chromatographic peaks revealed considerable tailing, and a special data evaluation method was developed in order to obtain precise results, by defining a 'uniform isotope ratio zone' inside the chromatographic peak. Precision of 0.03–0.05% RSD was determined on $^{32}S/^{34}S$, depending on the concentration injected. Single point isotope ratios drifted during peak elution, but no evidence was found for chromatographic fractionation.

In an attempt to determine possible mercury isotope fractionation in fish tissue, methylmercury (MeHg) and inorganic mercury (as $HgEt_2$) were measured by GC coupled to an Axiom MC-ICP-MS. A precision of better than 0.01% RSD was obtained for the $^{202}Hg/^{198}Hg$ ratio when about 50 pg (as Hg) was injected. Interestingly, for two samples highly concentrated in inorganic mercury and MeHg, the $^{202}Hg/^{198}Hg$ ratio was found to be different for MeHg and inorganic mercury, indicating an enrichment of the heavier isotope in MeHg.[347]

Wehmeier *et al*.[349] measured antimony isotope ratios in trimethylantimony ($SbMe_3$) produced by anaerobic digestion of sewage sludge in a laboratory fermenter by cryotrapping-cryofocusing capillary GC coupled to the Isoprobe MC-ICP-MS. Integration of the peak centre resulted in an isotope ratio precision of 0.02% RSD. Bracketing with gaseous $SbMe_3$ was chosen for mass bias correction. The chromatograms show that the isotopically heavier $^{123}SbMe_3$ eluted first from the column. $SbMe_3$ produced during anaerobic fermentation in laboratory sewage sludge digesters showed a significant enrichment of ^{123}Sb with a $\delta^{123}Sb$ of 19.6 and 10.4%, respectively, for two different fermentation experiments, contradictory to the hypothesis that lighter isotopes should be preferred and enriched during biologically mediated methylation reactions.

HPLC has been coupled to the Neptune MC-ICP-MS, and a significant drift of the point-to-point isotope ratios during peak elution for the measurement of the uranium isotope ratio $^{235}U/^{238}U$ was detected. To evaluate the reason for this drift, injections of the same sample via HPLC and via a flow injection system were compared. For both kinds of sample introduction, the drift in isotope ratio development during peak elution showed the same order of magnitude; thus, chromatographic fractionation on the HPLC column was excluded as the major source. It was stated that the observed isotope ratio drift is supposedly due to an instrumental shift in mass bias over the peak width.[350]

Clough *et al*.[163] reported a greatly improved uncertainty budget (as low as 0.7% RSD) in species-specific isotope dilution for the determination of methylmercury in the DORM-2 reference material when coupling HPLC to MC-ICP-MS, compared to 4.1% when using quadrupole ICP-MS. Data evaluation was performed on the basis of a steady-state approach, averaging data points for isotope pairs during the peak maximum. The instrumental mass bias was corrected for, by using the $^{203}Tl/^{205}Tl$ signal ratio obtained from thallium mixed with the mobile phase of the HPLC.

As interesting as these few experiments conducted for chromatography with MC-ICP-MS detection are, the results are not conclusive. Most experiments reveal a drift of the analyte isotope ratio during peak elution, and no common rule can be applied to explain this effect. So far, it has not been determined if this drift is of instrumental origin, as a result of the fact that multicollector detection systems are by default not conceived for fast transient signal acquisition. Also, it is not yet clear what effect this drift may have on the accuracy of isotope ratios obtained on transient signals.

Solving this problem will be an important step forward as speciation moves into new fields of application where highly precise isotope ratios are required, be it for single-shot laser ablation, CE, GC or nano-HPLC methods. Future research will be focused on these techniques.

References

1. Templeton, D. M., Ariese, F., Cornelis, R., Dabiellson, L.-G., Muntau, H., van Leeuwen, H. P., and Lobinski, R. (2000) Guidelines for terms related to chemical speciation and fractionation of elements. Definitions, structural aspects, and methodological approaches: IUPAC recommendations 2000. *Pure Appl. Chem.*, **72**, 1453–70.
2. Soderbergh, S. (Director) (2000) *Erin Brokovich* [Motion Picture] with Julia Roberts and Albert Finney, Universal/MCA.
3. Wood, J. M. (1974) Biological cycles for toxic elements in the environment. *Science*, **183**, 1049–52.
4. Larocque, A. C. L. and Rasmussen, P. E. (1998) An overview of trace metals in the environment, from mobilization to remediation. *Environ. Geol.*, **33**, 85–90.
5. Stein, E. D., Cohen, Y., and Winer, A. M. (1996) Environmental distribution and transformation of mercury compounds. *Crit. Rev. Environ. Sci. Technol.*, **26**, 1–43.
6. US EPA Brochure (2004) What you need to know about mercury in fish and shellfish. EPA-823 F-04009.
7. AFSSA recommendation (March 16, 2004) SalsIne no. 2003-S-A-0380.
8. Zoorob, G. K., McKiernan, J. W. and Caruso, J. A. (1998) ICP-MS for elemental speciation. *Microchim. Acta*, **128**, 145–68.
9. Lobinski, R. and Adams, F. C. (1997) Speciation analysis by gas chromatography with plasma source spectrometric detection. *Spectrochim. Acta B*, **52**, 1865–903.
10. Hintelmann, H., Harris, R., Heyes, A., Hurley, J. P., Kelly, C. A., Krabbenhoft, D. P., Lindberg, S., Rudd, J. W. M., Scott, K. J., and St. Louis, V. L. (2002) Reactivity and mobility of new and old mercury deposition in a boreal forest ecosystem during the first year of the METAALICUS study. *Environ. Sci. Technol.*, **36**, 5034–40.
11. Monperrus, M., Krupp, E., Amouroux, D., Donard, O. F. X., and Rodríguez Martín-Doimeadios, R. C. (2004) Potential and limits of speciated isotope-dilution analysis for metrology and assessing environmental reactivity. *Trends Anal. Chem.*, **23**, 261–72.
12. Rodríguez-Gonzáles, P., Ruiz-Encinar, J., García-Alonso, J. I., and Sanz-Medel, A. (2004) Development of a triple spike methodology for validation of butyltin compounds speciation analysis by isotope dilution mass spectrometry, Part I: Synthesis of the spike, characterisation and development of the mathematical equations. *J. Anal. At. Spectrom.*, **19**, 685–91.
13. Kingston, H. M., Dengwei Huo, S., Yusheng Lu, S., and Chalk, S. (1998) Accuracy in species analysis: speciated isotope dilution mass spectrometry (SIDMS) exemplified by the evaluation of chromium species. *Spectrochim. Acta B*, **53**, 299–309.
14. Cornelis, R., Crews, H., Donard, O., Ebdon, L., Pitts, L., and Quevauviller, Ph. (2001) Summary paper on the EC network on trace element speciation for analysts, industry and regulators – what we have and what we need. *J. Environ. Monit.*, **3**, 97–101.
15. Barceló, D. (ed.) (2003) *Comprehensive Analytical Chemistry*, Vol. XLI, Elsevier, Amsterdam.
16. Szpunar, J., Bouyssiere, B., and Lobinski, R. (2000) Sample preparation techniques for elemental speciation studies. In: *Comprehensive Analytical Chemistry*, Vol. XXXIII (ed. D. Barceló), Elsevier, Amsterdam, pp. 7–40.
17. Nerín, C. and Pons, B. (1994) Speciation of organolead compounds in air by GC-MS-SIM. *Appl. Organomet. Chem.*, **8**, 607–14.
18. Wang, Y., Turnbull, A. B., and Harrison, R. M. (1997) Concentrations, phase partitioning and deposition of specific alkyl-lead compounds in the atmosphere. *Appl. Organomet. Chem.*, **11**, 889–901.

19. Jenkins, R., Craig, P. J., Gössler, W., Miller, D., Ostah, N., and Irgolic, K. J. (1998) Biomethylation of inorganic antimony compounds by an aerobic fungus: *Scopulariopsis brevicaulis*. *Environ. Sci. Technol.*, **32**, 882–5.
20. Hirner, A. V., Feldmann, J., Krupp, E. M., Grümping, R., Goguel, R., and Cullen, W. R. (1998) Metal(loid) compounds in geothermal gases and waters. *Org. Geochem.*, **29**, 1765–78.
21. Haas, K. and Feldmann, J. (2000) Sampling of trace volatile metal(ioid) compounds in ambient air using polymer bags: a convenient method. *Anal. Chem.*, **72**, 4205–11.
22. Haas, K., Feldmann, J., Wennrich, R., and Stärk, K. J. (2001) Species-specific isotope-ratio measurements of volatile tin and antimony compounds using capillary GC-ICP-time-of-flight-MS. *Fresenius' J. Anal. Chem.*, **370**, 587–96.
23. Feldmann, J., Grümping, R., and Hirner, A. V. (1994) Determination of volatile metal and metalloid compounds in gases from domestic waste deposits with GC/ICP-MS. *Fresenius' J. Anal. Chem.*, **350**, 228–34.
24. Hirner, A. V., Krupp, E., Schulz, F., Koziol, M., and Hofmeister, W. (1998) Organometal(loid) species in geochemical exploration: preliminary qualitative results. *J. Geochem. Explor.*, **64**, 133–9.
25. Feldmann, J. (1995) *Erfassung fluechtiger metal-und metalloidverbindungen in der umwelt mittels GC/ICP-MS*, Ph.D. Thesis, Essen University, Cuvillier, Goettingen, Germany.
26. Pécheyran, C., Quetel, C., Martin Lecuyer, F. M., and Donard, O. F. X. (1998) Simultaneous determination of volatile metal (Pb, Hg, Sn, In, Ga) and nonmetal species (Se, P, As) in different atmospheres by cryofocusing and detection by ICPMS. *Anal. Chem.*, **70**, 2639–45.
27. Pavageau, M. P., Pécheyran, C., Desauziers, V., Krupp, E., Pinaly, H., and Donard, O. F. X. (2002) Echantillonneur cryogenique prix pour l'analyse des COV. *Info Chim. Mag.*, **434**, 92–5.
28. Namiesnik J. and Wardencki K. (1999) Water vapour removal from gaseous samples used for analytical purposes: a review. *Int. J. Environ. Anal. Chem.*, **73**, 269–80.
29. Feldmann, J., Naels, L., and Haas, K. (2001) Cryotrapping of CO_2-rich atmospheres for the analysis of volatile metal compounds using capillary GC-ICP-MS. *J. Anal. At. Spectrom.*, **16**, 1040–3.
30. Pavageau, M. P., Krupp, E., de Diego, A., Pécheyran, C., and Donard, O. F. X. (2003) Cryogenic trapping for speciation analysis. In: *Comprehensive Analytical Chemistry*, Vol. XLI (ed. D. Barceló), Elsevier, Amsterdam, pp. 495–531.
31. Quevauviller, Ph. and Donard, O. F. X. (1991) Organotin stability during storage of marine waters and sediments. *Fresenius' J. Anal. Chem.*, **339**, 6–14.
32. Gómez-Ariza, J. L., Giráldez, I., Morales, E., Ariese, F., Cofino, W., and Quevauviller, Ph. (1999) Stability and storage problems in organotin speciation in environmental samples. *J. Environ. Monit.*, **1**, 197–202.
33. Valkirs, A. O., Seligman, P. F., Olson, G. J., Brinckman, F. E., Matthias, C. L., and Bellama, J. M. (1987) Di- and tributyltin species in marine and estuarine waters. Inter-laboratory comparison of two ultratrace analytical methods employing hydride generation and atomic absorption of flame photometric detection. *Analyst*, **112**, 17–21.
34. Carter, R. J., Turocy, N. J., and Bond, A. M. (1989) Container adsorption of tributyltin (TBT) compounds: implications for environmental analysis. *Environ. Sci. Technol.*, **23**, 615–7.
35. Meinema, H. A., Burger-Wiersma, T., Versluis-deHann, G., and Gevers, E. C. (1978) Determination of trace amounts of butyltin compounds in aqueous systems by gas chromatography/mass spectrometry. *Environ. Sci. Technol.*, **12**, 288–93.
36. Maguire, R. J., Carey, J. H., and Hale, E. J., Degradation of the tri-*n*-butyltin species in water. *J. Agric. Food Chem.*, **31**, 1060–5.
37. Quevauviller, Ph., Bruchet, A., and Donard, O. F. X. (1991) Leaching of organotin compounds from poly(vinyl chloride) (PVC) material. *Appl. Organomet. Chem.*, **5**, 125–9.

38. Forsyth, D. S. and Jay, B. (1997) Organotin leachates in drinking water from chlorinated puly(vinyl chloride) (CPVC) pipe. *Appl. Organomet. Chem.*, **11**, 551–8.
39. Donard, O. F. X., Lespes, G., Amouroux, D., and Morabito, R. (2001) Organotin compounds in the environment: still a critical issue. In: *Trace Element Speciation for Environment, Food and Health* (eds L. Ebdon, L. Pitts, R. Cornelis, H. Crews, O. F. X. Donard, and Ph. Quevauviller), The Royal Society of Chemistry, Cambridge, pp. 142–75.
40. Morabito, R. Speciation of organotin compounds in environmental matrices. *Microchem. J.*, **51**, 198–206.
41. Morabito, R. (2000) *Proceedings of Metal Speciation in the Enviroment* (eds N. S. Thomaidis and T. D. Lekkas), Global Nest Publishers, Athens, pp. 49–64.
42. Quevauviller, Ph., de la Calle Guntiñas, M. B., Maier, E. A., and Cámara, C. (1995) A survey on stability of chemical species in solution during storage: the BCR experience. *Mikrochim. Acta*, **118**, 131–41.
43. Gómez-Ariza, J. L., Morales, E., Sánchez-Rodas, D., and Giráldez, I. (2000) Stability of chemical species in environmental matrices. *Trends Anal. Chem.*, **19**, 200–9.
44. Van Cleuvenbergen, R., Dirckx, W., Quevauviller, Ph., and Adams, F. C. (1992) Preliminary study on degradation of ionic alkyllead species in water. *Int. J. Environ. Anal. Chem.*, **47**, 21–32.
45. Gadner, M. and Gunn, A. (1997) Stability of mercury in seawater samples. *Anal. Commun.*, **35**, 245–6.
46. Hintelmann, H. (2003) Sample preparation for mercury speciation. In: *Comprehensive Analytical Chemistry*, Vol. XLI (ed. D. Barceló), Elsevier, Amsterdam, pp. 1063–80.
47. Leermakers, M., Lansen, P., and Baeyens, W. (1990) Storage and stability of inorganic and methylmercury solutions. *Fresenius' J. Anal. Chem.*, **336**, 655–62.
48. Gössler, W. and Kühnelt, D. (2003) Sample preparation for arsenic speciation. In: *Comprehensive Analytical Chemistry*, Vol. XLI (ed. D. Barceló), Elsevier, Amsterdam, pp. 1027–41 (and references herein).
49. Palacios, M. A., Gómez, M., Cámara, C., and López, M. A. (1997) Stability studies of arsenate, monomethylarsonate, dimethylarsinate, arsenobetaine and arsenocholine in deionised water, urine and clean-up dry residue from urine samples and determination by liquid chromatography with microwave-assisted oxidation-hydride generation atomic absorption spectrometric detection. *Anal. Chim. Acta*, **340**, 209–20.
50. Lindemann, T., Prange, A., Dannecker, W., and Neidhart, B. (2000) Stability studies of arsenic, selenium, antimony and tellurium species in water, urine, fish and soil extracts using HPLC/ICP-MS. *Fresenius' J. Anal. Chem.*, **368**, 214–20.
51. Ponce de León, C., Vonderheide, A. P., and Caruso, J. A. (2003) Sample preparation for speciation of selenium. In: *Comprehensive Analytical Chemistry*, Vol. XLI (ed. D. Barceló), Elsevier, Amsterdam, pp. 1045–61.
52. Kotas, J. and Stasicka, Z. (2000) Chromium occurrence in the environment and methods of its speciation. *Environ. Pollut.*, **107**, 263–83.
53. Quevauviller, Ph. (1998) *Method Performance Studies for Speciation Analysis*, The Royal Society of Chemistry, Cambridge.
54. Gómez-Ariza, J. L., Morales, E., Beltrán, R., Giráldez, I., and Ruiz-Benítez, M. (1994) Sampling and storage of sediment samples for organotin speciation. *Quim. Anal.*, **13**, S76–9.
55. Lamberty, A., Quevauviller, Ph., and Morabito, R. (1998) The recertification of the contents (mass fractions) of tributyltin and dibutyltin in coastal sediment CRM 462. EU Report EUR 18406 EN.
56. Craig, P. J. and Bartlett P. D. (1978) The role of hydrogen sulfide in environmental transport of mercury. *Nature*, **275**, 635–7.

57. Baldi, F., Parati, F., and Filipelli, M. (1993) Methylmercury resistance in *Desulfovibrio desulfuricans* strains in relation to methylmercury degradation. *Appl. Environ. Microbiol.*, **59**, 2479–85.
58. Quevauviller, Ph., Fortunati, G. U., Fillipelli, M., Baldi, F., Bianchi, M., and Muntau, H. (1996) Interlaboratory study to improve the quality control of methylmercury determination in sediment. *Appl. Organomet. Chem.*, **10**, 537–44.
59. Ashley, K., Howe, A. M., Demange, M., and Nygren, O. (2003) Sampling and analysis considerations for the determination of hexavalent chromium in workplace air. *J. Environ. Monit.*, **5**, 707–16.
60. Morabito, R. (2003) Sampling and sample treatment in the analysis of organotin compounds. In: *Comprehensive Analytical Chemistry*, Vol. XLI (ed. D. Barceló), Elsevier, Amsterdam, pp. 991–1026.
61. Olesik, J. W., Kinzer, J. A., and Olesik, S. V. (1995) Capillary electrophoresis inductively coupled plasma spectrometry for rapid elemental speciation. *Anal. Chem.*, **67**, 1–12.
62. Kannamkumarath, S. S., Wrobel, K., Wrobel, K., B'Hymer, C., and Caruso, J. A. (2002) Capillary electrophoresis-inductively coupled plasma-mass spectrometry: an attractive complementary technique for elemental speciation analysis. *J. Chromatogr. A*, **975**, 245–66.
63. Jandik, P. and Bonn, G. (1993) *Fundamentals of Capillary Electrophoresis*, VCH, Weinheim.
64. Camilleri, P. (1998) *Capillary Electrophoresis*, CRC Press, Boca Raton, FL.
65. Khaledi, M. G. (1998) *High-Performance Capillary Electrophoresis: Theory*, *Techniques, and Applications*, John Wiley & Sons, New York.
66. Weinberger, R. (2000) *Practical Capillary Electrophoresis*, Academic Press, New York.
67. Lu, G. H., Bird, S. M., and Barnes, R. M. (1995) Interface for capillary electrophoresis and inductively coupled plasma mass spectrometry. *Anal. Chem.*, **67**, 2949–56.
68. Michalke, B. and Schramel, P. (1996) Hyphenation of capillary electrophoresis to inductively coupled plasma mass spectrometry as an element-specific detection method for metal speciation. *J. Chromatogr.*, **750**, 51–62.
69. Majidi, V. and Millerihli, N. J. (1998) Two simple interface designs for capillary electrophoresis inductively coupled plasma mass spectrometry. *Analyst*, **123**, 803–8.
70. Van Holderbeke, M., Zhao, Y. N., Vanhaecke, F., Moens, L., Dams, R., and Sandra, P. (1999) Speciation of six arsenic compounds using capillary electrophoresis inductively coupled plasma mass spectrometry. *J. Anal. At. Spectrom.*, **14**, 229–34.
71. Taylor, K. A., Sharp, B. L., Lewis, D. J., and Crews, H. M. (1998) Design and characterisation of a microconcentric nebuliser interface for capillary electrophoresis-inductively coupled plasma mass spectrometry. *J. Anal. At. Spectrom.*, **13**(10), 1095–100.
72. Kirlew, P. W., Castillano, M. T. M., and Caruso, J. A. (1998) An evaluation of ultrasonic nebulizers as interfaces for capillary electrophoresis of inorganic anions and cations with inductively coupled plasma mass spectrometric detection. *Spectrochim. Acta B*, **53**, 221–37.
73. Kinzer, J. A., Olesik, J. W., and Olesik, S. V. (1996) Effect of laminar flow in capillary electrophoresis – model and experimental result on controlling analysis time and resolution with inductively coupled plasma mass spectrometry detection. *Anal. Chem.*, **68**, 3250–7.
74. Liu, Y., Lopezavila, V., Zhu, J. J., Wiederin, D. R., and Beckert, W. F. (1995) Capillary electrophoresis coupled on-line with inductively coupled plasma mass spectrometry for elemental speciation. *Anal. Chem.*, **67**, 2020–5.
75. Schaumlöffel, D. and Prange, A. (1999) A new interface for combining capillary electrophoresis with inductively coupled plasma-mass spectrometry. *Fresenius' J. Anal. Chem.*, **364**, 452–6.
76. Schaumlöffel, D. and Prange, A. (1998) German Patent No. 198 41 288.6, GKSS Forschungszentrum GmbH.

77. Nurmi, J., Köllensperger, G., and Stingeder, G. (2002) Interfacing capillary electrophoresis to inductively coupled plasma mass spectrometry. *ICP Inf. Newsl.*, **4**, 242–5.
78. Bendahl, L., Gammelgaard, B., Jons, O., Farver, O., and Hansen, S. H. (2001) Interfacing capillary electrophoresis with inductively coupled plasma mass spectrometry by direct injection nebulization for selenium speciation. *J. Anal. At. Spectrom.*, **16**, 38–42.
79. Rottmann, L. and Heumann, K. G. (1994) Determination of heavy metal interactions with dissolved organic materials in natural aquatic systems by coupling a high performance liquid chromatography system with an inductively coupled plasma mass spectrometer. *Anal. Chem.*, **66**, 3709–15.
80. Rottmann, L. and Heumann, K. G. (1994) Development of an on-line isotope dilution technique with HPLC-ICP-MS for the accurate determination of elemental species. *Fresenius' J. Anal. Chem.*, **350**, 221–7.
81. Heumann, K. G., Gallus, S. M., Radlinger, G., and Vogl, J. (1998) Accurate determination of element species by on-line coupling of chromatographic systems with ICP-MS using isotope dilution technique, *Spectrochim. Acta B*, **52**, 273–87.
82. Vogl, J. and Heumann, K. G. (1998) Development of an ICP-IDMS method for dissolved organic carbon determinations and its application to chromatographic fractions of heavy metal complexes with humic substances. *Anal. Chem.*, **70**, 2038–43.
83. Rosman, K. J. R. and Taylor, P. D. P. (1998) IUPAC, Isotopic composition of the elements. *Pure Appl. Chem.*, **70**, 217–35.
84. Nelms, S. M., Quetel, C. R., Prohaska, T., Vogl, J., and Taylor, P. D. P. (2001) Evaluation of detector dead time calculation models for ICP-MS. *J. Anal. At. Spectrom.*, **16**, 333–8.
85. Köllensperger, G., Hann, S., Nurmi, J., Prohaska, T., and Stingeder, G. (2003) Uncertainty of species unspecific quantification strategies in hyphenated ICP-MS analysis. *J. Anal. At. Spectrom.*, **18**, 1047–55.
86. Prange, A. and Schaumlöffel, D. (1999) Determination of element species at trace levels using capillary electrophoresis-inductively coupled plasma sector field mass spectrometry. *J. Anal. At. Spectrom.*, **14**, 1329–32.
87. Köllensperger, G., Nurmi, J., Hann, S., Stingeder, G., Fitz, W. J., and Wenzel, W. W. (2002) CE-ICP-SFMS and HPIC-ICP-SFMS for arsenic speciation in the rhizosphere. *J. Anal. At. Spectrom.*, **17**, 1042–7
88. Gine, M. F., Gervasio, A. P. G., Lavorante, A. F., Miranda, C. E. S., and Carrilho, E. (2002) Interfacing flow injection with capillary electrophoresis and inductively coupled plasma mass spectrometry for Cr speciation in water samples. *J. Anal. At. Spectrom.*, **17**, 736–8.
89. Song, Q. J., Greenway, G. M., and McCreedy, T. (2003) Interfacing microchip capillary electrophoresis with inductively coupled plasma mass spectrometry for chromium speciation. *J. Anal. At. Spectrom.*, **18**, 1–3.
90. Michalke, B. and Schramel, P. (1998) Application of capillary zone electrophoresis-inductively coupled plasma mass spectrometry and capillary isoelectric focusing-inductively coupled plasma mass spectrometry for selenium speciation. *J. Chromatogr. A*, **807**, 71–80.
91. Michalke, B. and Schramel, P. (1998) Selenium speciation by interfacing capillary electrophoresis with inductively coupled plasma-mass spectrometry. *Electrophoresis*, **19**, 270–5.
92. Michalke, B., Schramel, O., and Kettrup, A. (1999) Capillary electrophoresis coupled to inductively coupled plasma mass spectrometry (CE/ICP-MS) and to electrospray ionization mass spectrometry (CE/ESI-MS): an approach for maximum species information in speciation of selenium. *Fresenius' J. Anal. Chem.*, **363**, 456–9.
93. Institute of Medicine (2000) *Dietary Reference Intakes for Vitamin C, Vitamin E, Selenium and Carotenoids*, National Academy Press, Washington, DC.
94. Rayman, M. P. (2002) The argument for increasing selenium intake. *Proc. Nutr. Soc.*, **61**, 203–15.

95. Casiot, C., Donard, O. F. X., and Potin-Gautier, M. (2002) Optimization of the hyphenation between capillary zone electrophoresis and inductively coupled plasma mass spectrometry for the measurement of As-, Sb-, Se- and Te-species, applicable to soil extracts. *Spectrochim. Acta B*, **57**, 173–87.
96. Hansen, S. H., Bendahl, L., Gammelgaard, B., Jons, O., and Farver, O. (2002) Hyphenation of CE to ICP-MS and to sheathless electrospray-MS for high sensitivity and selectivity in bioanalysis. *Chromatographia*, **55**, 15–9.
97. Mounicou, S., McSheehy, S., Szpunar, J., Potin-Gautier, M., and Lobinski, R. (2002) Analysis of selenized yeast for selenium speciation by size-exclusion chromatography and capillary zone electrophoresis with inductively coupled plasma mass spectrometric detection (SEC-CZE-ICP-MS), *J. Anal. At. Spectrom.*, **17**, 15–20.
98. Day, J. A., Kannamkumarath, S. S., Yanes, E. G., Montes-Bayón, M., and Caruso, J. A. (2002) Chiral speciation of Marfey's derivatized DL-selenomethionine using capillary electrophoresis with UV and ICP-MS detection. *J. Anal. At. Spectrom.*, **17**, 27–31.
99. Sanz-Medel, A. and Blanco-González, E. (2001) Chiral speciation of trace elements: approaches to the speciation of selenoamino acid enantiomers in biological samples. *J. Anal. At. Spectrom.*, **16**, 957–63.
100. Prange, A. and Schaumlöffel, D. (2002) Hyphenated techniques for the characterization and quantification of metallothionein isoforms. *Anal. Bioanal. Chem.*, **373**, 441–53.
101. Mounicou, S., Polec, K., Chassaigne, H., Potin-Gautier, M., and Lobinski, R. (2000) Characterization of metal complexes with metallothioneins by capillary zone electrophoresis (CZE) with ICP-MS and electrospray (ES)-MS detection. *J. Anal. At. Spectrom.*, **15**, 635–42.
102. Prange, A., Schaumlöffel, D., Brätter, P., Richarz, A. N., and Wolf, C. (2001) Species analysis of metallothionein isoforms in human brain cytosols by use of capillary electrophoresis hyphenated to inductively coupled plasma-sector field mass spectrometry. *Fresenius' J. Anal. Chem.*, **371**, 764–74.
103. Polec, K., Szpunar, J., Palacios, O., González-Duarte, P., Atrian, S., and Lobinski, R. (2001) Investigation of metal binding by recombinant and native metallothioneins by capillary zone electrophoresis (CZE) coupled with inductively coupled plasma mass spectrometry (ICP-MS) via a self-aspirating total consumption micronebulizer. *J. Anal. At. Spectrom.*, **16**, 567–74.
104. Schaumlöffel, D., Prange, A., Marx, G., Heumann, K. G., and Brätter, P. (2002) Characterization and quantification of metallothionein isoforms by capillary electrophoresis-inductively coupled plasma-isotope-dilution mass spectrometry. *Anal. Bioanal. Chem.*, **372**, 155–63.
105. Wang, Z. X. and Prange, A. (2002) Use of surface-modified capillaries in the separation and characterization of metallothionein isoforms by capillary electrophoresis inductively coupled plasma mass spectrometry. *Anal Chem.*, **74**, 626–31.
106. Caruso, J. A. and Montes-Bayón, M. (2003) Elemental speciation studies – new directions for trace metal analysis. *Ecotoxicol. Environ. Saf.*, **56**, 148–63.
107. Sutton, K. L., Sutton, R. M. C., and Caruso, J. A. (1997) Inductively coupled plasma mass spectrometric detection for chromatography and capillary electrophoresis. *J. Chromatogr. A*, **789**, 85–126.
108. Blanco González, E. and Sanz-Medel, A. (2000) Liquid chromatography techniques for trace element speciation analysis. In: *Comprehensive Analytical Chemistry* (eds J. A. Caruso, K. L. Sutton, and K. L. Ackley), Elsevier, Amsterdam, pp. 81–115.
109. Michalke, B. (2002) The coupling of LC to ICP-MS in element speciation, I: General aspects. *Trends Anal. Chem.*, **21**, 142–53.
110. Sutton, K. L. and Caruso, J. A. (1999) Liquid chromatography-inductively coupled plasma mass spectrometry. *J.Chromatogr. A*, **856**, 243–58.

111. Montes-Bayón, M., DeNicola, K., and Caruso J. A. (2003) Liquid chromatography-inductively coupled plasma mass spectrometry. *J. Chromatogr. A*, **1000**, 457–76.
112. Szpunar, J. (2000) Trace element speciation analysis of biomaterials by high-performance liquid chromatography with inductively coupled plasma mass spectrometric detection. *Trends Anal. Chem.*, **19**, 127–37.
113. Casiot, C. (1999) *Développement de techniques analytiques couplées (HPLC-ICP-MS et EC-ICP-MS) pour la spéciation de métalloïdes (arsenic, sélénium, antimoine et tellure)*, Thèse de l'Université de Pau et des Pays de l'Adour.
114. Vanhaecke, F. and Köllensperger, G. (2003) Detection by ICP-mass spectrometry. In: *Handbook of Elemental Speciation: Techniques and Methodology* (eds R. Cornelis, H. Crews, J. Caruso, and K. Heumann), John Wiley & Sons, Chichester, pp. 281–312.
115. Larsen, E. H. (1998) Method optimization and quality assurance in speciation analysis using high performance liquid chromatography with detection by inductively coupled plasma mass spectrometry. *Spectrochim. Acta B*, **53**, 253–65.
116. Guérin, T., Astruc, A., and Astruc, M. (1999) Speciation of arsenic and selenium compounds by HPLC hyphenated to specific detectors: a review of the main separation techniques. *Talanta*, **50**, 1–24.
117. Cairns, W. R. L., Ebdon, L., and Hill, S. J. (1996) A high performance liquid chromatography-inductively coupled plasma-mass spectrometry interface employing desolvation for speciation studies of platinum in chemotherapy drugs. *Fresenius' J. Anal. Chem.*, **355**, 202–8.
118. Boorn, A. W. and Browner, R. F. (1982) Effects of organic solvents in inductively coupled plasma atomic emission spectrometry, *Anal. Chem.*, **54**, 1402–10.
119. Garraud, H., Woller, A., Fodor, P., and Donard, O. F. X. (1997) Trace elemental speciation by HPLC using microbore columns hyphenated to atomic spectrometry: a review. *Analusis*, **25**, 25–31.
120. Lindsay, S. (1992) *High Performance Liquid Chromatography*, John Wiley & Sons, Chichester.
121. Ishii, D. (ed.) (1998) *Introduction to Microscale High-Performance Liquid Chromatography*, VCH Publishers, New York.
122. Zoorob, G., Tomlinson, M., Wang, J., and Caruso, J. (1995) Evaluation of the direct injection nebulizer in the coupling of high-performance liquid chromatography to inductively coupled plasma mass spectrometry. *J. Anal. At. Spectrom.*, **10**, 853–8.
123. Shum, S. C. K. and Houk, R. S. (1993) Elemental speciation by anion exchange and size exclusion chromatography with detection by inductively coupled plasma mass spectrometry with direct injection nebulization. *Anal. Chem.*, **65**, 2972–6.
124. Powell, M. J., Boomer, D. W., and Wiederin, D. R. (1995) Determination of chromium species in environmental samples using high-pressure liquid chromatography direct injection nebulization and inductively coupled plasma mass spectrometry. *Anal. Chem.*, **67**, 2474–8.
125. Pergantis, S. A., Heithmar, E. M., and Hinners, E. M. (1995) Microscale flow injection and microbore high-performance liquid chromatography coupled with inductively coupled plasma mass spectrometry via a high-efficiency nebulizer. *Anal. Chem.*, **67**, 4530–5.
126. Shum, S. C. K., Pang, H.-M., and Houk, R. S. (1992) Speciation of mercury and lead compounds by microbore column liquid chromatography-inductively coupled plasma mass spectrometry with direct injection nebulization. *Anal. Chem.*, **64**, 2444–50.
127. Marchante-Gayón, J. M., Thomas, C., Feldmann, I., and Jakubowski, N. (2000) Comparison of different nebulizers and chromatographic techniques for the speciation of selenium in nutritional commercial supplements by hexapole collision and reaction cell. *J. Anal. At. Spectrom.*, **15**, 1093–102.

128. Ackley, K. L., Sutton, K. L., and Caruso, J. A. (2000) A comparison of nebulizers for microbore LC-ICP-MS with mobile phases containing methanol. *J. Anal. At. Spectrom.*, **15**, 1069–73.
129. Sun, Y. C., Lee, Y. S., Shiah, T. L., Lee, P. L., Tseng, W. C., and Yang, M. H, (2003) Comparative study on conventional and low-flow nebulizers for arsenic speciation by means of microbore liquid chromatography with inductively coupled plasma mass spectrometry. *J. Chromatogr. A*, **1005**, 207–13.
130. Todoli, J. L. and Mermet, J.-M. (2002) New torch design with an in-built chamber for liquid sample analysis by ICP-AES. *J. Anal. At. Spectrom.*, **17**, 345–51.
131. Chao, W.-S. and Jiang, S.-J. (1998) Determination of organotin compounds by liquid chromatography-inductively coupled plasma mass spectrometry with a direct injection nebulizer. *J. Anal. At. Spectrom.*, **13**, 1337–41.
132. Acon, B. W., McLean, J. A., and Montaser, A. (2001) A direct injection high efficiency nebulizer interface for microbore high-performance liquid chromatography-inductively coupled plasma mass spectrometry. *J. Anal. At. Spectrom.*, **16**, 852–7.
133. Lobinski, R., Pereiro, I. R., Chassaigne, H., Wasik, A., and Szpunar, J., (1998) Elemental speciation and coupled techniques – towards faster and reliable analyses. *J. Anal. At. Spectrom.*, **13**, 859–67.
134. Szpunar, J., Lobinski, R., and Prange, A. (2003) Hyphenated techniques for elemental speciation in biological systems. *Appl. Spectrosc.*, **57**, 102A–112A.
135. Bloxham, M. J., Gachanja, A., Hill, S. J., and Worsfold, P. J. (1996) Determination of mercury species in seawater by liquid chromatography with inductively coupled plasma mass spectrometric detection. *J. Anal. At. Spectrom.*, **11**, 145–8.
136. Huang, C. W. and Jiang, S. J. (1993) Speciation of mercury by reversed-phase liquid chromatography with inductively coupled plasma mass spectrometric detection. *J. Anal. At. Spectrom.*, **8**, 681–6.
137. Falter, R. and Ilgen, G. (1997) Coupling of the RP C18 preconcentration HPLC-UV-PCO-system with atomic fluorescence detection for the determination of methylmercury in sediment and biological tissue. *Fresenius' J. Anal. Chem.*, **358**, 407–10.
138. Aizpún, B., Fernández, M. L., Blanco, E., and Sanz-Medel, A. (1994) Speciation of inorganic mercury(II) and methylmercury by vesicle-mediated high-performance liquid chromatography coupled to cold vapour atomic absorption spectrometry. *J. Anal. At. Spectrom.*, **9**, 1279–84.
139. Falter, R. and Schöler, H. F. (1995) Determination of mercury species in natural waters at picogram level with online RP C18 preconcentration and HPLC-UV-PCO-CVAAS. *Fresenius' J. Anal. Chem.*, **353**, 34–38.
140. Eiden, R., Falter, R., Agustín-Castro, B., and Schöler, H. F. (1997) Distillation, on-line RP C18 preconcentration and HPLC-UV-PCO-CVAAS as a new combination for the determination of methylmercury in sediments and fish tissue. *Fresenius' J. Anal. Chem.*, **357**, 439–41.
141. Falter, R. and Ilgen, G. (1997) Determination of trace amounts of methylmercury in sediment and biological tissue by using water vapor distillation in combination with RP C18 preconcentration and HPLC-HPF/HHPN-ICP-MS. *Fresenius' J. Anal. Chem.*, **358**, 401–6.
142. Wan, C. C., Chen, C. S., and Jiang, S. J. (1997) Determination of mercury compounds in water samples by liquid chromatography-inductively coupled plasma mass spectrometry with an in situ nebulizer/vapor generator. *J. Anal. At. Chem.*, **12**, 683–7.
143. Darrie, G. (2001) The importance of chromium in occupational health. In: *Trace Element Speciation for Environment, Food and Health* (eds L. Ebdon, L. Pitts, R. Cornelis, H. Crews, O. F. X. Donard, and Ph. Quevauviller), The Royal Society of Chemistry, Cambridge, pp. 315–28.

144. Marqués, M. J., Salvador, A., Morales-Rubio, A., and de la Guardia, M. (2002) Chromium speciation in liquid matrices: a survey of the literature. *Fresenius' J. Anal. Chem.*, **367**, 601–13
145. Lintschinger, J., Kalcher, K., Gössler, W., and Novic, M. (1995) Simultaneous determination of chromium(III) and chromium(VI) by reversed-phase ion-pair HPLC with chromium-specific detection. *Fresenius' J. Anal. Chem.*, **351**, 604–9.
146. Posta, J., Alimonti, A., Petrucci, F., and Caroli, S. (1996) On-line separation and preconcentration of chromium species in seawater. *Anal. Chim. Acta*, **325**, 185–93.
147. Andrle, C. M., Jakubowski, N., and Broekaert, J. A. C. (1997) Speciation of chromium using reversed phase-high performance liquid chromatography coupled to different spectrometric detection methods. *Spectrochim. Acta B*, **52**, 189–200.
148. Chang, Y.-L. and Jiang, S.-J. (2001) Determination of chromium species in water samples by liquid chromatography-inductively coupled plasma-dynamic reaction cell-mass spectrometry. *J. Anal. At. Spectrom.*, **16**, 858–62.
149. Byrdy, F. A., Olson, L. K., Vela, N. P., and Caruso, J. A. (1995) Chromium speciation by anion-exchange high-performance liquid chromatography by both inductively coupled plasma atomic emission spectroscopic and inductively coupled plasma mass spectrometric detection. *J. Chromatogr. A*, **712**, 311–20.
150. Saverwyns, S., Van Hecke, K., Vanhaecke, F., Moens, L., and Dams, R. (1999) Evaluation of a commercially available microbore anion exchange column for chromium speciation with detection by ICP-mass spectrometry and hyphenation with microconcentric nebulization. *Fresenius' J. Anal. Chem.*, **363**, 490–4.
151. Vanhaecke, F., Saverwyns, S., de Wannemacker, G., Moens, L., and Dams, R. (2000) Comparison of the application of higher mass resolution and cool plasma conditions to avoid spectral interferences in Cr(III)/Cr(VI) speciation by means of high-performance liquid chromatography: inductively coupled plasma mass spectrometry. *Anal. Chim. Acta*, **419**, 55–64.
152. Barnowski, C., Jakubowski, N., Stuewer, D., and Broekaert, J. A. C. (1997) Speciation of chromium by direct coupling of ion exchange chromatography with inductively coupled plasma mass spectrometry. *J. Anal. At. Spectrom.*, **12**, 1155–61.
153. Pantsar-Kallio, M. and Manninen, P. K. G. (1996) Speciation of chromium in aquatic samples by coupled column ion chromatography-inductively coupled plasma-mass spectrometry. *Anal. Chim. Acta*, **318**, 335–43.
154. Pantsar-Kallio, M. and Manninen, P. K. G. (1996) Speciation of chromium in wastewaters by coupled column ion chromatography-inductively coupled plasma mass spectrometry. *J. Chromatogr. A*, **750**, 89–95.
155. Pantsar-Kallio, M. and Manninen, P. K. G. (1996) Speciation of chromium by coupled column HPLC-ICP-MS – the effects of interfering ions. *Fresenius' J. Anal. Chem.*, **355**, 716–8.
156. Séby, F., Charles, S., Gagean, M., Garraud, H., and Donard, O. F. X. (2003) Chromium speciation by hyphenation of high performance liquid chromatography to inductively coupled plasma-mass spectrometry – study of the influence of interfering ions. *J. Anal. At. Chem.*, **18**, 1386–90.
157. Rodríguez-cea, A., Fernández de la Campa, M.R., Blanco-González, E., Andón Fernández, B., and Sanz-Medel, A. (2003) Metal speciation analysis in eel (*Anguilla anguilla*) metallothioneins by anionic exchange-FPLC-isotope dilution-ICP-MS. *J. Anal. At. Spectrom.*, **18**, 1357–64.
158. Sariego Muñiz, C., Marchante-Gayón, J. M., García Alonso, J. I., and Sanz-Medel, A. (2001) Speciation of essential elements in human serum using anion-exchange chromatography coupled to post-column isotope dilution analysis with double focusing ICP-MS. *J. Anal. At. Spectrom.*, **16**, 587–92.

159. Radlinger, G. and Heumann, K. G. (1997) Determination of halogen species of humic substances using HPLC/ICP-MS coupling. *Fresenius' J. Anal. Chem.*, **359**, 430–3.
160. Hinojosa Reyes, L., Marchante-Gayón, J. M., García Alonso, J. I., and Sanz-Medel, A. (2003) Quantitative speciation of selenium in human serum by affinity chromatography coupled to post-column isotope dilution analysis ICP-MS. *J. Anal. At. Spectrom.*, **18**, 1210–6.
161. Yang, L., Mester, Z., and Sturgeon, R. E. (2002) Species-specific isotope dilution-based calibration for trace element speciation and its combined uncertainty evaluation: determination of tributyltin in sediment by HPLC-ICP-MS. *Anal. Chem.*, **74**, 2968–76.
162. Wahlen, R. and Wolff-Briche, C. (2003) Comparison of GC-ICP-MS and HPLC-ICP-MS for species-specific isotope dilution analysis of tributyltin in sediment after accelerated solvent extraction. *Anal. Bioanal. Chem.*, **377**, 140–8.
163. Clough, R., Belt, S. T., Evans, E. H., Fairman, B., and Catterick, T. (2003) Uncertainty contributions to species specific isotope dilution analysis, Part 2: Determination of methylmercury by HPLC coupled with quadrupole and multicollector ICP-MS. *J. Anal. At. Spectrom.*, **18**, 1039–46.
164. Ebdon, L., Hill, S. J., and Rivas, C. (1998) Lead speciation in rainwater by isotope dilution-high performance liquid chromatography-inductively coupled plasma-mass spectrometry. *Spectrochim. Acta B*, **53**, 289–97.
165. Hill, S. J., Pitts, L. J., and Fisher, A. S. (2000) High-performance liquid chromatography-isotope dilution inductively coupled plasma mass spectrometry for speciation studies: an overview. *Trends Anal. Chem.*, **19**, 120–6.
166. Kavanagh, P. E., Balder, D., and Franklin, G. (1999) Estimation of retention times of homologous series in temperature programmed gas chromatography. *Chromatographia*, **49**, 509–12.
167. Grob, R. L. (1995) Theory of gas chromatography. In: *Modern Practice of Gas Chromatography*, 3rd edn (ed. R. L. Grob), John Wiley & Sons, New York, pp. 51–122.
168. Barry, E. F. (1995) Columns: packed and capillary/column selection in gas chromatography. In: *Modern Practice of Gas Chromatography*, 3rd edn (ed. R. L. Grob), John Wiley & Sons, New York, pp. 123–224.
169. Krupp, E. (1999) *Analytik umweltrelevanter Metall(oid)spezies mittels gaschromatographischer Trennmethoden* (in German), Ph.D. Thesis, Essen University, Germany.
170. Feldmann, J. and Hirner, A. V. (1995) Occurrence of volatile metal and metalloid species in landfill and sewage gases. *Int. J. Environ. Anal. Chem.*, **60**, 339–59.
171. Pavageau, M. P., Pécheyran, C., Krupp, E. M., Morin, A., and Donard, O. F. X. (2002) Volatile metal species in coal combustion flue gas. *Environ. Sci. Technol.*, **36**, 1561–73.
172. Pavageau, M. P., Morin, A., Séby, F., Guimon, C., Krupp, E., Pécheyran, C., Poulleau, J., and Donard, O.F.X. (2004) Partitioning of metal species during an enriched fuel combustion experiment. Speciation in the gaseous and particulate phases. *Environ. Sci. Technol.*, **38**, 2252–63.
173. Amouroux, D., Tessier, E., Pécheyran, C., and Donard, O. F. X. (1998) Sampling and probing volatile metal (loid) species in natural waters by in-situ purge and cryogenic trapping followed by gas chromatography and inductively coupled plasma mass spectrometry (P-CT-GC-ICP/MS). *Anal. Chim. Acta*, **377**, 241–54.
174. Tseng, C. M., Amouroux, D., Brindle, I. D., and Donard, O. F. X. (2000) Field cryofocussing hydride generation applied to the simultaneous multi-elemental determination of alkyl-metal(loid) species in natural waters using ICP-MS detection. *J. Environ. Mon.*, **2**, 603–12.
175. Segovia García, E., García Alonso, J. I., and Sanz-Medel, A. (1997) Determination of butyltin compounds in sediments by means of hydride generation/cold trapping gas chromatography coupled to inductively coupled plasma mass spectrometry. *J. Mass Spectrom.*, **32**, 542–9.

176. Montes Bayón, M., Gutiérrez Camblor, M., García Alonso, J. I., and Sanz-Medel, A. (1999) An alternative GC-ICP-MS interface design for trace element speciation. *J. Anal. At. Spectrom.*, **14**, 1317–22.
177. Leal-Granadillo, I. A., García Alonso, J. I., and Sanz-Medel, A. (2000) Determination of the speciation of organolead compounds in airborne particulate matter by gas chromatography-inductively coupled plasma mass spectrometry. *Anal. Chim. Acta*, **432**, 21–9.
178. Wasik, A., Rodríguez-Pereiro, I., Dietz, C., Szpunar, J., and Lobinski, R. (1998) Speciation of mercury by ICP-MS after on-line capillary cryofocussing and ambient temperature multicapillary gas chromatography. *Anal. Commun.*, **35**, 331–5.
179. Slaets, S., Adams, F., Pereiro, I. R., and Lobinski, R. (1999) Optimization of the coupling of multicapillary GC with ICP-MS for mercury speciation analysis in biological materials. *J. Anal. At. Spectrom.*, **14**, 851–7.
180. Feldmann, J. (1997) Summary of a calibration method for the determination of volatile metal(loid) compounds in environmental gas samples by using gas chromatography-inductively coupled plasma mass spectrometry. *J. Anal. At. Spectrom.*, **12**, 1069–76.
181. Krupp, E. (2000) Speciation of volatile metal(loid) compounds by cryotrap-capillary-GC/ICP-MS. Poster presentation at *Winter Conference on Plasma Spectrochemistry 2000*, Ft. Lauderdale, FL.
182. Kresimon, J., Grüter, U. M., and Hirner, A.V. (2001) HG/LT-GC/ICP-MS coupling for identification of metal(loid) species in human urine after fish consumption. *Fresenius' J. Anal. Chem.*, **371**, 586–90.
183. Grüter, U. M, Kresimon, J., and Hirner, A. V. (2000) A new HG/LT-GC/ICP-MS multi-element speciation technique for real samples in different matrices. *Fresenius' J. Anal. Chem.*, **368**, 67–72.
184. Peters, G. R. and Beauchemin, D. (1992) Versatile interface for gas chromatographic detection or solution nebulization analysis by inductively coupled plasma mass spectrometry: preliminary results. *J. Anal. At. Spectrom.*, **7**, 965–9.
185. Peters, G. R. and Beauchemin, D. (1993) Characterization of an interface allowing either nebulization or gas chromatography as the sample introduction system in ICP-MS. *Anal. Chem.*, **65**, 97–103.
186. Glindemann, D., Ilgen, G., Herrmann, R., and Gollan, T. (2002) Advanced GC/ICP-MS design for high-boiling analyte speciation and large volume solvent injection. *JAAS*, **17**, 1386–1389.
187. DeSmaele, T., Verrept, P., Moens, L., and Dams, R. (1995) A flexible interface for the coupling of capillary gas chromatography with inductively coupled plasma mass spectrometry. *Spectrochim. Acta B*, **50**, 1409–16.
188. Prange, A. and Jantzen, E. (1995) Determination of organometallic species by gas chromatography inductively coupled plasma mass spectrometry. *JAAS* **10**, 105–9.
189. Pritzl, G., Stuer-Lauridsen, F., Carlsen, L., Jensen, A. K., and Thorsen, T. K. (1996) A versatile capillary gas chromatography inductively coupled plasma mass spectrometer interface. *Int. J. Environ. Anal. Chem.*, **62**, 147–59.
190. Kim, A., Hill, S. J., Ebdon, L., and Rowland, S. (1992) Determination of organometallic compounds by capillary gas chromatography-inductively coupled plasma mass spectrometry. *J. High Res. Chromatogr.*, **15**, 665–8.
191. Ebdon, L., Evans, E. H., Pretorius, W. G., and Rowland, S. J. (1994) Analysis of geoporphyrins by high-temperature gas chromatography inductively coupled plasma mass spectrometry and high-performance liquid chromatography inductively coupled plasma mass spectrometry. *J. Anal. At. Spectrom.*, **9**, 939–43.
192. Armstrong, H. E. L., Corns, W. T., Stockwell, P. B., O'Connor, G., Ebdon, L., and Evans, E. H. (1999) Comparison of AFS and ICP-MS detection coupled with gas chromatography for the determination of methylmercury in marine samples. *Anal. Chim. Acta*, **390**, 245–53.

193. Pretorius, W. G., Ebdon, L., and Rowland, S. J. (1993) Development of a high-temperature gas chromatography-inductively coupled plasma mass spectrometry interface for the determination of metalloporphyrins. *J. Chromatogr.*, **646**, 369–75.
194. Poehlmann, J., Pack, B. W., and Hieftje, G. M. (1999) A heated transfer line for coupling GC with plasma source spectrometry. *Int. Lab.*, July, 26–9.
195. Krupp, E. M., Yamanaka, M., Pécheyran, C., and Donard, O. F. X. (2000) Analysis of high boiling organtin compounds using GC/ICP-MS – a comparative study between different interfaces. Poster presentation at *Winter Conference on Plasma Spectrochemistry 2000*, Ft. Lauderdale, FL.
196. Rodríguez Martín-Doimeadios, R. C., Krupp, E., Amouroux, D., and Donard, O. F. X. (2002) Application of isotopically labeled methylmercury for isotope dilution analysis of biological samples using gas chromatography/ICPMS. *Anal. Chem.*, **74**, 2505–12.
197. Monperrus, M., Rodríguez Martín-Doimeadios, R. C., Scancar, J., Amouroux, D., and Donard, O. F. X. (2003) Simultaneous sample preparation and species-specific isotope dilution mass spectrometry analysis of monomethylmercury and tributyltin in a certified oyster tissue. *Anal. Chem.*, **75**, 4095–102.
198. Monperrus, M., Zuloaga, O., Krupp, E., Amouroux, D., Wahlen, R., Fairman, B., and Donard, O. F. X. (2003) Rapid, accurate and precise determination of tributyltin in sediments and biological samples by species specific isotope dilution-microwave extraction-gas chromatography-ICP mass spectrometry. *J. Anal. At. Spectrom.*, **18**, 247–53.
199. Rodríguez, I., Mounicou, S., Lobinski, R., Sidelnikov, V., Patrushev, Y., and Yamanaka, M. (1999) Species-selective analysis by microcolumn multicapillary gas chromatography with inductively coupled plasma mass spectrometric detection. *Anal. Chem.*, **71**, 4534–43.
200. Yamanaka, M. and Donard, O. F. X. (2003) Agilent Application Note 5980–0336E.
201. Krupp, E. M., Pécheyran, C., Brenner, I. B., Shaw, P., Nash, M., and Donard, O. F. X. (2003) Speciation analysis using a new commercial interface for the coupling of GC with ICP-MS. Oral presentation at *Post Symposium CSI XXXIII*, Almuñecar, Spain.
202. Nash, M. and Krupp, E. M. (2004) Determination of organotin species in sediment extracts using GC coupled with X Series ICP-MS. Thermo Electron Application Note 40698.
203. Ruiz Encinar, J., Leal Granadillo, I., García Alonso, J. I., and Sanz-Medel, A. (2001) Isotope ratio measurements using gas chromatography inductively coupled mass spectrometry for the assessment of organolead sources. *J. Anal. At. Spectrom.*, **16**, 475–80.
204. Feldmann, J., Koch, I., and Cullen, W. R. (1998) Complementary use of capillary gas chromatography-mass spectrometry (ion trap) and gas chromatography-inductively coupled plasma mass spectrometry for the speciation of volatile antimony, tin and bismuth compounds in landfill and fermentation gases. *Analyst*, **123**, 815–20.
205. Pécheyran, C., Lalere, B., and Donard, O. F. X. (2000) Volatile metal and metalloid species (Pb, Hg, Se) in a European urban atmosphere (Bordeaux, France). *Environ. Sci. Technol.*, **34**, 27–32.
206. Feldmann, J. (1999) Determination of $Ni(CO)_4$, $Fe(CO)_5$, $Mo(CO)_6$ and $W(CO)_6$ in sewage gas by using cryotrapping gas chromatography inductively coupled plasma mass spectrometry. *J. Environ. Monit.*, **1**, 33–7.
207. Fledmann, J. and Cullen, W. R. (1997) Occurrence of volatile transition metal compounds in landfill gas: synthesis of molybdenum and tungsten carbonyls in the environment. *Environ. Sci. Technol.*, **31**, 2125–9.
208. Feldmann, J., Riechmann, T., and Hirner, A.V. (1996) Determination of organometallics in intra-oral air by LT-GC/ICP-MS. *Fresenius' J. Anal. Chem.*, **354**, 620–3.
209. Feldmann, J. (2003) Sample preparation for the analysis of volatile metals species. In: *Comprehensive Analytical Chemistry*, Vol. XLI (ed. D. Barceló), Elsevier, Amsterdam, pp. 1211–32.

210. Mester, Z. J., Sturgeon, R., and Pawliszyn, J. (2001) Solid phase microextraction as tool for trace element speciation. *Spectrochim. Acta B*, **56**, 233–60.
211. Smith, L. M., Maher, W. A., Craig, P. J., and Jenkins, O.R. (2002) Speciation of volatile antimony compounds in culture headspace gases of *Cryptococcus humicolus* using solid phase microextraction and gas chromatography-mass spectrometry. *Appl. Organomet. Chem.*, **16**, 287–93.
212. Howard, A. G. (1997) (Boro)hydride techniques in trace element speciation. *JAAS*, **12**, 267–72.
213. Dedina, J. and Tsalev, D. L. (1995) *Hydride-Generation Atomic-Absorption Spectrometry*, John Wiley & Sons, New York.
214. Filipelli, M., Baldi, F., Brinckman, F. E., and Olson, G. J. (1992) Methylmercury determination as volatile methylmercury hydride by purge and trap gas chromatography in line with Fourier transform infrared spectroscopy. *Environ. Sci. Technol.*, **26**, 1457–60.
215. Jin, K., Shibata, Y., and Morita, M. (1991) Determination of germanium species by hydride generation-inductively coupled argon plasma mass spectrometry. *Anal. Chem.*, **63**, 986–9.
216. Rapsomanikis, S., Donard, O. F. X., and Weber, J. H. (1986) Speciation of inorganic tin and alkyltin compounds by atomic absorption spectrometry using electrothermal quartz furnace after hydride generation. *Anal. Chem.*, **58**, 772–7.
217. Ceulemans, M. and Adams, F. C. (1996) Integrated sample preparation and speciation analysis for the simultaneous determination of methylated species of tin, lead and mercury in water by purge-and-trap injection-capillary gas chromatography-atomic emission spectrometry. *J. Anal. At. Spectrom.*, **11**, 201–6.
218. Bergmann, K., Roehr, U., and Neidhart, B. (1994) Examination of the different procedural steps in the determination of organotin compounds in water samples. *Fresenius' J. Anal. Chem.*, **349**, 815–9.
219. Heisterkamp, M., DeSmaele, T., Candelone, J. P., Moens, L, Dams, R., and Adams, F. C. (1997) Inductively coupled plasma mass spectrometry hyphenated to gas chromatography as a detection system for the speciation analysis of organolead compounds in environmental waters. *J. Anal. At. Spectrom.*, **12**, 1077–81.
220. Gómez-Ariza, J. L., Morales, E., and Ruiz-Benitez, M. (1992) Simultaneous speciation of butyltin and phenyltin compounds in the waters of south-west Spain. *Analyst*, **117**, 641–4.
221. Gómez-Ariza, J. L., Morales, E., Beltrán, R., Giráldez, I., and Ruiz-Benítez, M. (1995) Ultrasonic treatment of molluscan tissue for organotin speciation. *Analyst*, **120**, 1171–4.
222. Donard, O. F. X., Lalere, B., Martin, F., and Lobinski, R. (1995) Microwave-assisted leaching of organotin compounds from sediments for speciation analysis. *Anal. Chem.*, **67**, 4250–4.
223. Dirkx, W. M., Lobinski, R., and Adams, F. C. (1995) Speciation analysis of organotin by GC-AAS and GC-AES after extraction and derivatization. In: *Quality Assurance for Environmental Analysis* (eds Ph. Quevauviller, E. A. Maier, and B. Griepink), Elsevier, Amsterdam, pp. 357–409.
224. Waldock, M. J. (1992) Speciation of trace metals in environmental samples at the fisheries laboratory, Burnham on Crouch. *Mikrochim. Acta*, **109**, 23–6.
225. Dowling, T. M. and Uden, P. C. (1993) Alkyltin speciation in seawater on-line hydride conversion and gas chromatography-atomic emission detection. *J. Chromatogr.*, **644**, 153–60.
226. Rapsomanikis, S. (1994) Derivatization by ethylation with sodium tetraethylborate for the speciation of metals and organometallics in environmental samples. *Analyst*, **119**, 1429–39.
227. Minganti, V., Capelli, R., and DePellegrini, R. (1995) Evaluation of different derivatization methods for the multi-element detection of Hg, Pb and Sn compounds by gas

chromatography-microwave induced plasma-atomic emission spectrometry in environmental samples. *Fresenius' J. Anal. Chem.*, **351**, 471–7.

228. DeSmaele, T., Moens, L., Dams, R., Sandra, P., Van der Eycken, J., and Vandyck, J. (1998) Sodium tetra(*n*-propyl) borate: a novel aqueous in situ derivatization reagent for the simultaneous determination of organomercury, -lead and -tin compounds with capillary gas chromatography-inductively coupled plasma mass spectrometry. *J. Chromatogr. A*, **793**, 99–106.
229. Hu, G. L., Wang, X. R., Wang, Y. R., Chen, X., and Jia, L. (1997) Determination of methylmercury in waters using sodium tetraphenylborate derivatization/solvent extraction and gas chromatography-ion trap mass spectrometry. *Anal. Lett.*, **30**, 2579–94.
230. Bloom, N. (1989) Determination of picogram levels of methylmercury by aqueous phase ethylation, followed by cryogenic gas chromatography with cold vapor atomic fluorescence detection. *Can. J. Fish. Aquat. Sci.*, **46**, 1131–40.
231. Hintelmann, H. (1999) Comparison of different extraction techniques used for methylmercury analysis with respect to accidental formation of methylmercury during sample preparation. *Chemosphere*, **39**, 1093–105.
232. Cai, Y., Jaffe, R., Alli, A., and Jones, R. D. (1996) Determination of organomercury compounds in aqueous samples by capillary gas chromatography atomic fluorescence spectrometry following solid-phase extraction. *Anal. Chim. Acta*, **334**, 251–9.
233. Lee, Y. H. (1987) Determination of methyl- and ethylmercury in natural waters at subnanogram per liter using SCF-adsorbent preconcentration procedure. *Int. J. Environ. Anal. Chem.*, **29**, 263–7.
234. Morrison, M. A. and Weber, J. H. (1997) Determination of monomethylmercury cation in sediments by vacuum distillation followed by hydride derivatization and atomic fluorescence spectrometric detection. *Appl. Organomet. Chem.*, **11**, 791–9.
235. Horvat, M., Bloom, N. S., and Liang, L. (1993) Comparison of distillation with other current isolation methods for the determination of methyl mercury compounds in low level environmental samples, I: Sediments. *Anal. Chim. Acta*, **281**, 135–52.
236. Horvat, M., Liang, L., and Bloom, N. S. (1993) Comparison of distillation with other current isolation methods for the determination of methyl mercury compounds in low level environmental samples, II: Water. *Anal. Chim. Acta*, **282**, 153–68.
237. Pawliszyn, J. B. (1997) *Solid-Phase Microextraction: Theory, Practice*, Wiley-VCH, Weinheim.
238. Zhang, Z., Yang, M. J., and Pawliszyn, J. B. (1994) Solid-phase microextraction. A solvent-free alternative for sample preparation. *Anal.Chem.*, **66**, 844A–854A.
239. Gorecki, T. and Pawliszyn, J. B. (1996) Determination of tetraethyllead and inorganic lead in water by solid phase microextraction/gas chromatography. *Anal. Chem.*, **68**, 3008–14.
240. DeSmaele, T., Moens, L., Sandra, P., and Dams, R. (1999) Determination of organometallic compounds in surface water and sediment samples with SPME-CGC-ICP-MS. *Microchim. Acta*, **130**, 241–51.
241. Aguerre, S., Pécheyran, C., Lespes, G., Krupp, E., Donard, O. F. X., and Potin-Gautier, M. (2001) Optimisation of the hyphenation between solid-phase microextraction, capillary gas chromatography and inductively coupled plasma atomic emission spectrometry for the routine speciation of organotin compounds in the environment. *J. Anal. At. Spectrom.*, **16**, 1429–33.
242. Moens, L., DeSmaele, T., Dams, R., van den Brock, P., and Sandra, P. (1997) Sensitive, simultaneous determination of organomercury, -lead and -tin compounds with headspace solid phase microextraction capillary gas chromatography combined with inductively coupled plasma mass spectrometry. *Anal. Chem.*, **69**, 1604–11.

243. Vercauteren, J., Peres, C., Devos, C., Sandra, P., Vanhaecke, F., and Moens, L. (2001) Stir bar sorptive extraction for the determination of ppq-level traces of organotin compounds in environmental samples with thermal desorption-capillary gas chromatography-ICP mass spectrometry. *Anal. Chem.*, **73**, 1509–14.
244. Morabito, R. (1995) Extraction techniques in speciation analysis of environmental samples. *Fresenius' J. Anal. Chem.*, **351**, 378–85.
245. Lobinski, R., Dirkx, W. M. R., Szpunar-Lobinska, J., and Adams, F. C. (1994) Speciation analysis of organolead compounds by gas chromatography with atomic spectrometric detection. *Anal. Chim. Acta*, **286**, 381–90.
246. Pellegrino, C., Massanisso, P., and Morabito, R. (2000) Comparison of twelve selected extraction methods for the determination of butyl- and phenyltin compounds in mussel samples. *Trends Anal. Chem.*, **19**, 97–106.
247. Ceulemans, M. and Adams, F. C. (1995) Evaluation of sample preparation methods for organotin speciation analysis in sediments: focus on monobutyltin extraction. *Anal. Chim. Acta*, **317**, 161–70
248. Simon, S., Bueno, M., Lespes, G., Mench, M., and Potin-Gautier, M. (2002) Extraction procedure for organotin analysis in plant matrices: optimisation and application. *Talanta*, **57**, 31–42.
249. Gómez-Ariza, J. L., Morales, E., Giráldez, I., Sánchez-Rodas, D., and Velasco, A. (2001) Sample treatment in chromatography-based speciation of organometallic pollutants. *J. Chromatogr. A*, **938**, 211–24.
250. Szpunar, J., Bouyssiere, B., and Lobinski, R. (2000) Sample preparation techniques for elemental speciation studies. In: *Elemental Speciation: New Approaches for Trace Element Analysis* (eds J. A. Caruso, K. L. Sutton, and K. L. Ackley), Elsevier, Amsterdam, Chapt. 2, pp. 7–40.
251. Arnold, C. G., Berg, M., Mueller, S. R., Dommann, U., and Schwarzenbach, R. P. (1998) Determination of organotin compounds in water, sediments, and sewage sludge using perdeuterated internal standards, accelerated solvent extraction, and large-volume-injection GC/MS. *Anal. Chem.*, **70**, 3094–101.
252. Chiron S., Roy S., Cottier R., and Jeannot R. (2000) Speciation of butyl- and phenyltin compounds in sediments using pressurized liquid extraction and liquid chromatography-inductively coupled plasma mass spectrometry. *J. Chromatogr. A*, **879**, 137–45.
253. Ruiz-Encinar, J., Rodríguez-González, P., Rodríguez Fernández, J., García Alonso, J. I., Diez, S., Bayona, J. M., and Sanz-Medel, A. (2002) Evaluation of accelerated solvent extraction for butyltin speciation in PACS-2 CRM using double-spike isotope dilution-GC/ICPMS. *Anal. Chem.*, **74**, 5237–42.
254. Liu, Y., López-Avila, V., Alcarez, M., and Beckert, W. F. (1993) Determination of organotin compounds in environmental samples by supercritical fluid extraction and gas chromatography with atomic emission detection. *J. High Resolut. Chromatogr.*, **16**, 106–12.
255. Bayona, J. M. and Cai, Y. (1994) The role of supercritical fluid extraction and chromatography in organotin speciation studies. *Trends Anal. Chem.*, **13**, 327–32.
256. Chau, Y. K., Yang, F., and Brown, M. (1995) Supercritical fluid extraction of butyltin compounds from sediment. *Anal. Chim. Acta*, **304**, 85–9.
257. Emteborg, H., Bjorklund, E., Odman, F., Karlsson, L., Mathiasson, L., Frech, W., and Baxter, D.C. (1996) Determination of methylmercury in sediments using supercritical fluid extraction and gas chromatography coupled with microwave-induced plasma atomic emission spectrometry. *Analyst*, **121**, 19–29.
258. Szpunar, J., Schmitt, V., Donard, O. F. X., and Lobinski, R. (1996) Low-power focused microwave technology as a new tool for rapid preparation of solid samples for speciation analysis. *Trends Anal. Chem.*, **15**, 181–7.

259. Donard, O. F. X., Krupp, E., Pécheyran, C., Amouroux, D., and Ritsema, R. (2000) Trends in speciation analysis for routine and new environmental issues. In: *Comprehensive Analytical Chemistry*, Vol. XXXIII (ed. D. Barceló), Elsevier, Amsterdam, pp. 451–500.
260. Hintelmann, H., Evans, R. D., and Villeneuve, J. Y. (1995) Measurement of mercury methylation in sediments by using enriched stable mercury isotopes combined with methylmercury determination by gas chromatography-inductively coupled plasma mass spectrometry. *J. Anal. At. Spectrom.*, **10**, 619–24.
261. Wilken, R. D., Falter, R., Ilgen, G., and Evans, H. E. (1997) Mercury as a global pollutant. *Fresenius' J. Anal. Chem.*, **358**, 363–70.
262. Westoeoe, G. (1966) Determination of methylmercury compounds in foodstuffs, I: Methylmercury compounds in fish, identification and determination. *Acta Chem. Scand.*, **20**, 2131–7.
263. Sumino, K. (1968) Analysis of organic mercury compounds by gas chromatography, I: Analytical and extraction method of organic mercury compounds. *Kobe J. Med. Sci.*, **14**, 115–30.
264. Tseng, C. M., de Diego, A., Martin, F. M., and Donard, O. F. X. (1997) Rapid and quantitative microwave-assisted recovery of methylmercury from standard reference sediments. *J. Anal. At. Spectrom.*, **12**, 629–35.
265. Vázquez, M. J., Carro, A. M., Lorenzo, R. A., and Cela, R. (1997) Optimization of methylmercury microwave-assisted optimization from aquatic sediments. *Anal. Chem.*, **69**, 221–5.
266. Rodríguez Martín-Doimeadios, R. C., Monperrus, M., Krupp, E., Amouroux, D., and Donard, O. F. X. (2003) Using speciated isotope dilution with GC-inductively coupled plasma mass spectrometry to determine and unravel the artificial formation of monomethylmercury in certified reference sediments. *Anal. Chem.*, **75**, 3202–11.
267. Sources of error in methylmercury determination during sample preparation, derivatisation, detection (Special Issue) (1999) *Chemosphere* **39**, 1037–224.
268. Wilken, R. D. and Falter, R. (1998) Determination of methylmercury by species-specific isotope addition method using a newly developed HPLC-ICP MS coupling technique with ultrasonic nebulization. *Appl. Organomet. Chem.*, **12**, 551–7.
269. Fischer, R., Rapsomanikis, S., and Andreae, M. O. (1993) Determination of methylmercury in fish samples using GC/AA and sodium tetraethylborate derivatization. *Anal. Chem.*, **65**, 763–6.
270. Rapsomanikis, S. and Craig, P. J. (1991) Speciation of mercury and methylmercury compounds in aqueous samples by chromatography-atomic absorption spectrometry after ethylation with sodium tetraethylborate. *Anal. Chim. Acta*, **248**, 563–7.
271. de la Calle-Guntiñas, M. B., Scerbo, R., Chiavarini, S., Quevauviller, Ph., and Morabito, R. (1997) Comparison of derivatization methods for the determination of butyl- and phenyltin compounds in mussel by gas chromatography. *Appl. Organomet. Chem.*, **11**, 693–702.
272. Morabito, R., Massanisso, P., and Quevauviller, Ph. (2000) Derivatization methods for the determination of organotin compounds in environmental samples. *Trends Anal. Chem.*, **19**, 113–9.
273. Krupp, E. M., Grümping, R., Furchtbar, U. R. R., and Hirner, A. V. (1996) Speciation of metals and metalloids in sediments with LTGC/ICP-MS. *Fresenius' J. Anal. Chem.*, **354**, 546–9.
274. Díaz-Bone, R. A., Felix, J., Kösters, F. J., and Hirner, A. V. (2003) Simultaneous multielement organometal(loid) speciation by pH gradient hydride generation. Poster presentation at *ICEBAMO 2003*, Pau, France.
275. Pannier, F., Astruc, A., and Astruc, M. (1994) Extraction and determination of butyltin compounds in shellfish by hydride generation-gas chromatography-quartz furnace atomic absorption spectrometry. *Anal. Chim. Acta*, **287**, 17–24.

276. Grüter, U. M., Hitzke, M., Kresimon, J., and Hirner, A. V. (2001) Derivatization of organometal(loid) species by sodium borohydride: problems and solutions. *J. Chromatogr.*, **938**, 225–36.
277. Koch, I., Feldmann, J., Lintschinger, J., Serves, S. V., Cullen, W. R., and Reimer, K. J. (1998) Demethylation of trimethylantimony species in aqueous solution during analysis by hydride generation/gas chromatography with AAS and ICP MS detection. *Appl. Organomet. Chem.*, **12**, 129–36.
278. de Diego, A., Chun Mao Tseng, T., Stoichev, T., Amouroux, D., and Donard, O. F. X. (1998) Interferences during mercury speciation determination by volatilization, cryofocusing, gas chromatography and atomic absortion spectroscopy: comparative study between hydride generation and ethylation techniques. *J. Anal. At. Spectrom.*, **13**, 623–9.
279. Chun Mao Tseng, T., de Diego, A., Martin, F. M., Amouroux, D., and Donard, O. F. X. (1997) Rapid determination of inorganic mercury and methylmercury in biological reference materials by hydride generation, cryofocusing, atomic absorption spectrometry after open focused microwave-assisted alkaline digestion. *J. Anal. At. Spectrom.*, **12**, 743–50.
280. Bergmann, K. and Neidhart, B. (1996) Speciation of organolead compounds in water samples by GC-AAS after in-situ butylation with tetrabutylammonium tetrabutylborate. *Fresenius' J. Anal. Chem.*, **356**, 57–61.
281. Demuth, N. and Heumann, K. G. (2001) Validation of methylmercury determinations in aquatic systems by alkyl derivatization methods for GC analysis using ICP-IDMS. *Anal. Chem.*, **73**, 4020–7.
282. Lobinski, R. and Adams, F. C. (1992) Ultratrace speciation analysis of organolead in water by gas chromatography-atomic emission spectrometry after in-liner preconcentration. *J. Anal. At. Spectrom.*, **7**, 987–92.
283. Bulska, E., Emteborg, H., Baxter, D. C., Frech, W., Ellingsen, D., and Thomassen, Y. (1992) Speciation of mercury in human whole blood by capillary gas chromatography with microwave-induced plasma emission detector system following complexometric extraction and butylation. *Analyst*, **117**, 657–63.
284. Bouyssiere, B., Baco, F., Savory, L., and Lobinski, R. (2002) Speciation analysis for mercury in gas condensates by capillary gas chromatography with inductively coupled plasma mass spectrometric detection. *J. Chromatogr.*, **976**, 431–9.
285. Emteborg, H., Snell, J., Qian, J., and Frech, W. (1999) Sources of systematic errors in mercury speciation using grignard reagents and capillary gas chromatography coupled to atomic spectrometry. *Chemosphere*, **39**, 1137–52.
286. San-Chik, S., Seong-Il, K., Yong, K., Min-Suk, L., Moo-Sung, K., Suk-Ki, K., and In-Hoo, C. (1996) Properties of carbon-doped InGaAs grown by atmospheric pressure metalorganic chemical vapor deposition using CCl_4. *J. Cryst. Growth*, **165**, 222–6.
287. Weber, J. H. (1999) Volatile hydride and methyl compounds of selected elements formed in the marine environment. *Marine Chem.*, **65**, 67–75.
288. Tanzer, D. and Heumann, K. G. (1991) Determination of dissolved selenium species in environmental water samples using isotope dilution mass spectrometry, *Anal. Chem.*, **63**, 1984–9.
289. Gallus, S. M. and Heumann, K. G. (1996) Development of a gas chromatography inductively coupled plasma isotope dilution mass spectrometry system for accurate determination of volatile element species, Part 1: Selenium speciation. *J. Anal. At. Spectrom.*, **11**, 887–92.
290. Bancon-Montigny, C., Yang, L., Sturgeon, R. E., Colombini, V., and Mester, Z. (2004) High-yield synthesis of milligram amounts of isotopically enriched methylmercury ($CH_3^{198}HgCl$). *Appl. Organomet. Chem.*, **18**, 57–64.
291. Rodríguez Martín-Doimeadios, R. C., Stoichev, T., Krupp, E., Amouroux, D., Holeman, M., and Donard, O. F. X. (2002) Microscale preparation and characterization of isotopically enriched monomethylmercury. *Appl. Organomet. Chem.*, **16**, 610–5.

292. Clough, R., Belt, S. T., Evans, E. H., Sutton, P., Fairman, B., and Catterick, T. (2003) Uncertainty contributions to species specific isotope dilution analysis, Part 1: Characterisation and stability of ^{199}Hg and ^{13}C isotopically enriched methylmercury by ^{1}H NMR. *J. Anal. At. Spectrom.*, **18**, 1033–8.
293. Ruiz-Encinar, J., García Alonso, J. I., and Sanz-Medel, A. (2000) Synthesis and application of isotopically labelled dibutyltin for isotope dilution analysis using gas chromatography-ICP-MS. *J. Anal. At. Spectrom.*, **15**, 1233–9.
294. Sutton, P. G., Harrington, C. F., Fairman, B., Evans, E. H., Ebdon, L., and Catterick, T. (2000) The small-scale preparation and NMR characterization of isotopically enriched organotin compounds. *Appl. Organomet. Chem.*, **14**, 691–700.
295. Ruiz-Encinar, J., Monterde Villar, M. I., and Gotor Santamaría, V., García Alonso, J. I., and Sanz-Medel, A. (2001) Simultaneous determination of mono-, di-, and tributyltin in sediments by isotope dilution analysis using gas chromatography-ICP-MS. *Anal. Chem.*, **73**, 3174–80.
296. Held, A. and Taylor, P. D. P. (1999) A calculation method based on isotope ratios for the determination of deadtime and its uncertainty in ICP-MS and application of the method to investigating some features of a continuous dynode multiplier. *J. Anal. At. Spectrom.*, **14**, 1075–9.
297. Jarvis, K. E., Gray, A. L., and Houk, R. S. (1992) *Handbook of Inductively Coupled Plasma Mass Spectrometry*, Blackie, London.
298. Longerich, H. P., Fryer, B. J., and Strong, D. F. (1987) Determination of lead isotope ratios by inductively coupled plasma-mass spectrometry (ICP-MS). *Spectrochim. Acta B*, **42**, 39–48.
299. Hintelmann, H. and Shengyong, L. (2003) High precision isotope ratio measurements of mercury isotopes in cinnabar ores using multi-collector inductively coupled plasma mass spectrometry. *Analyst*, **128**, 635–9.
300. Rodríguez Martín-Doimeadios, R. C., Krupp, E., Amouroux, D., and Donard, O. F. X. (2002) Application of isotopically labeled methylmercury for isotope dilution analysis of biological samples using gas chromatography/ICPMS. *Anal. Chem.*, **74**, 2505–12.
301. Krupp, E. M., Pécheyran, C., Pinaly, H., Motelica-Heino, M., Koller, D., Young, S. M. M., Brenner, I. B., and Donard, O. F. X. (2001) Isotopic precision for a lead species ($PbEt_4$) using capillary gas chromatography coupled to inductively coupled plasma-multicollector mass spectrometry. *Spectrochim. Acta B*, **56**, 1233–40.
302. Krupp, E. M., Pécheyran, C., Meffan-Main, S., and Donard, O. F. X. (2004) Precise isotope-ratio determination by CGC hyphenated to ICP-MCMS for speciation of trace amounts of gaseous sulfur, with SF_6 as example compound. *Anal. Bioanal. Chem.*, **378**, 250–5.
303. Prichard, E., Mackay, G. M., and Points, J. (1998) *Trace Analysis: Structured Approach to Obtaining Reliable Results* (ed. E. Prichard), The Royal Society of Chemistry, Cambridge, pp. 121–42.
304. Snell, J. P., Stewart, I. I., Sturgeon, R. E., and Frech, W. (2000) Species specific isotope dilution calibration for determination of mercury species by gas chromatography coupled to inductively coupled plasma or furnace atomisation plasma ionisation-mass spectrometry. *J. Anal. At. Spectrom.*, **15**, 1540–5.
305. Rodríguez-González, P., Ruiz-Encinar, J., García Alonso, J. I., and Sanz-Medel, A. (2002) Determination of butyltin compounds in coastal seawater samples using isotope dilution GC-ICP-MS. *J. Anal. At. Spectrom.*, **17**, 824–30.
306. Yang, L., Mester, Z., and Sturgeon, R. E. (2002) Improvement in measurement precision with SPME by use of isotope dilution mass spectrometry and its application to the determination of tributyltin in sediment using SPME GC-ICP-MS. *J. Anal. At. Spectrom.*, **17**, 944–9.

307. Hintelmann, H. and Evans, R. D. (1997) Application of stable isotopes in environmental tracer studies – measurement of monomethylmercury (CH_3HG^+) by isotope dilution ICP-MS and detection of species transformation. *Fresenius' J. Anal. Chem.*, **358**, 378–85.
308. Hintelmann, H., Falter, R., Ilgen, G., and Evans, R. D. (1997) Determination of artifactual formation of monomethylmercury (CH_3Hg^+) in environmental samples using stable Hg^{2+} isotopes with ICP-MS detection: calculation of contents applying species specific isotope addition. *Fresenius' J. Anal. Chem.*, **358**, 363–70.
309. Bloom, N. S., Evans, R. D., Hintelmann, H., and Wilken, R. D. (1999) Methyl mercury revisited. *Anal. Chem.*, **71**, 575A.
310. Quevauviller, Ph. Adams, F., Caruso, J., Coquery, M., Cornelis, R., Donard, O. F. X., Ebdon, L., Horvat, M., Lobinski, R., Morabito, R., Muntau, H., and Valcárcel, M. (1999) Artefact formation of methylmercury in sediments. *Anal. Chem.*, **71**, 155A–156A.
311. Hammerschmidt, C. R. and Fitzgerald, W. F. (2001) Formation of artefact methylmercury during extraction from a sediment reference material. *Anal. Chem.*, **73**, 5930–6.
312. Lambertsson, L., Lundberg, E., Nilsson, M., and Frech, W. (2001) Application of enriched stable isotope tracers in combination with isotope dilution GC-ICP-MS to study mercury species transformation in sea sediments, during in-situ ethylation and determination. *J. Anal. At. Spectrom.*, **16**, 1296–301.
313. Ruiz-Encinar, J., Rodríguez-González, P., García Alonso, J. I., and Sanz-Medel, A. (2002) Evaluation of extraction techniques for the determination of butyltin compounds in sediments using isotope dilution-GC/ICPMS with ^{118}Sn and ^{119}Sn-enriched species. *Anal. Chem.*, **74**, 270–81.
314. Sloth, J. J. and Larsen, E. H. (2000) The application of inductively coupled plasma dynamic reaction cell mass spectrometry for measurement of selenium isotopes, isotope ratios and chromatographic detection of selenoamino acids. *J. Anal. At. Spectrom.*, **15**, 669–72.
315. Larsen, E. H., Hansen, M., Fan, T., and Vahl, M. (2001) Speciation of selenoamino acids, selenonium ions and inorganic selenium by ion exchange HPLC with mass spectrometric detection and its application to yeast and algae. *J. Anal. At. Spectrom.*, **16**, 1403–8.
316. Larsen, E. H., Sloth, J., Hansen, M., and Moesgaard, S. (2003) Selenium speciation and isotope composition in ^{77}Se-enriched yeast using gradient elution HPLC separation and ICP-dynamic reaction cell-MS. *J. Anal. At. Spectrom.*, **18**, 310–6.
317. Chéry, C. C., Günther, D., Cornelis, R., Vanhaecke, F., and Moens L. (2003) Detection of metals in proteins by means of polyacrylamide gel electrophoresis and laser ablation-inductively coupled plasma-mass spectrometry: application to selenium. *Electrophoresis*, **24**, 3305–13.
318. Mazan, S., Gilon, N., Crétier, G., Rocca, J. L., and Mermet, J. M. (2002) Inorganic selenium speciation using HPLC-ICP-hexapole collision/reaction cell-MS. *J. Anal. At. Spectrom.*, **17**, 366–70.
319. Marchante-Gayón, J. M., Thomas, C., Feldmann, I., and Jakubowski, N. (2000) Comparison of different nebulisers and chromatographic techniques for the speciation of selenium in nutritional commercial supplements by hexapole collision and reaction cell ICP-MS. *J. Anal. At. Spectrom.*, **15**, 1093–102.
320. Marchante-Gayón, J. M., Feldmann, I., Thomas, C., and Jakubowski, N. (2001) Speciation of selenium in human urine by HPLC-ICP-MS with a collision and reaction cell. *J. Anal. At. Spectrom.*, **16**, 457–63.
321. Huerta, V. D., Sánchez, M. L. F., and Sanz-Medel, A. (2004) Quantitative selenium speciation in cod muscle by isotope dilution ICP-MS with a reaction cell: comparison of different reported extraction procedures. *J. Anal. At. Spectrom.*, **19**, 644–8.
322. Pröfrock, D., Leonhard, P., and Prange, A. (2003) Determination of sulfur and selected trace elements in metallothionein-like proteins using capillary electrophoresis hyphenated to

inductively coupled plasma mass spectrometry with an octopole reaction cell. *Anal. Bioanal. Chem.*, **377**, 132–9.
323. Hann, S., Köllensperger, G., Obinger, C., Furtmüller, P. G., and Stingeder, G. (2004) SEC-ICP-DRCMS and SEC-ICP-SFMS for determination of metal–sulfur ratios in metalloproteins. *J. Anal. At. Spectrom.*, **19**, 74–9.
324. Holliday, A. E., Krupp, E., Moldovan, M., Pécheyran, C., Beauchemin, D., and Donard, O. F. X. (2004) Poster presentation at *Winter Conference on Plasma Spectrochemistry 2004*, Ft. Lauderdale, FL, January 4–10, 2004.
325. Li, Y., Pradhan, N. K., Foley, R., and Low, G. K. C. (2002) Selective determination of airborne hexavalent chromium using inductively coupled plasma mass spectrometry. *Talanta*, **57**, 1143–53.
326. Chang, Y.-L. and Jiang, S.-J. (2001) Determination of chromium species in water samples by liquid chromatography-inductively coupled plasma-dynamic reaction cell mass spectrometry. *J. Anal. At. Spectrom.*, **16**, 858–62.
327. Chéry, C. C., De Cremer, K., Cornelis, R., Vanhaecke, F., and Moens, L. (2003) Optimisation of ICP-dynamic reaction cell-MS as specific detector for the speciation analysis of vanadium at therapeutic levels in serum. *J. Anal. At. Spectrom.*, **18**, 1113–8.
328. Liu, H. and Jiang, S.-J. (2002) Determination of vanadium in water samples by reaction cell inductively coupled plasma quadrupole mass spectrometry. *J. Anal. At. Spectrom.*, **17**, 556–9.
329. Xie, Q., Kerrich, R., Irving, E., Liber, K., and Abou-Shakra, F. (2002) Determination of five arsenic species in aqueous samples by HPLC coupled with a hexapole collision cell ICP-MS. *J. Anal. At. Spectrom.*, **17**, 1037–41.
330. Polya, D. A., Lythgoe, P. R., Abou-Shakra, F., Gault, A. G., Brydie, J. R., Webster, J. G., Brown, K. L., Nimfopoulos, M. K., and Michailidis, K. M. (2003) IC-ICP-MS and IC-ICP-HEX-MS determination of arsenic speciation in surface and groundwaters: preservation and analytical issues. *Mineral. Mag.*, **67**, 247–61.
331. Jakubowski, N., Moens, L., and Vanhaecke, F. (1998) Sector field mass spectrometers in ICP-MS. *Spectrochim. Acta B*, **53**, 1739–63.
332. Bandura, D. R., Baranov, V. I., and Tanner, S. D. (2000) Effect of collisional damping and reactions in a dynamic reaction cell on the precision of isotope ratio measurements. *J. Anal. At. Spectrom.*, **15**, 921–8.
333. Klueppel, D., Jakubowski, N., Messerschmidt, J., Stuewer, D., and Klockow, D. (1998) Speciation of platinum metabolites in plants by size-exclusion chromatography and inductively coupled plasma mass spectrometry. *J. Anal. At. Spectrom.*, **13**, 255–62.
334. Lesniewska, B. A., Messerschmidt, J., Jakubowski, N., and Hulanicki, A. (2004) Bioaccumulation of platinum group elements and characterization of their species in *Lolium multiflorum* by size-exclusion chromatography coupled with ICP-MS. *Sci. Total Environ.*, **322**, 95–108.
335. Feldmann, I., Jakubowski, N., Stuewer, D., and Thomas, C. (2000) Speciation of organic selenium compounds by reversed-phase liquid chromatography and inductively coupled plasma mass spectrometry, Part II: Sector field instrument with high mass resolution. *J. Anal. At. Spectrom.*, **15**, 371–6.
336. Jakubowski, N., Stuewer, D., Klockow, D., Thomas, C., and Emons, H. (2001) Speciation of organic selenium compounds using reversed-phase liquid chromatography and inductively coupled plasma mass spectrometry, Part III: Application of a sector field instrument with low and high mass resolution for selenium speciation in herring gull eggs. *J. Anal. At. Spectrom.*, **16**, 135–9.
337. Umweltprobenbank (1999) Umweltprobenbank des Bundes. Ergebnisse aus den Jahren 1996 und 1997, UBA Texte 61/99, Berlin.

338. Zheng, J., Hintelmann, H., Dimock, B., and Dzurko, M. S. (2003) Speciation of arsenic in water, sediment, and plants of the Moira watershed, Canada, using HPLC coupled to high resolution ICP-MS. *Anal. Bioanal. Chem.*, **377**, 14–24.
339. Zheng, J. and Hintelmann, H. (2004) Hyphenation of high performance liquid chromatography with sector field inductively coupled plasma mass spectrometry for the determination of ultra-trace level anionic and cationic arsenic compounds in freshwater fish. *J. Anal. At. Spectrom.*, **19**, 191–5.
340. Silva da Rocha, M., Soldado, A. B., Blanco-González, E., and Sanz-Medel, A. (2000) Speciation of mercury using capillary electrophoresis coupled to volatile species generation-inductively coupled plasma mass spectrometry. *J. Anal. At. Spectrom.*, **15**, 513–8.
341. De Smaele, T., Moens, L., and Dams, R. (1997) Coupling of GC with ICP-MS for trace metal speciation. In: *Plasma Source Mass Spectrometry – Developments, Applications* (eds G. Holland and S. D. Tanner), The Royal Society of Chemistry, Cambridge, pp. 109–23.
342. Yang, L., Mester, Z., and Sturgeon, R. E. (2003) Comparison of sector field- and quadrupole-ICP-MS for the determination of DBT and TBT in sediment following GC separation. *J. Anal. At. Spectrom.*, **18**, 1365–70.
343. Platzer, I. T. (1997) *Modern Isotope Ratio Mass Spectrometry*, John Wiley & Sons, Chichester.
344. Walder, A. J. and Freedman, P. A. (1992) Isotopic ratio measurement using a double focusing magnetic sector mass analyser with an inductively coupled plasma as an ion source. *J. Anal. At. Spectrom.*, **7**, 571–6.
345. Lauretta, D. S., Klaue, B., Blum, J. D., and Buseck, P. R. (2001) Mercury abundances and isotopic compositions in the Murchison (CM) and Allende (CV) carbonaceous chondrites. *Geochim. Cosmochim. Acta*, **65**, 2807–18.
346. Walczyk, T. (2004) TIMS versus multicollector-ICP-MS: coexistence or struggle for survival? *Anal. Bioanal. Chem.*, **378**, 229–31.
347. Donard, O. F. X., Krupp, E., Pécheyran, C., Amouroux, D., and Fitzgerald, W. F. (2003) Fractionation of mercury at the molecular level in tuna and whale from world oceans: potential and limits of this novel approach to assess global mercury cycling. In: *Goldschmidt Conference 2003*, Abstract A81.
348. Krupp, E. M., Pécheyran, C., Meffan-Main, S., and Donard, O. F. X. (2001) Precise isotope-ratio measurements of lead species by capillary gas chromatography hyphenated to hexapole multicollector ICP-MS. *Fresenius' J. Anal. Chem.*, **370**, 573–80.
349. Wehmeier, S., Ellam, R., and Feldmann J. (2003) Isotope ratio determination of antimony from the transient signal of trimethylstibine by GC-MC-ICP-MS and GC-ICP-TOF-MS. *J. Anal. At. Spectrom.*, **18**, 1001–7.
350. Günther-Leopold, I., Wernli, B., Kopajtic, Z., and Günther, D. (2004) Measurement of isotope ratios on transient signals by MC-ICP-MS. *Anal. Bioanal. Chem.*, **378**, 241–9.

Chapter 8
Collision and Reaction Cells

Gregory K Koyanagi, Diethard K Bohme and Dmitry R Bandura

8.1 FUNDAMENTALS

Gregory K Koyanagi and Diethard K Bohme

8.1.1 Introduction

One of the numerous technical hurdles to overcome for accurate trace element analysis using plasma mass spectrometry is that of isobaric interference in the spectrum of atomic metal ions, both between elemental ions and between elemental ions and diatomic (and larger) ions generated in the plasma. The existence of an isobaric interference causes degraded detection limits and decreased quantitative accuracy. One of the several methods for the resolution or reduction of isobaric interference is the use of chemical reactions in the analyte ion beam to selectively remove the interference ion(s) or generate a new analyte ion of differing mass (so-called chemical resolution). Several other methods exist for the resolution or reduction of some of these isobaric interferences such as: cold/cool plasma techniques,[1–4] plasma modification techniques,[5,6] collision activated dissociation[7] and high-resolution mass spectrometry,[8] but none is universally applicable and all have drawbacks.

The use of collision and reaction cells for differentiation or elimination of isobaric interferences in plasma mass spectrometry has become commonplace. The ability to rapidly select and advance a chemical reaction scheme for a single-element or multi-element analysis is therefore crucial for expeditious result generation. Implicit in determining an effective chemical reaction scheme is an understanding of the physics and physical chemistry underlying ion–molecule reactions.

Selection of the neutral species for use in a reaction/collision cell mass spectrometer is a balancing act between many competing factors. First, the neutral must be amenable to introduction into the cell in a convenient, controlled and reproducible manner. Also, the neutral must have a relatively low atomic or molecular mass so as to reduce the effects of collisional scattering.[9] Lastly, the neutral must react with the interference ion with a high efficiency per collision to effect rapid and quantitative conversion (preferably to a single product).

The choice of reagent gas admitted to the reaction/collision cell is influenced by the reactivity of that gas towards both the interference ion and the analyte ion. Furthermore 'chemical resolution' of an isobaric overlap can be effected either by removal of the interference ion (by chemical reaction) or by addition of a known mass to the analyte ion to move it to a 'cleaner' area further up in the mass spectrum. Although metal ions exhibit a diverse range of ion–molecule chemistries, it

Inductively Coupled Plasma Mass Spectrometry Handbook Edited by Simon M. Nelms
 ISBN: 978-1-405-10916-1

is precisely this diversity which permits judicious selection of reagent gases capable of resolving multiple isobaric interferences.

To exploit chemical resolution it is of course necessary to have full knowledge of the chemical reactivity of the interfering ions. Despite the considerable historical body of work covering ion–molecule reactions, atomic metal ion reactivity has only recently begun to be explored. Current databases by Ikezoe *et al.*,[10] Anicich and Huntress[11] and by Anicich[12,13] contain approximately 200 and approximately 150 rate coefficients, respectively, for reactions that would be of interest to plasma mass spectrometrists utilizing chemical-resolution to alleviate spectral interferences. This is a relatively modest number and furthermore, these databases contain overlapping information. In addition, few of these recent studies are available in a compact wide-in-scope database format. With an ever-widening importance and relevance to numerous fields, gas-phase metal ion chemistry should be indexed in a comprehensive database of reaction rate coefficients. At the Ion-Molecule Chemistry Laboratory, York University, an instrument (the ICP-SIFT) has been constructed specifically to make measurements of metal ion reaction rate constants and thus vastly expand the database for plasma mass spectrometrists.[14,15]

8.1.2 Ion–molecule collision rate

Ion–molecule reactions are driven strongly by charge-dipole and charge-induced dipole interactions. Stronger attractive forces bring reacting entities closer and provide a source of energy to overcome any activation barrier that might be present. This means that ion–molecule reactions often proceed at the collision rate. Ion–molecule collision theories have been developed at several levels and can be used to predict ion–molecule collision rate coefficients.[16,17] Pure polarization theory makes the assumption that the ion can be treated as a point charge and that the molecule is a point polarizable entity. The total effective interaction potential, V_{eff} is then

$$V_{\text{eff}}(r) = (L^2/2\mu r^2) - (\alpha q^2/2r^4) \tag{8.1.1}$$

where L is the orbital angular momentum between the two particles, μ is the reduced mass of the system, q is the charge on the ion, α is the spherically averaged polarizability of the neutral molecule and r is the separation between the center of mass of the ion and molecule. The predicted collision rate coefficient, k_{C}, often referred to as the Langevin collision rate coefficient, is then[16,17]

$$k_{\text{C}} = 2\pi q(\alpha/\mu)^{1/2} = 2.34 \times 10^{-9}(\alpha/\mu)^{1/2} \tag{8.1.2}$$

where a is expressed in Å^3 and μ is in atomic mass units. When the molecule also has a permanent dipole moment the total effective interaction potential of the ion and molecule becomes[17]

$$V_{\text{eff}}(r, \phi) = (L^2/2\mu r^2) - (\alpha q^2/2r^4) - (q\mu_D \cos\phi/r^2) \tag{8.1.3}$$

where μ_D is the permanent dipole moment of the neutral and ϕ is the angle between the dipole moment vector of the neutral and the distance vector to the ion. The locked dipole assumption proposes that the dipole vector remains aligned with the distance vector during ion–molecule interactions ($\cos\phi = 1$) and then the thermally averaged collision rate, k_{LD}, is given by

$$k_{\text{LD}} = 2\pi q\mu^{-1/2}[\alpha^{1/2} + \mu_{\text{D}}(2/\pi k_{\text{B}}T)^{1/2}] \tag{8.1.4}$$

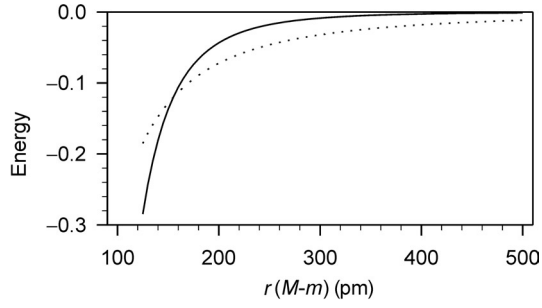

Figure 8.1 Plot of charge-induced dipole (solid line) and charge-permanent dipole (dotted line) interaction energy for a polarizability of 10^{-24} cm^3 and 1 Debye, respectively.

where T is the absolute temperature and k_B is Boltzmann's constant. However, it is generally accepted that molecular rotation is not completely quenched by the ion field and thus complete dipole 'locking' is not generally realized. So the averaged dipole orientation (ADO) description[18–20] was developed to account for the degree of dipole orientation caused by the ion field. The ADO theory uses an empirically parameterized locking constant, c, that is a function of $\mu_D \cdot \alpha^{-1/2}$. The ADO collision rate, k_{ADO}, is then

$$k_{ADO} = 2\pi q \mu^{-1/2}[\alpha^{1/2} + c\mu_D(2/\pi k_B T)^{1/2}] \tag{8.1.5}$$

The relative strengths of the charge-induced dipole and charge-permanent dipole forces are illustrated in Figure 8.1 for a singly charged ion, M, interacting with a neutral, n, of polarizability 10^{-24} cm^3 (solid line) and a neutral, n, with a permanent dipole moment of 1 Debye (dotted line). It can be clearly seen in Figure 8.1 that the charge-permanent dipole force acts over a larger ion–molecule separation distance.

Also, neutral species can possess a sizable electric quadrupole moment (similar to a dipole but involving the spatial arrangement of four charges) so ion–quadrupole interactions can be significant. Su and Bowers[21] introduced the average quadrupole orientation (AQO) formalism to describe these cases.

Currently state-of-the-art computations are achieved by the trajectory capture formalism developed by Chesnavich *et al.*[22] This is a classical trajectory calculation based on variational transition state theory. Computation of the trajectory capture rate (k_{TC}) has been simplified by creating the functional parameter x, which is dependent on the neutral dipole moment and the neutral polarizability and is computed using equation 8.1.6.

$$x = \mu_D(2\alpha k_B T)^{-1/2} \tag{8.1.6}$$

Once the parameter x is computed k_{TC} is computed using either equation (8.1.7) or (8.1.8).

$$k_{TC} = 2\pi q(\alpha\mu)^{1/2}[0.4767x + 0.6200], \quad \text{when } x \text{ is } \geq 2 \tag{8.1.7}$$

$$k_{TC} = 2\pi q(\alpha\mu)^{1/2}[((x + 0.5090)^2/10.526) + 0.9754], \quad \text{when } x \text{ is } \leq 2 \tag{8.1.8}$$

A comparison of theoretical collision rate constants can be found in Table 8.1, and further discussion of classical ion–molecule collision theory can be found in reference 23.

Table 8.1 Comparison of computed ion–molecule collision rates

	Sr^+/MeF	Sr^+/CH_4	MoO^+/N_2O
α	2.97	2.593	30.3
μ_D	1.85	0	1.67
$\mu_{D/\alpha}$	0.623	0	0.551
C	0.17	0	0.16
		$k_{coll}/10^9$	
k_{LC}	0.815	1.025	0.723
k_{LD}	4.245	1.025	3.445
k_{ADO}	1.398	1.025	1.159
k_{TC}	1.954	1.025	1.598

8.1.3 Thermodynamic control of reactions

Beyond the factors mentioned in the preceding section, thermodynamics is an underlying guide to whether or not a reaction will proceed at thermal energy. Extensive monographs exist in which enthalpies of formation for ionic and neutral species are tabulated.[24,25] Working through these tables on a reaction by reaction basis can be a tedious task, and leads to little or no insight into reactivity trends or periodicities in families of reactions. The task can be clarified by examining specific properties such as ionization energies or oxygen atom affinities and their relative values, viz. scales or ladders. Much like electrochemical cell reactions that are broken down into half reactions, ion–molecule reactions can also be broken down into half reactions. Reaction enthalpies are then derived, quite simply, from the difference of two numbers. Scales helpful to the mass spectroscopist are the ionization energy, proton affinity, H-atom affinity, O-atom affinity and Cl-atom affinity scales.

In extensive experiments with molecular oxygen, rate constants and product branching ratios for the reaction of 67 atomic metal cations were measured.[26,27] The reaction efficiencies are plotted as a function of metal cation oxygen affinity (OA) in Figure 8.2. A clear correlation between reaction efficiency and OA and between product channel and OA is evident. When the OA of the metal is below the bond dissociation energy (BDE) of O_2 (i.e. the OA of O) inefficient O_2 clustering occurs. When the OA of the metal is above the OA of O, efficient O-atom transfer to the metal cation occurs. Near the thermo-neutral threshold Mo^+ reacts with moderate efficiency by O-atom transfer. So it can be said that these reactions are thermodynamically controlled.

However, all exothermic reactions do not react with unit efficiency, as is clearly evident in the case of nitrous oxide reacting with atomic metal cations. In extensive experiments with nitrous oxide, rate constants and product branching ratios for the reaction of 67 atomic metal cations were measured.[27,28] The reaction efficiencies are plotted as a function of metal cation OA in Figure 8.3. In reactions with nitrous oxide a significant number of metal cations react with only moderate to low efficiency, despite being strongly exothermic. As discussed by Bohme and co-workers[28] and by Armentrout *et al.*,[29] this apparent lack of reactivity can be related to the electronic structure of reactants, products and possible interconnecting transition states.

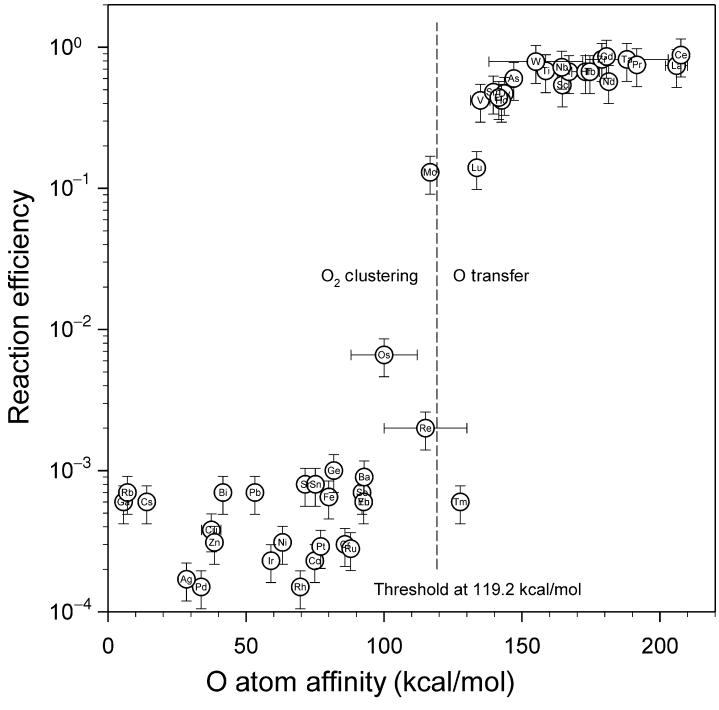

Figure 8.2 Plot of reaction efficiency and product-branching versus metal-ion-O-atom affinity for the reaction of 50 atomic cations reacting with molecular oxygen.

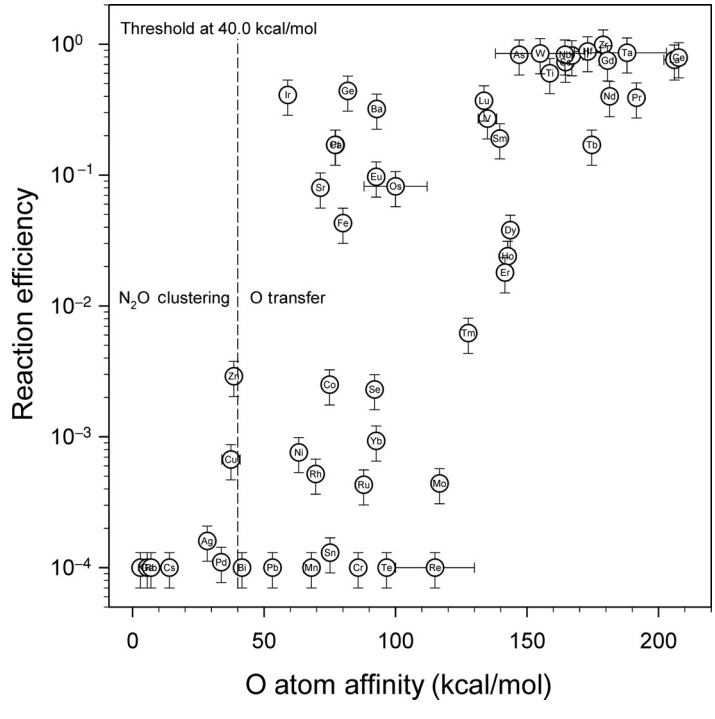

Figure 8.3 Plot of reaction efficiency and product-branching versus metal-ion-O-atom affinity for the reaction of 53 atomic cations reacting with nitrous oxide.

8.1.4 Driving endothermic reactions

The rf-energy field of the multipole device can be used as an energy source to drive (slightly) endothermic processes. It is important to note that, in assessing the energy available for driving endothermic reactions, one must consider the collision energy in the 'centre-of-mass' reference frame (E_{CM}) and not the laboratory-based translation energy (E_{LAB}) imparted by any lenses in the ion optical path. This is because in a collision of two freely moving bodies recoil of the target carries off some part of the collision energy. To convert from E_{LAB} to E_{CM} the relationship $E_{CM} = E_{LAB}m/(M + m)$, where m and M are the masses of the neutral and ionic species respectively, is used.

It is important to note that all the energy available in a collision is not necessarily converted to internal energy in the colliding pair. Armentrout and co-workers have observed collision-target dependent effects for the series of rare gas atoms as neutral targets.[30–32] In the collision induced dissociation (CID) of VO^+ the dissociation cross section was found to be notably different for Ne, Ar and Kr as target gas compared to Xe as target gas, where the dissociation threshold progressed to higher energy as the target gas was made lighter.[30] Armentrout and co-workers attribute this effect, and an associated reduction in the dissociation cross section, to a reduction in the lifetime of the collision complex as the target gas becomes lighter.[32]

While this may be the case for atomic target species, for polyatomic targets other factors such as the 'hardness' of the target may influence the extent of conversion of translation energy into internal energy.[33,34] Resorting to a classical-mechanical interpretation, we will introduce a term representing the coefficient of restitution or elasticity (e) of the collision, where $e = 0$ corresponds to an inelastic collision and $e = 1$ corresponds to a completely elastic collision. We can derive the following equation that relates the conversion of kinetic energy into internal energy (E_{INT}):

$$\Delta E_{INT} = (1/2)\mu V_{REL}{}^2(e^2 - 1) \tag{8.1.9}$$

where μ is the reduced mass ($Mm/(M + m)$) and the relative velocity, V_{REL}, is taken assuming a stationary target gas atom/molecule, $V_{REL} = (2E_{LAB}/M)^{1/2}$. Therefore,

$$\Delta E_{INT} = E_{LAB}m(e^2 - 1)/(M + m) \tag{8.1.10}$$

It is important to note that some part of this energy may indeed be stored rather inertly as internal energy in the neutral target and thus not be used to promote an endothermic reaction. Hence heavy atomic species are found to be best for promoting collision induced dissociation.[30] Conversely, a softer colliding partner may induce greater reaction efficiency by increasing the lifetime of the orbital ion–molecule complex (see below). Furthermore, product branching ratios could be altered when, in the case of multiple exit channels, removal of energy by the collision target removes, thermodynamically, one or more exit channels. Data for the degree of conversion of kinetic energy to internal energy for an ion of mass 80 colliding with target molecule of mass 16 as a function of collision elasticity and E_{LAB} of the ion are shown in Table 8.2.

8.1.5 Spin conservation rules

The first application of spin and symmetry considerations to chemical reactions was presented by Wigner and Witmer,[35] who published rules concerned with the conservation of spin and orbital angular momentum for reactions of diatomic molecules. Later extensions to this work by Hoffmann and by Fukui[36] earned them the Nobel Prize for Chemistry in 1981.

Table 8.2 Degree of conversion of kinetic energy to internal energy for an $m/z = 80$ ion colliding with an $m/z = 16$ target molecule as a function of collision elasticity and laboratory reference frame energy (E_{LAB}) of ion

	ΔE_{INT} (kcal/mol)				
E_{LAB}(eV)	$e = 0.1$	$e = 0.3$	$e = 0.5$	$e = 0.7$	$e = 0.9$
0.5	1.9	1.8	1.4	1.0	0.4
1.0	3.8	3.5	2.9	2.0	0.7
1.5	5.7	5.3	4.3	2.9	1.1
2.0	7.6	7.0	5.8	3.9	1.5
2.5	9.5	8.8	7.2	4.9	1.8
3.0	11.4	10.5	8.7	5.9	2.2

The important concept is that it is possible to make certain spin and symmetry based selection rules for the prediction of allowed and forbidden chemical reactions.[36] Also important is the so-called non-crossing rule introduced by Neumann and Wigner,[37] and independently by Teller[38] which states that two orbitals of the same symmetry cannot intersect in an orbital energy correlation diagram. Correlation diagrams can provide valuable information about the allowed transition state of a chemical reaction[36] and therefore about possible outcomes of a chemical reaction.

To formalize the concept of spin conservation we can borrow from Shuler[39] who stated: 'In order for reactants and products to correlate, it will be necessary that the intermediate complex formed during the reaction have at least one electronic species in its term manifold (the collection of micro-states falling under one term symbol) which arises from the combination both of the reactants and of the products'. This can be expressed via the reaction sequence shown in equation (8.1.11).

$$A^+ + B \rightarrow AB^+ \rightarrow C^+ + D \tag{8.1.11}$$

In this reaction sequence A^+, B, C^+ and D have spins s(A^+), s(B), s(C^+) and s(D), respectively. The set of spins in the reactant term manifold, s_1, is $\{s(A^+) + s(B), s(A^+) + s(B) - 1, \ldots, |s(A^+) - s(B)|\}$ (where the vertical bars indicate that the magnitude of the difference is to be taken) and that in the product term manifold, s_2, is $\{s(C^+) + s(D), s(C^+) + s(D) - 1, \ldots, |s(C^+) - s(D)|\}$, recalling that spins are added as vector quantities. For the reaction to be spin-allowed there must be an energetically accessible intermediate AB^+ with spin s(AB^+) such that s(AB^+) is in both set s_1 and set s_2.

The ramification, for example, is that a species with doublet spin multiplicity reacting with another species with doublet spin multiplicity can have the following product pairs: two triplet multiplicity species, two doublet multiplicity species, a triplet and a singlet or two singlet species (and other combinations of higher multiplicity). Perhaps more significantly, if the neutral reactant and neutral product of reaction (8.1.6) are both singlet species then the reactant and product ions must have the same multiplicity. Adherence to spin conservation rules can therefore govern the rate and branching ratio of a reaction.[40–42]

Table 8.3 presents reaction rate constants for Sr^+ reacting with several small neutral oxygen-containing reagents. The strontium cation has electronic configuration [Kr] $5s^1$ and electronic state term symbol ^2S. The fastest Sr^+ reaction studied in our lab is, by far, that with nitrogen

Table 8.3 Selected properties of reactant neutrals and reaction rate coefficients for reactions with strontium cations (Sr^+, ^2S)

Neutral	Ground state	$\Delta_r H^o_{298}$ (kcal/mol)	Primary product	Rate constant (cm^3/molecules/s)
NO_2	$^2A_1$	$\sim 0^a$	SrO^+	6.7×10^{-10}
N_2O	$^1\Sigma^+$	−31.4	SrO^+	6.3×10^{-11}
D_2O	$^1A'$	+45.6	$Sr(D_2O)^+$	3.5×10^{-12}
O_2	$^3\Sigma_g^-$	+47.8	$Sr(O_2)^+$	5.0×10^{-14}
CO	$^1\Sigma^+$	+185.9	$Sr(CO)^+$	$< 1 \times 10^{-14}$

[a] While the literature value is +2.1(6.0) kcal/mol, the computed value (B3LYP/DZVP) is −3.7 kcal/mol, so the reaction is taken to be approximately thermoneutral.

dioxide. Ground state nitrogen dioxide and Sr^+ are both doublet species. Similarly NO and SrO^+, the logical products for this reaction, are doublet species. This radical–radical reaction is spin-allowed, thermo-neutral to slightly exothermic and is observed to proceed essentially at the collision rate indicating an absence of any significant activation barrier. The absence of an entrance channel barrier is confirmed by quantum chemical calculations at the B3LYP/DZVP level. This designation contains the quantum chemical method, in this instance Becke's three-parameter exchange functional[43] with the Lee-Yang-Parr electron correlation functional (LYP)[44] and the orbital basis set, in this case Salahub's double zeta valence plus polarization (DZVP)[45] basis set. However, the O-atom transfer reaction with N_2O, although >30 kcal/mol more exothermic than that with NO_2, proceeds at a rate one order of magnitude more slowly than the latter reaction. Activation barriers to reaction could arise at either the entrance channel, where the closed shell nature of N_2O will introduce an activation barrier to the bond formation between Sr^+ and the terminal O-atom, or at the transition state for N_2 separation from SrO^+.

8.1.6 Electron transfer reactions

The ionization energy scale is also an important consideration when predicting the outcome of an ion–molecule reaction. A general trend apparent in reactions with benzene is that the outcome is, with few exceptions, either simple clustering of benzene to the metal ion or electron transfer from the benzene molecule to the metal. The transition from one mechanism to the other is sharply dependent on the first ionization energy of the metal cation. For example the first ionization energy of benzene is 9.2459 eV and that of Au is 9.226 eV, making the electron transfer from neutral benzene to cationic gold endothermic by a mere 0.02 eV (or 0.5 kcal/mol). SIFT studies show that Zn^+ (IE^1 Zn = 9.394 eV) and Hg^+ (IE^1 = 10.437 eV) remove an electron from benzene at or near the collision rate, while Cd^+ (IE^1 = 8.99 eV) and other lower IE^1 metals undergo clustering reactions. The near thermo-neutral Au^+/benzene reaction proceeds by both electron transfer and simple clustering in approximately equal ratio. It would appear that in a thermal ensemble, part of the population (in the high-energy tail) has sufficient kinetic energy to overcome the slight endothermicity of the electron transfer reaction.

The implication of these reaction rate coefficients and product distribution channels is that a reaction gas with high electron transfer efficiency and known ionization energy could be used as

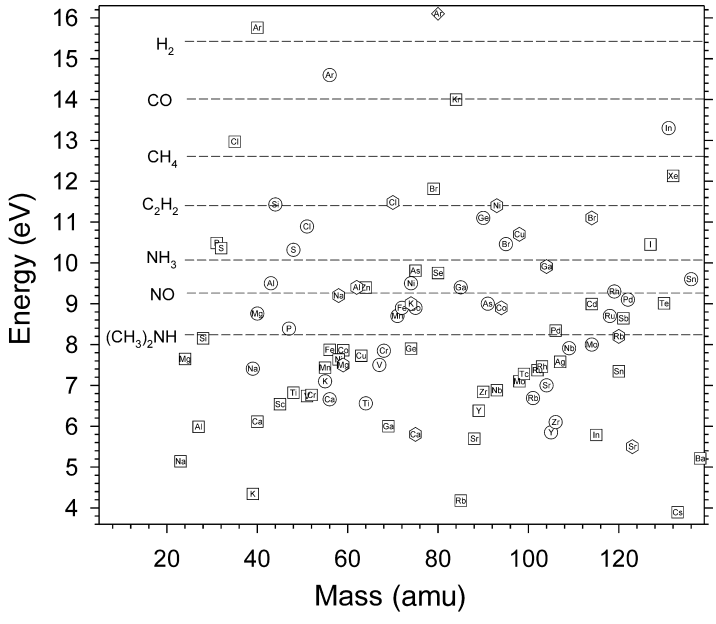

Figure 8.4 Plot of ionization energy versus mass (covering the range 20–140 amu) for known metals (squares), oxides (circles), dimers (diamonds) and chlorides (hexagons). The ionization energy of selected electron transfer reagents is denoted with horizontal dashed lines. This plot can serve as a graphical aid in forming strategies for using electron transfer reactions to chemically resolve isobaric interferences.

a so-called low-pass filter, discriminating against interference ions on the basis of first ionization potential. Indeed, neutral targets such as xenon and methane,[46] and ammonia[9] have been used as effective reagents for the removal of high-ionization energy interference ions. In Figure 8.4, literature values for ionization energy are plotted versus mass for: atomic metals, oxides, selected dimers and selected chlorides. The ionization energy of seven selected electron transfer reagents is denoted with horizontal dashed lines. This plot is intended to serve as a graphical aid in forming strategies for using electron transfer reactions to chemically resolve isobaric interference.

8.1.7 Ion–molecule complex lifetime (energy redistribution)

Once an ion–molecule collision complex has been created, the electronic structure of the two species must re-form to the product electronic configuration. The collisional complex must be permitted enough time for this electronic structure rearrangement to occur. Typically in ion–atom collisions, an elastic or near-elastic collision occurs and the colliding entities separate before a new electronic configuration is formed, thus ion–atom reactions are generally of low probability (i.e. inefficient on a per-collision basis). However, in an ion–molecule collision, energy redistribution from the reaction coordinate to vibrational modes of the complex causes an inelastic collision which results in a longer orbital-complex lifetime. This longer orbital-complex lifetime permits re-formation of the electronic wave function to that of the product channel.[47,48]

8.1.8 The kinetic isotope effect

Beyond simple quantitation of elemental composition, often the inherent isotope ratio of a single element is of interest in geology, geochronology and even in the forensic sciences. Of course the isotope dependent instrument sensitivity must be carefully understood to accurately make such measurements. Beyond this, when using reaction cell chemistry to simultaneously remove an isobaric interference and make isotope ratio determinations one must give consideration to the kinetic isotope effect inherent in the ion–molecule reaction being utilized.

The kinetic isotope effect (KIE) results in variation of the reaction rate constant as a function of isotopic variations in either of the reactants. A primary isotope effect occurs when the labeled bond is directly involved in the reaction coordinate and a secondary isotope effect occurs when the labeled bond is elsewhere in the ion or molecule. The effect is greater for larger changes in relative isotope mass. Often, a precise measure of the KIE can provide valuable information regarding the reaction mechanism. The predominant cause of the KIE is variation in the zero-point vibration energy (ZPE) as a function of isotope mass since changes to the ZPE may alter the reaction enthalpy of activation. Isotope substitution also effects changes in the translation, rotation and vibration partition functions, which in turn alters the reaction entropy of activation.

Moens and co-workers used the fluoride transfer reaction from methyl fluoride to Sr^+ (resulting in the formation of SrF^+) to separate the strontium isotope pattern from a rubidium-containing background matrix, with the aim of making Rb-interference free isotope ratio measurements of strontium.[49] However, it has been proposed that mass discrimination effects due to the ion–molecule reaction can alter the experimentally determined isotope pattern, thereby degrading the accuracy of isotope ratio measurements made using this approach.[50] Consider the reaction

$$CH_3F + Sr^+ \rightarrow \text{Transition State (TS)} \rightarrow CH_3 + SrF^+ \tag{8.1.12}$$

Transition state theory[51] (TST) predicts a rate coefficient k,

$$k = (k_B T/h)\exp\{\Delta^{\ddagger}S^{\circ}/R\}\exp\{-\Delta^{\ddagger}H^{\circ}/RT\} = (k_B T/h)\exp\{-\Delta^{\ddagger}G^{\circ}/RT\} \tag{8.1.13}$$

where $\Delta^{\ddagger}S^{\circ}$, $\Delta^{\ddagger}H^{\circ}$ and $\Delta^{\ddagger}G^{\circ}$ are the activation entropy, enthalpy and free energy, respectively, of the reaction. Alternately the TST rate can be written in terms of partition functions and activation energy:

$$k = (k_B T/h)(Q(TS)/Q(Sr^+)Q(\text{MeF}))\exp\{-\Delta E^{\circ}/RT\} \tag{8.1.14}$$

Writing a ratio of reaction rates for two isotope labeled reactions we arrive at

$$k/^*k = \exp\{-(\Delta^{\ddagger}G^{\circ} - \Delta^{\ddagger}G^{\circ *})/RT\} \tag{8.1.15}$$

To determine the KIE requires computation of the free energy of activation for the reaction. This is usually achieved using computational quantum chemistry. For the reaction in (8.1.12) the reaction surface and requisite stationary points were computed at the B3LYP/DZVP level of theory using the Gaussian98 quantum chemistry package. Exploration of the reaction surface revealed that the reaction lowest in energy was of C_3-symmetry. Figure 8.5 shows the r(SrF) − r(FC) potential energy surface where the C-H bond distance and H-C-H bond angle are relaxed to the lowest energy geometry at each point. The surface reveals that at the transition state the Sr-F bond has fully formed and that the C-F bond is breaking. Taking vibration frequencies at the B3LYP/DZVP level and electronic energy differences at CCSD(T)/DZVP level one (here

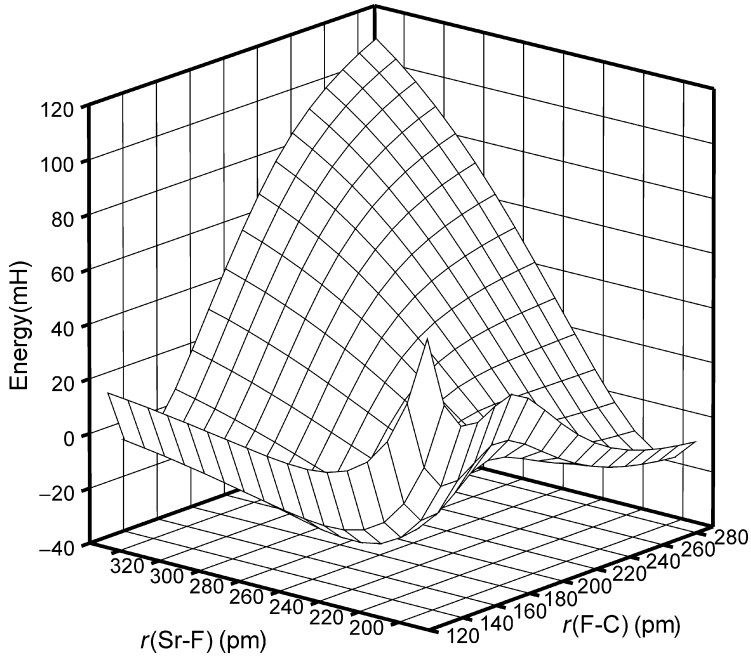

Figure 8.5 Potential energy surface (PES) for the reaction of Sr^+ reacting with methylfluoride in C_3 symmetry. The Sr–F bond distance is varied from 190 to 350 pm while the C–F bond distance is varied from 125 to 285 pm in 10 pm steps. Computations reveal that at the transition state geometry the Sr–F bond distance is near its equilibrium SrF^+ distance and that the C–F bond is breaking. The zero of energy is arbitrary.

CCSD(T) refers to a sophisticated coupled-clusters calculation[52]) derives activation free energies of: 26.3712 kcal/mol, 26.3700 kcal/mol, 26.3674 kcal/mol and 26.3643 kcal/mol for reactions involving ^{88}Sr, ^{87}Sr, ^{86}Sr and ^{84}Sr, respectively. Normalizing to the rate constant for the ^{88}Sr reaction the ^{87}Sr, ^{86}Sr and ^{84}Sr reactions are 0.203%, 0.643% and 1.172% slower, respectively. To determine the effect that the KIE will have on the observed isotope distribution pattern requires propagation of the KIE through to extent-of-reaction. This last step will depend on pressure conditions in the individual reaction cell. One can see that the KIE can impart a mass discrimination effect on measured isotope distribution patterns. This effect will be alleviated when the extent of reaction approaches 1 (i.e. 100% complete).

8.1.9 The York University ion–molecule reaction rate constant database

In an ongoing project in the Ion Chemistry Laboratory at York University, numerous ion–molecule reaction rate coefficients have been determined using a selected-ion flow tube (SIFT) tandem mass spectrometer modified to accept ions, generated by a plasma ion source, through an atmosphere–vacuum interface.[14,15] The SIFT technique is a powerful and versatile means for making accurate determinations of ion–molecule reaction rate coefficients and product branching ratios and has allowed the establishment of a significant new database. In the mid-1970s the SIFT

was developed out of the Flowing Afterglow (FA) apparatus, which in turn had been developed in the early 1960s for the study of atmospheric and interstellar chemistry.[53]

An extensive database of ion–molecule reaction rate constants and product branching ratios for possible ion–molecule reactions occurring within a reaction cell is required if reaction/collision cell chemical resolution is to gain wide and routine application. The task of accumulating the required database is sizable. For example, taking the cations from lithium to americium, and including their oxides, carbides, nitrides, hydrides, hydroxides and chlorides, one arrives at 651 potential reagent ions. Multiplying this by the 14 neutral reagent molecules (methane, ammonia, hydrogen, oxygen, nitrogen, water, nitric oxide, nitrous oxide, carbon monoxide, carbon dioxide, methyl chloride, methyl fluoride, benzene and nitrogen dioxide) currently being studied as chemical resolving agents results in a total of 9114 possible primary reactions. Of the previously noted databases, coverage of metal ion–molecule reactions is limited to approximately 300 primary and secondary reactions from the above matrix.

It is important to review the similarities and differences between a typical reaction/collision cell mass spectrometer and the ICP/SIFT instrument. In Figure 8.6, schematics for the ICP/SIFT and an Elan 6100DRC are illustrated. Both instruments utilize essentially identical plasma generators and atmosphere–vacuum interfaces. While the Elan 6100DRC simultaneously selects and reacts the primary ion in the dynamic reaction cell, the SIFT instrument first selects the primary reagent ion in one region and then reacts the ion in the flow tube in the presence of helium buffer gas. In the SIFT the reagent gas is a minor component of the helium buffer gas, so tube pressure and flow conditions do not change during the course of an experiment. However, in the DRC the reaction gas is the sole source of pressure so the cell conditions change as the reaction gas flow increases.

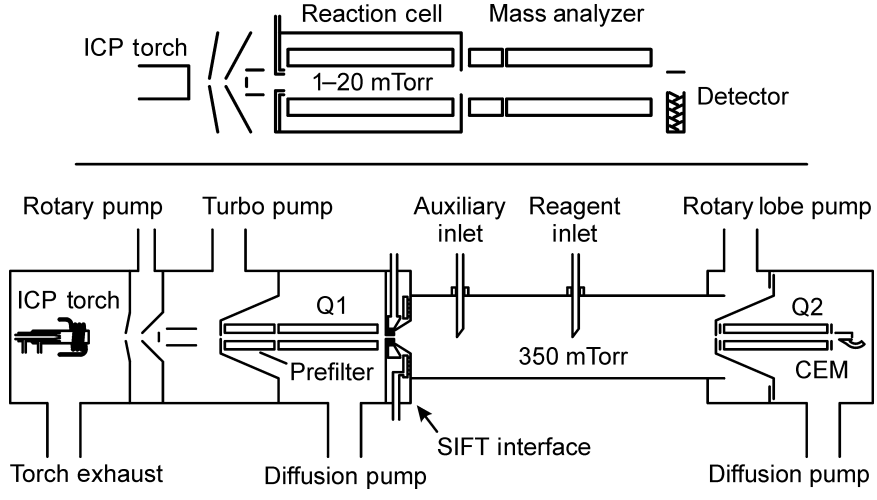

Figure 8.6 Schematic diagrams for the ICP/SIFT (top) and Elan 6100DRC (bottom) instruments. In the ICP/SIFT instrument ions are produced in a plasma source and sampled by a standard atmosphere-vacuum interface (see text). The ion of interest is mass-selected in Q1, after which it is passed to the flow tube via a Venturi inlet. The flow tube is kept at a constant pressure of 0.35 Torr. Thermalized ions react with a neutral admitted at the reagent inlet as they flow downstream (to the right). Product ions are mass analyzed by Q2. In the Elan 6100DRC, ions are produced and sampled as above but are then reacted in a bandpass quadrupole reaction cell (DRC). Unreacted ions and product ions are detected by the mass analyzer quadrupole.

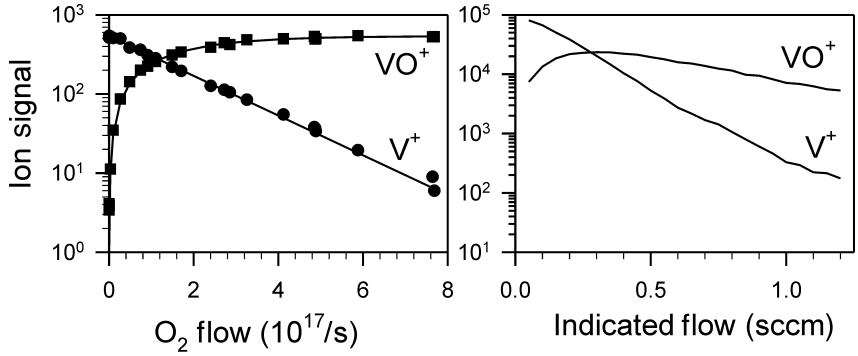

Figure 8.7 Reaction profiles for V^+ reacting with O_2 as a function of O_2 flow in the respective reaction regions. ICP/SIFT data above and Elan 6100DRC data below. Scattering loss as a function of reaction cell pressure is evident in the VO^+ signal for the DRC data.

The primary effect is that of collisional scattering which slowly increases at high cell pressures. Furthermore, since the SIFT flow tube is pressurized to 0.35 Torr with helium, the mass selected ion experiences approximately 10^5 collisions with He before being permitted to react with the neutral of interest. One can compare this to the DRC where transiting ions may experience between 1 and 20 collisions over the operating pressure range of the DRC. Figure 8.7 contains

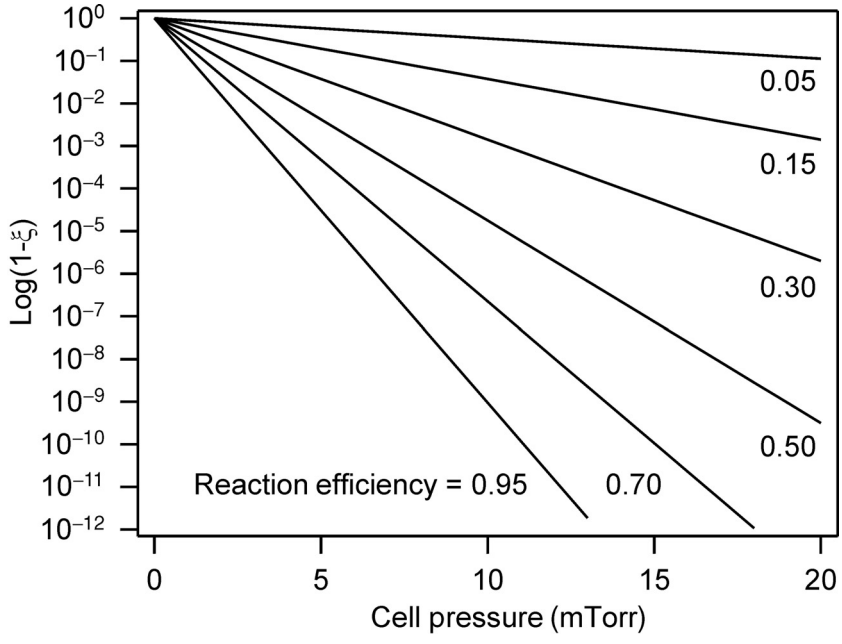

Figure 8.8 Plot of extent of reaction as a function of reaction cell pressure for six selected reaction efficiencies, assuming a typical DRC configuration. From this plot one can quickly determine the extent, in orders of magnitude, that an ion will be suppressed from the ion beam or converted to an alternate product (i.e. detection mass).

plots of reaction profile data for the ICP/SIFT and Elan 6100DRC. The similarity is encouraging and suggests that rate constant data are transportable between the two instruments. In addition, many other examples of identical reaction behavior have been observed.

Repetitive quantitative conversion of an analyte or interference is best achieved when the extent of reaction is high (near 1). Figure 8.8 is a plot of $\log(1 - \xi)$ as a function of reaction cell pressure for six selected reaction efficiencies, assuming a typical DRC configuration. From this plot one can quickly determine the extent, in orders of magnitude, that an interference ion will be suppressed from the ion beam or an analyte ion will be converted to an alternate product for subsequent detection and quantitation.

Currently the online database consists of reaction details for 11 neutral species reacting with a broad selection of atomic metal ions, as well as a table of selected plasma 'matrix' ion reactions. Also, various tables of thermodynamic data and physical property data are presented. The universal resource locator (URL) for the database Web page is: http://www.chem.yorku.ca/profs/bohme/research/research.html.

References

1. Montaser, A. (ed.) (1998) *Inductively Coupled Plasma Mass Spectrometry*, J. Wiley, New York.
2. Sakata, K. and Kawabata, K. (1994) Reduction of fundamental polyatomic ions in inductively coupled plasma mass spectrometry. *Spectrochim. Acta* B, **49**, 1027.
3. Nonose, N. S., Matsuda, N., Fudagawa, N., and Kubota, M. (1994) Some characteristics of polyatomic ion spectra in inductively coupled plasma mass spectrometry. *Spectrochim. Acta* B, **49**, 995.
4. Tanner, S. D. (1995) Characterization of ionization and matrix suppression in inductively coupled 'cold' plasma mass spectrometry. *J. Anal. At. Spectrom.*, **10**, 905.
5. Lam, J. W. and McLaren, J. W. (1990) Use of aerosol processing and nitrogen–argon plasmas for reduction of oxide interference in inductively coupled plasma mass spectrometry. *J. Anal. At. Spectrom.*, **5**, 419.
6. Lam, J. W. H. and Horlick, G. (1990) A comparison of argon and mixed gas plasmas for inductively coupled plasma-mass spectrometry. *Spectrochim. Acta* B, **45**, 1313.
7. Douglas, D. J. (1989) Some current perspectives on ICP-MS. *Can. J. Spectrosc.*, **34**, 38.
8. Turner, P. J., Mills, D. J., Schroder, E., Lapitajs, G., Jung, G., Iacone, L. A., Haydar, D. A., and Montaser, A. (1998) Instrumentation for low- and high-resolution ICPMS. In: *Inductively Coupled Plasma Mass Spectrometry*, Chapter 6 (ed. Akbar Montaser), Wiley-VCH, New York, pp. 421–501.
9. Tanner, S. D., Baranov, V. I., and Bandura, D. R. (2002) Reaction cells and collision cells for ICP-MS: a tutorial review. *Spectrochim. Acta* B, **57B**, 1361.
10. Ikezoe, Y., Matsuoka, S., Takebe, M., and Viggiano, A. (1987) *Gas Phase Ion–Molecule Reaction Rate Constants Through 1986*, Maruzen Company, Tokyo.
11. Anicich, V. G. and Huntress, W. T. (1986) A survey of bimolecular ion–molecule reactions for use in modeling the chemistry of planetary atmospheres, cometary comae, and interstellar clouds. *Ap. J. Supplement Series*, **62**, 553.
12. Anicich, V. G. (1993) A survey of bimolecular ion–molecule reactions for use in modeling the chemistry of planetary atmospheres, cometary comae, and interstellar clouds: *Astrophys. J. Suppl. Ser.*, **84**, 215.
13. Anicich, V. G. (1993) Evaluated bimolecular ion–molecule gas phase kinetics of positive ions for use in modeling planetary atmospheres, cometary comae, and interstellar clouds. *J. Phys. Chem. Ref. Data*, **22**, 1469.

14. Koyanagi, G. K., Lavrov, V. V., Baranov,V., Bandura, D., Tanner, S., McLaren, J., and Bohme, D. K. (2000) A novel inductively coupled plasma/selected-ion flow tube mass spectrometer for the study of reactions of atomic and atomic oxide ions. *Int. J. Mass Spectrom.*, **194**, L1.
15. Koyanagi, G. K., Baranov,V. I., Tanner, S. D., and Bohme, D. K. (2000) An inductively coupled plasma/selected-ion flow tube mass spectrometric study of the chemical resolution of isobaric interferences. *J. Anal. At. Spectrom.*, **15**, 1207.
16. Langevin, P. (1905) *Ann. Chim. Phys.*, **5**, 245.
17. Gioumousis, G. and Stevenson, D. P. (1958) Reactions of gaseous molecule ions with gaseous molecules: V. Theory. *J. Chem. Phys.*, **29**, 294.
18. Su, T. and Bowers, M. T. (1973) Theory of ion-polar molecule collisions. Comparison with experimental charge transfer reactions of rare gas ions to geometric isomers of difluorobenzene and dichloroethylene. *J. Chem. Phys.*, **58**, 3027.
19. Su, T. and Bowers, M. T. (1973) Ion-polar molecule collisions. Proton transfer reactions of H_3^+ and CH_5^+ to the geometric isomers of difluoroethylene, dichloroethylene, and difluorobenzene. *J. Am. Chem. Soc.*, **95**, 1370.
20. Su, T. and Bowers, M. T. (1973) Ion-polar molecule collisions. Effect of ion size on ion-polar molecule rate constants. Parameterization of the average-dipole-orientation theory. *Int. J. Mass Spectrom. Ion Phys.*, **12**, 347.
21. Su, T. and Bowers, M. T. (1975) Ion-polar molecular collisions: the average quadrupole orientation theory. *Int. J. Mass Spectrom. Ion Phys.*, **17**, 309. See also the erratum, Su, T. and Bowers, M. T. (1976) *Int. J. Mass Spectrom. Ion Phys.*, **21**, 424.
22. Chesnavich, W. J., Su, T., and Bowers, M. T. (1980) Collisions in a noncentral field: a variational and trajectory investigation of ion–dipole capture. *J. Chem. Phys.*, **72**, 2641.
23. Su, T. and Bowers, M. T. (1979) *Gas Phase Ion Chemistry*, Chapter 3 (ed. M. T. Bowers), Academic Press, New York.
24. JANAF Thermochemical Tables (1971) 2nd edn Nat. Stand. Ref. Data Ser., 37 National Bureau of Standards (U.S.).
25. Lias, S. G., Bartmess, J. E., Liebman, J. F., Holmes, J. L., Levin, R. D., and Mallard, W. G. (1988) Gas-phase ion and neutral thermochemistry. *J. Phys. Chem. Ref. Data*, **17**, (1).
26. Koyanagi, G. K., Caraiman, D., Blagojevic, V., and Bohme, D. K. (2002) Gas-phase reactions of transition-metal ions with molecular oxygen: room-temperature kinetics and periodicities in reactivity. *J. Phys. Chem.* A, **106**, 4581.
27. Koyanagi, G. K. and Bohme, D. K. (2001) Oxidation reactions of lanthanide cations with N_2O and O_2: periodicities in reactivity. *J. Phys. Chem.* A, **105**, 8964.
28. Lavrov, V. V., Blagojevic, V., Koyanagi, G. K., Orlova, G., and Bohme, D. K. (2004) Gas-phase oxidation and nitration of first, second and third-row atomic cations in reactions with nitrous oxide: periodicities in reactivity. *J. Phys. Chem.* A, **108**, 5610.
29. Armentrout, P. B., Halle, L. F., and Beauchamp, J. L. (1982) Reaction of Cr, Mn, Fe, Co, and Ni with O_2 and N_2O. Examination of the translational energy dependence of the cross section of endothermic reactions. *J. Chem. Phys.*, **76**, 2449.
30. Aristov, N. and Armentrout, P. B. (1986) Collision-induced dissociation of vanadium monoxide ion. *J. Phys. Chem.*, **90**, 5135.
31. Hales, D. A. and Armentrout, P. B. (1990) Effect of internal excitation on the collision-induced dissociation and reactivity of the cobalt diatomic monopositive ion. *J. Cluster Sci.*, **1**, 127.
32. Shultz, R. H., Crellin, K. C., and Armentrout, P. B. (1991) Sequential bond energies of iron carbonyl $Fe(CO)_x^+$ ($x = 1$–5): systematic effects on collision-induced dissociation measurements. *J. Am. Chem. Soc.*, **113**, 8590.

33. McLuckey, S. A. (1992) Principles of collisional activation in analytical mass spectrometry. *J. Am. Soc. Mass Spectrom.*, **3**, 599.
34. Horning, S. R., Vincenti, M., and Cooks, R. G. (1990) Angular dependence of internal energy distributions of activated $Fe(CO)_5^+$ and $W(CO)_6^+$ ions. The contributions of vibrational and electronic excitation mechanisms in kiloelectron volt collisions. *J. Am. Chem. Soc.*, **112**, 119.
35. Wigner, E. and Witmer, E. E. (1928) Molecular spectra of diatomic molecules in modern quantum-mechanics. *Z. Phys*., **51**, 859.
36. Hargittai, I. and Hargittai, M. (1995) *Symmetry through the Eyes of a Chemist*, 2nd edn, Plenum, New York, p. 299.
37. von Neumann, J. and Wigner, E. (1929) On the behaviour of eigenvalues in adiabatic processes. *Phys. Z.*, **30**, 467.
38. Teller, E. (1937) Crossing of potential surfaces. *J. Phys. Chem.*, **41**, 109.
39. Shuler, K. E. (1953) Adiabatic correlation rules for reactions involving polyatomic intermediate complexes and their application to the formation of $OH(^2\sum^+)$ in the H_2-O_2 flame. *J. Chem. Phys.*, **21**, 624.
40. Armentrout, P. B. (1990) Electronic state-specific transition metal ion chemistry . *Ann. Rev. Phys. Chem.*, **41**, 313.
41. Clemmer, D. E., Aristov, N., and Armentrout, P. B. (1993) Reactions of scandium oxide (ScO^+), titanium oxide (TiO^+) and vanadyl (VO^+) with deuterium: M^+-OH bond energies and effects of spin conservation. *J. Phys. Chem.*, **97**, 544.
42. Schroder, D., Shaik, S., and Schwarz, H. (2000) Two-state reactivity as a new concept in organometallic chemistry. *Acc. Chem. Res.*, **33**, 139.
43. Becke, A. D. (1993) Density-functional thermochemistry: III. The role of exact exchange. *J. Chem. Phys.*, **98**, 5648.
44. Lee, C., Yang, W., and Parr, R. G. (1988) Development of the Colle–Salvetti correlation-energy formula into a functional of the electron density. *Phys. Rev.* B, **37**, 785.
45. Godbout, N., Salahub, D. R., Andzelm, J., and Wimmer, E. (1992) Optimization of Gaussian-type basis sets for local spin density functional calculations: Part I. Boron through neon, optimization technique and validation. *Can. J. Chem.*, **70**, 560.
46. Rowan, J. T. and Houk, R. S. (1989) Attenuation of polyatomic ion interferences in inductively coupled plasma mass spectrometry by gas-phase collisions, *Appl. Spectrosc*., **43**, 976.
47. Chesnavich, W. J. and Bowers, M. T. (1979) *Gas Phase Ion Chemistry*, Chapter 4 (ed. M. T. Bowers), Academic Press, New York.
48. Hase, W. L. (1998) Some recent advances and remaining questions regarding unimolecular rate theory. *Acc. Chem. Res.*, **31**, 659.
49. Moens, L. J., Vanhaecke, F. F., Bandura, D. R., Baranov V. I., and Tanner, S. D. (2001) Elimination of isobaric interferences in ICP-MS, using ion–molecule reaction chemistry: Rb/Sr age determination of magmatic rocks, a case study. *J. Anal. At. Spectrom.*, **16**, 991.
50. Vanhaecke, F., Balcaen, L., Deconinck, I., De Schrijver, I., Almeida, C. M., and Moens, L. (2003) *J. Anal. At. Spectrom.*, **18**, 1060.
51. Laidler, K. J. (1987) *Chemical Kinetics*, 3rd edn, Harper Collins Publishers, Inc, New York.
52. Cizek, J. (1969) Use of the cluster expansion and the technique of diagrams in calculations of correlation effects in atoms and molecules. *Adv. Chem. Phys.*, **14**, 35.
53. Bohme, D. K. (2000) Experimental studies of positive ion chemistry with flow-tube mass spectrometry: birth evolution, and achievements in the 20th century. *Int. J. Mass Spectrom.*, **200**, 97.

8.2 IMPLEMENTATION AND APPLICATIONS

Dmitry R Bandura

8.2.1 Introduction

The first reported work on the use of gas phase ion–molecule processes for the reduction of isobaric interferences in ICP-MS was published by Douglas, in 1989.[1] He observed that the loss of atomic ions in collisions with argon in a triple quadrupole mass spectrometer coupled to an ICP was comparable to the loss of molecular ions, suggesting that collision induced decomposition (CID) is a relatively inefficient process for reducing molecular ion interferences. However, Douglas also suggested that ion–molecule chemistry may provide a way around some persistent interferences. Significant enhancement of metal to metal-oxide ratio (Tb^+ to CeO^+ ratio) was shown when both were measured as products of oxidation reactions (TbO^+ and $CeO_2{}^+$) performed in the middle quadrupole (Tb^+ formed oxide ions readily in collisions with oxygen admitted into the collision cell while CeO^+ did not further oxidize). Rowan and Houk in the same year reported on preferential loss of argide ions in ion–molecule reactions with Xe and CH_4 while analyte ions were almost unaffected. Elevation of background from the products of side reactions was also observed and kinetic energy discrimination was used in order to suppress the unwanted product ions.[2] Publications by Barinaga, Koppenaal and Eiden[3–5] between 1994 and 1997 made a significant impact on the resurgence of the method, with their observations that application of ion–molecule chemistry with hydrogen, oxygen and methane was effective for resolving isobaric interferences in ICP-MS. There are currently several commercially available quadrupole-based ICP-MS instruments that use collision cells and reaction cells. These are the Platform™ (GV Instruments), the ELAN® DRC™-e and ELAN® DRC™-II (PerkinElmer-SCIEX), the X Series ICP-MS (Thermo Electron Corp.) and the Agilent 7500cs and 7500ce systems. A collision cell is used in place of an electrostatic analyzer on the double focusing mass analyzer of the multicollector sector field IsoProbe instrument (GV Instruments). Schematics of the Platform™, ELAN® DRC™-II, X Series ICP-MS and 7500cs are shown in Figure 8.9. The principal difference between the instruments lies in the method of controlling unwanted side reactions and their products. In hexapole and octapole cell instruments this is done by post-cell kinetic energy discrimination (KED) that suppresses transport of the products of the side reactions to the analyzer. The unique stability characteristics of the quadrupole cell allow formation of the unwanted side product ions to be suppressed by selecting an appropriate mass bandpass of the quadrupole. The details of the KED and bandpass approaches are discussed later.

Since its commercial introduction in 1997, collision cell and reaction cell ICP-MS has come a long way and is now well accepted. A recent tutorial review by Tanner *et al.*[6] covered the fundamentals of the operation of such devices, and listed the applications published up until September 2001. This section examines implementation and use of the ion–molecule processes enabled in the linear radio-frequency driven (r.f.) collision cells and reaction cells used in ICP-MS, partially drawn from the Tanner *et al.* review. Special attention is paid to ion dynamics, since the outcome of the ion–molecule processes strongly depends on it. Examples of the principle applications are given along with a discussion of the fundamental processes occurring in pressurized r.f. multipole devices.

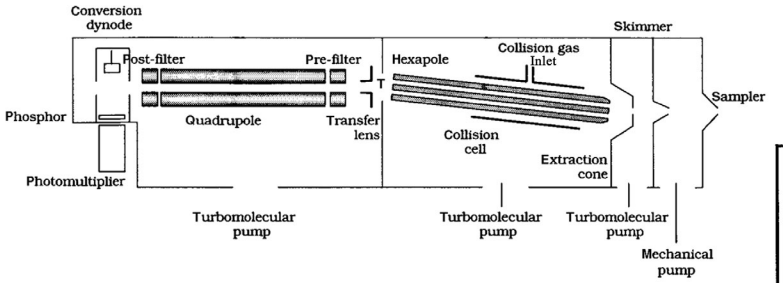

GV Instruments Platform

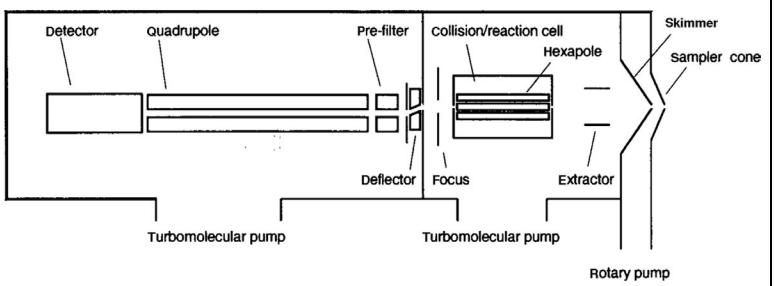

Thermo Electron Corporation X-7 ICP-MS

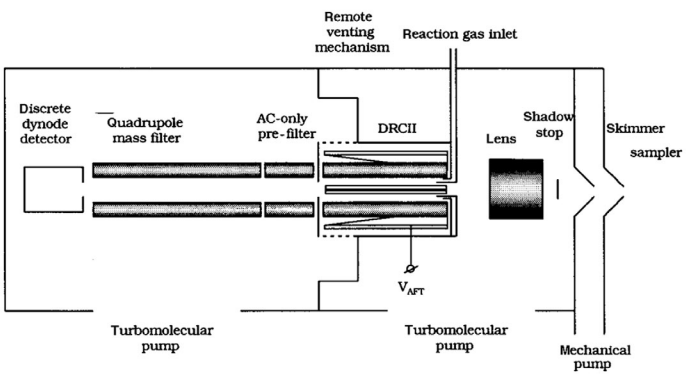

PerkinElmer SCIEX ELAN®DRCII

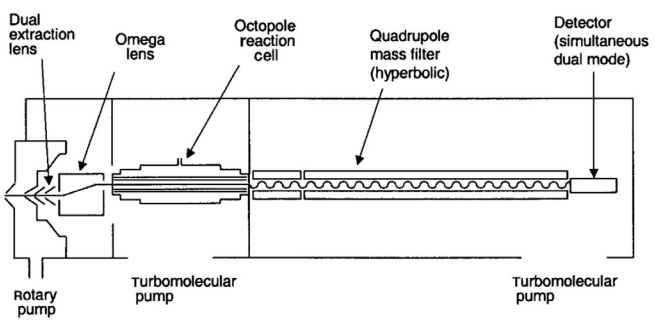

Agilent 7500cs

Figure 8.9 Schematics of the Platform™ (courtesy of Zenon Palacz, GV Instruments), ELAN® DRC™-II, X7-CCT (courtesy of Jonathan Batey, Thermo Electron Corporation) and 7500cs (courtesy of Noriyuki Yamada, Agilent).

8.2.2 Ion motion in nonpressurized r.f. multipoles

Consider an array of an even number, $2n$, of parallel rods of length L placed evenly about an axis of symmetry, z, with the minimum distance between the opposite rods of $d_0 = 2r_0$ (d_0 *and* r_0 are usually called inscribed diameter and radius, respectively, of the multipole). The opposite rods are electrically connected to each other, making n pairs of the rods. The pole pairs are supplied with an AC voltage $V_{AC} = 0.5V_{rf} \cos \omega t$ of a radio frequency $f = \omega/2\pi$ and amplitude $0.5V_{rf}$, with a phase shift of $2\pi/n$ rad between rod pairs.

In addition, a DC voltage, V_{dc}, can be applied between the pole pairs (in the case of the quadrupole filter, $n = 2$, this voltage is often called the 'resolving DC'). Further, all of the rods are supplied with an identical DC voltage, V_{RO}, which defines a rod offset potential (also called the pole bias). Thus, at any particular moment, the potential of the particular rod (pair) is defined by V_{AC} and its phase, V_{dc} and V_{RO}, of which V_{RO} is the same for all rods.

The simplistic description of the ion motion in an r.f. multipole is easiest for a quadrupole ($n = 2$). The (positively charged) ion within the array experiences an oscillating field and is at one moment attracted to the nearest pole at negative voltage, and at the next (*1/2f* s later) to the neighboring rod. If the ion mass is sufficiently small, the V_{rf} is sufficiently high or the frequency is sufficiently low, the amplitude of ion trajectory oscillations rises rapidly and after a few oscillations it reaches r_0, i.e. the ion hits the rods and is lost from the beam. If the frequency is sufficiently high, the V_{rf} is sufficiently low, or the ion sufficiently heavy, its inertia will prevent it from reaching very high amplitude oscillations, and the ion will transfer through the rod array taking $L \cdot f/v_z$ r.f. field cycles, where v_z is the ion velocity component along the axis (which is not changed by the fields applied radially). Operation in this 'r.f. only' mode (i.e. $V_{dc} = 0$) provides a high-pass mass filter, i.e. only ions having masses above a 'low mass cut-off' are transmitted.

When V_{dc} is applied between pole pairs, the ion will feel a continuous attraction toward the more negatively biased (DC) pole pair. If the AC frequency is sufficiently low, or the ion is heavy enough so that it cannot respond to the AC field sufficiently, the ion will drift toward the DC-negative pole, eventually striking that pole. Lighter ions, at the same time, can respond to the AC more readily and thus be protected from the defocusing action of the DC potential. Thus, the addition of a DC bias between pole pairs potentially provides a high mass cut-off in addition to the low mass cut-off of the r.f. The combination of AC and DC components gives a certain mass pass-band. If the ion mass, AC frequency and DC voltage are just right, the ion will have a stable (i.e. finite) trajectory through the array.

Theoretical description of ion motion in a general n-order multipole positioned along axis z is determined by classical equations of motion:

$$\frac{\partial^2 x}{\partial t^2} = -\frac{e}{m}\frac{\partial \Phi}{\partial x}, \qquad \frac{\partial^2 y}{\partial t^2} = -\frac{e}{m}\frac{\partial \Phi}{\partial y} \tag{8.2.1}$$

where

$$\Phi = \frac{1}{2}\left(\frac{\left(x^2 + y^2\right)^{1/2}}{r_0}\right)^n \cos\left(n \times \operatorname{atan}\frac{y}{x}\right)\left(V_{dc} - V_{rf}\cos(\omega t)\right) \tag{8.2.2}$$

is the time-variable potential of the multipole field[7] expressed in Cartesian coordinates and e and m are ion charge and mass, respectively. It can be shown that for $n = 2$ (quadrupole) the equations of motion (8.2.1) are linear and decoupled, are of the Mathieu type[8] and can be written

in canonical form as:[9]

$$\frac{d^2u}{d\xi^2} + (a_u - 2q_u \cos 2(\xi - \xi_0))\ u = 0 \tag{8.2.3}$$

where $u = x, y$; $\xi = \omega t/2$; $2\xi_0$ is the initial r.f. phase and

$$a_u = a_x = -a_y = \frac{4eV_{dc}}{m\omega^2 r_0^2}, \qquad q_u = q_x = -q_y = \frac{2eV_{rf}}{m\omega^2 r_0^2} \tag{8.2.4}$$

Solutions for this equation have been thoroughly investigated by analytical approximation methods, matrix methods and numeric methods (all providing approximate solutions[9,10]) and, after recent development of algebraic methods to compute Mathieu functions,[11] by an analytical method providing exact solutions for cos confining waveforms.[12] The solutions allow an a–q space, for which ions of mass m and charge e will have finite (stable) trajectory through the ideal infinite length quadrupole, to be mapped. This space is best visualized via the Mathieu stability diagram, for which the first region of ion stability is shown as a shaded area in Figure 8.10. This region is in fact an intersection of two regions characterizing stability of ion motion in xz and yz planes. Since the two motions are completely decoupled, such an intersection describes a binary state i.e. the ion is either stable or unstable (depending on its mass, for a given combination of V_{rf}, V_{dc}, r_0 and ω). The mass filtering application of a quadrupole (as discussed in Chapter 2) requires operation near the apex of the stability diagram to achieve unit mass resolution. Operation of a quadrupole as an ion guide or a reaction/collision cell does not require unit mass resolution, thus low a and medium q (selection of values for which will be discussed below) are usually used. One of the important differences between these two modes of operation is larger acceptance in the latter case. Acceptance, which describes the ion displacement–velocity phase

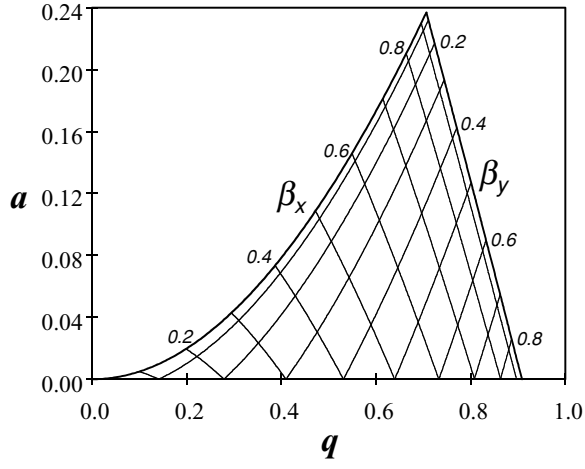

Figure 8.10 Stability diagram for an infinitely long and perfect quadrupole in the dimensionless space of (a, q), where a and q are the Mathieu parameters given by equations (8.2.4) in the text. Ions that are within the enclosed region have finite (stable) trajectories, independent of their initial displacement and initial phase of the applied r.f. Ions that are outside this region have amplitude of their oscillations exponentially increasing and are thus unstable in the field – independent of their initial displacement and initial phase of the applied r.f. Also shown are the iso-beta lines: ions of the same beta have same frequencies of trajectory oscillation in the field.

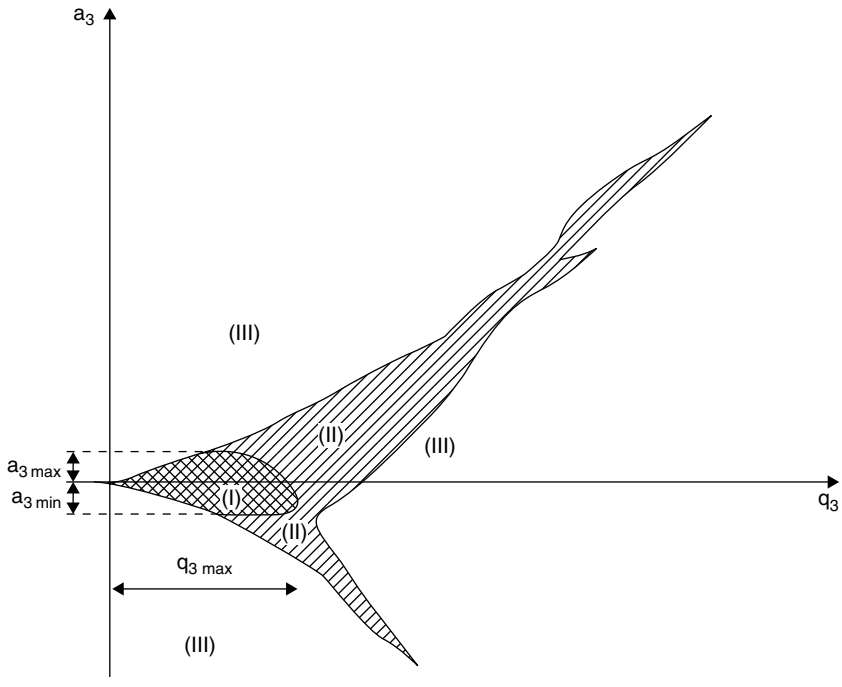

Figure 8.11 Stability diagram for a hexapole for ions introduced at radial displacement $r = 0.1r_0$, obtained by numerical modeling. (Adapted with permission from reference 15.)

space for which the amplitude of movement of an ion on a stable trajectory through the multipole is always less than the inscribed radius r_0, is directly related to ion transmission efficiency.

By substituting (8.2.2) in (8.2.1), one can show that for $n > 2$ (higher order multipoles) the equations of motion (8.2.1) are nonlinear and coupled. It has been shown by Dawson and Whetten[13] that the stability of the ion motion for $n > 2$ multipoles depends strongly on the initial conditions (ion position velocity and r.f. phase). The generalization of stability parameters (a, q) for multipoles of $n > 2$ has been attempted.[7,14] Numerical simulations of ion trajectories in ideal r.f. hexapoles and octapoles were reported by Hägg and Szabo who confirmed that the shape of the stability diagrams in the (a, q) plane is dependent on the initial conditions.[15,16] Results of such simulations for ions starting at displacement $r = 0.1r_0$ presented in the form of a stability diagram for a hexapole are shown in Figure 8.11. Three areas of stability are shown, namely, I (stable), II (partially stable) and III (unstable). The corresponding stability diagram for octopoles has similar areas of partial stability. The interesting fact is that the regions of stability for both hexapoles and octopoles propagate to very high q (crossing the $a = 0$ axis at approximately $q = 5.7$ and 61, respectively, for ions starting at $r = 0.1r_0$).[15,16] Although these numbers are derived from simulations for specific initial conditions and will be different for other conditions, it is a general trend of higher order multipoles to have broader (along the q axis) stability regions. This makes hexapoles and octopoles convenient ion guides, since this property means that they can transmit a large range of masses simultaneously (since q is inversely proportional to the ion m/z). Also, simultaneous retention in the field of high m/z precursor ions and low m/z product ions makes higher order multipoles convenient CID cells in tandem organic mass spectrometry, where analysis of the fragment ions produced in the cell is necessary. It is

apparent from Hägg and Szabo's results that the instability of the ion in higher order multipoles is always partial, i.e. dependent on the initial conditions. Even for ions corresponding to region III (unstable), there were stable trajectories observed for some initial displacements. Thus, there is no unconditional low-mass cut-off (at a set a, q) for higher order multipoles, although for ions with particular initial characteristics, mass-dependent instability can be induced by operating at appropriately high q. Note that the potential function Φ describes the potential in the multipole, using the approximation that space charge effects are negligible. The space charge effects on ion trajectories can be considered negligible provided the perveance of the beam, P (defined by equation (8.2.5) and adopted from Szilagyi[78]), is below $10^{-8}\mathrm{A/V}^{3/2}$:

$$P = IU^{-3/2}(M/m_e)^{1/2} < 10^{-8}A/V^{3/2}, \tag{8.2.5}$$

where I is the ion beam current (in ampere, A), $U = KE/e$ (in volt, V), KE is the ion kinetic energy (in electron volt, eV), e is the elementary ion charge (in coulomb, C), M is ion mass and m_e is mass of electron. Under nonpressurized conditions, a cell which is operated as a collision-free ion guide transmits typically a current of 16 nA (10^{11} ions/s of predominantly Ar^+) at an ion kinetic energy of 20 eV. The perveance for such a beam $P = 5 \times 10^{-8}A/V^{3/2}$, i.e. the space charge effects have to be considered. From Douglas'[79] estimations of charge storage limit of a linear quadrupole (based on an effective potential approximation valid generally only for $q < 0.3$) it can be shown that for $q = 0.2, m/z = 40$, $f = 1$ MHz, maximum charge density is 7×10^{-13} C/cm^3. For an ion beam of KE = 20 eV occupying total cross section of a quadrupole of $r_0 = 4.1$ mm this charge density limit translates to an ion flux of 2×10^{12} ions/s, indicating that the maximum charge density is not reached in a nonpressurized cell that transmits an ion beam typical for ICP-MS even at a relatively low q. If the ion kinetic energy is significantly reduced (by energy damping through collisions with cell gas) and the charge is conserved, maximum charge density may potentially be reached and space charge effects may significantly affect ion trajectories. The effects of space charge in pressurized multipoles are discussed later.

8.2.3 Processes induced by collisions

Two distinct classes of processes induced by collisions between ions and target gas atoms/molecules (neutrals) can be considered, namely (i) momentum and energy transfer processes (or collisional processes) and (ii) particle transfer processes (or ion–molecule reactions). The former are elastic and/or inelastic processes in which the identity of the ion does not change. Momentum and energy transfer processes may result in damping of the ion kinetic energy, collisional focusing and excitation of the internal degrees of freedom of the ion or the neutral. Excitation can further cause a collision induced decomposition (see for example, the review by K.R. Jennings[17]) of an ion or a neutral. Momentum transfer can also change the radial component of ion velocity in such a way that its displacement and velocity fall out of the acceptance of the r.f. multipole. Such collisions then cause ions to be lost from the multipole (observed as a reduction in the ion signal), a process often referred to as scattering loss.

The second process, particle transfer, results in a change of identity of the ion (for example, the ion can be neutralized by electron transfer from the neutral, and an ion of new identity is produced from the neutral). Momentum and energy transfer processes can have a significant impact on the outcome of ion–molecule reactions (for example, endothermic reactions discussed in Part 8.1 of Chapter 8 by Koyanagi can potentially be promoted if enough energy is transferred during the collision).

8.2.3.1 Momentum and energy transfer

In an elastic (no internal excitation) nonreactive collision of an ion of mass m_1 and kinetic energy E_1 (in the laboratory frame of reference, LAB) with a stagnant ($E_2 = 0$) neutral of mass m_2, the energies after collision are given by[18]

$$E_1^{'} = E_1 \left[\frac{m_1^2 + m_2^2}{(m_1 + m_2)^2} + \frac{2m_1 m_2}{(m_1 + m_2)^2} \cos\theta_{CM} \right] \tag{8.2.6}$$

where θ_{CM} is the scattering angle in the center-of-mass coordinate, and

$$E_2^{'} = E_1 - E_1^{'} = \Delta E_1 \tag{8.2.7}$$

The average scattering angle, $|\theta_{CM}|$, is equal to $\pi/2$ rad, so from (8.2.6) and (8.2.7) , the average ion energy loss per collision is

$$\frac{\overline{\Delta E_1}}{E_1} = \frac{2m_1 m_2}{(m_1 + m_2)^2} \tag{8.2.8}$$

As $m_2 \to 0$, no energy transfer takes place. At $m_2 = m_1$, the collision partners exit with equal energy, so that the incident ion loses half of its initial energy. Multiple collisions of the ion result in a sequential loss of kinetic energy together with a reduction in the width and magnitude of the kinetic energy distribution (referred to as collisional energy relaxation, or energy damping).[18] A larger neutral/ion mass ratio increases the rate of energy relaxation of the ion. Concurrent with energy damping, several processes that have important ramifications in the operation of pressurized multipoles occur. These are (i) an increase in collision cross section and increase in probability of ion–molecule reactions, (ii) collisional focusing of ion trajectories toward the axis, (iii) an increase in space charge density in the cell, (iv) an increase in ion transit time through the multipole and (v) temporal homogenization of ion density fluctuations.

Before considering these processes, it is worth recalling that the extent to which a process depletes the ion population can be described by Beer's law:

$$I = I_0 e^{-n} \tag{8.2.9}$$

where I_0 describes the initial population of the ions, I describes the population of those ions that 'survived' the process and n is the number of the process enabling events. For example, four reactive collisions of charge exchange (i.e. reaction probability on collision = 1) cause depletion of the original ion population by a factor of $e^4 = 55$. If the probability of reaction on each collision is 0.1 and nonreactive collisions do not cause other kinds of ion loss, the same degree of depletion requires 40 collisions.

8.2.3.2 Increase of the ion–molecule collision cross section at lower kinetic energies

At high energy, the interaction of the ion with the neutral is sufficiently short and the collision cross section, σ_{HS}, can be described by the hard-sphere collision model and determined via the sum of the physical radii r_1 and r_2 of the collision partners, using the equation $\sigma_{HS} = \pi(r_1 + r_2)^2$. As the energy is decreased, the ion interactions with permanent and induced dipole moments of the molecule start to define the interaction potential, and at some energy (generally

considered as <1 eV) ion–dipole interaction becomes dominant.[19] The cross section of such an interaction can be calculated using different models, of which average dipole orientation (ADO[20]) or its refinement AADO (which includes angular momentum transfer[21]) is a good enough approximation for all practical purposes.

Figure 8.12 shows evaluated (ADO) cross section of collisions of Ar^+ with H_2, CH_4 and NH_3 as a function of kinetic energy. At low energy, the interaction is defined by charge–dipole interaction and the cross section is many times larger than hard-sphere cross section. Under these conditions, the difference in collision cross sections of atomic and polyatomic ions of the same charge and mass is diminished.

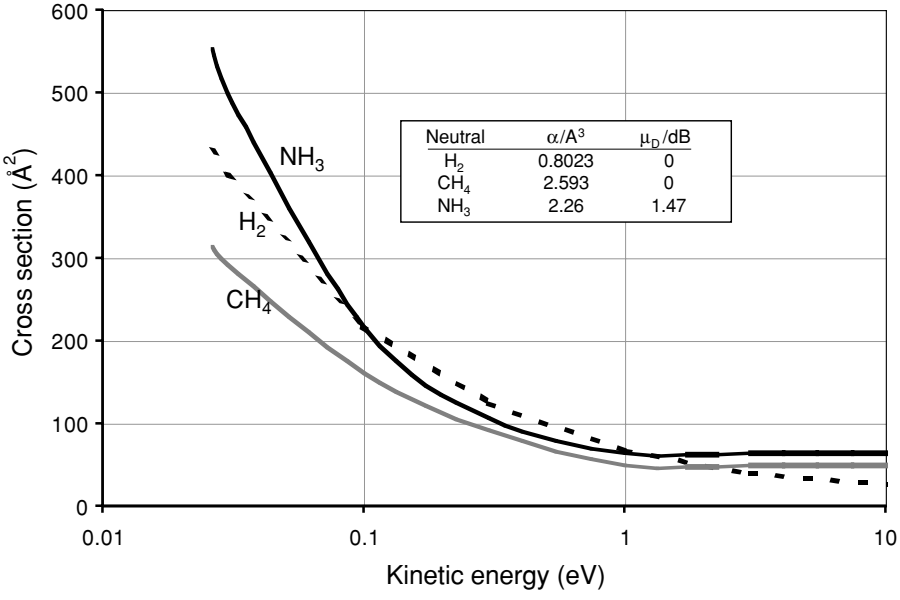

Figure 8.12 Calculated collision cross sections as a function of ion kinetic energy.

8.2.3.3 Collisional focusing

As the ion energies are relaxed, collisional focusing improves the transmission efficiency through an on-axis exit aperture of the cell.[18] This is accompanied by substantial changes in the kinetic energy distributions of the ions. In the usual instance for ICP-MS, the axial kinetic energy of the ion is significantly greater than the radial energy, and the first step in the collisional damping of the ion's axial energy is transfer to (excitation of) the ion's radial energy. In an electrostatic collision cell (without r.f. applied), this radial excitation would likely lead to an increased probability of ion loss. In the r.f. driven collision cell, the restoring force provided by the r.f. drives the radially excited ions back toward the cell axis. Transfer of energy from axial to radial excitation continues until the two modes approach equilibrium, and then both translational degrees of freedom relax together. Eventually, the axial energy should be completely relaxed to near-thermal, under which conditions the ion motion in the axial direction is close to Brownian.

However, the radial energy does not completely relax, as it continues to be excited to a degree by the r.f. field. At pseudo-equilibrium, the total ion energy is distributed between the radial (x, y) and axial degrees of freedom, with radial degrees being dominant due to the r.f. excitation. The magnitude of the total pseudo-equilibrium energy is a function of the operating parameters (a, q), and of the number of collisions per r.f. cycle (and is thus dependent on the pressure and r.f. frequency). Figure 8.13 shows the energy transfer and relaxation due to collisions in an r.f. quadrupole calculated with the model of thermalization described by *Baranov and Tanner*.[22] For typical operating conditions ($q < 0.6$), the kinetic energy at pseudo-equilibrium is of the order of 0.1 eV, which is near-thermal. As can be seen from Figure 8.14, ion displacement collapses due to collisional relaxation toward the quadrupole axis, resulting in better ion transmission. At low q and $a = 0$, an improvement in ion transmission of up to a factor of 5 for nonreactive ions has been reported.[23] Similar effects were reported for a r.f. only hexapole collision and reaction cell.[24] It should be noted that the factors of improvement of ion transmission due to collisional focusing strongly depend on the characteristics of the ion beam extracted from the plasma, such that beams with a larger energy spread will show more improvement in transmission due to collisional focusing than energetically 'tight' ion beams.[25] Improvement of ion transmission can also be accompanied by improvement of the abundance sensitivity of the quadrupole analyzer used downstream of the pressurized multipole.[26,75,76] As the resolution of the quadrupole is related to the square of the number of cycles the ions spend in the field,[9] the contribution of high energy ions to the peak width at its base is reduced through collisional damping of the ion energies. The degree of abundance sensitivity improvement due to collisional focusing then depends on the initial energy spread of the ion beam.

8.2.3.4 Temporal homogenization, axial fields and space charge effects

Energy damping to levels close to the thermal condition means that the ion simply executes an essentially 'random walk' through the cell. As a result, the time distribution of ion arrival (at the detector) can be modified, resulting in collisional broadening of transient signals. Such broadening has been used for converting the pulsed beam of MALDI-generated ions into a quasi-continuous beam in a collisional damping ion transmission device described by Krutchinski *et al*.[27] The degree of collisional broadening in a pressurized r.f. quadrupole depends on the pole bias, the entrance and exit aperture potentials, the Mathieu parameter q of the quadrupole and the properties of the target gas. For the same target thickness (which is a value calculated as the length of the cell multiplied by the number density of the collision gas), polyatomic gases generally produce more significant broadening due to their higher polarizability (and thus larger (thermal) collision cross section) and also greater energy deposition into internal degrees of freedom (Figure 8.15). Since the broadening occurs on the scale of several milliseconds, fluctuations of the ion current at high and intermediate frequencies are smoothed,[28] resulting in better correlation of sequentially sampled ion populations (if a sequential mass analyzer is employed). This results in an improvement in the short-term precision of isotope ratio measurements. It has been shown that collisional homogenization allows isotope ratio internal precision performance equivalent to the counting statistics limit to be achieved.[28] When atomic gases are used for collisional homogenization, the number of collisions needed to achieve sufficient (on a millisecond scale) temporal homogenization can be large enough to induce scattering losses of the ion signal, so that the absolute value of the ratio precision (for a given sample concentration), although being

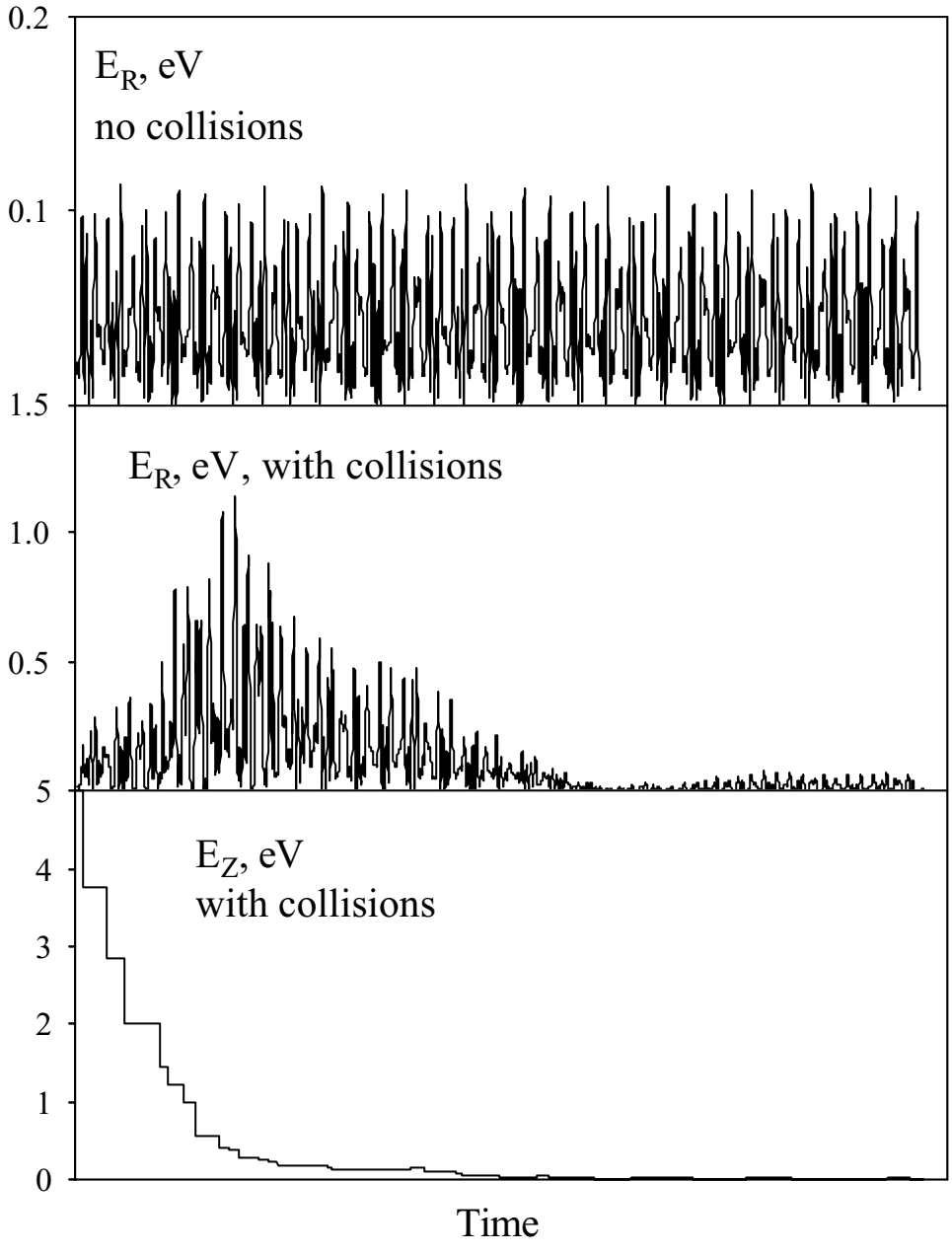

Figure 8.13 Calculated radial and axial energy as a function of time for an ion in an r.f. only quadrupole. The upper figure shows the radial energy in the absence of collisions. The middle figure shows the initial increase and then decay of radial energy resulting from conversion of axial energy to radial energy, followed by an approach to equilibrium, caused by collisions with the gas. The lower figure shows the decay of the axial energy caused by collisions with the gas. (Adapted with permission from reference 22.)

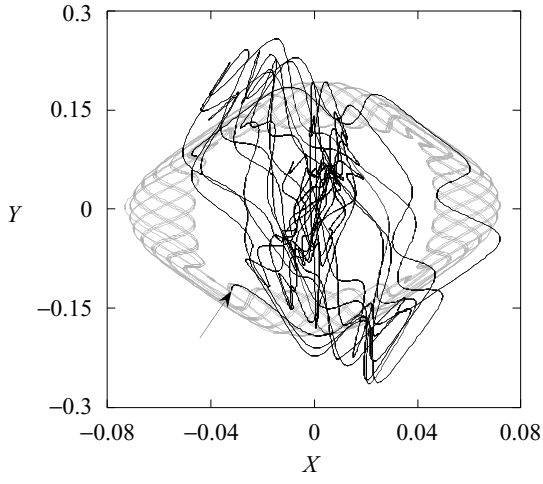

Figure 8.14 Calculated trajectories with (darker shaded) and without (lighter shaded) collisions for an ion in a quadrupole r.f. field at (a, q) = (0, 0.4). The same initial modeling conditions were used, and the initial displacement is indicated by the arrow. Without collisions, the ion trajectory is bound by an outside and an inside surface, as a result of the requirement for conservation of the total energy and the angular momentum, respectively. Collisions involve transfer of energy (axial to radial, and ion to neutral), and the ion displacement initially increases and then collapses toward the quadrupole axis. (Adapted with permission from reference 22.)

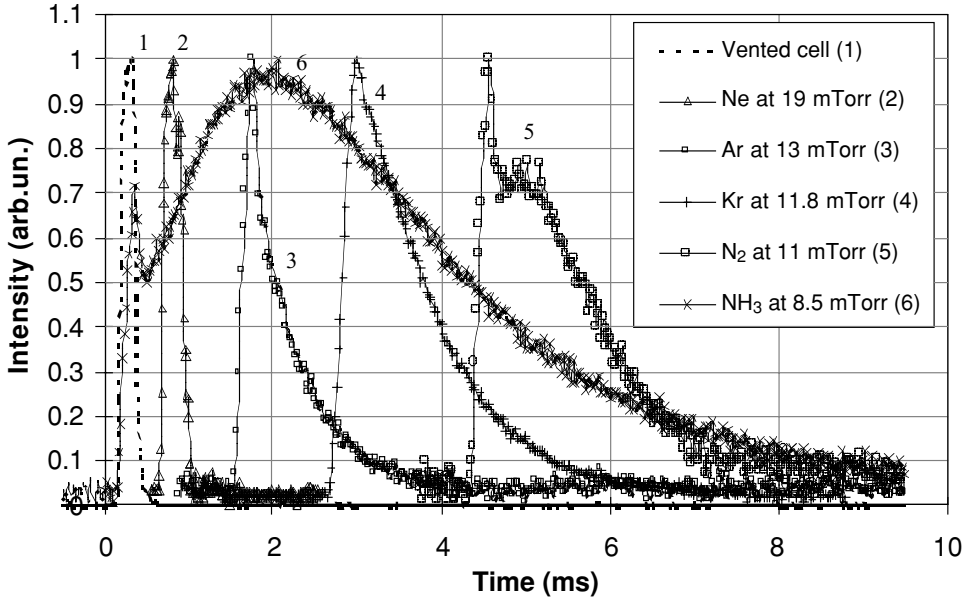

Figure 8.15 $^{107}Ag^{+}$ ion packets collisional broadening in the DRC with different target gasses. The plots (except for 1 and 6) are shifted along the horizontal axis for clarity of displaying, and horizontal coordinate does not reflect ion drift time from $t = 0$. (Adapted with permission from reference 28.)

at its statistical limit, may not improve compared to nonpressurized cell operation. The most practical case of collisional homogenization is with the use of a polyatomic gas for the chemical resolution of isobaric interferences. Use of a reactive gas such as NH_3 allows simultaneous reactive removal of isobaric interferences and collisional homogenization of the analyte ion populations. It has been shown that the ratios of the normally interfered isotopes ^{54}Fe, ^{56}Fe and ^{57}Fe can be measured by quadrupole ICP-MS at the counting statistics limited internal precision of 0.05–0.1% for a sample concentration of 50 ng/mL.[28]

The ion transmission after collisional damping depends largely on the gas drift through the cell. If the gas (1 sccm (standard cm^3/min)) is introduced coaxially (annular area 0.06 cm^2) with the ion beam at the entrance of the cell (pressure $\sim$ 20 mTorr), the gas will have a velocity at the entrance of the cell that is of the order of 10^4cm/s. While the gas flow will also be damped in collisions, the impulse of the gas at the entrance of the cell induces a net drift velocity through the cell, and even the thermalized ions will be carried with this gas flow, transiting the cell in a few milliseconds. Hence, the flow of gas can provide an axial flow field that assists with ion penetration into the cell. Ion penetration into the cell and exit from the cell are also assisted by axial electric fields established by the entrance and exit aperture potentials. At the entrance region the field is usually retarding for the positive ions inside the cell, and at the exit, accelerating (since the entrance and exit aperture plates are usually biased negatively compared to the V_{CRO}). Those fields are most effective over a length of the order of r_0.[29] Note that when ions are slowed down by collisions to an ion energy of $\sim$0.2 eV, the perveance is of the order of 10^{-5} $A/V^{3/2}$, i.e. much higher than 10^{-8} space charge negligibility limit. Hence the combined axial field consists of gas flow field, entrance and exit fields and significant space charge field.

One of the effects of slowing the ions by collisions is increased transit time through the cell, which can increase the settling time of the cell. This phenomenon is known in organic mass spectrometry, where the pressurized collision cell is usually capacitively coupled to a mass filter. When the mass filter is adjusted to a different mass, a certain time is required for the ions to redistribute within the collision cell. If the measurement is taken within too short a time after the mass change, either or both of two observations might be made: (i) the apparent ion signal corresponding to the new mass may be suppressed because these ions have not yet 'filled' the collision cell, or (ii) ions that were present in the prior state are still apparent (sometimes referred to as 'cross-talk'). The matter has been discussed by several authors for organic MS/MS applications.[30,31] Lock and Dyer[31] showed that a voltage gradient applied along the cell can alleviate the cross-talk effect. Several means to provide this axial field have been proposed and/or evaluated.[31–34] In one of them,[32,34] the axial field is generated by the addition of auxiliary electrodes inserted between the rods of the cell quadrupole and tapered in the longitudinal direction.

The cross-talk effect is somewhat different in ICP-MS. Due to high ion current, space charge density in the cell (which is increased dramatically by the energy damping process) has a significant effect on ion transmission. When an abrupt change of the cell electrical parameters occurs (for example, the mass transmission window is changed), space charge distribution in the cell may change (for example, due to a change in stability of the dominant ion in the r.f. field) and need to be re-established to a new steady state in order for ion transmission to stabilize. Hattendorf and Günther[35] showed that cell stabilization can take several hundreds of milliseconds. For a mass jump from $m/z = 238$ to $m/z = 24$, the $^{24}Mg^+$ signal was suppressed when insufficient time was allowed for cell stabilization, as shown in Figure 8.16 (a). Increasing the dwell (measurement) time, which essentially allows longer time for stabilization of the ion distribution in the cell following the mass adjustment, eliminated the signal suppression. When

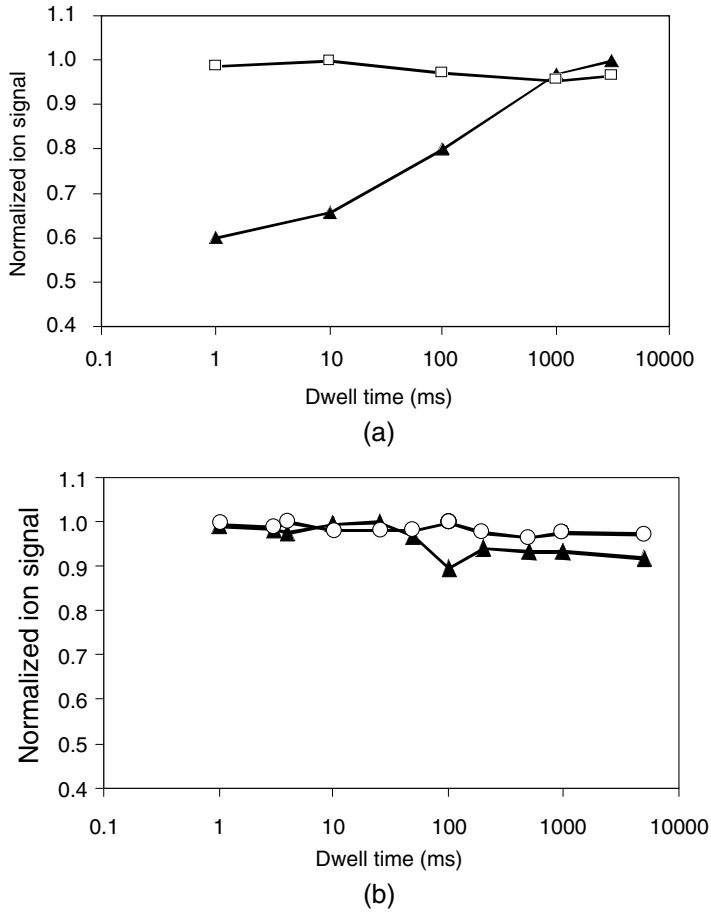

Figure 8.16 Normalized ion signals for $^{24}Mg^+$ (▲) and $^{238}U^+$ (□) or $^{208}Pb^+$ (○) with dwell time in a pressurized cell. The ions were sequentially measured with a settling time of 3 ms with $(a, q) = (0, 0.45)$. Accordingly, Mg^+ was rejected from the cell (outside the bandpass) when the high mass ion was measured. (a) Without axial field, the Mg^+ signal is significantly suppressed at short dwell times (insufficient time to re-establish the ion distribution within the cell). (b) With an axial field, the ion distribution within the cell is rapidly re-established and the measured signals are largely independent of the dwell time. (Figure (a) adapted with permission from reference 35.)

the cell of the same instrument was equipped with auxiliary electrodes for axial field generation,[36] the need for additional recovery time following a mass jump from high mass was eliminated, and the cell could be operated with a settling time similar to that of the quadrupole analyzer and short dwell times, as shown in Figure 8.16(b). The principal benefits of incorporating a DC axial field obtained for a thermal (or near-thermal) cell include compression of the transit time distribution (allowing for more rapid scanning), suppression of clustering reactions (because these reactions are very sensitive to the effective collision temperature) and increase of the space charge limit.[36] It is our understanding that the space charge limit is increased most significantly in the entrance region of the cell, where some ions after the first collision are turned around by

the retarding entrance field (thus passing through the zero-kinetic energy turn-around point). It has been our experience that the most robust operation of the cell (i.e. no concomitant element effects observed) is achieved when the axial field is of the order of 40 V/m (corresponding to an applied DC potential of $\geq +350$ V). It has been shown that the additional axial field electrodes have little effect on the stability characteristics of the r.f. field of the pressurized quadrupole cell.[6] Hence, the bandpass control of sequential chemistry (discussed below) in a quadrupole reaction cell is not compromised.

8.2.3.5 Collision induced decomposition and kinetic energy discrimination

The relaxation of ion kinetic energies to levels close to thermal values insures that endothermic processes are not promoted. However, before thermalization occurs, endothermic processes may take place. One of the endothermic processes that can potentially occur is collision induced decomposition (CID). The maximum energy ($E_{\text{int,max}}$) that can be converted into internal degrees of freedom of the polyatomic ion (of mass m_1) on collision can be calculated as[37]

$$E_{\text{int,max}} = E_{\text{CM}} = E_1 \frac{m_2}{m_1 + m_2} \tag{8.2.10}$$

For single collision dissociation, it is thus desirable to have a neutral having as large a mass (m_2) as possible, and as high a value of kinetic energy (E_1) as is practical. For dissociation of strongly bound polyatomic ions, for example O_2^+ (bond dissociation energy 6.66 eV),[38] which interferes with the detection of S^+, conditions under which single collision dissociation is promoted may also cause loss of S^+ via charge exchange if the collision gas atoms/molecules have an ionization energy, IE, that is lower than the sum of the collision energy and ionization energy of the analyte. In this example, the high ionization energy of sulfur (10.36 eV) limits the choice of collision gases to neon (IE = 21.56 eV) and helium (IE = 24.59 eV). With these gases, minimum LAB energies (E_{LAB}) of 17.3 eV and 60 eV, respectively, are required to provide the possibility of a single-collision dissociation of $^{16}O_2^+$. Unfortunately, under such conditions, scattering losses are significant.[1,39]

Sequential pumping of vibrational degrees of freedom by collisions at low energy ('slow heating') has been found to be efficient for fragmentation of organic molecular ions in tandem mass spectrometry employing ion traps.[40] However, the extent of interference removal required in ICP-MS is usually much higher than the extent of fragmentation required in organic mass spectrometry. To achieve three orders of magnitude suppression, at least seven dissociating collisions – or 70 or more total collisions, if each collision delivers 10% or less of the required internal excitation – are needed. Such collision numbers are not usually accessible in linear r.f. multipoles and, furthermore, if a high neutral number density is used to attempt to facilitate such high number of collisions, significant scattering loss of the analyte ions occurs, making pumped dissociation of strongly bound polyatomics impractical.

Another suprathermal process that is used for suppression of unwanted ions is kinetic energy discrimination (KED). It was first used by *Rowan and Houk* to prevent polyatomic ions formed in-cell from entering the analyzer,[2] by providing a potential energy barrier between the cell and the analyzer. Ions formed in the cell originate at a potential that is close to the cell rod bias (V_{CRO}) and have little residual kinetic energy (which may be acquired from the precursor ion).

Thus, setting the analyzer rod bias (V_{QRO}) to a high enough value should stop in-cell formed ions from being transmitted through the analyzer. The efficiency of KED separation of the analyte and ions formed in-cell depends on the number of collisions that are used to suppress an unwanted in-plasma formed interference and on the rate of collisional cooling of the analyte ion. A large extent (several orders of magnitude) of interference suppression requires a high number of collisions (especially when the interfering ion is not removed on every collision). High mass and polyatomic gases induce rapid cooling of the analyte ions. The resulting overlap in energy distributions for the analyte and in-cell produced ions causes KED suppression of both.[6]

Recently, KED has been used for suppression of polyatomic ions formed in the plasma.[44] This approach is based on the difference of collision cross section between polyatomic and atomic ions at suprarthermal energies. In our example, $^{16}O_2^+$ and S^+ diameters can be estimated (from $O–O^+$ bond length and radii of O and S)[45] as 2.5 Å and 1.9 Å, respectively . If Xe is used as the collision gas (atomic radius 1.24 Å), hard-sphere collision cross sections can be calculated as $\sigma_{HS}(O_2^+) = 19.5$ Å^2 and $\sigma_{HS}(S^+) = 15$ Å^2. Thus, for the same target thickness, $^{16}O_2^+$ on average will experience 1.3 times more collisions than $^{32}S^+$, losing more translational energy per unit of ion trajectory length. As was discussed above, at low kinetic energy, the collision cross section is dependent on the ion charge and reduced mass rather than the size of the ion. Thus the KED approach can only be used under cell conditions that yield a low number of collisions, before significant energy damping occurs and analyte and interference ions can no longer be distinguished on the basis of their energy differences.

Suppression of $^{16}O_2^+$ interference on S^+ discussed by *Pröfrock et al.*,[42] can result from several processes, namely CID, KED and charge exchange reactions. CID could be utilized in collisions with xenon (the maximum energy that can be converted into excitation of the $O–O^+$ bond on the first collision at $E_{LAB} = 44$ eV used in this work was $E_{int,max.} = E_{CM} = 35.4$ eV), and KED was utilized using a 37 eV post-cell energy barrier between the analyzer quadrupole and the cell multipole. Charge exchange for O_2^+ with Xe is nearly resonant ($\Delta H_r = 0.06$ eV) and under thermal conditions is determined to occur in around 6% of collisions (based on data from Anicich's reaction kinetics index[43] and from the calculated ADO capture rate[20]). It should be noted that the improvement of the $^{32}S^+$ detection limit (to 3.2 μg/L) measured with the cell pressurized with Xe, using a post-cell energy barrier of 37 eV, was accompanied by a deterioration in the detection limits for ^{52}Cr, ^{55}Mn, ^{58}Ni, ^{59}Co, ^{63}Cu, ^{66}Zn and ^{114}Cd by factors of 44, 625, 33, 50, 100, 20 and 330 compared to nonpressurized mode, respectively.[42] Such deterioration was caused by collisional scattering at a relatively high E_{LAB} and due to energy discrimination of elemental ions that had lost energy in collisions with the heavy collision gas used in this work.

Yamada *et al.*[44] used a lighter gas (He) to study CID of ArH^+ and the relatively weakly bound polyatomic ions Ar_2^+ and ArO^+ (bond dissociation energies $D_0 = 4.0$; 1.2 and 0.56 eV, respectively[38]) introduced into an octopole cell at LAB energy of 17.5 eV. They observed virtually no suppression of ArH^+ and Ar_2^+, ruling out dissociation via accumulation of internal excitation in multiple collisions. A three-fold reduction in the ArO^+ signal was observed at a very low flow of He, consistent with single collision dissociation (which should reduce the ArO^+ population by $e^1 = 2.7$ times). It is interesting that, according to equation (8.2.8), the average loss of the kinetic energy of an ion of $m_1 = 56$ in collisions with He ($m_2 = 4$) is only 12.4% of the incident energy per collision, which means that even the fourth collision should have $E_{CM} > D_0 = 0.6$ eV. Thus, theoretically, the ArO^+ population should be depleted by CID by a factor of $e^4 = 55$ even without accounting for internal excitation of the ion by the preceding collisions. However, this was not observed.[44] Use of CID in a collision cell pressurized with He, with no post-cell

energy barrier applied, was reported by Niemelä *et al.*[46] as being inefficient for suppression of ArO^+, $ArCl^+$ and $Ar_2{}^+$. More efficient CID has been claimed for weakly bound $NaAr^+$ ($D_0 = 0.2$ eV) and $MgAr^+$ ($D_0 = 0.16$ eV) in collisions with He at approximately 16–18 eV LAB energy.[47] The data were collected with a 1 eV post-cell energy barrier, making it difficult to estimate the net effect of the CID. A combination of KED and CID for suppression of the $ArCl^+$ interference on As^+ has been reported to provide a blank equivalent concentration (BEC) of ~60 ng/L for As, allowing detection of As^{III}, As^V and monomethylarsonic acid at detection limits of 22, 21 and 25 ng/L, in a sample containing 2% chloride.[48] In this work, an ion exclusion chromatograph coupled to the ICP-MS was used, with the collision cell pressurized with He at 6 mL/min. A helium-flow-dependent fall in the As^+ signal was also observed, probably as a result of KED suppression of analyte transmission, with ~100 counts per second per 1 μg/L As^+ signal being obtained at the helium flow that produced the optimum BEC.

It has been shown[6] that for KED to be efficient, ion thermalization should not occur, otherwise both analyte ions and unwanted ions assume similar energy distributions and cannot be separated by the post-cell energy barrier. This necessarily limits the number of collisions that can be used, and hence the extent of collisional or reactive suppression of interferences. When a high number of collisions are used even with low mass gas, significant suppression of analyte ions is observed. McCurdy and Woods[81] have reported suppression of ClO^+ and $ClOH^+$, ArC^+ interferences on V^+ and Cr^+, respectively, by more than four orders of magnitude due to KED utilized by 3.5 eV post-cell energy barrier when collisions with nonreactive gas (He at 5.5 mL/min) were used. Analyte ion suppression of more than two orders of magnitude was observed under these conditions.

A different way of kinetic energy discrimination has been discussed by Bandura *et al.*[36] This approach was based on establishing a continuous retarding field inside the pressurized cell. Application of an in-cell continuous retarding field decelerates and scatters slower polyatomic ions, before the energies of the analyte ions are equilibrated by collisions to the point of being indistinguishable from those of the in-cell produced ions. As a result, a higher discrimination efficiency of in-cell produced $^{127}IH_2{}^+$ compared to post-cell KED was observed. When O_2 was used as the reaction/collision gas for suppression of $^{129}Xe^+$, in-cell energy discrimination reduced the background at $m/z = 129$ to around 3×10^{-8} of the $^{127}I^+$ signal.

The difference in ionic radii between isobaric isotopes of different elements is too small for KED to be practical for suppression of atomic isobaric interferences. In our view, the most universal method of interference suppression in ICP-MS is chemical resolution via ion–molecule reactions, since it can provide a way of resolving both atomic and polyatomic interferences, and can be more specific compared to the use of energy and momentum transfer processes.

Under multiple collision conditions, most of the collisions occur after the ion energy is damped to close to thermal values, and the inherent specificity of thermal chemistry can be used for chemical resolution of isobaric ions. Appropriate reaction gases can be simply selected on the basis of the available thermal rate constant data for ion–molecule reactions of the analyte ion and interference ion. These rate constants have for the most part been measured under thermal conditions using techniques such as flowing afterglow[49] and the selected ion flow tube (as discussed earlier in this chapter).[50,51] For exothermic reactions that do not have large activation barriers, reaction cross sections usually maximize at thermal or close to thermal energy, as has been shown in several studies using the guided ion beam method.[52] Introduction of ions into the collision cell at high kinetic energy, although potentially increasing the dissociation cross section for some weakly bound polyatomic ions, will also necessarily increase the energy available for promoting ion–molecule reactions that are endothermic or have an activation barrier (in some

cases undesirable reactions of the analyte ions). This can reduce the specificity and efficiency of the selected reaction chemistry.

8.2.4 Applications of ion–molecule reactions used in ICP-MS

The most abundant interferences in ICP-MS are usually those caused by argide ions (Ar^+ and ArX^+, where X may be Ar, O, Cl, C, N and so on). The corresponding ArX neutrals (if they existed) would likely have relatively high ionization potentials. Hence, in ICP-MS applications, the most useful type of reactions is charge transfer of the type:

$$A^+ + B \rightarrow B^+ + A \text{ (for example: } Ar^+ + NH_3 \rightarrow {NH_3}^+ + Ar) \quad (8.2.11)$$

which in the case of argide ions is highly exothermic for a wide variety of neutrals. The enthalpy of a charge transfer reaction, ΔH_r, can be approximately calculated as the difference between the ionization potentials of the reactants. Thus the selection of the candidate reaction gas is relatively simple: its ionization potential has to be higher than that of the analyte but lower than that of the interference. A convenient way to qualitatively visualize charge transfer energetics is to plot the ionization potential against mass (or identity) of the analyte and interference ions and overlay on this plot horizontal lines that correspond to the ionization potential of candidate reaction gases, as shown in Figure 8.17. The (positive) ions of species that are above a particular candidate gas line in Figure 8.17 are exothermic in charge transfer reactions with that gas, and those that are below the line are endothermic. For example, Ar^+ and ${N_2}^+$ are exothermic for charge transfer with H_2, but all other ions shown are endothermic. On the other hand, charge

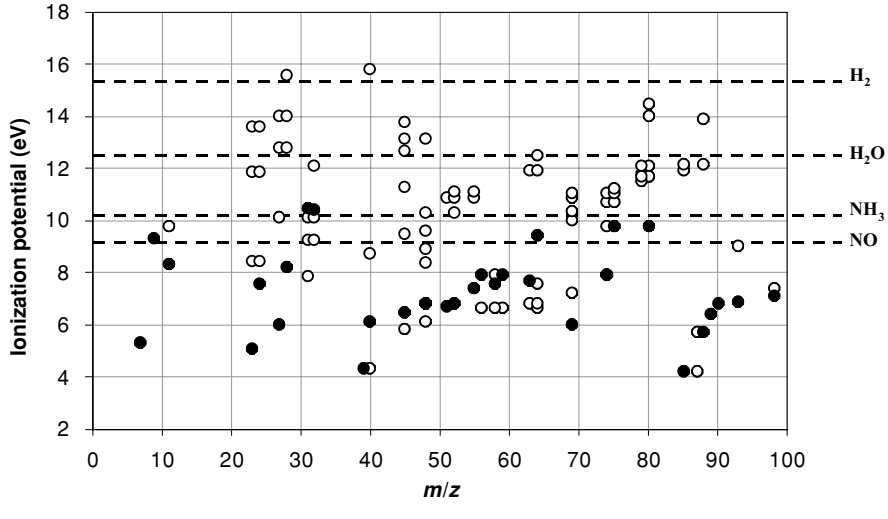

Figure 8.17 Ionization potentials of some atomic ions and potential atomic and polyatomic interference ions. Solid circles represent the atomic ions usually of interest in inorganic analysis, and the open circles represent argon, argide, oxide, hydroxide and other potential interference ions. The horizontal lines indicate the ionization potentials of candidate reaction gases. Ions above a horizontal line are thermodynamically favorable (though not necessarily kinetically favorable) for charge transfer with the indicated neutral.

exchange with NO is exothermic for the majority of interference ions and endothermic for most analyte ions (although other reactions, such as oxidation, can be exothermic and thus have to be considered when assessing the candidate gas).

At thermal energies, electron transfer is efficient even for highly exothermic (and thus far from resonant) reactions – in contrast with charge transfer at high energies, which is relatively inefficient at non-resonant conditions. For example, Xe^+ charge transfer with NH_3 (ionization potential of NH_3 is 1.97 eV lower than that of Xe) is highly exothermic and occurs under thermal conditions of SIFT at around 52% of the collision rate, while with O_2 it is nearly resonant ($\Delta H_r = -0.06$ eV) but occurs only at around 2% of the collision rate (data from Anicich[43] and ADO calculations[20]).

The efficiency of charge-exchange reactions can be very high. Tanner *et al*. have demonstrated eight orders of magnitude of suppression of Ar^+ in reactions with ammonia, while retaining $^{40}Ca^+$ sensitivity,[23] and more than five orders of magnitude of suppression of ArO^+ while retaining Fe^+ sensitivity has been reported by Kawabata *et al.*[53] This high efficiency allows achievement of the very low BECs and detection limits required for analysis of materials used in semiconductor manufacturing (see Chapter 9). BECs for normally interfered $^{39}K^+$ (interfered by $^{38}ArH^+$), $^{40}Ca^+$($^{40}Ar^+$), $^{52}Cr^+$($^{40}Ar^{12}C^+$), Mn^+($^{40}Ar^{15}N^+$), $^{56}Fe^+$($^{40}Ar^{16}O^+$) of 2.6, 0.10, 0.12, 0.54, 0.40 ng/L, respectively, have been measured for deionized water, with corresponding 3σ detection limits of 0.27, 0.10, 0.12, 0.17 and 0.12 ng/L, respectively, obtained using 1 s integration per isotope. These results were achieved using standard sample introduction apparatus under normal (hot) plasma conditions. Charge exchange of Ar_2^+ with CH_4 has been used by Sloth and Larsen for detection of all six isotopes of Se, with a BEC and detection limit for $^{80}Se^+$ of ~30 ng/L and 6 ng/L, respectively.[54] Reduction of Ar_2^+ signal intensity by five orders of magnitude with concomitant (due to collisional focusing) increase of ^{80}Se+ signal was reported.

It is apparent from Figure 8.17 that there are cases for which an appropriate reaction gas which will remove the interference by charge exchange without also reacting with the analyte is not (currently) available. This is a particular problem when the ionization potential of the interference is lower than that of the analyte. One case that is important in practice is the interference of CaO^+ on Fe^+ (ionization potentials of the neutrals are 6.7 eV and 7.9 eV, respectively). In these cases, other types of reactions have to be applied. One such reaction is hydrogen-containing particle transfer. There are several types of this reaction:

$$\text{Proton transfer: } AH^+ + B \rightarrow BH^+ + A \text{ (e.g. } ArH^+ + H_2 \rightarrow H_3^+ + Ar) \quad (8.2.12)$$

Hydrogen atom transfer:

$$A^+ + BH \rightarrow AH^+ + B \text{ (e.g. } CaO^+ + CH_4 \rightarrow CaOH^+ + CH_3) \quad (8.2.13)$$

Hydride ion (H^-) transfer:

$$A^+ + BH \rightarrow B^+ + AH \text{ (e.g. } Br^+ + CH_4 \rightarrow CH_3^+ + HBr) \quad (8.2.14)$$

Reaction (8.2.13) was used for enhanced detection of Fe, Ni and Zn in a Ca-rich matrix.[55] In this study, the BEC for $^{56}Fe^+$, $^{58}Ni^+$ and $^{64}Zn^+$ in the presence of 200 mg/L Ca in the samples was shown to improve by factors of 2200, 20 and 15, respectively, when the reaction cell was pressurized with methane compared to the standard (non-pressurized) mode. The major application of hydrogen-containing particle transfer is in suppression of Ar^+, Ar_2^+ and ArO^+ in collision cells pressurized with hydrogen. Detection limits of 42 ng/L for Ca, 17 ng/L for ^{56}Fe and 1.4 ng/L for ^{80}Se have been reported by Boulyga *et al.*[56] for a hexapole collision cell

instrument pressurized with helium and hydrogen (the numbers quoted here are for the standard Meinhard nebulizer). Improvement of the ^{56}Fe detection limit to 9 ng/L in ultrapure water has been shown for an octopole reaction cell pressurized with hydrogen.[47] Using the same approach, a BEC of 60 ng/L, with a 3σ detection limit (12 s signal integration time) of 14 ng/L for ^{80}Se was obtained by Reyes *et al.*[57]

Niemelä *et al.*[46] reported on the determination of iron, selenium and arsenic using a hexapole collision cell instrument pressurized with a mixture of hydrogen (7%) in helium, without the use of post-cell energy discrimination. Detection limits for ^{56}Fe and ^{80}Se of 15.5 ng/L and 29 ng/L in 2% v/v nitric acid were obtained under optimized conditions. A detection limit for As in 5% v/v hydrochloric acid of 153 ng/L was achieved.

So-called 'condensation reactions' involving transfer of atoms other than hydrogen, and often resulting in rearrangement to a thermodynamically stable form, are also an option. Oxidation reactions (reaction (8.2.15)) are promising due to their apparent selectivity and speed:

$$A^+ + BO \rightarrow AO^+ + B \text{ (e.g. } Ba^+ + N_2O \rightarrow BaO^+ + N_2) \quad (8.2.15)$$

Atom transfer is very sensitive to the thermodynamic stabilities of the product oxide ions and of the residual (neutral) leaving molecule. For example, N_2O and CO_2 are attractive as oxidizing agents because the corresponding reactions include N_2 and CO as leaving groups, which are very stable. O_2 and NO have different applications because a very strong A^+–O bond is required for these reactions to proceed. As a result, reactions with O_2 and NO can be very specifically selected to oxidize the chosen cations. Selection of a candidate oxidation gas can be made on the basis of the oxygen-atom affinity of the ion of interest and of the leaving group. Conveniently, O-atom affinities of many cations are shown in a periodic chart available from the web page of Diethard K. Bohme's research group at York University, Toronto, Canada.[58] Figure 8.18 shows O-atom affinities for atomic isobars of naturally occurring isotopes as well as affinities of potential leaving groups for oxidation by O_2, NO, N_2O, NO_2 and CO_2, calculated using the gas phase ion and neutral thermochemical data collected by Lias *et al.*[77] Atomic ions shown above the horizontal line of a particular gas have a thermodynamically allowed (exothermic) oxidation channel with

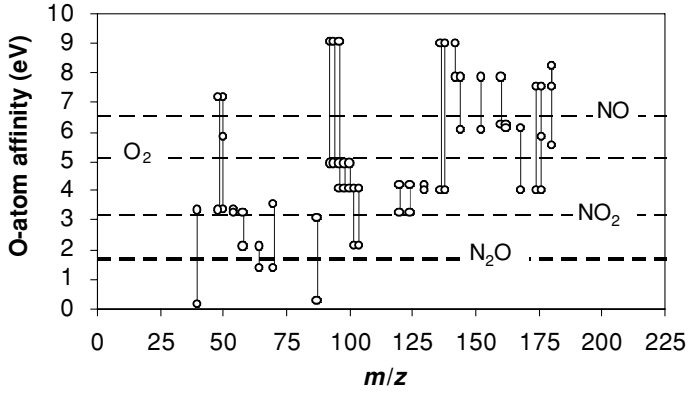

Figure 8.18 O-atom affinities of positive ions of naturally occurring atomic isobars (open circles, isobars connected by vertical lines) and of the leaving groups of oxidation reactions with NO, O_2, NO_2 and N_2O (horizontal dotted lines). Oxidation of ions above a horizontal line corresponding to a particular gas is thermodynamically allowed.

the gas. Eiden *et al.*[5] have demonstrated selective oxidation of Zr^+ and Y^+ while leaving the Sr^+ signal unaffected, using O_2 as the collision cell gas, suggesting that very low levels of ^{90}Sr may be detected in the presence of ^{90}Zr and ^{90}Y. In contrast selective oxidation of Sr^+ in reactions with N_2O has been shown to allow detection of ^{87}Sr (as $^{87}SrO^+$) in the presence of ^{87} Rb ($^{87}Rb^+$ did not react with N_2O).[19] Recently, the feasibility of selective oxidation reactions has been shown for resolving the atomic isobars $^{135,137}Cs/^{135,137}Ba$ (Ba^+ was reduced by five orders of magnitude by oxidation with N_2O while Cs^+ did not react), $^{176}Lu/^{176}Hf$ (Hf^+ was reduced by 3.5 orders of magnitude by oxidation with NO while Lu^+ did not react) and $^{187}Os/^{187}Re$ (Os^+ was removed by six orders of magnitude by oxidation with N_2O while the more slowly reacting Re^+ was suppressed only two-fold).[59] Selective oxidation has also been used for the detection of As in the presence of high chloride levels.[60] In this work, As^+ was quantitatively oxidized by reaction with O_2 and detected as AsO^+, while the interfering $ArCl^+$ was not oxidized. In this way, single digit ng/L detection limits could be achieved for As in 10% HCl (v/v)[60]. Since the potentially interfering Zr^+ ion (at $m/z = 91$) reacts quickly and efficiently with O_2,[5,19] this method can tolerate a relatively high (up to five orders of magnitude higher than As) abundance of Zr in the samples.

Oxidation of ZrO^+, NbO^+, HfO^+ and TaO^+ to higher oxides in reactions with oxygen was used by Simpson *et al.* to effect improved detection of Ag, Au, Pd and Pt.[61]

Another O-atom transfer reaction is O-atom abstraction of the type:

$$AO^+ + B \rightarrow A^+ + BO \text{ (e.g. } ArO^+ + CO \rightarrow Ar^+ + CO_2) \tag{8.2.16}$$

The high O-atom affinity of CO and thermodynamic stability of the leaving neutral (CO_2) allows O-atom abstraction even from relatively strongly bound oxide cations, such as CaO^+. A BEC of ~100 ng/L for $^{56}Fe^+$ in the presence of 10 mg/L of Ca has been demonstrated[19] and this approach has also been used for measurement of Fe isotope ratios in human serum.[62]

Since oxygen is not monoisotopic, isotope ratios of the product oxide ions are complicated by the superimposition of oxygen's isotope ratios. To avoid this complication, Vanhaecke *et al.*[63] used monoisotopic F-atom transfer to selectively fluorinate Sr^+ in reactions with CH_3F, in order to overcome isobaric overlap of ^{87}Rb on ^{87}Sr. The Sr isotope ratios were then measured as SrF^+ ratios. The Sr/Rb age of magmatic rocks determined using this approach was in close correlation with TIMS data. Kinetic isotope effects (discussed in Section 8.1.8 of Part 8.1 of Chapter 8) and mass bias were compensated for by using matrix-matched external isotope standard.

Another type of reaction – association, or clustering – generally plays a negative role in reaction cell ion chemistry when applied to ICP-MS. Ammonia is a good clustering ligand, which means that it forms adducts readily and hence can be an analytical complication unless steps are taken to control the appearance of cluster ions. This type of reaction is also observed with water molecules. The presence of water in the cell can also facilitate oxidation, hydroxylation, H-atom transfer, proton transfer or electron-transfer reactions. The effects of adventitious water in an ICP-ion trap pressurized with He were observed in the early work of Koppenaal's group.[3,4] They found that Ar^+ suppression in the ion trap was attributable to possible reactions with water impurities in the He collision gas used in the study. Dexter *et al.*[64] reported domination of the cell chemistry by water when an unreactive gas such as He was used. Thus, tight control of water impurities in the cell is desirable, especially when low reactivity gases are used. One of the sources of water and other impurities in the collision/reaction cell is gas flow from the ion source, since ICP can contain atomized water which contributes H and O to the bulk argon at up to 17%.[65] The expansion of gas from the ICP imparts a directed supersonic flow which can produce an impact pressure at the

cell entrance (usually coaxially aligned with the expanding flow). This impact pressure is of the order of 10–50 mTorr, depending on the flow characteristics and the position of the cell.[66] If the cell pressure is lower than the impact pressure, source gas flows into the cell, modifying the composition of the cell gas. Positioning of the cell at right angles to the expansion or disruption of the directed flow by the use of a chicane lens or a shadow-stop in front of the cell reduces the impact pressure and minimizes incursion of the source gas into the cell.[6,67] Yamada *et al.*[44] reported that reactivity of Ar^+ toward H_2 was not affected by cell gas impurities, when they were introduced into the cell gas supply. Yet increased formation of CeO^+ in the cell was observed when even highest purity H_2 (99.9998%) was used. Hattendorf[68] observed significant reduction in LaO^+ when H_2 (99.9993% purity) was introduced into the reaction cell through a gas purifier.

In some limited cases, clustering reactions can be used for detecting an interfered analyte ion as its cluster ion at a less interfered m/z. Kawabata and Kishi[53] used $TiNH^+ \cdot (NH_3)_3$ at $m/z = 114$ and $Zn^+ \cdot (NH_3)_3$ at $m/z = 115$ for detection of Ti and Zn in 10% sulfuric acid, obtaining BECs of 4.4 ng/L and 14 ng/L, and detection limits of 3.4 ng/L and 16 ng/L, respectively. Liu and Jiang[69] used $Cu^+(NH_3)_n$ clusters to detect Cu in fly ash in the presence of high Ti in the samples.

More complicated multistep ion–molecule reactions may be observed in the reaction cell environment, but are usually considered as a nuisance. This does not mean that they cannot be used to advantage, for example the sequential oxidation of Sr^+ by N_2O followed by H-atom transfer from CH_4[19] or the sequential oxidation of Os^+ to OsO_4 in reactions with N_2O that allow simultaneous detection of ^{187}Re and ^{187}Os.[59] Since KED equally discriminates against unwanted in-cell formed polyatomic ions and against desired product ions (e.g. oxidation, fluorination or clustering in the instances where these are promoted for analytical benefit), it does not facilitate measurement of an analyte as a product ion. This approach can potentially be applied if the cell is operated under non-KED conditions, with the quadrupole bias potential set more negative than the collision cell bias. However, sequential chemistry of lighter-than-the-analyte precursor ions will produce new ions that in the absence of the kinetic energy barrier downstream of the cell will be transmitted through the analyzer and may elevate chemical background at the m/z of the analyte production.

So far we have considered only one method of suppressing unwanted ions formed in the cell, namely KED (originally demonstrated by Rowan and Houk in 1989).[2] It is important to realize that the application of the kinetic energy barrier does not affect the formation of the new 'interference ions' within the cell; they are formed at the same rate, independent of the difference between V_{CRO} and V_{QRO}. Only the transmission of these ions through the mass filter, and hence their detection, is affected by the energy barrier, which in many cases reduces the new interferences by 1–2 orders of magnitude.[56] A different method of control of ions produced in the cell is dynamic bandpass tuning suggested by Tanner and Baranov.[70] It is based on the unique (among r.f. multipoles) properties of the quadrupole field, in which for a given V_{rf}, V_{dc} and ω, the stability of the ion trajectory depends only on the m/z of the ion and does not depend on its initial displacement or field phase, as discussed above.

8.2.4.1 Dynamic bandpass control of unwanted collision/reaction cell chemistry

The extent of interference suppression required in ICP-MS is very high, the most obvious example being the $^{40}Ar^+$ interference on $^{40}Ca^+$. Since ICP is used to analyze samples with as high as 0.3% (m/v) total dissolved solids, interferences from polyatomic ions originating from the sample and plasma matrix can be of the same order. Certainly, many collisions are required to suppress

such large interferences. A simple calculation from Beer's law (equation (8.2.9)) shows that to achieve five orders of magnitude interference suppression, at least 12 reactive collisions are required (more if the interference ion is not removed on every collision). A high ion current (10^{11}–10^{12} ions/s) constantly enters the cell, with the majority of ions being of relatively high ionization potential (Ar^+ and ArH^+). Under these conditions, sequential reaction chemistry takes place. Even if the gas is nonreactive, reactive contaminants present in the gas will be ionized by the high Ar^+, ArH^+ current and will participate in multiple secondary reactions. If a charge-conservative multipole ion guide with a wide stability region is used as a reaction cell, the newly formed ionized species are stable in the rf field and the initial ion current is distributed among many m/z channels, thereby producing a ubiquitous chemical background. Let us consider for example the use of CH_4 as the reaction gas for removal of the Ar^+ interference on Ca^+. The primary reaction:

$$\begin{aligned} Ar^+ + CH_4 &\rightarrow CH_2{}^+ + Ar + H_2 \\ &\rightarrow CH_3{}^+ + Ar + H \\ &\rightarrow CH_4{}^+ + Ar \end{aligned} \tag{8.2.17}$$

is fast ($k_r/k_c = 0.88$, where k_r is the reaction rate constant[43] and k_c is the collision rate constant calculated via ADO model[20]), and the branching ratios are 0.12, 0.85 and 0.03, respectively[43]. The product ions, if retained in the cell, react further with CH_4, producing $C_2H_4{}^+$, $C_2H_5{}^+$ and $CH_5{}^+$ ions. $CH_2{}^+$ is also known to react with water producing CH_2OH^+. $C_2H_5{}^+$ reacts further with CH_4, producing $C_3H_7{}^+$.[43] Concurrently, other plasma or sample matrix ions can react with CH_4 and impurities. For example, $C_2{}^+$ is reactive toward CH_4 producing $C_3H_3{}^+$.[43] Reactions of plasma and sample matrix ions with impurities of acetone or acid vapors can produce higher mass $C_3H_7O^+$ ions or MOH^+ ions (e.g. $Mg^+ + HNO_3 \rightarrow MgOH^+ + NO_2$). A rich array of hydrocarbon and other ions can thus be produced in the cell. Figure 8.19(b) shows overlaid mass spectra for high purity water and a solution containing 1 μg/L each of K, Ca, Cr, Mn, Fe, Ni, Cu, Zn, Se and Sr collected with a quadrupole cell pressurized with methane and operated in a manner that allows simultaneous stability of precursors and products of the reactions discussed above (at quadrupole stability parameters $a = 0$ and $q = 0.15$) and with no post-cell energy discrimination. While some of the argide ions are substantially reduced in intensity compared to a standard (no gas in the cell) mode (e.g. $Ar_2{}^+$, see Figure 8.19(a) for the standard mode spectra), a generally elevated spectral background is observed. The detection power of the instrument for the elements that are not normally interfered is therefore degraded (thus making analysis of noninterfered isotopes in pressurized mode, which can enhance sensitivity via collisional focusing, impractical). Moreover, despite the fast removal of Ar^+ by the primary reaction, ultimate detection at $m/z = 40$ cannot be achieved due to a combination of polyatomic ions produced in the cell contributing to the background. Tanner *et al.*[6] have shown that CH_4 is very efficient in damping ion kinetic energy and causes overlap of cell-formed and analyte ion energy distributions, even at a relatively low gas pressure in the cell. This limits the applicability of KED and since only low flows of methane can be used if KED is employed, the extent of suppression of the original interferences using this gas is also reduced.

In most practical cases, the sequential chemistry involves primary ions (either plasma-based matrix ions or primary in-cell produced product ions) that are significantly different in m/z compared to the analyte ion of interest. Our example of sequential (in time) chemistry with CH_4 can be presented on the mass scale, as shown in Figure 8.20. Let us assume that the instrument is operated in such a manner that when the analyzing quadrupole downstream of the cell is detecting $^{40}Ca^+$ ions, the Mathieu parameters of the quadrupole field of the cell are set

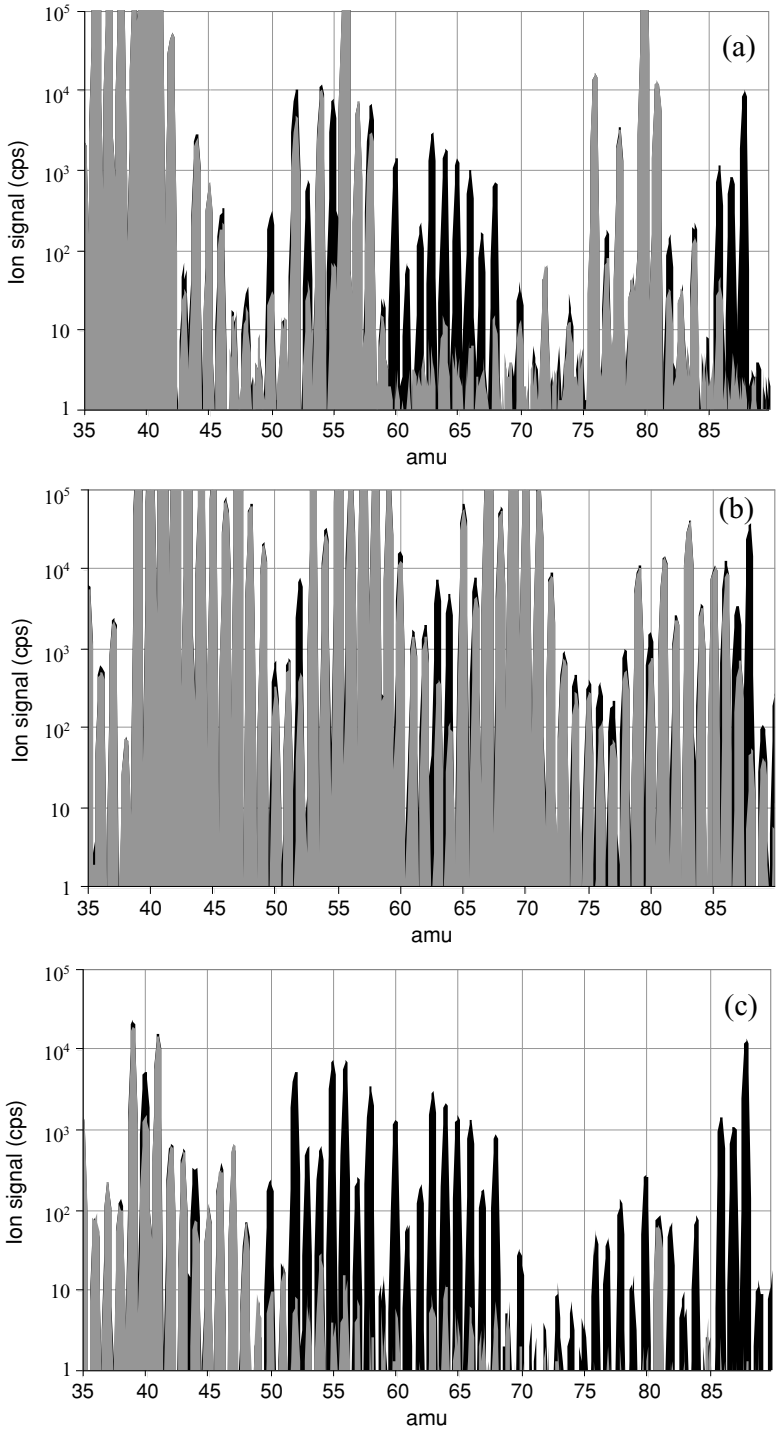

Figure 8.19 Mass spectra obtained on Elan DRC^{plus} instrument for 1 μg/L each of K, Ca, Cr, Mn, Fe, Ni, Cu, Zn, Se and Sr collected with a quadrupole cell vented to a pressure of $\sim 10^{-5}$ Torr (a); pressurized with methane and operated in a manner that allows simultaneous stability of precursors and products (at quadrupole stability parameters $a = 0$ and $q = 0.15$) and with no post-cell energy discrimination (b); and at the same methane pressure and conditions but at $(a, q) = (0, 0.7)$, i.e. with narrower mass bandpass of the quadrupole (c).

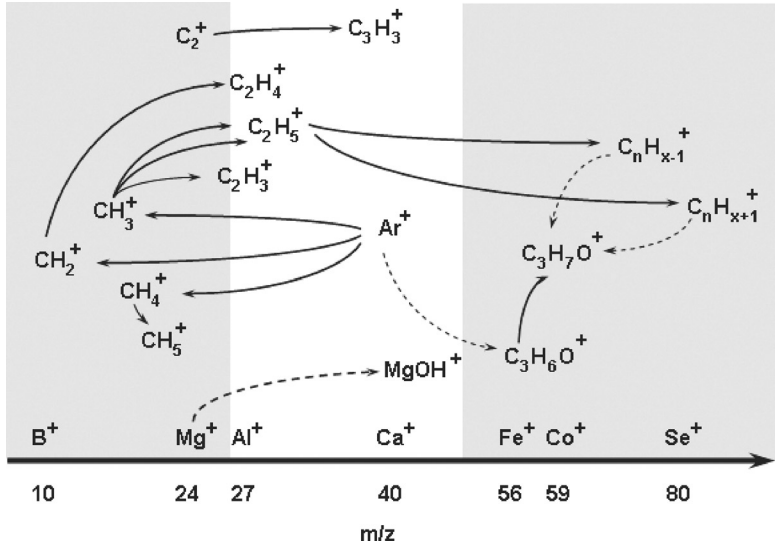

Figure 8.20 Sequential chemistry with methane (solid lines) and impurities (dotted lines) plotted along the m/z scale. When $m/z = 40$ is transmitted through the quadrupole field at Mathieu parameters $a = 0.1$, $q = 0.5$, the ions of $m/z < 26$ or $m/z > 49$ (inside shaded area) are unstable in the quadrupole field, and the chemistry with these ions is aborted.

to $(a, q) = (0.1, 0.5)$ for $m/z = 40$. Referring to equations (8.2.4) one can calculate what Mathieu parameters will correspond to $m/z = 26$ and $m/z = 49$. For these masses, the parameter values are (0.15, 0.77) and (0.082, 0.41), respectively. Consulting the quadrupole stability diagram (Figure 8.10) one can establish that these points are just outside the boundaries of stability. Operating the quadrupole cell at $(a, q) = (0.1, 0.5)$ for $m/z = 40$ establishes a mass bandpass around the ion of interest (Ca^+) of approximately 23 amu width. This bandpass is wide enough not to affect the analyte transmission significantly. All ions of $m/z < 26$ or $m/z > 49$ (in gray areas in Figure 8.20) are unstable in the quadrupole and are thus ejected from the field. This ejection occurs within 1–2 r.f. cycles which, for a cell operated at a few hundred kHz frequency, is much shorter than the average time between collisions at a few mTorr pressure. The sequential chemistry is thus aborted very quickly, so significant levels of further, new unwanted polyatomic ions are not formed in the cell.

When the analyte of a different m/z (e.g. $^{59}Co^+$) is measured at the same Mathieu parameter values of $(a, q) = (0.1, 0.5)$, the bandpass is established from $m/z = 38$ to $m/z = 72$, and some of the precursors of $C_3H_7O^+$ are ejected from the cell. If ejection of Ar^+ is desirable during measurements of $m/z = 59$, a higher operating point inside the stability diagram can be used. Operation of the cell in a manner that moves the mass bandpass in concert with the mass scan of the analyzing quadrupole establishes a dynamic bandpass. It is this approach that the Dynamic Reaction Cell™ (DRC™) employs to automatically tune the bandpass in concert with the analyzer, according to user-selectable (a, q) values that can be the same or different for different analytes. To minimize the effect of r.f. heating on the ion energies, the amplitude of the r.f. voltage is kept constant and relatively low, and bandpass tuning is accomplished by adjusting the r.f. frequency. Figure 8.19(c) shows a mass spectrum obtained under the same

conditions as that in Figure 8.19(b), but with the cell operated at $(a, q) = (0, 0.7)$ for every mass channel. The increase in low-mass cut-off clarifies the mass spectrum, while the sensitivity of the analyte ions remains comparable to that of Figures 8.19(a) and 8.19(b). The reduction of plasma-derived interference ions is obtained through reactions with methane, and the secondary reaction chemistry is aborted as a result of rejection of lower mass ions that otherwise would react, leading to the ubiquitous background seen in Figure 8.19(b).

In most practical cases, operation at $(a, q) = (0, 0.5)$, while being close to the optimum for transmission of the analyte ions in pressurized mode, is sufficient to abort unwanted sequential chemistry. In some cases, however, a narrower bandpass is required. Hattendorf *et al.*[71] investigated the problem of the $CrAr^+$ interference on isotopes of Nb^+ and Zr^+. Reactions with hydrogen suppressed metal argide ions, allowing detection of Nb and Zr in Cr-rich matrix, with estimated detection limits of 2 ng/g and 5 ng/g, respectively, in pure chromium metal. Rejection of the precursors of potential in-cell formed $CrO_2{}^+$ and CrO_2H^+ interferences on Zr^+ was accomplished using $(a, q) = (0, 0.7)$ when measuring $^{90}Zr^+$ and $^{93}Nb^+$, establishing a low-mass cut-off at $m/z = 70$ and 73, respectively.

Olesik *et al.*[72] investigated the removal of ClO^+ by charge exchange with ammonia for the detection of $^{51}V^+$, and in doing so, observed an additional interference on ^{51}V, due to minor production of $ClNH_2{}^+$ in the cell from Cl^+. Operation of the cell at $(a, q) = (0, 0.65)$ provided ejection of Cl^+ from the cell, thereby aborting formation of the new interference while reducing the original interference to a BEC of 3 ng/L.

Operation of the DRC with narrower bandpass affects analyte transmission: 3- to 10-fold suppression of analyte signals have been reported[68,70] for the pressurized cell operated at $(a, q) = (0, 0.75)$ when compared to operation at optimum parameters $(a, q) = (0, 0.45)$. Collisional focusing partially compensates for these transmission losses. The net effect – many orders of magnitude suppression of in-cell formed ions with some three-fold reduction of analyte transmission (as shown in Figures 8.19(a)–8.19(c)) – results in many orders of magnitude improved detection limits compared to wide open bandpass operation. Hattendorf and Günther[68] studied suppression of in-cell generated interferences in a reaction cell ICP-MS by bandpass tuning and KED and concluded that elemental sensitivity is higher by approximately a factor of 5 and the abundance of the cell produced ions is reduced more efficiently with bandpass tuning approach compared to KED.

In some cases, metal-oxide interferences can be suppressed by using oxidation reactions to form higher oxides.[61] If the reaction gas that is used for oxidation of the metal oxide ion also reacts with the metal ion at a significant rate, the original metal-oxide interference will be produced in the cell and exacerbate the challenge. The quadrupole cell can be operated at a relatively high q in order to eject the precursor metal ion and prevent formation of the interference. In the case of $a = 0$, the minimum value of q required to prevent oxide formation can be calculated as

$$q \geq 0.908 \frac{m - 16}{m}, \tag{8.2.18}$$

where m is m/z of the analyte ion, and $q = 0.908$ is the intersection of the stability region with axis $a = 0$ (see Figure 8.10). We observed suppression of the MoO^+ interference on Cd^+ by oxidation of MoO^+ to MoO_2^+ in reactions with O_2 (occurring almost at the collision rate[73]), while formation of new MoO^+ in the cell was prevented by operating at $(a, q) = (0, 0.75)$. This allowed reduction of the MoO^+ background at $m/z = 114$ to ~1 ng/L BEC for Cd, at 10 µg/L Mo in the sample.[6]

Obviously, if product ions are to be used as analyte ions, both precursor and product have to be stable in the quadrupole field. At $a = 0$ this requirement can be satisfied at

$$q \leq 0.908\frac{m_1}{m_2}, \tag{8.2.19}$$

where m_1 and m_2 are the m/z of the precursor ion and the product analyte ion, respectively. Since optimum transmission in a pressurized quadrupole cell occurs at $q_{opt} = 0.45–0.55$,[23] a compromise condition for the best transmission of both precursor and product ions can be found (for $a = 0$) at

$$q_{m_2} = \frac{m_1 + m_2}{2m_2} q_{opt}. \tag{8.2.20}$$

8.2.4.2 Method development

If the analytes are not interfered at the level of interest, operating in conventional (no gas in the cell) mode is advisable. The experienced user could take advantage of collisional focusing in order to improve sensitivity; however, as was discussed above, cell gas impurities can produce new interferences even when low reactivity gases are used. Increased oxide formation in reactions with impurities has been reported for collision cells pressurized with He[44,62] and H_2[68]. Collisional focusing[18] can improve sensitivity by as much as a factor of 5 or 10. [23,24,74] For maximum collisional focusing effect use of post-cell KED is not desirable because enhancement in sensitivity can be compromised by the energy discrimination of the analyte. Jakubowski *et al.*[24] have shown that increase in sensitivity of 5–8 fold with no KED was reduced to 1.5–3 fold with KED. One more fact has to be considered when using collisional focusing: there is an inherent mass bias associated with thermal collision rate constant inverse proportionality to the square root of the reduced mass[20,21]. This mass bias, however, in most cases is smaller than mass biases related to other processes in ICP-MS (space charge suppression of lighter ions, mass dependence of electrostatic optics focusing due to the ion kinetic energy dependence on mass). Since the collisional mass bias is monotonic with mass, usual methods of internal or external mass bias correction can be used in isotope ratio measurements. Other advantages of the collisional mode of operation are the improved precision of isotope ratio measurements and improved abundance sensitivity discussed above, also useful when detecting noninterfered analytes. The mass bias effects for reactive ions are discussed in detail by Koyanagi *et al.* in this book. Vanhaecke *et al.* found that the most accurate compensation for the mass bias of the product ion isotope ratios is achieved when the sample matrix of the external isotope ratio standard is similar to that of the sample[80].

If the analyte of interest is interfered, reactive gas or nonreactive collision gas has to be used. In many applications, only few analytes require interference background suppression, while most analytes can be successfully analyzed without cell gas. Most of the commercially available cell-based instruments allow operation without any gas introduced into the cell, switching between nonpressurized and pressurized modes within the same sample measurement. There are many publications on practical methods developed for detection of interfered analytes, that describe the use of NH_3, CH_4, H_2, He + H_2 mixture, O_2, He and other gases. To be of greatest value, these methods should be transferable between instruments and laboratories. Certainly, achievable detection limits will depend on the level of contamination of the method blank, which may differ between the laboratories, but the method itself should be consistent. One of the potential

inconsistencies can be attributed to the composition of the cell gas, since the role of impurities in suppression of interferences can be significant for low reactivity or inert gases. This may result in significant variability of the optimum cell gas flows and parameters that affect transmission of in-cell produced ions. Olesik *et al.*[72] has recently published a list of reaction gases and optimum parameters used in different applications of the quadrupole reaction cell. Strategies of method development for the quadrupole reaction cell equipped instruments have been described by Tanner *et al.*,[6] Hattendorf and Günther[82] and by Olesik *et al.*[72]. The cited papers, as well as the author's experience, are related to the method development for the dynamic reaction cell ICP-MS. Certain principles, though, may be applicable, in the author's view, to method development for other cell-based instruments.

Method development comprises stages of identifying suitable reaction gas, finding its optimum flow and determining optimum values of parameters that control production or transmission of unwanted in-cell produced ions. In all cases, optimization should be performed on true sample blanks and spiked by the element of interest standards. Suppression of the interfering ion by many orders of magnitude cannot be used as a criterion for successful interference rejection. Net analyte signal should not decay with gas flow faster than the standard deviation of the background signal – otherwise no improvement of detection limit will be achieved.

Selection of gas can be based on known reactivities of the interfering ions and analytes toward the gas, which generally correlate with published reaction rate constants (see reference 43 for most recent compilation). Ideally, the interfering ion should be very reactive with the candidate gas and the analyte should not react at all. If such a gas is found, method development is relatively straightforward and consists of the following steps.

(1) Select 'intermediate' value of in-cell produced ion control parameter. In the case of DRC, $q = 0.45 - 0.5$ is a good starting point. For other instruments, where transmission of in-cell produced ions is controlled by KED, a post-cell potential energy barrier of 1–2 eV is commonly used.
(2) Measure signal at the analyte m/z as a function of the cell gas flow (so-called cell gas profile) for the blank. If there is interest in determining the products of the reaction, signals at other m/z can also be monitored. It is advisable to run a mass scan in the mass range that includes the analyte m/z and the potential products m/z. If true blank is impractical to obtain, the sample of interest can be used as a blank. If the (interference) signal is decayed significantly, then step 2 can be taken. If not, another reaction gas should be used.
(3) Measure cell gas profile for the standard (spiked blank or the sample spiked with the analyte).
(4) Plot and analyze the data (in many cases this can be done within the software of the instrument). In most cases when the interference reacts fast and the analyte signal is nonreactive, the signals measured will look similar to the signals measured at $m/z = 112$, shown as an example in Figure 8.21. At low cell gas flow the signal is dominated by the interference and decays fast with increase of the gas flow until most of interfering species ($^{96}MoO^+$ in our example) are removed in reaction with the cell gas (O_2) to a different m/z (to $MoO_2{}^+$, not shown). Then the rate of signal decay measured for the spiked blank changes: remaining ions (predominantly $^{112}Cd^+$) react with the cell gas at a different rate. Background equivalent concentration is calculated as a ratio of the background to the net sensitivity and plotted as a function of the cell gas flow. Detection limit is calculated (or estimated) and plotted as a function of the gas flow. The cell gas flow at which the detection limit is at a minimum is then selected as a preliminary optimum.

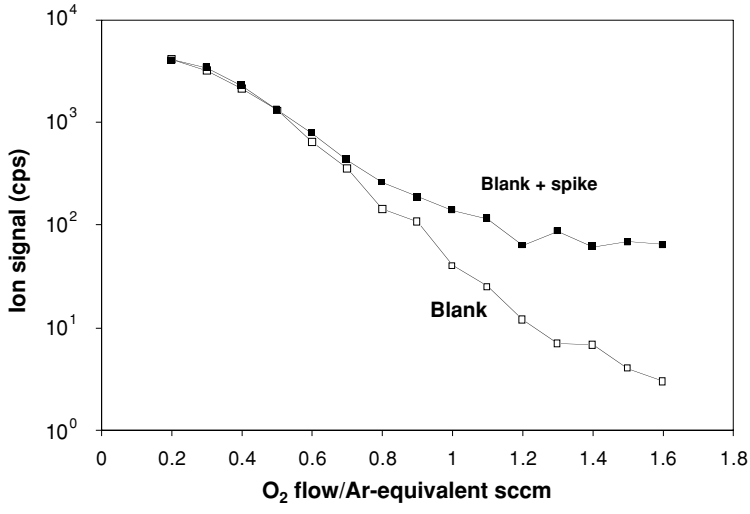

Figure 8.21 Cell gas profiles at $m/z = 112$ for the blank (Mo at 10 ng/mL) and the blank spiked with 10 pg/mL Cd.

(5) At the selected cell gas flow, signals for the blank and for the spiked blank are measured as a function of the q (for the DRC) or the KED barrier (for other cells). The q (or the KED barrier) at which the detection limit is at minimum can then be selected as an optimum for the control of in-cell produced ions. In some cases use of nonzero a may prove to be useful since the stability boundaries of the pressurized quadrupole are somewhat sharper at $a > 0$[6].

(6) Cell gas profiles can be measured again at the optimum q (or KED barrier) to obtain a more precise optimum of the cell gas flow.

(7) If the instrument software permits selection of individual values of the cell gas flow and (a, q) or KED barrier for the analytes in the same method run, each analyte can be measured at its optimum and ultimate detection limits can be achieved. Alternatively, compromise conditions of universal gas flow and other parameters can be chosen – with trade-offs in detection capabilities.

For the strategy of method development when the analyte ions are reacted to form new ions at a less interfered m/z, the reader is referred to the work of Olesik *et al*[72].

8.2.5 Summary and future perspectives

In a relatively short time since their commercial introduction, r.f.-driven reaction cells and collision cells became a major every-day tool for reducing spectral interferences in ICP-MS. The major process that enables interference suppression in such cells is ion–molecule reactions that can be selected on the basis of different reactivities of an interference and an analyte. In many practical cases, many orders of magnitude of interference suppression are achieved through multiple reactive collisions of the interfering ions with a reaction gas. Efficient primary ion–molecule chemistry that distinguishes analyte ions from plasma-based interference ions is accompanied by efficient secondary reactions that create new isobaric interferences within the

cell. Two methods are commonly used to suppress the appearance of these secondary interference ions: post-cell kinetic energy discrimination and in-cell bandpassing. The former is most efficient when the number of collisions is low enough to allow in-plasma produced ions to retain some of their initial kinetic energy. Operation of the cell with a bandpass that suppresses the formation of the secondary interference ions by excluding their precursors from the cell allows operation of the cell under many-collision conditions, optimizing the efficiency of the primary chemistry. Rf-driven reaction and collision cells in ICP-MS are best suited for quadrupole mass analyzers. Since individual cell gas flows and in-cell produced ion control parameters are often needed for each analyte for achieving ultimate detection limits, use of 'simultaneous' analyzers will probably be possible only with some compromise in interference suppression or for a limited number of isotopes. High ion energy, which is needed in sector field instruments for achieving their exceptional sensitivity, may limit application of cells to suppression of interfering ions that have vastly different reactivity toward a reaction gas compared to analyte ions, since input of high kinetic energy into reaction enthalpy may result in loss of reaction specificity. In our view, this will delay – if not restrict – appearance of the 'dream instrument', a high sensitivity high resolution multicollector sector instrument with reaction cell.

Acknowledgments

The author thanks Dr Scott D. Tanner and Dr Vladimir I. Baranov, without whom this overview would be impossible to write and whose data, ideas and thoughts are used throughout.

References

1. Douglas, D. J. (1989) Some current perspectives on ICP-MS. *Can. J. Spectrosc.*, **34**, 38–49.
2. Rowan, J. T. and Houk, R. S. (1989) Attenuation of polyatomic ion interferences in inductively coupled plasma mass spectrometry by gas-phase collisions. *Appl. Spectrosc.*, **43**, 976–80.
3. Barinaga, C. J. and Koppenaal, D. W. (1994) Ion-trap mass spectrometry with an inductively coupled plasma source. *Rapid Commun. Mass Spectrom.*, **8**, 71–6.
4. Eiden, G. C., Barinaga, C. J., and Koppenaal, D. W. (1996) Selective removal of plasma matrix ions in plasma source mass spectrometry. *J. Anal. At. Spectrom.*, **11**, 317–22.
5. Eiden, G. C., Barinaga, C. J., and Koppenaal, D. W. (1997) Beneficial ion/molecule reactions in elemental mass spectrometry. *Rapid Commun. Mass Spectrom.*, **11**, 37–42.
6. Tanner, S. D., Baranov, V. I., and Bandura, D. R. (2002) Reaction cells and collision cells for ICP-MS: a tutorial review. *Spectrochim. Acta* B, **57**, 1361–452.
7. Gerlich, D. (1992) Inhomogeneous RF fields: a versatile tool for the study of processes with slow ions. In. *State-Selected and State-to-State Ion–Molecule Reaction Dynamics*: *Part 1. Experiment*, *Adv. Chem. Physics Series*, Vol LXXXII, (eds C-Y Ng and M. Baer), John Wiley & Sons, New York, pp. 1–176.
8. Mathieu, E. (1868) Mémoire sur le mouvement vibratoire d'une membrane de forme elliptique. *J. Math. Pures Appl. (J. Liouville)*, **13**, 137–48.
9. Dawson, P. H. (1995) *Quadrupole Mass Spectrometry and its Applications*, American Institute of Physics, Woodbury, NY.
10. Konenkov, N. V., Sudakov, M., and Douglas, D. J. (2002) Matrix methods for the calculation of stability diagrams in quadrupole mass spectrometry. *J. Am. Soc. Mass Spectrom.*, **13**, 597–613.

11. Frenkel, D. and Portugal, R. (2001) Algebraic methods to compute Mathieu functions. *J. Phys. Math. Gen.*, **34**, 3541–51.
12. Baranov, V. I. (2003) Analytical approach for description of ion motion in quadrupole mass spectrometer. *J. Am. Soc. Mass Spectrom.*, **14**, 818–24.
13. Dawson, P. H. and Whetten, N. R. (1971) *Dynamic Mass Spectrometry* (ed. D. Price), Heyden & Son, London, Vol. 2.
14. Szabo, I. (1986) New ion-optical devices utilizing oscillatory electric fields: I. Principle of operation and analytical theory of multipole devices with two-dimensional electric fields. *Int. J. Mass Spectrom. Ion Processes*, **73**, 197–235.
15. Hägg, C. and Szabo, I. (1986) New ion-optical devices utilizing oscillatory electric fields: II. Stability of ion motion in a two-dimentional hexapole field. *Int. J. Mass Spectrom. Ion Processes*, **73**, 237–75.
16. Hägg, C. and Szabo, I. (1986) New ion-optical devices utilizing oscillatory electric fields: II. Stability of ion motion in a two-dimensional octopole field. *Int. J. Mass Spectrom. Ion Processes*, **73**, 277–94.
17. Jennings, K. R. (2000) The changing impact of the collision-induced decomposition of ions on mass spectrometry. *Int. J. Mass Spectrom.*, **200**, 479–93.
18. Douglas, D. J. and French, J. B. (1992) Collisional focusing effects in radio frequency quadrupoles. *J. Am. Soc. Mass Spectrom.*, **3**, 398–408.
19. Bandura, D. R., Baranov, V. I., and Tanner, S. D. (2001) Reaction chemistry and collisional processes in multipole devices for resolving isobaric interferences in ICP-MS. *Fresenius' J. Anal. Chem.*, **370**, 454–70.
20. Bass, L., Su, T., Chesnavich, W. J., and Bowers, M. T. (1975) Ion-polar molecule collisions. A modification of the average dipole orientation theory: the cosθ model. *Chem. Phys. Lett.*, **34**, 119–22.
21. Su, T., Su, E. C. F., and Bowers, M. T. (1978) Ion-polar molecule collisions. Conservation of angular momentum in the average dipole orientation theory. The AADO theory. *J. Chem. Phys.*, **69**, 2243–50.
22. Baranov, V. I. and Tanner, S. D. (1999) A dynamic reaction cell for inductively coupled plasma mass spectrometry (ICP-DRC-MS): I. The RF-field energy contribution in thermodynamics of ion–molecule reactions. *J. Anal. At. Spectrom.*, **14**, 1133–42.
23. Tanner, S. D., Baranov, V. I., and Vollkopf, U. (2000) A dynamic reaction cell for inductively coupled plasma mass spectrometry (ICP-DRC-MS): III. Analytical performance. *J. Anal. At. Spectrom.*, **15**, 1261–9.
24. Feldmann, I., Jakubowski, N., and Steuwer, D. (1999) Application of a hexapole collision and reaction cell in ICP-MS: part I. Instrumental aspects and operational optimization. *Fresenius' J. Anal. Chem.*, **365**, 415–21.
25. Austin, W. E., Holme, A. E., and Leck, J. H. (1995) The mass filter: design and performance. In: *Quadrupole Mass Spectrometry and its Applications*, (ed. P. H. Dawson), AIP Press, New York, pp. 121–52.
26. Boulyga, S. F. and Becker, J. S. (2002) Improvement of abundance sensitivity in a quadrupole-based ICP-MS instrument with a hexapole collision cell. *J. Anal. At. Spectrom.*, **17**(9), 1202–6.
27. Krutchinsky, A. N., Loboda, A. V., Spicer, V. L., Dworschak, R., Ens, W., and Standing, K. G. (1998) Orthogonal injection of matrix-assisted laser desorption/ionization ions into a time-of-flight spectrometer through a collisional damping interface. *Rapid Commun. Mass Spectrom.*, **12**, 508–18.
28. Bandura, D. R., Baranov, V. I., and Tanner, S. D. (2000) Effect of collisional damping and reactions in a dynamic reaction cell on the precision of isotope ratio measurements. *J. Anal. At. Spectrom.*, **15**, 921–8.

29. Londry, F. A. and Hager, J. W. (2003) Mass selective axial ion ejection from a linear quadrupole ion trap. *J. Am. Soc. Mass Spectrom.*, **14**, 1130–47.
30. Morris, M., Thibault, P., and Boyd, R. K. (1994) Characterization of a high-pressure quadrupole collision cell for low-energy collision-induced dissociation. *J. Am. Soc. Mass Spectrom.*, **5**, 1042–63.
31. Lock, C. M. and Dyer, E. (1999) Characterisation of high pressure quadrupole collision cells possessing direct current axial fields. *Rapid Commun. Mass Spectrom.*, **13**, 432–48.
32. Thomson, B. A. and Jolliffe, C. L. (1998) Spectrometer with axial field. U.S. patent 5,847,386.
33. Javahery, G. and Thomson, B. (1997) A segmented radiofrequency-only quadrupole collision cell for measurements of ion collision cross section on a triple quadrupole mass spectrometer. *J. Am. Soc. Mass Spectrom.*, **8**, 697–702.
34. Loboda, A., Krutchnisky, A., Loboda, O., McNabb, J., Spicer, V., Ens, W., and Standing, K. (2000) Novel LINAC II electgrode geometry for creating an axial field in a multipole ion guide. *Eur. J. Mass Spectrom.*, **6**, 531–6.
35. Hattendorf, B. and Gunter, D. (2000) Characteristics and capabilities of an ICP-MS with a dynamic reaction cell for dry aerosols and laser ablation. *J. Anal. At. Spectrom.*, **15**, 1125–31.
36. Bandura, D. R., Baranov, V. I., and Tanner, S. D. (2002) Inductively coupled plasma mass spectrometer with axial field in a quadrupole reaction cell. *J. Am. Soc. Mass Spectrom.*, **13**, 1176–85.
37. Dawson, Douglas (1983) *Tandem Mass Spectrometry* (ed. F. W. McLafferty), Chapter 6, John Wiley & Sons, New York.
38. Nonose, N. S., Matsuda, N., Fudagawa, N., and Kubota, M. (1994) Some characteristics of polyatomic ion spectra in inductively coupled plasma mass spectrometry. *Spectrochim. Acta*, **49B**, 955–74.
39. King, F. L. and Harrison, W. W. (1989) Collision-induced dissociation of polyatomic ions in glow discharge mass spectrometry. *Int. J. Mass Spectrom. Ion Processes*, **89**, 171–85.
40. Mcluckey, S. A. and Goeringer, D. E. (1997) Slow heating methods in tandem mass spectrometry. *J. Mass Spectrom.*, **32**, 461–74.
41. Mason, P. R. D., Kaspers, K., and vanBergen, M. J. (1999) Determination of sulfur isotope ratios and concentrations in water samples using ICP-MS incorporating hexapole ion optics. *J. Anal. At. Spectrom.*, **14**, 1067–74.
42. Pröfrock, D., Leonhard, P., and Prange, A. (2003) Determination of sulfur and selected trace elements in metallothionein-like proteins using capillary electrophoresis hyphenated to inductively coupled plasma mass spectrometry with an octopole reaction cell. *Anal. Bioanal. Chem.*, **377**, 132–9.
43. Anicich, V. G. (2003) An index of the literature for bimolecular gas phase cation-molecule reaction kinetics. *JPL Publication*, Jet Propulsion Laboratory, Pasadena, CA, pp. 03–19.
44. Yamada, N., Takahashi, J., and Sakata, K. (2002) The effect of cell-gas impurities and kinetic energy discrimination in an octopole collision cell ICP-MS under non-thermalised conditions. *J. Anal. At. Spectrom.*, **17**, 1213–22.
45. Handbook of Chemistry and Physics, (1986) 66 edn. CRC Press, Boca Raton, FL, pp. F164–67.
46. Niemelä, M., Perämäki, P., Kola, H., and Piispanen, J. (2003) Determination of arsenic, iron and selenium in moss samples using a hexapole collision cell, inductively coupled plasma-mass spectrometry. *Anal. Chim. Acta*, **493**(1), 3–12.
47. Leonhard, P., Pepelnik, R., Prange, A., Yamada, N., and Yamada, T. (2002) Direct analysis of seawater at the ng L^{-1} level using an ICP-MS with an octapole reaction cell. *J. Anal. At. Spectrom.*, **17**, 189–96.
48. Nakazato, T., Tao, H., Taniguchi, T., and Isshiki, K. (2002) Determination of arsenite, arsenate, and monomethylarsonic acid in seawater by ion-exclusion chromatography combined

with inductively coupled plasma mass spectrometry using reaction cell and hydride generation techniques. *Talanta*, **58**(1), 121–32.
49. Fensenfeld, F. C., Schmeltekopf, A. L., Goldan, P. D., Shiff, H. I., and Ferguson, E. E. (1966) Thermal energy ion-neutral reaction rates: 1. Some reactions of helium ions. *J. Chem. Phys*., **44**, 4078–94.
50. Adams, N. G. and Smith, D. (1976) The selected ion flow tube (SIFT): a technique for studying ion-neutral reactions. *Int. J. Mass Spectrom. Ion Phys*., **21**, 349–59.
51. Bohme, D. K. (2000) Experimental studies of positive ion chemistry with flow-tube mass spectrometry: birth, evolution, and achievements in the 20th century. *Int. J. Mass Spectrom*., **200**, 97–136.
52. Armentrout, P. B. (2000) Kinetic energy dependence of ion–molecule reactions: guided ion beams and threshold measurements. *Int. J. Mass Spectrom*., **200**, 219–41.
53. Kawabata, K., Kishi, Y., and Thomas, R. (2003) The benefits of dynamic reaction cell ICP-MS technology to determine ultra trace metal contamination levels in high-purity phosphoric and sulfuric acid. *At. Spectrosc*., **24**, 57–65.
54. Sloth, J. J. and Larsen, E. H. (2000) The application of inductively coupled plasma dynamic reaction cell mass spectrometry for measurement of selenium isotopes, isotope ratios and chromatographic detection of selenoamino acids. *J. Anal. At. Spectrom*., **15**(6), 669–672.
55. Tanner, S. D. and Bandura, D. R. (2003) Determination of Fe, Ni, Co, Cu and Zn in high-Ca samples using methane as a reaction cell gas. In: *Plasma Source Mass Spectrometry: Applications and Emerging Technologies* (eds G. Holland and S. D. Tanner), The Royal Society of Chemistry, Cambridge, pp. 292–303.
56. Boulyga, S. F., Dietze, H. J., and Becker, J. S. (2001) Performance of ICP-MS with hexapole collision cell and application for determination of trace elements in bio-assays. *Microchim. Acta*, **137**(1–2), 93–103.
57. Reyes, L. H., Gayon, J. M. M., Alonso, J. I. G., and SanzMedel, A. (2003) Determination of selenium in biological materials by isotope dilution analysis with an octapole reaction system ICP-MS. *J. Anal. At. Spectrom*., **18**(1), 11–6.
58. Bohme, D. K. Research Page. Thermodynamics and physical properties. Thermodynamically derived O-atom affinities. http://www.chem.yorku.ca/profs/bohme/research/research.html
59. Bandura, D. R., Litherland, A. E., Baranov, V. I., and Tanner, S. D. (2003) Chemical resolution of isobaric atomic interferences by ICP-DRC-MS. *30th Federation of Analytical Chemistry and Spectroscopy Societies Conference*, Ft. Lauderdale, FL, October 19–23. Book of Abstracts, p. 119.
60. Kishi, Y. and Kawabata, K. (2002) Analysis of semiconductor-grade HCl with the ELAN DRC ICP-MS: elimination of chloride-based interferences. *At. Spectrosc*., **23**(5), 165–9.
61. Simpson, L. A., Thomsen, M., Alloway, B. J., and Parker, A. (2001) A dynamic reaction cell (DRC) solution to oxide-based interferences in inductively coupled plasma mass spectrometry (ICP-MS) analysis of the noble metals. *J. Anal. At. Spectrom*., **16**(12), 1375–80.
62. Vanhaecke, F., Balcaen, L., DeWannemacker, G., and Moens, L. (2002) Capabilities of inductively coupled plasma mass spectrometry for the measurement of Fe isotope ratios. *J. Anal. At. Spectrom*., **17**(8), 933–43.
63. Moens, L. J., Vanhaecke, F. F., Bandura, D. R., Baranov, V. I., and Tanner, S. D. (2001) Elimination of isobaric interferences in ICP-MS, using ion–molecule reaction chemistry: Rb/Sr age determination of magmatic rocks, a case study. *J. Anal. At. Spectrom*., **16**(9), 991–4.
64. Dexter, M. A., Appelblad, P. K., Ingle, C. P., Batey, J. H., Reid, H. J., and Sharp, B. L. (2002) The effect of adventitious water in hexapole collision cell inductively coupled plasma mass spectrometry. *J. Anal. At. Spectrom*., **17**(3), 183–8.

65. Niu, H. and Houk, R. S. (1996) Fundamental aspects of ion extraction in inductively coupled plasma mass spectrometry. *Spectrochim. Acta* B, **51**(8), 779–815.
66. Olney, T. N., Chen, W., and Douglas, D. J. (1999) Gas dynamics of the ICP-MS interface: impact pressure probe measurements of gas flow profiles. *J. Anal. At. Spectrom.*, **14**, 9–17.
67. Tanner, S. D., Bandura, D. R., and Baranov, V. I. (2003) Device and method preventing ion source gases from entering reaction/collision cells in mass spectrometry. U.S. patent # 6,630,665, Oct 7.
68. Hattendorf, B. and Günther, D. (2004) Suppression of in-cell generated interferences in a reaction cell ICP-MS by bandpass tuning and kinetic energy discrimination. *J. Anal. At. Spectrom.*, **19**, 600–6.
69. Liu, H. T. and Jiang, S. J. (2003) Determination of copper in coal fly ash in the presence of excess titanium by dynamic reaction cell inductively coupled plasma mass spectrometry. *Anal. Bioanal. Chem.*, **375**(2), 306–9.
70. Tanner, S. D. and Baranov, V. I. (1999) A dynamic reaction cell for inductively coupled plasma mass spectrometry (ICP-DRC-MS): II. Reduction of interferences produced within the cell. *J. Am. Soc. Mass Spectrom.*, **10**(11), 1083–94.
71. Hattendorf, B., Gunther, D., Schonbachler, M., and Halliday, A. (2001) Simultaneous ultra-trace determination of Zr and Nb in chromium matrixes with ICP-dynamic reaction cell MS. *Anal. Chem.*, **73**(22), 5494–8.
72. Olesik, J. W., Jones, D. R., and Olesik, Susan V. (accepted, 2004) Strategies to develop methods using ion-molecule reactions in a quadrupole reaction cell to overcome spectral overlaps in inductively coupled mass spectrometry. *J. Anal. At. Spectrom.*,
73. Koyanagi, G. K., Caraiman, D., Blagojevic, V., and Bohme, D. K. (2002) Gas-phase reactions of transition-metal ions with molecular oxygen: room temperature kinetics and periodicities in reactivity. *J. Phys. Chem. A*, **106**, 4581–90.
74. Boulyga, S. F. and Becker, J. S. (2001) ICP-MS with hexapole collision cell for isotope ratio measurements of Ca, Fe, and Se. *Fresenius' J. Anal. Chem.*, **370**(5), 618–23.
75. Thomson, B. A., Douglas, D. J., Corr, J. J., Hager, J. W., and Jolliffe, C. L. (1995) Improved collisionally activated dissociation efficiency and mass resolution on a triple quadrupole mass spectrometer system. *Anal. Chem.*, **67**, 1696–704.
76. Turner, P., Merren, T., Speakman, J., and Haines, C. (1997) Interface studies in the ICP-mass spectrometer. In: *Plasma Source Mass Spectrometry: Development and Applications* (eds G Holland and S. D. Tanner), The Royal Society of Chemistry, Cambridge, pp. 28–34.
77. Lias, S. G., Bartmess, J. E., Liebman, J. F., Holmes, J. L., Levin, R. D., and Mallard, W. G., (1988) Gas-phase ion and neutral thermochemistry. *J. Phys. Chem. Ref. Data*, **17**(Suppl. 1), 1–861.
78. Szilagyi, M. (1988) *Electron and Ion Optics*., Plenum Press, New York, NY pp. 497–513.
79. Douglas, D. J. (1993). Multipole inlet system for ion traps. U.S. patent # 5,179,278, Jan. 12.
80. Vanhaecke, F., Balcaen, L., Deconinck, I., DeSchrijver, I., Almeida, C. M., and Moens, L. (2003) Mass discrimination in dynamic reaction cell (DRC)-ICP-mass spectrometry. *J. Anal. At. Spectrom.*, **18**(9), 1060–5.
81. McCurdy, E. and Woods, G. (2004) The application of collision/reaction cell inductively coupled plasma mass spectrometry to multi-element analysis in variable sample matrices, using He as a non-reactive cell gas. *J. Anal. At. Spectrom.*, **19**(5), 607–15.
82. Hattendorf, B. and Günther, D. (2003) Strategies for method development for an inductively coupled plasma mass spectrometer with bandpass reaction cell. Approaches with different reaction gases for the determination of selenium. *Spectrochim. Acta* B, **58**(1), 1–13.

Chapter 9
ICP-MS Applications

Jackie Morton, Zoë A Quinn, Vladimir I Baranov, Scott D Tanner, Bill Spence, David Wray, Yuichi Takaku, Jean-Marie Collard and Yoko Kishi

9.1 CLINICAL APPLICATIONS OF ICP-MS

Jackie Morton

9.1.1 Introduction

Clinical applications of ICP-MS have increased significantly in the past decade. The types of biological samples analysed by ICP-MS have diversified and now include whole blood, plasma, serum, urine, interstitial fluids, internal organs, teeth, bones, hair, nails, metal-binding proteins as well as various types of human and animal cells.

The determination of trace elements in such matrices is crucial since they play a role in both normal biological function and toxicity. ICP-MS has become a very important tool for measuring concentrations of both essential and toxic metals at trace levels using small volumes of sample. The reliable measurement of trace elements has become an important aspect of many clinical, industrial and governmental laboratories.[1] The trace element status of patients is often of clinical importance and multi-elemental analysis of biological samples can provide rapid analysis and quantification, which allows a quick diagnosis. ICP-MS replaces time-consuming analysis procedures of previous single elemental methods such as atomic absorption spectrometry (AAS). Biological monitoring of workers exposed to high levels of elements is of concern in industrial environments. In these cases, environmental levels of elements in biological materials must be determined to help establish control levels, which subsequently allow interpretation in cases where exposure has occurred. In many cases the detection limits of existing AAS techniques are not sensitive enough for environmental levels of metals in urine and other biological materials.[2]

The use of ICP-MS in hospitals is increasing slowly but this is hampered by the large capital cost of such an instrument, whereas in other areas ICP-MS has become the instrument of choice, e.g. the pharmaceutical industry. As hospitals and other laboratories replace atomic absorption spectrometers with ICP-MS, there is a requirement for robust and routine methodology using simple methods. The improved detection limits are very appealing, as well as the multi-elemental ability of ICP-MS. In order for hospitals and routine laboratories to invest in ICP-MS, it is important that sample preparation be as simple as possible.

Biological sample analysis by ICP-MS is not without problems. In biological samples, interferences from atomic and molecular ions produced in the plasma from argon and matrix constituents of the aspirated solutions plague the quantification of several elements,[3–4] e.g. $^{27}Al/^{12}C^{15}N/^{12}C^{14}NH$, $^{39}K/^{38}Ar^{1}H$, $^{40}Ca/^{40}Ar$, $^{51}V/^{35}Cl^{16}O$, $^{75}As/^{40}Ar^{35}Cl$,

Inductively Coupled Plasma Mass Spectrometry Handbook Edited by Simon M. Nelms
 ISBN: 978-1-405-10916-1

$^{77}Se/^{40}Ar^{37}Cl$, $^{80}Se/^{40}Ar_2$, $^{82}Se/^{12}C^{35}Cl_2$, $^{63}Cu/^{40}Ar^{23}Na/^{31}P^{16}O_2$, $^{59}Co/^{43}Ca^{16}O$, $^{64}Zn/^{32}S^{16}O_2$, $^{52}Cr/^{40}Ar^{12}C/^{36}Ar^{16}O/^{35}Cl^{16}O^1H$, $^{79}Br/^{40}Ar^{39}K$, $^{58}Ni/^{42}Ca^{16}O$, $^{55}Mn/^{39}K^{16}O/^{38}Ar^{16}O^1H$, $^{48}Ti/^{32}S^{16}O$, $^{54}Fe/^{40}Ar^{14}N$, $^{56}Fe/^{40}Ar^{16}OH/^{40}Ca^{16}O$ and $^{57}Fe/^{40}Ar^{16}OH/^{40}Ar^{17}O$. Selection of different isotopes of the same element has allowed the measurement of elements using quadrupole ICP-MS,[1] e.g. using ^{65}Cu instead of ^{63}Cu, ^{68}Zn instead of ^{64}Zn or ^{66}Zn, and ^{53}Cr instead of ^{52}Cr. Also, the selection of a well-matched internal standard helps reduce the matrix effects of biological samples. It is necessary to choose internal standards that are not present in the biological sample. Depending on the samples it is not always possible to select gallium and bismuth as internal standards because these elements may occur endogenously in some people. For multi-elemental analysis, often internal standards are chosen from Y, Ge, Sc, Rh, In and Pt because generally these elements exist in very low concentrations in biological samples and would not have any effect on the internal standard.

The introduction of collision cell technology (CCT) means that the capabilities of ICP-MS continue to push the boundaries of clinical sample analysis. It is now possible by introducing reaction/collision gases to analyse elements like selenium and chromium in urine, which would not be possible using traditional quadrupole ICP-MS as a result of isobaric interferences. It is possible to measure such elements in urine and other matrices using high-resolution/sector-field ICP-MS; however, the increase in resolution required to resolve the interferences is inherently correlated to a loss in sensitivity. This means that for elements with low concentrations (e.g. Cr is around 1 μg/L in urine for normal levels), the high-resolution ICP-MS may have insufficient limits of detection. Sector-field instruments have been used for the determination of trace elements[6–8] in biological samples that traditionally have interferences (Co, Cr, Cu, Fe, Mn, Ni, Sc, V, Zn) when using quadrupole ICP-MS. It has been reported that it is possible to determine 37 elements in urine[7] following a 20-fold dilution with 0.14 mol/L nitric acid over a wide dynamic range 9.3 ng/L for U to 4700 mg/L for Si.

Several factors are still of concern in the analysis of trace elements in biological matrices with ICP-MS. Most biological fluids contain large amounts of organic compounds and inorganic salts, which can lead to spectral and non-spectral interferences. The introduction of CCT has eliminated several of the spectral interferences from elements such as bromide, selenium, vanadium and chromium in biological fluids. However, for multi-elemental analysis careful consideration must be given to the application of collision gases because the gas may reduce the interferences on certain elements whilst at the same time reduce the sensitivity of other elements being measured. It may be necessary to use in-sample switching modes to measure all the required elements. It is also necessary to be aware that the proteins, other organic compounds and high concentration of inorganic salts in biological media may block the sample introduction system of an ICP-MS during an analytical run.

Often the low levels of the elements are being determined in a heavy matrix, and so historically, samples were always analysed using matrix-matched standards and standard addition methods. Using ICP-MS, it is possible with the selection of the appropriate isotopes and internal standards to measure trace elements in biological matrices using external aqueous calibrations for matrices such as urine and serum. Blood samples with a simple dilution usually require matrix-matched standards, whereas if digested, it is possible to use aqueous standards.

However, the introduction of CCT for quadrupole ICP-MS means that a lot of the previous problems of interferences on elements in biological samples could be removed. The challenge for CCT is to now have an optimum gas that will allow the quantitative analysis of many elements simultaneously.

9.1.2 Sample preparation

Following collection, biological samples should be frozen or refrigerated. In preparation for analysis, biological samples should be gradually allowed to reach room temperature and then homogenised by vigorously rolling/inverting and then swirling prior to aliquotation.[2]

There have been many publications on the subject of sample preparation of biological samples. It is necessary to dilute biological samples because the large amounts of proteins and salts can cause an irreversible reduction of the analyte signal intensity due to clogging of the nebuliser, torch, sample and skimmer orifices. Dilution reduces the matrix effects and improves the accuracy on the internal calibration.[1]

Digestion of samples is really only necessary for solid materials (unless using laser ablation). Urine and blood samples can simply be diluted and then analysed. Urine and serum samples are commonly diluted in acidic solutions and whole blood samples in alkaline media.[9] It would be possible to analyse urine and blood in the same analysis if the blood samples were acid digested prior to determination by ICP-MS. The need for matrix-matched blood standards makes it difficult to dilute the blood sample and analyse *in situ* with urine samples.

The dilution factor of blood and urine can very much depend on the element of interest because some of the elements are present in biological samples at very high concentrations, e.g. Mg, Ca, Fe and Br in urine are typically more than 1 mg/L; some at moderate concentrations, e.g. Pb in whole blood is less than 50 μg/L for unexposed persons; and others at low concentrations, e.g. Co and Tl in urine are less than 2 μg/L in normal persons whilst Cr in whole blood is around 0.2 μg/L.

9.1.2.1 Urine

An advantage of ICP-MS over AAS is that matrix-matched standards are no longer necessary as internal standards can adequately compensate for the matrix effects on many of the elements measured. Also, the need for complicated separations to remove the analyte from the matrix is generally no longer necessary, e.g. for molybdenum in urine,[10] arsenic in urine and vanadium (with CCT).[11]

Urine samples are generally diluted ten-fold with 1% v/v nitric acid solution.[5] Five-fold dilutions may be necessary for elements present in lower concentrations, e.g. cobalt and thallium. Fifty-fold dilutions may be carried out on elements present in higher concentrations, e.g. bromide. In urine, some elements are present only at ng/L levels and depending on the detection limit of the ICP-MS, flow injection of undiluted urine samples may be necessary, e.g. for platinum and uranium. To establish occupational exposure to chemotherapy drugs, platinum in urine has been analysed using flow injection[12] or ultrasonic nebulisation[13,14] to improve the detection limits. Morrison *et al.* reported a detection limit of 1 ng/L Pt in only 100 μL matrix. The use of a torch shield has been seen to improve the detection limits of Pd, Pt and Rh (0.5, 0.5, 0.2 ng/L) in urine using sector-field ICP-MS.[15] Using a hexapole collision cell ICP-MS with an ultrasonic nebuliser, Boulyga and Becker reported a detection limit of 3 pg/L for ^{236}U, which is not present in natural uranium, and they attributed the low detection limit to both low blanks (this isotope would not be in blanks) and the increased sensitivity from the plasma shielded torch.[16]

It has been published that it is possible to analyse uranium isotopes in urine at low levels using high-resolution ICP-MS.[17,18] In both papers the ICP-MS used was in low-resolution mode, which

is similar to the resolution achieved using a quadrupole system. There have been differences reported in the sample preparation for analysis: the urine is either simply diluted 10-fold in acid[17] or digested by UV-photolysis.[18] Krystek and Ritsema[17] reported uranium levels of 9 ng/L in a urine sample, with five replicates reporting an RSD of 3.3%. Similarly, Schramel[18] reported precision levels of 3% on U^{238} and 10% on U^{235} on an in-house urine sample spiked with 10 ng/L uranium, with an overall 2.5% standard deviation on the isotope ratio (138.1 ± 3.4) on a urine sample with 10 ng/L total uranium. Uranium analysis is possible by quadrupole ICP-MS and Ejnik *et al.* prepared urine samples for this method by firstly dry-ashing and then wet-ashing.[19] Using this method, it was possible to calculate an isotope ratio for $^{235}U/^{238}U$, which allows the identification of depleted urine, when the total concentration was greater than 14 ng/L.

Using quadrupole ICP-MS, it has not been fully possible to use mathematical corrections to correct for the interferences of Se, V and Cr in urine. With the advances in CCT it is now possible to determine elements such as selenium, vanadium and chromium in urine by introducing gases in a collision cell to remove the interference. The introduction of CCT effectively means that AAS will no longer be required in the clinical laboratory for such analysis.

Recent work 'discusses the analysis of 23 elements in urine using ICP-MS with CCT. In this methodology by Heitland *et al.*' different cell gases were employed for selenium (hydrogen) than for the other elements (helium). This work does not mention the capability of CCT gas 'switching' mode where in theory it should be possible to purge one collision gas from the cell and introduce another.

Selenium speciation in urine samples has been carried out using a mix of H_2 and He in a hexapole collision–reaction cell ICP-MS.[20] Selenium metabolites occur at very low concentrations in urine and so the use of high-resolution ICP-MS with the inherent loss in sensitivity is not practical. In the case of selenium, helium is used as the collision gas, which improves the ion transmission, and hydrogen is the reaction gas, which is useful in reducing most argide interferences by orders of magnitude.[20] Ammonia has been used as a collision/reaction gas for removing the ArC^+ and OCl^+ interferences for chromium and vanadium respectively. Using reaction cell technology it has been seen that the detection limits of chromium in urine samples are 2.5 times lower than those measured by Zeeman graphite furnace AAS and the detection limits of vanadium are approximately 50 times lower.[21] In this study internal standards yttrium and gallium were used, as well as matrix-matched standards.

For elements such as iodine, it has been suggested that urine samples are diluted in alkaline medium to improve the ionisation in the plasma, stability and reduce memory effects, because at low pH HI and I_2 may be formed.[22]

Mercury analysis in urine still requires special treatment and often better results are obtained when the element is determined on its own and not as part of a multi-elemental analysis. Prior to ICP-MS total mercury concentrations in urine and blood were determined using cold vapour AAS. The sample was first digested and then reacted with stannous chloride and the elemental mercury detected by AAS. However, this is not always an ideal method for mercury in urine samples because the presence of cysteine or an oxidising agent such as iodine in urine can prevent the effective reduction of mercury by stannous chloride.[23] The volatility of mercury at room temperature and the residual mercury signal following analysis from tubing and spray chamber are well-documented problems associated with mercury analysis. To maintain a stable mercury signal it is necessary to add gold to the diluent and the rinse/wash solution. If the rinse solution is allowed to equilibrate (at 1 mL/min for 1 h prior to analysis), loss of mercury from samples and thus drift is reduced. For urinary mercury analysis, the best results have been seen

when all solutions containing gold (standards, samples, diluent and wash) are all prepared freshly for each analysis. It has been suggested that adding dichromate with hydrochloric acid instead of gold also helps the stability of the analytical run and reduces the memory effects in the spray chamber.[23] However, as a result of the carcinogenicity of dichromate solutions, adding gold (up to 1 mg/L) would be the method of choice.

The determination of arsenic in urine samples to determine exposure requires the hyphenation of hydride generation with ICP-MS. This is because total arsenic analysis, which has been vastly improved with the introduction of CCT and the removal of the ArCl interference, still includes some arsenic species that are present in urine as a result of seafood contributions. The reduction of As^{5+}, DMA and MMA (dimethylarsinic acid and monomethylarsonic acid) to As^{3+} with L-cysteine and hydrochloric acid and subsequent hydride generation by mixing with sodium borohydride will measure all the arsenic species except arsenobetaine and arsenocholine. The hydride gas line can be simply connected to the spray chamber (replacing the nebuliser gas) and arsenic is measured using a dry plasma. The hydride generator system removes both the chloride interference (because only the AsH_3 gas enters the plasma) and the dietary component of exposure (because AB and AC are not reduced to As^{3+}).

9.1.2.2 Whole blood

Depending on the concentration of the elements in whole blood samples, generally a 10-fold dilution with an alkaline diluent will allow adequate analysis of most elements. The most commonly used diluent for direct analysis of whole blood contains ammonia to lyse the red blood cells, EDTA to prevent loss of the metals by precipitation or absorption and Triton X-100 to reduce blockages of the sample introduction system. Such diluents have been successfully used for multi-elemental determination in whole blood samples.[9,24] White and Sabbioni[10] used 0.3 M ammonia, 0.05% EDTA and 0.05% Triton X-100 in the whole blood diluent, and to reduce matrix suppression effects used matrix-matched calibration standards and internal standardisation. However, this study used flow injection for the blood samples to prevent blocking of the injector. Sector-field ICP-MS in medium resolution has been used to measure Mo, Co, Cr, Ni in whole blood following a ten-fold alkaline dilution.[25] It has been suggested that whole blood needs to be digested or deproteinised by the addition of an acid[24]; however, simply diluting the blood samples with an alkaline diluent is quicker and more reproducible. Matrix-matched standards are commonly used with diluted blood samples, using a standard addition procedure where the blank diluent is used to calculate endogenous levels. This standard addition is then converted to an external calibration graph.

Problems with blockages have been reported using such diluents when large numbers of whole blood samples have been analysed.[26] Rodushkin *et al.* found that the sample introduction system failed following ten-fold dilution of blood samples in such a diluent. They also had problems disinfecting the tubing and the glassware and so decided to digest the whole blood samples. The method was described using microwave digestion with nitric acid and deionised water and subsequent dilution with water. This allowed the analysis of 60 elements in whole blood by using a sector-field mass spectrometer. The digestion of many blood samples in a microwave system means that there has to be rigorous cleaning of the vials between digest to ensure that there is no cross contamination. Blockages of the sample introduction system can be avoided by using an appropriate rinse solution. In the case of whole blood it is helpful to also use an alkaline wash when

running blood samples containing Triton X-100 and TMAH (tetraammonium hydroxide) this will help prevent blockages/adhesion to the tubing/probe. When TMAH is used as a wash solution, it is also useful to note that, in addition to preventing blockages, TMAH cleans the ion lens/lenses if solutions of 0.05% v/v are used. If mercury in blood is being determined then it is advantageous to add between 100 μg/L and 1 mg/L of gold to both the wash solution and the diluent.

The determination of chromium in blood on a quadrupole ICP-MS requires digestion of the samples to decrease the carbon content.[24]

9.1.2.3 Serum

Serum can be diluted in either acid[5] or alkaline diluent.[24] Often it is easy to analyse urine and serum samples at the same time following dilution with acidic diluents. Some laboratory practices prefer to precipitate the proteins in a serum solution with nitric acid, and then centrifuge and dilute the sample with water.[1] Enzymatic digestions have also been used, e.g. non-specific protease enzymes, to break down a wide range of proteins, which would reduce blockages in the ICP-MS and improve ionisation efficiencies.[27]

The determination of selenium in serum and whole blood has required the addition of an organic solvent to suppress the affect of the argon adducts that interfere with all six selenium isotopes. It is thought that with the addition of propanol, ethanol, methanol or butanol the argon adducts become involved in the formation of carbides, nitrides and oxides through charge-transfer mechanisms, which effectively shifts the mass of polyatomic ions away from the region of interest.[28] This methodology has successfully measured selenium in serum, whole blood and erythrocytes diluting in an alkaline diluent with indium as the internal standard. Since the introduction of collision/reaction cells it has been possible to measure selenium at masses 78 and 80 with the introduction of methane gas to the reaction cell.[29] Nixon *et al.* added 10% v/v ethanol to 1% v/v nitric acid and 0.5% Triton X-100, with gallium and indium as internal standards.

9.1.3 Isotope ratios and biological materials

Isotopically enriched iron tablets have been used to study absorption of iron from nutritional sources.[20] Iron is a very problematic element for ICP-MS in biological samples because there are significant interferences from Ar-based and Ca-based molecular ions. Vanhaecke *et al.*[31] compared sector-field ICP-MS with a collision cell ICP-MS for the determination of iron isotopes in serum. The problem exists mostly because typical levels of calcium in serum are approximately 50 times higher than those of iron. This study found that sector-field ICP-MS at a mass resolution of 3000 allows accurate determination of iron isotope ratios in human serum but only $^{54}Fe/^{56}Fe$ ratios could be determined with sufficient accuracy and precision using CO as a reaction gas with a DRC-ICP-MS. This was due to the DRC-ICP-MS not being able to correct for both the argon and calcium interferences.

The use of stable isotopes as tracers in clinical studies is becoming more commonplace. Human metabolism studies have been reported with enriched ^{25}Mg and ^{26}Mg measuring plasma, faecal and urine samples.[31] In another study using ^{25}Mg, the absorption of magnesium was seen to increase when certain 'fatty acids' were also administered.[32] Enriched boron stable isotopes have also been determined in rat urine and faeces to establish excretion pathways and found that

the isotope ratios changed in urine samples but returned to normal in 24 h.[33] Yeast has been isotopically enriched with ^{77}Se and used in a human clinical study.[34] Using an ICP-DRC-MS, isotopes of selenium were measured in urine, faeces and plasma. ^{80}Se was also measured and was used to determine the normal selenium concentrations present in the diet. The results were used to estimate the absorption rates of selenium. Stable isotopes have been used to study the dietary absorption in humans for cadmium, using ^{106}Cd, in wheat made into porridge.[35] The study suggested that the absorption of cadmium might be more than previous estimates. Rat and human serum and urine have been measured by ICP-MS for the determination of ^{61}Ni as part of a study looking at the biokinetics of nickel.[36]

9.1.4 Tissue samples

Tissue samples normally have to be digested for the analysis of metals by direct nebulisation ICP-MS. Laser ablation can be used on some biological samples; however, because of the inhomogeneity of biological tissues total digestion offers a more accurate analysis. Microwave digestion systems have been used extensively for the digestion of biological tissue, with samples such as hair,[37,38] muscle,[39] lung,[40] renal cortex,[37,41] liver,[37,40,42] cerebellum,[37] kidney,[40] brain,[40] teeth.[43] Digestion normally involves the addition of concentrated nitric acid and hydrogen peroxide, although perchloric acid, sulfuric acid and hydrofluoric acid have been used.

Certified references are available mostly in powder form for tissues like hair, liver and muscle. For speciation analysis of tissue samples, it may be necessary to cold digest the tissue sample; e.g. methyl mercury in hair samples will be destroyed if microwave digested.[44]

9.1.5 Speciation

The absorption, distribution, reactivity to binding sites, bioavailability, toxicity and excretion of elements can be better understood if information about the chemical species is available.[45] Speciation can provide additional information that just total elemental analysis. Although the speciation of trace elements in biological fluids and tissues has been approached in many different ways during the last decades, it is extremely difficult because of the complexity of the biological systems.[46] Approximately 15 elements, 20 oxidation states and 25 organic compounds have been involved in the speciation of biological samples.[45] Several biological matrices have been considered but blood, serum and urine are the most analysed, with tissue being found to be a relevant matrix for copper, zinc and cadmium. Organic compounds (such as ethyl, methyl and aryl derivatives) have been demonstrated for arsenic, mercury, lead and selenium, and other organic compounds (e.g. complexes with amino acids, proteins and macromolecules) have been demonstrated for silver, cadmium, copper, chromium, lead, selenium and zinc. Among the procedures for the separation and identification of species are various chromatographic techniques, as well as chemical chelation, extraction, acid-modified separation, heating and distillation.

Common elements speciated using liquid chromatography (LC) coupled with ICP-MS include arsenic, selenium, mercury, antimony in mostly urine samples. Arsenic speciation is usually achieved using an anion-exchange column. Selenium compounds may be separated under conditions similar to those for arsenic, or by a reverse phase column with ion pairing

chromatography.[47] Selenium speciation in urine has been carried out using a desolvator to remove organic solvent between the reverse phase and ion-pair chromatography, and the ICP-MS with a collision and reaction cell[20] showed improved detection limits of 30–80 ng/L for ^{80}Se. Aluminium in serum has been separated by fast protein liquid chromatography with ICP-MS,[48] and iron has been separated from human serum transferrins using HPLC-ICP-MS.[49]

Antimony compounds in the pentavalent state are administered to people suffering from leishmaniaisis, a tropical disease caused by parasites. Using antimony speciation, the ion exchange-ICP-MS method was capable of separating the intense drug peak from its inorganic species and thus permitting the first studies in the biotransformation of *N*-methyl megulmine antimonite to Sb^{5+} and Sb^{3+} in the human body.[50]

Iodine speciation has been successfully carried out using capillary electrophoresis coupled to inductively coupled plasma mass spectrometry.[51] The status of iodine species (such as thyroxine, triiodothyronine or iodide) in serum or urine can give information about the malfunction of the thyroid gland and can explain other metabolic abnormalities. Chromium speciation is not normally required in biological samples because the body converts all of the Cr^{6+} to Cr^{3+} and so the measurement of 'total chromium' in blood and urine is referred to when in fact Cr^{3+} has been determined. Chromium speciation has been carried out in bacteria culture medium,[52] which has used to convert Cr^{6+} to Cr^{3+}.

Mercury speciation in hair samples has been carried out using reverse phase chromatography following a digestion at room temperature.[44] Methyl and inorganic mercury were determined using this method in less than 7 min, which is a vast improvement on lengthy extractions used previously to remove methyl mercury from hair.

It is possible to introduce oxygen as a gas to the spray chamber to help with the organic solvent content of some mobile phases. In speciation methods where a lot of organic solvent is required for the chromatography, e.g. for lead compounds, if the concentrations of the analytes are high then it would be possible to split the flow from the LC column and mix with an aqueous solution to reduce the carbon contamination of the sample cones.

9.1.6 New areas of analysis

The use of ICP-MS for the determination of metals in biological materials, such as skin, skin cells and organs, will help provide a better understanding of metabolism and uptake pathways of the human body. The analysis of platinum–DNA adducts in peripheral blood leukocytes by ICP-MS[53] has been achieved.

ICP-MS analysis has also been of use in forensic cases where samples have been analysed to determine exposure to toxic metals, e.g. arsenic in supernatant of stomach contents.[54]

There will be an increase in demand for ICP-MS in biological areas that require the identification of metals in proteins,[55] drugs[56] and drug uptake,[57] biotransformations, metabolic, proteomics and other biological processes. Using ICP-MS it was possible to see that Cu^{2+} and Zn^{2+} binding is crucial in the modulation of the aggregation and neurotoxic properties of prion peptides.[58] ICP-MS has also been used to measure cadmium isotopes in metallothionein in liver cytosol samples.[59] This work has been shown to successfully replace the need for radiolabelled compounds where an enriched isotope can be used. Enriched selenium isotopes have also been used in nutritional and dietary studies.[60] Trace elements in brain samples from patients with Alzheimer's disease (AD) have also been analysed.[61] The results showed that there were

significantly different levels of metals in the AD brain samples and suggested that oxidative processes are occurring between the metallothioneins in the brain. Antimony is being measured by ICP-MS as a marker for sentinel lymph nodes in melanoma patients.[62]

Methodology and research to date have focused on measuring concentrations of toxic and essential elements and their potential health effects. Future uses of ICP-MS could concentrate more on the role of inorganic species in disease states and cellular mechanisms.

References

1. Hsiung, C. S., Andrade, J. D., Costa, R., and Ash, K. O. (1997) Minimising interferences in the quantitative multielemental analysis of trace elements in biological fluids by inductively coupled plasma mass spectrometry. *Clin. Chem.*, **43**, 2303–11.
2. Schramel, P., Wendler, I., and Angerer, J. (1997) The determination of metals (antimony, bismuth, lead, cadmium, mercury, palladium, platinum, tellurium, thallium, tin and tungsten) in urine samples by inductively coupled plasma mass spectrometry. *Int. Arch. Occup. Environ. Health*, **69**, 219–23.
3. Krachler, M. and Irgolic, K. J. (1999) The potential of inductively coupled plasma mass spectrometry for the simultaneous determination of trace elements in whole blood, plasma and serum. *J. Trace Elem. Med. Bio.,* **13**, 157–69.
4. Apostoli, P. (2002) Elements in environmental and occupational medicine. *J. Chromatogr. B*, **778**, 63–97.
5. Vanhoe, H. (1993) A review of the capabilities of ICP-MS for trace element analysis in body fluids and tissues. *J. Trace Elem. Electrolytes Health Dis.*, **7**, 131–9.
6. Begerow, J., Turfeld, M., and Dunemann, L. (2000) New horizons in human biomonitoring of environmentally and occupationally relevant metals-sector-field ICP-MS versus electrothermal AAS. *J. Anal. At. Spectrom.*, **15**, 347–52.
7. Roduskin, I. and Odman, F. (2001) Application of inductively coupled plasma sector field mass spectrometry for elemental analysis of urine. *J. Trace Elem. Med. Bio.*, **14**, 241–7.
8. Krystek, P., de Boer, J. L. M., and Ritsema, R. (2002) Performance testing of HR-ICP-MS instrumentation and first applications for analysing biomedical samples under routine laboratory conditions. *ICP Inf. Newsl.*, **27**, 233–7.
9. White, M. A. and Sabbioni, E. (1998) Trace element reference values in tissues from inhabitants of the European Union, X: A study of 13 elements in blood and urine of a UK population. *Sci. Total Environ.*, **216**, 253–70.
10. Minoia, C., Gatti, A., Aprea, C., Ronchi, A., Sciarra, G., Turci, R., and Bettinelli, M. (2002) Inductively coupled plasma mass spectrometric determination of molybdenum in urine. *Rapid Commun. Mass Spectrom.*, **16**, 1313–19.
11. Heitland, P., Koster, H. D., and Köster. (2004) Fast, simple and reliable routine determination of 23 elements in urine by ICP-MS. *J. Anal. At. Spectrom.*, **19**, 1552–8.
12. Mason, H. J., Morton, J., Grafitt, S. J., Iqbal, S., and Jones, K. (2003) Cytotoxic drug contamination on the outside of vials delivered to a hospital pharmacy. *Ann. Occup. Hyg.*, **47**, 681–5.
13. Turci, R., Sottani, C., Ronchi, A., and Minoia, C. (2002) Biological monitoring of hospital personnel occupationally exposed to antineoplastic agents. *Toxicol. Lett.*, **134**, 54–7.
14. Morrison, J. G., White, P., McDougall, S., Firth, J. W., Woolfrey, S. G., Graham, M. A., and Greenslade, D. (2000) Valiadation of a highly sensitive ICP-MS method for the determination of platinum in biofluids: application to clinical pharmacokinetic studies with oxiplatin. *J. Pharm. Biomed. Anal.*, **24**, 1–10.

15. Petrucci, F., Bocca, B., and Alimonti, A. (2002) Determination of Pt-group elements in human urine: advantages of the torch shield in sector field mass spectrometry. *ICP Inf. Newsl.*, **27**, 246–51.
16. Boulyga, S. and Becker, J. S. (2000) Inductively coupled plasma mass spectrometry with hexapole collision cell: figures of merit and applications. *Ber. Forschungszent. Juelich*, 13–44.
17. Krystek, P. and Ritsema, R. (2002) Determination of uranium in urine – measurement of isotope ratios and quantification by use of inductively coupled plasma mass spectrometry. *Ana. Bioanal. Chem.*, **374**, 226–9.
18. Schramel, P. (2002) Determination of ^{235}U and ^{238}U in urine samples using sector field inductively coupled plasma mass spectrometry. *J. Chromtaogr. B*, **778**, 275–8.
19. Ejnik, J. W., Carmicheal, A. J., Hamilton, M. M., McDiarmid, M., Squibb, K., Boyd, P., and Tardiff, W. (2000) Determination of the isotopic composition of uranium in urine by inductively coupled plasma mass spectrometry. *Health Phys.*, **78**, 143–6.
20. Marchante-Gayon, J. M., Feldman, I., Thomas, C., and Jakubowski. (2001) Speciation of selenium in human urine by HPLC-ICP-MS with a collision and reaction cell. *J. Anal. At. Spectrom.*, **16**, 457–63.
21. Nixon, D. R., Neubauer, K. R., Eckdahl, S. J., Butz, J. A., and Burritt, M. F. (2002) Evaluation of a tunable bandpass reaction cell for an inductively coupled plasma mass spectrometer for the determination of chromium and vanadium in serum and urine. *Spectrochim. Acta B*, **57**, 951–66.
22. Patriarca, M., Kratochwil, N. A., and Sadler, P. J. (1999) Simultaneous determination of Pt and I by ICP-MS for studies of the mechanism of reaction of diiodoplatinum anticancer complexes. *J. Anal. At. Spectrom.*, **14**, 633–7.
23. Nixon, D., Burritt, M. F., and Moyer, T. P. (1999) The determination of mercury in whole blood and urine by inductively coupled plasma mass spectrometry. *Spectrochim. Acta B*, **54**, 1141–53.
24. Barany, E., Bergdahl, I. A., Schutz, A., Skerfving, S., and Oskarsson, A. (1997) Inductively coupled plasma mass spectrometry for direct multielemental analysis of diluted human blood and serum. *J. Anal. At. Spectrom.*, **12**, 1005–9.
25. Case, C. P., Ellis, L., Turner, J. C., and Fairman, B. (2001) Development of a routine method for the determination of trace metals in whole blood by magnetic sector inductively coupled plasma mass spectrometry with particular relevance to patients with total hip and knee arthroplasty. *Clin. Chem.*, **47**, 275–80.
26. Roduskin, I., Odman, F., Olofsson, R., and Axelsson, M. D. (2000) Determination of 60 elements in whole blood by sector field inductively coupled plasma mass spectrometry. *J. Anal. At. Spectrom.*, **15**, 937–44.
27. Abou-Shakra, F. R., Rayman, M. P., Ward, N. I., Hotton, V., and Bastian, G. (1997) Enzymatic digestion for the determination of trace elements in blood serum by inductively coupled plasma mass spectrometry. *J. Anal. At. Spectrom.*, **12**, 429–33.
28. Sieniawska, C. E., Mensikov, R., and Delves, H. T. (1999) Determination of total selenium in serum, whole blood and erythrocytes by ICP-MS. *J. Anal. At. Spectrom.*, **14**, 109–12.
29. Nixon, D. R., Neubauer, K. R., Eckdahl, S. J., Butz, J. A., and Burritt, M. F. (2002) Evaluation of a tunable bandpass reaction cell for an inductively coupled plasma mass spectrometer for the determination of selenium in serum and urine. *Spectrochim. Acta B*, **58**, 97–110.
30. Vanhaecke, F., Balcaen, L., De Wannemacker, G., and Moens, L. (2002) Capabilities of inductively coupled plasma mass spectrometry for the measurement of Fe isotope ratios. *J. Anal. At. Spectrom.*, **17**, 933–43.
31. Benech, H., Batel, A., Pruvost, A., Thomas, J.-L., and Grognet, J.-M. (1998) Magnesium isotopic abundance measurement in humans: comparison of two mass spectrometric methods. *Magnes. Res.*, **11**, 91–102.

32. Tahiri, M., Tressol, J. C., Arnaud, J., Bornet, F., Bouteloup-Demange, C., Feillet-Coudray, C., Ducros, V., Pepin, D., Brouns, F., Roussel, A. M., Rayssiguier, Y., and Coudray, C. (2001) Five-week intake of short-chain fructooligiosaccharides increases intestinal absorption and status of magnesium in postmenopausal women. *J. Bone Miner. Res.*, **16**, 2152–60.
33. Vanderpool, R. A., Hoff, D., and Johnson, P. E. (1994) Use of inductively coupled plasma mass spectrometry in boron-19 stable isotope experiments with plants, rate and humans. *Environ. Health Perspect.*, **102**, 13–20.
34. Sloth, J. J., Larsen, E. H., Bugel, S. H., and Moesgaard, S. (2003) Determination of total selenium and ^{77}Se in isotopically enriched human samples by ICP-dynamic reaction cell-MS. *J. Anal. At. Spectrom.*, **18**, 317–22.
35. Crews, H. M., Owen, L. M., Langford, N., Fairweather-Tait, S. J., Fox, T. E., Hubbard, L., and Phillips, D. (2000) Use of stable isotope ^{106}Cd for studying dietary cadmium absorption in humans. *Toxicol. Lett.*, **112–113**, 201–7.
36. Templeton, D. M., Xu, S. X., and Stuhne-Sekalec, L. (1994) Isotope-specific analysis of Ni by ICP-MS: applications of stable isotope tracers to biokinetic studies. *Sci. Total Environ.*, **148**, 253–62.
37. Hac, E., Krzyzanowski, M., and Krechniak, J. (2000) Total mercury in human renal cortex, liver, cerebellum and hair. *Sci. Total Environ.*, **248**, 37–43.
38. Morton, J., Carolan, V. A., and Gardiner, P. H. E. (2002) Removal of exogenously bound elements from human hair by various washing procedures and determination by inductively coupled plasma mass spectrometry. *Anal. Chim. Acta*, **455**, 23–34.
39. Eilola, K. and Peramaki, P. (2001) Microwave heated vapour-phase digestion method for biological materials. *Fresenius' J. Anal. Chem.*, **369**, 107–12.
40. Garcia, F., Ortega, A., Domingo, J. L., and Corbella, J. (2001) Accumulation of metals in autopsy tissues of subjects living in Tarragon County, Spain. *J. Environ. Sci. Health A*, **36**(9), 1767–86.
41. Lopez-Artiguez, M., Camean, A., Gonzalez, G., and Repetto, M. (1995) Cadmium concentration in human renal cortex tissue (necropsies). *Bull. Environ. Contam. Toxicol.*, **54**, 841–7.
42. Delves, H. T., Sieniawska, C. E., Fell, G. S., Lyon, T. D. B., Dezateux, C., Cullen, A., Variend, S., Bonham, J. R., and Chantler, S. M. (1997) Determination of antimony in urine, blood, serum and in liver and lung tissues of infants by inductively coupled plasma mass spectrometry. *Analyst*, **122**, 1323–29.
43. Prohaska, T., Latkoczy, C., Schultheis, G., Teschler-Nicola, M., and Stingeder, G. (2002) Investigation of Sr isotope ratios in prehistoric human bones and teeth using laser ablation ICP-MS and ICP-MS after Rb/Sr separation. *J. Anal. At. Spectrom.*, **17**, 887–91.
44. Morton, J., Carolan, V. A., and Gardiner, P. H. E. (2002) The speciation of inorganic and methylmercury in human hair by high performance chromatography coupled with inductively coupled plasma mass spectrometry. *J. Anal. At. Spectrom.*, **17**, 377–81.
45. Apostoli, P. (1999) The role of element speciation in environmental and occupational medicine. *Fresenius' J. Anal. Chem.*, **363**, 499–504.
46. Das, A. K., Chakraborty, R., Cervera, M. L., and de la Guardia, M. (1996) Metal speciation in biological fluids – a review. *Mikrochim. Acta,* **122**, 209–46.
47. Zheng, J., Shibata, Y., and Tanaka, A. (2002) Study of the stability of selenium compounds in human urine and determination by mixed ion-pair reverse-phase chromatography with ICP-MS detection. *Anal. Bioanal. Chem.*, **374**, 348–53.
48. Belen Soldado Cabezuelo, A., Montes Bayon, M., Blanco Gonzalez, E., Garcia Alonso, J. I., and Sanz-Medel, A. (1998) Speciation of basal aluminium in human serum by fast protein liquid chromatography with inductively coupled plasma mass spectrometry. *Analyst*, **123**, 865–9.

49. Harada, K., Kuniyasu, A., Nakayama, H., Nakayama, M., Matsunga, T., Uji, Y., Sugiuchi, H., and Okabe, H. (2002) Separation of human serum transferrins with different iron-binding states by high performance liquid chromatography using a pyridinium polymer column. *J. Chromatogr. B*, **767**, 45–51.
50. Miekeley, N., Mortari, S. R., and Schuhbach, A. O. (2002) Monitoring of total antimony and its species by ICP-MS and on-line ion chromatography in biological species from patients treated for leishmaniasis. *Anal. Bioanal. Chem.*, **372**, 495–502.
51. Michalke, B. and Schramel, P. (1999) Iodine speciation in biological samples by capillary electrophoresis inductively coupled plasma mass spectrometry. *Electrophoresis*, **20**, 2547–53.
52. Chardin, B., Chaspoul, F., Gallice, P., and Bruschi, M. (2002) Chromium speciation in bacterial culture medium by combining strong anion exchange liquid chromatography with inductively coupled plasma mass spectrometry. Application to the reduction of Cr(VI) by sulphate-reducing bacteria. *J. Liquid Chromatogr. Related Technol.*, **25**, 877–87.
53. Bonetti, A., Apostoli, P., Zaninelli, M., Pavanel, F., Colombatti, M., Cetto, G. L., Franceschi, T., Sperotto, L., and Leone, R. (1996) Inductively coupled plasma mass spectroscopy quantitation of platinum–DNA adducts in peripheral blood leukocytes of patients receiving cisplatin or carboplatin based chemotherapy. *Clin. Cancer Res.*, **2**, 1829–35.
54. Tanaka, T., Hara, K., Tanimoto, A., Kasai, K., Kita, T., Tanaka, N., and Takayasu, T. (1996) Determination of arsenic in blood and stomach contents by ICP-MS. *Forensic Sci. Int.*, **81**, 43–50.
55. Inagaki, K., Umemura, T., Matsuura, H., and Haraguchi, H., (2000) Speciation of trace elements, binding and non-binding with proteins in human blood serum, by surfactant-mediated HPLC with element selective detection by ICP-MS. *Anal. Sci.*, **16**, 787–88.
56. Smith, C. J., Wilson, I. D., Abou-Shakra, F., Payne, R., Grisedale, H., Long, A., Roberts, D., and Malone, M., (2002) Analysis of a ^{14}C-labelled platinum anticancer compound in dosing formulations and urine using a combination of HPLC-ICP-MS and flow scintillation counting. *Chromatogr. Suppl.*, **55**, S151–5.
57. Sessa, C., Capri, G., Gianni, L., Peccatori, F., Grasselli, G., Bauer, J., Zucchetti, M., Vigano, L., Gatti, A., Minoia, C., Liati, P., Van den Bosch, S., Bernareggi, A., Camboni, G., and Marsoni, S. (2000) Clinical and pharmacological phase I study with accelerated titration design of a daily times five schedule of BBR3464, a novel cationic triplatinum complex. *Ann. Oncol.*, **11**, 977–83.
58. Jobling, M. F., Huang, X., Stewart, L. R., Barnham, K. J., Curtain, C., Volitakis, I., Perugini, M., White, A. R., Cherny, R. A., Masters, C. L., Barrow, C. J., Collins, S. J., Bush, A. I., and Cappai, R. (2000) Copper and zinc binding modulates the aggregation and neurotoxic properties of the prion peptide PrP106-126. *Biochemistry*, **40**, 8073–84.
59. Valles Mota, J. P., Linde Arias, A. R., Fernandez de la Campa, M. R., Garcia Alonso, J. I., and Sanz-Medel, A. (2000) Development of a stable isotope approach for inductively coupled plasma mass spectrometry determination of oxidised metallothionein in biological materials. *Anal. Biochem.*, **282**, 194–9.
60. Suzuki, K. T. (1996) Simultaneous speciation of endogenous and exogenous elements by HPLC-ICP-MS with enriched stable isotopes. *Tohoku J. Exp. Med.*, **178**, 27–35.
61. Richarz, A. N. and Bratter, P. (2000) Speciation analysis of trace elements in the brains of individuals with Alzheimer's disease with special emphasis on metallothioneins. *Anal. Bioanal. Chem.* **372**, 412–7.
62. Dawson, M., Doble, P., Beavis, A., Li, L. X., Soper, R., Scolyer, R. A., Uren, R. F., and Thompson, J. F. (2003) Antimony by ICP-MS as a marker for sentinel lymph nodes in melanoma patients, *Analyst*, **128**, 217–9.

9.2 EMERGING BIOANALYSIS APPLICATIONS FOR ICP-MS

Zoë A Quinn, Vladimir I Baranov and Scott D Tanner

9.2.1 Introduction

New technology that enables accurate protein quantitation is required in the booming area of proteomics and drug discovery as well as in areas of clinical and diagnostic testing. It is also important in biological research aimed at analyzing protein development, function and disease at the molecular level. Currently, there are several existing techniques that are widely used for estimating protein concentration, including Western blotting, Bradford and Lowry assays, UV spectroscopy, organic mass spectrometry, HPLC, flow cytometry, ligand binding assays, ELISA (enzyme linked immunosorbent assay), RIA (radioimmunoassay) and protein microarrays. Nevertheless, this extensive assortment of well-established analytical tools and research techniques remains insufficient for today's challenges. The usual complaints are related mostly to limitations in sensitivity, selectivity, dynamic range, and the ability to determine the concentrations of several proteins simultaneously in an accurate and absolute manner.

The realization that elemental analysis offers significant advantages to the field of protein quantitation has directed the development of several new methods of protein quantitation via inductively coupled plasma mass spectrometry (ICP-MS) linked immunoassays.[1–5] This new technique provides an innovative arena for ICP-MS in the analysis of biological samples.

The ICP-MS technique has acquired its well-deserved place in the analysis of biological samples through its wide use for the quantitation of toxic elements, study of transport of metals and monitoring of the absorption and metabolism of metals and metallo-drugs, metallo-amino acids and metallo-proteins. In all of these cases, the biomolecules being analyzed are already associated with a metal component. In contrast, the ICP-MS-linked immunoassays provide a means to determine the concentrations of proteins that do not necessarily naturally contain a metal. To achieve this, ICP-MS immunoassays rely on the use of affinity products that include a metal containing tag. The most straightforward approach includes antibodies that have been raised specifically against the antigens (e.g. proteins) of interest and tagged with a metal.

Antibodies bind specific antigens with great affinity (having association constants between 10^6 and 10^9 M^{-1}) and can be conjugated to a traceable tag (fluorochrome, radioisotope, enzyme or metal). In a typical immunoassay, the sample containing the antigen of interest is mixed with tagged antibodies, after which the newly formed antigen–tagged-antibody complexes are separated from unreacted tagged antibodies and other contaminant materials, and then quantitated using the tag. Typically in the past, ELISA with fluorescent tags and RIAs have been found to be very sensitive, capable of detecting pg/mL of protein. Unfortunately, the means of detection of fluorochromes and radioisotopes suffer from both a limited dynamic range (2–3 orders of magnitude) and the ability to multiplex (detect multiple proteins simultaneously). However, these methods are under continuing development, with recent advances in microsphere immunoassays and flow cytometry, reporting the ability to quantitate up to 15 targets almost simultaneously[6,7] with somewhat limited dynamic range. Flow cytometers are now capable of accumulating data very rapidly, analyzing up to 20 000 beads per second as beads flow singly through a focused laser beam. The difficulties encountered upon analyzing a large number of targets are not surprising because of the cross-reactivity of the required antibodies,[8] the differences in conjugation

efficiency to antibodies, and possible steric interferences inhibiting the binding of antigens and tagged antibodies. These deficiencies are largely independent of the employed technique and are related to using the antibody as an affinity reagent. Specifically for cytometry these limitations also include limited dynamic range due to some spectral overlap and detector capabilities, the beads' surface capacity, background due to nonspecific binding of antibodies, and variability in tag response (tag integrity problem).

ICP-MS as an analytical detector possesses several advantages that enhance the performance of immunoassays, including (i) high precision, (ii) low detection limits, (iii) large dynamic range, (iv) lower matrix effects from other components of the biological sample (contaminating proteins in the sample have no effect on elemental analysis), (v) lower background from plastic containers and plates (plastic containers do not cause interference on elemental detection as they can with fluorescence), (vi) independence of nonspecific background and analytical response from incubation or storage times (as protein degradation does not affect analysis of an elemental tag), (vii) larger multiplexing potential (potentially, up to 167 isotopes; realistically, around 100 distinguishable tags), and (viii) better spectral resolution (abundance sensitivity).[1–5]

This section of the book details various methods and applications of measuring specific protein concentrations using the ICP-MS-linked metal-tagged immunoassays.

9.2.2 Method and results

9.2.2.1 Metal tagging

In metal-tagged immunoassays, proteins of interest are captured using surface chemistries as a means of separating proteins from other sample constituents (buffer, plasma, cell fragments and so on). It also helps to reduce any nonspecific binding of antibodies, resulting in decreased background. Once reacted with the metal-tagged antibodies and separated from unbound tagged antibodies, the sample can be analyzed for the tag content.

As specific tags for elemental analysis have not yet been developed, commercially available immunoreagents that contain elemental tags for unrelated purposes can be used. Fortunately, there are a variety of metal-containing immunoreagents such as gold-tagged antibodies that are routinely used in electron microscopy. It has been found that small gold clusters (1.4 nm diameter)[9] and colloidal gold particles can be successfully analyzed by ICP-MS.[1–5,10,11] In addition, four lanthanide (Eu, Tb, Dy and Sm) tagged antibodies[12] produced for fluorescence-based ELISA methods were also found to be good candidates for ICP-MS-based immunoassays.[4] Both the 1.4 nm nanogold and lanthanide tags were determined to have several valuable characteristics for elemental analysis including (i) uniform size (number of atoms), (ii) more than one tag atom per conjugate, (iii) covalent attachment to antibodies, (iv) biological inactivity with low steric hindrance and (v) a reproducible ratio of tag to antibody.

Traditionally, antibodies have been tagged with radioisotopes, enzymes (e.g. horseradish peroxidase) or fluorochrome molecules. Thus the chemistry of antibody tagging has been well established and typically involves using accessible primary amines (e.g. lysines) and thiol groups (reduced cysteine disulfide bonds) for binding. The same methods are also used for coupling metal tags to antibodies.

9.2.2.2 Immunoassay strategies and techniques

There are three basic stages in an immunoassay method. Firstly, the antigens (e.g. proteins) of interest in the biological sample must be harvested, separated from contaminants, and allowed to react with tagged antibodies (or other interacting molecules). Then, it is necessary to remove any unreacted tagged reagent and retain the reacted tagged products. The third stage includes the quantitation by a method that is specific for the given tag – detector combination. In order to adapt this to the elemental analysis, a variety of immunoseparation strategies can be used. Several of them are discussed in the following sections, including centrifugal filtration, protein A affinity, size exclusion gel filtration, antibody-coated microspheres, sandwich ELISA using primary and secondary antibodies (96 well plate format) and direct ELISA using maleic anhydride and nitrocellulose filter plates.

The advantages and disadvantages of each method were systematically analyzed. The protein targets examined included Smad proteins (which play a role in cardiac muscle development) and various regulatory proteins found in human serum which are involved in the immune response, including immunoglobin (IgG), interleukin-1beta (IL-1β), interleukin-6 (IL-6), interleukin-8 (IL-8), interleukin-13 (IL-13), interferon-gamma (IFN-γ) and tumor necrosis factor-alpha (TNF-α).

(a) Detection and quantitation of specific proteins using centrifuge filters and ICP-MS

Centrifugal filtration of the immunoprecipitation mixture followed by ICP-MS detection was found to provide a reproducible, sensitive method with a linear relationship between signal and antigen concentration. Concentrations of antigen as low as 2.5 ng protein/250 μL can be detected. In this method, samples containing the antigen of interest (e.g. human IgG) were mixed with a metal-tagged antibody (Fab' fragments or whole molecule IgG) and allowed to react (see Figure 9.1). Size exclusion filter units were used to separate antigen – antibody complexes from free antibody. The pore size of the filter should be selected appropriately to allow free reagents to pass easily through the filter. After separation, both the retained volume and the filtered volume were analyzed by ICP-MS to determine the amount of metal in each fraction. When compared to a standard curve prepared using a known amount of antigen, the concentration of antigen in an unknown sample can be determined.

It was assumed that all of the reacted complexes of protein–metal-tagged antibodies plus nonspecifically bound metal-tagged antibody would be retained on the top of the filter and the remainder of the unbound metal-tagged antibodies would pass through the filter. However, it should be pointed out that these filters were not originally designed to perform this task and the extent of nonspecific adsorption of the filters is not known. In addition, the distribution of pore size, the susceptibility of the filter to clogging, and interaction of the metal tag with the filter's material remains to be characterized.

Although it was observed that clogging did not occur in the experiments performed, to prevent other factors from affecting the method an antigen-free negative control was used. It was advantageous to degrade the complexes in a spiked acid solution that would be suitable for elemental analysis and would also provide an internal standard for ICP-MS quantitation. The internal standard chosen in each experiment is selected so that it has similar atomic mass as the elemental tag and also has a similar first ionization potential.

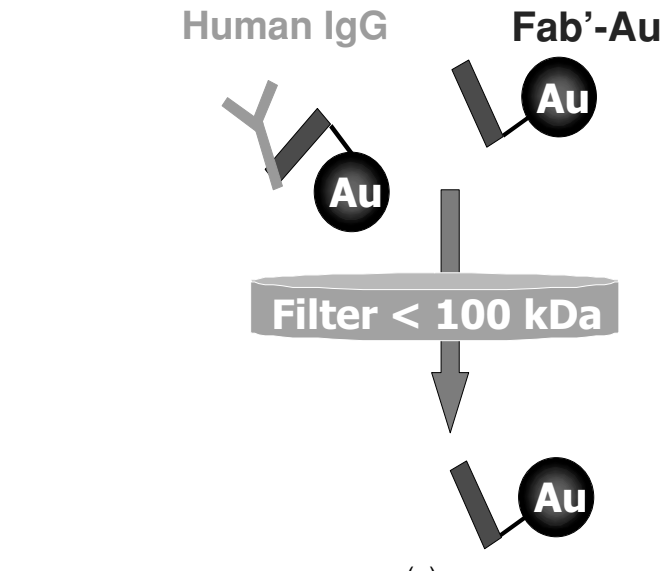

(a)

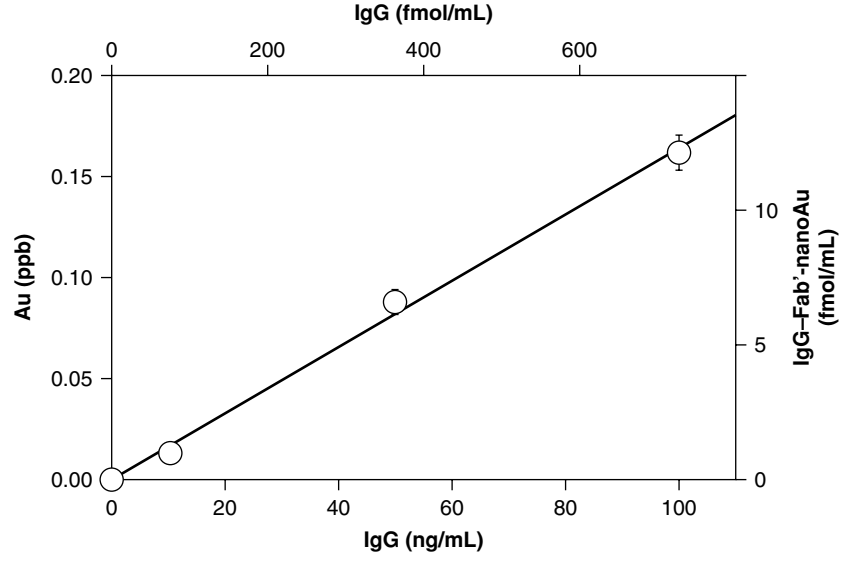

(b)

Figure 9.1 Schematic diagram depicting size exclusion centrifugal filtration immunoassay coupled to ICP-MS. (b) Calibration curve of the ICP-MS-coupled centrifugal filtration immunoassay of human IgG using concentrations of 0–100 ng protein/mL. An excess of prefiltered anti-human Fab'-nanoAu was reacted with human IgG for 2 h at room temperature.[3] After centrifugal filtration, both the retained volume and the filtered volume were analyzed by ICP-MS to determine the amount of the element in each fraction. The amount of nanoAu retained by the filter is plotted in units of ppb Au, and derived fmol/mL of IgG–Fab'-nanoAu complex.

To reduce the nonspecific binding of the metal-tagged antibody to the filter, these experiments were performed using a 1% BSA/1 × PBS buffer as a blocking agent and Fab'-nanoAu that was prefiltered to remove any large and sticky gold clusters. However, it was found that significant levels of analyte signal (equivalent to ~7 fmol/mL of the nanoAu clusters) were present in the negative control, probably because of nonspecific binding. The molar concentration of the complex was significantly lower than expected, indicating that the complex cannot be extracted efficiently from the filter. Taken together, it is estimated that the detection limit of this method will be ~3 ng protein/mL for human IgG (where the detection limit is defined as three standard deviations of the analyte signal in the blank solutions divided by the net signal in the sample solutions).

Overall, this method was found to provide a quick and easy means of assessing specific protein concentrations in the range of 10–5000 ng/mL target protein.

(b) Determination of K_D values of protein–protein interactions using gel filtration coupled to ICP-MS detection

Size exclusion gel filtration can also be coupled directly to the ICP-MS detector. This technique was effective in enabling the determination of the dissociation constant (K_D) between proteins (see Figure 9.2). In addition, it was noted that the ICP-MS provides a method by which metal-tagged antibodies can be purified after labeling. However, because of the inherent dilution effects of gel filtration, this method was found not to be sensitive in detecting low levels of protein and therefore not appropriate for accurately measuring small amounts of protein in complex biological samples. Therefore, despite the advantages of this technique for K_D value determination and metal-tag purification, there are a few limitations including the length of time required for a sample to pass through the column, the resolution of the gel and detection limits of only ~10 fmol Fab'-nanoAu (with ICP-MS detection).

(c) Sensitive quantitation of specific proteins by coupling sandwich and competitive ELISA with ICP-MS

Sandwich ELISA and competitive ELISA are the methods of choice for accurate quantitation of low levels of protein in diagnostic testing of such samples as human serum. ELISA plates are readily available that contain adsorptive surfaces such as coatings of primary or secondary antibodies. In general, sandwich ELISA utilizes antibodies bound to the surfaces of 96 well plates to capture specific antigens from complex mixtures and allow for their detection and quantitation using tagged detection antibodies. In a similar manner, competitive ELISA utilizes capture antibodies to anchor specific antigens. However, unlike sandwich ELISA, competitive ELISA uses tagged antigens of known concentration instead of tagged detection antibodies. Traditionally, enzyme, radioisotope and fluorochrome tags are utilized for detection and quantitation in ELISA.

Sandwich and competitive ELISA coupled to the ICP-MS detector yield reproducible and linear responses to antigen concentration. They also enable 96 immunoassays to be run per plate. Primary antibody plates were found to be more sensitive than secondary antibody plates, allowing lower levels of protein to be detected. This is probably due to the restricted well capacity of secondary antibody plates resulting from the steric hindrance of overlying antibodies. Comparative study of three analytes [estriol, α-fetoprotein(AFP) and human chorionic gonadotropin(hCG)] in 81 patient samples has been performed,[3] where it was found that ICP-MS detection reproduced results currently achieved on the same plates with fluorometers (Figure 9.3).

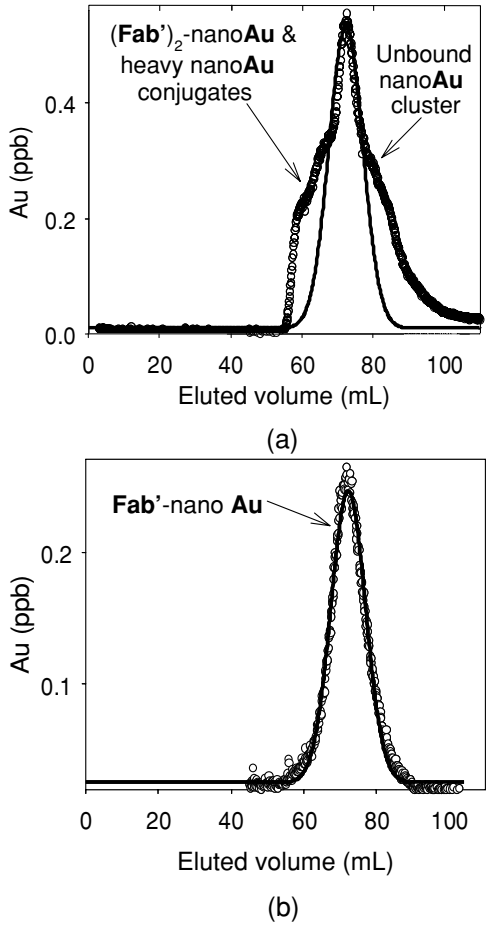

Figure 9.2 Purification of metal-tagged antibodies and determination of K_D values of protein–protein interactions using ICP-MS. As shown in panel (a), despite purification by the manufacturer, Fab′-nanoAu was found to contain unbound nanoclusters and heavier conjugates. In order to determine the K_D values of the interaction between anti-human Fab′-nanoAu and human IgG, it was necessary to obtain a higher purity of Fab′-nanoAu. Therefore, this run on the Sephacryl S200 column was repeated and an 8 mL portion of the peak was collected. The concentration of Fab′-nanoAu in this fraction was found to be 51.3 fmol/mL. One half of this purified fraction (4 mL) was rerun through the Sephacryl column, and the acquired ICP-MS spectrum shown in panel (b) indicates that the majority of nanoAu contaminants has been removed. The second half of the fraction was mixed with 4 μg of human IgG (290 pmol) and after a 1 h shaken incubation at room temperature, it was run through the Sephacryl column [panel (c)]. An internal spike of 1 ppb Ir in the running buffer was used to account for the overall signal stability during the run. The quantitation of both the IgG–Fab′-nanoAu complex and the free Fab′-nanoAu could be determined by the best fit of the data to area. The K_D for the antibody–antigen complex was determined in the next set of runs that contained mixtures of one of four serial dilutions of purified Fab′-nanoAu reacted with 10 μg aliquots of human IgG. From Scatchard plot calculations, the K_D was found to be $(2.3 \pm 0.8) \times 10^{-8}$ M. The solid lines represent fitted curves [panels (a) and (b), Fab′-nanoAu; and panel (c), IgG–Fab′-nanoAu and Fab′-nanoAu].[3]

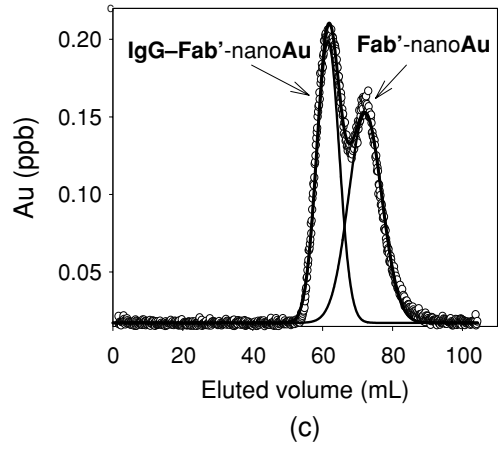

Figure 9.2 (*Continued*)

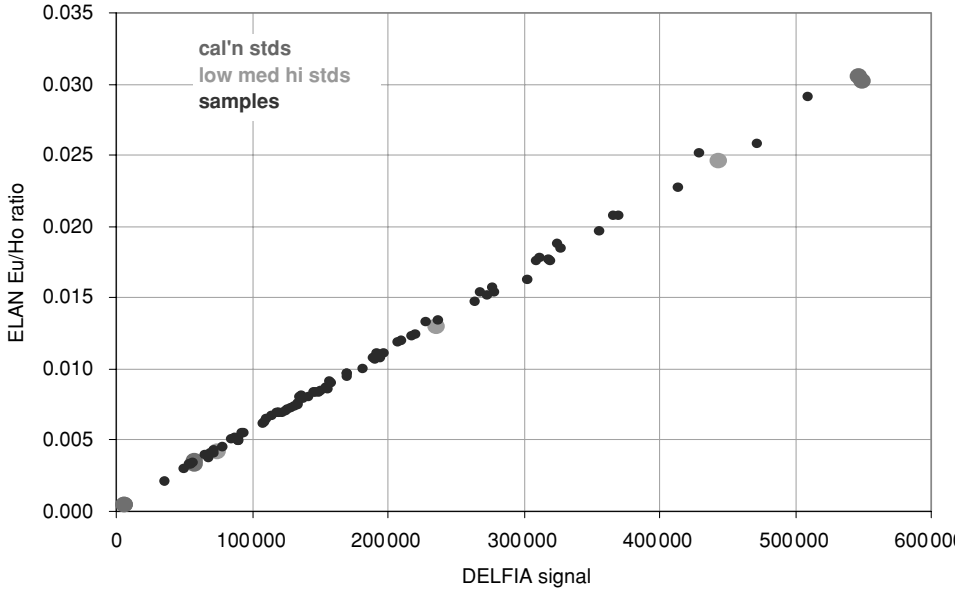

Figure 9.3 Comparison data of fluorescence detection to elemental detection of an hCG immunoassay. Through collaboration with North York General Hospital, the DELFIA system was compared directly with ICP-MS detection. In this assay, DELFIA sandwich ELISA for patient hCG was quantitated as directed by the manufacturer using Eu-tagged anti-hCG antibodies. After analysis using the DELFIA fluorometer, the assay was diluted for elemental analysis by ICP-MS with 50 µL concentrated HCl containing an internal standard of 1 ppb Ho.[3] Cal'n stds: calibration standards; low med hi stds: low, medium, and high standards.

(d) Sensitive quantitation of specific proteins by coupling direct ELISA with ICP-MS

ICP-MS detection can be used to analyze direct ELISA mixtures, preferably in 96-well format. This method was found to yield reproducible, linear responses to increasing antigen (protein) concentrations. However, they were not as sensitive as the sandwich ELISA results (see previous section), probably because of limited well capacity and nonspecific binding of detection antibodies. However, direct ELISA offers an inexpensive alternative to sandwich ELISA.

In Figure 9.4, Nunc Maxisorp plates were used. According to the manufacturer, these plates have both hydrophobic and hydrophilic binding pockets, which allow most proteins to be anchored at the bottoms of each well plate for immunoreaction and separations. Using Maxisorp plates, accurate calibration curves could be generated by incubating the plates with the protein of interest, blocking the wells with BSA, probing with specific metal-tagged antibodies, washing off excess antibodies, drying the wells, dissolving the metal tag with spiked acid, and sampling into the ICP-MS.

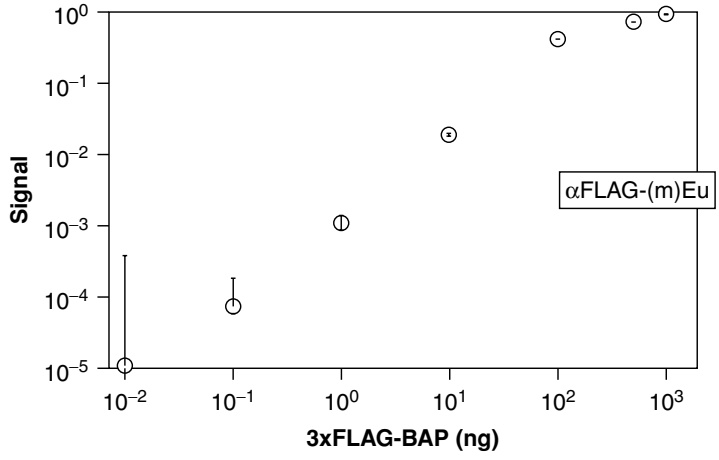

Figure 9.4 A direct ELISA linked ICP-MS assay of 3xFLAG-BAP (bacterial alkaline protein). In this assay, serial dilutions of 3xFLAG-BAP over a concentration range of 0.01–1000 ng/mL were incubated overnight at 4°C in the wells of a Maxisorp plate. Negative controls consisted of PBS without protein. The wells were then blocked for 1 h with 3% BSA/1 × PBS buffer at room temperature, washed, and exposed to anti-FLAG-Eu antibodies for 2 h in a shaken incubation. The wells were washed, dried, and the residue dissolved in 10% HCl spiked with 1 ppb Ho and 1 ppb Ir prior to sampling into the ICP-MS.

As a support system for ICP-MS-linked immunoassays, the Maxisorp plates are limited by capacity and are thus not suited to the detection of minor proteins in complex mixtures. However, these plates have the advantage of being able to bind all proteins, making the detection and quantitation of multiple analytes in a single sample possible. In the following section, another type of direct ELISA plate (maleic anhydride) is investigated for its potential use in the simultaneous quantitation of two proteins using ICP-MS-linked immunoassays.

9.2.2.3 Multiplexing

It should be evident that antigens having independent antibodies that are distinguishably tagged can be determined simultaneously, or multiplexed. Five available tags (Au, Sm, Eu, Dy and Tb) enable a 5-plex assay, assuming that the antibodies are not cross-reactive. Although multiplexing is in a very early stage of research and feasibility studies, it is already apparent that more than five could be accurately detected simultaneously using the ICP-MS. The current limits in performing multiplexed immunoassay of higher order include the availability of discrete isotopically enriched tags for biologically active materials, the limited capacity of commercially available capture surfaces, and obtaining groups of antibodies that do not cross-react.

(a) Simultaneous detection and quantitation of two proteins using ICP-MS

As a first step toward multiplexing, the ICP-MS detector was coupled with direct ELISA for the simultaneous detection of two proteins (human IgG and 3xFLAG-BAP). Linear calibration curves, low background and low standard deviation between triplicate samples (see Figure 9.5) are among the positive features of this method. In this experiment, maleic anhydride plates were used to anchor the proteins in the sample through the maleylation reaction that occurs between the primary amine groups of proteins and the coating on the bottom of the 96 well plates. The principal advantage of this technique is that it is an inexpensive means of anchoring multiple proteins simultaneously. Two differently tagged antibodies were used containing either nanogold (Nanoprobes) or Eu (Wallac, PerkinElmer) for this experiment. The difference in signal can be attributed to the differences in the sizes of the tags as nanogold has approximately

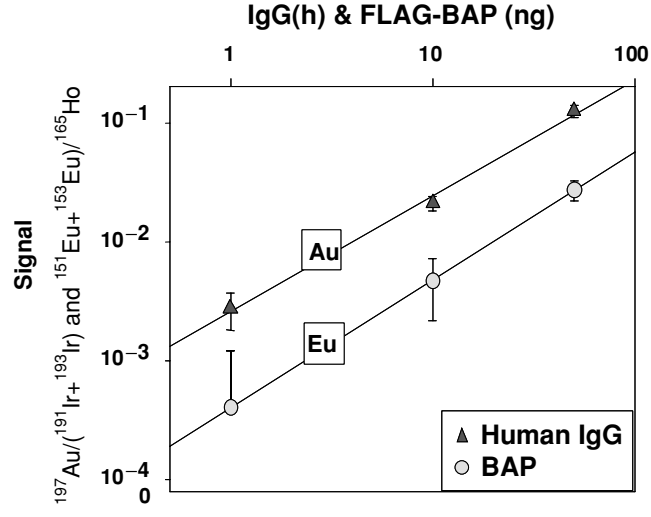

Figure 9.5 Simultaneous quantitation of two proteins using a direct ELISA coupled to the ICP-MS detection. In this experiment, two proteins (human IgG and 3xFLAG-BAP) in 1xPBS were incubated in triplicate for 1 h at room temperature to allow binding to the surfaces of the maleic anhydride plate. Negative controls consisted of 100 µL PBS without protein. The plate was probed with primary antibodies anti-human Fab'-nanoAu and anti-FLAG-Eu, washed, and acidified with 10% HCl, 1 ppb Ir and 1 ppb Ho.[5]

70 (monoisotopic) Au atoms and the Eu-tagged antibody has 6–10 atoms of Eu (3–5 atoms of each of two nearly equally abundant isotopes) per IgG molecule as specified by the manufacturer. One can expect that with larger tags (i.e. more atoms of a given isotope per tag), this technique, like the other ICP-MS-linked immunoassays, would improve linearly in terms of sensitivity.

9.2.2.4 Enhanced dynamic range

Experimental data demonstrate that detection of up to 4 orders of magnitude in protein concentration could be achieved [see Figure 9.6(a)]. One could speculate that the ICP-MS-linked immunoassays could measure protein over an even wider dynamic range (of 8 orders of magnitude) potentially starting at very low levels of protein (<pg/mL) since the ICP-MS technique allows such dynamic range measurement of a sample concentration. However, the characteristics of antibody–antigen equilibrium are not consistent with such dynamic range unless the complex is extremely strongly bound, to suppress the dissociation reaction in the presence of excessive quantity of the antibody. The sensitivity of element tag detection by ICP-MS is a linear function of the number of atoms of a given isotope in the tag and therefore it is expected that elemental tags of $\geq$100 atoms (preferably as large as possible) would be extremely valuable. It is also clear that the distribution of the number of atoms per tag must be narrow in order to achieve maximum accuracy. Therefore, limits of practical implementation of an extended dynamic range are external to those of ICP-MS detection. In addition to larger elemental tags, greater surface capacity and better affinity products are instrumental in enhancing the dynamic range.

(a) Use of sensitive microsphere-based ICP-MS immunoassays for enhanced dynamic range

Microspheres or beads are an attractive option for supporting surface chemistries of immunoassays. In a manner similar to 96 well plates, various compositions, coatings or conjugated groups can be constructed or added to provide the required surface chemistry. One of the advantages of microspheres is the ability to increase the reaction surface area per volume of the reaction mixture, which provides a reliable means of increasing the capacity and dynamic range potential of an immunoassay. In the following example, microsphere immunoassays were coupled with ICP-MS detection. Specifically, immunoprecipitation on protein A Sepharose beads was studied. In this method, capture antibodies were anchored to the surface of the beads through the high affinity of protein A for the Fc region of antibodies. As with other means of affinity purification, these beads were used to bind antigens of interest and separate them from other nonbinding molecules. Furthermore, after probing antigen-bound beads with metal-tagged antibodies, the antigens of interest can be quantified via ICP-MS detection. The bead complexes can be either directly sampled into the ICP-MS or dissociated in a spiked acid solution, allowing the metal tag to be dissolved and sampled without the bead matrix [Figure 9.6(b)]. This method was found to be reproducible, yielding linear calibration curves over more than 4 orders of magnitude. It was also noted to be very sensitive with detection limits of 0.1 ng protein/mL. Because of the affinity of protein A for the Fc regions of antibodies, this method requires a capture antibody and element-tagged detection Fab' fragments or proteins. Therefore, another expected advantage of this method is the ability to detect protein–protein interactions.

In a comparison study, Western blot detection, a common method of protein quantitation, was evaluated against ICP-MS detection [Figure 9.6(b)].[3] In Western blot analysis, proteins are separated by mass in a polyacrylamide gel. The proteins are then transferred to nitrocellulose using

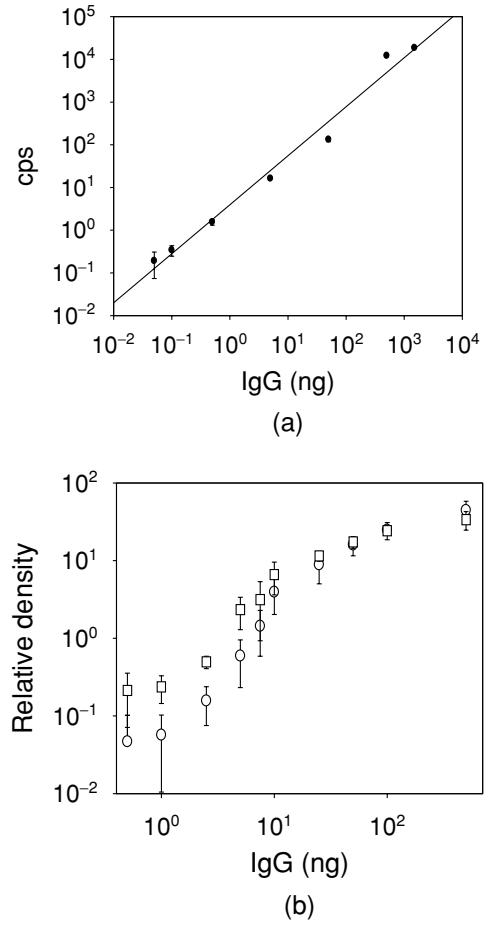

Figure 9.6 Comparison of Western blot and densitometry analysis with ICP-MS detection. (a) Calibration curve of the ICP-MS-linked immunoprecipitation assay of 3xFLAG-BAP. Anti-FLAG M2 Affinity Gel (Sigma) was used to immunoprecipitate triplicate samples of serially diluted 3xFLAG-BAP over a concentration range of 0.05–1500 ng/100 μL. 3xFLAG-BAP was detected using an anti-BAP primary antibody and an anti-mouse-nanoAu secondary antibody. Diluted HCl spiked with 1 ppb Ir and 1 ppb Ho was used to dissolve the nanogold tag for ICP-MS sampling. (b) Human IgG was quantitated using Western blot analysis after protein A Sepharose immunoprecipitation. In this experiment, a concentration range of 0.5–500 ng/20 μL of human IgG was prepared in triplicate and loaded into the wells of a 7.5% SDS-PAGE, which was then run and transferred to nitrocellulose. The nitrocellulose was blocked and then exposed to anti-human horseradish peroxidase-tagged antibody followed by ECL substrate (Super Signal, Pierce). The IgG band intensities were quantified using an imager at 5 and 20 s intervals.

electroblotting, and proteins of interest can be detected by probing with horseradish peroxidase-tagged antibodies. Exposing the blot to chemiluminescent substrate and sensitive film paper allows the protein of interest to be analyzed. In the experiment shown in Figure 9.6(b), it is apparent that 1 ng in the longest exposure (20 s) is the lowest amount of human IgG that could be detected, while 2.5 ng could be reliably detected in both exposures (5 and 20 s). The expected linear relationship between signal and protein concentration was observed only between 2.5 and

25 ng of IgG, which may be due in part to the limited capability of the imager (256 levels of gray) in data acquisition. Western blotting has one advantage that is currently beyond the reach of ICP-MS detection, which is that low volumes of sample can be easily analyzed. However, compared to ICP-MS detection, the sensitivity and the linear dynamic range of signal to protein concentration of Western blotting are poor. In terms of multiplexing potential, it is apparent that the resolution of the gel limits the number of proteins that can be analyzed simultaneously, whereas the number of distinguishable isotope tags that are available limits the ICP-MS approach.

(b) Silver enhancement of nanogold signal in ICP-MS coupled immunoassays

In electron microscopy, silver is frequently used to enhance the gold signal, by making the particles appear larger under the microscope. Enhancement of the nanogold signal using silver reagent (Nanoprobes) was attempted in an immunoprecipitation-coupled ICP-MS study (Figure 9.7). It was found that the silver improved the detection limit of antigen to 0.01 pg protein/mL.

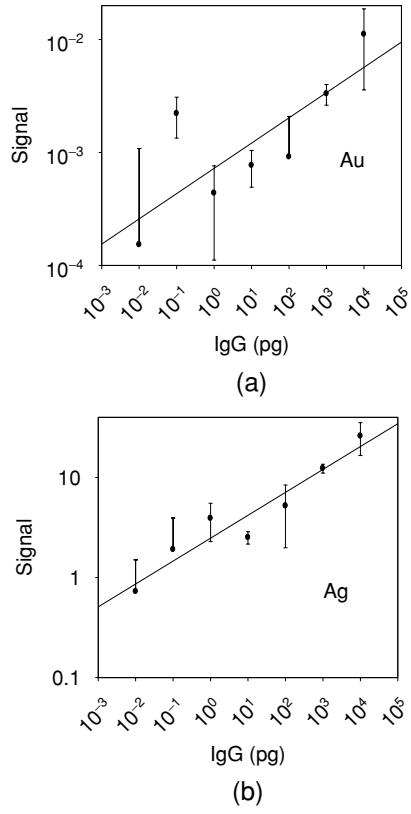

Figure 9.7 Silver enhancement of nanogold signal in the ICP-MS-coupled immunoassays. A series of immunoprecipitation reactions were set up containing 8 µL of 25% protein A Sepharose with serial dilutions of human IgG (0.01 pg to 10 ng). Samples were prepared in triplicate. After a shaken incubation for 1 h at room temperature, 20 µL of 1:50 anti-human Fab'-nanoAu was added and mixed for 2 h. The beads were washed four times and then exposed to 300 µL of fresh developer (Nanoprobes). After washing the beads, nanogold and silver were dissolved in acid spiked with 1 ppb Ir for sample uptake into the ICP-MS. The gold signal is shown in panel (a) and the silver signal is shown in panel (b).

However, the silver aggregates were found to not be uniform, in part because the silver development protocol is time sensitive and did not yield a 1:1 signal with increasing protein concentration. Although silver enhancement is successfully used for its intended purpose in enhancing particle detection in electron microscopy, it was found to be less suitable for the present method.

9.2.3 Conclusion

Several novel biological applications of ICP-MS in which various proteins were quantitated through the use of distinguishable elemental tags have been demonstrated. It has been found that the sensitivity of ICP-MS-linked immunoassay is comparable with that of radioisotope detection. In addition, it has been demonstrated that the simultaneous detection and quantitation of more than one analyte in a complex mixture yields reproducible and linear results. Overall, ICP-MS was found to offer several benefits over traditional immunoassay methods, such as enhanced precision, sensitivity, dynamic range, and ability to directly analyse the tag eliminating the need for a substrate or chelator. In addition, with ICP-MS elemental analysis is not affected by biological impurities or contaminants, nonspecific background is not a function of time, elemental analysis is not affected by protein degradation, which allows for long-term storage prior analysis and sensitivity is improved linearly with the number of atoms of a given isotope in the tag.

References

1. Baranov, V. I., Bandura, D. R., and Tanner, S. D. (2001) ICP-MS as an elemental detector in immunoassays. Speciation without chromatography. In *European Winter Conference on Plasma Spectrochemistry*, Hafjell, Norway, 2001, Book of Abstracts, p. 85.
2. Zhang, C., Zhang, Z., Yu, B., Shi, J., and Zhang, X. (2002) Application of the biological conjugate between antibody and colloid Au nanoparticles as analyte to inductively coupled plasma mass spectrometry. *Anal. Chem.*, **74**, 96–9.
3. Baranov, V. I., Quinn, Z. A., Bandura, D. R., and Tanner, S. D.(2002) A sensitive and quantitative element-tagged immunoassay with ICP-MS detection. *Anal. Chem.*, **74**, 1629–36.
4. Baranov, V. I., Quinn, Z. A., Bandura, D. R., and Tanner, S. D. (2002) The potential for elemental analysis in biotechnology. *J. Anal. At. Spectrom.*, **17**, 1148–52.
5. Quinn, Z. A., Baranov, V. I., Tanner, S. D., and Wrana, J. L. (2002) Simultaneous determination of proteins using an element-tagged immunoassay coupled with ICP-MS detection. *J. Anal. At. Spectrom.*, **17**, 892–6.
6. Carson, R. T. and Vignali, D. A. (1999) Simultaneous quantitation of 15 cytokines using a multiplexed flow cytometric assay. *J. Immunol. Methods*, **227**, 41–52.
7. De Jager, W., te, V. H., Prakken, B. J., Kuis, W., and Rijkers, G. T. (2003) Simultaneous detection of 15 human cytokines in a single sample of stimulated peripheral blood mononuclear cells. *Clin. Diagn. Lab. Immunol.*, **10**, 133–9.
8. MacBeath, G. (2002) Protein microarrays and proteomics. *Nat. Genet.*, **32**(*Suppl.*), 526–32.
9. Nanogold Conjugates, Nanoprobes, http://www.nanoprobes.com.
10. Andreu, E. J., Martin de Llano, J. J., Moreno, I., and Knecht, E. (1998) A rapid procedure suitable to assess quantitatively the endocytosis of colloidal gold and its conjugates in cultured cells. *J. Histochem. Cytochem.*, **46**, 1199–201.
11. Martin de Llano, J. J., Andreu, E. J., and Knecht, E. (1996) Use of inductively coupled plasma-mass spectrometry for the quantitation of the binding and uptake of colloidal gold-low-density lipoprotein conjugates by cultured cells. *Anal. Biochem.*, **243**, 210–7.
12. DELFIA, Perkin Elmer. Life Sciences, http://www.perkinelmer.com.

9.3 ENVIRONMENTAL ANALYSIS

Bill Spence

9.3.1 Some history of environmental legislation of concern to ICP-MS

During the latter half of the twentieth century, public awareness of environmental issues began to increase because of heightened publicity of such issues as the undesirable effects of herbicides, pesticides, toxic metals, smog, global warming and the greenhouse effect. There became a groundswell of public opinion towards cleaning up the environment, which inevitably provoked some political action. Consequently, a number of countries began forming government bodies to act upon the public's growing concern. Notably, in 1970, the U.S. government formed the Environmental Protection Agency (EPA). Many other countries formed similar bodies, for example the British government formed central and local government departments such as the National Rivers Authority, Her Majesty's Inspectorate of Pollution and local authority waste management departments. In 1990, with the passing of the Environment Act, these were consolidated, forming the Environment Agency in England and Wales and the Scottish Environmental Protection Agency in Scotland.

The main objectives for these bodies are to protect and improve the environment. In order to do this the environment must be monitored to judge if and when pollution incidents occur, what the pollutant is, how much of it is present, what the effect will be (principally on human health) and who or what is responsible for it. This requires that such bodies heavily employ chemical analysis for environmental monitoring purposes. One such example is the analysis of environmental samples for elemental content. Environmental scientists employed atomic absorption spectrophotometry (AAS) and ICP atomic emission spectrometry for such measurements for many years, but there was always a need to measure lower concentrations for greater numbers of analytes and to produce results more rapidly. Consequently, the advent of ICP-MS triggered much interest from environmental scientists. By the mid-1980s, the first commercially available quadrupole ICP-MS instruments were being used globally by environmental analytical chemists. The technique was seen as a logical progression from the already highly successful optical ICP technique, combining the multi-element character of ICP with the low detection limits of graphite furnace AAS.

By this time there was a great push for standardisation of analytical methodology within the now powerful US EPA. Driven by the more prolific organic compound analysis techniques, the EPA set about producing prescriptive standard methodologies for common analytical measurements. The documents they prepared prescribed the acceptable analytical techniques for analysing particular parameters and gave an overview of how to perform the analysis, specifying quality control procedures including the type, frequency and acceptability of each. Table 9.1 gives the important US EPA methods for ICP-MS. These can be downloaded in full from the EPA website[1] free of charge.

At around the same time, much of the rest of the world was putting together regional or local performance-based method standardisation; i.e. statistical performance characteristics were specified instead of analytical techniques.

Table 9.1 EPA methods for ICP-MS

Office responsible	Method	Matrix	Date
Office of Water	200.8	Waters	1991
Office of Solid Waste	6020	Multiple matrices	1994
Office of Solid Waste	6020A	Multiple matrices	1998
Contract Laboratory Program	ILM05.3	Multiple matrices	2004

9.3.2 Environmental sample types

Environmental analysts may be interested in measuring metal concentrations in potentially any type of environmental material. The most common sample types for ICP-MS analysis include drinking waters, process waters, surface waters, groundwaters, effluents, and digests of sewage sludges, soils, sediments and biota. Sample preparation for these is a large topic in its own right and the most appropriate preparation method may depend upon the analyte(s) of primary interest. The US EPA has produced methods for sample preparation, including a number of digestion techniques for various matrices.[2]

9.3.3 Drinking water analysis in the United States

Drinking water is analysed to enforce compliance with legislation dictating the quality of water fit for human consumption. In the United States, this type of analysis is performed to ensure that supplied water complies with the requirements of the Primary Drinking Water Standard,[3] a national standard enforced by the EPA. Simply put, all supplied waters for human consumption must contain less than the maximum contaminant level (MCL) for each monitored analyte. Tables 9.2 and 9.3 give the MCLs for metallic species in the Primary Drinking Water Standard

Table 9.2 Metals MCLs from the Primary Drinking Water Standard (40CFR141.51)

Contaminant	MCL (mg/L)
Barium	2
Cadmium	0.005
Chromium	0.1
Mercury	0.002
Selenium	0.05
Antimony	0.006
Beryllium	0.004
Thallium	0.002
Arsenic	0.01

Table 9.3 Metals MCLs from Secondary Drinking Water Standard (40CFR143.3)

Contaminant	Level (mg/L)
Aluminium	0.05 to 0.2
Copper	1.0
Iron	0.3
Manganese	0.05
Silver	0.1
Zinc	5

and the levels in the Secondary Drinking Water Standard.[4] The Secondary Drinking Water Standard represents reasonable goals for drinking water quality. Provided that public health and welfare are not adversely affected, each state may establish higher or lower levels, which may be appropriate depending upon local conditions such as lack of availability of alternative water sources.

The EPA's Method 200.8, entitled 'Determination of Trace Elements in Waters and Wastes by Inductively Coupled Plasma Mass Spectrometry', is the approved ICP-MS method for the measurement of analytes in water and is applied to drinking water to check compliance with the Primary and Secondary Drinking Water Standards. The corresponding ICP-AES method is 200.7, which also includes 'major' elements, such as calcium and sodium. Since acquiring 40CFR 141 approval, Method 200.8 has found widespread use in the United States and elsewhere and it forms the core of many newer EPA procedures. Large numbers of water samples are determined using Method 200.8 for regulatory compliance monitoring as well as private water analysis. Method 200.8 provides guidelines on general laboratory practices such as sample preparation, calibration standards and correction equations. It also provides specific rules on various analytical practices that must be followed, including elements covered, required isotopes, quality control practices and instrument validation. Method 200.8 covers the determination of the following elements: Al, Sb, As, Ba, Be, Cd, Cr, Co, Cu, Pb, Mn, Hg, Mo, Ni, Se, Ag, Tl, Th, U, V and Zn. Some current ICP-MS instruments are also suitable for the measurement of group I and II elements at the typical high mg/L concentrations found in most natural waters, although the technique is not approved for these measurements in the United States. Since technology invariably moves faster than environmental legislation, it is likely that the technique will become approved in the near future.

Method 200.8 describes a protocol for determining the method detection limit (MDL) as well as the linear dynamic range (LDR). For the MDL, the analyst sets up the instrument hardware and method as intended for the analysis, and then analyses a reagent blank solution spiked at 2–5 times the estimated detection limit. Seven repeats are required over three non-consecutive days. The standard deviation is determined for each of the sets and multiplied by 3.14 to arrive at the MDL. The data for the MDL calculation must have all the required calculations included, e.g. interference correction equations, as these can have a substantial influence on the MDL. Table 9.4 lists some typical MDL values obtained as per the method for a standard quadrupole ICP-MS instrument.

Table 9.4 Typical method detection limits

Element	MDL (μg/L)	Element	MDL (μg/L)	Element	MDL (μg/L)
Be	0.01	Ni	0.1	Cd*	0.01
B	0.1	Cu	0.05	Sb	0.005
Al	0.05	Zn	0.05	Cs	0.005
Ti	0.02	As*	0.05	Ba	0.01
V*	0.01	As†	0.2	Hg	0.01
V†	0.5	Se*	0.2	Tl	0.005
Cr	0.01	Sr	0.01	Pb	0.005
Mn	0.005	Mo	0.005	Tl	0.005
Co	0.005	Ag	0.005	U	0.001

* Interference correction equation applied.
† MDL in presence of 0.5% HCl/2% HNO_3.

In general, the MDL is a function of sensitivity, background signal or contamination, and signal stability. The ICP-MS technique generally produces a high signal-to-background ratio and good, signal stability, which facilitates achievement of MDLs that easily meet most environmental analysis requirements when sufficient integration time per element is used. It is important that contamination is kept under control, especially for environmentally abundant elements such as Al, Zn, etc., since any contamination will degrade the MDL. Some elements are limited in their MDL by spectral background features. Interference equations also affect the MDL (see Table 9.4), since they employ the monitoring of additional peaks and, accordingly, propagate their errors. Whilst MDL values are important, it is often at higher concentration ranges where ICP-MS technology is challenged to meet everyday sample needs. It would be desirable to employ an analytical technique capable of measuring tens to hundreds of mg/L in environmental samples, as concentration ranges can vary enormously from sample to sample. The upper-range limit is termed the linear dynamic range (LDR). Method 200.8 defines the upper LDR to be the concentration at which an observed signal deviates by less than 10% from that extrapolated by the lower standards. Sample dilution can facilitate the measurement of high concentrations, but at additional effort, cost and error. Recent generations of some instruments have introduced specialised interface designs and sensitivity attenuation technologies to allow calibrations for matrix elements, e.g. Na, K, Mg and Ca, well in excess of 100 ppm.

The instrument performance must be validated prior to the sample run according to the 200.8 method. This includes a 30 min instrument warm-up, mass calibration, peak resolution and stability check using the tuning solution (a multi-element mix spanning the mass range, e.g. Be, Mg, Co, Y, In, Ba, Tb, Pb, U). Peak scanning of ^{24,25,26}Mg and ^{206,207,208}Pb is used to verify the mass calibration of the low-and high-mass elements and the peak width at 5% peak height is used to check the resolution. If the position of the measured peak maximum is >0.1 amu from the current calibration position, this indicates that a mass calibration must be performed to correct the mass position. The resolution must be set to approximately 0.75 amu at 5% peak height. Some instrument software suites allow for these parameters to be conveniently checked using an automated sequence.

Methods like 200.8 were written prior to the introduction of the dual mode (pulse/analog) detectors that are most frequently used in current instrumentation; therefore no mention is made of adjustment or calibration of the detector. Such detectors should regularly be adjusted in three manners:

(1) The analog voltage should be set to a level that provides the required cross-calibration factor (i.e. analog to pulse count scaling factor).
(2) The pulse count voltage should be optimised to give a signal plateau.
(3) The two detector modes should be calibrated to generate the conversion factor from analog counts to equivalent pulse counts.

This stage is important for such detectors as a non-optimised detector will produce long-term sensitivity drift during the analysis. Similarly, the detector cross-calibration must be performed regularly if accurate concentrations are to be measured above the pulse counting threshold. The frequency of performing these routines depends upon the magnitude of signal exposure. Most laboratories may perform the voltage optimisations perhaps once per week, while the cross-calibration should be performed daily for maximum accuracy on analog measurements. Analog accuracy is best when a cross-calibration factor has been calculated for the actual analyte of interest, rather than interpolating the factor from a cross-calibration factor versus mass curve (see Chapter 3 for a detailed description of ICP-MS detectors). The software of most currently available instruments allow for these routines to be performed in a convenient automated sequence.

ICP-MS methods use internal standardisation to correct for matrix effects, particularly with environmental samples where high mg/L levels of matrix elements, relative to the calibration standards in dilute nitric acid, are frequently found. Internal standards also correct for long-term sensitivity drift associated with deposition of refractory matrix-based material around the cone orifices. Recent interface design improvements in some instruments resist such matrix deposition, improving long-term stability. Furthermore, after moderate exposure to matrix, most interfaces undergo a 'conditioning' effect, whereby the initial drift observed subsides to a more tolerable level. Method 200.8 lists nine candidate isotopes for internal standard use: ^{6}Li, ^{45}Sc, ^{89}Y, ^{103}Rh, ^{115}In, ^{159}Tb, ^{165}Ho, ^{175}Lu and ^{209}Bi. It requires that at least three are used, spanning the mass range of interest and these are generally associated with analytes of similar mass. For acceptance as a valid 200.8 run, the responses for all the internal standards relative to the original response of the calibration blank ('x') must stay within (x + 25%) or (x − 40%). Anything outside of this range mandates greater dilution, rinsing or reanalysis. Internal standards either are added manually as a multi-element mix to each blank, standard and sample or may be added on-line via a mixing T- or Y-piece.

The text of the method includes details on standard preparation, but does not prescribe calibration concentrations or the number of standards. Calibration concentrations should ideally span the typical sample concentration range, and for this reason the elements should be grouped according to their anticipated concentrations.

Method 200.8 specifies a variety of quality control standards. The first of these are the ICV and ICB (initial calibration verification and blank, respectively) samples. These must be run immediately after calibration and must be prepared from an alternative source to the calibration solutions. This test is designed to check the accuracy of the calibration. The CCV and CCB (continuing calibration verification and blank, respectively) samples are a similar check

that must be analysed once every 10 samples. There is no requirement for these to be prepared from an alternative source. Both quality control (QC) samples must measure within ±10% of the known concentration for compliance. Periodic running of a QC sample is also required. This sample is used as a check on the accuracy of the analytical process. It should be a reference standard from a second source that has been subjected to the sample preparation procedure. Analysis of this sample must have results within ±10% of the known value to be compliant with the method. Three types of blanks are involved with Method 200.8: (1) the rinse blank, (2) the calibration blank and (3) the reagent blank. The latter must be subjected to the sample preparation procedure. Except for the rinse blank, the others have minimum requirements that must be met. These are related to the reported MDL. A further quality control measure is a spiked blank that accompanies each batch of samples. This is termed the laboratory fortified blank (LFB) and its spike recovery must be within the range 85–115%.

A spike of known concentration into the sample matrix is required to verify recovery of the analyte in the matrix. This is termed the laboratory fortified matrix (LFM) and must be performed on each different matrix, for a minimum of 10% of all samples. For compliance, the results for the spike recovery must be between 70 and 130% of the spiked concentration. Often, adding spikes to true 'unknowns' is difficult, since 200.8 dictates that the spike must be 1–5 times greater than the concentration of the element in the unknown to be used as a QC test. In those cases where the spike is too low to verify performance (<30% of the indigenous sample concentration) the recovery calculation is not required.

Interferences related to environmental samples have been well documented.[5,6] While they may limit the ultimate detection capability of the technique, accuracy problems can be corrected, to a degree, using interference correction equations. Method 200.8 provides recommended equations that function well for common interferences, e.g. chloride-based interferences on vanadium and arsenic. Table 9.5 gives the equations listed in 200.8. The lead (Pb) equation is not a correction for interferences, but corrects for potential isotopic abundance variations that can be found in lead from natural sources.

Table 9.5 Correction equations for the 200.8 method

Equation	Purpose
$^{75}As = {}^{75}M - 3.127 \times ({}^{77}M - 0.815 \times {}^{82}M)$	Corrects for the ArCl interference on As, taking into account the Se contribution at *m/z* 77
$^{111}Cd = {}^{111}M - 1.073 \times ({}^{108}M - 0.712 \times {}^{106}M)$	Corrects for the MoO interference on cadmium, taking into account the cadmium contribution at *m/z* 108
$^{98}Mo = {}^{98}M - 0.146 \times {}^{99}M$	Corrects for the ^{98}Ru isobaric overlap on ^{98}Mo
$^{208}Pb = {}^{206}M + {}^{207}M + {}^{208}M$	Corrects for natural lead isotopic abundance variations
$^{51}V = {}^{51}M - 3.127 \times ({}^{53}M - 0.113 \times {}^{52}M)$	Corrects for the ClO interference on V, taking into account the Cr contribution at *m/z* 53

For many elements, Method 200.8 requires more than one isotope to be monitored. This is intended as an alternative or to provide information on potential interferences. In most cases one isotope will always be preferred for quantification. Table 9.6 gives the recommended isotopes and additional masses that must be monitored.

Table 9.6 Required isotopes for monitoring in Method 200.8

Isotope	Element
27	Aluminium
121, **123**	Antimony
75	Arsenic
135, **137**	Barium
9	Beryllium
106, 108, **111**, 114	Cadmium
52, 53	Chromium
59	Cobalt
63, 65	Copper
206, **207**, **208**	Lead
55	Manganese
95, 97, **98**	Molybdenum
60, 62	Nickel
77, **82**	Selenium
107, 109	Silver
203, **205**	Thallium
232	Thorium
238	Uranium
51	Vanadium
66, 67, 68	Zinc
83	Krypton
99	Ruthenium
105	Palladium
118	Tin

Note. Isotopes in bold indicate that they are the recommended isotopes for reporting.

9.3.4 Drinking water analysis in Europe

The European legislation covering drinking water is European 'Council Directive 98/83/EC of 3 November 1998 on the quality of water intended for human consumption'. Each European Member State was required to transcribe this into their local legislation. Again, the legislation prescribes a set of maximum allowable concentrations or 'parametric values' for each analyte and analysis is performed to ensure that these figures are complied with. Table 9.7 gives 98/83/EC parametric values for elements that can be measured by ICP-MS.

Table 9.7 Parametric values from 98/83/EC and analytical methodology performance requirements

Element	Parametric values (mg/L)	Trueness % of parametric value	Precision % of parametric value	Required limit of detection (mg/L)
Antimony	0.005	25	25	0.00125
Arsenic	0.01	10	10	0.001
Boron	1	10	10	0.1
Cadmium	0.005	10	10	0.0005
Chromium	0.05	10	10	0.005
Copper	2	10	10	0.2
Lead	0.01	10	10	0.001
Mercury	0.001	20	10	0.0002
Nickel	0.02	10	10	0.002
Selenium	0.01	10	10	0.001
Aluminium	0.2	10	10	0.02
Iron	0.2	10	10	0.02
Manganese	0.05	10	10	0.005
Sulfate	250	10	10	25
Sodium	200	10	10	20

Unlike the United States, there is no specific standard methodology that is applicable to the European legislation. The European approach is performance-based rather than prescriptive. The legislation lays out many of the analytical performance characteristics required, in terms of accuracy, precision and detection limit but does not stipulate the methodology to use in order to achieve the required performance levels. Some Member States suggest how methods should be validated; for example in the United Kingdom, the government body responsible for enforcing the water supply regulations, the Drinking Water Inspectorate, has produced a document that gives guidance on how to translate the European legislation.[7] This suggests the use of analytical performance evaluation following the guidance of a publication by the Water Research Centre (WRc) entitled 'NS30 A Manual of Analytical Quality Control for the Water Industry'. This manual is widely used as the basis for the performance testing of analytical methods, even for non-regulatory analysis. Performance testing normally consists of analysing at least 11 batches of the following sample types, run in duplicate:

(1) Blank samples
(2) Quality control standards at two levels prepared from an alternative source to that of the calibration
(3) Typical matrix samples spiked at two levels with the analytes of interest
(4) Where possible, reference materials of similar matrix.

From the data obtained, a variety of statistical figures may be determined, including the detection limit, the accuracy, the recovery in typical sample matrices (hence identifying any matrix effects) and the precision (within and between batch). Furthermore, an ongoing statistical process control system can be set up for day-to-day quality control purposes. This normally

consists of running QC at a given frequency. The results of all QC standards are plotted on a control chart and the validity of each QC-bracketed batch of unknowns is assessed by comparing the QC standard results with the standard deviations of the previously collected data. Normally, results within 2 standard deviations of the mean are deemed acceptable, those between 2 and 3 standard deviations are classed as a warning and those outside 3 standard deviations are classed as a failure. Two consecutive warning values, for the same analyte, are also classed as a failure. If a QC standard produces a failure, the samples associated with it must be reanalysed.

9.3.5 Drinking water analysis in the rest of the world

Many other countries have their own legislation on the quality of drinking water, for example, Japan. The Japanese legislation is similar to the European one in that it does not specify how the analysis should be performed. The Japanese drinking water limits are given in Table 9.8.

Table 9.8 Japanese maximum permissible concentrations for drinking water

Analyte	Maximum permissible concentration (mg/L)	Analyte	Maximum permissible concentration (mg/L)
Al	0.2	Mo	0.07
Sb	0.002	Na	200
As	0.01	Ni	0.01
B	0.2	Pb	0.05
Cd	0.01	Hg	0.0005
Cr	0.05	Se	0.01
Cu	1	U	0.002
Fe	0.3	Zn	1
Mn	0.05		

Although there are no specific methods defined for the analysis of drinking waters within the legislation of countries outside the United States, an ISO ICP-MS method has recently been published [ISO/CD 17294-1 'Water quality – Determination of 61 elements by inductively coupled plasma mass spectrometry (ICP-MS)']. This standard method is not yet widely used.

9.3.6 Other environmental sample types

Environmental sample types other than drinking water are covered by a multitude of legislation the world over. Again, the United States has prescribed methods for these, while other countries tend to operate performance-based approaches to method validation. The vast majority of solid environmental materials that can be digested in some way can be analysed using the EPA's Method 6020, 6020A or ILM05.3, although these were primarily developed for the analysis of solid wastes, contaminated soils and associated groundwater.[8–10]

The EPA's Office of Solid Waste (OSW) regulates waste under the Resource Conservation and Recovery Act (RCRA). The act's goals are to

(1) protect the public from the hazards of waste disposal,
(2) conserve energy and natural resources by recycling and recovery,
(3) reduce or eliminate waste, and
(4) clean up waste, which may have spilled, leaked, or been improperly disposed of.

The EPA publication SW-846, entitled 'Test Methods for Evaluating Solid Waste, Physical/Chemical Methods', is the OSW's official compendium of analytical and sampling methods that have been evaluated and approved for use for analysis relating to the RCRA regulations. SW-846 functions primarily as a guidance document setting forth acceptable methods for use in RCRA-related sampling and analysis requirements. The SW-846 volume 6020 describes the use of ICP-MS instrumentation for determining a variety of metallic elements in aqueous and solid media. In draft edition IVA, the method was replaced with 6020A.

Much like Method 200.8, Methods 6020 and 6020A provide guidelines on general laboratory practices such as sample preparation, instrument set-up, calibration of analytes and interference correction. They also provide specific rules on various analytical practices that must be followed, including elements covered, required isotopes, quality control practices and instrument validation. Since both methods are well established and readily available in the public domain they have become widely adopted as templates for methodologies used by a host of laboratories undertaking environmental analysis worldwide. The requirements of these methods are broadly similar, having the aim of ensuring a consistently high quality of analytical data by enforcing compliance with a variety of stringent instrument and analytical performance checks, as outlined in Tables 9.9 to 9.11. Method 6020A extended the analytical scope to include mercury (after fixing all analytical solutions with 2 mg/L gold) and increased the interferent concentrations in the interference check solutions.

The US EPA Contract Laboratory Program (CLP) is a national network of EPA personnel, commercial laboratories and support contractors. The CLP supports the EPA's Superfund program, created under the 1980 Comprehensive Environmental Response, Compensation, and Liability Act (CERCLA), and currently under the 1986 Superfund Amendments and Reauthorization Act (SARA). The CLP's primary service is the provision of analytical data of known and documented quality, through its routine analytical services, to its customers. All analytical services are performed by EPA-approved contract laboratories that must meet stringent requirements and standards in order to be a part of the CLP.

Each sample processed by the CLP is properly documented to ensure timely and accurate analysis for all requested parameters. This process creates robust analytical data that can be used in potential enforcement actions. CLP data is used for a variety of purposes such as defining the nature and extent of contamination at Superfund sites, determining appropriate clean-up action, determining emergency response and remedial actions, and enforcement or litigation activities.

The inorganic analysis undertaken by CLP laboratories is described in the document ILM05.3, entitled 'US EPA Contract Laboratory Program Statement of Work for Inorganic Analysis, Multi-Media, Multi-Concentration'. Exhibit D, Part B, describes the use of ICP-MS instrumentation for determining a range of metallic elements. ILM05.3 provides guidelines similar to those set out in the SW-846 methods. The aim of ILM05.3 is to ensure a consistently high quality of analytical data by enforcing compliance with stringent instrument and analytical performance checks outlined in Tables 9.9 to 9.11.

Table 9.9 Summary of instrument calibration and check requirements

Check code	Check name	Purpose	Frequency	6020A limits	ILM05.3 limits
–	Mass calibration/ resolution setting	Ensures the correct mass is measured at its maximum and that peaks are properly resolved	Prior to each analytical run (daily)	Masses must not deviate by >0.1 amu from their nominal position and peak width must be <0.9 amu at 10% peak height	Mass calibration must be within the manufacturer's specifications
–	Stability and precision	Ensures the instrument is properly optimised and thermally stable	Prior to each analytical run (daily)	<5% RSD on at least four measurements	<5% RSD on at least five measurements
–	Calibration	Calibrates the instrument response for measurement	Daily or when required	Recalibration must be performed when QC samples are outside of specification	Recalibration must be performed when QC samples are outside of specification
IDL	Instrument detection limit	Estimates the detection limit of the instrument from seven analyses of a blank over three non-consecutive days	Every 3 months or after major instrument maintenance or hardware replacement	–	–
MDL	Method detection limit	Assesses the detection limit of the method according to 40CFR136	Annually or after major instrument maintenance or hardware replacement	–	<50% of contract required quantitation limit value
LDR	Linear dynamic range	Assesses the linear range of the instrument using three or more standards	Quarterly or after major instrument maintenance or hardware replacement	–	High standard must be within ±10% of the expected value extrapolated from the low standards

Table 9.10 Summary of method calibration check requirements

Code	Check name	Purpose	Frequency	6020A limits	ILM05.3 limits
ICV	Initial calibration verification	Checks the accuracy of the calibration against a second calibration source	After initial calibration	90–110%	90–110%
ICB	Initial calibration blank	Initial check of read-back at blank level	After initial calibration	Within ±3 IDL	Within ±3 IDL
ICS A	Interference check solution A	Checks for freedom from interference at blank level in the presence of interfering species	After initial calibration	No specific require-ments	<3 × contract required quantitation limit value (CRQL)
ICS AB	Interference check solution AB	Checks that analytes are measured accurately in the presence of interfering species	After initial calibration	No specific require-ments	Within ±3 CRQL or within 20% of the true value (whichever is the greater)
CRI	Contract required quantitation limit check	Checks accuracy at the required quantitation limit	After each calibration and every 20 samples	–	70–130%, or 50–150% for Co, Mn, Zn

Territories outside the United States do not have such prescriptive methods and consequently many laboratories base their methods on those of the EPA or design their own.

9.3.7 Best practice for environmental analysis

This section details some hints and tips for best practice when performing the analysis of environmental samples by ICP-MS. Some important factors to consider include the following:

(1) Sample transport effects
(2) Matrix-induced signal suppression effects
(3) Matrix-induced signal drift
(4) Spectral interferences, such as plasma gas and matrix-based polyatomic interferences

Inaccuracies due to sample transport effects arise from differences (from calibration to sample) in the physical properties that govern the transport efficiency of the solution from its container

Table 9.11 Summary of quality control requirements

QC code	QC name	Purpose	Frequency	6020A limits	ILM05.3 limits
CCV	Continuing calibration verification	A continuing periodic check on accuracy and drift	After calibration and once every 10 samples	90–110%	90–110%
CCB	Continuing calibration blank	A continuing periodic check on the read-back at blank levels	After calibration and once every 10 samples	Within ±3 IDL	Less than contract required quantitation limit value
MXS	Matrix spike	Checks the recovery of a pre-preparation (normally pre-digestion) spike on an unknown sample	1 per sample delivery group (batch)	–	75–125%
PDS	Post-digestion spike	Checks the recovery of analytes spiked into an unknown sample after preparation (normally digestion)	Once per 20 samples per matrix	75–125%	75–125%
DUP	Duplicate	Checks the reproducibility of results by analysing an unknown sample in duplicate	Once per 20 samples per matrix	±20% relative percentage difference	±20% relative percentage difference
SER	Serial dilution	Checks for matrix effects by assessing the variation of results for an unknown sample before and after dilution	Once per 20 samples per matrix	±10% of the original undiluted sample result after dilution correction	±10% of the original undiluted sample result after dilution correction
LCS	Laboratory control sample	Checks the accuracy of the entire analytical process	Once every 20 samples	80–120%	80–120%

to the plasma.[11,12] As an exaggerated example, consider a calibration solution prepared in dilute nitric acid and a digested sludge material. The two samples have different viscosities (greater for the digested sample) and surface tensions, and so the sample will have greater resistance to being pumped along the narrow bore uptake tube to the nebuliser. Furthermore, the sample will not produce an aerosol with exactly the same efficiency as the calibration solution and the droplet size distribution of the aerosol may be markedly different. These effects will impact upon the accuracy of the analysis because of the variation in the overall mass flow of solution into the plasma.

Matrix-induced suppression effects occur because of differences (from calibration to sample) in the concentration of the sample matrix. For example, a 1 ppb solution of an analyte in dilute nitric acid might give a signal of 100 000 cps. The same concentration of analyte in seawater might give a signal of only 50 000 cps (after correction for transport effects). This effect is principally due to two phenomena: ionisation suppression[13] in the plasma and space-charge effects in the interface region of the instrument.[14,15] Although matrix-induced enhancement effects can occur, these are rare in environmental sample matrices.

Matrix-induced signal drift generally occurs as a result of deposition of matrix-based material onto the cones. This normally manifests itself as a downward signal drift with time because of the progressive constriction of the cone apertures.[16]

These three phenomena can be corrected, to a degree, by the use of internal standardisation techniques (see Chapter 4). For matrix-induced signal drift, an external drift correction technique may also be used, whereby the drift is corrected by use of drift correction standards run at intervals during the analysis. Spectral interferences are discussed in detail in Chapters 4 and 8. The effects of most of these problems can be minimised through careful instrument set-up and/or selection of an appropriate instrument configuration or sample introduction components.

9.3.7.1 Instrument set-up

Because of the generally high levels of total dissolved solids found in environmental samples, it is normally best to introduce as little sample as possible to the instrument. The less sample matrix introduced per unit time, the more effective the decomposition in the plasma. This results in lower matrix effects and lower formation of polyatomic species. However, most nebulisers have an optimum sample uptake rate and therefore performance may be adversely affected if the sample flow rate is set below a threshold value. This must be taken into consideration when setting sample uptake rates and selecting nebulisers. For environmental analysis it is normally best to pump the sample into the nebuliser, rather than allowing the nebuliser to 'free aspirate', as this will reduce the severity of viscosity-induced transport effects. An uptake rate between 0.4 and 0.8 mL/min is generally appropriate. Lower uptake rates (e.g. 0.1–0.4 mL/min) can be desirable if a suitable nebuliser is used. The liquid uptake rate is best set using a combination of the peristaltic pump speed and the internal diameter of the pump tube. The pump tube should be narrow enough to enable the use of a reasonably fast pump rate so as to minimise the effect of pulsing caused by the action of the peristaltic pump rollers against the tube.

The choice of nebuliser is also of importance because of the risk of blockage or 'salting-up' when high matrix samples are aspirated over extended periods of time. Although concentric devices give good sensitivity and stability, this is the design that is most prone to blockage. Alternative designs such as the cross-flow, V-groove or Babington types may provide better resistance to blockage along with more recent designs such as the Burgener parallel path nebulisers.

Whichever nebuliser is selected, the nebuliser gas flow rate should be carefully optimised by monitoring the cerium oxide (CeO^+, m/z 156) to cerium (Ce^+, m/z 140) ratio whilst aspirating a solution containing cerium at a reasonable signal level, e.g. 1–100 μg/L. Most instruments are capable of producing a CeO^+/Ce^+ ratio of <0.02. The magnitude of this ratio is a good indicator of the processing ability of the plasma. When the nebuliser gas flow is too high, the oxide will be high, indicating that the central channel of the plasma is relatively diffuse and cool and will therefore not break up refractory species (such as CeO) as effectively. Conversely, when the nebuliser gas flow is at its optimum, the oxide ratio will be at its minimum, indicating that the central channel is hot and is efficiently processing the sample. Nebuliser gas flow rate optimisation curves will vary with plasma RF power, with higher power plasmas requiring higher optimum nebuliser flows and vice versa. Similar oxide behaviour is observed when adjusting the ion sampling position along the axis of the plasma (oxides show a relative decrease in signal intensity as the sampling depth is increased owing to an increase in the residence time in the plasma, leading to improved decomposition).[6] The conditions producing the oxide minimum may not exactly correspond to the sensitivity maximum for non-refractory elements, but for environmental analysis it is preferable to run the most robust, stable set of conditions rather than the most sensitive.

The choice of spray chamber is also important, for two reasons: the aerosol droplet size distribution affects the sample processing characteristics in the plasma and the material of construction and the design of the spray chamber will influence the aerosol transport efficiency and sample washout characteristics. There is some evidence to show that double-pass spray chamber designs produce a higher proportion of easily processed, small droplets when compared to single-pass designs, although single-pass designs lend themselves to lower internal surface areas and internal volumes, producing more favourable washout characteristics.

The torch design also influences the sample processing ability of the plasma. The internal diameter of the injector tube will affect the sample aerosol velocity (and hence the residence time in the plasma) and the aerosol density. The longer the sample aerosol particle resides in the plasma and the less dense the aerosol spray entering the plasma, the more efficient the decomposition. Wider injector tubes tend to produce lower velocities through the plasma, resulting in better matrix decomposition. This has the effect of breaking down many of the interfering polyatomic species, such as metal oxides, and of reducing the build-up of material on the cones.

The cone and interface design itself have a dramatic effect on the performance of an instrument for the analysis of environmental samples. Some ICP-MS manufacturers have recently developed cone designs specifically for environmental analysis. These have different characteristics than traditional designs in that their materials of construction and geometric design yield better resistance to the deposition of sample matrix salts, produce a lower contribution from polyatomic species (for example iron may be analysed, without further performance enhancing hardware, at m/z 56 with background equivalent concentrations of the order of 0.03 mg/L), and alter the response curve of the instrument such that major elements (low mass species) may be analysed up to levels of hundreds of mg/L, while trace elements can be measured down to ng/L levels. The effects of deposition of matrix salts will be reduced by the use of the parameters discussed above and by using a slightly retracted sampling position, i.e. with the torch and load coil moved further back from the interface cones. Again, this prolongs the sample droplet residence time in the plasma, producing more complete decomposition. A further effect of concern is one frequently referred to as ‘conditioning’ the cones. This is the process of intentionally coating the cones with matrix-based material. When using a brand new or freshly cleaned set of cones, analysts

frequently report an initial drift of the signal intensity upon aspirating the sample matrix. As the sample matrix continues to be aspirated the signal appears to settle. This initial stabilisation period is known as the conditioning period, and many analysts condition their cones with a typical sample matrix for a few hours after replacing or cleaning the cones. To save time this may also be done for a shorter duration with a higher concentration of a synthetic solution containing similar matrix ions, e.g. 200 mg/L calcium. Reoptimising the lens system after conditioning can frequently regain some of the sensitivity that may have been lost. Figures 9.8 and 9.9 show that conditioning the cones produces better stability in the matrix.

The mass calibration and resolution set-up should be verified prior to analysis. This can be performed using an automated sequence on some systems and should be done by acquiring a

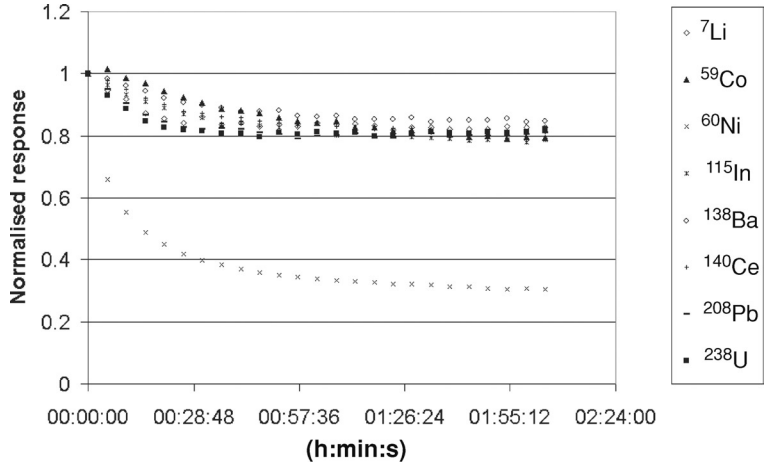

Figure 9.8 The effect of cone conditioning for a 1 ppb spike of the analytes shown in borehole water containing approximately 80 ppm Ca, 30 ppm Na, Mg and 5 ppm K – cone run from clean.

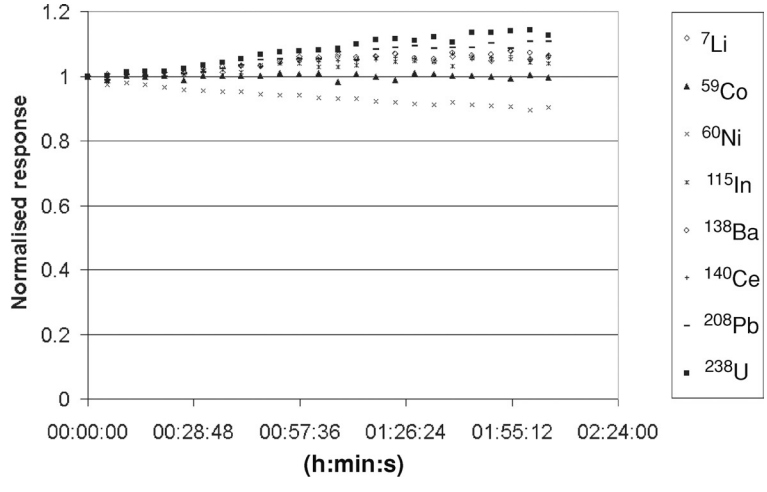

Figure 9.9 The effect of cone conditioning for a 1 ppb spike of the analytes shown in borehole water containing approximately 80 ppm Ca, 30 ppm Na, Mg and 5 ppm K – cone conditioned.

mass spectrum for a solution that contains analytes spanning the mass range of interest. If the peak maximum is more than 0.1 amu from the nominal position, a new mass calibration should be performed. If the peaks are wider than 0.8 amu at 5% peak height, the resolution should be adjusted accordingly. The detector voltage set-up should be checked weekly in accordance with the manufacturers' instructions. If a dual mode detector is used, a cross-calibration should be performed daily prior to analysis (see Chapter 3).

9.3.7.2 Analytical considerations

An important consideration for all ICP-MS analyses is the effect of contamination. This can be avoided for the most part by careful handling and common sense. Certain environmentally abundant elements such as zinc and aluminium are likely to present a significant contamination hazard. Ordinary household dust contains a high proportion of such metals. Similarly, many plastics contribute amounts of contamination upon addition of an acidified sample, prior to being cleaned. Care must be taken with the selection and pretreatment of all containers, tubes and volumetric ware. It is best to avoid glassware and instead use plastic. The ideal material is PFA (a fluoropolymer), although high-density polyethylene (HDPE) and polypropylene (PP) are cheaper alternatives that will suffice in most cases. All containers should be precleaned (surface leached) by soaking with 10% nitric acid for at least 24 h, followed by thorough rinsing with deionised water. It is best to dedicate containers to the storage of particular solutions, so that, for example, stock bottles used to store mg/L concentration solutions are never subsequently used for preparing μg/L solutions by mistake. It is best to avoid using glass pipettes; instead piston-type pipettes with disposable plastic tips are preferable. Tips should be used only once to avoid cross-contamination. Coloured tips should be avoided as the pigment can contain metals which will leach out and contaminate the solution. It is advisable to preclean pipette tips in a manner similar to the precleaning of containers described above. The addition of contamination to samples and standards may be prevented by avoiding pipetting directly from the storage container. All such containers should be opened for the absolute minimum of time. Contamination from the skin during handling can be avoided by wearing powder-free gloves. Although a clean-hood or bench fitted with a HEPA filter or a laminar flow cabinet is desirable for sample and standard preparation, they are not essential for most environmental work and satisfactory results can be obtained provided the analyst takes the appropriate precautions and keeps a clean working area. Autosamplers are frequently used for environmental analysis because of high sample numbers. An autosampler without exposed metallic components is desirable as corrosion products from such components can be a source of metallic contamination. Relatively cheap Perspex covers or cabinets are available for most autosamplers. These are a simple method of preventing sample contamination during long unattended runs.

As mentioned above, transport effects, suppression effects and drift can cause accuracy problems in ICP-MS. In environmental analysis, this is most commonly corrected for by the use of internal standards. An internal standard can be added to each solution either by volumetric addition or by mixing the flow of the internal standard solution and the sample (pumped separately) using a T- or Y-piece prior to the nebuliser. The latter option is often preferred as it does not require each sample to be accurately dispensed into a test tube. Since suppression and drift effects can be somewhat mass dependent, several internal standard isotopes are normally

selected, reflecting the mass range of interest. The criteria for the selection of appropriate internal standard isotopes (see also Chapter 4) are that a candidate isotope

(1) is not present in significant quantities in the sample;
(2) is not interfered by any of the species created from the sample matrix;
(3) does not produce any new interferences on the analytes of interest;
(4) does not produce any chemical incompatibilities with the analytes of interest;
(5) has mass similar to that of the analyte to be corrected;
(6) has a first ionisation potential similar to that of the analyte to be corrected; and
(7) behaves similarly to the analytes of interest such that it can correct for their signal changes in varying composition solutions.

For a suite of elements spanning a wide mass range, at least three internal standard isotopes are normally used: those representing each of the low-, mid- and high-mass regions. The list of candidate isotopes for use in the EPA Methods 200.8, 6020, etc., (described earlier) is a good set of options, although it is not necessary to use all of these. For an analysis spanning the full mass range, isotopes such as ^{6}Li (this must be isotopically pure), ^{45}Sc, ^{103}Rh and ^{209}Bi are a good choice. It is particularly difficult to find reliable low-mass isotopes for use as internal standards. For example, Li is often present at significant concentrations in environmental samples. To reduce the effect of this, the internal standard concentration may be set a little higher than normal, and in the case of lithium, a correction should be made for the contribution from the sample to the ^{6}Li signal by measuring the ^{7}Li signal. The EPA methods give a theoretical correction equation for this. Scandium suffers from interference from calcium hydride ($^{44}Ca^{1}H^{+}$) in samples containing high concentrations of calcium and $^{12}C^{16}O_{2}{}^{1}H^{+}$ in samples containing elevated levels of carbon. Again, the effect of these interferences can be masked by setting the scandium concentration at a level that gives a signal that is somewhat higher than that of the interfering species. Another frequently used isotope is ^{89}Y. This works well as an internal standard for most water samples, but is a poor choice for digests of soils, sediments, etc. as it frequently occurs in these materials at significant concentrations. Gallium can also be a good choice for a low-mid mass internal standard element, but care must be taken to use the ^{71}Ga isotope and not the ^{69}Ga isotope, as this is interfered by the doubly charged barium ion $^{138}Ba^{2+}$.

When multiple internal standards are used, most instrument software packages give the option either to interpolate analyte responses between the internal standards or to reference each analyte to a particular internal standard isotope. This is normally done on the basis of the internal standard that is closest in mass to the target analyte. Sometimes, some analytes behave unlike the internal standard, because of, for example, differences in ionisation. In such cases some analysts attempt to match this behaviour by utilising an internal standard of similar ionisation potential.

In cases where the internal standard isotope is indigenous in the sample, an enhanced signal for only this internal standard isotope will be observed. Most software packages have functionality to allow the affected isotope to be removed from the calculation for only the affected sample.

The example below shows the effect of internal standard correction on the accuracy of an analysis for cadmium in river water. Rhodium is used as the internal standard element. Raw counts per second data is given in Table 9.12.

An internal standard factor is calculated for each sample by dividing the rhodium count rate for the initial sample (blank) by that of each sample. Each cadmium count rate is multiplied by the factor to correct it for suppression, drift, etc. The corrected count rates are then used to calculate the sensitivity and this is used to calculate the concentration.

Table 9.12 Raw signal count rates for cadmium and rhodium

Sample	^{103}Rh	^{111}Cd
Blank	89045	2
50 ppb	85907	50389
NIST 1640	83819	21784

Tables 9.13 and 9.14 show how internal standard correction can improve the accuracy of an analysis. Prior to correction the recovery is 95% (Table 9.13) and after correction this increases to 97% (Table 9.14). This example shows a fairly modest change in the internal standard intensity from a blank to the sample, but internal standard correction is also effective in more extreme cases. When the suppression or drift effect becomes too extreme, however, the correction becomes questionable. EPA Method 6020 states that the internal standard recovery [100 × (sample internal standard counts)/(initial blank internal standard counts)] must be between 70 and 125% for the sample result to be valid. If the recovery falls outside this range owing to drift, the analysis must be terminated, the problem corrected and the sample must be reanalysed after full recalibration. If the recovery falls outside this range owing to suppression effects, the sample must be reanalysed after a dilution to reduce the matrix effect.

Table 9.13 Uncorrected data

Sample	^{111}Cd count rate	^{111}Cd concentration (ppb)	Sensitivity (cps/ppb)
Blank	2	0.0	1008
50 ppb	50 389	50.0	
NIST 1640	21 784	21.6	
Known		22.8	
Recovery %		95	

Table 9.14 Corrected data

Sample	^{103}Rh Count rate	^{111}Cd Uncorrected count rate	Internal standard factor	^{111}Cd corrected count rate	^{111}Cd corrected concentration (ppb)	corrected sensitivity (cps/ppb)
Blank	89045	2	1.000	2	0.0	1045
50 ppb	85907	50389	1.037	52229	50.0	
NIST 1640	83819	21784	1.062	23142	22.2	
Known					22.8	
Recovery %					97	

It is important to fully assess the effect of spectral interferences as these can seriously impair the accuracy of an analysis. For many of the problematic interferences that are commonly found in environmental analysis, mathematical correction methods can be used with reasonable success. There are two types of interference correction equation: those with theoretically derived factors

and those with empirically derived factors. Both types monitor the interferent at a mass other than the analyte mass of interest and then deduct the interference contribution from the mass of interest by use of a correction factor. Theoretical corrections monitor an alternative isotope of the interfering species and then use the isotopic abundance ratio to calculate the correction factor. An example is the polyatomic isobar $^{35}Cl^{16}O^+$ on ^{51}V. Here, the polyatomic species may be monitored at an alternative mass of 53 ($^{37}Cl^{16}O^+$ at m/z 53). The abundance ratio of $^{35}Cl/^{37}Cl$ is 3.127.[17] This ratio can be substituted into a correction equation that infers the ClO contribution at mass 51 from the measured signal at mass 53:

$$^{51}V = {}^{51}M - 3.127 \times {}^{37}Cl^{16}O$$

In this example, there is a complication due to the fact that chromium has an isotope at m/z 53. This contribution to the $^{37}Cl^{16}O^+$ signal must also be corrected. This can be done by monitoring chromium at m/z 52. The abundance ratio of $^{53}Cr/^{52}Cr$ is 0.1134.[17] This can be substituted into an equation to correct for the chromium contribution to the signal at m/z 53:

$$^{53}ClO = {}^{53}M - 0.1134 \times {}^{52}Cr$$

This approach can also correct for elemental isobaric contributions (for multi-isotopic elements). An example is the elemental isobar ^{114}Sn on ^{114}Cd. Tin may be monitored at an alternative isotope, e.g. m/z 118. The abundance ratio of $^{114}Sn/^{118}Sn$ is 0.0272.[17] This may be substituted into an equation to correct for the presence of tin when measuring cadmium at mass 114:

$$^{114}Cd = {}^{114}M - 0.0272 \times {}^{118}Sn$$

The advantages of this type of correction are that the abundance ratio does not change and the correction factor is therefore constant. The disadvantages are that it does not take mass-dependent sensitivity effects (mass bias) into account and that the accuracy depends on the type and magnitude of interference relative to the analyte. Also, there are some cases where theoretical corrections simply cannot be used because there is no alternative isotope of the interfering species to monitor. In such cases the interference may often be monitored indirectly and the correction factor may be calculated empirically.

An example is the polyatomic isobar $^{44}Ca^{16}O^+$, interfering with ^{60}Ni. In this case calcium oxide cannot be monitored at an alternative isotope since it falls in a complex region of the mass spectrum. However, the calcium content of samples can be monitored using ^{43}Ca (this isotope is selected as it is of low abundance and will give good dynamic range and is relatively free from interference). The formation of calcium oxide per unit quantity of calcium must be measured in order to calculate a correction factor. This is best done using a blank and several pure calcium standards, spanning the likely calcium concentration in the samples. Plots of signal intensity (y) versus calcium concentration (x) for ^{43}Ca and $^{44}Ca^{16}O^+$ (at mass 60) can be produced. The slopes of the two plots (in units of counts per second per unit calcium concentration) are then used to calculate the correction factor.

$$f = S_{CaO}/S_{Ca}$$

where f is the correction factor, S_{CaO} is the slope for calcium oxide at mass 60 and S_{Ca} is the slope for calcium at mass 43. This can then be substituted into a correction equation for ^{60}Ni:

$$^{60}Ni = {}^{60}M - f \times {}^{43}Ca$$

The advantage of this technique is that it produces accurate correction factors that take mass bias into account. The disadvantages are that the factor may change from day to day and with cone conditioning and that extra solutions must be analysed in order to calculate the factor.

The vast majority of interferences can be tackled using similar techniques. However, the use of such equations does have some limitations. When the interference is present, the detection limit for analytes using equations is compromised as the error in measuring the monitored species is propagated with that of the analyte. Furthermore, the correction will become increasingly inaccurate as the magnitude of the interference grows relative to the analyte.

9.3.8 Future development

Currently ICP-MS is an excellent technique for the analysis of environmental samples. By using some of the methods and techniques discussed it can be employed very successfully to perform regulatory analyses to check compliance with environmental law and can be used for research purposes.

One of the long-standing problems of the technique – polyatomic interferences – has been addressed to a degree with the advent of collision and reaction cell technology in ICP-MS (see Chapter 8). As this technology matures it will undoubtedly be utilised more frequently for environmental analysis. This technology is certainly of use for more accurate analysis at lower levels for analytes such as arsenic, selenium and vanadium in environmental matrices. An environmental application that is particularly likely to benefit from the use of collision and reaction cell technology is the direct analysis of seawater after only a dilution step. Until recently it would have been unthinkable to introduce seawater diluted by a factor of 1:10 into an ICP-MS because of both physical and spectral interference problems. In order to perform such an analysis with any degree of success would have required a matrix separation technique such as solid-phase chelation. However, recent developments in instrumentation, including sampling interface design improvements and the use of collision/reaction cells for interference removal, have allowed some success with ultratrace determinations in such matrices.[18]

The other area of considerable research that is likely to become part of the routine environmental analysis spectrum is speciation. As we continue to develop our understanding of the underlying variation in toxicity of the various metallic species, there will inevitably be a drive towards quantifying the actual species present rather than just the total elemental content. Californian environmental law is already poised to implement legislation on MCLs for hexavalent chromium [Cr(VI)]. The Californian EPA is currently investigating the possibility of implementing an MCL for this species following much publicity due to the release of the film *Erin Brockovich* in March of 2000 (see reference 19 for the latest information on this issue). ICP-MS can be used very effectively for the determination of Cr(VI) by using it as an element-specific detector coupled to a separation technique such as ion chromatography, liquid chromatography or capillary electrophoresis (e.g. reference 20). Similar hyphenated techniques can be used for determination of arsenic oxidation sates and species, antimony species and selenium species. Other species of interest are organomercury and organotin species for which GC-ICP-MS has been used (see Chapter 7 for further details).

With these new areas of development and the constant improvements to instrument design driving achievable detection limits lower and lower, ICP-MS has a bright future in environmental analysis.

References

1. US EPA website, www.epa.gov.
2. US EPA website, Office of Solid Waste, SW-846 Sample Preparation Methods for Metals Analysis, http://www.epa.gov/epaoswer/hazwaste/test/3_series.htm.
3. GPO website, page for 40 CFR part 141, http://a257.g.akamaitech.net/7/257/2422/14mar20010800/edocket.access.gpo.gov/cfr_2002/julqtr/40cfr141.62.htm.
4. GPO website, page for 40 CFR part 143, http://a257.g.akamaitech.net/7/257/2422/14mar20010800/edocket.access.gpo.gov/cfr_2002/julqtr/40cfr143.3.htm.
5. May, T. W. and Weidmeyer, R. H. (1998) *J. At. Spectrosc.*, **19**(5), 150–4.
6. Jarvis, K. E., Gray, A. L., and Houk, R. S. (1992) *Handbook of Inductively Coupled Plasma Mass Spectrometry*, Blackie, Glasgow, pp. 18–20.
7. Draft Guidance on Water Supply (Water Quality) Regulations 2000, available from http://www.dwi.gov.uk/regs/regulations.shtm.
8. EPA Office of Solid Waste website, SW-846 6000 series methods, http://www.epa.gov/epaoswer/hazwaste/test/6_series.htm.
9. EPA Office of Solid Waste website, SW-846 6000 series methods, Update IVA, http://www.epa.gov/SW-846/up4a.htm#6_series.
10. EPA Superfund website, Contract Laboratory Program Inorganic Methods Web page, http://www.epa.gov/superfund/programs/clp/ilm5.htm.
11. Stewart, I. I. and Olesik, J. W. (1998) Transient acid effects in inductively coupled plasma optical emission spectrometry and inductively coupled plasma mass spectrometry. *J. Anal. At. Spectrom.*, **13**, 843–54.
12. Stewart, I. I. and Olesik, J. W. (1998) The effect of nitric acid concentration and nebulizer gas flow retes on aerosol properties and transport rates in inductively coupled plasma sample introduction. *J. Anal. At. Spectrom.*, **13**, 1249–56.
13. Tan, S. H. and Horlick, G. (1987) Matrix-effect observations in inductively coupled plasma mass spectrometry. *J. Anal. At. Spectrom.*, **2**, 745–63.
14. Allen, L. A., Leach, J. J., and Houk, R. S. (1997) Spatial location of the space charge effect in individual icon clouds using monodisperse dried microparticulate injection with a twin quadrupole inductively coupled plasma mass spectrometer. *Anal. Chem.*, **69**, 2384–91.
15. Olivares, J. A. and Houk, R. S. (1986) Suppression of analyte signal by various concomitant salts in inductively coupled plasma mass spectrometry. *Anal. Chem.*, **58**, 20–5.
16. Douglas, D. J. and Kerr, L. A. (1988) Study of solids deposition on inductively coupled plasma mass spectrometry samplers and skimmers. *J. Anal. At. Spectrom.*, **3**, 749–52.
17. Rosman, K. J. R. and Taylor, P. D. P. (1997) *IUPAC Isotopic Composition of the Elements.* Available from http://www.iupac.org/reports/1998/7001rosman/iso.pdf.
18. Leonhard, P., Papelnik, R., Prange, A., Yamada, N., and Yamada, T. (2002) Analysis of diluted sea-water a the ng L^{-1} level using an ICP-MS with an octopole reaction cell. *J. Anal. At. Spectrom.*, **17**, 189–96.
19. California Department of Health Services, Chromium VI in Drinking Water: Regulation and Monitoring Update website, http://www.dhs.cahwnet.gov/ps/ddwem/chemicals/Chromium6/Cr^{+}6index.htm.
20. Gurleyuk, H. and Wallschlager, D. (2001) Determination of chromium(III) and chromium(VI) using suppressed ion chromatography inductively coupled plasma mass spectrometry. *J. Anal. At. Spectrom.*, **16**, 926–30.

9.4 GEOLOGICAL ANALYSIS

David Wray

9.4.1 Introduction

The technique of ICP-MS was rapidly embraced by the geoscience community during the early stages of instrument development and is today accepted as a routine analytical technique in many geochemical laboratories. It had immediate appeal for the geoscience community because it offered a relatively quick and simple route to the determination of geochemically important metals present at low concentration without the need for chromatographic separation procedures (in the case of rare earth elements) or access to a nuclear reactor (for neutron activation analysis). The importance of the technique to the geosciences is reflected in many of the early publications, which investigated the analysis of geological materials.[1–5] Indeed, it could be argued that the geoscience community fostered and sponsored the development of the technique through orders for instruments whilst the instruments themselves were still at the prototype stage.[6]

Over time, geoscience applications of the basic technique have proliferated, aided by the development of a variety of sample introduction systems, most notably laser ablation. More recently, the use of single- and double-focusing mass spectrometers has enabled workers to resolve interferences not readily resolved on quadrupole-based systems and to determine isotope ratios with high precision. This chapter aims to provide an overview of the geoscience applications of this multifaceted technique.

9.4.2 Quadrupole ICP-MS

9.4.2.1 Solution-based analysis

For geochemists seeking trace element data from bulk rock samples, dissolution followed by ICP-MS analysis is today the route of choice. With careful consideration of the preparation methodology it is possible to determine most, if not all, trace metals of interest to geochemists. Although manufacturers are striving to extend the upper limit of the detector's dynamic range by varying the resolution of the quadrupole, elements forming major components of rocks (such as Al, Si, Mg, etc.) are still best determined using complementary techniques such as ICP-OES or XRF. This section seeks to discuss some of the practical considerations relating to ICP-MS analysis of solutions derived from the dissolution of geological materials.

Most geological materials can be digested either by fusing the sample with an alkali flux followed by dissolution in weak nitric acid, or by using strong acids.[7] In most fusion methods, a flux-to-sample ratio of 5:1 is employed and the resultant solution is normally made up to give a 1000-fold dilution of the original rock sample. This dilution is adequate for ICP-OES analysis (for the analysis of major and some trace elements) but results in the rapid formation of deposits on the sampler and skimmer cones of an ICP-MS, followed by blockage, principally because of the high dissolved solids contribution from the flux material. Blockage can be mitigated by undertaking a further 10-fold dilution of the sample solution, but in first and second generation instruments this has a significant impact on limits of quantitation for low-abundance

elements when undertaking routine multi-element analysis. In addition, even at this level of dilution, drift of the instrument signal over time is a significant consideration requiring, in the author's experience, the use of both internal and external standard drift correction (and frequent recalibration). Digestion using strong acids (commonly a combination of hydrofluoric acid and perchloric acid in open or closed vessels) enables a more concentrated sample solution to be aspirated into the plasma (typically 10 times more concentrated that a fusion-based solution) because of the absence of a flux component. This route also allows determination of more volatile metals, such as cadmium. However, acid digestions are not without their limitations. Open vessel digestions in particular are vulnerable to contamination problems, and so great care has to be taken to avoid this. It is also well documented that acid attack may not quantitatively digest resistate minerals, such as zircon and chromite, which are important mineral phases for some trace metals.[7] In addition, large Cl-based interferences are generated on As and V because of the use of perchloric acid. Microwave digestion using hydrofluoric acid and *aqua regia* has been investigated by a number of workers[8–10] as a means of negating some of the issues associated with open vessel digestions. This approach has attractions but preparation times are relatively long in comparison to both open vessel digestions and fusion procedures. Invariably, the microwave methods described include either an overnight pretreatment period in which the sample is cold-soaked in the acid mixture, or a mini-fusion step to dissolve post-digestion residues. Furthermore, the relatively small number of samples that can be treated in the microwave oven, even when using more than one set of digestion vessels, results in a significant increase in preparation times for the large sample batches often encountered in geochemical projects.

The above, rather complex situation has been resolved to a large extent by the current generation of instruments whose routine limits of quantitation are significantly lower than those of earlier instruments. This in turn enables the use of fusion-based preparations for the analysis of most geologically important trace and rare earth elements in a single measurement cycle, with limits of quantitation well below levels commonly encountered in geological materials. Signal drift over time due to sample/flux deposition on the sampling and skimmer cones remains an important consideration. In the author's laboratory, short-term drift in instrument signal is monitored and corrected through the use of internal standardisation, and recalibration is undertaken after every 10 samples with a further correction applied for inter-calibration drift, assuming linear drift between calibrations.

Calibration is commonly achieved through the use of matrix-matched synthetic standard solutions. For fusion-based samples, a relatively simple matrix-matching exercise using a fusion blank is usually all that is required as the flux is the dominant matrix component (typically a 5:1 ratio of flux to sample, as described earlier) influencing ionisation within the plasma. Premixed multi-element stock solutions are commercially available, but these tend to be oriented towards environmental analysis and either do not contain all the elements of interest to geochemists, or contain elements with relative abundances that are at variance to that commonly found in geological materials. Therefore, multi-element standards reflecting the expected analyte concentrations should be made from high purity, certified single element stock solutions either by the analyst or by special order to a reputable manufacturer. The long tradition of using reference materials (RMs) within the geosciences means that a selection of suitable RMs should be incorporated into analytical protocols to validate results, although for some elements finding materials with an adequate range of certified values remains a challenge. Needless to say, reagent purity and sample contamination issues are vital considerations – instrument constraints and project requirements mean that many elements of interest will be at low ppb to low ppt levels in solution. Whilst some

elements of geological interest are not commonly found in the laboratory environment, e.g. the heavy rare earth elements, many others such as copper, zinc and lead are ubiquitous and their quantification at low level requires clean-room preparative conditions, ultrapure reagents and, as a minimum, a protective environment for the instrument auto-sampler.

In most instances, the effect of the common interferences reported for the technique (e.g. inter-element, oxide and Ar-based) can be minimised by careful matching of standard solutions to the values expected to be found in the samples. If rare earth elements are required then consideration must be given to the impact of barium and light rare earth element oxides on middle rare earth elements (most notably Eu, Tb and Gd) and it is common to apply a correction factor to mitigate these interferences. However, where elements such as barium are present at percent levels, automatic correction may not be effective because of the size of the interfering peak relative to the analyte signal.

9.4.2.2 Application of collision/reaction cells

To date, collision/reaction cell technologies have had a relatively minor impact on classical, solution-based geochemical determinations by ICP-MS. Elements whose quantitation is most assisted by this technology either are normally present at relatively high levels and are more readily determined by other techniques (e.g. iron by ICP-OES) or are normally lost during preparation (e.g. arsenic, selenium). The use of a He/H_2 mixture in a collision cell has however been demonstrated to reduce the proportion of metal oxides relative to atomic ions for analysis of the lanthanides.[11] A more novel approach[12] nearly quantitatively oxidised all the lanthanides, effectively moving the atomic spectrum 16 amu further up the mass range, thereby alleviating the spectral overlap of the Ba oxides on the mid-range rare earth elements (although this has significant implications for the quantitation of other trace metals such as hafnium and tantalum).

Some geological materials such as phosphorites, metalliferous ore minerals and shales contain appreciable quantities of sulfur or phosphorus, which, if not lost or removed during sample preparation, will result in significant oxide interferences on at least some of the isotopes of copper and zinc as well as minor interferences on isotopes of gallium and germanium. There has as yet been little published research on the successful removal of these interferences with or without the application of cell-type technologies, although the addition of ethene to the nebuliser gas has been shown to reduce the magnitude of both sulfur- and phosphorous oxide-based interferences.[13] Collision/reaction cell technologies are however important in laser ablation analysis of geological materials, as discussed later in this chapter.

9.4.2.3 Analysis of solutions derived from sequential extraction procedures

In the fields of environmental and exploration geochemistry, considerable use has been made of sequential extraction procedures in order to determine the bioavailability and geomobility of trace metals (including V, Cr, As, Se, Cd and Pb). More recently, sequential extractions have been used to elucidate information relating to the speciation of metals in soils and sediments. The extraction protocol developed by Tessier[14] has traditionally been used (with modifications) and involves the sequential use of a variable cocktail of extractants including acetic acid, sodium acetate, magnesium chloride, EDTA, acidified hydroxylamine hydrochloride, oxalic acid, sodium

dithionite, *aqua regia*, and often finishing with a hydrofluoric and perchloric acid stage to dissolve resistate materials (see the reviews by Chao[15] and Gleyzes *et al.*[16]). Analysis has traditionally been undertaken by flame- and graphite-furnace-atomic absorption spectroscopy. More recently, workers have tended to use ICP-based instrumentation as they strive for lower limits of quantitation and rapid multi-element measurements.[17–20] The cocktail of extractants often prevents direct analysis by ICP-MS either because of the interferences generated by the extractant or because of the high dissolved solid levels in the extracted solutions. Attempts to resolve some of these issues include gentle evaporation of the extracts to near-dryness, taking up the residue in weak nitric acid, and the potentially less satisfactory approach of applying a large dilution to the extract. Although there is little published work, it would appear that at least some of the interferences generated by the extractants could be mitigated through the use of collision cell-based technology enabling direct quantification of extracts. An alternative sequential extraction protocol currently under development uses sequential aliquots of weak nitric acid to effect the extraction, with a chemometric analysis of the resultant data.[21,22] This approach lends itself to analysis by ICP-MS and might become more widely applied if the full chemometric methodology were published.

9.4.2.4 Analysis of the noble metals

The analysis of the noble metals (Pt, Pd, Rh, Ru, Ir, Os, Re and Au) is another key attraction of ICP-MS to the geochemist. Prior to the introduction of ICP-MS, analysis of the noble metals was undertaken either by instrumental neutron activation analysis, requiring access to a nuclear reactor, or by atomic absorption/emission spectroscopy. ICP-MS is rapidly becoming the technique of choice for the determination of these metals because of its relative simplicity, freedom from interferences and low limits of quantitation.[23,24] In a recent round robin analysis of noble metals in reference materials it was found that, whilst instrumental neutron activation analysis produced slightly more precise data, both analytical methods produced satisfactory data for geological samples rich in noble metals and ICP-MS produced superior results for crustal rocks with relatively low noble metal content.[25] Nickel sulfide fire assay procedures remain the preparation method of choice, but acid digestion protocols have been proposed that require smaller sample weights than those used in NiS procedures.[10,26] Further simplifications of the preparation procedure have also been investigated with variable success; noble metal recoveries after digestion with *aqua regia* have not been found to be quantitative in all types of geological samples.[27] The more novel approach of direct slurry nebulisation into an ICP-MS[28] requires the prior production of a very fine powder to minimise nugget effects and has not gained widespread acceptance. Laser ablation ICP-MS (LA-ICP-MS) has also been used successfully in the quantification of noble metals in NiS fire assay beads and a variety of natural materials, as discussed later in this chapter.

9.4.3 Application of magnetic sector ICP-MS in the geosciences

Whilst quadrupole ICP-MS instruments dominate geoanalytical laboratories in terms of sheer number of instruments and diversity of application, they have sensitivity and precision limitations which can be overcome by the use of single and multiple collector magnetic sector ICP-MS

instruments. Single collector magnetic sector ICP-MS instruments were developed to offer more sensitivity than quadrupole-based systems, with the option to increase mass resolution to resolve interferences (albeit with a resultant loss of sensitivity). Multiple collector instruments were developed to obtain true simultaneous measurements of ions in order to obtain high-precision isotope ratio measurements comparable or better in quality than those attainable with thermal ionisation mass spectrometry. These instruments are inherently more expensive than quadrupole-based systems and improvements in sensitivity of the latest quadrupole-based systems may negate some of the perceived benefits of single collector magnetic sector instruments (see, for example, reference 29). Both magnetic sector instrument types have found important applications within the geosciences; these have been reviewed recently[30] and are discussed below.

9.4.3.1 Single collector magnetic sector ICP-MS

These instruments have primarily been used for elemental analysis requiring ultra-high sensitivity, or high resolution to resolve interferences. The number of true geoscience studies using these instruments is relatively small but in areas relating to marine studies and volcanic processes they have proved to be a valuable tool. A considerable body of work exists on the measurement of trace metals in seawater and ice using single collector instruments. The high resolution capability of these instruments combined with a low-flow nebuliser has been used to aspirate undiluted seawater and remove seawater-based interferences on a range of trace metals.[31] The alternative strategy of ion exchange separation of seawater followed by ICP-MS analysis at low resolution has also been applied to give very high sensitivities for multi-element trace analysis.[32] Volcanic fluids with a high ionic strength have also been analysed by single collector magnetic sector instruments, using a combined strategy of sample dilution to minimise matrix effects and high mass resolution to overcome spectral interferences.[33] The high sensitivity of the technique has also proved to be beneficial for analysis of trace metals in ice and snow at sub-pg/g levels.[34] Sector instruments have also been used to measure rare earth element concentrations in small samples taken from marine particulate matter and hydrothermal plumes as well as in more routine geological materials.[35,36]

Sample introduction of geoscience materials via laser ablation has been investigated by a number of authors seeking to use the additional capabilities that high-resolution single collector ICP-MS can offer over quadrupole-based systems.[37–39]

9.4.3.2 Multi-collector magnetic sector ICP-MS

Whilst both quadrupole and single collector magnetic sector instruments are capable of undertaking isotope ratio measurements, the precision of the measurements is inadequate for most geoscience applications. The principal reason for this is the intrinsic short-term instability of the plasma source (often referred to as *plasma flicker*), which, when combined with a single detector scanning system, results in unacceptable levels of imprecision. A recent study[40] presented short-term stability data (five measurements) for a 1:1 $^{235}U/^{238}U$ solution, which illustrates the point: quadrupole ICP-MS – 0.2% RSD; quadrupole ICP-MS with collision cell – 0.07% RSD; multi-collector magnetic sector ICP-MS – 0.002% RSD. By having matched, fixed detectors combined with a magnetic sector ICP-MS operating in static, low-resolution mode, instrumental

precision similar to or better than that obtainable with thermal ionisation mass spectrometry (TIMS) can be achieved. Furthermore, the plasma source allows the ionisation of metals that are difficult or impossible to be analysed using TIMS and that are of considerable interest to the geoscience community (for example hafnium and tungsten). This technique is normally called multi-collector ICP-MS (MC-ICP-MS) but is described by some authors as plasma ionisation multi-collector mass spectrometry (PIMMS). In addition to the new opportunities provided by MC-ICP-MS for isotopic measurements, it is likely that over time MC-ICP-MS will replace TIMS as the routine technique of choice for isotopic measurements in the geosciences, with TIMS instruments being used only for specific, niche applications.

It is perhaps worth highlighting that although a magnetic sector instrument is used, it is operated in low-resolution mode for the majority of MC-ICP-MS applications, and inter-element and polyatomic interferences must still be considered. Indeed, in most instances it is necessary to undertake ion exchange procedures prior to analysis to separate out the element of interest from the sample matrix. Some workers are now investigating the potential for determinations without matrix separation and are producing promising results for some isotope systems.[41] Mention should also be made of samples introduced using laser ablation MC-ICP-MS, which, by their very nature, will contain matrix elements. At the present time only one instrument offers the ability to perform high precision measurements at high-resolution – the recently introduced Nu 1700 MC-ICP-MS (Nu Instruments) – which is designed to undertake high-precision measurements at resolutions of up to 10 000, enabling the removal of many polyatomic interferences and multiply charged species.[42]

While applications of MC-ICP-MS are now expanding across many areas of isotopic analysis, much of the early development work was associated with geochemical and cosmochemical problems. The technique was first introduced by VG Elemental (now Thermo Electron Corporation) in the early 1990s, with the launch of the Plasma 54 instrument,[43,44] and its application to the geoscience community was quickly demonstrated.[45,46] The success of these initial studies increased the commercial interest in the technique and a number of companies produced second generation instruments in the mid- to late-1990's, offering a variety of modifications and potential improvements over the Plasma 54. Despite the quality of data attained so far, developments of the technique and in particular the detailed understanding of mass bias corrections are still under investigation[47,48] and should result in yet further improvements in precision and data quality.

Reviews of the current and potential applications of the technique in the geosciences have been presented.[49,50] The technique has now developed to the extent that it has comparable performance characteristics to TIMS for some radiogenic elements and is far superior for others (e.g. Hf and W). The precision of Sr, Pb, Th and U isotope determinations are all at least as good as those attainable by TIMS. In the case of Pb, data are a factor of 3–4 more precise than conventional TIMS results and approach the precision attainable by the double-/triple-spiking TIMS methods.[50,51] For the analysis of Hf isotopes, MC-ICP-MS has become the technique of choice, rapidly displacing TIMS and secondary ion mass spectrometry (SIMS) methods, which are slower and suffer from poor precision. This in turn has permitted Hf isotopic measurements to become a routine geochemical tool.[52] Prior to the introduction of MC-ICP-MS relatively little isotopic data were available for W owing to the difficulty of obtaining precise results by negative ion TIMS. The efficient ionisation of W in an ICP has resulted in a rapid increase in our knowledge of this isotopic system, and in particular its usefulness in understanding the early evolution of the Earth's core, meteorite parent bodies and the moon.[49,53] Similar developments are likely for the ^{92}Nb–^{92}Zr isotope system, which again is useful for investigating early solar system development.[54]

The application of MC-ICP-MS to stable isotope analysis has again resulted in significant improvements in our understanding of these elements in geological systems as well as simplifying analytical procedures. For light elements such as Li and B the precision is comparable to that produced by TIMS but sample preparation is simplified and mass discrimination during analysis can be more reliably controlled.[55,56] Many other isotope systems are only poorly understood mainly because of analytical difficulties (e.g. Mg, Si, Ca, Ti, Fe, Cu, Zn, Ge, Mo, platinum group elements and Tl). With the introduction of MC-ICP-MS, many of these difficulties have been reduced or removed and workers are beginning to investigate natural fractionation within these systems.[57–67] Most of these studies are aimed at demonstrating the validity of the analytical methodology and present initial data from restricted sample suites. Over the next 5 to 10 years it is this area of ICP-MS-based geoscience research that is likely to see the most fundamental developments to improve our understanding of the isotopic fractionation of these little studied systems.

9.4.4 Laser ablation ICP-MS in the geosciences

Geochemists were quick to recognise the potential for LA-ICP-MS in the spot and bulk analysis of minerals and powdered rocks. Previously the commonly used technique was the electron microprobe, often coupled to a scanning electron microscope. This technique has limitations, particularly in the quantification of geochemically important trace metals at the levels commonly encountered in geological samples (a few μg/g or less). The combination of laser ablation with ICP-MS offers a ready route to the analysis of trace metals in geological materials at the microscale. In addition, its use reduces or removes many of the sources of contamination associated with mineral separation and solution preparation. The introduction of LA-ICP-MS had an immediate and significant impact on igneous and metamorphic petrology, resulting in major advances in ore, sedimentary rocks and environmental studies.

The analysis of geological samples using LA-ICP-MS was first explored using a ruby laser to ablate rock powders[68] and was developed further using both CO_2 and Nd:YAG pulsed lasers to investigate the composition of fused rock pellets (prepared for XRF analysis), pressed pellets and glass microprobe standards.[69]

Early problems of the technique included the coupling efficiency of the lasers to the sample and the lack of a suitable standardisation protocol. The parallel commercial development of suitable laser ablation systems has aided considerably in their application. Commercial laser ablation systems available in the late 1980s and early 1990s normally utilised the fundamental infrared wavelength of the Nd:YAG laser (1064 nm), which is poorly absorbed by many rock-forming minerals. The introduction of harmonic generators enabled Nd:YAG lasers to produce outputs in the UV, initially at 266 nm and more recently at 213 nm, which couples much more efficiently to minerals and can be focused to a smaller spot size.[70] Lasers using these two wavelengths are now relatively commonplace and have enabled LA-ICP-MS to develop and mature into an almost routine technique in the geosciences with widespread application. The latest development has been the application of the 193 nm excimer laser, which gives a more uniform distribution of laser energy over the sample surface, producing a flat-top beam profile. Comparative studies have indicated that the 193 nm excimer laser produces a finer ablated particle size, fewer memory effects and less element fractionation than does a 266 nm UV laser.[71,72]

LA-ICP-MS can perform two main roles for the geoscientist: bulk analysis of a sample and spot analysis of a feature of interest. For many workers the latter role is more important

but the attraction of bulk analysis with minimal sample preparation requires consideration. In both instances early workers recognised that sample-to-sample variations in ablation efficiency requires the use of internal standards to derive quantitative data, either using an element of known concentration already present in the sample or by the addition of an element which is effectively absent from the sample.

9.4.4.1 Bulk analysis using LA-ICP-MS

Bulk analysis of geological samples for trace metals using LA-ICP-MS has the potential to mitigate many of the difficulties encountered with solution-based approaches. The use of a dry plasma reduces or removes completely oxide-, nitride-, chloride- and hydride-based interferences and obviates issues relating to incomplete sample digestion. With a considered approach to sample preparation it is possible to determine some metals that are often lost during solution preparation (although mercury is likely to remain problematic). There are also potential savings in both the cost and time required to prepare samples. Challenges presented by this approach include the need to ensure that the sample presented to the laser is representative of the bulk and the need for continuous operator attendance. Bulk samples are normally presented to the laser in one of two forms: pressed pellets or fused discs/glasses. In the absence of physical constraints in the laser sample cell, sample preparation is identical to that required for XRF analysis, enabling all major and trace elements to be determined on the same sample aliquot.

In the case of pressed powders, key requirements for geological samples include that the ground material is of a suitably fine grain size such that it can be considered homogeneous and that all samples and standards are ground to a common grain size and pressed to a constant packing density. This is of considerably more importance than in XRF analysis (where it is nevertheless a key factor) because of the relatively small surface area ablated by the laser. Geoscience studies reported in the literature include references 68 and 73–75.

Issues of sample homogeneity are negated to a large extent by the preparation of a fused disc using lithium metaborate and/or lithium tetraborate as a flux, and this is the preferred route for many geoscience studies. Workers have demonstrated that the fused discs can be considered to be homogeneous with typical relative standard deviations on 10 measurements of 2–7%,[76,77] with long-term reproducibility of about 10%.[78] A variety of approaches have been used to achieve standardisation for LA-ICP-MS, ranging from the analysis of reference materials prepared as fused discs in the same manner as the unknowns through to the nebulisation of a standard solution whilst simultaneously ablating a fused disc flux blank.[78] Accuracy of measurements is generally found to be within $\pm 15\%$ but can be $\pm 30\%$ or more depending on the abundance of the element in the sample and on issues such as contamination derived from the flux.

Whilst bulk LA-ICP-MS has the potential to supply good quality data with minimal sample preparation over and above that required for major element analysis, it is the current absence of an integrated auto-sampler for the laser ablation accessory that limits its application. The requirement for attended operation, combined with the purchase cost of the laser, means that bulk LA-ICP-MS is unlikely to replace routine solution-based analysis in most laboratories.

9.4.4.2 Spot analysis using LA-ICP-MS

Spot analysis of samples using LA-ICP-MS has proven to be an excellent technique for researchers investigating the trace element composition of a variety of geological materials.[79,80]

The ability to obtain accurate data from spot and raster analysis of minerals, glasses, shards and melt or fluid inclusions had an immediate and significant effect on many areas of study. Preparation is relatively simple for most sample types, usually only consisting of the production of an over-thick (typically 100 μm) polished thin section. As with bulk LA-ICP-MS a key early issue was the development of suitable standardisation protocols. Commonly used external standards are synthetic glasses doped with known amounts of trace elements (e.g. the series of silicate NIST glasses) or homogeneous natural minerals of known composition. Once again internal standardisation is required to correct for variations in ablation efficiency and this is usually achieved by measurement using an independent technique (such as an electron microprobe) or from mineral stoichiometry.[81–84]

In the study of basaltic magmas and mantle evolution, LA-ICP-MS has enabled the rapid analysis of selected phases such as phenocrysts, xenocrysts and primary melts to disentangle the relative contributions that each are making to the bulk and allows examination of the resultant data from large suites of samples on a common basis.[85] Likewise, LA-ICP-MS has proved invaluable in determining trace element distribution coefficients between minerals and melts, essential for the construction of realistic models of igneous processes.[86–88] It has also proved invaluable in tephrochronology through the analysis of volcanic shards, providing both a chemical composition of the primary magma and the potential to characterise and chemostratigraphically correlate volcanic events.[89–91] Within metamorphic petrology, LA-ICP-MS has been successful in making selective measurements of complex, compositionally zoned minerals. As with igneous studies, one of the key outputs has been numerous studies focusing on trace element partitioning between coexisting metamorphic minerals, permitting in turn the determination of pressure–temperature conditions or the diffusion properties of trace elements and the subsequent implications for isotopic dating.

Palaeoenvironmental analysis of shell material has also benefited from LA-ICP-MS, negating the need for microdrilling to obtain samples. The technique enables researchers to investigate changes in ocean chemistry, water temperature and aquatic pollution over time. Using LA-ICP-MS it is possible to undertake analysis of individual microfossils (such as foraminifera)[92–94] and to derive elemental profiles across growth layers of shells and corals to determine changes in water chemistry over time.[95–97] Studies of sediment provenance using LA-ICP-MS analysis of individual heavy mineral grains (especially garnets and zircons) have the potential to expand considerably on earlier work which used electron microprobe techniques.[98] The ready determination of a large additional suite of elements means that in the medium term, LA-ICP-MS is likely to replace the electron microprobe as the technique of choice for spot analysis especially when combined with isotopic analysis using LA-MC-ICP-MS.

LA-ICP-MS has been successfully used for *in situ* U-Pb geochronology using uranium-rich minerals such as zircon and monazite. Initial studies using infrared lasers observed significant variations in U/Pb isotope ratios, probably because of isotopic fractionation associated with the wavelength of the laser, but measurements of $^{207}Pb/^{206}Pb$ yielded ages precise to 0.5–0.6%.[99,100] The use of UV lasers with active focusing significantly reduces the degree of observed fractionation in U/Pb ratios, which, with other methodological developments, enables the concordance of the zircon population under investigation.[101,102] The principal application of this technique has been the dating of zircon grains in sedimentary rocks to elucidate information about their provenance and tectonic history.[103,104] Although LA-ICP-MS produces data that are less precise than that obtained from ion microprobe or LA-MC-ICP-MS determinations, the agreement in results from both techniques is excellent, and the relatively low cost of LA-ICP-MS combined with the speed of analysis means that it is now the technique of choice for many workers.

The analysis of fluid inclusions in minerals has also benefited from LA-ICP-MS, where the combination of a UV laser capable of ablating transparent minerals such as quartz with the elemental sensitivity of ICP-MS has enabled significant advances in several areas of research. Early work rapidly validated the approach and the technique is now gaining widespread acceptance across many facets of the geosciences.[105–108] Examples of applications include the analysis of inclusions in halite,[109] evaluation of the emplacement history of mineral deposits,[110–112] and the evaluation of hydrothermal history of granitic bodies.[113]

LA-ICP-MS analysis for noble metals in NiS fire assay beads has also been undertaken by a number of workers. The approach is attractive because it negates the need to undertake several of the preparation stages associated with solution analysis (including crushing and dissolution of the bead, precipitation of dissolved noble metals using tellurium co-precipitation, filtering to trap the precipitate, dissolution of the filter). Each of the preparation stages increases the risk of contamination and workers are also concerned about losses of noble metals at some stages of the assay. Initial work demonstrated the viability of the technique and confirmed the even distribution of noble metals within the NiS bead.[114] This work used an infrared laser but produced detection limits that were too high for general use. The use of a UV laser combined with a higher sensitivity instrument demonstrated the true potential of the technique, attaining the limits of quantitation necessary to determine the noble metal content of low-level mineralised samples.[115,116] Noble metals have also been directly measured in natural basaltic glasses, ferromanganese crusts and mineral deposits using LA-ICP-MS.[117–119]

The use of collision/reaction cell technologies with LA-ICP-MS has also received attention as suitable instruments have become more generally available. As mentioned previously the use of a laser reduces or removes many of the interferences associated with solution-based analysis but the inclusion of cell technology offers the potential for the removal of Ar-based interferences and improvements in ion transmission to the detector.[120,121] In the geosciences this has considerable potential in the study of fluid inclusions where elements such as Ca and Fe are of key importance and suffer from Ar-based interferences. Using a reaction cell, the detection capabilities for Ca and Fe have been reported to be improved by factors of 250 and 20 respectively.[122] The significant improvement in Ca signal to background is a consequence of the elimination of ^{40}Ar by charge exchange processes and/or chemical reactions in the cell, which permits the measurement of the most abundant Ca isotope at m/z 40. Although similar improvements in signal to background can be achieved using the cool plasma approach (see Chapter 1), the attraction of cell-based interference reduction is that it permits simultaneous determination of refractory metals whose signal is virtually lost under cool plasma conditions.[123,124]

9.4.4.3 Laser ablation MC-ICP-MS

The coupling of a laser to an MC-ICP-MS instrument (LA-MC-ICP-MS) was investigated at an early stage in the development of the technique, firstly through the isotopic analysis of lead in NIST 610 glass[125] and subsequently by the hafnium isotope ratio analysis of zircon[126] and the strontium isotope ratio analysis of feldspar and marine carbonates.[127] LA-MC-ICP-MS offers the potential for *in situ* isotopic determinations with minimal preparation. The preliminary studies demonstrated the potential of the technique by producing a reproducibility of spot analysis a factor of 2 better than that reported for comparable ion microprobe studies and a precision approaching that of TIMS. Because of the relatively small amount of material being ablated from the mineral surface, optimum precision is attained with analyte contents ranging from 1000 ppm

and upwards in the mineral and with relatively large laser spot sizes of 50–150 μm in diameter. A limiting factor in many early studies was the reliance on Faraday detectors for ion counting. These have relatively poor sensitivity and hence required high analyte concentrations and/or large spot sizes. With the incorporation of one or more electron multipliers into detector assemblies it is possible to count much weaker ion beams, enabling the simultaneous determination of low abundance, but often important, isotopes.

Since these early studies, efforts have concentrated on expanding the number of isotope systems to which LA-MC-ICP-MS can be applied, and mechanisms to correct for inter-element interference, mass bias and laser-induced isotopic fractionation.[128] Where possible, internal normalisation of data using fractionation factors determined from a pair of stable isotopes of the element under investigation is the preferred route of data correction. Where this is not possible, external normalisation using another element at similar mass is used but, especially at light masses, this approach may not readily correct for laser-induced preferential volatilisation of lighter isotopes which may vary on an element-by-element basis.[128–130]

Studies have been completed on a variety of geological materials for a number of different isotope systems. Strontium isotopes have been determined in both igneous and sedimentary materials with accuracies approaching those attainable by TIMS.[127,131,132] Laser ablation studies of iron,[133] hafnium,[134,135] osmium,[136,137] magnesium,[138] lead,[139] uranium-thorium,[140] uranium-lead[141] and zirconium[142] have all been successfully performed. The majority of these studies used relatively small sample suites and were primarily designed to test the analytical methodology. Some geoscience studies incorporating large data sets derived from LA-MC-ICP-MS are now emerging and it is likely that over the next few years spot isotopic analysis using LA-MC-ICP-MS will make a key contribution to many facets of the geosciences.

9.4.5 Conclusions

It is impossible to overemphasise the impact that ICP-MS has had on the geosciences over the last 20 years. Quadrupole ICP-MS, even in the early stages of development, was able to provide data for a vast range of trace metals with greater speed, sensitivity and analytical simplicity than was previously available. The development of magnetic sector instruments enabled significant improvements in sensitivity and/or mass resolution to remove difficult interferences. The introduction of multi-collector ICP-MS facilitated the routine determination of isotope ratios for a greater number of elements than was possible using earlier technologies and with greater speed and precision. Coupling a laser to an ICP-MS enables the geochemist to perform spot trace element and isotopic analysis of minerals and fluid inclusions, determinations that were previously very problematic or impossible to achieve. In many ways the technique is mature in terms of instrument development but its application within the geosciences, especially in the measurement of isotope ratios, will continue to expand for many years to come.

References

1. Date, A. R. and Gray, A. L. (1983) Progress in plasma source mass spectrometry. Determination of rare earth elements in geological samples by inductively coupled plasma source mass spectrometry. *Spectrochim. Acta Part B At. Spectrosc.*, **38**(1–2), 29–37.

2. Date, A. R. and Gray, A. L. (1985) Determination of trace elements in geological samples by inductively coupled plasma source mass spectrometry. *Spectrochim. Acta Part B At. Spectrosc.*, **40**(1–2), 115–22.
3. Date, A. R. and Hutchison, D. (1986) The determination of trace-elements in geochemical-exploration samples by ICP-MS. *Spectrochim. Acta Part B At. Spectrosc.*, **41**(1–2), 175–81.
4. Date, A. R. and Hutchinson, D. (1987) Determination of rare earth elements in geological samples by inductively coupled plasma source mass spectrometry. *J. Anal. At. Spectrosc.*, **2**, 269–76.
5. Doherty, W. and Vander Voet, A. (1985) The application of inductively coupled plasma mass spectrometry to the determination of rare-earth elements in geological materials. *Can. J. Spectrosc.*, **30**, 135–41.
6. Riddle, C., Vander Voet, A., and Doherty, W. (1988) Rock analysis using inductively coupled plasm mass spectrometry: a review. *Geostand. Newsl.*, **12**(1), 203–34.
7. Jarvis, I. (1992) Sample preparation for ICP-MS. In: *Handbook of Inductively Coupled Plasma Mass Spectrometry* (eds K. E. Jarvis, A. L. Gray, and R. S. Houk), Blackie, Glasgow, pp. 172–224.
8. Totland, M., Jarvis, I., and Jarvis, K. E. (1992) An assessment of dissolution techniques for the analysis of geological samples by plasma spectrometry. *Chem. Geol.*, **95**(1–2), 35–62.
9. Ivanova, J., Djingova, R., Korhammer, S., and Markert, B. (2001) On the microwave digestion of soils and sediments for determination of lanthanides and some toxic and essential elements by inductively coupled plasma source mass spectrometry. *Talanta*, **54**(4), 567–74.
10. Jarvis, I., Totland, M. M., and Jarvis, K. E. (1997) Determination of the platinum-group elements in geological materials by ICP-MS using microwave digestion, alkali fusion and cation-exchange chromatography. *Chem. Geol.*, **143**(1–2), 27–42.
11. Du, Z. Y. and Houk, R. S. (2000) Attenuation of metal oxide ions in inductively coupled plasma mass spectrometry with hydrogen in a hexapole collision cell. *J. Anal. At. Spectrom.*, **15**(4), 383–8.
12. Baranov, V. I., Bandura, D. R., and Tanner, S. D. (2000) Reaction cell approach to the oxide problem. In: *Winter Conference on Plasma Spectrochemistry 2000*, Ft Lauderdale, FL, p. 375.
13. Ebdon, L., Ford, M. J., Hutton, R. C., and Hill, S. J. (1994) Evaluation of ethene addition to the nebulizer gas in inductively-coupled plasma-mass spectrometry for the removal of matrix-gas-derived, solvent-gas-derived, and support-gas-derived polyatomic ion interferences. *Appl. Spectrosc.*, **48**(4), 507–16.
14. Tessier, A., Campbell, P. G. C., and Bisson, M. (1979) Sequential extraction procedure for the speciation of particulate trace metals. *Anal. Chem.*, **51**, 844–51.
15. Chao, T. T. (1984) Use of partial dissolution techniques in geochemical exploration. *J. Geochem. Explor.*, **20**, 101–35.
16. Gleyzes, C., Tellier, S., and Astruc, M. (2002) Fractionation studies of trace elements in contaminated soils and sediments: a review of sequential extraction procedures. *TrAC Trends Anal. Chem.*, **21**(6–7), 451–67.
17. Hall, G. E. M., Gauthier, G., Pelchat, J. C., Pelchat, P., and Vaive, J. E. (1996) Application of a sequential extraction scheme to ten geological certified reference materials for the determination of 20 elements. *J. Anal. At. Spectrom.*, **11**(9), 787–96.
18. Hall, G. E. M. (1998) Analytical perspective on trace element species of interest in exploration. *J. Geochem. Explor.*, **61**(1–3), 1–19.
19. Quevauviller, P., Rauret, G., LopezSanchez, J. F., Rubio, R., Ure, A., and Muntau, H. (1997) Certification of trace metal extractable contents in a sediment reference material (CRM 601) following a three-step sequential extraction procedure. *Sci. Total Environ.*, **205**(2–3), 223–34.

20. Goergen, M. G., Murshak, V. F., Roettger, P., Murshak, I., and Edelman, D. (1992) ICP-MS analysis of toxic characteristics leaching procedure (TCLP) extract – advantages and disadvantages. *At. Spectrosc.*, **13**(1), 11–8.
21. Cave, M. R. and Wragg, J. (1997) Measurement of trace element distributions in soils and sediments using sequential leach data and a non-specific extraction system with chemometric data processing. *Analyst*, **122**(11), 1211–21.
22. Santamaria-Fernandez, R., Moreda-Pineiro, A., and Hill, S. J. (2002) Optimization of a multielement sequential extraction method employing an experimental design approach for metal partitioning in soils and sediments. *J. Environ. Monit.*, **4**(2), 330–6.
23. Barefoot, R. R. and Van Loon, J. C. (1999) Recent advances in the determination of the platinum group elements and gold. *Talanta*, **49**(1), 1–14.
24. Barefoot, R. R. (1998) Determination of the precious metals in geological materials by inductively coupled plasma mass spectrometry. *J. Anal. At. Spectrom.*, **13**(10), 1077–84.
25. Bedard, L. P. and Barnes, S. J. (2002) A comparison of the capacity of FA-ICP-MS and FA-INAA to determine platinum-group elements and gold in geological samples. *J. Radioanal. Nucl. Chem.*, **254**(2), 319–29.
26. Totland, M. M., Jarvis, I., and Jarvis, K. E. (1995) Microwave digestion and alkali fusion procedures for the determination of the platinum-group elements and gold in geological-materials by ICP-MS. *Chem. Geol.*, **124**(1–2), 21–36.
27. Juvonen, R., Kallio, E., and Lakomaa, T. (1994) Determination of precious metals in rocks by inductively-coupled plasma-mass spectrometry using nickel sulfide concentration – comparison with other pretreatment methods. *Analyst*, **119**(4), 617–21.
28. Totland, M., Jarvis, I., and Jarvis, K. E. (1993) Determination of the platinum-group elements and gold in solid samples by slurry nebulization ICP-MS. *Chem. Geol.*, **104**(1–4), 175–88.
29. Louie, H., Wu, M., Di, P., Snitch, P., and Chapple, G. (2002) Direct determination of trace elements in sea-water using reaction cell inductively coupled plasma mass spectrometry. *J. Anal. At. Spectrom.*, **17**(6), 587–91.
30. Gäbler, H. E. (2002) Applications of magnetic sector ICP-MS in geochemistry. *J. Geochem. Explor.*, **75**(1–3), 1–15.
31. Field, M. P., Cullen, J. T., and Sherrell, R. M. (1999) Direct determination of 10 trace metals in 50 μL samples of coastal seawater using desolvating micronebulization sector field ICP-MS. *J. Anal. At. Spectrom.*, **14**(9), 1425–31.
32. Sohrin, Y., Iwamoto, S., Akiyama, S., Fujita, T., Kugii, T., Obata, H., Nakayama, E., Goda, S., Fujishima, Y., Hasegawa, H., Ueda, K., and Matsui, M. (1998) Determination of trace elements in seawater by fluorinated metal alkoxide glass-immobilized 8-hydroxyquinoline concentration and high-resolution inductively coupled plasma mass spectrometry detection. *Anal. Chim. Acta*, **363**(1), 11–9.
33. Fischer, T. P., Shuttleworth, S., and O'Day, P. A. (1998) Determination of trace and platinum-group elements in high ionic-strength volcanic fluids by sector-field inductively coupled plasma mass spectrometry (ICP-MS). *Fresenius' J. Anal. Chem.*, **362**(5), 457–64.
34. Barbante, C., Cozzi, G., Capodaglio, G., van de Velde, K., Ferrari, C., Boutron, C., and Cescon, P. (1999) Trace element determination in alpine snow and ice by double focusing inductively coupled plasma mass spectrometry with microconcentric nebulization. *J. Anal. At. Spectrom.*, **14**(9), 1433–8.
35. Prohaska, T., Hann, S., Latkoczy, C., and Stingeder, G. (1999) Determination of rare earth elements U and Th in environmental samples by inductively coupled plasma double focusing sector field mass spectrometry (ICP-SFMS). *J. Anal. At. Spectrom.*, **14**(1), 1–8.
36. Cullen, J. T., Field, M. P., and Sherrell, R. M. (2001) Determination of trace elements in filtered suspended marine particulate material by sector field HR-ICP-MS. *J. Anal. At. Spectrom.*, **16**(11), 1307–12.

37. Axelsson, M. D. and Rodushkin, I. (2001) Determination of major and trace elements in sphalerite using laser ablation double focusing sector field ICP-MS. *J. Geochem. Explor.*, **72**(2), 81–9.
38. Shuttleworth, S. and Kremser, D. T. (1998) Assessment of laser ablation and sector field inductively coupled plasma mass spectrometry for elemental analysis of solid samples. *J. Anal. At. Spectrom.*, **13**(8), 697–9.
39. Ødegård, M. and Hamester, M. (1997) Preliminary investigation into the use of a high resolution inductively coupled plasma-mass spectrometer with laser ablation for bulk analysis of geological materials fused with $Li_2B_4O_7$. *Geostand. Newsl.*, **21**(2), 245–52.
40. Becker, J. S. and Dietze, H. J. (2000) Precise and accurate isotope ratio measurements by ICP-MS. *Fresenius' J. Anal. Chem.*, **368**(1), 23–30.
41. Halicz, L. and Ehrlich, S. (2002) Precise isotope ratio analysis by MC-ICP-MS without matrix separation Sr, Pb and U case study. *Geochim. Cosmochim. Acta*, **66**(15A), A303.
42. Halliday, A. N., Freedman, P. A., Oberli, F., Baur, H., Hollins, S., Levasseur, S., Leya, I., Poitrasson, F., Quitte, G., Teutsch, N., Wiechert, U., Williams, H., and Williams, J. (2002) Nu 1700: a new large-geometry high-resolution multiple collector ICP-MS. *Geochim. Cosmochim. Acta*, **66**(15A), A303.
43. Walder, A. J. and Freedman, P. A. (1992) Isotopic ratio measurement using a double focusing magnetic sector mass analyser with an inductively coupled plasma as an ion source. *J. Anal. At. Spectrosc.*, **7**, 571–5.
44. Walder, A. J. (1997) Advanced isotope ratio mass spectrometry, II: Isotope ratio measurement by multiple collector inductively coupled plasma mass spectrometry. In: *Modern Isotope Ratio Mass Spectrometry* (ed. I. T. Platzner), John Wiley & Sons, London, pp. 83–108.
45. Halliday, A. N., Lee, D. C., Christensen, J. N., Walder, A. J., Freedman, P. A., Jones, C. E., Hall, C. M., Yi, W., and Teagle, D. (1995) Recent developments in inductively-coupled plasma magnetic-sector multiple cdollector mass-spectrometry. *Int. J. Mass Spectrom. Ion Processes*, **146**, 21–33.
46. Lee, D.-C., Halliday, A. N. (1995) Precise determinations of the isotopic compositions and atomic weights of molybdenum, tellurium, tin and tungsten using ICP magnetic sector multiple collector mass spectrometry. *Int. J. Mass Spectrom. Ion Processes*, **146–147**, 35–46.
47. Thirlwall, M., Anczie wicz, R., Vance, D., and Munday, D. (2002) Accuracy and long-term precision of MC-ICP-MS isotope ratios. *Geochim. Cosmochim. Acta*, **66**(15A), A771.
48. Vance, D. and Thirlwall, M. (2002) An assessment of mass discrimination in MC-ICP-MS using Nd isotopes. *Chem. Geol.*, **185**(3–4), 227–40.
49. Halliday, A. N., Lee, D. C., Christensen, J. N., Rehkämper, M., Yi, W., Luo, X. Z., Hall, C. M., Ballentine, C. J., Pettke, T., and Stirling, C. (1998) Applications of multiple collector-ICPMS to cosmochemistry, geochemistry, and paleoceanography. *Geochim. Cosmochim. Acta*, **62**(6), 919–40.
50. Rehkämper, M., Schonbachler, M., Stirling, C. H. (2001) Multiple collector ICP-MS: introduction to instrumentation, measurement techniques and analytical capabilities. *Geostand. Newsl.*, **25**(1), 23–40.
51. White, W. M., Albarede, F., and Telouk, P. (2000) High-precision analysis of Pb isotope ratios by multi-collector ICP-MS. *Chem. Geol.*, **167**(3–4), 257–70.
52. Blichert-Toft, J. (2001) On the Lu–Hf isotope geochemistry of silicate rocks. *Geostand. Newsl.*, **25**(1), 41–56.
53. Halliday, A. N. and Lee, D. C. (1999) Tungsten isotopes and the early development of the Earth and Moon. *Geochim. Cosmochim. Acta*, **63**(23–24), 4157–79.
54. Schonbachler, M., Rehkämper, M., Halliday, A. N., Lee, D. C., Bourot-Denise, M., Zanda, B., Hattendorf, B., and Gunther, D. (2002) Niobium–zirconium chronometry and early solar system development. *Science*, **295**(5560), 1705–8.

55. Lecuyer, C., Grandjean, P., Reynard, B., Albarede, F., and Telouk, P. (2002) B-11/B-10 analysis of geological materials by ICP-MS Plasma 54: application to the boron fractionation between brachiopod calcite and seawater. *Chem. Geol.*, **186**(1–2), 45–55.
56. Tomascak, P. B., Carlson, R. W., and Shirey, S. B. (1999) Accurate and precise determination of Li isotopic compositions by multi-collector sector ICP-MS. *Chem. Geol.*, **158**(1–2), 145–54.
57. Galy, A., Pomies, C., Day, J. A., Pokrovsky, O. S., and Schott, J. (2003) High precision measurement of germanium isotope ratio variations by multiple collector-inductively coupled plasma mass spectrometry. *J. Anal. At. Spectrom.*, **18**(2), 115–9.
58. Rehkamper, M. and Halliday, A. N. (1999) The precise measurement of Tl isotopic compositions by MC-ICP-MS: application to the analysis of geological materials and meteorites. *Geochim. Cosmochim. Acta*, **63**(6), 935–44.
59. Rehkämper, M., Halliday, A. N., Fitton, J. G., Lee, D. C., Wieneke, M., Arndt, N. T. (1999) Ir, Ru, Pt, and Pd in basalts and komatiites: new constraints for the geochemical behavior of the platinum-group elements in the mantle. *Geochim. Cosmochim. Acta*, **63**(22), 3915–34.
60. Marechal, C. N., Telouk, P., and Albarede, F. (1999) Precise analysis of copper and zinc isotopic compositions by plasma-source mass spectrometry. *Chem. Geol.*, **156**(1–4), 251–73.
61. Guo, Y., Makishima, A., Zhu, X. K., Belshaw, N. S., O'Nions, R. K., and Russell, S. S. (2002) High precision measurement of Ti isotopes in terrestrial and extraterrestrial materials. *Geochim. Cosmochim. Acta*, **66**(15A), A298.
62. Galy, A., Belshaw, N. S., Halicz, L., and O'Nions, R. K. (2001) High-precision measurement of magnesium isotopes by multiple-collector inductively coupled plasma mass spectrometry. *Int. J. Mass Spectrom.*, **208**(1–3), 89–98.
63. Zhu, X. K., O'Nions, R. K., Guo, Y., Belshaw, N. S., and Rickard, D. (2000) Determination of natural Cu-isotope variation by plasma-source mass spectrometry: implications for use as geochemical tracers. *Chem. Geol.*, **163**(1–4), 139–49.
64. Belshaw, N. S., Zhu, X. K., Guo, Y., and O'Nions, R. K. (2000) High precision measurement of iron isotopes by plasma source mass spectrometry. *Int. J. Mass Spectrom.*, **197**, 191–5.
65. Halicz, L., Galy, A., Belshaw, N. S., and O'Nions, R. K. (1999) High-precision measurement of calcium isotopes in carbonates and related materials by multiple collector inductively coupled plasma mass spectrometry (MC-ICP-MS). *J. Anal. At. Spectrom.*, **14**(12), 1835–8.
66. Alleman, L., Cardinal, D., Ziegler, K., and Andre, L. (2002) New developments in measuring silicon isotopes by MC-ICP-MS. *Geochim. Cosmochim. Acta*, **66**(15A), A14.
67. Siebert, C., Nagler, T. F., and Kramers, J. D. (2001) Determination of molybdenum isotope fractionation by double-spike multicollector inductively coupled plasma mass spectrometry. *Geochem. Geophys. Geosystems*, 2:art. no.-2000GC000124.
68. Gray, A. L. (1985) Solid sample introduction by laser ablation for inductively coupled plasma source mass spectrometry. *Analyst*, **110**, 551–6.
69. Arrowsmith, P. (1987) Laser ablation of solids for elemental analysis by inductively coupled plasma mass spectrometry. *Anal. Chem.*, **59**, 1437–44.
70. Jackson, S. E. (2001) The application of Nd:YAG lasers in LA-ICP-MS. In: *Laser-Ablation-ICPMS in the Earth Sciences: Principles and Applications* (ed. P. Sylvester), Mineralogical Association of Canada, Ottawa, pp. 29–46.
71. Gunther, D. and Heinrich, C. A. (1999) Comparison of the ablation behaviour of 266 nm Nd:YAG and 193 nm ArF excimer lasers for LA-ICP-MS analysis. *J. Anal. At. Spectrom.*, **14**(9), 1369–74.
72. Günther, D. and Hattendorf, B. (2001) Elemental fractionation in LA-ICP-MS. In: *Laser-Ablation-ICPMS in the Earth Sciences: Principles and Applcations* (ed. P. Sylvester), Mineralogical Association of Canada, Ottawa, pp. 83–92.

73. Klemm, W. and Bombach, G. (2001) A simple method of target preparation for the bulk analysis of powder samples by laser ablation inductively coupled plasma mass spectrometry (LA-ICP-MS). *Fresenius' J. Anal. Chem.*, **370**(5), 641–6.
74. Perkins, W. T., Pearce, N. J. G., and Jeffries, T. E. (1993) Laser ablation inductively coupled plasma mass-spectrometry – a new technique for the determination of trace and ultra-trace elements in silicates. *Geochim. Cosmochim. Acta*, **57** (2), 475–82.
75. Jarvis, K. E. and Williams, J. G. (1993) Laser-ablation inductively-coupled plasma-mass spectrometry (La-ICP-MS) – a rapid technique for the direct, quantitative determination of major, trace and rare-earth elements in geological samples. *Chem. Geol.*, **106**(3–4), 251–62.
76. Ødegård, M., Dundas, S. H., Flem, B., and Grimstvedt, A. (1998) Application of a double-focusing magnetic sector inductively coupled plasma mass spectrometer with laser ablation for the bulk analysis of rare earth elements in rocks fused with $Li_2B_4O_7$. *Fresenius' J. Anal. Chem.*, **362**(5), 477–82.
77. Pickhardt, C., Becker, J. S., and Dietze, H. J. (2000) A new strategy of solution calibration in laser ablation inductively coupled plasma mass spectrometry for multielement trace analysis of geological samples. *Fresenius' J. Anal. Chem.*, **368**(2–3), 173–81.
78. Sylvester, P. (2001) Trace element analysis of fused whole rock glasses by laser ablation ICPMS. In: *Laser-Ablation-ICPMS in the Earth Sciences: Principles and Applications* (ed. P. Sylvester), Mineralogical Association of Canada, Ottawa, pp. 147–62.
79. Nesbitt, R. W., Hirata, T., Butler, I. B., and Milton, J. A. (1997) UV laser ablation ICP-MS: some applications in the earth sciences. *Geostand. Newsl.*, **21**(2), 231–43.
80. Sylvester, P. (ed.) (2001) *Laser-Ablation-ICPMS in the Earth Sciences: Principles and Applications*, Mineralogical Association of Canada, Ottawa.
81. Pearce, N. J. G., Perkins, W. T., Abell, I., Duller, G. A. T., and Fuge, R. (1992) Mineral microanalysis by laser ablation inductively coupled plasma mass-spectrometry. *J. Anal. At. Spectrom.*, **7**(1), 53–7.
82. Pearce, N. J. G., Westgate, J. A., and Perkins, W. T. (1996) Developments in the analysis of volcanic glass shards by laser ablation ICP-MS: quantitative and single internal standard-multi-element methods. *Quat. Int.*, **34–36**, 213–27.
83. Longerich, H. P., Jackson, S. E., and Gunther, D. (1996) Laser ablation inductively coupled plasma mass spectrometric transient signal data acquisition and analyte concentration calculation. *J. Anal. At. Spectrom.*, **11**(9), 899–904.
84. Košler, J. (2001) Laser-ablation ICPMS study of metamorphic minerals and processes. In: *Laser-Ablation-ICPMS in the Earth Sciences: Principles and Applications* (ed. P. Sylvester), Mineralogical Association of Canada, Ottawa, pp. 185–202.
85. Norman, M. D. (2001) Applications of laser-ablation ICPMS to the trace element geochemistry of basaltic magmas and mantle evolution. In: *Laser-Ablation-ICPMS in the Earth Sciences: Principles and Applications* (ed. P. Sylvester), Mineralogical Association of Canada, Ottawa, pp. 163–84.
86. Jeffries, T. E., Perkins, W. T., and Pearce, N. J. G. (1995) Measurements of trace-elements in basalts and their phenocrysts by laser probe microanalysis inductively-coupled plasma-mass spectrometry (LPMA-ICP-MS). *Chem. Geol.*, **121**(1–4), 131–44.
87. Thompson, G. M. and Malpas, J. (2000) Mineral/melt partition coefficients of oceanic alkali basalts determined on natural samples using laser ablation-inductively coupled plasma-mass spectrometry (LAM-ICP-MS). *Mineral. Mag.*, **64**(1), 85–94.
88. Eggins, S. M., Rudnick, R. L., and McDonough, W. F. (1998) The composition of peridotites and their minerals: a laser-ablation ICP-MS study. *Earth Planet. Sci. Lett.*, **154**(1–4), 53–71.
89. Perkins, W. T., Pearce, N. J. G., and Westgate, J. A. (1997) The development of laser ablation ICP-MS and calibration strategies: examples from the analysis of trace elements in volcanic glass shards and sulfide minerals. *Geostand. Newsl.*, **21**(2), 175–90.

90. Eastwood, W. J., Pearce, N. J. G., Westgate, J. A., and Perkins, W. T. (1998) Recognition of Santorini (Minoan) Tephra in lake sediments from Golhisar Golu, southwest Turkey by laser ablation ICP-MS. *J. Archaeol. Sci.*, **25**(7), 677–87.
91. Pearce, N. J. G., Eastwood, W. J., Westgate, J. A., and Perkins, W. T. (2002) Trace-element composition of single glass shards in distal Minoan tephra from SW Turkey. *J. Geol. Soc.*, **159**, 545–56.
92. Wu, G. P. and Hillairemarcel, C. (1995) Application of LP-ICP-MS to benthic foraminifers. *Geochim. Cosmochim. Acta*, **59**(2), 409–14.
93. Stecher, H. A., Krantz, D. E., Lord, C. J., Luther, G. W., and Bock, K. W. (1996) Profiles of strontium and barium in *Mercenaria mercenaria* and *Spisula solidissima* shells. *Geochim. Cosmochim. Acta*, **60**(18), 3445–56.
94. Eggins, S., De Deckker, P., and Marshall, J. (2002) Laser ablation-ICP-MS compositional profiling of chamber walls in planktonic Foraminifera: implications for Mg/Ca thermometry. *Geochim. Cosmochim. Acta*, **66**(15A), A207.
95. Toland, H., Perkins, B., Pearce, N., Keenan, F., and Leng, M. J. (2000) A study of sclerochronology by laser ablation ICP-MS. *J. Anal. At. Spectrom.*, **15**(9), 1143–8.
96. Bellotto, V. R. and Miekeley, N. (2000) Improvements in calibration procedures for the quantitative determination of trace elements in carbonate material (mussel shells) by laser ablation ICP-MS. *Fresenius' J. Anal. Chem.*, **367**(7), 635–40.
97. Vander Putten, E., Dehairs, F., Keppens, E., and Baeyens, W. (2000) High resolution distribution of trace elements in the calcite shell layer of modern *Mytilus edulis*: environmental and biological controls. *Geochim. Cosmochim. Acta*, **64**(6), 997–1011.
98. Morton, A., Knox, R. W. O., and Hallsworth, C. (2002) Correlation of reservoir sandstones using quantitative heavy mineral analysis. *Petroleum Geosci.*, **8**(3), 251–62.
99. Fryer, B. J., Jackson, S. E., and Longerich, H. P. (1993) The application of laser-ablation microprobe-inductively coupled plasma-mass spectrometry (LAM-ICP-MS) to in-situ U–Pb geochronology. *Chem. Geol.*, **109**(1–4), 1–8.
100. Feng, R., Machado, N., and Ludden, J. (1993) Lead geochronology of zircon by laser probe-inductively coupled plasma-mass spectrometry (LP-ICP-MS). *Geochim. Cosmochim. Acta*, **57**(14), 3479–86.
101. Hirata, T. and Nesbitt, R. W. (1995) U–Pb isotope geochronology of zircon – evaluation of the laser probe-inductively coupled plasma-mass spectrometry technique. *Geochim. Cosmochim. Acta*, **59**(12), 2491–500.
102. Horn, I., Rudnick, R. L., and McDonough, W. F. (2000) Precise elemental and isotope ratio determination by simultaneous solution nebulization and laser ablation-ICP-MS: application to U–Pb geochronology. *Chem. Geol.*, **164**(3–4), 281–301.
103. Košler, J., Fonneland, H., Sylvester, P., Tubrett, M., and Pedersen, R. B. (2002) U–Pb dating of detrital zircons for sediment provenance studies – a comparison of laser ablation ICP-MS and SIMS techniques. *Chem. Geol.*, **182**(2–4), 605–18.
104. Machado, N. and Gauthier, G. (1996) Determination of Pb-207/Pb-206 ages on zircon and monazite by laser-ablation ICP-MS and application to a study of sedimentary provenance and metamorphism in southeastern Brazil. *Geochim. Cosmochim. Acta*, **60**(24), 5063–73.
105. Shepherd, T. J. and Chenery, S. R. (1995) Laser-ablation ICP-MS elemental analysis of individual fluid inclusions – an evaluation study. *Geochim. Cosmochim. Acta*, **59**(19), 3997–4007.
106. Ghazi, A. M., McCandless, T. E., Vanko, D. A., and Ruiz, J. (1996) New quantitative approach in trace elemental analysis of single fluid inclusions: applications of laser ablation inductively coupled plasma mass spectrometry (LA-ICP-MS). *J. Anal. At. Spectrom.*, **11**(9), 667–74.
107. Moissette, A., Shepherd, T. J., and Chenery, S. R. (1996) Calibration strategies for the elemental analysis of individual aqueous fluid inclusions by laser ablation inductively coupled plasma mass spectrometry. *J. Anal. At. Spectrom.*, **11**(3), 177–85.

108. McCandless, T. E., Lajack, D. J., Ruiz, J., and Ghazi, A. M. (1997) Trace element determination of single fluid inclusions in quartz by laser ablation ICP-MS. *Geostand. Newsl.*, **21**(2), 279–87.
109. Shepherd, T. J., Ayora, C., Cendon, D. I., Chenery, S. R., and Moissette, A. (1998) Quantitative solute analysis of single fluid inclusions in halite by LA-ICP-MS and cryo-SEM-EDS: complementary microbeam techniques. *Eur. J. Mineral.*, **10**(6), 1097–108.
110. Harlov, D. E., Andersson, U. B., Forster, H. J., Nystrom, J. O., Dulski, P., Broman, C. (2002) Apatite–monazite relations in the Kiirunavaara magnetite–apatite ore, northern Sweden. *Chem. Geol.*, **191**(1–3), 47–72.
111. Ulrich, T., Gunther, D., and Heinrich, C. A. (2001) Evolution of a porphyry Cu–Au deposit, based on LA-ICP-MS analysis of fluid inclusions: Bajo de la Alumbrera, Argentina. *Econ. Geol. Bull. Soc. Econ. Geologists*, **96**(8), 1743–74.
112. Audetat, A., Gunther, D., and Heinrich, C. A. (1998) Formation of a magmatic-hydrothermal ore deposit: insights with LA-ICP-MS analysis of fluid inclusions. *Science*, **279**(5359), 2091–4.
113. Audetat, A., Gunther, D., and Heinrich, C. A. (2000) Magmatic-hydrothermal evolution in a fractionating granite: a microchemical study of the Sn-W-F-mineralized mole granite (Australia). *Geochim. Cosmochim. Acta*, **64**(19), 3373–93.
114. Jarvis, K. E., Williams, J. G., Parry, S. J., and Bertalan, E. (1995) Quantitative-determination of the platinum-group elements and gold using NiS fire assay with laser ablation-inductively coupled plasma-mass spectrometry (LA-ICP-MS). *Chem. Geol.*, **124**(1–2), 37–46.
115. Jorge, A. P. D., Enzweiler, J., Shibuya, E. K., Sarkis, J. E. S., and Figueiredo, A. M. G. (1998) Platinum-group elements and gold determination NiS fire assay buttons by UV laser ablation ICP-MS. *Geostand. Newsl.*, **22**(1), 47–55.
116. Figueiredo, A. M. G., Enzweiler, J., Sarkis, J. E. S., Jorge, A. P. S., and Shibuya, E. K. (2000) NAA and UV laser ablation ICP-MS for platinum group elements and gold determination in NiS fire assay buttons: a comparison between two methods. *J. Radioanal. Nucl. Chem.*, **244**(3), 623–5.
117. Sylvester, P. J. and Eggins, S. M. (1997) Analysis of Re, Au, Pd, Pt and Rh in NIST glass certified reference materials and natural basalt glasses by laser ablation ICP-MS. *Geostand. Newsl.*, **21**(2), 215–29.
118. Sylvester, P. (2001) A practical guide to platinum-group element analysis of sulphides by laser-ablation ICPMS. In: *Laser-Ablation-ICPMS in the Earth Sciences: Principles and Applications* (ed. P. Sylvester), Mineralogical Association of Canada, Ottawa, pp. 203–12.
119. Garbe-Schonberg, C. D. and Mcmurtry, G. M. (1994) In-situ microanalysis of platinum and rare-earths in ferromanganese crusts by laser-ablation ICP MS (LA-ICP-MS). *Fresenius' J. Anal. Chem.*, **350**(4–5), 264–71.
120. Mason, P. R. D. and Kraan, W. J. (2002) Attenuation of spectral interferences during laser ablation inductively coupled plasma mass spectrometry (LA-ICP-MS) using an rf only collision and reaction. *J. Anal. At. Spectrom.*, **17**(8), 858–67.
121. Tanner, S. D., Baranov, V. I., and Bandura, D. R. (2002) Reaction cells and collision cells for ICP-MS: a tutorial review. *Spectrochim. Acta Part B At. Spectrosc.*, **57**(9), 1361–452.
122. Hattendorf, B. and Gunther, D. (2000) Characteristics and capabilities of an ICP-MS with a dynamic reaction cell for dry aerosols and laser ablation. *J. Anal. At. Spectrom.*, **15**(9), 1125–31.
123. Gunther, D., Hattendorf, B., and Audetat, A. (2001) Multi-element analysis of melt and fluid inclusions with improved detection capabilities for Ca and Fe using laser ablation with a dynamic reaction cell ICP-MS. *J. Anal. At. Spectrom.*, **16**(9), 1085–90.
124. Günther, D. (2001) Quantitative fluid inclusion analysis using a 193 nm excimer laser-ablation system coupled to ICP-MS. In: *Laser-Ablation-ICPMS in the Earth Sciences: Principles and Applications* (ed. P. Sylvester), Mineralogical Association of Canada, Ottawa, p. 243.

125. Walder, A. J., Abell, I. D., Platzner, I., and Freedman, P. A. (1993) Lead isotope ratio measurement of Nist 610 glass by laser ablation inductively coupled plasma mass-spectrometry. *Spectrochim. Acta Part B At. Spectrosc.*, **48**(3), 397–402.
126. Thirlwall, M. F. and Walder, A. J. (1995) In situ hafnium isotope ratio analysis of zircon by inductively coupled plasma multiple collector mass spectrometry. *Chem. Geol.*, **122**(1–4), 241–7.
127. Christensen, J. N., Halliday, A. N., Lee, D. C., and Hall, C. M. (1995) In-situ Sr isotopic analysis by laser-ablation. *Earth Planet. Sci. Lett.*, **136**(1–2), 79–85.
128. Jackson, S. E., Pearson, N. J., and Griffin, W. L. (2001) In situ isotope ratio determination using laser-ablation (LA)-magnetic sector-ICP-MS. In: *Laser-Ablation-ICPMS in the Earth Sciences: Principles and Applications* (ed. P. Sylvester), Mineralogical Association of Canada, Ottawa, pp. 105–20.
129. Jackson, S. E. and Gunther, D. (2002) Studies of the source of laser-induced isotopic bias in LA-MC-ICP-MS. *Geochim. Cosmochim. Acta*, **66**(15A), A359.
130. Jackson, S. E. and Guther, D. (2003) The nature and sources of laser induced isotopic fractionation in laser ablation-multicollector-inductively coupled plasma-mass spectrometry. *J. Anal. At. Spectrom.*, **18**(3), 205–12.
131. Bizzarro, M., Simonetti, A., Stevenson, R. K., and Kurszlaukis, S. (2003) In situ Sr-87/Sr-86 investigation of igneous apatites and carbonates using laser-ablation MC-ICP-MS. *Geochim. Cosmochim. Acta*, **67**(2), 289–302.
132. Outridge, P. M., Chenery, S. R., Babaluk, J. A., and Reist, J. D. (2002) Analysis of geological Sr isotope markers in fish otoliths with subannual resolution using laser ablation-multicollector-ICP-mass spectrometry. *Environ. Geol.*, **42**(8), 891–9.
133. Hirata, T. and Ohno, T. (2001) In-situ isotopic ratio analysis of iron using laser ablation-multiple collector-inductively coupled plasma mass spectrometry (LA-MC-ICP-MS). *J. Anal. At. Spectrom.*, **16**(5), 487–91.
134. Griffin, W. L., Pearson, N. J., Belousova, E., Jackson, S. E., van Achterbergh, E., O'Reilly, S. Y., and Shee, S. R. (2000) The Hf isotope composition of cratonic mantle: LAM-MC-ICPMS analysis of zircon megacrysts in kimberlites. *Geochim. Cosmochim. Acta*, **64**(1), 133–47.
135. Chu, N. C., Taylor, R. N., Chavagnac, V., Nesbitt, R. W., Boella, R. M., Milton, J. A., German, C. R., Bayon, G., and Burton, K. (2002) Hf isotope ratio analysis using multi-collector inductively coupled plasma mass spectrometry: an evaluation of isobaric interference corrections. *J. Anal. At. Spectrom.*, **17**(12), 1567–74.
136. Hirata, T., Hattori, M., and Tanaka, T. (1998) In-situ osmium isotope ratio analyses of iridosmines by laser ablation multiple collector inductively coupled plasma mass spectrometry. *Chem. Geol.*, **144**(3–4), 269–80.
137. Pearson, N. J., Alard, O., Griffin, W. L., Jackson, S. E., and O'Reilly, S. Y. (2002) In situ measurement of Re–Os isotopes in mantle sulfides by laser ablation multicollector-inductively coupled plasma mass spectrometry: analytical methods and preliminary results. *Geochim. Cosmochim. Acta*, **66**(6), 1037–50.
138. Pearson, N. J., Griffin, W. L., O'Reilly, and Delpech, G. (2002) Magnesium isotopic composition of the lithospheric mantle: an in-situ study of mantle-derived olivine. *Geochim. Cosmochim. Acta*, **66**(15A), A584.
139. Christensen, J. N., Halliday, A. N., Godfrey, L. V., Hein, J. R., Rea, D. K. (1997) Climate and ocean dynamics and the lead isotopic records in Pacific ferromanganese crusts. *Science*, **277**(5328), 913–8.
140. Stirling, C. H., Lee, D. C., Christensen, J. N., and Halliday, A. N. (2000) High-precision in situ U-238–U-234–Th-230 isotopic analysis using laser ablation multiple-collector ICP-MS. *Geochim. Cosmochim. Acta*, **64**(21), 3737–50.
141. Machado, N. and Simonetti, A. (2001) U–Pb dating and Hf isotopic composition of zircon by laser ablation-MC-ICP-MS. In: *Laser-Ablation-ICP-MS in the Earth Sciences: Principles*

and Applications (ed. P. Sylvester), Mineralogical Association of Canada, Ottawa, pp. 121–46.
142. Hirata, T. and Yamaguchi, T. (1999) Isotopic analysis of zirconium using enhanced sensitivity-laser ablation-multiple collector-inductively coupled plasma mass spectrometry. *J. Anal. At. Spectrom.*, **14**(9), 1455–9.

9.5 MEASUREMENT OF ENVIRONMENTAL AND BIOLOGICAL RADIONUCLIDES

Yuichi Takaku

9.5.1 Introduction

Naturally occurring and artificial radionuclides are useful in many fields of science. For radiation protection of the general public, these nuclides need to be analysed in different environments at natural levels and at elevated concentrations, following accidents at nuclear facilities. When radionuclides are released after accidents, they are transported by air and water. Since the half-lives of many released nuclides are very long, people will be radiated internally and externally for long periods by contact with the environment (for example, air and water), by food intake and so on. Plutonium isotopes are especially important in ecotoxicology since it seems that they significantly affect the human body.

In geochemistry, radionuclides are used as tracers for materials and elements in different environments. It is relatively straightforward to understand the behaviour of these nuclides in controlled systems in the laboratory, because the source terms are fixed and measurable. However, for real-world environmental samples, the activity determination of long-lived radionuclides is more difficult, because of their low concentration and low specific activity (low radioactivity per unit mass). The isotopes ^{234,230}Th, ^{231}Pa and ^{210}Pb, which are daughter products in the uranium and thorium decay series, can be applied as tracers of non-conservative materials in water systems because these nuclides are particle-reactive and insoluble in lake and sea waters. In the field of geochronology, these isotopes have been used as 'clocks' in samples, because their decay rate is inherent under various physical and chemical conditions. Estimation of the accumulation rate of surface sediments has been carried out by measuring ^{210}Pb ($t_{1/2} = 22.3$ years) in lake and coastal areas. Ages of hypolimnitic waters in sea and archaeometric samples have been determined from ^{14}C ($t_{1/2} = 5740$ years) measurements. For older samples, such as rocks and meteorites, similar dating methods (for example, U-Th, K-Ar, U-Pb, Rb-Sr) have also been used. Traditionally, radionuclides have been determined using a low background activity counting method such as α-, β- or γ-ray spectrometry, coupled with radiochemical separations using a yield tracer. These methods require large volume samples and complicated chemical separations. Depending on the particular case, lengthy activity measurements (from one day to several weeks) are often required. For example, to measure ^{237}Np at the global fallout level in soil using α-ray spectrometry, it takes a week or more to obtain just a few tens of counts.[1] In terms of sample throughput this is neither suitable nor satisfactory. Therefore, a more rapid, sensitive and accurate method for measuring long-lived radionuclides in the general environment is needed and it was these requirements that first led nuclear scientists to investigate the potential of ICP-MS.

In 1989, when ICP-MS was only just starting to gain recognition in the field of analytical chemistry, Kim *et al.*[2] applied the technique to the analysis of long-lived radionuclides in

environmental samples. Following this work, the number of papers discussing the measurement of long-lived radionuclides using ICP-MS increased rapidly, and it is not an exaggeration to say that this technique is now regarded as a standard approach for analysis of these isotopes in a broad range of samples.

In this chapter, the history and current state-of-the-practice of ICP-MS analysis of long- lived radionuclides in environmental samples is presented.

9.5.2 Detection limits of long-lived radionuclides

The detection limits (DL) obtained by magnetic sector-ICP-MS with an ultrasonic nebuliser are shown in Table 9.15. These DLs were defined to be equal to three times the standard deviation of repeated measurements ($n = 10$) of a blank solution, and were determined to be at the sub fg g^{-1} level for most elements. In this work, the blank level for each isotope was equivalent to the instrument background, so the achieved DLs were almost equivalent to the theoretical DL of the instrument.

Table 9.15 The detection limits (DL) obtained using magnetic sector-ICP-MS with ultrasonic nebuliser

Nuclide	Half-life (years)	CPS per pg g^{-1}	DL (fg g^{-1})	DL (Bq g^{-1})
^{99}Tc	2.14×10^5	2.28×10^2	2.6	1.60×10^{-6}
^{226}Ra	1.60×10^3	1.01×10^4	0.1	3.70×10^{-6}
^{232}Th	1.41×10^{10}	7.78×10^3	0.2	8.00×10^{-13}
^{237}Np	2.14×10^6	5.83×10^3	0.2	5.20×10^{-9}
^{238}U	4.47×10^{10}	8.02×10^3	0.2	2.40×10^{-12}
^{239}Pu	2.41×10^4	6.21×10^3	0.2	4.28×10^{-7}
^{240}Pu	6.56×10^3	6.21×10^3	0.2	1.57×10^{-6}
^{243}Am	7.37×10^3	6.56×10^3	0.2	1.40×10^{-6}

Calibration curves for the isotopes measured are shown in Figure 9.10. For almost all the target isotopes, linear calibrations could be obtained at the fg g^{-1} concentration level. For Np, it was possible to calibrate below the fg g^{-1} level. The detection and determination limits were almost the same, because the instrument background was so low. These results clearly demonstrated the possibility of measuring ^{99}Tc and shorter half-life nuclides such as ^{226}Ra and ^{243}Am below 10^{-5} Bq g^{-1} and other longer half-life nuclides below 10^{-8} Bq g^{-1} in the sample solution, i.e. at the levels found in environmental samples. For example, the ^{237}Np concentration in Japanese soil is 0.4–4 mBq kg^{-1}, which could be detected in this work using a soil sample quantity of less than 1 g.[3] This detection capability is three orders of magnitude lower than that of α-ray spectrometry.

A comparison of the half-life, number of atoms and corresponding activity for several radionuclides is shown in Figure 9.11.[4] This figure shows that for ^{226}Ra (half-life: approximately 1000 years), for example, the number of atoms in 1 fg of this isotope (i.e. 10 times the DL) is around 10^7. The activity of this number of atoms is about 10^{-2} dpm (disintegrations per minute), which means that it takes roughly 10 days to detect only 100 counts. It is therefore apparent that magnetic sector-ICP-MS has a great time advantage over counting methods for detecting low levels of radionuclides whose half-lives are 1000 years or more.

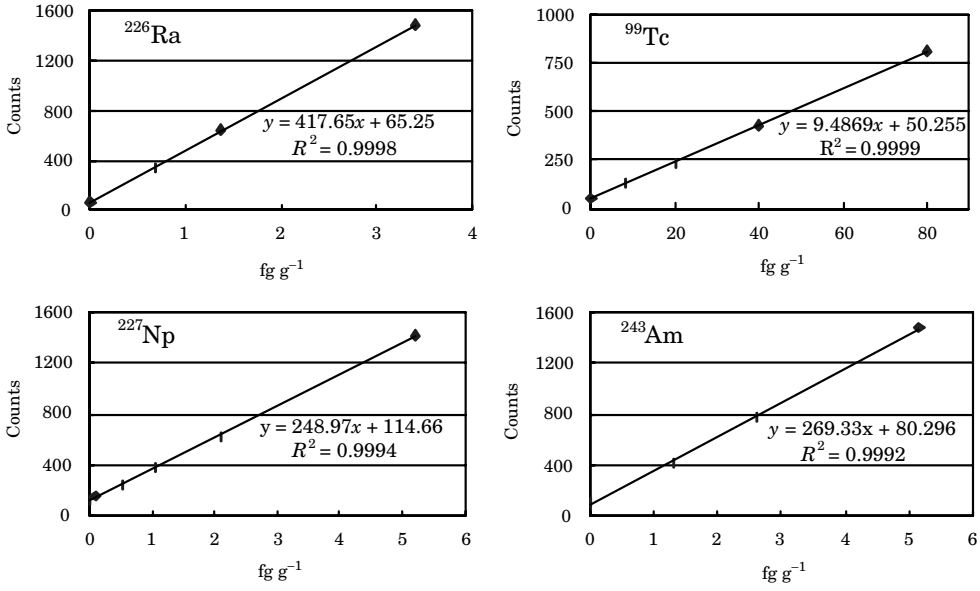

Figure 9.10 Calibration curves of long-lived radionuclides using magnetic sector-ICP-MS.

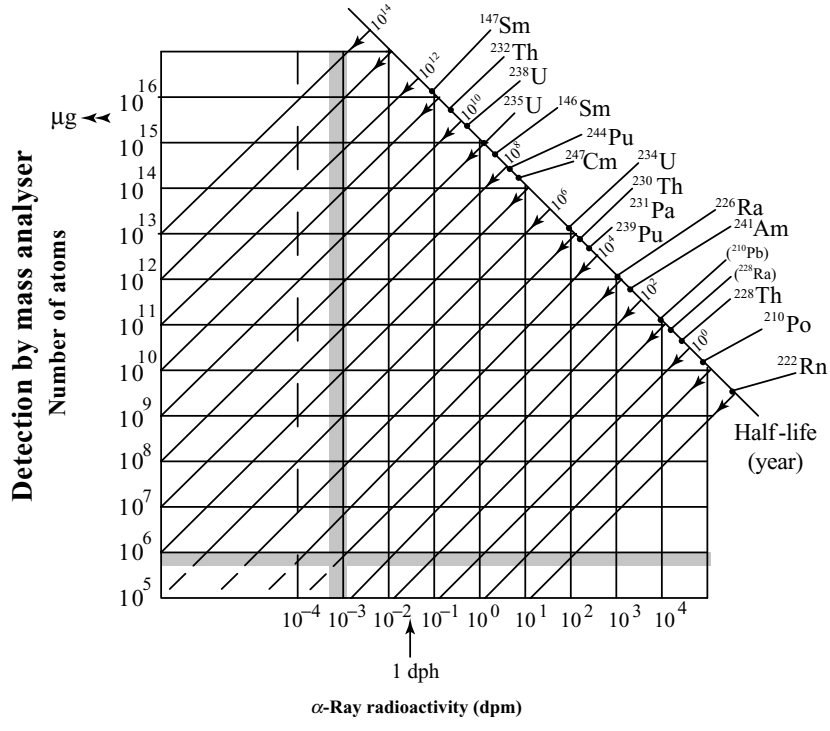

Figure 9.11 Comparison of number of atoms and activity.

9.5.3 Thorium and uranium

The first application of ICP-MS for environmental radionuclide analysis was probably for the determination of thorium and uranium. The first paper describing uranium analysis of environmental samples was published by Boomer and Powell in 1987.[5] In this work, they analysed seven environmental standard reference materials (SRMs). Igarashi *et al*.[6] reported results for Th and U concentration in human bone and tissues in 1991. In addition, another (unique) report was also presented by Igarashi *et al*. in 1991.[7] In this study, the authors determined Th in a thorotrast patient's liver. After these publications, the number of Th and U analysis papers rapidly increased, and ICP-MS is now the most popular analytical technique for determining these elements in both environmental and biological samples.

In 1999, a serious accident happened at the JCO uranium conversion facility in Tokai-mura, Japan, resulting in a large release of uranium isotopes into the local environment. Yoshida *et al.*,[8] collected soil samples just after this accident from around the JCO factory and determined both the concentration of U and the $^{235}U/^{238}U$ isotope ratio in these samples. They reported that the $^{235}U/^{238}U$ isotope ratio in the soil around the JCO factory was elevated compared to the natural U ratio, illustrating how and where the enriched U material released from the facility was distributed following the accident.

In the geochemical field, the application of $^{230}Th/^{232}Th$ and $^{234}U/^{238}U$ analysis is increasing. For these two isotope ratio analyses, α-ray spectrometry[9] or thermal ionisation mass spectrometry (TIMS)[10] has traditionally been mainly used, because of the need to generate accurate and precise results. The precision of isotope ratio analysis using quadrupole-based ICP- MS is not sufficient for these applications, but magnetic sector-ICP-MS (especially multicollector ICP-MS), with its enhanced isotope ratio precision capability offers the required performance.[11] A sample digestion and chemical separation procedure for measuring Th in sediment samples is shown in Figure 9.12. The sample was first digested using HF, HNO_3 and $HClO_4$. The digested sample was then diluted with 8 M HNO_3 (to 50 mL) and passed through an anion-exchange resin (Dowex

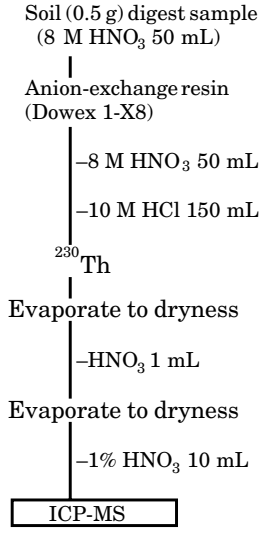

Figure 9.12 Sample digestion and chemical separation procedure for ^{230}Th in sediment samples.

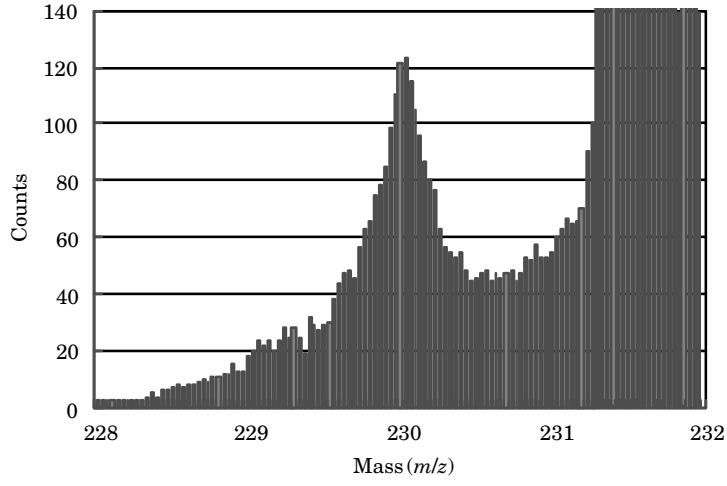

Figure 9.13 Mass spectrum ^{230}Th in lake sediment sample by magnetic sector-CP-MS.

1-X8, Dow Chemical®, USA), preconditioned with 10 M HCl. The resin (5.5 mL) was loaded into a glass column with a quartz wool plug at the bottom. The sample flow rate through the resin column was 2 mL min^{-1}. Finally, thorium was eluted with 150 mL 10 M HCl. In Figure 9.13, the mass spectrum of ^{230}Th in lake sediment is shown. In this spectrum, the tail from the large ^{232}Th peak can clearly be seen, which shows that the abundance sensitivity of conventional magnetic sector-ICP-MS, although high (around 1×10^{-6}), is insufficient for accurate ^{230}Th analysis in environmental samples. A mass analyser with higher abundance sensitivity, such as a large mass dispersion magnet system, or a second electrostatic analyser[11] or similar ion energy filter, is required to solve this problem. Multicollector magnetic sector-ICP-MS instrumentation equipped with such a system for improving abundance sensitivity will be highly beneficial for ^{230}Th analysis in environmental samples in the future, because it is simpler and much quicker than other conventional methods.

9.5.4 Neptunium

Although the present level of ^{237}Np concentration in the environment is generally low relative to some other actinide nuclides, it is expected that the quantities of ^{237}Np will increase with increasing nuclear fuel reprocessing, in addition to the fallout from nuclear weapons testing. Neutron activation analysis[3] and α-ray spectrometry[1] analysis have historically been the generally available techniques for ^{237}Np determination in environmental samples. For this application, these methods have some disadvantages. For instance, α-ray spectrometry demands a higher degree of radiochemical purity of ^{237}Np to avoid interference from ^{234}U, ^{231}Pa and ^{230}Th, while neutron activation analysis requires irradiation of the sample for a long time with a high neutron flux followed by post-irradiation separation.

The first paper describing ^{237}Np analysis in environmental samples using ICP-MS was that of Kim *et al*. in 1989.[2] These authors suggested the possibility of using ICP-MS for ^{237}Np determination and demonstrated the potential of this technique by analysing two soil samples. They also measured the global fallout level for ^{237}Np in Japanese soil, soil contaminated by

weapons testing at Bikini and UK sediments contaminated by nuclear fuel reprocessing activities. Following this work, Assinder *et al.*[12] compiled a review of global Np levels in 1991. Yamamoto *et al.*[13] presented results detailing the Np concentration in paddy fields in Japan using magnetic sector-ICP-MS in 1994. Neptunium can be regarded as one of the most promising analytes for ICP-MS among the long-lived artificial radionuclides in environmental samples.

9.5.5 Plutonium

Plutonium has accumulated in the environment from several sources, such as atmospheric nuclear weapons testing, the accidental burn up of satellites carrying nuclear batteries and discharges from nuclear facilities. The isotopic composition of Pu is characteristic for each origin, and so it is possible to estimate the source location from the $^{239}Pu/^{240}Pu$ isotope ratio of the samples.[14] In addition, this ratio gives important geochemical information about the behaviour of Pu in marine and terrestrial water environments.[15] Usually, the $^{239}Pu/^{240}Pu$ ratio cannot be measured by conventional α-ray spectrometry. For isotope measurement of Pu, TIMS has been the most commonly used method,[15] although occasionally the fission tracks (FT) method[16] has been applied.

The first paper reporting Pu determination and isotope ratio measurement in environmental samples using ICP-MS was published by Kim *et al.* in 1989.[17] They measured $^{239}Pu/^{240}Pu$ isotope ratios using quadrupole-ICP-MS and compared the results with those obtained by FT. In this study, samples were collected from areas where (a) global fallout was known to have deposited (Okuetsu, Japan), (b) extensive radioactive rain (so-called black rain) had fallen after explosion of the Pu bomb over Nagasaki, Japan, and (c) high contamination had occurred as a result of releases from nuclear fuel reprocessing facilities (Ravenglass, UK). In this paper, ICP-MS results were shown to compare well with FT data. However, the precision of the results was typically several percent, which was poorer than could be obtained using TIMS. Recently, Taylor *et al.*[18] presented Pu isotope analysis results using multicollector ICP-MS. They were able to measure the $^{240}Pu/^{239}Pu$ isotope ratio to better than 1% (RSD) precision at a total Pu concentration of just 50 fg mL^{-1}. These results were similar to those obtained using TIMS. In this paper, they also succeeded in measuring the $^{242}Pu/^{239}Pu$ isotope ratio to a precision of better than 3% on solutions containing only 10 fg of ^{242}Pu.

Kim *et al.*[19] described a sample pretreatment system for online determination of Pu using magnetic sector-ICP-MS with isotope dilution. They used a computer-controlled online sample preparation system (the PrepLab, Thermo Electron Corp., Winsford, UK) with Sr-Spec and TEVA-Spec resin micro-columns for Pu preconcentration. These resins, obtained from Eichrom Industries Inc. (Darien, Illinois, USA), were highly selective for radionuclide elements. To reduce the effect of the $^{238}U^{1}H$ interference on ^{239}Pu, a microconcentric nebuliser with integrated desolvation system (the MCN 6000, Cetac, Omaha, Nebraska, USA) was used as the sample introduction method. Using this approach, the authors were able to determine less than 10 pg of Pu in soil samples.

9.5.6 Technetium

Technetium-99 has a long half-life ($t_{1/2} = 2.14 \times 10^5$ years) and relatively high fission yield. Like Pu, it has been accumulating in the environment as a result of nuclear weapons testing and discharges resulting from nuclear power production, fuel reprocessing and waste storage

activities. In addition, the use of ^{99m}Tc (which decays directly to ^{99}Tc, with a half-life of 6.01 h) in nuclear medicine is another source of this isotope. The conventional method for determining ^{99}Tc was β-counting using a low background gas flow proportional counter.[20] However, this method has disadvantages, such as the demand for precise positioning of the ^{99}Tc sample in order to achieve accurate activity counting, the high degree of radiochemical purification of ^{99}Tc required to eliminate β-emitting nuclides coexisting in the samples and the rather long counting times required.

The first paper describing ^{99}Tc analysis in environmental samples using ICP-MS was that of Kim *et al*. in 1989.[21] These authors suggested the possibility of analysing Tc using ICP-MS, but could not obtain accurate results from real soil samples. The reason was that it was difficult to develop a method that efficiently separated ^{99}Tc from ^{99}Ru. Since ^{99}Ru has a relatively high isotopic abundance (12.7%), this interference cannot be mathematically subtracted from the low ^{99}Tc signals obtained from environmental samples without inducing very large errors.

Morita *et al*.[22] developed a separation method based on a solvent extraction procedure and used this to analyse the global fallout level of ^{99}Tc in Japanese soil. In this paper, they used an anion-exchange column to pre-separate Tc from the sample matrix elements in soil leachate solutions. Then, Tc was separated from Ru by solvent extraction with cyclohexanone before detection using ICP-MS. This separation procedure was, however, very complicated and time-consuming. Recently, Tagami and Uchida[23] developed a simpler separation method using TEVA resin. Using this method, ^{99}Tc could be separated directly from soil leachate solutions. Kondo and Seki[24] have successfully determined ^{99}Tc in water samples using a similar method.

9.5.7 Radium

Radium (^{226}Ra) is of particular environmental concern because of its long half-life (1600 years) and because, when ingested, it significantly increases the internal radiation dose of individuals and population groups. ^{226}Ra is also important from the viewpoint of studying aerosols in air, matter in the ocean, and sediment chronology in seas or lakes. The determination of ^{226}Ra in environmental samples is not always easy because of its low concentration. For this reason, there has been much interest in the development of improved methods for its determination in a variety of sample types. Generally, the determination of ^{226}Ra has been carried out as follows: (1) β-counting with liquid scintillation counting of ^{226}Ra and its daughters,[25] (2) γ-ray spectrometry, using a Ge semiconductor detector for ^{226}Ra (186.1 keV) and/or its daughter, ^{214}Pb (295.2, 351.9 keV),[26] and (3) α-ray spectrometry, using a surface barrier Si(Au) semiconductor detector for ^{226}Ra (and yield monitor, ^{225}Ra) after chemical purification and electrodeposition on a stainless steel disk.[27] These methods all have the same disadvantage, in that they require a long counting time to obtain sufficient counts to determine ^{226}Ra.

Kim *et al*.[28] first proposed the possibility of measuring ^{226}Ra using magnetic sector-ICP-MS in 1991. Then, in 1999, Kim *et al*.[29] developed a new analytical method that provided better accuracy and was less time-consuming. In this work, the new method was applied for the determination of ^{226}Ra in hot spring water. A chemical separation procedure for extracting ^{226}Ra from hot spring water in the author's laboratory is shown in Figure 9.14. With this method, the hot spring water sample (100 mL) is acidified with HCl to 0.1 M. A cation-exchange resin (Bio-Rad AG 50W-X12), which is preconditioned with 0.3 M HCl before use, is used to retain ^{226}Ra. The resin (5.5 mL) is loaded into a glass column with a quartz wool plug at the bottom and the sample solution passed through it at a flow rate of 2 mL min^{-1}. Finally, radium is eluted

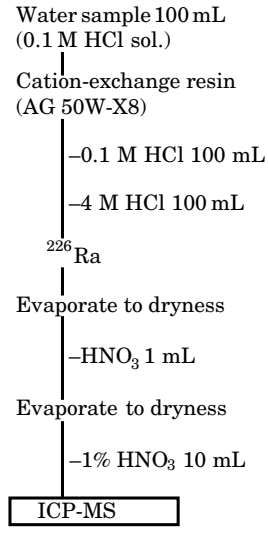

Figure 9.14 Chemical separation procedure of ^{226}Ra.

with 10 mL 4 M HCl. In this method, an enrichment factor of 10 is obtained, allowing ^{226}Ra to be determined down to a level of 0.4 fg g^{-1} in water samples.

Recently, a radium-specific disk, which is highly selective for Ra, has been developed by Empore. Joannon and Pin[30] used this disk for chemical separation and determination of Ra in spring water with ICP-MS detection. In this paper, conventional separation methods using cation-exchange resins were compared to Sr-Spec and the Ra-disk method. The Ra-disk method can be applied to other environmental water samples, such as river and ground waters. Since these waters are used for drinking, determination of ^{226}Ra in them will be important for radiation dose estimation in the future.

9.5.8 Iodine

Iodine is one of the essential elements for the human body. It is mainly enriched in the thyroid gland and plays an important role in metabolism. It is of great interest to investigate the environmental behaviour of iodine from the viewpoint of both health science and public hygiene. It is also important to radioecology. ^{129}I (half-life: 1.57×10^7 years) is produced naturally by the interaction of cosmic rays with xenon atoms in the atmosphere and by the spontaneous fission of ^{238}U in the Earth's subsurface. Since 1945, nuclear activities, such as weapons testing and fuel reprocessing, and accidents at nuclear power plants have added a relatively large amount of ^{129}I to the environment. About 10 Ci of ^{129}I is estimated to have been released into the atmosphere from nuclear weapons tests. Also, about 3700 Ci of ^{129}I has been accumulated in spent fuel from nuclear plants worldwide and from that, about 7.4 Ci of ^{129}I has been released into the atmosphere during fuel reprocessing.[31]

Accurate analysis of ^{129}I at low levels is difficult using β- and γ-ray spectrometry, because this nuclide emits only low-energy β (maximum energy: 0.15 MeV) and γ (0.035 MeV) rays. ^{129}I in

environmental samples has therefore generally been determined using the neutron activation method.[32] In this method, the short half-life (12.4 h) ^{130}I isotope which is produced from ^{129}I(n,γ) is determined by γ-ray spectrometry (at 536 keV). However, this method is very time-consuming and risks exposing the analytical workers to high γ-ray doses from activated samples. Recently, accelerator mass spectrometer has been widely used for ^{129}I analysis[33] but the instrumentation required for this approach is complicated and very expensive.

As discussed throughout this section, ICP-MS has been widely used for analysing long-lived radionuclides, such as Pu, Np and Tc in environmental samples including soil and water samples. For ^{129}I analysis, however, argon-based ICP-MS has not been so useful because of interference from ^{129}Xe, which is a common impurity in Ar gas. In an attempt to solve this problem, Uezu *et al*.[34] applied nitrogen MIP-MS (the P-6000 Hitachi instrument) for ^{129}I determination. Nitrogen MIP-MS produces almost no ^{129}Xe interference because the concentration of Xe in N_2 gas is usually very low. However, the plasma temperature of the MIP system is not so high (about 5000°C) and at this temperature, the ionisation efficiency of iodine is low. For this reason, the DL of ^{129}I was not particularly good. Using this system, the achievable ^{129}I/^{127}I isotope ratio was limited to 1×10^{-6} and this level was not enough to measure the ^{129}I/^{127}I in uncontaminated environments.

Recently, ICP-MS with dynamic reaction cell (DRC)technology has been developed. With this system it is possible to significantly reduce several polyatomic ion interferences, such as ArO and Ar_2.[35] Kawabata *et al*.[36] have recently described the use of DRC-ICP-MS for the determination of ^{129}I in environmental samples. In this work, oxygen was used as the reaction cell gas, and in Figure 9.15, the effect of the volume of O_2 introduced into the cell on the ^{129}Xe signal is shown. As oxygen was introduced into the cell, the iodine signal stayed almost constant while the ^{129}Xe signal decreased very rapidly, from about 50,000 counts per second (cps) before gas introduction to around 10 cps with O_2 introduced. The calibration curve derived for ^{129}I is shown

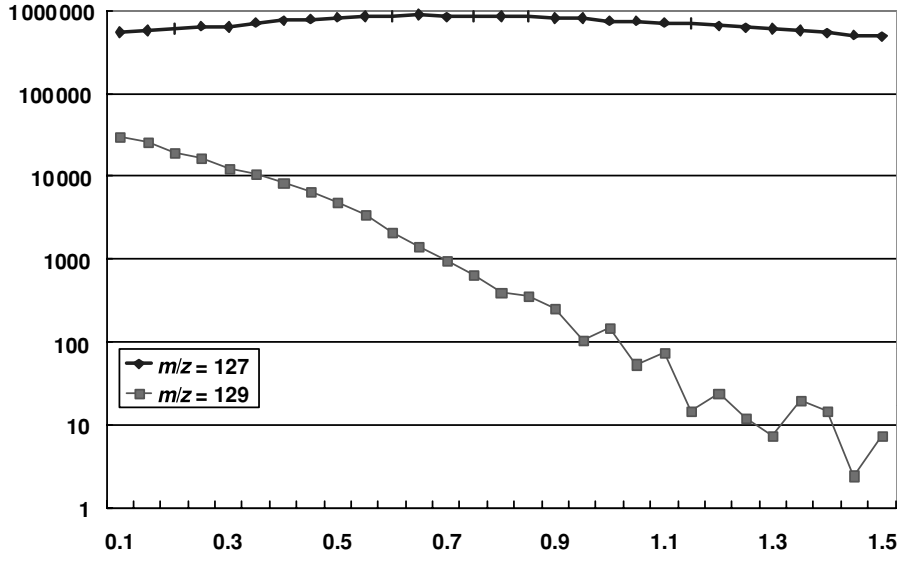

Figure 9.15 Cell gas optimisation for ^{129}Xe background.

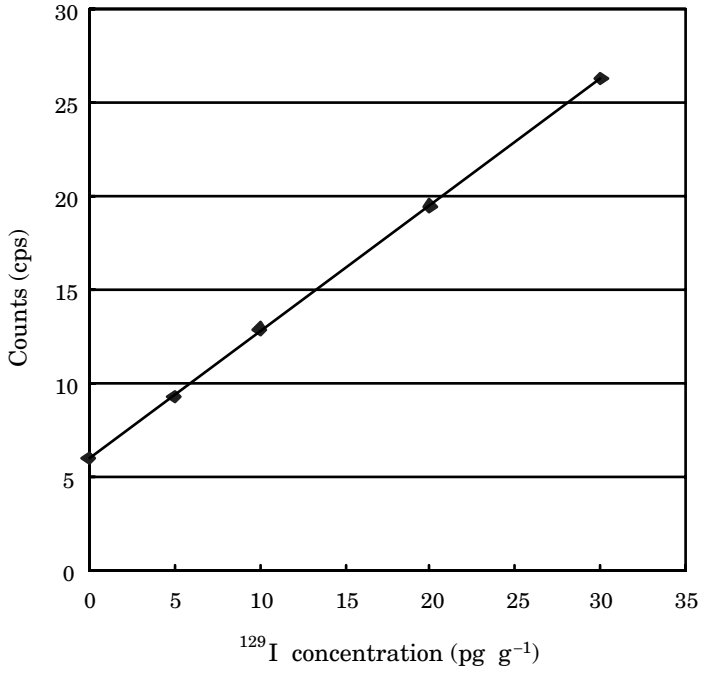

Figure 9.16 Calibration curve of ^{129}I in 40 μg g^{-1} ^{127}I in 1% tetramethylammonium hydroxide.

in Figure 9.16. In this experiment, ^{129}I standard was diluted using 1% tetramethylammonium hydroxide solution and 40 μg g^{-1} of ^{127}I was added to allow the ^{129}I/^{127}I ratio to be determined. Using this method, calibrating below the 100 pg g^{-1} level was possible. A DL for ^{129}I of about 0.5 pg g^{-1} could be obtained, together with a lowest achievable ^{129}I/^{127}I ratio of 4×10^{-7}. This analytical method, although only early in its development at this stage, is advantageous for ^{129}I analysis and it is anticipated that this method will be widely used in the environmental field in the future.

References

1. Sakanoue, M., Yamamoto, M., and Komura, K. (1987) Determination of environmental actinide nuclides and ^{210}Pb (^{210}Po) by low-energy photon spectrometry with alpha-spectrometry. *J. Radioanal. Nucl. Chem.*, **115**, 71–82.
2. Kim, C. K., Takaku, Y., Yamamoto, M., Kawamura, H., Shiraishi, K., Igarashi, Y., Igarashi, S., Takayama, H., and Ikeda, N. (1989) Determination of ^{237}Np in soil samples using inductively coupled plasma mass spectrometry. *Radioisotopes*, **38**, 153–4.
3. Kim, C. K., Seki, R., and Ikeda, N. (1988) Determination of ^{237}Np in soil samples by neutron activation analysis. *Radioisotopes*, **37**, 229–30.
4. Igarashi, Y. (1993) Long-lived radionuclides and ICP-mass spectrometry. *BUNSEKI*, **3**, 174–80 (in Japanese).
5. Boomer, D. W. and Powell, J. (1987) Determination of uranium in environmental samples using inductively coupled plasma mass spectrometry. *Anal. Chem.*, **59**, 2810–3.

6. Igarashi, Y., Ishikawa, Y., Takaku, Y., Masuda, K., Shiraishi, K., and Seki, R. (1991) Concentrations of Th and U in human tissues determined by inductively coupled plasma mass spectrometry. *Radioisotopes*, **40**, 226–33.
7. Igarashi, Y., Ishikawa, Shiraishi, K., Takaku, Y., and Masuda, K. (1991) Determination of thorium in thorotrast patient's liver by inductively coupled plasma mass spectrometry. *Radioisotopes*, **40**, 197–9.
8. Yoshida, S., Muramatsu, Y., and Tagami, K. (2000) Concentrations of uranium and $^{235}U/^{238}U$ ratios in soil and plant samples collected around the uranium conversion bulding in the JCO campus. *J. Environ. Radioactivity*, **50**, 161–72.
9. Cherdyntsev, V. V., Chalov, P. L., Khitrik, M. E., Mamebetov, D. M., and Khaidarov, G. Z. (1955) Transactions of 3rd Session of Committee for Determination of Absolute Ages of Geologic Formations. *Izv. Akad. Nauk SSSR*, 175.
10. Yokoyama, T., Makishima, A., and Nakura, E. (1999) Separation of thorium and uranium from silicate rock samples using two commercial extraction chromatographic resin. *Anal. Chem.*, **71**, 135–41.
11. Nakai, S., Fukuda, S., and Nakada, S. (2001) Thorium isotopic measurements on silicate rock samples with a multi-collector inductively coupled plasma mass spectrometer. *Analyst*, **126**, 1707–10.
12. Assinder, D. J., Yamamoto, M., Kim, C. K., Seki, R., Takaku. Y., Yamauchi, Y., Komura, K., Ueno, K., and Bourne, G. S. (1991) Neptunium in intertidal coastal and estuarine sediments in the Irish sea. *J. Environ. Radioactivity*, **14**, 135–45.
13. Yamamoto, M., Kofuji, H., Tsumura, A., Yamasaki, S., Yuita, K., Komamura, M., Komura, K., and Ueno, K. (1994) Temporal feature of global fallout ^{237}Np deposition in paddy field through the measurement of low-level ^{237}Np by high resolution ICP-MS. *Radiochem. Acta*, **64**, 217–24.
14. Yamamoto, M., Komura, K., and Sakanoue, M. (1983) ^{241}Am and plutonium in Japanese rice-field surface soils. *J. Radiat. Res.*, **24**, 250–8.
15. Buesseler, K. O. and Sholkovitz, E. R. (1987) The geochemistry of fallout plutonium in the North Atlantic, 2: $^{240}Pu/^{239}Pu$ ratios and their significance. *Geochim. Cosmochim. Acta*, **51**, 2623–37.
16. Nakanishi, T., Seki, Y., and Sakanoue, M. (1979) *Proceedings of the 23rd Symposium on Radiochemistry*, p. 72.
17. Kim, C. K., Oura, Y., Takaku, Y., Nitta, H., Igarashi, Y., and Ikeda, N. (1989) Measurment of $^{240}Pu/^{239}Pu$ ratio by fission track method and inductively coupled plasma mass spectrometry. *J. Radioanal. Nucl. Chem. Lett.*, **136**, 353–62.
18. Taylor, R. N., Warneke, T., Milton, J. A., Croudace, I. W., Warwick, P. E., and Nesbitt, R. W. (2001) Plutonium isotope ratio analysis at femtogram to nanogram levels by multicollector ICP-MS. *J. Anal. At. Spectrom.*, **16**, 279–84.
19. Kim, C. S., Kim, C. K., Lee, J. I., and Lee, K. J. (2000) Rapid determination of Pu isotopes and atom ratios in small amounts of environmental samples by an on-line sample pre-treatment system and istope dilution high resolution inductively coupled plasma mass spectrometry. *J. Anal. At. Spectrom.*, **15**, 247–55.
20. Holom, E., Rioseco, J., Ballestra, S., and Walton, A. (1988) Radiochemical measurements of ^{99}Tc: sources and environmental levels. *J. Radioanal. Nucl. Chem.*, **123**, 167–79.
21. Kim, C. K., Otsuji, M., Takaku, Y., Kawamura, H., Shiraishi, K., Igarashi, Y., Igarashi, S., and Ikeda, N. (1989) Application of inductively coupled plasma mass spectrometry to the determination of ^{99}Tc in soil samples. *Radioisotopes*, **38**, 151–2.
22. Morita, S., Kim, C. K., Takaku, Y., Seki, R., and Ikeda, N. (1991) Determination technetium-99 in environmental samples by inductively coupled plasma mass spectrometry. *Appl. Radiat. Isot. Part A*, **42**, 531–4.

23. Tagami, K. and Uchida, S. (1999) A rapid separation method for determination of Tc-99 in environmental waters by ICP-MS. *Radioact. Radiochem.*, **10**, 30–4.
24. Kondo, M. and Seki, R. (2002) *Proceeding of the Third Workshop on Environmental Radioactivity*, KEK, Tsukuba, Japan, March 5–7, 2002, p. 63.
25. Higuchi, H., Uesugi, M., Satoh, K., and Ohashi, N. (1984) Determination of radium in water by liquid scintillation counting after preconcentration with ion-exchange resin. *Anal. Chem.*, **56**, 761–3.
26. Michel, J., Moore, W. S., King, P. T. (1985) Gamma-ray spectrometry for determination of radium-228 and radium-226 in natural waters. *Anal. Chem.*, **56**, 1885–9.
27. Ishikawa, Y., Murakami, H., Sekine, T., Saito, T., and Yoshihara, K. (1994) Non-destructive determination of low level ^{210}Pb and ^{226}Ra with an ordinary high-purity Ge-detector. *J. Radioanal. Nucl. Chem.*, **178**, 301–10.
28. Kim, C. K., Seki, R., Morita, S., Yamasaki, S., Tsumura, A., Takaku, Y., Igarashi, Y., and Yamamoto, M. (1991) Application of a high resolution inductively coupled plasma mass spectrometer to the measurement of long-lived radionuclides. *J. Anal. At. Spectrom.*, **6**, 205–9.
29. Kim, Y. J., Kim, C. K., Kim, C. S., Yun, J. Y., and Rho, B. H. (1999) Determination of ^{226}Ra in environmental samples using high resolution inductively coupled plasma mass spectrometry. *J. Radioanal. Nucl. Chem.*, **240**, 613–8.
30. Joannon, S. and Pin, C. (2001) Ultra-trace determination of ^{226}Ra in thermal waters by high sensitivity quadrupole ICP-mass spectrometry following selective extraction and concentration using radium-specific membrane disks. *J. Anal. At. Spectrom.*, **16**, 32–6.
31. National Council on Radiation Protection and Measurement [NCRP] (1983) Iodine-129: evaluation of releases from nuclear power generation. NCRP Report No. 75, NCRP, Bethesda.
32. Muramatsu, Y. and Yoshida, S. (1995) Determination of ^{129}I and ^{127}I in environmental samples by neutron activation analysis (NAA) and inductively coupled plasma mass spectrometry (ICP-MS). *J. Radioanal. Nucl. Chem.*, **197**, 149–59.
33. Rao, U. and Fehn, U. (1999) Sources and reservoirs of anthropogenic iodine-129 in western New York. *Geochim. Cosmochim. Acta*, **63**, 1927–38.
34. Uezu, Y., Morita, S., Nakano, M., Watanabe, K., and Katagiri, Y. (2000) Analytical method developed for determination of iodine-129 in environmental samples by means of MIP-MS. *Radioisotopes*, **49**, 136–9.
35. Tanner, S. D. and Baranov, V. I. (1999) A dynamic reaction cell for inductively coupled plasma mass spectrometry (ICP-DRC-MS), 2: Reduction of interferences produced within the cell. *J. Am. Soc. Mass Spectrom.*, **10**, 1083–94.
36. Kawabata, K., Kishi, Y., and Takaku, Y. (2003) *Abstract of Winter Plasma Conference*.

9.6 SEMICONDUCTOR APPLICATIONS

Jean-Marie Collard and Yoko Kishi

9.6.1 Introduction

Because of some of its intrinsic qualities such as high throughput, high sensitivity and wide coverage, ICP-MS technology became the technique of choice in the semiconductor industry as soon as it was released for elemental analysis of numerous materials involved in semiconductor

manufacturing, including not only ultrapure water and most liquid chemicals, but also solid materials and even gases.

The key parameter in regard to semiconductor applications has always been the best achievable detection limits, because of the never-ending requirement for higher purity materials from the semiconductor manufacturers.

As an example, specifications for maximum metallic impurity levels in high-purity hydrogen peroxide, as published by the Semiconductor Equipment and Materials International Organization (SEMI®), went down from less than 10 ppb for each cation to less than 10 ppt (i.e. 3 orders of magnitude) in far less than 10 years.[1]

At such a level of purity, two big issues are faced:

- Contamination control, which is not covered here but has been well described in the literature.[2]
- Difficulties with method validation, because of the lack of reference materials in this specific field. In order to circumvent this obstacle, SEMI has developed a specific approach,[3] mainly based on a spike recovery study and determination of the method detection limits.[4] Full application examples of this approach are presented in the literature.[5,6]

Although ICP-MS technology has been used extensively for many years now in the semiconductor industry, the total number of publications is comparatively small because of the typical 'secrecy' covering these applications. Moreover, continuous interactions between users and suppliers have led to rapid instrument improvements in performance, making 10-year-old publications look prehistoric. Consequently, in this chapter, literature references are mainly limited to papers published after 1994.

The semiconductor manufacturing process may be divided into three stages: material preparation, wafer fabrication and packaging. ICP-MS has been mainly used in the first two stages.

There are a large number of sequences and operations in the complete fabrication process; therefore it is impossible to comment on all of the materials and chemicals used in the semiconductor industry. Table 9.16 shows the typical materials and chemicals that can be monitored by ICP-MS along the process.

Cleaning steps, along with the various processing steps, are inevitable, and the number of cleaning steps has increased considerably over the years because of the ever increasing number of process steps and the introduction of new materials requiring specific cleaning technology.[7] The following sections describe some applications for each material.

9.6.2 Ultrapure water

Ultrapure water (UPW) is one of the essential materials used in semiconductor manufacturing and a considerable amount of water (as much as 6000–8000 L) is used to process each 200 mm wafer. The paramount importance of water purity is reflected in the Book of SEMI Standards, where three standards are fully devoted to UPW.[8–10]

In the production of high-purity water, boron is the first ion to breakthrough into purified water when the ion-exchange resin approaches depletion and ICP-MS can be used for investigating the water purification process and technique.[11] An optimized pure water system configuration has been proposed, that includes the combination of reverse osmosis and electro-deionization technologies in the pretreatment phase, followed by an ion-exchange resin stage and finally

Table 9.16 Typical materials and chemicals used in semiconductor manufacturing

Process step	Materials and chemicals
Wafer making	Polysilicon Si wafer
Photoresist coating	Photoresist PGMEA, NMP, EL Antireflective coating (ARC)
Development	TMAH
Etch	
SiO_2	HF/NH_4F (BOE)
Si_3N_4	H_3PO_4
Si	HF/HNO_3
Metal (Al, Ni)	$H_3PO_4/HNO_3/CH_3COOH$
Photoresist strip	H_2SO_4/H_2O_2
Doping	AsH_3, PH_3, BF_3, B_2H_6
Deposition	
Chemical vapor deposition	TEOS, $TiCl_4$, TDMAT
Physical vapor deposition	Al, TiN, Co, TaN, W, Mo
Electroplating	Cu
Evaporation	Al
Planarization	SiO_2, CeO_2
Cleaning	
Organics	H_2SO_4/H_2O_2(Piranha or SPM)
SiO_2	HF
Particles	NH_4OH/H_2O_2 (SC-1 or APM)
Metals	HCl/H_2O_2 (SC-2 or HPM)
Drying	IPA

Note: PGMEA: propylene glycol 1-mono-methyl-ether-2-acetate; NMP: *n*-methyl pyrrolidone; EL: ethyl lactate; TMAH: tetramethyl ammonium hydroxide; BOE: buffered oxide etch; TEOS: tetraethyl orthosilicate; TDMAT: tetrakis(dimethylamido) titanium; IPA: isopropyl alcohol or 2-propanol.

a specific chelating adsorbent stage, that results in the efficient removal of boron.[12] The final product was analyzed by an ICP-MS and the concentration, as the blank equivalent concentration, was below 2 ng/L.[13] A two-step approach was demonstrated for analyzing a high number of samples: the reference analysis and the routine analysis.[14] A 'reference water' was analyzed with the method of standard additions, after preconcentration. Several parameters such as the sample introduction system, stabilization time and signal integration time were investigated in attempts to achieve the lowest possible detection limit. For the routine analysis, external calibration was used with the subtraction of the reference water value.

Sample preconcentration is a good way to extend the capability to analyze lower concentrations. However, special care must be taken since volatile elements such as B, Ge, Sb and Sn can be easily vaporized as molecular compounds. It is well known that mannitol can be used to avoid

the volatilization of B. Mannitol has been used for sample preparation along with nonboiling conditions, e.g. 85–90°C.[15] In this case the sample was successfully concentrated from an initial quantity of between 50 and 750 g to 5 mL final volume, without any loss of 28 elements, including the four elements mentioned above. Preconcentration using a column packed with analytical-grade ion-exchange resin has also been applied to the monitoring of UPW used in semiconductor manufacturing.[16] Retained elements were eluted with 1 M nitric acid. The eluate was then diluted in high-purity water and analyzed using high-resolution ICP-MS (HR-ICP-MS). Good recoveries were obtained down to the 0.5 ng/L level. HR-ICP-MS has also been applied to direct determination of traces of silicon in ultrahigh-purity water.[17] Because of the high atomizing and ionizing power of the plasma, total Si concentration results are obtained, regardless of the chemical state of Si. Consequently, by subtracting ionic Si determined by colorimetric analysis, one can estimate the concentration of nonionic Si (colloidal) present in the sample. High mass resolving power is used to remove the numerous interferences from polyatomic ions encountered on all major Si isotopes. Unfortunately, besides interferences, Si analysis by ICP-MS also suffers from high blanks thought to come from the sample introduction system. To overcome the problem, Takaku *et al.*[17] applied sample preconcentration by evaporation in a clean environment and were able to achieve accurate Si determination down to 0.5 μg/L using an optimized sample introduction system configuration (platinum injector with a fluorinated polymer spray chamber and nebuliser).

9.6.3 Liquid chemicals

A wide variety of chemicals are used throughout the manufacturing process (Table 9.16). Typically, liquid chemicals delivered to the semiconductor industry must comply with many tightly defined specific criteria and for most of them, specifications are well defined in the Book of SEMI Standards, under the 'Process Chemicals' section. Table 9.17 shows a summary of the SEMI specifications for some common chemicals. Some references covering analysis of these chemicals by ICP-MS are also listed in this table.

The analysis of process chemicals is without doubt the main application of ICP-MS in the semiconductor field besides UPW quality monitoring. However, in the analysis of most chemicals, there are some specific isobaric interferences as well as universal interferences such as Ar^+, ArH^+ and ArO^+. Since its inception, the cool/cold plasma technique has been widely used in semiconductor sample analysis, since it can effectively eliminate these universal interferences. The cool plasma technique can also remove C-related polyatomic ions such as C_2 and ArC interferences. This technique has been applied to organic solvents, organic photoresist removers and post-etch cleaning chemicals, after dilution with de-ionized (DI) water.[39] By selecting appropriate hardware conditions, including sample introduction components, organic solvents can be directly analyzed by the technique. The analysis of isopropyl alcohol, acetone, kerosene, photoresist, stripper, etc., has been demonstrated with a cooled spray chamber, appropriate sample tubing and torch injector.[37] Another key point for enabling direct analysis of organic solvents is the addition of a small amount of oxygen into the argon carrier gas, which transports the sample aerosol into the plasma. This prevents deposition of carbon on the sampling cone since the carbon in the sample is decomposed by reaction with oxygen to form CO_2.

To eliminate isobaric interferences derived from the sample matrix and matrix suppression effects, specific sample preparation approaches, such as evaporation followed by dissolution of

Table 9.17 Current SEMI specifications for some common process chemicals (as of July 2004)

Chemical	H_2O_2	HF	HCl	H_2SO_4	HNO_3	H_3PO_4	NH_4OH	TMAH	NH_4F	IPA	BOE
STD number	C30	C28	C27	C44	C35	C36	C21	C46	C20	C41	C23
Grade 1	×	×	×	×	×	×	×	–	×	×	×
Grade 2	×	×	×	×	×	×	×	–	–	×	×
Grade 3	×	–	–	–	–	×	×	–	–	–	–
Grade 4	×	–	–	–	–	–	×	–	–	–	–
Grade 5	×	–	–	–	–	–	–	–	–	–	–
Tier A	–	–	–	–	–	–	–	×	×	–	–
Tier B	–	×	×	×	×	–	–	–	×	×	–
Tier C	–	×	×	×	–	–	–	–	–	×	–
Tier D	–	–	–	–	–	–	×		–	–	–

Table 9.17 (*Continued*)

Chemical	H_2O_2	HF	HCl	H_2SO_4	HNO_3	H_3PO_4	NH_4OH	TMAH	NH_4F	IPA	BOE
STD number	C30	C28	C27	C44	C35	C36	C21	C46	C20	C41	C23
Lowest specification	Grade 5	Tier C	Tier C	Tier C	Tier B	Grade 3	Tier D	Tier A	Tier B	Tier C	Grade 2
Assay (%)	30–32	48.9–49.1	37–38	95.0–97.0	69.0–70.0	79.0–81.0 or 85.0–87.0	28–30	25.0 ± 0.1	39–41	99.8 min	
Concentration unit (see Note)						ppb		ppb			ppb
Al	×	×	×	×	×	50	×	×	×	×	10
As and Sb (as As)					×						
Sb	×	×	×	×		1000	×	×	×	×	10
As	×	×	×	×		50	×	×	×	×	10
Ba	×	×	×	×	×	50	×	×	×	×	–
Be					×			×			
Bi					×			×			
B	×	×	×	×	×	50	×	×	×	×	20
Cd	×	×			×	50	×	×	×	×	
Ca	×	×	×	×	×	150	×	×	×	×	10
Cr	×	×	×	×	×	50	×	×	×	×	5
Co			×		×	50		×			
Cu	×	×	×	×	×	50	×	×	×	×	5
Ga					×			×			
Ge					×			×			

(*Continued*)

Table 9.17 (*Continued*)

Chemical	H_2O_2	HF	HCl	H_2SO_4	HNO_3	H_3PO_4	NH_4OH	TMAH	NH_4F	IPA	BOE
STD number	C30	C28	C27	C44	C35	C36	C21	C46	C20	C41	C23
Lowest specification	Grade 5	Tier C	Tier C	Tier C	Tier B	Grade 3	Tier D	Tier A	Tier B	Tier C	Grade 2
Assay (%)	30–32	48.9–49.1	37–38	95.0–97.0	69.0–70.0	79.0–81.0 or 85.0–87.0	28–30	25.0 ± 0.1	39–41	99.8 min	
Concentration unit (see Note)						ppb		ppb			ppb
Au					×	50		5			10
Fe	×	×	×	×	×	100	×	5	×	×	5
Pb	×	×	×	×	×	50	×	×	×	x	10
Li	×	×			×	10		×	×	×	
Mg	×	×	×	×	×	50	×	×	×	×	10
Mn	×	×	×	×	×	50	×	×	×	×	10
Mo					×			×			
Ni	×	×	×	x	×	50	×	×	×	×	10
Nb					×						
K	×	×	×	×	×	150	×	5	×	×	5
Si					×	50					
Ag					×			×			
Na	×	×	×	×	×	250	×	5	×	×	5
Sr					×	10		×			
Ta			×		×						

Table 9.17 (*Continued*)

Chemical	H_2O_2	HF	HCl	H_2SO_4	HNO_3	H_3PO_4	NH_4OH	TMAH	NH_4F	IPA	BOE
STD number	C30	C28	C27	C44	C35	C36	C21	C46	C20	C41	C23
Lowest specification	Grade 5	Tier C	Tier C	Tier C	Tier B	Grade 3	Tier D	Tier A	Tier B	Tier C	Grade 2
Assay (%)	30–32	48.9–49.1	37–38	95.0–97.0	69.0–70.0	79.0–81.0 or 85.0–87.0	28–30	25.0 ± 0.1	39–41	99.8 min	
Concentration unit (see Note)						ppb		ppb			ppb
Tl					×			×			
Sn	×	×	×	×	×		×	×	×	×	10
Ti	×	×	×	×	×	50	×		×	×	10
V	×	×			×				×	×	
Zn	×	×	×	×	×	50	×	×	×	×	5
Zr					×			×			
References	5, 6, 15, 18–25	19, 20–22, 25–27	19, 20, 25, 28–32	19, 20, 25, 27, 33, 34	18–20, 25, 31	19, 20, 35	36	19–21, 25, 35	22	33, 37, 38	19–21, 26

Note: Concentration levels, unless otherwise specified.

Specification name	Concentration level	Specification name	Concentration level
Grade 1	<0.1 ppm	Tier A	<10 ppb
Grade 2	<10 ppb	Tier B	<1 ppb
Grade 3	<1 ppb	Tier C	<100 ppt
Grade 4	<100 ppt	Tier D	<10 ppt
Grade 5	<10 ppt		

Comment: Tier applies to a grade for which full validation has not yet been demonstrated for the analytical methodology recommended for that specific level of purity.

the residue with diluted nitric acid, have been performed.[40] Another merit of evaporative sample preparation methods is that the target analytes can be preconcentrated prior to analysis. But again, care must be taken to avoid losses of volatile elements as described in Section 9.6.2. Similarly to mannitol, dulcitol, which is a polyhydric alcohol having two or more hydroxyl groups in the *cis*-position, has been used to minimize volatile element losses for sample preparation of ammonium hydroxide.[36] The recovery results for 28 elements were in the range of 86–117%.

Boron is one of the difficult elements to analyze with an evaporation step because of its volatility. Since mannitol has been known to contain significant levels of boron, a mixture of hydrofluoric acid and KF has been used instead during preconcentration for boron determination in various high-purity alcohols.[38] The recovery results shown were 100–116% and the concentrations found were in the range of pg/g to ng/g.

For organic chemicals such as bottom antireflective coating and photoresist, matrix elimination using open-focused microwave digestion has been applied successfully.[41] Recoveries for 13 elements were in the 80–120% range, except for Ca, for which the results were affected by the CO_2^+ interference.

Electrothermal vaporization (ETV) has also been applied as a sample introduction technique for ICP-MS in order to evaporate matrix-derived interferences prior to the analysis of the target elements.[26,28,29] However, ETV is typically limited to a few elements, since furnace conditions are difficult to optimize for many elements simultaneously.

Since sample preparation is both tedious and a potential source of contamination, any technique that allows 'interference free' direct analysis is very beneficial. Cool/cold plasma techniques are known to suffer from some major drawbacks, notably poor ionization of elements having higher ionization potentials (such as Zn, As and Se), high oxide formation and poor tolerance of heavy sample matrices. This led semiconductor analysts to investigate other, more effective techniques. Chronologically, the first successful alternative approach to the cool/cold plasma method to be developed was HR-ICP-MS. Since its commercial release in the late 1980s, HR-ICP-MS has been widely adopted in the semiconductor industry. Analysis of several chemicals using HR-ICP-MS has been reported in the literature.[18,19,30] The determination of nonmetals (e.g. Si, P, S, Cl, As, Se and Br) by quadrupole ICP-MS is difficult owing to the presence of ubiquitous molecular spectral interferences from H, C, N, O and Ar and the high ionization energies of these elements (8–13 eV), which prevents the application of cool/cold plasma techniques. Determination of these anion-forming elements has been traditionally accomplished by ion chromatography, but the alternative approach of HR-ICP-MS has been investigated by different authors and found to be successful for measuring these elements in a wide variety of chemicals.[20,21]

However, price and complexity have always limited expansion of the HR-ICP-MS technique, and so other techniques for interference elimination have continued to be researched. Recently, collision and reaction cell techniques have emerged as new techniques to solve the interference problem. Since application of these techniques is independent of the plasma conditions, hot plasma operation can be used to minimize matrix suppression and to improve ionization of high ionization potential elements,[22] thereby eliminating two of the major drawbacks of cool/cold plasma techniques. Hydrochloric acid has been analyzed using one of the collision cell techniques, dynamic reaction cell (DRC), resulting in complete elimination of chlorine-based interferences such as ClO^+, $ClOH^+$ and $ArCl^+$.[31,32] The reaction/collision technique has also been applied successfully to the analysis of various other aqueous chemicals such as H_2O_2, HNO_3, HF, NH_4F, H_3PO_4, H_2SO_4 and TMAH,[6,23,31,33,35] and organic solvents.[33,42]

Wet cleaning procedures, using several types of chemicals, are commonly used in the semiconductor manufacturing process and failure in the wet chemical baths can turn products into tremendous amounts of scrap. Currently, the solutions in the baths are periodically analyzed off-line, which can easily take a few hours, or the bath integrity is determined indirectly through wafer inspection. Different successful approaches for in-line monitoring of the rinse solutions based on ICP-MS technology have been recently reported,[43,44] allowing the wafer fabrication plant to switch its mode of operation from product outgoing monitoring to process input monitoring.

9.6.4 Si wafer–substrate, thin films and ion implantation

The silicon wafer surface is routinely analyzed for many purposes. Before a bare wafer is processed, the surface must be checked for impurities. Later on in the process, the wafer surface is analyzed to check the thermal oxide layer or the thin layer after deposition. The wafer surface can also be used to monitor the contamination coming from atmosphere, cleaning baths or tools.

With the exception of the geological community, direct solid analysis is not traditionally an application field for ICP-MS, mainly because ICP-MS, like its predecessors ICP-OES and flame AAS/AES, was originally built and developed around the concept of a liquid sample being converted to a fine aerosol for introduction into the atomization/ionization source. In the past, wafer surface analysis was performed by (T)XRF or (TOF-)SIMS, but since the evolution of ICP-MS, new approaches have become practical, such as the vapor phase decomposition (VPD) technique. The basic principle of VPD is as follows: a Si wafer is placed in a Teflon container and exposed to HF vapor. After the SiO_2 layer is decomposed in the HF vapor phase, the Si wafer is scanned with a small droplet across the entire surface of the wafer. The impurities released from the decomposed oxide layer are collected in the droplet during the scanning process and then analyzed by ICP-MS. The sample volume obtained from the VPD is very small, typically around 200 μL, and so initially, ICP-MS coupled with ETV was investigated for measuring the sample droplets.[45–47] However, the limitations of the ETV technique (see Section 9.6.3 above) restricted development of the VPD technique. Fortunately, in recent years, nebulisers that can operate at sample flow rates of well below 100 μL/min have become commercially available from several vendors and such devices are now widely used for VPD sample analysis, since they allow simple direct analysis. This has allowed rapid expansion of the VPD-ICP-MS technique[35,48–57] to such an extent that it now competes favorably with TXRF and SIMS techniques, owing its comparatively cheaper price, ease of use, extended low mass range measurement ability and lower detection limits, compared to TXRF, and ability to more easily obtain quantitative data, compared to the SIMS technique. These advantages have been recognized by SEMI and VPD-ICP-MS is now recommended in numerous standards.[58,59]

Understanding the chemistry of the scanning solution in VPD is important to ensure accurate data.[60,61] It has been demonstrated that a mixture of H_2O_2 and HF shows better extraction rates than HF only, or mixtures of HNO_3 and HF, especially for copper. In addition, the extraction rate reportedly changes for different wafer types.[62] In this study, four wafer types (p, p^+, n and n^+ type polished Si wafers) were used to investigate the extraction rate for 14 elements.

Copper has received attention lately, since it is used as a replacement for aluminum for on-chip wiring between devices. The possibility of Cu contamination at the bevel edge of the wafer

from a front opening unified pod (FOUP) was investigated using a special tool that enables etching of only the bevel edge of the wafer with an HF/H_2O_2 mixture which is then analyzed by ICP-MS.[63]

The formation of a thin film is a very common step in the integrated circuit manufacturing process. There are several ways to form the thin layer, such as chemical vapor deposition, physical vapor deposition or thermal deposition. Three types of oxide layers, formed from different sources, showed significant differences in the level of residual metallic contamination into the oxide film.[40] Polycrystalline silicon germanium (poly-SiGe) has become one of the key layers. The impurities in a poly-SiGe film were determined as follows, in order to avoid Ge-related matrix effects during measurement.[64] After a typical HF/HNO_3 etching step, *aqua regia* was added to the etching solution to remove the residual Si, followed by 20% HCl to remove the Ge matrix as $GeCl_4$. The final residue was dissolved in diluted acid and submitted to the ICP-MS. The method was used to evaluate the cleanliness of two deposition processes and also to obtain the depth profile of Hf contamination in poly-SiGe films.

Uniformly copper-doped[65] and boron-doped[66] silicon thin films fabricated by the ion beam sputter deposition method were analyzed by HR-ICP-MS using an isotope dilution approach to provide a certified reference material for quantitative surface analysis by SIMS.

Ion implantation has become the dominant doping technique, particularly in the fabrication of bipolar-CMOS devices and in the formation of shallow junctions. Laser ablation sampling coupled with ICP-MS was applied recently to the determination of total dopant dose.[67,68] Since this technique spatially and temporally separates the sampling and ionization steps, it has the potential to produce more quantitative results than SIMS for trace elements in a given matrix. Wafer surface analysis can also be used to monitor the contamination induced by different process steps. The importance, in terms of contamination contribution, of the chamber components used for film deposition and ion implantation was demonstrated,[69] as was the effect of cleaning bath solution purity.[70]

9.6.5 High-purity materials

High-purity materials used in semiconductor manufacturing are included in this chapter. They are used in many places, such as interconnects, insulators and capacitors.

Higher dielectric constant (k) materials are becoming increasingly important because it is considered that transistor performance using these materials as gate dielectrics can be improved compared to conventional silicon dioxide. Hence, it is expected that impurity analysis in these materials will become more and more important. There are several materials currently being researched as high-k materials, such as HfO_2, Al_2O_3 and ZrO_2.[71]

High-purity metals are also used as silicides to make contact layers (metal-Si sputtered layers). Matrix suppression (due to the high matrix concentration) and the numerous possible isobaric interferences derived from the matrix element mean that matrix separation is commonly applied prior to the analysis of these materials. Mo, Mo oxide, $MoSi_x$, W, W oxide, WSi_x and also As, P and Re have been analyzed after online matrix separation and analyte preconcentration using ion chromatography coupled to ICP-MS (IC-ICP-MS).[72,73] The basis of the separation resides in the ability to convert those particular matrix elements to anionic species through reaction with H_2O_2. When the reacted sample is passed through the ion-exchange column, which contains a

cation-exchange material, these anions pass through unaffected while the cationic impurities are retained and preconcentrated. The cations are then eluted with HNO_3 directly into the ICP-MS. Results for 19 elements compared with those obtained from reference methods such as thermal ionization mass spectrometry with isotope dilution quantification and radiochemical neutron activation analysis show good accuracy for most elements and contamination problems with ubiquitous elements. The same principle has been applied to analysis of high-purity aluminum[74] and high-purity tantalum.[75]

An attempt to directly analyze high-purity aluminum oxide after decomposition with H_2SO_4 using HR-ICP-MS was reported.[76] Use of HR-ICP-MS allowed most matrix-induced polyatomic ions interferences to be resolved. However, there was severe matrix suppression, preventing the effective use of internal standardization, and therefore the method of standard additions had to be used for quantification.

Since phosphorus is one of the most common dopant elements, monitoring the level of this element as an impurity in semiconductor materials is very important. Phosphorus in high-purity tantalum materials has been determined using an online separation technique.[77] In the first step, the tantalum matrix in the sample solution was trapped on an anion-exchange column while phosphorus (as the phosphate ion) was eluted with a HF/HNO_3 carrier solution (the same mixture as used for sample dissolution). The eluted solution was then mixed with bismuth solution and aqueous ammonia to coprecipitate the phosphate with bismuth hydroxide. This precipitate was collected on an in-line membrane filter and then washed out with pure water. Finally the washed precipitate was dissolved with HCl and injected directly into the plasma. Phosphorus was determined at m/z 47 as $^{31}P^{16}O^+$. The detection limit (3σ) achieved was 1.3 ng/L of sample solution, translating to a determination limit of the order of 40 ng P per g of tantalum (10σ). Results found for four tantalum metal samples were in fairly good agreement with those obtained by glow discharge mass spectrometry (GD-MS). By carefully adjusting the eluent composition and strength, the same basic methodology (matrix separation using an anion exchanger) was applied successfully to the determination of low levels of boron[78] and various metals[79] in tantalum materials.

It was reported that phosphorus in high-purity silicon could be determined down to a level of 0.01 μg/g, by converting P to molybdophosphate, followed by the formation of molybdophosphate-dodecyltrimethyl-ammonium bromide.[80] Phosphorus was then indirectly quantified by analyzing Mo by isotope dilution-ICP-MS.

Trace metal characterization of high-purity gallium is also required, since impurities are detrimental to semiconductor materials such as GaAs, GaP and GaInAs. Trace impurities in gallium samples have been determined both with and without matrix separation.[81] For matrix separation, the samples were first dissolved with a mixture of HCl and HNO_3, and then filtered and extracted with a solution of HCl–MIBK prior to ICP-MS measurement. The results were compared with those from graphite furnace atomic absorption spectrometry (GF-AAS) measurements. Very good agreement was found between GF-AAS data and ICP-MS data obtained through matrix separation (correlation coefficient $= 0.995$). The high dilution factor imposed by the presence of the Ga matrix led to determination limits for the direct ICP-MS analysis that were higher than the impurity levels observed by the other two methods.

HR-ICP-MS after matrix separation was evaluated for the analysis of very high purity (>99.9995%) GaAs single crystals.[82] The matrix was separated from the impurity or dopant elements, Zn, B, Si, Ge, Sn, Sb, P, S, Se and Te, by chlorination of GaAs in a chlorine–argon

stream at 280°C, to selectively volatilize the matrix elements. Very good recoveries were observed for most elements and the detection limits obtained were better by about 1 order of magnitude as compared with the values obtained without matrix separation. The results were also comparable with those obtained by more conventional direct solid analysis techniques such as SIMS or GD-MS. The latter method shows detection limits that are better than those achieved by ICP-MS, even after matrix separation, but has the disadvantage of requiring solid certified reference materials for calibration.

As mentioned in the previous section, the coupling of laser ablation (LA) with ICP-MS can be used for direct solid sample analysis. It does not require time-consuming sample preparation and can avoid contamination risks inherent during sample digestion and dissolution procedures. However, quantification is often limited by the lack of suitable standard reference materials. A strategy using solution-based calibration for multielement determination was investigated for the analysis of high-purity platinum.[83] Multielement standard solutions were nebulized by an ultrasonic nebuliser coupled to the LA-ICP-MS. The high-purity platinum target was ablated during the standard solution analysis. The results for a reference material were in good agreement with the certified values.

Besides the determination of impurities in bulk materials, LA-ICP-MS can be used for identifying the nature of unknown particles in a material that shows defects, and can also be applied to other applications such as film consistency (depth profiling) or spatial mapping.[68] More recently, LA-ICP-MS has even been applied to the determination of impurities in photoresist samples after deposition on a wafer surface using a spin coating/baking procedure.[84]

9.6.6 Miscellaneous

9.6.6.1 Gases

High-purity gases are also essential raw materials for semiconductor manufacturing and a wide range is necessary, including common gases such as nitrogen, oxygen and hydrogen; inert gases, such as helium or argon; and highly toxic and/or reactive gases, such as arsine (see the Book of SEMI Standards, section 'Gases'). Although ICP-MS is not the method of choice for characterizing impurities in gaseous media, it can be used under specific conditions. Typically, an impinger method or particle filtering method is used for gas analysis by ICP-MS. The impinger method was applied to HCl analysis[85] and CO analysis[86] for evaluation of new gas packages. It is usually recommended to add acid to facilitate dissolution of metallic impurities and to avoid any adsorption issues. The filtering method was applied to analysis of silane.[87] A Teflon membrane filter of 0.1 μm pore size was used for trapping. The trapped particles were dissolved in concentrated HCl. The analytical results for six elements showed that the total metallic impurity in silane was <1ng/g. Alternatively, silane can be analyzed by direct introduction into the ICP-MS under optimum conditions.[88] In order to improve the energy transfer process between the bulk plasma and the central analyte channel, hydrogen was added to the argon carrier gas. By doing so, condensation of sample material onto the cones could be reduced and signal integrity could be maintained for reasonably long working periods. With this approach, sub-ppb detection limits were achieved for arsenic and iodine.

A comparison between the filtering and impinger techniques for the determination of particulate metal impurities in gases has been performed using NaCl particles.[89] The recovery

result using the impinger was found to be higher than that obtained with the filter (0.2 μm pore size) method. A direct analysis was also performed in the study, and showed detection limits in the pg/L range with only a minute of signal accumulation, compared to hours for the indirect methods.

9.6.6.2 Liquid/gas distribution system

In integrated circuit manufacturing plants, the chemicals and gases are normally transported from the storage tank to the point-of-use through a distribution system. Therefore, the quality of the materials used to construct these distribution systems impacts on the actual purity of chemicals and gases used in the process. SEMI has acknowledged the importance of this issue for many years and a significant number of standards (more than 30!) are related to liquid or gas distribution systems and components (see the Book of SEMI Standards, section 'Facilities'). Unfortunately, although a lot of work has been done in this field, very few publications are available.

To evaluate new filter and/or purifier technology placed in distribution or recirculation lines, ICP-MS has been applied to analyze impurities in ethyl lactate, ethyl 3-ethoxy propionate, propylene glycol monomethyl ether acetate and 2-heptanone,[90] DI[Q1] water and IPA,[91] or diluted HF.[92] ICP-MS is also the recommended technique to evaluate the purity of polymer components used in UPW and liquid chemical distribution systems.[93–95] It has also been applied to evaluate the relative effectiveness of various acids for extracting impurities from components made of different types of fluorinated polymers.[96]

9.6.7 Conclusions

In summary, application of ICP-MS in the semiconductor industry has expanded rapidly (and continues to expand), as the number of materials used in this field increases and the required monitoring concentration level decreases. The sample types that need to be analyzed have also spread widely from very clean samples, such as UPW, to difficult samples such as chemical mechanical polishing materials. The constant drive to produce ever smaller, ever cleaner microelectronic components, coupled with the continuing performance enhancement occurring in ICP-MS, ensures that this technology will remain at the forefront of ultratrace elemental analysis for several years to come.

References

1. SEMI (2000) Specifications and Guidelines for Hydrogen Peroxide, SEMI C30, SEMI, San Jose.
2. Kawabata, K., Kishi, Y., Li, F., and Anderson, S. (2003) Sample preparation for semiconductor materials. In: *Comprehensive Analytical Chemistry XLI*, Elsevier, Amsterdam, The Netherlands.
3. SEMI (2001) Guide for the Analysis of Liquid Chemicals, SEMI C1, SEMI, San Jose.
4. SEMI (1999) Guide for Determination of Method Detection Limits, SEMI C10, SEMI, San Jose.

5. Collard, J.-M., Kishi, Y., and Costanza, C. (2001) Analytical method validation in the semiconductor industry applied to high purity hydrogen peroxide. Presented at the *2001 Semiconductor Pure Water and Chemicals Conference*, Monterey, CA, USA.
6. Collard, J.-M., Kawabata, K., Kishi, Y., and Thomas, R. (2002) Implementing enhanced ICP-MS technology to attain SEMI grade 5 purity levels. *MICRO Mag.*, **20**(1), 39–46.
7. Hand, A. (2001) Wafer cleaning confronts increasing demands. *Semiconductor Int.*, **24**(9), 62–6.
8. SEMI (2001) Guide for Ultrapure Water System Used in Semiconductor Processing, SEMI F61, SEMI, San Jose.
9. SEMI (2001) Guidelines for Ultrapure Water Used in Semiconductor Processing, SEMI F63, SEMI, San Jose.
10. SEMI (2002) Guide for Quality Monitoring of Ultrapure Water Used in Semiconductor Manufacturing, SEMI F75, SEMI, San Jose.
11. Tanabe, M. and Kaneko, S. (1996) Application of boron selective resin in ultra-pure water system. Presented at the *1996 Semiconductor Pure Water and Chemicals Conference*, Santa Clara, CA, USA.
12. Darbouret, D. and Kano, I. (2000) Ultrapure water blank for boron trace analysis. *J. Anal. At. Spectrom.*, **15**(10), 1395–9.
13. Mabic, S., Kano, I., and Darbouret D. (April/May 2003) Matching purified water quality to experimental detection limits. *LabPlus Int.*, 16–8.
14. Hoelzl, R., Fabry, L., Kotz, L., and Pahlke, S. (2000) Routine analysis of ultra pure water by ICP-MS in the low- and sub-ng/L level. *Fresenius' J. Anal. Chem.*, **366**(1), 64–9.
15. Takeda, K., Watanabe, S., Naka, H., Okuzaki, J., and Fujimoto, T. (1998) Determination of ultra-trace impurities in semiconductor-grade water and chemicals by ICP-MS following a concentration step by boiling with mannitol. *Anal. Chim. Acta*, **377**(1), 47–52.
16. Kitami, K., Mizuniwa, T., Ito, M., Miwa, R., and Yabe K. (1997) Ultrapure water quality and analytical technology for advanced semiconductor manufacturing. Presented at the *1997 Semiconductor Pure Water and Chemicals Conference*, Santa Clara, CA, USA.
17. Takaku, Y., Masuda, K., Takahashi, T., and Shimamura, T. (1994) Determination of trace silicon in ultra-highpurity water by inductively coupled plasma mass spectrometry. *J. Anal. At. Spectrom.*, **9**(12), 1385–7.
18. Dahmen, J., Pfluger, M., Martin, M., Rottmann, L., and Weichbrodt, G. (1997) Trace element determination of high-purity chemicals for the processing of semiconductors with high-resolution ICP-MS using stable isotope dilution analysis (IDA). *Fresenius' J. Anal. Chem.*, **359**(4–5), 410–13.
19. Wildner, H. and Hearn, R. (1998) Application of high resolution (sector field) ICP-MS to the fast and sensitive quality control of process chemicals in semiconductor manufacturing. *Fresenius' J. Anal. Chem.*, **360**(7–8), 800–3.
20. Wildner, H. (1998) Application of inductively coupled plasma sector field mass spectrometry for the fast and sensitive determination and isotope ratio measurement of non-metals in high-purity process chemicals. *J. Anal. At. Spectrom.*, **13**(6), 573–8.
21. Pourmotamed, Z. and Gupta, P. (1996) Parts per billion detection of non metallic elements on silicon surfaces and in semiconductor processing chemicals. Presented at the *1996 Semiconductor Pure Water and Chemicals Conference*, Santa Clara, CA, USA.
22. Collard, J.-M. (2002) Advantages of reaction cell ICP-MS technology for trace metals analysis in the semiconductor industry. Presented at the *2002 International Conference on Plasma Souce Mass Spectrometry*, Durham, UK.
23. Vollkopf, U. Klemm, K., and Pfluger, M. (1999) The analysis of high purity hydrogen peroxide by dynamic reaction cell ICP-MS. *At. Spectrosc.*, **20**(2), 53–9.

24. Thomas, J., Mortensen, R., and Gluodenis, T. (2000) Determination of critical elements in hydrogen peroxide at the Tier D level using ICP-MS. Presented at the *2000 Winter Conference on Plasma Spectrochemistry*, Fort Lauderdale, FL, USA.
25. Blodorn, W. and Potter, D. (2003) Analysis of ultra high purity (UHP) chemicals by ICP-MS: tasks, possibilities and limitations. Presented at the *2003 Winter Conference on Plasma Spectrochemistry*, Garmish, Germany.
26. Hub, W. and Amphlett, H. (1994) Application of ETV-ICP-MS in semiconductor process control. *Fresenius' J. Anal. Chem.*, **350**, 587–92.
27. Anderson, S., Schleisman, A., Bollinger, D., and Kaun, R. (2000) Examination of complete metal recovery following evaporation/concentration of process chemicals used in the semiconductor industry. Presented at the *2000 Winter Conference on Plasma Spectrochemistry*, Fort Lauderdale, FL, USA.
28. Laly, S., Nakagawa, K., Arimura, T., and Kimijima, T. (1996) Optimization of electrothermal vaporization, ICP-MS conditions for the determination of iron, copper, nickel and zinc in semiconductor grade acids. *Spectrochim. Acta*, **51B**, 1393–401.
29. Laly, S., Nakagawa, K., and Kimijima, T. (1996) Optimization of ETV-ICP-MS conditions for the determination of multi-elements in semiconductor grade acids. *Fresenius' J. Anal. Chem.*, **356**, 31–6.
30. Wills, J. and Settembre, G. (2003) Analysis of semiconductor grade mineral acids by sector field ICP-MS. Presented at the *2003 Winter Conference on Plasma Spectrochemistry*, Garmish, Germany.
31. Bollinger, D. S. and Schleisman, A. J. (1999) Analysis of high purity acids using a dynamic reaction cell ICP-MS. *At. Spectrosc.*, **20**(2), 60–3.
32. Kishi, Y. and Kawabata, K. (2002) Analysis of semiconductor grade HCl with the ELAN DRC ICP-MS: elimination of chloride-based interferences. *At. Spectrosc.*, **23**(2), 165–9.
33. Ping, C. M., Kishi, Y., Kawabata, K., and Thomas, R. (2003) Achieving high trace-metal purity levels using dynamic reaction cell ICP-MS. *MICRO Mag.*, **21**(4), 37–43.
34. Hernandez, M. and Radle, M. (2000) The determination of trace metal impurities in semiconductor grade sulfuric acid by inductively coupled plasma mass spectrometry (ICP-MS). Presented at the *2000 Winter Conference on Plasma Spectrochemistry*, Fort Lauderdale, FL, USA.
35. Kawabata, K. and Kishi, Y. (2001) Determination of various chemicals used in the semiconductor industry by DRC-ICP-MS. Presented at the *2001 Semiconductor Pure Water and Chemicals Conference*, Monterey, CA, USA.
36. Takeda, K., Ikushima, S., Okuzaki, J., Watanabe, S., Fujimoto, T., and Nakahara, T. (2001) Inductively coupled plasma mass spectrometric determination of ultra-trace elements in electronic grade water and chemicals using dulcitol. *Anal. Chim. Acta*, **426**(1), 105–9.
37. McCurdy, E. and Potter, D. (October 2001) Applications of ICP-MS for trace and ultratrace metal quantitation in organic matrices. *Semiconductor Int.* Web exclusive: www.reed-electronics.com/semiconductor/article/CA179126?text=mccurdy%20%26%20potter.
38. Kozono, S., Yagi, M., and Takashi, R. (1998) Determination of ultratrace amounts of boron in high purity alcohols by ICP-MS with hydrofluoric acid/potassium fluoride treatment. *Anal. Chim. Acta*, **368**(3), 275–80.
39. Harrison, I. and Tollan, F. (2001) Material monitoring. *Eur. Semiconductor*, **23**(1), 31–4.
40. Balazs, M. K. (1998) Wet chemical analysis for the semiconductor industry – a total view. Presented at the *1998 International Conference on Characterization and Metrology for ULSI Technology*, Gaithersburg, MD, USA.
41. Lu, J. K., Ko, F. H., Chu, T. C., Sun, Y. C., Wang, M. Y., and Wang, T. K. (2000) Evaluation of cleaning efficiency with a radioactive tracer and development of a microwave digestion method for semiconductor processes. *Anal. Chim. Acta*, **407**(1–2), 291–300.

42. Spence, B. and Lee, K. (2001) How can collision cell technology enhance the analysis of organic solvents? Presented at the *2001 Annual Conference of the Federation of Analytical Chemistry and Spectroscopy Societies*, Detroit, MI, USA.
43. Shive, L. W., Ruth, K., and Schmidt, P. (1999) Using ICP-MS for in-line monitoring of metallics in silicon wafer – cleaning baths. *MICRO Mag.*, **17**(2), 27–31.
44. Kishi, Y., Kawabata, K., Palsulich, D., and Wiederin, D. (2003) On-line analysis of process chemicals by ICP-MS. Presented at the *2003 International Conference on Characterization and Metrology for ULSI Technology*, Austin, TX, USA.
45. Takenaka, M., Yamada, Y., Hayashi, M., Omori, H., Ito, S., and Okada, A. (1997) Determination of ultratrace metallic impurities in silicon wafers by acid vapor decomposition/electrothermal vaporization ICP-MS. *Bunseki Kagaku*, **46**(9), 743–7.
46. Komoda, M., Chiba, K., and Uchida, H. (1996) Determination of trace impurities on silicon-wafer surface by isotope dilution analysis using electrothermal vaporization/ICP-MS. *Anal. Sci.*, **12**(2), 21–5.
47. Tsoupras, G. (1996) ICP-MS application to semiconductor processing chemical materials analysis. *Analusis Mag.*, **24**(9/10), M23–M28.
48. Fujiwara, K., Toumori, Y., Mitsumata, H., Inada, M., and Nakahara, T. (1999) Determination of ultra-trace germanium on a silicon wafer by hydrofluoric acid vapor-decomposition/microconcentric nebulizer-ICP-MS. *Bunseki Kagaku*, **48**(7), 681–5.
49. Ferrero, E. and Posey, D. (2002) Improving the detection limits for VPD-ICP-MS analysis. *J. Anal. At. Spectrom.*, **17**(9), 1194–201.
50. Meyer, F., White, J. B., and Radle, M. (June 1999) Characterizing wafer contaminants. *Semiconductor Int.*, **22**(6), 125–32.
51. Lovejoy, L. and Hues, S. (July 2002) Assessment of VPD/ICP-MS for routine contamination monitoring in a high-volume production fab. *Future Fab Intl.*, **13**, 140–9.
52. Palsulich, D., Coyle, K., and Weston, L. (2002) Using VPD and magnetic sector ICP-MS to characterize contaminants. *MICRO Mag.*, **20**(6), 75–85.
53. Wang, J. and Balazs, M. K. (March 2000) Analytical technique compares dopants in fab air and on wafers. *Semiconductor Int.*, **23**(3), 99–104.
54. Radle, M., Lian, H., Nicoley, B., and Howard, A. J. (July 2001) Characterizing thermal oxide metals. *Semiconductor Int.*, **24**(8), 217–24.
55. Krushevska, A., Tan, S., Passer, M., and Liu, X. R. (2000) Advances in trace element analysis of silicon wafer surfaces by vapor phase decomposition (VPD) and inductively coupled plasma mass spectrometry. *J. Anal. At. Spectrom.*, **15**(9), 1211–6.
56. Takenaka, M., Yamada, Y., Yabuki, M., Nakamura, S., and Kozuka, S. (2001) Determination of the ultratrace metallic impurities distribution in silicon wafers by sub-area chemical etching/microflow nebulizer-ICP-MS. *Bunseki Kagaku*, **50**(6), 399–404.
57. Yamada, Y., Tachibe, T., Shimazaki, A., Takenaka, M., and Kozuka, S. (2001) Determination of ultratrace phosphorus and titanium on silicon wafer surface by high resolution ICP-MS. *Bunseki Kagaku*, **50**(6), 453–8.
58. SEMI (2001) Test Method for the Determination of Inorganic Contamination from Mini-environments Using VPD-TXRF, VPD-AAS or VPD-ICP-MS. SEMI E45-1101, SEMI, San Jose.
59. SEMI (2002) Specifications for Polished Monocrystalline Silicon Wafers. SEMI M1-0302, SEMI, San Jose.
60. Meyer, F. and White, J. B. (July 1999) Acid etching chemistry characterizes silicon wafer surface metals. *Semiconductor Int.*, **22**(8), 137–44.
61. Wang, J., Balazs, M. K., Tansy, B., Pianetta, P., Baur, K., and Brennan, S. (2002) Quantification issues for the measurement of copper contaminant on silicon wafer surfaces. Presented at the *2002 SEMI Technology Symposium.* San Francisco, CA, USA.

62. Chung, H. Y., Kim, Y. H., Cho, H. Y., Lee, B. O., Yoo, H. D., and Lee, S. H. (2001) Collection efficiency of metallic contaminants on Si wafer by VPD-droplet collection. *Anal. Sci.*, **17**(5), 653–8.
63. Beebe, M., Sparks, C., and Rudack, A. (2003) Detection of copper in the edge exclusion area of wafers transported in 300 mm FOUPs. Presented at the *2003 Materials Integrity Management Symposium*, Santa Clara, CA, USA.
64. Yamada, Y., Kozuka, S., Shimazaki, A., and Takenaka, M. (2002) Evaluation of ultratrace metallic elements in poly-SiGe thin films. Presented at the *2002 UCPSS Conference*, Ostende, Belgium.
65. Park, C. J., Cha, M. J., and Lee, D. S. (2001) Determination of copper in uniformly-doped silicon thin films by isotope-dilution ICP-MS. *Bull. Korean Chem. Soc.*, **22**(2), 205–9.
66. Park, C. J., Kim, K. J., Cha, M. J., and Lee, D. S. (2000) Determination of boron in uniformly-doped silicon thin films by isotope dilution inductively coupled plasma mass spectrometry. *Analyst*, **125**, 493–7.
67. Li, F., Balazs, M. K., and Pong, R. (2000) Total dose measurement for ion implantation using laser ablation ICP-MS. *J. Anal. At. Spectrom.*, **15**(9), 1139–41.
68. Li, F. and Anderson, S. (2003) Using direct solid sampling ICP-MS to complement SEM-EDX and SIMS in characterizing semiconductor materials. Presented at the *2003 International Conference on Characterization and Metrology for ULSI Technology*, Austin, TX, USA.
69. Tan, S., Chen, N., and Liu, S. (2003) Cleaning and qualification of semiconductor process chamber components for yield improvement. Presented at the *2003 SEMI Technology Symposium: Innovations in Semiconductor Manufacturing*, San Francisco, CA, USA.
70. Schneider, G. (2001) Requirements of chemicals used in semiconductor manufacturing at INFINEON Dresden. Presented at the *2001 SEMICON Europa Standards Workshop: Analytical Methods for Process Chemicals*, Munich, Germany.
71. Singer, P. (February 2003) High-k gate dielectrics: no easy solution. *Semiconductor Int.*, **26**(2), 38.
72. Seubert, A. (1996) On-line coupling of ion chromatography and atomic spectrometry for ultra trace analysis in high purity molybdenum and tungsten silicides. *Fresenius' J. Anal. Chem.*, **354**, 788–96.
73. Seubert A. (1999) A critical comparison of on-line coupling IC-ICP-(AES, MS) with competing analytical methods for ultra trace analysis of microelectronic materials. *Fresenius' J. Anal. Chem.*, **364**(5), 404–9.
74. Coedo, A.-G., Dorado, M. T., and Padilla, I. (2002) On-line ion-exchange matrix separation and inductively coupled plasma mass spectrometric determination of trace impurities in high-purity aluminum. *J. Anal. At. Spectrom.*, **17**(5), 502–6.
75. Kozono, S., Sakamoto, H., Takashi, R., and Haraguchi, H. (1998) Multielement determination of ultratrace impurities in high purity tantalum metals by flow injection/ICP-MS. *Anal. Sci.*, **14**, 757–62.
76. Nakane, K., Uwamino, Y., Morikawa, H., Tsuge, A., and Ishizuka, T. (1998) Determination of trace impurities in high-purity aluminum oxide by high resolution ICP-MS. *Anal. Chim. Acta*, **369**(1–2), 79–85.
77. Kozono, S., Takahashi, S., and Haraguchi, H. (2002) Determination of trace phosphorus in high purity tantalum materials by inductively coupled plasma mass spectrometry subsequent to matrix separation with on-line anion exchange/coprecipitation. *Anal. Bioanal. Chem.*, **372**, 542–8.
78. Kozono, S., Takahashi, S., and Haraguchi, H. (2002) Determination of boron in high purity tantalum materials by on line matrix separation/ICP-MS. *Analyst*, **127**, 930–4.

79. Kozono, S., Takahashi, S., and Haraguchi, H. (2000) Determination of ultratrace impurities in high purity tantalum materials by on-line anion exchange matrix separation and ICP-MS. *Anal. Sci.*, **16**, 69–74.
80. Fujimoto, K., Ito, M., Shimura, M., and Yoshioka, K. (1998) Determination of trace amounts of P in high-purity silicon by ICP-MS after acid-vapor decomposition under elevated pressure and isolation as a molybdophosphate-dodecyltrimethylammonium bromide ion pair. *Bunseki Kagaku*, **47**(5), 187–93.
81. Kumar, S. J., Meeravali, N. N., and Arunachalam, J. (1998) Determination of trace impurities in high purity gallium by ICP-MS and cross validation of results by transverse heated graphite furnace AAS. *Anal. Chim. Acta*, **371**(2–3), 305–16.
82. Becker, J. S., Soman, R. S., Becker, T., Panday, V. K., and Dietze, H.-J. (1998) Trace and ultratrace analysis of gallium arsenide by different mass spectrometric techniques. *J. Anal. At. Spectrom.*, **13**(9), 983–7.
83. Becker, J. S., Pickhardt, C., and Dietze, H.-J. (2001) Determination of trace elements in high purity platinum by laser ablation inductively coupled plasma mass spectrometry using solution calibration. *J. Anal. At. Spectrom.*, **16**(6), 603–6.
84. Chi, P.-H., Ko, F.-H., Hsu, C.-T., Chen, H.-L., Yang, C.-K., Sun, Y.-C., and Yang, M.-H. (2002) Direct impurity analysis of semiconductor photoresist samples with laser ablation ICP-MS. *J. Anal. At. Spectrom.*, **17**, 358–65.
85. Torres, R., Vininski, J., Yucelen, B., Houlding, V., Treadwell, D., and Felbaum, J. W. (2001) An ultra-high-purity bulk specialty gas package for 300 mm wafer fabrication. *Semiconductor Fabtech*, **14**, 131–7.
86. Anderson, P. C., Cooper, G., and Houlding, V. H. (April 1998) The cylinder's impact on metal impurities in CO. *Semiconductor Int.*, **21**(4), 127–9.
87. Laly, S., Nakagawa, K., Kimijima, T., Taguchi, S., Ikeda, T., and Hasaka, S. (1996) Determination of particle-bound metallic impurities in semiconductor grade gases, 1: Silane. *Anal. Chem.*, **68**, 4312–5.
88. Hutton, R. C., Bridenne, M., Coffre, E., Marot, Y., and Simondet, F. (1990) Investigations into the direct analysis of semiconductor grade gases by inductively coupled plasma mass spectrometry. *J. Anal. At. Spectrom.*, **5**, 463–6.
89. Suzuki, I. and Tarutani, K. (1997) Comparison of sampling techniques for the analysis of particulate metal impurities in gases. *Anal. Sci.*, **13**(10), 833–6.
90. Capitanio, D., Mizuno, Y., and Leeca, J. (1999) Metal ion removal from photoresist solvents. Presented at the *1999 Microlithography Conference*, Santa Clara, CA, USA.
91. Parekh, B., Hashimoto, Y., and Amari, M. (2003) Purification of wet etch and cleaning chemicals and DI rinse water using high performance membrane purifiers. Presented at the *2003 Semiconductor Pure Water and Chemicals Conference*, Santa Clara, CA, USA.
92. Grant, D. C., Kelly, P. K., Anantharaman, V., and Shyu, J.-H. (1997) Purity control in dilute HF baths using point of use purifiers. Presented at the *1997 Semiconductor Pure Water and Chemicals Conference*, Santa Clara, CA, USA.
93. SEMI (1999) Practice for Preparing Liquid Chemical Distribution Components for Chemical Testing, SEMI F40-0699, SEMI, San Jose.
94. SEMI (2000) Test Method for Determining Trace Metals in Polymer Materials, SEMI F48-0600, SEMI, San Jose.
95. SEMI (2001) Provisional Specification for Polymer Components used in UltraPure Water and Liquid Chemical Distribution Systems, SEMI F57-0301, SEMI, San Jose.
96. Chilcote, D., Grant, D., Tan, S., and Carrieri, D. (1998) The extraction of surface and bulk trace metal impurities from typical fluoropolymers. Presented at the *1998 SEMI Workshop on Contamination in Liquid Chemical Distribution Systems*, San Francisco, CA, USA.

Index

Inductively Coupled Plasma Mass Spectrometry Handbook Edited by Simon M. Nelms

ISBN: 978-1-405-10916-1